
STEEL FORGINGS

Nisbett / Melilli editors



STP 903

STEEL FORGINGS

A symposium
sponsored by
ASTM Committee A-1
on Steel, Stainless Steel,
and Related Alloys
Williamsburg, VA, 28–30 Nov. 1984

ASTM SPECIAL TECHNICAL PUBLICATION 903
Edward G. Nisbett, National Forge Co.,
and Albert S. Melilli, General Electric,
editors

ASTM Publication Code Number (PCN)
04-903000-02



AMERICAN SOCIETY FOR TESTING AND MATERIALS
1916 Race Street, Philadelphia, PA 19103

Library of Congress Cataloging-in-Publication Data

Steel forgings.

(ASTM special technical publication; 903)

Includes bibliographies and index.

“ASTM publication code number (PCN) 04-903000-02.”

1. Steel forgings—Congresses. I. Nisbett, E. G. (Edward G.). II. Melilli, Albert S. III. American Society for Testing and Materials. Committee A-1 on Steel. IV. Series. TS320.S745 1986 672.3'32 86-14066
ISBN 0-8031-0465-0

Copyright © by AMERICAN SOCIETY FOR TESTING AND MATERIALS 1986

Library of Congress Catalog Card Number: 86-14066

NOTE

The Society is not responsible, as a body,
for the statements and opinions
advanced in this publication.

Printed in Ann Arbor, MI
September 1986

Foreword

The symposium on Steel Forgings was held in Williamsburg, Virginia on 28–30 Nov. 1984. The American Society for Testing and Materials' Committee A01 sponsored the symposium. E. G. Nisbett, National Forge Co., and Albert S. Melilli, General Electric, served as cochairmen of the symposium and as coeditors of this publication.

Related ASTM Publications

Through-Thickness Tension Testing of Steel, STP 794 (1983), 04-794000-02

Rolling Contact Fatigue Testing of Bearing Steels, STP 771 (1982), 04-771000-02

Application of 2-1/4Cr-1Mo Steel for Thick-Wall Pressure Vessels, STP 775 (1982), 04-755000-02

Toughness of Ferritic Stainless Steels, STP 706 (1978), 04-706000-02

Properties of Austenitic Stainless Steels and Their Weld Metals (Influence of Slight Chemistry Variations), STP 679 (1979), 04-679000-02

A Note of Appreciation to Reviewers

The quality of the papers that appear in this publication reflects not only the obvious efforts of the authors but also the unheralded, though essential, work of the reviewers. On behalf of ASTM we acknowledge with appreciation their dedication to high professional standards and their sacrifice of time and effort.

ASTM Committee on Publications

ASTM Editorial Staff

David D. Jones
Janet R. Schroeder
Kathleen A. Greene
Bill Benzing

Contents

Overview	1
-----------------	---

TURBINE AND GENERATOR FORGINGS

Keynote Address

The Development of Improved Forgings for Modern Steam Turbines—R. M. CURRAN	9
--	---

Steel Production for Rotors

Influence of Advanced Steelmaking Technology on Specification Trends for Rotor Forgings—J. E. STEINER AND R. I. JAFFEE	35
Discussion	43

The Effect of Alloying Elements and Steelmaking Processes on the “A” Segregation Occurrence in Large Ingots—J. T. KIM, M. R. PYO, Y. S. CHANG, AND H. S. CHIANG	45
--	----

Rotor Manufacture

Development of Integral High-Pressure–Low-Pressure Combination Rotor Forgings—M. YAMADA, M. MIYAZAKI, O. WATANABE, AND M. KAWAI	59
Discussion	71

Manufacture of Differentially Heat-Treated Turbine Rotor Forgings—A. SUZUKI, S. KINOSHITA, AND H. KIKUCHI	74
Discussion	85

Manufacturing of Welded Polyblock Turbine Rotors for Pressurized Water Reactor Nuclear Plants; Optimization of the Steel Grade; Effect of Impurities—J. PISSELOUP, I. S. POITRAULT, A. DE BADEREAU, AND P. G. BOCQUET	87
Discussion	102

Steels for Rotors

New 2Cr-Mo-Ni-W-V Steel for High-Pressure Rotors—H. FINKLER AND E. POTTHAST	107
Mechanical Properties of Advanced Technology 1Cr-Mo-V Steam Turbine Rotor Forgings—V. P. SWAMINATHAN, R. I. JAFFEE, AND J. E. STEINER	124
Discussion	141
Soft-Martensitic Stainless Cr-Ni-Mo Steel for Turbine Rotors in Geothermic Power Stations—K. SCHÖNFELD AND E. POTTHAST	143
Discussion	154

Rotor Assessment

Metallurgical Analysis of Flaws in Carbon-Molybdenum and Nickel- Molybdenum-Vanadium Turbine Rotor Forgings—S. TONEY, W. KIM, A. S. MELILLI, AND S. G. LEONE	157
Discussion	177
The Fracture Toughness of Actual and Simulated Large Rotor Forgings Made from 3.5Ni Steel—J. ALBRECHT, J.-E. BERTILSSON, AND B. SCARLIN	178
Discussion	196
Integrity of Full-Integral, Low-Pressure Nuclear Turbine Forgings—S. KAWAGUCHI, N. KANNO, T. IWADATE, AND T. OHHASHI	203
Discussion	214
In-Service Inspection Test and Evaluation Techniques for Large Generator Rotors—R. H. BELLOWS, R. J. ZAWOYSKY, AND D. N. WALKER	219
Discussion	234

Generator Retaining Rings

The Development of New Materials for Nonmagnetizable Retaining Rings and Other Applications in the Power Generating Industry—G. STEIN	237
Discussion	256

18–18 Corrosion-Resistant Retaining Rings for Nuclear Power Plant Generators—J. B. RAMBAUD AND R. H. CAZENAVE	258
Discussion	272

PRESSURE VESSEL AND NUCLEAR FORGINGS

Review

Seamless Shell Course Forgings for Heavy-Wall Reactor Vessels: A Forgemaster's Critical Review—P. BERNABEI, L. CALLEGARI, M. SCEPI, AND T. SALINETTI	275
---	-----

Steels for Pressure Retaining Components

Evaluation of Modified 9Cr-1Mo Steel Forging—A. K. KHARE AND V. K. SIKKA	303
Discussion	327

Evaluation of the Modified 9Cr-1Mo Steel Forging by French Laboratories—A. GEIPI	328
Discussion	345

Optimizing Mechanical Properties of Specialty, Stainless, and Heat-Resistant Alloy Steel Forgings by Thermomechanical Processing—G. W. KUHLMAN, R. PISHKO, W. S. DARDEN, AND W. L. KRUBSACK	346
Discussion	362

Forging Processing for Pressure Vessel and Nuclear Application

Application of New Types of Ingots to the Manufacturing of Heavy Pressure Vessel Forgings—P. G. BOCQUET, J.-C. SAINT-IGNAN, AND R. P. BLONDEAU	367
---	-----

Integral Forged Pump Casing for the Primary Coolant Circuit of a Nuclear Reactor: Development in Design, Forging Technology, and Material—W. AUSTEL AND H. KÖRBE	385
---	-----

Manufacturing of Large and Integral-Type Steel Forgings for Nuclear Steam Supply System Components—S. KAWAGUCHI, H. TSUKADA, K. SUZUKI, I. SATO, AND S. ONODERA	398
--	-----

Advanced Technology of Heavy-Section Tube Sheets for Nuclear Power Generation—T. A. SKAMLETZ AND W. W. GRIMM	410
Discussion	423

Best Possible Heat Treatment of Steel SA 336 F22 for the Production of Forged Shells with Heavy Walls—J. P. BADEAU, I. S. POITRAULT, A. DE BADEREAU, AND R. P. BLONDEAU	425
Discussion	438

Production of a 304 Stainless Steel Nuclear Reactor Forging from a Very Large Electroslag Refined Ingot—E. J. WATKINS AND E. L. TIHANSKY	439
Discussion	449

GENERAL INDUSTRIAL FORGINGS

Equipment and Forging Process

Survey of New Developments in Forging Techniques and Equipment—N. M. KRAMAROW	453
--	-----

Forging Force Requirements with Special Regard to Shear Resistance of the Forge Material—L. J. JAVORIK	476
---	-----

Forging of Long-Stroke Crankshafts by the TR Method—T. RUT	504
---	-----

Manufacture and Application

Cryogenic Mechanical Properties of A286 Alloy and 304LN Stainless Steel Used in Fabrication of Support Struts for Superconducting Magnets—T. ABE, M. KOHINO, A. SUZUKI, AND R. M. SCANLAN	523
Discussion	539

Steel Forgings for a Tension Leg Platform Anchoring System—The Design and Management Contractor's Experience of Their Manufacture and Testing—P. J. WHITEHOUSE	540
Discussion	548

Test Methods and Forging Assessment

High-Sensitivity, Immersion, Ultrasonic Testing of Steel Forgings—J. G. GENSURE, A. S. MELILLI, AND S. M. BRUEGGEMANN	553
--	-----

Hydrogen—Its Occurrence, Determination, and Control in Steel	
Forgings—E. L. MURPHY AND J. E. STEINER	573
Discussion	582
Failure Analysis of Hot Forging Dies—R. EBARA AND K. KUBOTA	583
Author Index	593
Subject Index	595

Overview

This symposium was sponsored by ASTM Committee A01 on Steel, Stainless Steel, and Related Alloys. It was organized by Subcommittee A01.06 on Steel Forgings and Billets and was international in terms of both the contribution of papers and the attendance. The object was to reflect on the scope of the work of the subcommittee and its four sections, as well as to provide a forum for the presentation of developments in ferrous forgings. An anticipated outcome of the symposium would be a significant contribution to the range, momentum, and quality of the expertise applied to the standards work of the subcommittee, but this special technical publication will serve more widely as a benchmark on the technology of steel forgings, particularly the larger sizes.

The symposium format followed the organization of A01.06, reflecting that subcommittee's diverse interest in steel forgings. The sessions, then, included general industrial forgings, turbine and generator forgings, pressure vessel and nuclear forgings, and test methods. Assistance was given by Subcommittee A01.08 on Wrought Stainless Steel Products for the session on stainless steel forgings. In the spirit of all ASTM activity, the symposium contributors included those who produce, those who use, and those who have a general interest in forgings, with an added contribution from a forging equipment manufacturer. The subject matter of the papers covers all of the salient manufacturing stages on which the production of quality forgings depends, namely, steel melting, refining and re-melting procedures, control of segregation and solidification in both large and specialized ingots, forging procedures, and achievements which contribute to improved integrity in response to application demands. It is laudable that the symposium was held so successfully at a time when demands on forging capacity were and currently are steadily receding. The trends in heat-treatment procedures for forgings are evident from the details given in several of the papers. Forgings present particular problems for nondestructive test methods because of the range in size and the variety in shape. The papers include reference to immersion ultrasonic examination as well as to specialized techniques for in-service inspection.

As a summary paper on the development and current status of turbine and generator rotor forgings, the keynote address by Curran reflects the growth of the industry in terms of the sheer size of the present-day central generating plant, made possible in part by the steadily improved quality of the forgings. It is indeed fitting that this paper marked the retirement of the author after a distinguished

2 STEEL FORGINGS

career devoted to these essential products. The integrity required in a huge spinning mass of forged alloy steel, confined within a steam chest or stator housing, is not generally subject to debate, and it should come as no surprise that papers concerned with this equipment constituted the longest session of the symposium, the subjects covering not only the rotors themselves but also the generator retaining rings.

The control of segregation in the massive ingots needed to make rotors is specifically the subject of a paper by Kim et al., giving confirmation of the beneficial effects of low silicon practice and adding to the data available on the important subject of ingot segregation. A glimpse of the possible future melt practice for super clean steel for large rotor production is the Electric Power Research Institute (EPRI) paper by Steiner and Jaffee on the manufacture of an experimental Ni-Cr-Mo-V turbine rotor forging. The full evaluation of this rotor is underway, and one challenge will be the assimilation of the evolving requirements into economic manufacture.

The mechanical property requirements of high-temperature steam turbine operation are at odds with those for the lower pressure operation of the same unit, and developments aimed at satisfying both requirements in an acceptable manner recently have resulted in production units being made. The development and manufacture of such turbine rotor forgings are discussed in papers by Yamada et al. and Suzuki et al. and depend on a novel dual heat-treatment procedure. These papers are reference works for this application. In similar fashion, the information included on the advanced technology 1Cr-Mo-V turbine forgings from more EPRI work by Swaminathan et al. and on the new 2Cr-Mo-Ni-W-V steel by Finkler and Potthast for high-pressure rotors will provide a fund of reference data.

The current status for large welded rotors by one of the European manufacturers also is discussed by Pisseloup et al., while the subject of large monobloc forgings in Ni-Cr-Mo-V steels, already touched on in discussion of the ingot segregation control, is addressed in a status paper by Kawaguchi et al., with test data from among the largest rotors produced, including deep-seated notch toughness properties.

A paper by Albrecht et al. on the subject of the Ni-Cr-Mo-V steel commonly used for LP rotor forgings was aimed at mass effects associated with the hardenability of the material and was based on some actual rotor test data, together with test results on test material heat-treated to simulate much larger forgings. As has been noticed often in other such comparisons, the degree of reduction in toughness concluded for large section sizes appears to be in some contradiction with actual measurement. This remains a lively topic for further work.

Many rotor forgings which predate such significant developments as vacuum degassing and ultrasonic examination are still in use. Such units are now commonly examined as far as is possible by modern test methods. The metallurgical examinations reported by Toney et al. of Cr-Mo and Ni-Mo-V rotors taken out of service after nondestructive testing add to the data on the significance of flaw indications. It will be helpful to those responsible for the continued use of older

equipment. The condition of operating power generator equipment is also the subject of a paper by Bellows and Walker. The paper addresses the use of ultrasonic and magnetic particle examination techniques for large rotors. The data obtained is considered with regard to service-related issues such as crack growth.

In the power generator industry, the electroslag remelting (ESR) process has found a niche in the manufacture of both the martensitic and duplex chromium stainless steel rotor forgings. The use of one such alloy for service in the arduous conditions of geothermic power stations is described by Schönfeld and Potthast.

As with the high chromium steels, the ESR process also lends itself to the production of nonmagnetic retaining rings for generator forgings. This highly specialized product requires high integrity to withstand the daunting forming procedures and the demanding service. The paper by Stein and the paper by Rambaud and Cazenave discuss the latest thinking on the materials used and their properties.

In other conventional applications of the ESR process, a large nuclear forging in Type 304 austenitic stainless steel is described by Watkins and Tihansky as is an assessment of an open die test forging in the new modified 9Cr-1Mo steel by Khare and Sikka and by Gelpi. The material is now known in ASTM as Grade F91 for forgings. The information on the latter forging contributes to the data required for designers wishing to use this versatile heat-resisting steel.

The introduction of electroslag remelting under pressure is described in the Stein paper, in the context of introducing nitrogen as well as excluding possible hydrogen sources. There is some indication that this development will see the introduction of new nitrogen-containing alloy steels, but the system may prove to be of great significance (without the addition of nitrogen) in the control of hydrogen, always a problem in the electroslag remelting of high-strength, low-alloy steels, and particularly so with the very low sulfur contents possible with the ESR process.

Forging procedures are covered on both the theoretical and application sides by a paper on forging force requirements with regard to shear resistance of the material by Javorik and by a detailed description of a procedure for manufacturing very large continuous grain flow, marine-type crankshafts by Rut. The latter paper again gives the current status for an established method of forging such shafts.

Thermomechanical processing for austenitic stainless and heat resisting forgings, including some high-strength precipitation hardening grades, is authoritatively described by Kuhlman et al., and an unusual forging application of austenitic stainless and the high-strength A286 material is described by Abe and his coworkers for cryogenic application in a fusion test facility in California. The details on forgings in these specialty steels will be welcomed by those using or working with them.

In the pressure vessel field, the papers included an account by Bocquet et al. on the directionally solidified ingots manufactured by what is known as the LSD process and used for specialized applications. Hollow ingots for pressure vessel

shells and disk-type ingots for large tube sheets are discussed, particularly on the segregation characteristics of these ingot types. It will be of great interest to watch the popularity of these procedures. In particular, the disk-type ingot without hot tops may be the subject for future papers.

The offshore oil and gas industry has developed quality and design restraints as a result of service experience that includes several tragic failures and is faced with the difficulties of working in deep waters. Sophisticated designs requiring material of high integrity are now appearing, and an example of this is in the paper by Whitehouse, while illustrates the use of low-alloy steel forgings for a tension leg platform (TLP) anchor design.

Heat treatment figured heavily in at least two papers in this session, one by Badeau et al. covering the 2 1/4Cr-1Mo material for petrochemical vessel shells, and the other by Skamletz and Grimm on large nuclear power system tube sheets in ASTM 508 class 3 type material. The latter example described the use of the intercritical heat-treatment system to enhance toughness. Standards action to positively admit this type of heat treatment is probably overdue at this time. Another paper from Europe by Austel and Körbe and from Japan by Kawaguchi et al. illustrate the state of development of very large and intricate open die forgings for specialized components for nuclear reactors and pumps. These papers convey very well to designers the forging capability for high-integrity components with the minimum of welds for later in-service examination. Just as the keynote paper gave the review of rotor forgings, the paper by Bernabei et al. on seamless shell course forgings gives an excellent overview of the nuclear forging status.

Forgings, because of their variability in size, shape, and cross-section size, impose specific requirements and restrictions on test methods not encountered or required for the more regularly-sized product forms such as rolled shapes or plate. The development of an immersion ultrasonic examination method for steel forgings and described in the paper by Gensure et al. in the test methods session describes the use of such a system, not currently covered by the methods of A 388,¹ A 418,² A 456,³ or A 745,⁴ all of which are ultrasonic examination methods for forgings. An update on hydrogen in steel forgings by Murphy and Steiner also was included in this session as a review of current thinking on this important subject. Failure analysis commonly is not addressed in a general symposium of this type, but the paper by Ebara and Kubota on forging die failure assessment, on a fracture mechanics basis, introduces factors of interest directly to the forging producers. The state of the art review of current forging equipment by Kramarow is also of great interest to forging producers and users alike by indicating the limitations as well as the capabilities of the various approaches.

¹ ASTM Recommended Practice for Ultrasonic Examination of Heavy Steel Forgings (A 388-84).

² ASTM Method for Ultrasonic Inspection of Turbine and Generator Steel Rotor Forgings [A 418-77 (1982)].

³ ASTM Specification for Magnetic Particle Inspection of Large Crankshaft Forgings (A 456-83).

⁴ ASTM Recommended Practice for Ultrasonic Examination of Austenitic Steel Forgings (A 745-84).

The quality of the papers and the breadth of their contents amply justified the decision to hold the symposium and indeed indicate that it was overdue. This record of the first symposium on Steel Forgings will, both with the papers and the frank discussion, assist the industry in showing what has been attained, warn of possible troublesome aspects, and serve as a reference for further development and application.

An aspect worthy of note is that where there has been a demonstrated need, there has been astonishing development of processes and procedures, as may be seen in the accounts of the large turbine and generator rotor forgings and the nuclear reactor forgings. Conversely, where demand has been absent, understandably there has been little development. This is being demonstrated in the United States, and the domestic forging community must be on guard against becoming a follower rather than a technical leader in steel forgings.

Edward G. Nisbett

National Forge Co., Irvine, PA; symposium
cochairman and coeditor

Turbine and Generator Forgings

Keynote Address

The Development of Improved Forgings for Modern Steam Turbines

REFERENCE: Curran, R. M., "The Development of Improved Forgings for Modern Steam Turbines," *Steel Forgings, ASTM STP 903*, E. G. Nisbett and A. S. Melilli, Eds., American Society for Testing and Materials, Philadelphia, 1986, pp. 9–32.

ABSTRACT: This paper describes the developments that have taken place during the past 40 years in the manufacture of the large rotor forgings that are required for the turbine and generator sets in electric utility, central station applications. Modifications in steelmaking practices—such as the changes from open hearth to the electric practice, the introduction of vacuum pouring, and changes in ingot mold design—are discussed, as well as evaluations of newer remelt techniques such as vacuum consumable electrode melting, electros slag remelting, and electros slag hot topping. Changes in alloy content and heat-treating practices and the improvements that have resulted in the mechanical properties and fracture toughness are illustrated.

The progress that has been made in reducing the incidence of internal flaws and the improvements that have been made in nondestructive testing and evaluation to quantitatively appraise the effect of such flaws on the probable performance are discussed.

It is concluded that in low-pressure rotors, as a result of the improved cleanliness, detection methods, and fracture toughness, the probability of an undetected critical size defect has been decreased by several orders of magnitude. In the case of the high-temperature rotors, the improvements in properties, together with improved designs and operating procedures, have substantially improved the life expectancy of these rotors in spite of increases in forging size and unit ratings.

The important contributions that ASTM committees have made to this progress are described and acknowledged.

KEY WORDS: large alloy steel forgings; turbine and generator steels; fracture toughness, rupture strength, and ductility of steels

The purpose of this paper is to describe the developments that have taken place in forgings for steam turbine-generator rotors during the past 40 years and to acknowledge the important role that ASTM has played.

Historical Perspective

The early steam turbine-generators manufactured by General Electric were similar to the 5000-kW vertical units installed in the Fisk Station of Common-

¹ Manager, Turbine Materials Engineering, General Electric Co., Schenectady, NY 12345.



FIG. 1—5000-kW vertical Curtis steam turbine-generator at the Schenectady plant of the General Electric Co. (designated as a national historic mechanical engineering landmark by the American Society of Mechanical Engineers, 28 May 1975).

wealth Edison Company in the early 1900s (Fig. 1). These early units operated at very low steam temperature and pressure and were very inefficient by modern standards. Figure 2 [1] shows the improvements in heat rate (British thermal units/kilowatt-hours) as the inlet temperatures and pressures have increased since those early years (Fig. 3) [2]. The vertical lines in this figure show specific machines that were built with inlet steam pressures and temperatures higher than prevailing steam conditions.

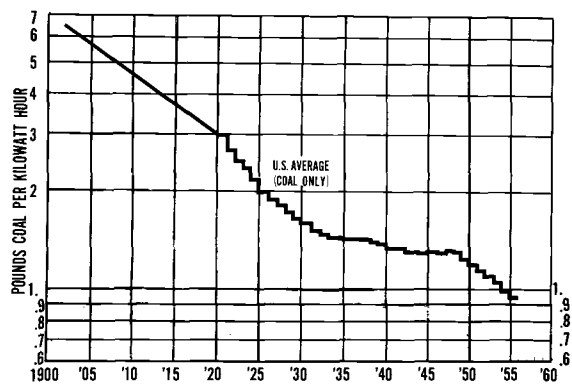


FIG. 2—U.S. coal rate (average fuel consumption rate per kilowatt-hour).

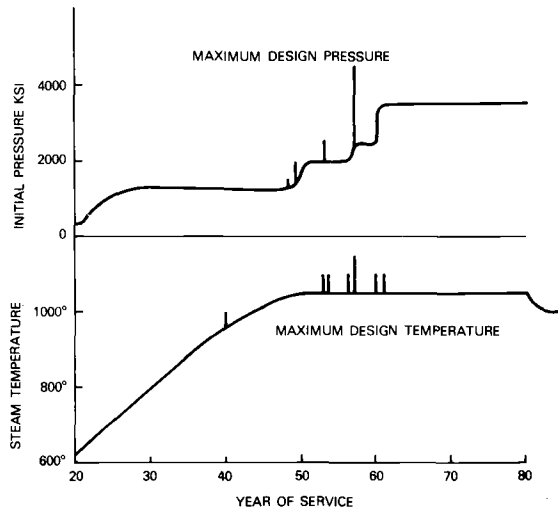


FIG. 3—Trends in large steam-turbine inlet pressures and temperatures.

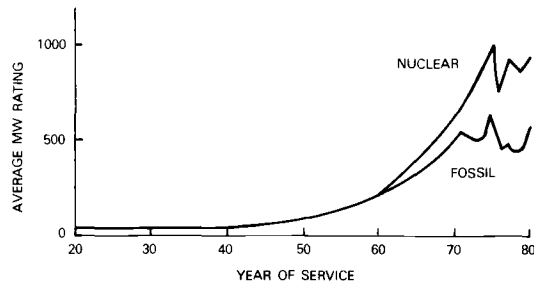


FIG. 4—Trends in large steam-turbine ratings.

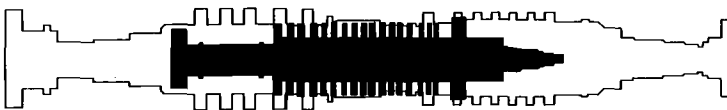


FIG. 5—Superimposed outline of typical 1945-hp steam turbine rotor on typical current high pressure-reheat (HP-RHT) rotor.

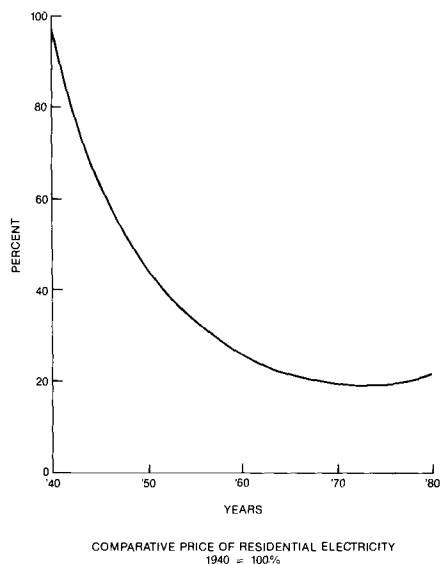


FIG. 6—Comparative price of residential electricity (1940 = 100%).

As utility systems grew in size, the demand for larger unit ratings also grew (Fig. 4), requiring larger, heavier rotor forgings.

Figure 5 compares a high-pressure rotor in a 30-MW unit, typical of those shipped in the 1940s, with a 500-MW unit shipped in the 1980s. It is interesting to note that the power generated per pound of rotor forgings in the smaller unit was only 0.45 kW/kg (1 kW/lb), while in the modern unit the ratio is 1.13 kW/kg (2.5 kW/lb).

Since gross stresses, such as average bursting stress, are a function of diameter, the strength levels required of the larger forgings are correspondingly higher.

Thus the requirements for forging development were established by the industry's dedication to lowering the cost of electricity by lowering fuel costs through advanced steam conditions and by lowering construction and operating and maintenance costs through larger unit ratings. The overall success in keeping power cost low may be judged by reference to Fig. 6, which shows the inflation-adjusted average price of residential electricity service since 1940.

Forging Developments

One of the earliest concerns in turbine rotor development was the change in properties that resulted from the increase in inlet operating temperatures during the 1920s. The ASTM-ASME Joint Committee on the Effect of Temperature on the Properties of Metals was formed in 1925 to address these questions. This committee did valuable work in developing test methods for hot tensile testing and later creep rupture testing. In the 1950s, the Data and Publication Panel provided a further service by publishing the first of a continuing series of special

technical summaries of high-temperature properties of alloys [3]. Although most of the work of the Joint Committee was concerned with piping and pressure vessel material, the data bases generated by the Committee provided a valuable reference in evaluating the high-temperature characteristics of rotor forgings.

Prior to 1940, requirements on rotor forgings were not demanding because the temperatures (with relatively few exceptions) were below the creep range, small unit ratings required relatively small forgings, and many of the units with larger ratings operated with low stresses at speeds less than 3600 rpm.

Most of the rotors were monoblock construction, but the low-pressure sections for 1800-rpm machines were made from a built-up construction using disks shrunk on a central shaft.

Rotor forgings of that era had mechanical properties specified to provide a generous margin between tensile strength and bulk design stresses. In many cases, the steel chemistry was decided by the steelmaker. The analyses chosen included 0.5Mo-2.5Ni-2.5Ni-V and 2.5Ni-0.5Mo-0.1V, with the latter steel applied to the larger rotors where higher strengths were required. ASTM Specification A293 on steel forgings for turbine rotors and shafts, issued in 1943, covered the requirements for these components.

The forgings of that era were manufactured from acid and basic open hearth steel. In the early 1940s, electric furnace melting facilities began to appear in large sizes as reductions in the cost of electricity made this practice more economical. The acid open hearth (AOH) steel tended to be dirtier because the slag had a lesser tendency to float out and because this process lacked the ability to lower phosphorus and sulfur levels during the refining periods. The AOH process did tend to provide lower hydrogen in the steel, in part because the slag materials were less hygroscopic; therefore, this practice was preferred for high-hardenability steels where hydrogen flaking threatened to be a problem.

The basic open hearth (BOH) practice provided steel that had somewhat higher hydrogen content than steel produced by AOH but was lower in phosphorus and sulfur content. The electric furnace practice was capable of providing the cleanest steel of all three methods and of achieving much lower phosphorus and sulfur levels. However, electric furnace (EF) steel tended to have the highest levels of hydrogen. (Typical values for phosphorus and sulfur were 0.035% for AOH, 0.025% for BOH, and 0.015% or lower for EF.)

Before 1940, forgings were evaluated using the heat stability test, magnetic particle test of the periphery, visual inspection and kerosene-and-whiting test of the bore, and tension tests from rotor prolongs. Although no subsurface non-destructive test method was available, the test of the bore after heat treatment and boring did give an opportunity to evaluate the internal soundness to some extent. Some of these examinations did show that hydrogen flaking had occurred, and steel mill practices were modified to include prolonged soaking periods at elevated temperatures to permit some of the hydrogen to diffuse before final heat treatment.

In the later 1940s, there was a rapid increase in inlet temperatures and pressures and in unit ratings of 3600-rpm designs. Considerable progress had been made

in high-temperature testing during the early 1940s, but the only technique available for predicting long-time strength was a log stress versus log-time extrapolation. Nevertheless, the data available indicated that the carbon and low-alloy steels used successfully in the 1930s would not provide suitable design margins for long-time service at higher temperatures. The Cr-Mo-V steels, which had been under development, were introduced into service for the high-temperature rotors. The strength characteristics of this grade were emphasized, an austenitizing temperature of 1283 K (1850°F) was selected, and the forgings were heat-treated to a relatively high tensile strength. The need for better high-temperature ductility and lower-temperature fracture toughness was not fully appreciated at that time.

The larger ratings required larger forgings and higher tensile strength than previously required for low pressure (LP) rotors. The Ni-Mo-V alloy was introduced to provide this strength with a reasonably high tempering temperature. This grade also was used in some high-temperature applications with a heat treatment designed to provide somewhat better creep rupture characteristics. Work had begun in the industry to evaluate the importance of impact energy, based on the ship plate failures of the early 1940s. Although the importance of fracture toughness was becoming understood, most design and materials acceptance criteria were based on tensile and yield strength criteria.

Rotors were evaluated on the basis: of tensile and impact tests of specimens removed from the body of the rotor and the prolong; of magnetic particle tests of the periphery and bore; and, in the later 1940s, of the periphery ultrasonic test.

Modern Rotor Forging Technology

The era of modern rotor forging technology began in the early 1950s after a series of failures in high- and low-temperature turbine rotors and generator rotors indicated that the improvements in rotor forgings had not kept pace with the demands made in the units then being built. Failures that occurred in the blade attachment area of several Cr-Mo-V turbine rotors were caused by inadequate creep ductility, and several failures in Ni-Mo-V turbine rotors were related to insufficient high-temperature strength [4,5]. Brittle fractures occurred in a Ni-Mo-V low-temperature turbine rotor [6] and several generator rotors of this material [7,8].

More extensive programs were undertaken to improve the overall mechanical property balance of rotors for both high- and low-temperature service. Other programs were directed at a better understanding of the causes of the failures and developing the ability to predict fracture strength from material properties obtained from laboratory tests, rotational and thermal stresses, and discontinuities detected by nondestructive testing.

Many rotor development programs [9] were initiated with the individual forging suppliers, and considerable efforts were devoted to developing improved steel chemical compositions and heat treatment that would provide better balances of

properties for high-temperature turbine rotors and low-temperature turbine and generator rotors.

The overall effort consisted of fundamental metallurgical studies on small heats processed to simulate the conditions existing in large masses. There was a considerable body of data, however, indicating that simulation of the thermal cycle experienced in the centers of large masses did not produce the same result as experienced in the actual product, presumably because of the favorable effect of the compressive stresses associated with transformation in the large section sizes. Consequently, considerable work was done in evaluating full-size forgings with large sections of test metal forged onto one of the couplings. This work provided material for large-disk bursting tests, as well as for more conventional testing techniques. A typical configuration of one of the development rotors is shown in Fig. 7. Rotors included in the program are shown in Table 1. The program was aimed at characterizing the steel then currently utilized, examining process improvements to improve properties, and investigating alternate compositions. Some of the forgings in this program were found to be unacceptable and were scrapped. Only those that were shown by extensive testing to be equal to or better than conventional forgings were placed in service.

Studies of a variety of Cr-Mo-V compositions showed that higher vanadium contents tended to improve rupture strength at the expense of rupture ductility, while higher nickel contents provided improved fracture toughness at the expense of rupture strength. Faster quenching provided some improvement in surface toughness at the expense of surface rupture strength but had little effect on center toughness or rupture strength.

The 3Cr-1Mo-0.25V compositions with a differential heat treatment, austenitizing from 1010°C (1850°F) on one end of the body to 899°C (1650°F) on the opposite end, appeared to offer some advantage for rotors that had high-temperature stages and exhaust stages on the same rotor. However, changes in the overall design configuration on the larger machines eliminated the need for this type of forging in the large steam turbine-generator rotor forgings.

For the balance of the high-temperature rotors, the basic 1Cr-1Mo-0.25V composition with an optimized chemical analysis and lower final austenitizing heat treatment was considered to provide the best balance of rupture strength, rupture ductility, and fracture toughness. There is considerable interest in several new compositions that have been suggested in recent years that offer an improved balance in properties. It must be remembered, however, that considerable testing must be done to demonstrate the long-time smooth- and notch-bar rupture char-

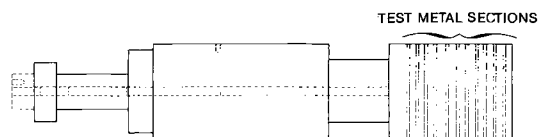


FIG. 7—Typical configuration of development rotor forgings with test metal prolongations.

TABLE 1—Some rotors evaluated in the rotor development program described by DeForest, Newhouse, and Sequin [9].

No.	Rotor Type	Type	Alloy Content, %				Process			Treatment		
			Ni	Cr	Mo	V	BE	AOH	VP	AC	OQ	WQ
2	LP turbine	Ni-Mo-V	2.8	...	0.5	0.1	1	1	...	1
1	test forging	Ni-Cr-Mo-V	2.6	0.9	0.7	0.3	1	1
3	LP turbine	Ni-Cr-Mo	2.6	1.5	0.6	...	2	1	...	1
1	LP turbine	Ni-Cr-Mo-V	2.0	1.4	0.4	0.1	1	...	1	...	1	...
2	LP turbine	3Cr-1/2Mo	...	3.2	0.5	...	1	1	...	1	...	1
2	LP turbine	Ni-Cr-Mo-V	2.7	1.6	0.6	0.1	2	2
2	LP turbine	Ni-Mo-V	2.7	1.5	0.6	0.1	2	...	2	2
1	LP turbine	Ni-Cr-Mo-V	3.3	1.8	0.6	0.1	1	...	1	1
1	generator	Ni-Cr-Mo	2.6	1.5	0.6	...	1	1
2	generator	Ni-Cr-Mo-V	2.0	1.4	0.6	0.1	1	1	1	1	1	...
1	generator	Ni-Cr-Mo-V	2.7	1.4	0.5	0.1	...	1	1
1	generator	Ni-Mo-V	1.9	...	0.5	0.1	1	1
3	generator	Ni-Mo-V	2.8	...	0.5	0.1	3	...	3	3
1	generator	Ni-Mo-V	3.0	...	0.3	0.1	...	1	...	1
2	generator	Ni-Mo-V	3.5	...	0.3	0.1	2	...	2	2
1	generator	Ni-Mo-V	2.5	...	0.3	0.1	1	1
2	generator	Ni-Mo-V	4.0	...	0.4	0.1	2	...	2	2
1	generator	Ni-Mo-V	3.5	...	0.6	0.1	1	...	1	1
1	generator	Ni-Cr-Mo-V	3.5	1.8	0.4	0.1	1	...	1	1
1	HP turbine	Cr-Mo-V	...	1.9	1.3	0.3	1	1
2	HP turbine	Cr-Mo-V	...	1.1	1.3	0.2	...	1	...	2 ^a	...	2
2	HP turbine	Cr-Mo-V	...	3.4	1.0	0.2	2	2 ^b
1	HP turbine	12Cr-Mo-WV	0.9	11.0	1.1	0.3	0.6W	1	...	1	...	1
3	2HP, 11P	Cr-Mo-V	...	3.6	1.9	0.9	3	3
1	IP	Cr-Mo-V	...	1.1	1.2	0.3	1	...	1	1
1	test forging	11Cr-Mo-V Cb	...	11.0	1.0	0.2	0.6Cb	1	...	1	...	1
1	HP	11Cr-Mo-V Cb	...	11.0	1.0	0.2	0.3Cb	1	...	1	...	1
7	HP	11Cr-Mo-V Cb	...	11.0	1.0	0.2	0.1Cb	7	...	7	...	7

NOTE: Melting and pouring practice: BE = Basic Electric, AOH = Acid Open Hearth, VP = Vacuum Pour. Treatment, cool from austenitize: AC = Air Cool, OQ = Oil Quench, WQ = Water Quench.

^a 1 rotor gradient heat-treated, 1 rotor instrumented air cool and water quench.

^b 1 rotor given gradient austenitize and temper.

acteristics and embrittlement tendencies and the heat-to-heat variability of these properties before they can be considered as alternates for the present Cr-Mo-V composition that has been well-qualified by hundreds of thousands of hours of testing and millions of hours of satisfactory service performance.

Other projects were directed toward understanding the mechanics of the failures and the role of varying microstructural discontinuities and service conditions. Large notched and unnotched spin disks were used to model the performance of rotors with and without stress concentrators. Winne and Wundt [10] applied the Griffith-Irwin theory of crack propagation to quantify the effects of discontinuities of various sizes and locations on the bursting strength of rotors and disks.

These relatively early applications of fracture mechanics were used in the

design, material acceptance, and evaluation of the adequacy of the characteristics of new forgings and those already in service.

Steelmaking Improvements

Cooperative programs with forgemasters were expanded to explore every facet of steelmaking that might have an influence on the incidence of internal discontinuities and mechanical characteristics of the steel. These studies included consideration of the control of scrap and slag-making constituents, ingot-stool-hot-top designs, top and bottom discard practice, the adequacy of forging practices, and the uniformity and control of heat treatment.

Some of the sources of internal discontinuities—such as oxide inclusions, inclusion arrays, porosity, and linear sulfides associated with V and inverted V segregation—have their origin in the ingot. Efforts were directed toward developing a method of analyzing the processes of solidification in large ingots and relating solidification parameters to various measures of ingot quality. A general purpose transient heat transfer program for a large digital computer was used for this purpose. The principles and assumptions used early in the program were described by Fischer [17], who showed that calculated solidification profiles could account for bridging under the hot-top and for formation of secondary pipe.

More than 100 ingot practices used by suppliers of rotor forgings and other steel products have been analyzed since this method was developed, and the results have been correlated with performance. Studies have included the effects: of variations in geometry of ingot mold, stool, and hot-top geometry; of the density, heat capacity, and conductivity of hot-top refractories and insulating cover powders; and of exothermic insulating materials of various types and characteristics on ingot soundness and V segregation. Figure 8 shows one of the products of solidification analysis, a diagram with solidification isochrons, showing the shape of the still-molten pool at various times after pouring.

Ingot solidification analysis can show if an ingot will be clearly prone to bridging and secondary pipe or whether it will be marginal with respect to V segregation and soundness. V segregation depends on other factors, such as pouring temperature, as well as ingot design parameters. Such analysis is especially useful in examination of the effects of changes in details of ingot and hot-top design and materials.

During the mid-1950s, there were substantial advances in the quality of steelmaking facilities and the techniques for the evaluation of the characteristics of forgings. The ability of the electric furnaces to provide higher quality steel and the introduction of vacuum pouring to provide for hydrogen removal made forgings available that were substantially better than had been possible prior to that time. The vacuum-pouring technology was first introduced in Europe using mechanical pumps that provided tank pressures of the order of 133 Pa (3 torr) (1 atm = 760 torr). In 1958, an American steel supplier pioneered with an instal-

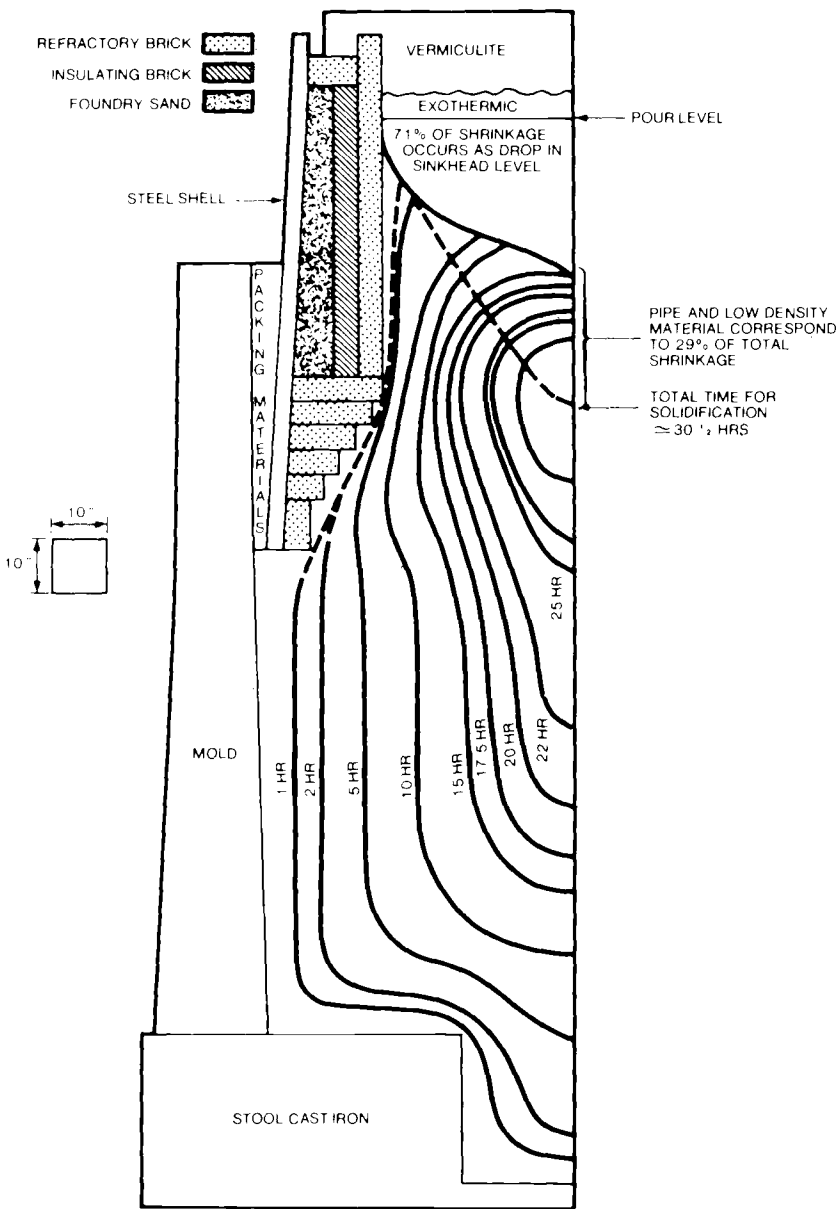


FIG. 8—Results of analysis of the solidification of a large ingot.

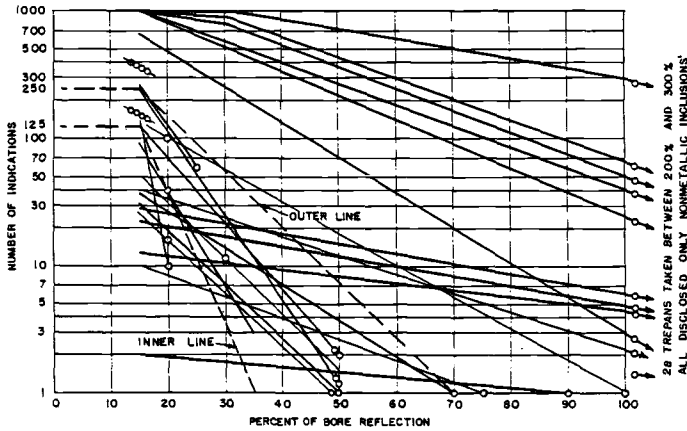


FIG. 9—Total number/magnitude plots of rotor forgings on which trepanning of stationary indications disclosed only nonmetallic inclusions. Reflection magnitudes of trepanned inclusions shown by small circles.

lation using steam ejector pumps that were capable of pumping down to 40 Pa (0.3 torr) [12-14]. This lower pressure, in addition to hydrogen removal, broke up the pouring stream into fine droplets, resulted in less oxidation of the stream, and apparently greatly reduced the size and number of nonmetallic inclusions in the ingot.

Thus, the development of improved steelmaking practices made a giant improvement in rotor cleanliness, while virtually eliminating hydrogen flaking.

A measure of the improvement in freedom from sonic indications that has been achieved is demonstrated in Fig. 9, extracted from a 1955 paper by Rankin and Moriarty [15]. This figure shows the number of sonic indications in rotors of that era versus their amplitude, as detected by the standard ultrasonic test then in use. Detection of any sonic indications with amplitude greater than 5% with their referenced test is a rarity in modern rotor forgings.

Alloy and Forge Processing Improvements

During the Diamond Jubilee annual meeting of the American Society of Mechanical Engineers (ASME) in November 1955, six papers concerned with large turbine and generator rotor forgings were presented at a joint session of the Power and Metals Engineering divisions. Included were descriptions of two turbine and two generator forging failures that had occurred during the preceding two years. A companion paper by A. O. Schaefer, "Work of the Task Group on Brittle Failure of Steel Forgings" [16], outlined the program undertaken by a special committee formed under ASTM to study the problem on an industry-wide basis.

Each of the fractures of the large turbine and generator rotors in 1954 and a later failure in 1956 occurred at stress levels far below the tensile and yield strength of the material in the presence of defects representing an extremely small

fraction of the total cross section. In general, the failures were attributed to inadequate fracture toughness for the magnitude of the stress concentrators, the stress level, and the operating temperature involved.

The basic specifications under which these forgings were produced were the responsibility of Subcommittee A01.06 on Steel Forgings and Billets of ASTM Committee A-1 on Steel, and it was recognized that a group study of the problems associated with their manufacture should come under the Subcommittee's jurisdiction. Accordingly, at the January 1955 meeting of the Subcommittee, a task force was appointed to study the "cause of brittle fracture in steel forgings with the aim of establishing a criterion by means of which the tendency of a material to fracture in a brittle manner may be appraised . . . and to discover the causes of brittle fracture and its cure." A review of the history of any committee exploring a problem of the magnitude, importance, and complexity of the brittle fracture of rotor forgings might be expected to disclose many false starts and much misdirected effort. It is, therefore, a tribute to the caliber of the original members of the Special Task Force on Large Forgings² that the activities of this committee were well directed and well supported from the beginning.

In its early work, the Committee met regularly at 2- to 3-month intervals, with additional meetings held by various subgroups appointed to study and report on various phases of the problem.

While the topics covered by the Committee were many and varied, the discussions may be grouped under a few broad categories:

1. Defining the problem.
2. Developing a measure of resistance to brittle fracture and the relationships among defect size, material properties, and the stress necessary to initiate brittle fracture.
3. Establishing ultrasonic testing techniques and the relationship between defect size and sonic indication size.
4. Developing steels with improved fracture toughness.
5. Improving steelmaking procedures to produce cleaner, sounder, and tougher rotor forgings.

Although ultrasonic testing had been developed and applied to rotor forgings in the late 1940s, there was little exchange of technical information concerning the procedures used on the interpretation made of the sonic test results. Since the incidence and size of defects in forgings were obviously as important as their resistance to brittle fracture, a considerable part of the Committee's early activity was directed toward this subject. There was an active exchange of information concerning the correlation of ultrasonic test results with the size and nature of defects and in the preparation of "Recommended Practices for Ultrasonic In-

² The activities of this committee have continued to the present time as A01.06.04.01, "Subsection on Research and Technology for Large Rotating Forgings for Central Station Power Generation."

spection of Large Rotor Forgings.” The Task Force demonstrated its recognition of the importance of continued progress in the detection and interpretation of internal defects in forgings with the formation of an Ultrasonic Group within the Task Force.

One of the earliest actions of the Special Task Force was the formation of a research group, with representation from each of the member companies, to establish cooperative research programs and to coordinate the activities in the various company laboratories. The objective was to develop stronger and tougher rotor forging materials. The difficulty of predicting the superiority or even the suitability of a new composition in a large rotor forging on the basis of laboratory heats and small-scale laboratory tests was well recognized. However, the substantial cost of even the modest-sized turbine and generator rotors made it imperative that every effort be made to ensure that a usable product would result from each of the full-sized experiments, and extensive laboratory testing preceding these production trials was essential. Although it seems almost elementary at this time, much of the Committee’s early activity was devoted to a study of hydrogen in forgings, establishing test methods for its measurements, and determining its effect on deep-seated properties. The clear evidence of the tremendous effect of hydrogen on tensile ductility served as a powerful stimulant to the installation of vacuum-pouring facilities in the later 1950s.

The investigations of alternate chemistries and heat-treating procedures ranged from consideration of minor chemistry variations in established grades and slight changes in heat-treating temperatures to substantial modifications in the entire melting, pouring, and heat-treating procedures. The Committee reviewed in detail the properties of several hundred forgings in evolving the practices used to produce today’s improved forgings. While the earlier forgings were evaluated on the basis of test prolongations added to the forgings, bore trepanning equipment added by all of the steel mills in the late 1950s made it possible to obtain center properties on all production forgings and greatly accelerated both the rate at which this information became available and the pace of the overall development program.

The work of the Special Task Force was described in a series of papers presented at a symposium at the 68th Annual Meeting of ASTM in 1965 [17,18]. Perhaps the best measure of the progress that has been made in providing improved rotor forgings for the power generation industry in that time period can be obtained by a comparison of the 1955 ASTM specification A 293 and ASTM Specification for Vacuum-Treated Carbon and Alloy Steel Forgings for Turbine Rotors and Shafts (A 470-82), issued in 1962, as shown in Table 2. The lower phosphorus and sulfur contents specified were indicative of the cleaner electric furnace steel now being utilized. While the improvement in tensile ductility shown here is substantial, the actual improvement was even greater because the 1955 values represent specimens artificially aged to remove hydrogen that reduced ductility to about one half the values specified. Although no transition temperatures were specified in the 1955 forgings, the average transition temperature in Ni-Mo-V

TABLE 2—Turbine rotors.

	1955 Specification A293 Class 6	1962 Specification A470 Class 6
CHEMICAL REQUIREMENTS		
Carbon max	0.40	0.28
Manganese max	1.00	0.20 to 0.60
Phosphorus max	0.05	0.015
Sulfur	0.05	0.018
Silicon	0.15 to 0.35	0.15 to 0.30
Nickel min	2.5	3.25 to 4.0
Chromium max	0.50	1.25 to 2.0
Molybdenum	0.45 to 0.65	0.30 to 0.60
Vanadium min	0.03	0.05 to 0.15
TENSILE AND NOTCH TOUGHNESS REQUIREMENTS		
Tensile strength min, psi	105 000	105 000
Yield strength min, psi	85 000	85 000
Elongation min, %	14	17
Reduction in area min, %	24	50
Transition temperature max, °F ^a	none specified	40
Room temperature impact min, ft-lb ^a	none specified	45

^a Conversion factors: 1 ft-lb = 0.138 m · kg; °C = °F - 32/1.8; 1 psi = 0.00029 m²/kg.

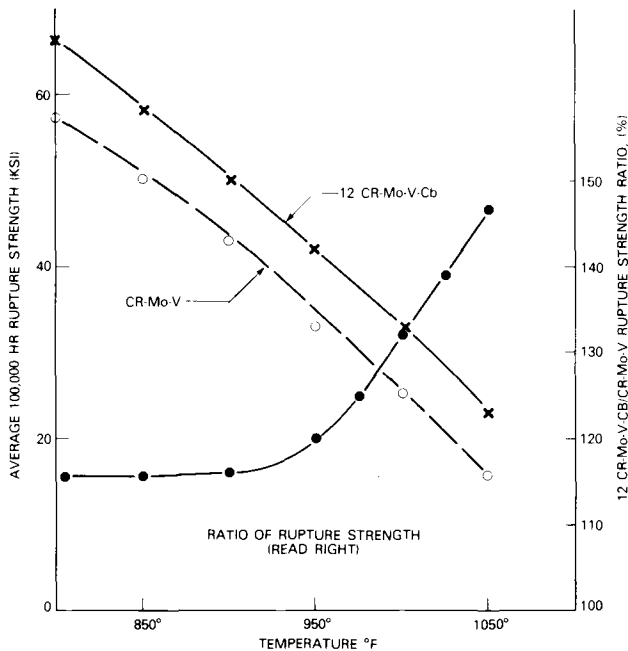


FIG. 10—Comparison of the mean predicted rupture strengths of 12Cr-Mo-V-Cb and Cr-Mo-V rotors.

forgings was well above 65.6°C (150°F) and, in many forgings, higher than 93.3°C (200°F).

During the 1960s, further work was performed to effect additional improvements in the properties and qualities of both high- and low-temperature rotor forgings by the industrial turbine manufacturers. In the case of high-temperature rotors, the practice of conducting parameter rupture tests from both the bore and periphery by General Electric provided a data base to permit further improvements in high-temperature strength and rupture ductility of Cr-Mo-V rotors. These data, together with extensive laboratory studies, demonstrated that, with minor changes in the chemical analysis and heat treatment, better rupture ductility could be achieved and the minimum rupture strength could be considerably increased.

In the early 1960s, the 12Cr-Mo-V-Cb rotor forging steelmaking practice was developed by two domestic steel suppliers [19,20]. This material, which provides a substantial improvement in rupture strength over the Cr-Mo-V analysis, has been used in more than 50 large turbines in ratings up to 1000 MW, with a total generation capacity of 34 000 MW. Some of these forgings have been in service over 20 years. Figure 10 shows a comparison between the mean values of the predicted 100 000-h rupture strength of Cr-Mo-V and 12Cr-Mo-V-Cb rotors, as produced using practices developed by General Electric with the steel suppliers. The superior strength of the latter material, especially at the higher temperatures, is apparent. Steel mill developments in the 1960s also were directed to providing the larger higher-strength, low-pressure rotors required to carry longer last-stage buckets, the very large forgings required for nuclear high-pressure rotors, and the still larger generator field forgings required for nuclear units. The large turbine wheel forgings required for the large nuclear low-pressure sections were also the subject of extensive developments.

Although the Ni-Cr-Mo-V low-pressure rotor material represented a substantial improvement in fracture toughness over the Ni-Mo-V alloy, fracture mechanics evaluations indicated that increased toughness was needed, particularly in the larger, higher-strength forgings required to carry the longer last-stage buckets introduced during the 1960s.

Early work by Danner and Dyble [21] suggested that improvements might be made in cleanliness and other characteristics by vacuum carbon deoxidation (VCD) instead of conventional silicon deoxidation. The higher capacity and lower pressures provided by the steam ejector pumps which had become available made it possible to rely on the carbon-oxygen reaction and to remove oxygen as gaseous carbon monoxide instead of as silicates which form nonmetallic inclusions when not adequately removed. Small-scale experiments indicated that this process would have some advantage in the Ni-Cr-Mo-V steels. Other work being done at that time indicated that a very severe quench provided an enhancement of the toughness in forgings in this alloy, particularly in the center portions of the forging. Prior to vacuum pouring, severe quenches in such large masses certainly would have resulted in internal hydrogen flaking.

In the early 1960s, full-size tests were made on a number of Ni-Cr-Mo-V low-

pressure rotors that were made by the VCD process and water-quenched cold. The results of these experiments were extremely gratifying. With tensile strengths over 827 MPa (120 ksi), impact tests of samples from the center core showed the transition temperatures to be 225 K (0°F) or below. Furthermore, tension tests on the core showed a substantial improvement in ductility in the transverse direction, as compared to the results achieved in silicon deoxidized forgings. There were no indications of hydrogen flaking, either in the rotors (as determined by extensive sonic testing) or in the core. The Ni-Cr-Mo-V analysis and the VCD practice has now been adopted almost universally for high-strength low-pressure rotors, shafts, and bucket wheels. A limited number of Cr-Mo-V forgings were produced in the 1960s and 1970s using the vacuum carbon deoxidation practice. These forgings appeared to have relatively higher rupture strength and ductility than the silicon deoxidized forgings, but with somewhat lower toughness. Thus the advantages of vacuum carbon deoxidation for the Cr-Mo-V alloy are not clear-cut, as in the case for Ni-Cr-Mo-V.

In the mid-1960s, an extensive long-time aging program was begun by General Electric to determine the extent of temper embrittlement that might be expected to occur in Cr-Mo-V, 12Cr-Mo-V-Cb, and Ni-Cr-Mo-V rotor steels. Samples from 650 rotors are not included in this program, with the longest aging times well beyond 120 000 h. The average embrittlement indicated for the Cr-Mo-V and 12Cr-Mo-V-Cb steels at 454°C (850°F) and the Ni-Cr-Mo-V steel at 343 and 371°C (650 and 700°F) is shown in Fig. 11.

The results of these tests show that relatively minor embrittlement can be expected in 30 years in 12Cr-Mo-V-Cb and Cr-Mo-V rotors made by modern electric furnace practice that can provide low phosphorus contents and close control of other embrittling tramp elements. This minor embrittlement is in sharp contrast to the serious embrittlement found in the higher phosphorus open hearth steels used in the 1940s and 1950s, where an increase in Fracture Appearance Transition Temperature (FATT) of more than 167 K (300°F) upon embrittlement was sometimes measured. In the case of the Ni-Cr-Mo-V steels, substantial decreases in embrittlement tendencies were achieved by reductions in phosphorus and tramp elements, but significant embrittlement was still observed at 644 K (700°F) in 120 000 h. Although the average embrittlement occurring at 616 K (650°F) in 120 000 h was 42 K (75°F), there was no indication in the latest data of a saturation in the embrittlement phenomena. These data have been taken into account in low-pressure rotor designs.

In spite of the relatively limited embrittlement in modern high-temperature rotor steels and the temperature limitations imposed on low-pressure rotors, some embrittlement is anticipated in service and is taken into account in evaluating the suitability of new forgings.

Considerable interest in this subject was generated by an ASTM symposium, *Temper Embrittlement in Steels*, ASTM STP 407, organized by the Special Task Force on Large Forgings in Philadelphia in 1967. Work is continuing in this area, under Electric Power Research Institute (EPRI) sponsorship, to investigate the

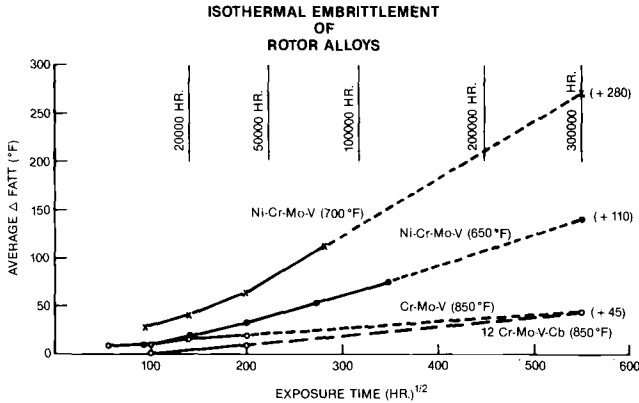


FIG. 11—Average increase in FATT for three rotor forging alloys.

characteristics of steels with very low levels of elements suspected of contributing to this phenomenon. Long-term aging tests will be necessary to establish the level of embrittlement that may be expected in these ultrapure materials.

Advances in Forging Evaluation Techniques

The introduction of center core trepanning equipment and the development of bore sonic tests were of tremendous assistance in providing a quantitative evaluation of rotor forging quality since the 1950s. Figure 12 shows the testing pattern that has been used on a typical fossil LP rotor to permit a thorough evaluation of the forging characteristics from the surface and the center and from end to end. In addition to providing material property information useful for determining the suitability of each forging for its particular application, the results of core and surface tests on several thousand forgings provided a valuable data base that has been useful in optimizing chemical analyses and heat-treatment cycles.

For large turbine and generator forgings, the across-the-board application of the bore sonic test in 1959 provided a sensitive test of forging quality in other areas of the forging where defects are most likely to occur. It also provided an additional means for in-service inspection.

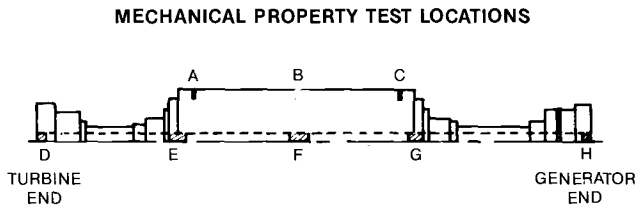


FIG. 12—Typical test locations for large rotor forgings.

TABLE 3 —*Chronology of significant events—approximate time of application to rotors.*

Year	Event
1933	magnetic particle testing
1947	Periphery ultrasonic testing
1951	Larson-Miller time-temperature parameter
1953	1750°F (1228 K) austenitize for Cr-Mo-V rotors
1956	large disk spin testing
1956	Charpy fracture appearance transition temperature
1957	application of Griffith-Irwin theory of crack propagation to rotors and disks
1957	analytical modeling of ingot solidification
1958	vacuum pouring for rotor ingots
1958	general application of electric furnace melting
1958	improved steelmaking practice for improved cleanliness
1958	bore trepanning, evaluation of center core properties
1959	Ni-Cr-Mo-V for low pressure rotors
1959	boresonic testing
1960	12Cr-Mo-V-Cb for high temperature rotors
1960	"excess temperature" concept (T-FATT) or normalizing fracture transition behavior
1961	water quenching low pressure rotors
1961	VCD of LP rotor steels
1964	fracture analysis diagram for rotors
1967	high sensitivity periphery sonic test
1968	correlation between K_{IC} and excess temperature
1970	vacuum arc remelting high temperature rotors
1972	higher sensitivity magnetic particle testing
1973	higher resolution periphery sonic test
1974	improved steel-making practices to minimize effects of segregation
1977	DATAQ TM system for boresonic testing
1978	electroslag remelting high temperature rotors
1979	electroslag topping (EST) for ingots for high temperature rotors
1982	angle beam boresonic test
1983	notch rupture ductility test

To permit proper interpretation of the results of bore sonic inspection, as well as other sonic tests, more than 100 rotors and other large forgings have been sectioned. The center cores also have provided a means for calibrating the periphery sonic test by comparing the results of sonic tests before removal of the center core with discontinuities captured in the core.

These data have been valuable in appraising the probable effect of sonic indications on the integrity of forgings with sonic indications, and evaluation of the nature of the indications has been valuable to the steel mills in determining the nature and probable source of the indications to suggest remedial action. Table 3 shows a chronology of some of the events that represent significant progress in the industry's ability to evaluate the suitability of forgings to perform satisfactorily in service and to provide superior forgings capable of meeting the stringent criteria established. In almost every instance, several years of development work preceded the application of these processes to regular production. Figures 13 and 14 show the trends in properties of high-temperature and low-temperature forgings that resulted from the changes described. These figures

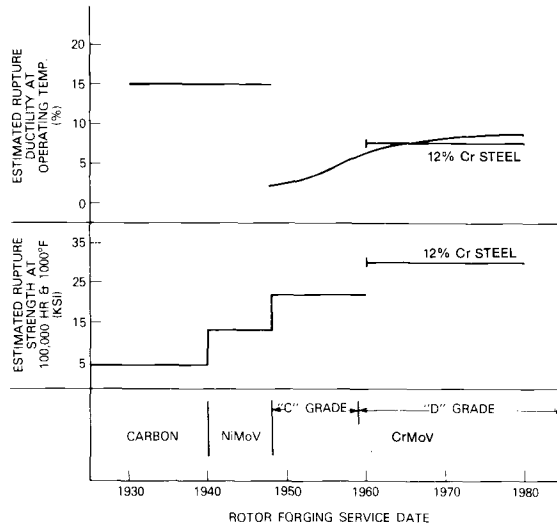


FIG. 13—Trends in high-temperature rupture strength and rupture ductility with rotor service date and type of rotor steel.

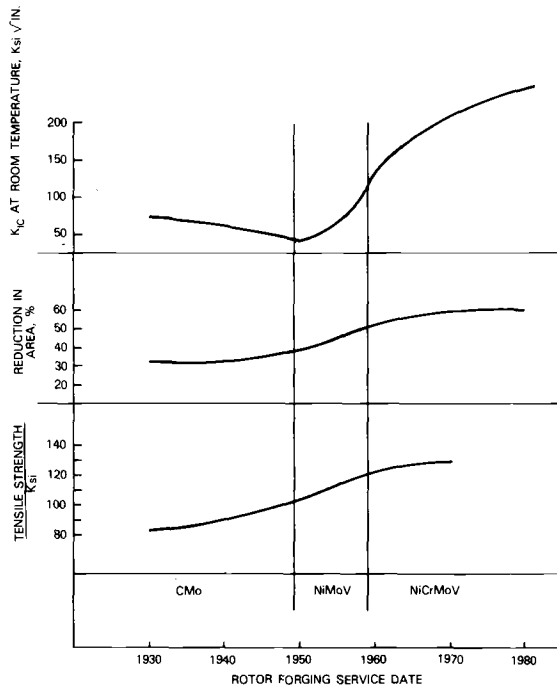


FIG. 14—Trends in tensile strength and ductility and in fracture toughness (K_{IC}) with rotor service date and type of rotor steel.

indicate that the changes made in order to achieve the strength characteristics required by increased ratings and steam conditions in the 1940s and early 1950s resulted in lower toughness and ductility. These curves also demonstrate that the work done since the 1950s has resulted in a much-improved balance in properties.

A measure of the success of the previously discussed developments toward solving the conditions that produced the failures in the 1950s and created the need to replace some of the rotors on the basis of after-service inspections is the fact that only one turbine rotor shipped by General Electric after 1960 has required replacement for metallurgical reasons.

New Steelmaking Processes

Cooperative programs with the steel mills have continued in several important areas to provide better properties that might permit further design improvements in order to improve reliability and minimize or eliminate procurement difficulties.

During the late 1960s and early 1970s, 23 Cr-Mo-V rotor forgings and 6 turbine wheels for special applications were obtained from steel remelted in a 1524-mm (60-in.) vacuum arc remelt (VAR) furnace, described by Schumann [22], that was installed by a domestic supplier.

In general, the properties of the forgings made with VAR were comparable to those achieved with conventional electric furnace, vacuum-poured practice. The incidence of sonic indications was much lower than for conventionally melted rotors. The performance in the heat test was somewhat better and, as would be expected, segregation and its effects were much less severe. The VAR facility, however, was capable of making ingots of approximately 50 000 kg (55 tons) that would provide forgings sufficiently large for many replacement rotors but for only about half of the rotors required for the larger units being built at that time. Rupture strength, rupture ductility, and fracture toughness showed no improvement with the use of the VAR process, as evaluated by radial trepans and longitudinal core specimens. In order to provide a more positive solution to the rotor forging problem and to achieve some benefits in other products as well, another of our domestic suppliers installed a large electroslag remelting (ESR) facility in 1976 that is capable of manufacturing the largest Cr-Mo-V and 12Cr-Mo-V-Cb rotors required for modern units. Evaluations of the products of this facility were first begun on smaller turbine parts and later on full-size forgings. To date, 27 high-temperature rotor forgings (Cr-Mo-V and 12Cr-Mo-V-Cb) have been made and have passed an acceptance test program. In 1976, a Cr-Mo-V rotor and several Ni-Cr-Mo-V bucket wheels also were ordered from a second steel supplier [23]. Extensive testing of all the ESR forgings has shown that, although there is some slight evidence of segregation as measured by etching and high-current density magnetic particle tests, this segregation does not affect the transverse tensile ductility in the core.

In 1978 a program to evaluate the product of an electroslag hot topping practice was begun [24,25]. A Cr-Mo-V rotor forging was produced that had acceptable

bore and surface characteristics and no problem with center core transverse ductility. A second experimental forging was manufactured for one rotor from an ingot using another electroslag topping practice [26,27]. Unfortunately, this rotor was not considered usable for reasons other than the hot-topping practice. There has been little activity in the use of electroslag hot topping in recent years because modern electric furnace steel provides forgings with completely satisfactory characteristics. During this period, numerous steel mill rotor forging processing modifications were evaluated. Examples of these processing developments are "low sulfur" melting practices, the use of smaller diameter ingots, modified discard practices, more effective forging techniques, and changes in preliminary and final heat-treating cycles.

Figure 15 illustrates the beneficial effect of low-sulfur melting practices on transverse bore core mechanical properties. The adverse effect of the possibly severe centerline segregation that is present at the top of the ingot can be reduced by melting to low sulfur levels and also by employing various consumable electrode remelting processes.

The most recent chapter in the development of rotor forging technology is the application of the Ni-Cr-Mo-V analysis to the large monoblock forgings required for nuclear low-pressure rotors.

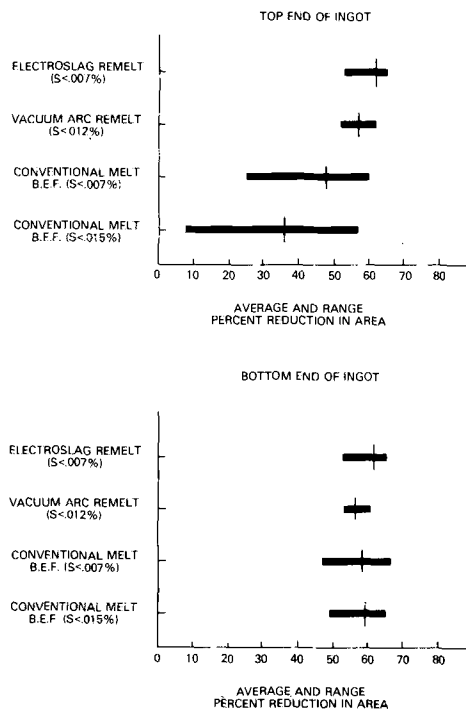


FIG. 15—Comparison of transverse bore core ductility of rotors made by conventional basic electric practice with that of rotors made by ESR, VAR, and low-sulfur basic electric practices.

As indicated earlier, the large rotors for 1800-rpm, low-pressure sections were of built-up construction using a shaft and shrunk-on disk design. On the basis of more than 30 years of satisfactory service on fossil machines, this design was introduced on nuclear low-pressure sections. After considerable periods of service, some of these machines have exhibited stress corrosion cracks emanating from the keyway in the bore of the wheels. Although the tough Ni-Cr-Mo-V wheels used in this type of construction have considerable tolerance for cracks, the potential for growth to unacceptable size has required periodic inspection and reinspection. New designs of the keyway, which greatly reduced the stress level and eliminated a chemical concentration mechanism, permit rebuilding these rotors using the existing wheels and buckets. In some circumstances, however, where time for rebuilding is limited, new rotors are required.

Figure 16 shows the size of forgings for the largest fossil low-pressure rotor, nuclear high-pressure rotor, and nuclear generator field compared to the forgings required for monoblock nuclear LP rotors. On the basis of data core samples from these forgings, excellent fracture toughness at the strength levels required has been obtained. Results on the monoblock forgings have confirmed expectations, and these results support the results published by the steelmakers [28]. The fracture toughness results obtained on actual rotors are considerably better than might be expected from laboratory tests on small samples simulating the thermal cycle in the center of the large monoblocks. A possible explanation for this difference, as indicated previously, is the presence of compressive transformation stresses in the large pieces, which may have the effect of delaying transformation. This delay probably results in the formation of finer, tougher bainite than would be predicted by the laboratory experiments.

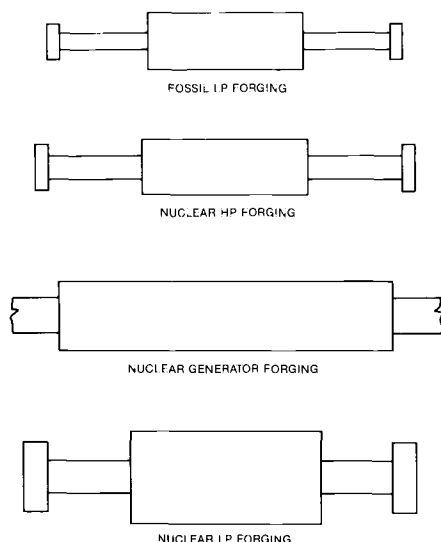


FIG. 16. --Comparable sizes of monoblock forgings for various turbine and generator applications.

Although the large monoblocks represent a modest technical extrapolation from previous experience, the investment in facilities and process development has been substantial, and the steelmakers who provided these facilities are to be congratulated for their foresight.

Summary and Conclusions

As a result of continuing cooperative programs between turbine manufacturers and forgemasters, and substantial contributions on their part, very significant improvements have been made in the quality of forgings available for the manufacture of turbine and generator rotors for large modern turbine-generator sets. The ASTM committees have been very helpful in this effort.

Inspection methods have been improved so that there is greater assurance that internal discontinuities can be detected and properly appraised. The cleanliness of forgings has been greatly improved. Increases in fracture toughness, particularly in low-pressure rotors, has considerably increased the critical defect size and decreased the probability of an undetected critical flaw by several orders of magnitude.

The high-temperature strength characteristics of Cr-Mo-V and 12Cr alloy rotors are better understood, and notch rupture ductility has greatly improved. With improved properties, designs, and operating procedures, the life expectancy of modern high-temperature rotors is expected to be considerably greater than those of the earlier vintages, in spite of the increase in forging size and unit ratings. It is encouraging to note from the papers presented at this symposium that work is continuing in many diverse areas supported by EPRI and individual manufacturers. The synergism provided by ASTM symposia such as this conference will provide valuable rewards in improved forging technology to all of the participants.

References

- [1] Elston C. W. and Downs, J. E., "Future of the Steam Turbine Cycle," American Power Conference Proceedings, March 1957.
- [2] Curran, R. M., Newhouse, D. L., and Newman, J. C., "The Development of Improved Rotor Forgings for Modern Large Steam Turbines," ASME 82-JPGC-PWR-25, American Society of Mechanical Engineers, New York.
- [3] Miller, R. F. and Heger, J. J., *Report on the Strength of Wrought Steels at Elevated Temperatures*, ASTM STP 100, March 1950, American Society for Testing and Materials, Philadelphia.
- [4] Conrad, J. D. and Mochel, N. L., "Operating Experiences with High Temperature Steam Turbine Rotors and Design Improvements in Rotor Blade Fastening," ASME Paper 57-PWR-10, ASME Power Division Conference, Allentown, PA, 21-23 Oct. 1957, American Society of Mechanical Engineers, New York.
- [5] Rankin, A. W. and Sequin, B. R., *ASME Transactions*, Vol. 78, Oct. 1956, pp. 1527-1546, American Society of Mechanical Engineers, New York.
- [6] Emmert, H. D., *ASME Transactions*, Vol. 78, No. 7, Oct. 1956, pp. 1547-1566, American Society of Mechanical Engineers, New York.
- [7] Schabtach, C., Foglenan, E. L., Rankin, A. W., and Winne, D. H., *ASME Transactions*, Vol. 78, No. 7, Oct. 1956, pp. 1567-1584, American Society of Mechanical Engineers, New York.
- [8] DeForest, D. R., Grobel, L. P., Schabtach, C., and Seguin, B. R., ASME Paper 57-PWR-12, ASME Power Division Conference, Allentown, PA, 21-23 Oct. 1957, American Society of Mechanical Engineers, New York.

- [9] DeForest, D. R., Newhouse, D. L., and Seguin, B. R., "Progress in the Development of Steam Turbine-Generator Rotor Materials," ASME Paper 57-A-280, ASME Annual Meeting, New York City, 1-6 Dec. 1957, American Society of Mechanical Engineers, New York.
- [10] Winne, D. H. and Wundt, B. M., *ASME Transactions*, Vol. 80, 1958, pp. 1643-1658, American Society of Mechanical Engineers, New York.
- [11] Fischer G. A., in *ASTM Proceedings*, Vol. 62, 1962, pp. 1137-1155, American Society for Testing and Materials, Philadelphia.
- [12] Hornak, J. N. and Orchoski, M. A., "Vacuum Casting of Steel," *Journal of Metals*, July 1958.
- [13] Stoll, J. H., "Vacuum Pouring of Ingots for Heavy Forgings," *Journal of the Iron and Steel Institute*, Vol. 191, January 1959.
- [14] Reid, E. A., "Vacuum Pouring for Large Forging Production," American Society of Plant Engineers Convention, Cleveland, OH, 26 Sept. 1958.
- [15] Rankin, A. W. and Moriarty, C. D., *ASME Transactions*, Vol. 78, No. 7, Oct. 1956, pp. 1603-1622, American Society of Mechanical Engineers, New York.
- [16] Schaefer, A. O., *ASME Transactions*, Vol. 78, No. 7, Oct. 1956, pp. 1623-1626, American Society of Mechanical Engineers, New York.
- [17] Curran, R. M., "The History of the Special ASTM Task Force on Large Turbine and Generator Rotors," ASTM Annual Meeting, Purdue University, Lafayette, Indiana, 13-18 June 1965, American Society for Testing and Materials, Philadelphia.
- [18] Boyle, C. J., Curran, R. M., DeForest, D. R., and Newhouse, D. L., "Further Progress in the Development of Large Steam Turbine and Generator Rotors," ASTM Annual Meeting, Purdue University, West Lafayette, Indiana, 13-18 June 1965, American Society for Testing and Materials, Philadelphia.
- [19] Newhouse, D. L., Boyle, C. J., and Curran, R. M., "A Modified 12% Chromium Steel for Large High-Temperature Steam Turbine Rotors," ASTM Annual Meeting, Purdue University, West Lafayette, Indiana, 13-18 June 1965, American Society for Testing and Materials, Philadelphia.
- [20] Boyle, C. J. and Newhouse, D. L., *Metal Progress*, March 1965, pp. 61-62.
- [21] Danner, G. E., and Dyble, E., *Metals Progress*, May 1961, Vol. 79, No. 5, pp. 74-79.
- [22] Schumann, R., "The Production of Heavy Forging Ingots by Remelting Processes," *Proceedings*, Fifth International Conference on Vacuum Metallurgy and Electroslag Remelting Processes, Munich, Germany, 11-15 Oct. 1976, pp. 229-232.
- [23] Jauch, R., Choudhury, A., Tince, F., and Lemor, W. R., *Ironmaking and Steelmaking*, 1979, No. 2, pp. 75-83.
- [24] Ramacciotti, A., Repetto, E., Sommovigo, P., Crisafulli, A., Basevi, S., Marianeschi, E., Toni, L. and Scepi, M., *Bollettino Tecnico Insider*, No. 370, Dec. 1977, pp. 777-795.
- [25] Basevi, S., Repetto, E., and Scepi, M., "The TREST Process for Manufacturing a CrMoV HP Rotor Shaft," International Conference on Special Melting, San Diego, CA, 23-27 April 1979.
- [26] Ploeckinger, E., Kuehnelt, G., Machner, P., and Straube, H., "Boehler-Electro-Slag-Topping—A New Process for the Production of High Quality Forging Ingots," AIME Electric Furnace Conference, Houston, TX, 9-12 Dec. 1975, American Institute of Mining, Metallurgical, and Petroleum Engineers, New York.
- [27] Machner, P., Kuehnelt, G., Jaeger, H., Ploeckinger, E., and Weiss, F. J., "Better Heavy Forgings by ESR and the B.E.S.T. Process," *Proceedings*, Fifth International Conference on Vacuum Metallurgy and Electroslag Remelting Processes, Munich, Germany, 11-15 Oct. 1976, pp. 223-227.
- [28] Kawaguchi, S., Kanno, N., Iwadata, T., and Ohhashi, T., "The Reliability of Full-Integral Low-Pressure Turbine Forgings for Nuclear Power Plants," this publication.

Turbine and Generator Forgings

Steel Production for Rotors

Influence of Advanced Steelmaking Technology on Specification Trends for Rotor Forgings

REFERENCE: Steiner, J. E. and Jaffee, R. I., "Influence of Advanced Steelmaking Technology on Specification Trends for Rotor Forgings," *Steel Forgings*, ASTM STP 903, E. G. Nisbett and A. S. Melilli, Eds., American Society for Testing and Materials, Philadelphia, 1986, pp. 35-44.

ABSTRACT: Advanced steelmaking equipment and processes that are state of the art for the production of rotor forgings are described. The Electric Power Research Institute (EPRI) has sponsored a study on high-pressure (HP) rotor forgings of 1Cr-Mo-V steel with 0.001 to 0.002% sulfur content produced by conventional vacuum carbon deoxidation (VCD) and electroslag remelting processes. Low phosphorus, low hydrogen, and residual element control were also objectives of this study.

Laboratory studies show that combined low levels of manganese (Mn), phosphorus (P), silicon (Si), and residual elements improve the toughness and resistance to temper embrittlement of rotor steels. In a recent EPRI program with Vereinigte Edelstahlwerke, the process combination basic electric arc furnace melting and ladle furnace refining with vacuum treatment successfully produced a 25-metric-ton model rotor in which levels of 0.02Mn, 0.002P, 0.001S, 0.04Si, and 0.005Al at 27 ppm oxygen were achieved.

Specification implications of these trends to high-purity rotor steels suggest that requirements for Mn, Si, and sulfur (S) will trend to lower content levels.

KEY WORDS: rotor forgings, advanced steelmaking, secondary refining processes, ladle refining furnace, ladle injection, vacuum carbon deoxidation, high purity steels, temper embrittlement

The quality of steel used in large steam turbine and generator rotor forgings continues to improve. Sulfur (S), phosphorus (P), and undesirable tramp element contents in modern rotors are usually only a small fraction of what was considered the absolute minimum levels attainable 20 years ago. Soundness and cleanliness, especially with respect to large isolated nonmetallic inclusion or porosity clusters, have also markedly improved in this period.

These improvements are largely the result of the technological impact of the rotor failures of the early fifties [1-4] on rotor steelmaking technology. A disparate set of concepts and technologies, including vacuum degassing of steel,

¹ Consultant—Forgings, Engineering Materials & Processes, Inc., Pittsburgh, PA 15217.

² Senior technical advisor, R & D Staff, Electric Power Research Institute, Palo Alto, CA.

vacuum carbon deoxidation, hydrogen analysis methods, ultrasonic testing, fracture mechanics, electroslag processes, ladle refining technology, special hot topping, and argon technology, have come together in making possible the high quality now available.

This brilliant record inevitably prompts the question with regard to quality, "How much is enough?" In the days when discontinuities occasionally could be large and toughness could be poor, most producers and users agreed that tighter standards were justifiable. Now, many feel that present soundness and mechanical property standards are more than adequate for safe and reliable rotor performance.

The steelmaking advances that have made possible today's high quality and those that promise even more for the future are discussed in this paper. Factors affecting specification considerations also are discussed. These factors bear on the just-cited question of what level of steel quality is necessary in large rotors.

Discussion

A survey, "Advanced Steelmaking Processes for Rotor Forgings" [5], was conducted for the Electric Power Research Institute (EPRI) by Engineering Materials & Processes, Inc. Results revealed that recent major advances in steelmaking technology for large rotor forgings lie largely in the secondary refining and casting phases of steelmaking. Processes such as argon-oxygen decarburization (AOD), ladle injection, ladle refining furnace (LRF), electroslag remelting (ESR), electroslag hot topping (ESHT), and exothermic hot topping have been of particular interest to the steelmaker and forgemaster.

Traditionally, both steelmaker-forgemaster and turbine builder have been seeking lower S contents in rotor steels. In the recent past, S contents in the range 0.004 to 0.008% as produced in the basic electric arc furnace have become the industry standard. This level of S content represents the practical limit of capability of the basic-electric arc-furnace (BEF) process without supplemental secondary refining.

Within the past ten years, secondary refining, mainly in the form of ladle metallurgy, has come of age. It has been demonstrated in many shops that 0.001 to 0.002% S contents can be consistently achieved in rotor steels by any one of several ladle processes, principally the injection, static agitation, or LRF methods. In addition, the ESR and AOD processes can achieve similarly low S contents. The EPRI survey report [5] provides description and detailed comparisons among these and other processes.

All these processes are capable of producing high-quality, low-S low-phosphorus (P) steel. The advantages of one over the other depend largely upon product mix (size of forging produced), existing shop limitations, operating cost, and capital investment.

As S, P, and oxygen (O) specification levels decrease, as they surely will, and

as silicon (Si) and manganese (Mn) levels decrease, as they may well, demands upon steel refining processes will increase. Fortunately, as just cited, the forgings producer has available a variety of attractive processes, any one of which can produce low S content and, to varying degrees, the other objectives of high-purity steel. Furthermore, to the extent that these processes remove the refining operations from the BEF, they increase shop melting capacity and can lower overall costs. Thus, the steelmaker can be placed in the highly desirable position of producing higher quality at lower cost.

For smaller rotors, where one or more forgings are produced from a single heat of steel, selection of an advanced secondary refining process is largely a question of economic considerations and best fit with existing facilities. Where the producer anticipates competing in the high purity area, where low Mn, P, S, Si, aluminum (Al), O, nitrogen (N), and hydrogen (H) may be required in combination, the field of selection narrows. Here the LRF with a vacuum capability generally is accepted as the ultimate process for close control of composition.

For large rotors, where multiple heats are required to produce a single ingot for the forging, the LRF approach has a further advantage in its ability to reheat and hold liquid steel in storage. Thus, for large rotor production, the optimum facility and process chain is BEF melting, LRF, and vacuum stream degassing (VSD) during casting.

For all large rotor ingot production, VSD during casting is most desirable, especially for the flake-sensitive rotor steels. For improved forging yield, homogeneity, and soundness, hot topping by means of ESHT, although not widely employed at this time, also appears to be desirable for rotor ingot production.

High Purity Rotor Steels

A remarkable extension of advanced steelmaking technology in the production of high-purity rotor steels has occurred at Vereinigte Edlstahlwerke (VEW), Kapfenberg, Austria under EPRI project RP1403-8. In this project, VEW employed BEF melting, vacuum ladle degassing with argon stirring, and LRF with induction and argon stirring capability. A 33-metric-ton ingot of Ni-Cr-Mo-V rotor steel was produced. Chemical composition, in percent, was as shown in Table 1.

The processing of a test rotor forging from this heat is in progress, and results will be reported later by VEW and EPRI.

This demonstration in a commercial size heat dramatically illustrates the capability of modern advanced technology secondary refining processes to achieve the extreme objectives of highly restrictive composition limits. The significance of this feat lies in the virtual elimination of the major deoxidizers Al and Si through the use of VCD while holding P, S, Mn, and O at very low levels.

Thus, it can be done.

TABLE 1—*Chemical composition of a high purity 33-metric-ton ingot of Ni-Cr-Mo-V rotor steel, %.*

	C	Mn	P	S	Si	Ni	Cr	Mo
Max	...	0.05	0.005	0.002	0.05
Aim	0.25/0.27	0.02	0.002	0.001	0.02	3.50	1.65	0.45
Ladle	0.30	0.02	0.0024	0.001	0.04	3.44	1.68	0.41
	V	Al	Sb	As	Sn	O, ppm	N, ppm	H, ppm
Max	...	0.005	0.002	0.005	0.005	25	50	0.5
Aim	0.10	LAP ^a	0.001	0.002	0.002	LAP	...	LAP
Ladle	0.09	0.005	<0.005	0.002	0.003	27	44	0.7

^a LAP stands for low as possible.

Discussion

Having established what can be accomplished in a 25-ton ingot and accepting that projection to the largest ingots produced will come, the question returns to, “Where next?”

Under EPRI Project RP2060 on “High-Purity Steels for Utility Components,” laboratory scale studies showed that low Mn and Si contents in rotor steels promoted improved resistance to temper embrittlement, even when the nickel (Ni) content was high. Furthermore, the extremely low S content required to permit lowering of the Mn content (without risking the formation of intergranular iron sulfide) greatly improves fracture toughness and ductility. Results of these studies suggest that low S combined with low Mn and Si can double fracture toughness at room temperature in Cr-Mo-V rotors. These findings interest the turbine builders and boost their confidence in the reliability and safety of future rotor forgings. Improved resistance to temper embrittlement becomes important in the larger low-pressure rotors designed for higher inlet temperatures or where cooling is not efficient. However, with few such exceptions, because of the more than adequate quality of current rotors on most counts, turbine builders and forgings producers quickly reduce the question of further quality improvements to economic considerations.

Addressing the question of specification trends, both quality and economics, therefore, promise to influence industry actions. One effect of economics on forgings producers in the current depressed market may be to use the high-purity approach as a sales tool in marketing rotors and other highly specialized forgings. From the other side, most turbine builders rely heavily on what is available in establishing their specifications. These purchasers will tighten limits on P, S, arsenic (As), antimony (Sb), and tin (Sn) to the level available and will watch for the results of development work on rotors with lower Mn and Si. Other turbine builders that rely more on mechanical properties and fracture toughness analysis in establishing specification limits will nevertheless be interested in the possibility of supertough high-purity steels in their rotors. As in the past, there will be a

complex system of subtle pressures on all concerned to continue the process of ever-tightening specifications.

In the face of all this, a comment on where the specification for each of the several elements of interest might trend is ventured.

Manganese

Work at the University of Pennsylvania under McMahon [8] suggests that Mn and Si play a major role in sensitizing the Ni-Cr-Mo-V steels to temper embrittlement (Fig. 1). In work under EPRI RP2060, such steels without Mn and Si exhibited reduced temper embrittlement even at high levels of P, Sb, As, and Sn. Current RP2060 work is evaluating Mn at less than 0.05% and at intermediate 0.10 to 0.15% levels. The results of these studies, together with those of the EPRI-VEW model rotor made from a 33-ton ingot, should provide a more quantitative estimate of an optimum level of Mn.

Hardenability is a concern in lowering or eliminating Mn. Fortunately, in the

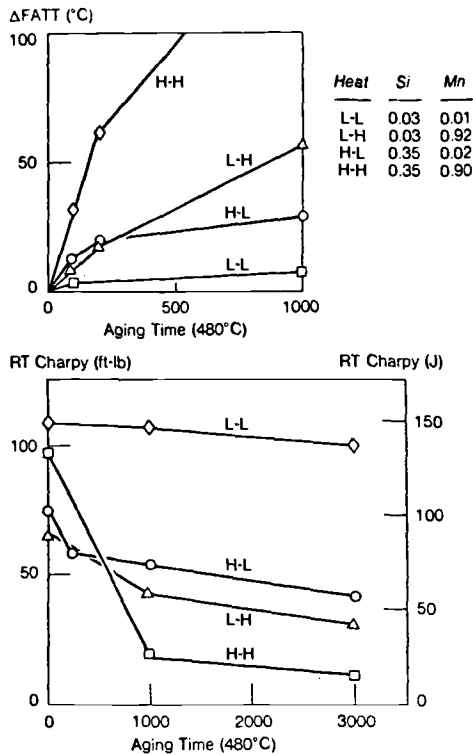


FIG. 1—Effect of manganese and silicon contents on the room temperature Charpy energy and Δ FATT of HY130 steel after 480°C aging.

Ni-Cr-Mo-V steels, where temper embrittlement is of greatest concern, it appears that Mn can be eliminated with no impairment of hardenability. For the 1Cr-Mo-V steel, an intermediate Mn level may be suitable if an effect of Mn on hardenability is demonstrated.

Thus, it might be expected that specifications for Mn content may trend to virtual elimination of Mn in the Ni-Cr-Mo-V steel and possibly to intermediate levels in the 1Cr-Mo-V steel. Mn content may be expressed as a maximum rather than as a range to accomplish such objectives.

Phosphorus

Reduction of P has not received much emphasis in recent years, probably because temper embrittlement during heat treatment could be kept within satisfactory limits in the Ni-Cr-Mo-V steel by maintaining P below 0.01% and Sb, As, and Sn at levels attainable in current practice. P may be readily reduced to levels of 0.002 to 0.003% by secondary refining using oxidizing slags. In contrast, Sn, As, and Sb are difficult to remove. P, like S, is an undesirable residual that reduces fracture toughness, and its removal will always be attractive. Strong emphasis for removal of P below current levels may not be necessary if extremely low Mn and Si eliminates or minimizes the effect of P, Sn, As, and Sb on temper embrittlement. This could affect economics in steelmaking in that the melting-dephosphorization period in the electric-arc furnace might be shortened.

It might be expected that specification trends will be affected by the detrimental effect of P on toughness and temper embrittlement susceptibility on the one hand, and a relaxed pressure for lower P on the other hand, if the promise from lower Mn and Si content is fulfilled. A moderate tightening of P specifications is anticipated.

Sulfur

The ease with which S is removed in all the advanced secondary refining processes should ensure continuation of the historical trend to lower S contents. The trend to lower Mn contents, especially the elimination of Mn, will require reduction of S to the 0.002% S level as well. Economics, in terms of product marketability, also will be a major factor in this trend. Improved toughness will be a lesser factor in that current production rotors with S contents in the range 0.004 to 0.008% exhibit adequate toughness in Ni-Cr-Mo-V steels. Low S in the 0.001 to 0.002% level is probably more important in Cr-Mo-V rotor steels. Minor pressure will persist to reduce S no further because of machinability considerations.

It is expected that S content specifications will gradually be tightened to reflect the levels achievable in modern steelmaking practice. With demonstrations of

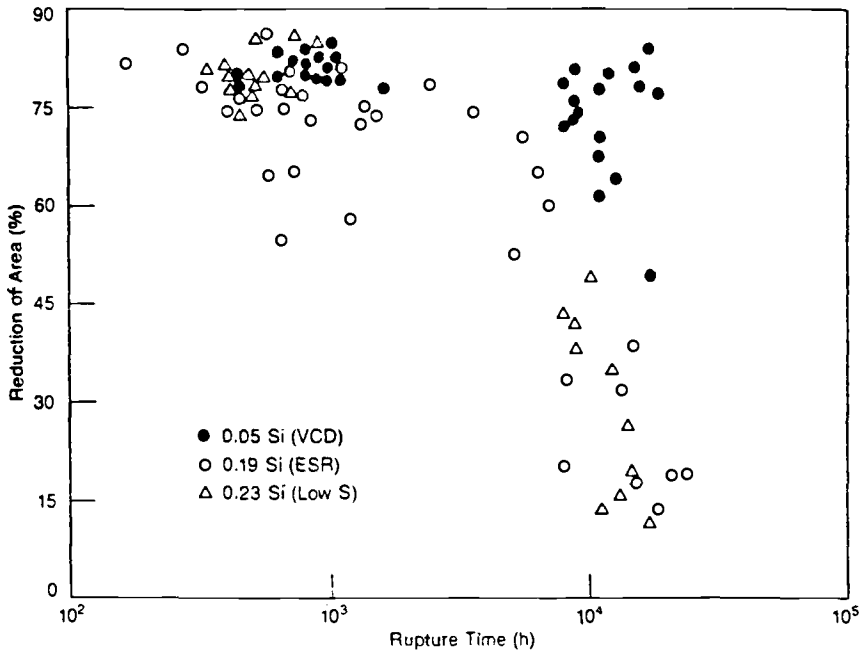


FIG. 2—Effect of deoxidation practice on creep reduction of area in 1Cr-Mo-V steel.

benefit from the elimination of Mn and Si, S content specifications will tighten concurrently.

Silicon

All modern rotor forging steels in the United States and many worldwide have been deoxidized with Si, that is, Si killed. Prior to and after the introduction of vacuum treatment, an Si range of 0.15 to 0.35% has been employed. With the introduction of VCD in the 1960s, a large improvement in the toughness of the Ni-Cr-Mo-V steels was noted at the low Si levels achievable with VCD. An additional advantage of the reduced Si content achievable through VCD is its effect in reducing the dendrite size and the thickness of the “mushy” zone in the solidification of Ni-Cr-Mo-V steel ingots. This effect minimizes the severity of segregation streaks in the ingot and enhances homogeneity. Work reported by Swaminathan [9] indicates that using VCD for 1Cr-Mo-V and reducing Si to the 0.02 to 0.05% range results in a significant improvement in long-term creep rupture ductility (Fig. 2).

It is expected that there will be no serious trend to further reduce the Si content of the Ni-Cr-Mo-V rotor steel. It is probable that the VCD process, and hence lower Si content, will be applied more frequently to the 1Cr-Mo-V rotor steel.

The Residual (Tramp) Elements: Antimony, Arsenic, and Tin

Advanced steelmaking technology relies primarily on scrap selection to control the tramp elements Sb, As, and Sn. These elements promote temper embrittlement in rotor steels at low levels. However, removal of Mn and Si and control of P to low levels may render these elements innocuous at current or even somewhat higher levels. This would give great relief to steelmakers that have been having difficulty obtaining clean low-residual scrap. Thus, the impact of advanced steel-making practice could be to maintain or possibly permit slight relaxation in specification limits on Sb, As, and Sn.

Aluminum

The use of Al in the production of rotor steels has been strictly avoided in the United States and limited in most shops worldwide. The industry standard maximum of 0.010% Al is established for turbine rotor steels. This limit recognizes the adverse effect of Al on the elevated temperature rupture ductility of the 1Cr-Mo-V steel. Steelmakers who use Al together with Ca for inclusion shape control in ladle injection processes or who use Al to achieve the low level of oxygen necessary for S removal argue that this limit, although justifiable for the 1Cr-Mo-V steel, is unnecessary for the Ni-Cr-Mo-V steel.

Furthermore, with argon purging of the ladle, the problem with alumina inclusions is minimized. However, with advanced steelmaking methods, the ability to achieve low oxygen levels without Al through in-process VCD provides an attractive alternative.

Thus, it is expected that there will be some tendency to relax the Al limit on Ni-Cr-Mo-V steels, while the limit for Cr-Mo-V steel will not change. There appear to be no pressures to tighten Al content limits.

Hydrogen

Most steel for rotor forgings is vacuum-stream degassed, especially steel for the larger rotors. This vacuum treatment has proved adequate for the processing of all rotor forging steels. Thus, no change in rotor forging specifications related to present requirements for vacuum treatment is anticipated as a result of recent advances in steelmaking technology.

Conclusion

Exciting advances are being made in the technology of steelmaking for rotor forgings. A variety of advanced technology processes such as LRF, ladle injection, ESR, and AOD are available and capable of achieving 0.001 to 0.002% S levels. Although most of these processes are attractive, the optimum combination for large rotor forging production appears to be BEF for melting and dephosphorization and LRF with vacuum and vacuum stream degassing for refining followed by special hot topping (possibly ESHT).

This modern steelmaking technology permits composition control to meet or exceed the requirements of current specifications as well as those of projected high-purity steel programs. If the prospect of improved resistance to temper embrittlement through reduction of Mn and Si content should be proved, it will not long remain a laboratory curiosity. The demonstration by EPRI-VEW that the extreme composition objectives of the high-purity rotor steels essentially can be met in commercial steelmaking practice is of primary importance in achieving credible evaluation and industry acceptance of the high-purity steels approach.

The steelmaker is fortunate that facilities are available to meet the most restrictive requirements that may evolve from current research in improved rotors and high-purity steel programs. Most forging producers have installed or are seriously considering installation of ladle metallurgy facilities, heavily favoring the LRF.

References

- [1] Bush, S. H., "Failures in Large Steam Turbine Rotors" in *Workshop Proceedings: Rotor Forgings for Turbines and Generators*, EPRI WS-79-235 Proceedings, Electric Power Research Institute, Palo Alto, CA, Sept. 1981, pp. 1-1 to 1-27.
- [2] Hagaman, R. T., "Failure Experience with Generator Rotors" in *Workshop Proceedings: Rotor Forgings for Turbines and Generators*, EPRI WS-79-235 Proceedings, Electric Power Research Institute, Palo Alto, CA, pp. 1-32 to 1-39.
- [3] Schabtach, C., Fogleman, E. L., Rankin, A. W., and Winne, D. H., "Report of the Investigation of Two Generator Rotor Fractures" in *Transactions ASME*, Vol. 78, American Society of Mechanical Engineers, New York, NY, Oct. 1956, pp. 1567-1584.
- [4] DeForest, D. R., Grobel, L. P., Schabtach, C., and Seguin, B. R., "Investigation of the Generator Rotor Burst at the Pittsburgh Station of the Pacific Gas and Electric Company," ASME paper 57-PWR-12, ASME Power Division Conference, Allentown, Pa., Oct. 21-23 1957, American Society of Mechanical Engineers, New York, NY.
- [5] Steiner, J. E., Busby, P. E., Jaffee, R. I., Murphy, E. L., Newhouse, D. L., and Wriedt, H. A., "Advanced Steelmaking Processes for Rotor Forgings," EPRI RD-3336, Contract 82-628, final report, Electric Power Research Institute, Palo Alto, CA, Dec. 1983.
- [6] McMahon, D. J. et al., "Elimination of Impurity-Induced Embrittlement in Steel. Part I: Impurity Segregation and Temper Embrittlement," EPRI Report NP-1501, Sept. 1980 and EPRI Report CS-3248, Nov. 1983, Electric Power Research Institute, Palo Alto, CA.
- [7] Newhouse, D. L., "Discussion on Temper/Hydrogen Embrittlement," *Workshop Proceedings: Rotor Forgings for Turbines and Generators*, EPRI WS-79-235, Proceedings, Sept. 1981, Electric Power Research Institute, Palo Alto, CA, pp. 5-80 to 5-82.
- [8] Takeda, Y. and McMahon, C. J., "Effects of Compositional Variations and Aging Treatments on the Fracture Behavior of HY130 Steel in Air and Hydrogen," *Metallurgical Transactions of AIME*, 13A (1982) III.
- [9] Swaminathan, V. P. and Jaffee, R. I., this publication.

DISCUSSION

*J. Ewald*¹ (written discussion)—It is to be expected that in future times copper (Cu) contents in rotor forging steels will increase. Are there current investigations

¹ Kraftwerk Union AG, D-4330 Muelheim a.d. Ruhr, Germany.

which could show the tolerable Cu contents in future specifications for 1Cr-Mo-Ni-V and a 3% to 3.5Ni-Cr-Mo-V steels?

J. E. Steiner and R. I. Jaffee (authors' closure)—The authors know of no current research that might show the tolerable limits of copper content in rotor steels. Fortunately, the levels of copper and other tramp elements in modern rotor steels have been suitably controlled by careful scrap selection. We agree that the future trends for availability of clean scrap are not encouraging; however, the "clean steels" approach with low manganese, sulfur, and phosphorus contents should provide greater tolerance for slightly higher levels of tramp elements.

G. Hartman² (written discussion)—I would like to comment on Dr. Jaffee's comment as to "the ease of being able to produce low manganese (0.02%) via the basic electric steelmaking process." To make steel to a low manganese content such as 0.02% requires that the steelmaker oxidize almost all of the carbon from the bath (less than 0.03%). This will require an extensive oxygen blow or the use of large amounts of iron ore resulting in very hot bath temperatures with an excessive amount of oxygen (≈ 1000 ppm) in the steel. The decarburization and low manganese will result in very high ferrous oxide (FeO) contents in the slag that has to be carefully removed from the furnace prior to proceeding with the heat. The heat has to be recarburized to at least 10 points above the tap carbon aim of 0.25% so it can be reoxidized to get the steel bath into the proper gas content and temperature prior to proceeding with the refining period.

This excessive level of oxygen is contrary to the established turbine rotor furnace practice utilized in the United States. This type of practice will result in extensive furnace time, refractory erosion, and yield loss which will dramatically increase the cost to produce the steel. This will be especially true when multiheat (three, four, or five) furnaces are being utilized to pour the ingot.

Low manganese steel can be produced in the electric furnace, but the consuming industry should thoroughly evaluate the level of manganese needed such as 0.10% max, 0.06% max, or 0.02% max, as the level permitted will determine the economics and feasibility of obtaining it.

J. E. Steiner and R. I. Jaffee (authors' closure)—In addition to dephosphorization by oxidation in the electric furnace, it is possible to remove manganese and silicon at the same time. While it is true that it is difficult to reduce Mn and Si to the level of 0.01%, reduction to the level of 0.05% is easy to achieve using conventional practice. Thus, it is possible to achieve the low P, Mn, and Si levels desired in clean steel production with conventional electric furnace practice.

² A. Finkl & Sons Co., Chicago, IL 60614.

Jeong Tae Kim,¹ Moon Ryang Pyo,² Yun Souk Chang,²
and Hyuk Soon Chang³

The Effect of Alloying Elements and Steelmaking Processes on the “A” Segregation Occurrence in Large Ingots

REFERENCE: Kim, J. T., Pyo, M. R., Chang, Y. S., and Chang, H. S., “The Effect of Alloying Elements and Steelmaking Processes on the ‘A’ Segregation Occurrence in Large Ingots,” *Steel Forgings, ASTM STP 903*, E. G. Nisbett and A. S. Melilli, Eds., American Society for Testing and Materials, Philadelphia, 1986, pp. 45–56.

ABSTRACT: Investigations on segregation in various sizes of ingots of 13, 25, 54, 104, 180, 210, and 430-ton weight were carried out at Korea Heavy Industries and Construction Co.

The results of the segregation examined reveal that silicon-deoxidized (SD) carbon steel ingots have much more segregation than have vacuum carbon-deoxidized (VCD) low-alloy steel ingots. That is, the total carbon segregation ratio is 41% in the 210-ton SD carbon steel ingot, whereas it is 38% and 21% in the 430 and 104-ton VCD, low-alloy steel ingots, respectively. From these results, “A” segregation is not found when the ratio of carbon segregation is less than 30 to 40% in both steel ingots. Since silicon and manganese increase the change of liquid density during solidification and molybdenum decreases it, it is possible to minimize the macrosegregation by increasing molybdenum and decreasing silicon and manganese within the specified range.

KEY WORDS: “A” segregation, segregation ratio, steelmaking process, vacuum carbon deoxidation, ingot solidification, carbon steel, Ni-Cr-Mo-V steel, alloy design, solute-enriched liquid, change of liquid density

As the size of ingots increases, the problem of micro- and macrosegregation is inevitable. Therefore, special attention has been given to the control of macrosegregation. “A” segregation sometimes is considered to be unavoidable in gigantic ingots, and no satisfying solution has been reported as yet.

Scepi et al. [1] studied the effect of the solidification course, the slenderness

¹ Assistant section chief, Research & Development, Korea Heavy Industries & Construction Co., Changwon, Korea 615, presently on leave as graduate student, Department of Materials Science Engineering, Korea Advanced Institute of Science & Technology, Seoul, Korea.

² Section chief and manager, respectively, Research & Development, Korea Heavy Industries & Construction Co., Changwon, Korea 615.

³ Director, Casting & Forging Division, Korea Heavy Industries & Construction Co., Changwon, Korea 615.

(H/D) ratio, the hot top volume, and the pouring temperature on the internal soundness of forging ingots. They found that the smaller the slope of the solidification front becomes, the higher the probability becomes that internal defects will be trapped. The optimum conditions to obtain sound forgings ingots are as follows: (1) The slenderness ratio is to be less than 1.20; (2) The minimum hot top volume is 28%; (3) Pouring temperature is to be higher than 1580°C.

Tashiro et al. [2] studied the relationship between the rate of vertical solidification and the soundness of forging ingots. They showed that the rate of vertical solidification relates to the mold design, that is, the H/D ratio and the ratio of the hot top diameter to ingot diameter (ζ). They found that, as the H/D decreases and the ζ increases, the critical rate of vertical solidification decreases and the suppression of internal defects is more effective.

The influence of alloying elements on the segregation of ingots has been studied [3,4]. Common et al. found that the contents of alloying elements such as carbon, nickel, chromium, manganese, copper, and tin had not shown any significant influence on the level of segregation of carbon. Their detailed analysis indicates that molybdenum and vanadium suppress the segregation of carbon.

However, Miyamoto and Suzuki [5] argued that vanadium did not influence the segregation of carbon but had properties to promote shrinkage cavities in ingots.

Suzuki et al. [5,6] studied the influence of alloying elements on the occurrence of ‘‘A’’ segregation and on the dendrite structure, using 14-kg ingots solidified horizontally and unidirectionally. Furthermore, Fujii et al. [7] developed the macrosegregation theory to predict the formation of channel-type segregation considering heat, mass, and momentum transport for a multicomponent system and suggested a methodology of alloy design to avoid channel-type segregation by adjusting chemical compositions.

There is no report about the results, however, when their segregation theory [7] is applied to the gigantic ingots. In this paper, the authors found that the Fujii macrosegregation theory [7] is applicable to the gigantic ingots of vacuum carbon deoxidized (VCD) alloy steel. The effect of ingot dimensions and steel-making processes on the segregation also is studied.

Experimental Procedure

The shapes of ingots investigated are shown in Table 1. Ingots smaller than 25 tons were teemed by bottom pouring in air with argon gas screening, and ingots larger than 30 tons were teemed by top pouring in the vacuum stream degassed system. Specimens for ladle analysis (of each ingot) were sampled in the ladle furnace for ingots smaller than 25 tons and in the pony ladle for ingots larger than 30 tons.

To investigate an aspect of segregation, the carbon steel 13-ton ingot, as cast, was cut using a band saw to a size of 100 by 100 mm along the axis. Figure 1 shows specimens used to analyze the chemical compositions and examine the

TABLE 1—Weight and shapes of ingots investigated.

Weight, ton	Description, mm				
	H^a	D_L^b	D_U^c	D^d	H/D^e
13	1852	849	1034	942	1.97
25	2256	1140	1320	1230	1.83
54	2323	1747	1933	1840	1.26
104	2887	2195	2425	2310	1.25
180	3195	2590	2850	2720	1.18
210	3960	2530	2850	2690	1.47
430	4370	3396	3740	3568	1.23

^a Height of ingot.^b Lower diameter of ingot.^c Upper diameter of ingot.^d Mean diameter of ingot $[(D_U + D_L)/2]$.^e Slenderness ratio.

dendritic structure of the 13-ton ingot. For the other ingots, except the 430-ton ingot, specimens were taken from forgings corresponding to parts of the hot tops and bottoms of ingots. Specimens from the 430-ton ingot were taken from the discarded hot top at positions shown in Fig. 2. Specimens for the center axis of the ingot were taken from the bored core bar, while specimens from the surface part were taken during rough machining.

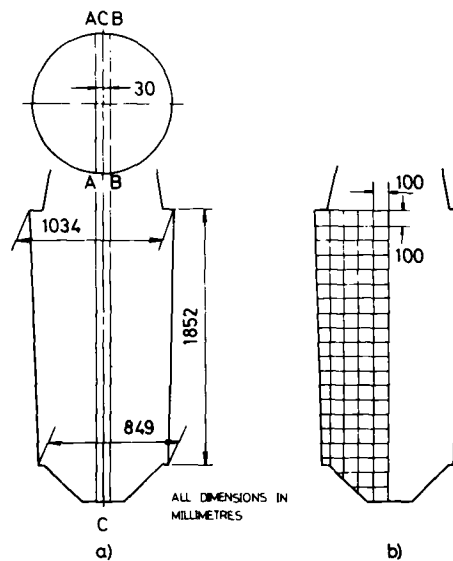


FIG. 1—Specimens used to analyze the chemical composition and dendrite structure of the 13-ton carbon steel ingot as cast: (a) ingot dimension; (b) specimens.

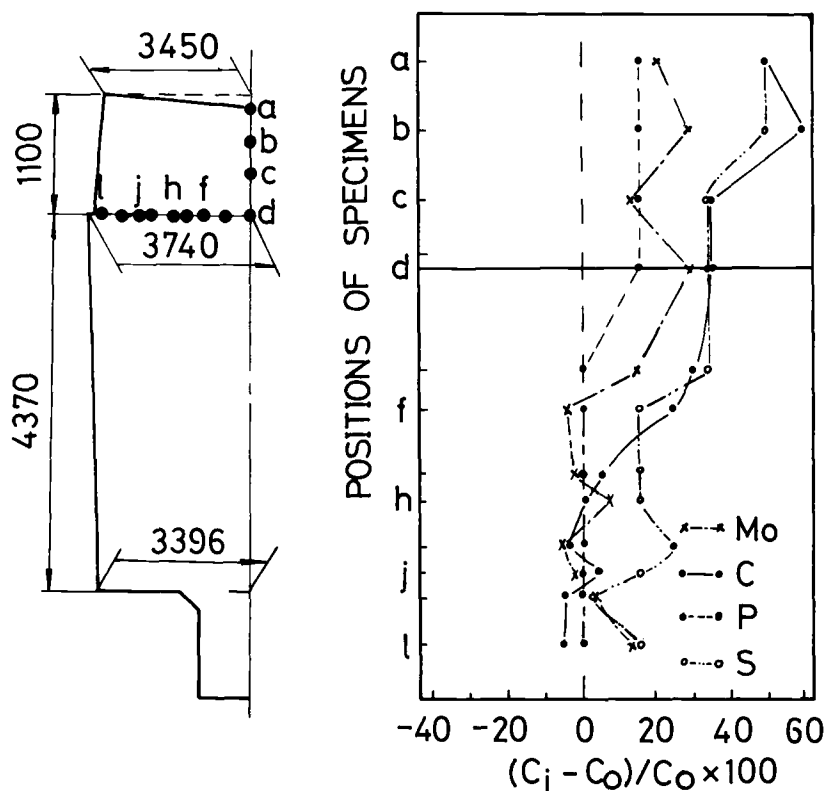


FIG. 2—Segregation ratio along the central axis and transverse direction in the hot top of a 430-ton steel ingot of VCD steel. NOTE: C_i is the chemical composition (percent by weight) of component i of the ingot; C_o is the ladle analysis of component i .

TABLE 2—Weights of ingots and their ladle analysis.

Ingot No.	Ingot Weight, ton	Chemical Composition, percent by weight											
		C	Si	Mn	P	S	Ni	Cr	Mo	V	As	Sn	Sb
1	13	0.29	0.22	0.48	0.006	0.006	0.010
2	25	0.56	0.27	0.81	0.009	0.007	1.72	0.77	0.35	0.08
3	54	0.37	0.21	1.16	0.008	0.007	0.17	0.18	0.014	...	0.003	0.004	0.003
4	54	0.25	0.07	0.39	0.007	0.006	2.17	1.40	0.49	0.07
5	54	0.25	0.08	0.31	0.007	0.007	3.41	1.70	0.48	0.12	0.013	0.006	...
6	54	0.56	0.26	0.80	0.009	0.008	1.71	0.78	0.34	0.09
7	104	0.28	0.09	0.48	0.007	0.006	2.28	1.65	0.40	0.10	0.009	0.006	0.013
8	180	0.36	0.25	1.00	0.007	0.008	0.05	0.08	0.160	0.047	0.004	0.004	0.003
9	210	0.37	0.26	0.99	0.007	0.007	0.03	0.07	0.010	0.045	0.003	0.004	0.003
10	430	0.20	0.04	0.32	0.006	0.006	2.97	1.59	0.39	0.10	0.006	0.003	0.002

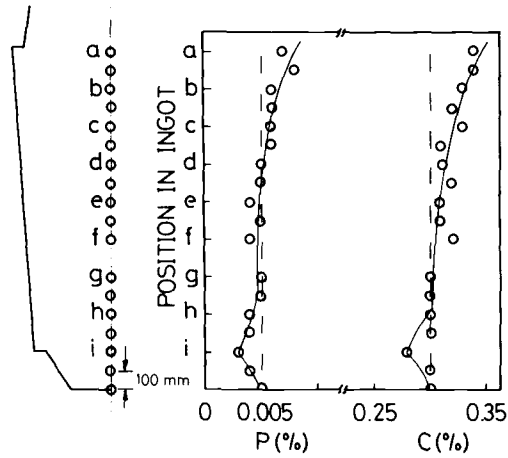


FIG. 3--The distribution of carbon and phosphorus along the central axis of a 13-ton carbon steel ingot of SD steel.

To investigate the effect of ingot size on the segregation ratio, ten sizes of ingots from 13 to 430 tons were investigated. Table 2 shows the weights of the ingots investigated and their ladle analyses.

In order to investigate the effect of the steelmaking process on the segregation, silicon deoxidation (SD) and VCD processes were compared.

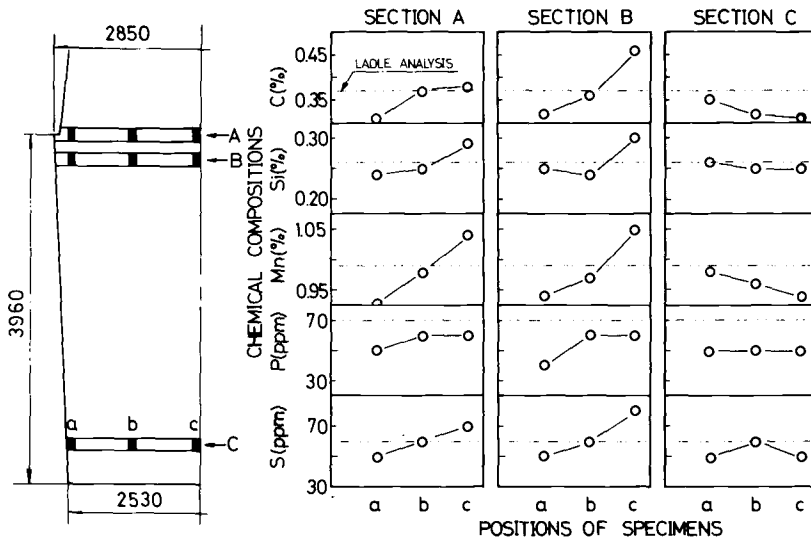


FIG. 4--Transverse distribution of chemical compositions in the top and bottom parts of a 210-ton carbon steel ingot of SD steel.

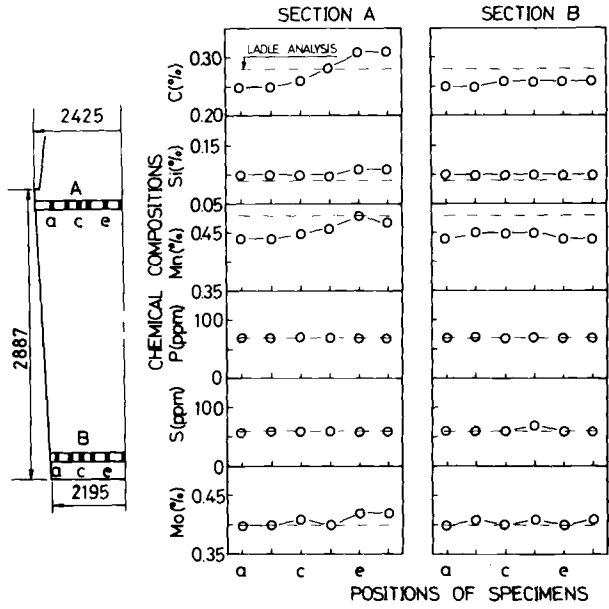


FIG. 5—Transverse distribution of chemical compositions in the top and bottom parts of a 104-ton low alloy steel ingots of VCD steel.

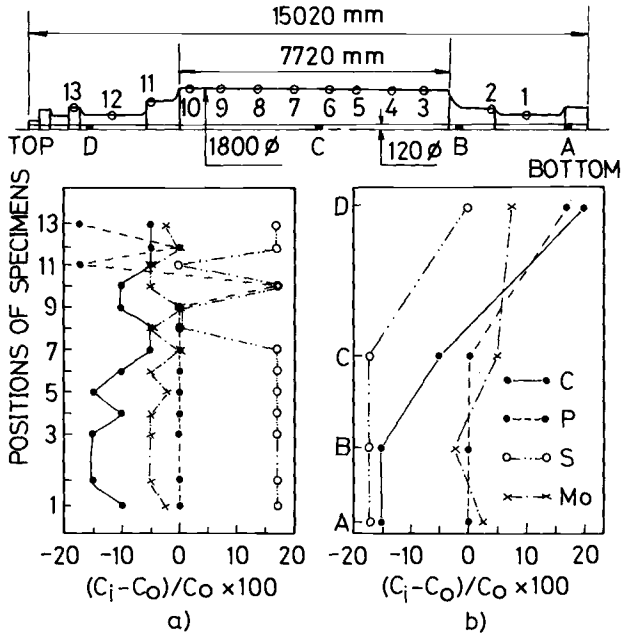


FIG. 6—Segregation ratio of chemical compositions at the surface part and bored core bar of a generator rotor shaft made with a 430-ton low alloy steel ingot of VCD steel: (a) surface part; (b) bored core bar.

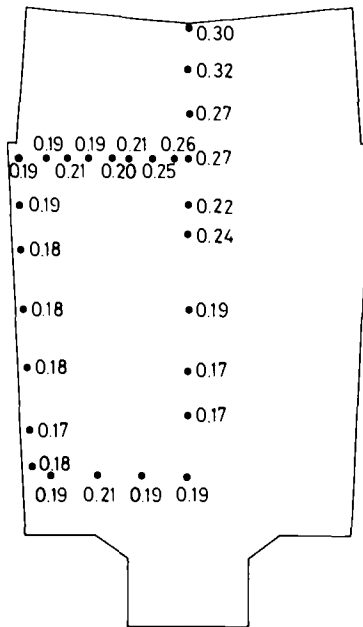


FIG. 7—Mean carbon content in ladle: 0.20%. Distribution of carbon in 3Ni-Cr-Mo-V steel 430-ton ingot.

Results

The aspect of segregation along the center axis of a 13-ton carbon steel ingot of SD steel is shown in Fig. 3. Prominent positive segregation occurred in the top area, but negative segregation occurred at the bottom. Figure 4 illustrates the transverse distribution of the chemical composition at the top and bottom parts of a 210-ton carbon steel ingot of SD steel. In the transverse section of the top, an aspect of segregation changes from negative at the surface to positive at the center. In the transverse bottom section, however, negative segregation in the center is much larger than that in the surface. The negative segregation in the bottom part of the large carbon steel ingot results from the development of a sedimental zone, which originates in the deposition and accumulation of pure crystalline fragments. Although the rate of carbon segregation was 41%, "A" segregation was not found in the 210-ton ingot of SD steel.

Figure 5 illustrates the transverse distribution of chemical composition in the top and bottom parts of a 104-ton, low-alloy steel ingot of VCD steel. The segregation ratio both along the center axis and in the transverse direction at the hot top of the 430-ton VCD, low-alloy steel ingot is shown in Fig. 2. These results are similar to those obtained from the top parts of the carbon steel ingots. But the segregation of low-alloy steel ingots is not so pronounced as that of carbon steel ingots. Figure 6 illustrates the segregation ratio in the surface parts

TABLE 3—The rate of carbon segregation of ingots investigated.

Ingot No.	Weight, ton	C _o ^a	C _{max}	C _{min}	ΔC/C _o , Observed ^b	ΔC/C _o , Calculated ^c
1	13	0.29	0.35	0.28	0.24	0.22
2	25	0.56	0.63	0.53	0.20	0.25
3	54	0.37	0.44	0.33	0.30	0.40
4	54	0.25	0.27	0.24	0.12	0.18
5	54	0.25	0.26	0.24	0.08	0.16
6	54	0.56	0.72	0.53	0.34	0.33
7	104	0.28	0.31	0.25	0.21	0.23
8	180	0.36	0.44	0.32	0.33	0.61
9	210	0.37	0.46	0.31	0.41	0.69
10	430	0.20	0.27	0.19	0.38	0.31

^a Percent by weight.
^b The rate of carbon segregation investigated.
^c The rate of carbon segregation calculated using the equation of J. Common [4].

and bored core bar taken from a generator shaft made with the 430-ton ingot. The negative segregation occurred in the surface part, whereas negative and positive segregation occurred at the bottom and top part of the generator shaft, respectively. When the distribution of carbon in the generator shaft was matched with the real position of the ingot, the results were as shown in Fig. 7.

Table 3 indicates the rate of carbon segregation of the ingots investigated. C_{max} is the maximum carbon content in the ingot body, C_{min} is the minimum carbon content in the ingot body, and C_o is the ladle analysis of carbon. ΔC is equal to the difference between C_{min} and C_{max}.

The ratio of carbon segregation (ΔC/C_o) versus ingot dimensions for VCD, low-alloy steel ingots and SD carbon steel ingots is shown in Fig. 8. The ratio of carbon segregation in carbon steel ingots is larger than that of the low-alloy steel ingots for the same dimensions.

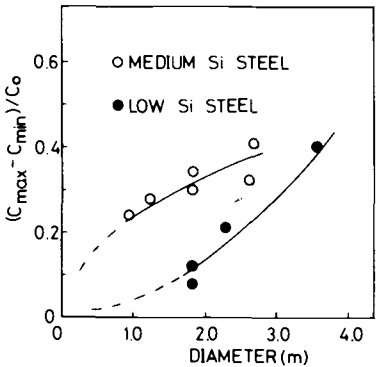


FIG. 8—The ratio of carbon segregation versus ingot dimensions for VCD steel ingots and slag deoxidized steel ingots. NOTE: C_{max} is the maximum concentration of component i in the ingot. C_{min} is the minimum concentration of component i in the ingot.

"A" segregation was not found when the ratio of carbon segregation was less than 30 to 40% in both carbon and alloy steel ingots.

Discussion

Figure 9 shows the dendrite structure of the carbon steel of the 13-ton ingot and the low-alloy steel of the 430-ton ingot. The mean spacing of dendrites in low-alloy steel ingots is smaller than that of carbon steel ingots. The effect of alloying elements on the formation of dendrite structure is significant. By increasing molybdenum and decreasing silicon content within a specified range, the radius of dendrite curvature becomes smaller, and higher dendritic arms are more easily formed. This result is consistent with the work of Taniguchi and Suzuki [6]. Since molybdenum promotes the formation of higher dendritic arms during solidification, it is suggested that molybdenum restrains the formation of macrosegregation in large ingots.

It is well-known [5,7] that the change of liquid density during solidification is the driving force in causing convection of solute-enriched liquid in the mushy zone. The natural convection of solute-enriched liquid in the mushy zone significantly influences the occurrence of the macrosegregation. So, it is necessary to adjust the relationship between alloying elements to minimize the change of liquid density. In order to suppress the change of liquid density during solidification, the relationship between alloying elements is calculated from the integral I [7].

$$I = \int_{g_L = g_E = 0.04}^{g_L = 1} \left| \frac{\Delta \zeta_L}{\zeta_L} \right| g_L dg_L \quad (1)$$

where

g_L = the volume fraction of liquid,

g_E = the volume fraction of liquid in the hot top portion, and

ζ_L = the density of liquid.

Since the amount of retained liquid to obtain the sound ingot body is to be at least 4%, the boundary condition of the integral I is $g_L = g_E = 0.04$ and $g_L = 1$. This condition is calculated from the simulated results of the isotherm curve versus time during solidification in large ingots. The relationship among the alloying elements such as silicon, manganese, and molybdenum in relation to the change of liquid density is calculated from the integral I , using the alloy parameters of Fujii et al. [7].

$$I = -1.022 \text{ Si} - 0.049 \text{ Mn} + 0.208 \text{ Mo} \quad (2)$$

Here, the amount of each element is percent by weight.

Figure 10 shows the interrelationship of manganese, silicon, and molybdenum in minimizing the change of liquid density under conditions where phosphorus

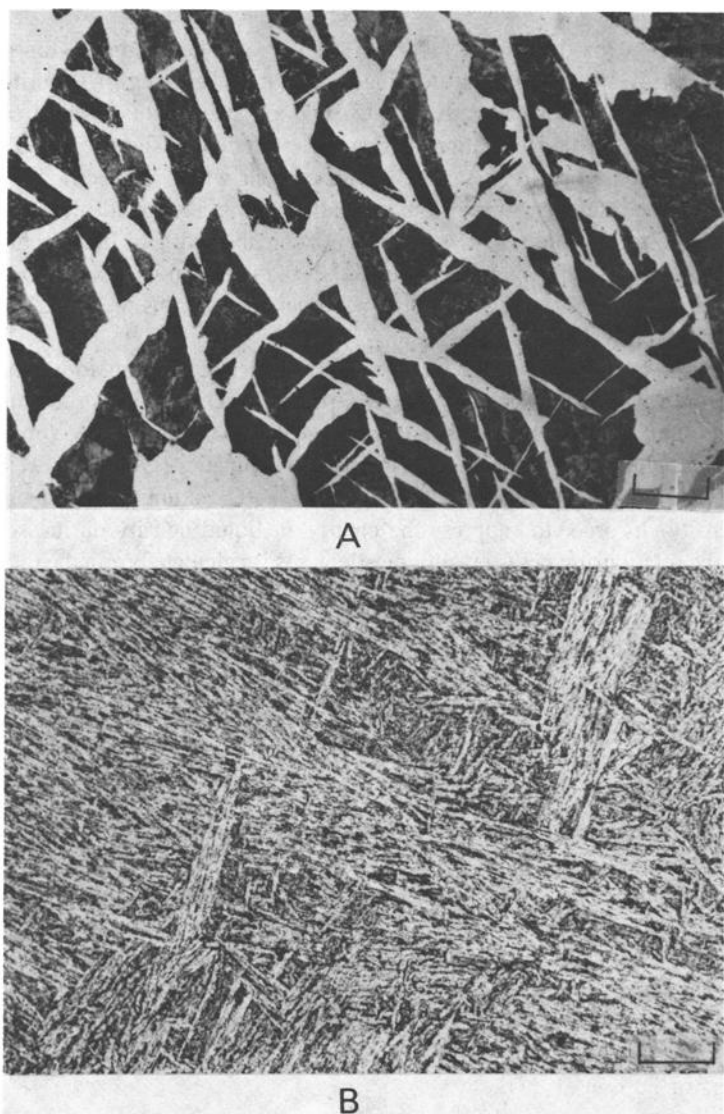


FIG. 9—Dendrite structure in (a) a 13-ton carbon steel ingot of slag deoxidized steel; (b) the hot top part of a 430-ton ingot of VCD steel. NOTE: The scale indicates 100 μm , nital etch.

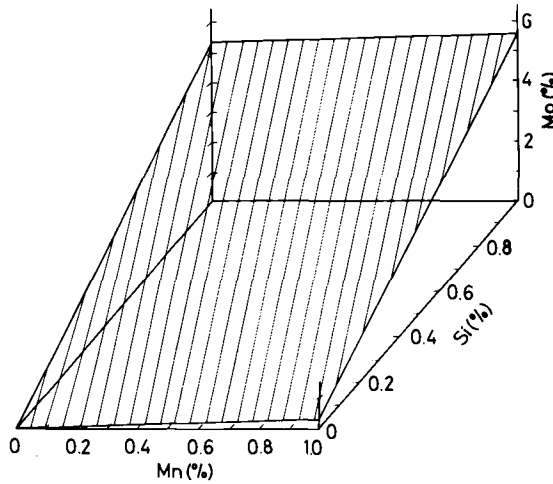


FIG. 10 The relationship among the concentrations of each component to minimize the change of liquid density at no phosphorus and sulfur content.

and sulfur are negligible. The alloying elements of negative values such as silicon and manganese increase the change of liquid density, while molybdenum element of positive values decreases it. That is, silicon and manganese promote the macrosegregation, whereas, molybdenum suppresses the micro- and macrosegregation.

Consequently, it is possible to minimize the macrosegregation by increasing molybdenum and decreasing silicon and manganese within the specified range. This methodology of alloy design coincides with the results of segregation in

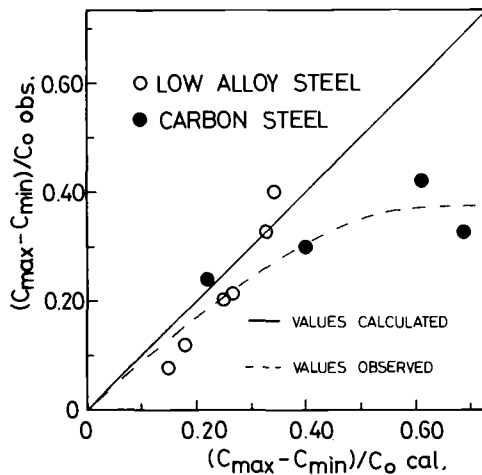


FIG. 11— Comparison of the observed carbon segregation ratio with calculated values.

VCD, low-alloy steel gigantic ingots. A possible explanation of this result is that the integral I is a parameter which characterizes the occurrence of segregation in gigantic ingots of low-alloy steel.

Figure 8 lends support to the effect of alloy elements, steelmaking processes, and ingot dimensions on the segregation. Reporters [4] presented an equation to estimate the ratio of carbon segregation with ingot dimensions, alloy, and impurity contents such as silicon, molybdenum, vanadium, phosphorus, and sulfur. But this is in conflict with the results investigated in large ingots as shown in Fig. 11. That is, the observed values of carbon segregation in gigantic ingots of SD steel are less than the calculated values.

Summary and Conclusions

For the purpose of minimizing macrosegregation in gigantic ingots, the results of investigations of the effects of alloying elements, ingot dimensions, and steel-making processes are summarized as follows:

1. Since the ratio of retained liquid in the hot top to total weight of the ingot is 0.04 in the 430-ton ingot, the relationship between alloying elements to minimize the change of liquid density follows the following equation

$$I = -1.022 \text{ Si} - 0.049 \text{ Mn} + 0.208 \text{ Mo}$$

2. This methodology of alloy design to minimize macrosegregation by adjusting the relationship among concentrations of alloying elements is applicable to gigantic ingots of vacuum-deoxidized, low-alloy steel.

3. Although the total carbon segregation ratio was 41% in the 210-ton ingot of SD carbon steel and 38% in the 430-ton ingot of VCD steel, "A" segregation was not found in either steel ingot.

References

- [1] Scepi, M., Andreoli, B., Basevi, S., and Giorgetti, A., "Thermal and Metallurgical Control of the Efficiency of Ingot Moulds for Forging Ingots," 9th International Forging Conference, Commission of European Communities, 4 to 9 May 1981.
- [2] Tashiro, K., Watanabe, S., Kitagawa, I., and Tamura, I., "Influence of Mould Design on the Solidification and Soundness of Heavy Forging Ingots," *Tetsu to Hagane*, Vol. 67, Jan. 1981, pp. 103-112.
- [3] Gibb, J. M. in *Casting and Solidification of Steel*, Vol. 1, information symposium, 6th technical paper, IPC Science and Technology Press, Ltd., Guildford, England, 1977, pp. 176-214.
- [4] Common, J., Delorme, J., and Bastien, P., "The Heterogeneity in Heavy Forging Ingots Study of the Influence of Impurities and Alloy Elements on Segregation," the 6th International Forgemasters Meeting, 1972.
- [5] Suzuki, K., and Miyamoto, T., "Influence of Alloying Elements on the Formation of "A" Segregates in Steel Ingot," *Tetsu to Hagane*, Vol. 65, Oct. 1979, pp. 63-72.
- [6] Suzuki, K. and Taniguchi, K., "The Elimination Mechanism of "A" Segregates of Steel Ingot," *Tetsu to Hagane*, Vol. 65, Oct. 1979, pp. 73-80.
- [7] Fujii, T., Poirier, D. R., and Flemings, M. C., "Macrosegregation in a Multicomponent Low Alloy Steel," *Metallurgical Transactions B*, Vol. 10B, Sept. 1979, pp. 332-339.

Turbine and Generator Forgings

Rotor Manufacture

Masayuki Yamada,¹ Matsuo Miyazaki,¹ Osamu Watanabe,¹ and Mitsuo Kawai²

Development of Integral High-Pressure–Low-Pressure Combination Rotor Forgings

REFERENCE: Yamada, M., Miyazaki, M., Watanabe, O., Kawai, M., “Development of Integral High-Pressure–Low-Pressure Combination Rotor Forgings,” *Steel Forgings*, ASTM STP 903, E. G. Nisbett and A. S. Melilli, Eds., American Society for Testing and Materials, Philadelphia, pp. 59–73.

ABSTRACT: Integral high pressure (HP)-low pressure (LP) combination rotor forgings for single-cylinder turbines used under the steam condition over 773 K require good toughness and elevated temperature strength. Conventional Ni-Cr-Mo-V or Cr-Mo-V steel forgings are undesirable from the viewpoint of material properties. We developed integral HP-LP combination rotor forgings by alloy modifications (niobium and nickel addition) based upon Cr-Mo-V steel and the application of differential heat treatment. An actual dimensional prototype sample forging (1650 mm in diameter) was manufactured and evaluated. The forging exhibited high quality, and superior creep rupture strength at the HP zone and excellent toughness at the LP zone were obtained simultaneously. These developed rotor forgings have been applied for several turbine units of about the 100-MW class.

KEY WORDS: steam turbine, rotor, creep rupture strength, toughness, tensile strength, proof stress, differential heat treatment, nickel, niobium

A steam turbine unit used under the steam condition over 773 K (500°C) normally consists of high-pressure (HP), intermediate-pressure (IP), and low-pressure (LP) cylinders. Recently, there has been a trend of single-cylinder design to make the total size compact for small and medium turbines.

Both creep rupture strength and toughness are simultaneously required in this integrated HP-LP turbine rotor: 1Cr-1.25Mo-0.25V steel (called Cr-Mo-V steel hereafter), which has been conventionally used for the HP (IP) rotor, is not sufficient in its toughness, and 3.5Ni-Cr-Mo-V steel used for the LP rotor is short in its creep rupture strength, and temper embrittlement in the HP zone also is apprehensive.

¹ Engineer, manager, and engineer, respectively, Toshiba Corp., Heavy Apparatus Engineering Laboratory, Yokohama, Japan 230.

² Senior researcher, Toshiba Research and Development Center, Toshiba Corp., Yokohama, Japan 230.

Consequently, we started development of an integral HP-LP combination rotor to satisfy both creep rupture strength and toughness simultaneously. The first step of study was to optimize the chemical composition and the heat treatment condition. Thereafter, we trially manufactured an integral HP-LP combination rotor so as to verify its quality and mechanical properties, thus completing the developmental study.

The obtained results follow.

Modification of Chemical Composition

Specimen

The specimen is made of either one of twelve kinds of steel (No. 1 to No. 12) shown in Table 1 that are mainly composed of Cr-Mo-V steel used as a conventional HP rotor and added with niobium and nickel in a single or compound form. Each specimen of 2 kg was melted in a high-frequency vacuum induction furnace. Then, it was subjected to forging, annealing, and further austenitization at 1243 K (970°C) for 7.2 ks (2 h). Subsequently, it was cooled at a cooling rate of 1.4×10^{-2} K/s (50°C/h), which is equivalent to the simulated cooling rate obtained at the center of a rotor barrel with 1600 to 1700 mm in diameter where water spray is applied. It was further subjected to tempering at 943 K (670°C) for 43.2 ks (12 h).

Test Results and Consideration

The effect of added niobium and nickel influencing the impact value is shown in Fig. 1. In Specimens 2 to 5 to which niobium is added, the grain size is small

TABLE 1—Chemical composition of specimens investigated and sample forging.

No.	C	Si	Mn	Ni	Cr	Mo	V	Cb	Fe	Remarks
1	0.25	0.19	0.70	0.31	1.08	1.25	0.22	...	balance	
2	0.23	0.20	0.65	0.30	1.10	1.18	0.22	0.021	balance	
3	0.23	0.20	0.68	0.29	1.11	1.26	0.24	0.038	balance	
4	0.24	0.21	0.66	0.28	1.07	1.20	0.23	0.050	balance	
5	0.26	0.23	0.64	0.32	1.06	1.23	0.22	0.084	balance	
6	0.22	0.19	0.73	0.61	1.12	1.17	0.24	...	balance	
7	0.25	0.20	0.71	1.03	1.10	1.22	0.22	...	balance	2-kg melts
8	0.24	0.18	0.70	1.51	1.12	1.23	0.25	...	balance	
9	0.22	0.21	0.64	0.60	1.10	1.18	0.23	0.035	balance	
10	0.25	0.22	0.67	1.10	1.08	1.19	0.23	0.035	balance	
11	0.26	0.20	0.71	0.57	1.11	1.21	0.24	0.085	balance	
12	0.23	0.19	0.70	1.08	1.07	1.24	0.25	0.091	balance	
13	0.28	0.05	0.69	0.29	1.10	1.24	0.23	...	balance	50-kg melts
14	0.23	0.03	0.66	0.90	1.07	1.13	0.22	0.035	balance	
Model	0.26	0.08	0.62	0.93	1.25	1.25	0.24	0.030	balance	sample forging

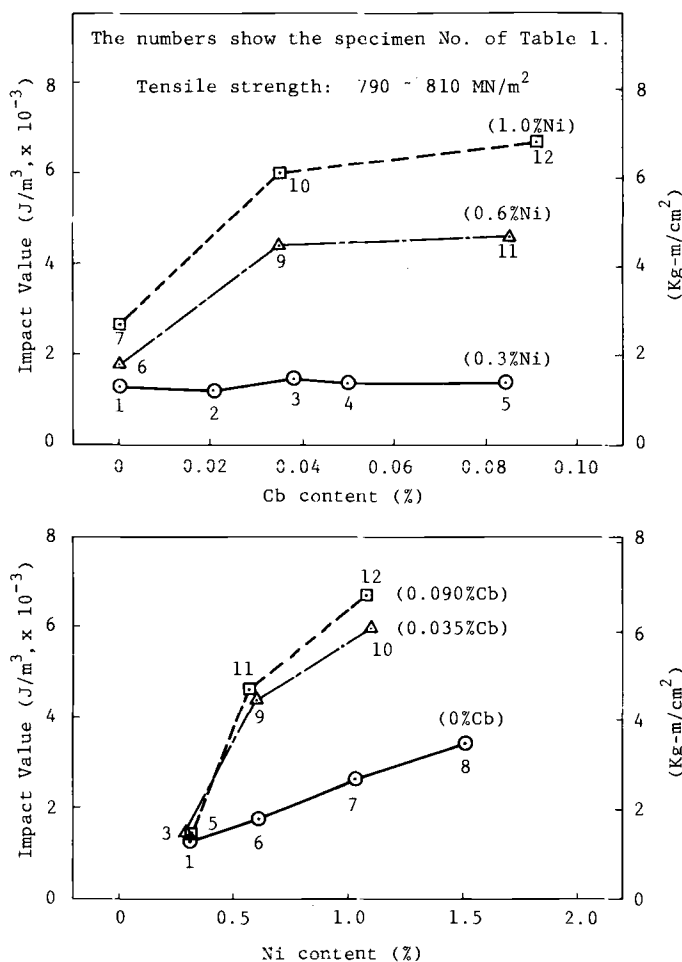


FIG. 1—Effect of niobium and nickel contents on impact value.

in comparison with those of Specimen 1 comprising the basic composition, but the impact value is hardly increased. Specimens 6 to 8 added with nickel are improved in their impact properties in comparison with Specimen 1. However, temper embrittlement at the high temperature portion is also apprehensive if the added content of nickel increases, and, according to the opinion [1] of Fukui et al., addition of more than 1.2% nickel may cause significant deterioration in proof stress or creep rupture strength or both. Therefore, added content of nickel was limited at most to 1% or so, and addition of niobium in compound form was investigated instead.

Specimens 9 to 12 added with niobium and nickel are significantly improved in view of impact properties. However, as may be clearly observed in Fig. 1,

niobium is effective on toughness, provided that about 0.6% or more nickel is added, and the impact property is enhanced as the added content of niobium increases, but 0.04% or more addition tends to get its effect saturated. Furthermore, toughness may be reduced as a large quantity of added niobium is liable to segregate coarse niobium carbides in the central portion of a rotor ingot. Therefore, about 0.04% addition of niobium is considered desirable.

Accordingly, Cr-Mo-V steel added with niobium and nickel possibly can be considered applicable as an integral HP-LP combination rotor forging from the view of its tensile properties and toughness.

Optimum Condition of Heat Treatment

Specimen

Two kinds of specimens were assigned (Nos. 13,14) as mentioned in Table 1, one of which is the Cr-Mo-V steel added with niobium and nickel and the other of which is the Cr-Mo-V steel used as a conventional HP rotor. The content of silicon was reduced to the possible minimum to increase the toughness by application of vacuum carbon oxidation (VCD). Each specimen of 50 kg was melted in a high-frequency vacuum induction furnace and then subjected to forging. Subsequently, annealing was applied to these specimens; then quality heat treatment was carried out. Two kinds of austenitizing temperature, that is, 1243 and 1293 K (970 and 1020°C), were employed. In addition, the cooling rate corresponds to each of the simulated rates of cooling equivalent to those of respective positions distributed from the outer surface [16.8×10^{-2} K/s (600°C/h)] to the center [1.4×10^{-2} K/s (50°C/h)] of the 1600 to 1700-mm barrel diameter.

Test Results and Consideration

The results of the tension test and impact test are shown in Fig. 2. The tensile properties of each specimen stay approximately at equal level. Specimen 14 is significantly improved in its impact properties in comparison with Specimen 13. In addition, the impact properties depend on the cooling rate, and the impact value increases, while 50% fracture appearance transition temperature (FATT) decreases as the cooling rate increases. Furthermore, Specimen 14 shows smaller variation in the impact properties than Specimen 13.

The result of the creep rupture test is shown in Fig. 3. The creep rupture strength of Specimen 14 is smaller than that of Specimen 13. Therefore, the mechanical properties-induced creep rupture strength of Specimen 14 were investigated after raising the austenitizing temperature up to 1293 K (1020°C). The obtained results are shown in parallel in both Figs. 2 and 3. When the austenitizing

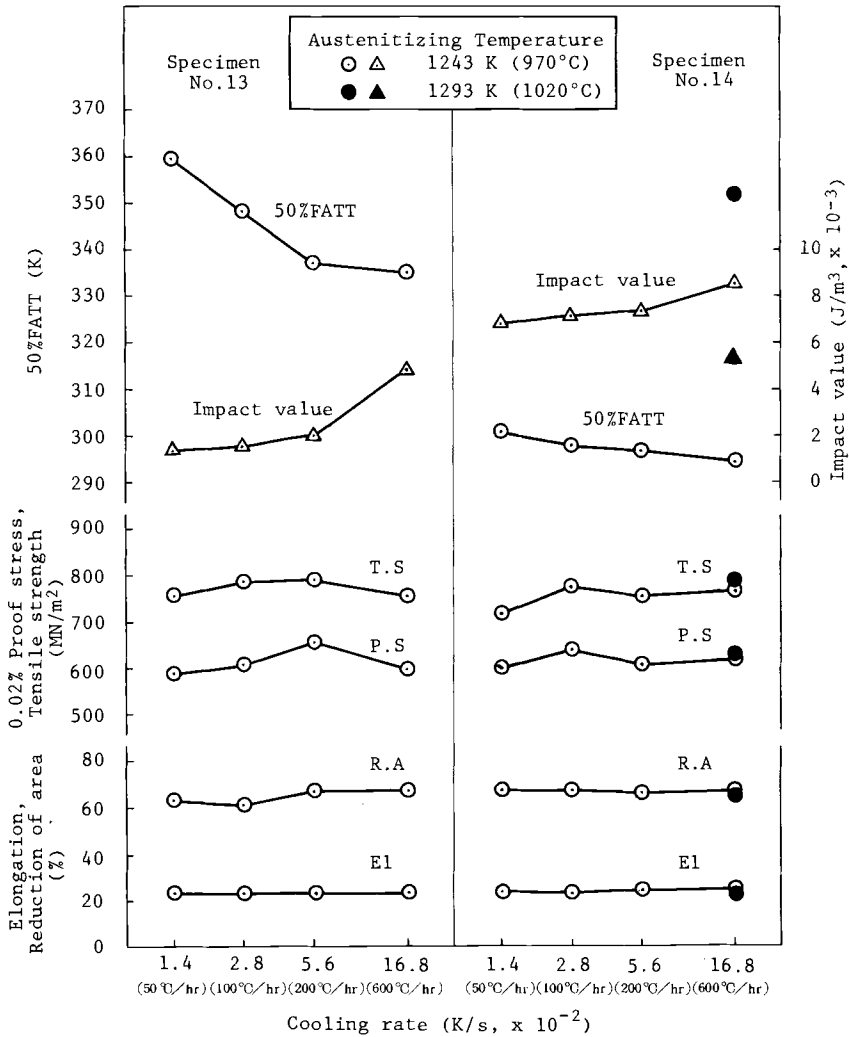


FIG. 2—Effect of heat treatment conditions on mechanical properties.

temperature is raised, the creep rupture strength is increased up to the level higher than that of Specimen 13, but the toughness is reduced.

Accordingly, in order to simultaneously satisfy both the creep rupture strength of the HP zone and the toughness of the LP zone, a process of combining the different heat treatment conditions for both the HP and LP zones of a rotor, respectively, as well as a process of adding niobium and nickel to Cr-Mo-V steel, can be taken into consideration. The examples of the heat treatment condition are shown in Fig. 4. The heat treatment on Model A shows a process to raise

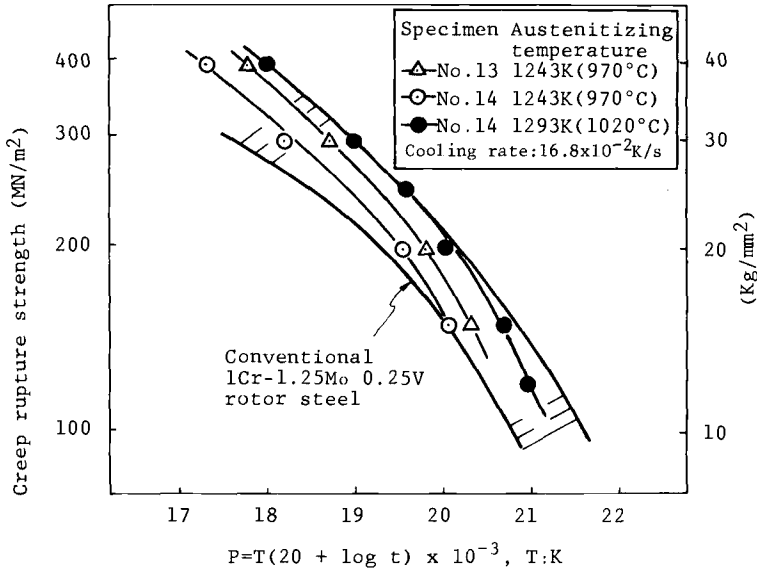


FIG. 3—Creep rupture strength of 1Cr-1.25Mo-0.25V steel containing niobium and nickel.

the austenitizing temperature of the HP zone compared with that of the LP zone. On the other hand, the heat treatment on Model B shows a process to expedite the cooling rate of the LP zone compared with that of the HP zone. Further, the heat treatment on Model C implies a process of combining Model A and Model B together. Application of these differential heat treatment processes is considered effective to materialize an integral HP-LP combination rotor forging.

Figure 5 shows the austenitizing temperature distribution obtained through the finite-element method (FEM). Difference in austenitizing temperatures of the HP and LP zones can be realized clearly.

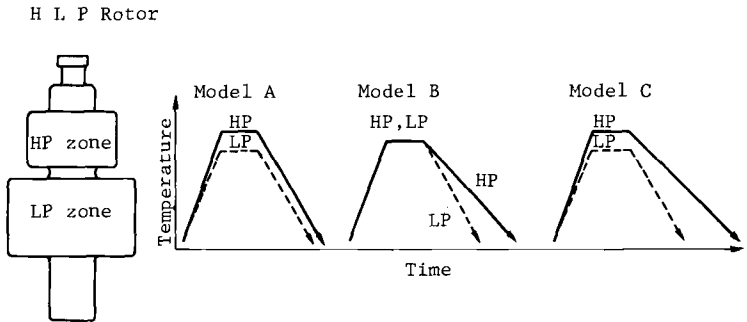


FIG. 4—Schematic illustration of the differential heat treatment for the integral HP-LP combination rotor.

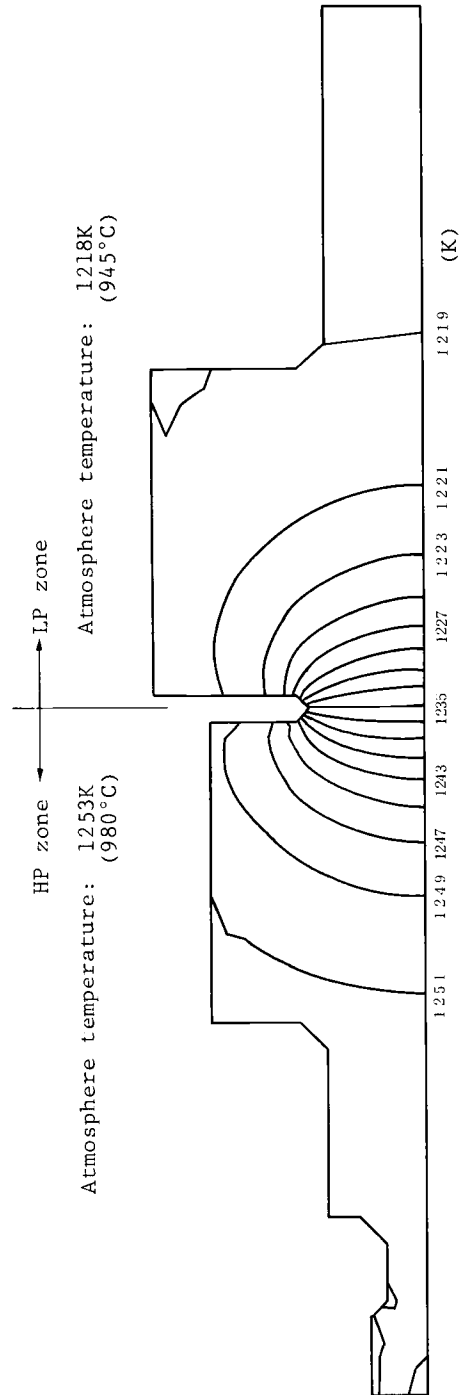


FIG. 5—One example of the finite-element method analysis of the differential heat treatment (austenitizing).

Verification by Sample Forging

Manufacturing Procedure of Sample Forging

The scale of the model rotor is the maximum 1650-mm barrel diameter and 50×10^3 kg drum weight. The chemical composition of this rotor is shown in Table 1, which is added with niobium and nickel as mentioned before. The material was subjected to vacuum casting after melting in a basic electric furnace and VCD. Thereafter, it was subjected to forging followed by annealing; then it was subjected to differential heat treatment of Model C shown in Fig. 4. The conditions for the heat treatment were set up by holding the austenitizing temperature at 1253 K (980°C) in the HP zone and at 1218 K (945°C) in the LP zone for 86.4 ks (24 h) and subsequently cooling these zones through fan cooling and water spray cooling, respectively. Thereafter, it was subjected to tempering at 933 K (660°C) for 252 ks (70 h).

After completion of a nondestructive inspection, a tension test, an impact test, and a creep rupture test were carried out together with microstructure observation on each location of the model rotor. The temper embrittlement sensitivity also was tested.

Test Results and Consideration

Figure 6 shows the measured results of the austenitizing temperature and the cooling rate for each part of the model rotor. It was clarified as expected through FEM analysis that a difference in the austenitizing temperature is distinctly observable on both sides of a slit. In addition, it was confirmed that the cooling rate also can be clearly differentiated.

A visual inspection, magnetic particle test, and ultrasonic test (2.25 MHz) on the inner surface of a rotor center bore and a high sensitivity ultrasonic test (2.25 MHz) from the outer periphery of the rotor were carried out. As a result, there were no segregation and defects, confirming satisfactory quality of the rotor.

Figure 7 summarizes the mechanical properties obtained. The tensile properties of HP and LP zones are nearly equal. Furthermore, the 50% FATT shows 318 K (45°C) even in the center core of a rotor in the LP zone that is far lower than the value 353 to 393 K (80 to 120°C) [2,3] of conventional Cr-Mo-V rotor forgings. Since this value is lower than the steam temperature 323 to 333 K (50 to 60°C) at the LP last stage in a steam turbine, safety margin against brittle fracture seems to be well provided [4]. The creep rupture strength in the HP zone is in the scattered band for conventional Cr-Mo-V steel. The temper embrittlement sensitivity was evaluated by means of a step cool method, suggesting none of this problem. The microstructures of each part of the rotor were tempered bainite, and the prior-austenite grain size numbers were 5.0 and 6.0, respectively, in the center core of the HP and LP zones.

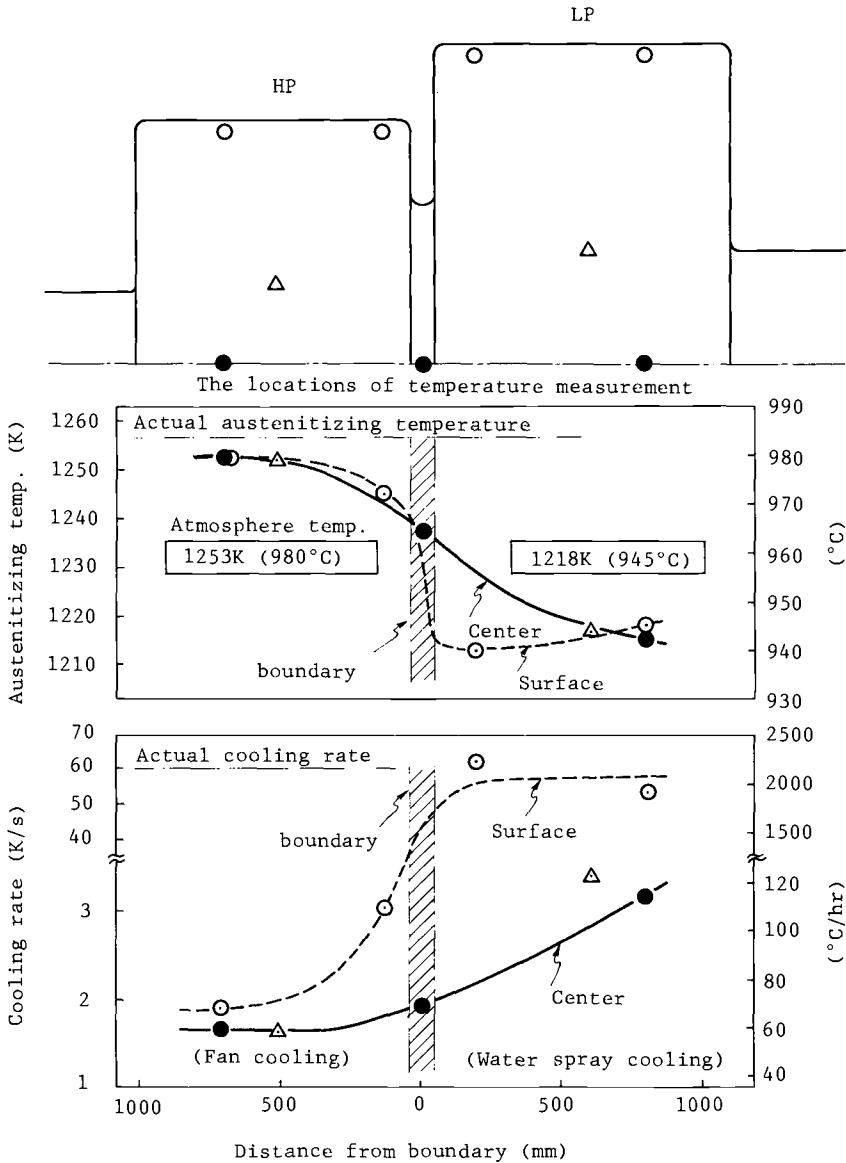


FIG. 6—The austenitizing temperature and cooling rate measured at the several locations.

By the aid of the just-mentioned verification by sample forging, it has been practicable to produce an integral HP-LP combination rotor forging which is capable of satisfying both creep rupture strength in the HP zone and toughness in the LP zone simultaneously and free from any qualitative problem.

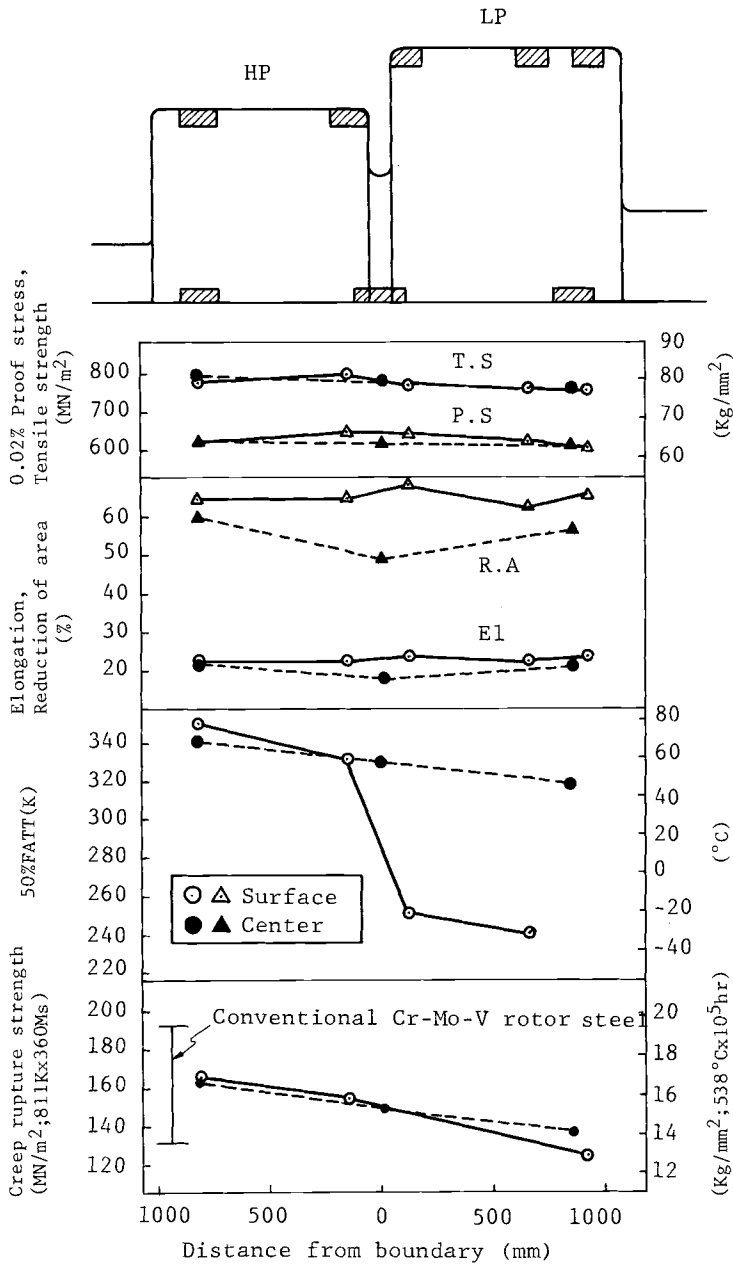


FIG. 7—Mechanical properties at various locations after quality heat treatment.

TABLE 2—Applications of integral HP-LP combination rotor forgings developed in Toshiba.

Plant	Rating, MW	Steam Temperature, K(°C)	Rotor Weight, kg	Maximum Diameter, mm	Heat Treatment	Start of Operation, Year/Month
Model A	50×10^3	1650	differentially	...
Model B	64×10^3	1650	differentially	...
A	75	811/811 (538/538)	40×10^3	1350	differentially	1980/2
B	75	811/811 (538/538)	40×10^3	1350	differentially	1980/2
C	100	783 (510)	45×10^3	1650	uniformly	1981/3
D	100	783 (510)	45×10^3	1650	uniformly	1981/11
E	47.5	811 (538)	22×10^3	1100	differentially	1983/6
F	33	755 (482)	30×10^3	1150	uniformly	1985/5

Applications of Integral HP-LP Combination Rotor Forgings

Applications of the developed integral HP-LP combination rotor forgings are shown in Table 2. Figure 8 shows the 50% FATT in the center core of rotors plotted with respect to the rotor diameter. Although the 50% FATT tends to increase to a certain extent as the rotor diameter increases, 50% FATT in the center core of rotors is below 323 K (50°C), thus satisfying the target value in

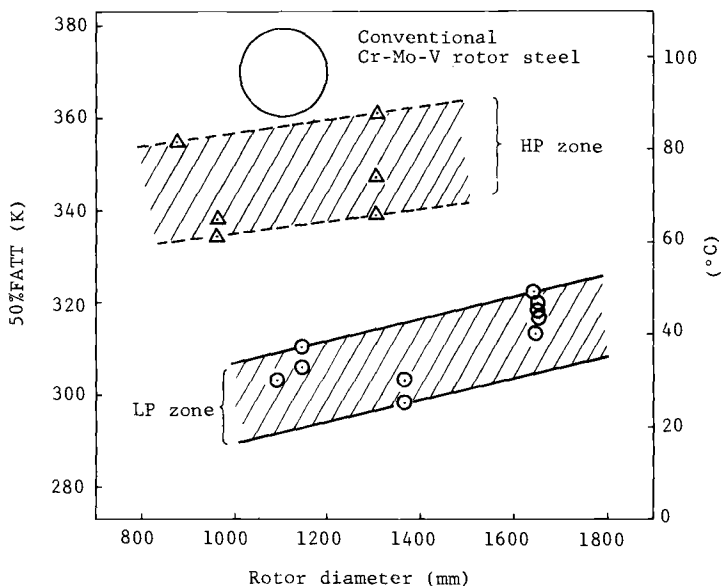


FIG. 8—The relationship of 50% FATT (center core) and rotor diameter.

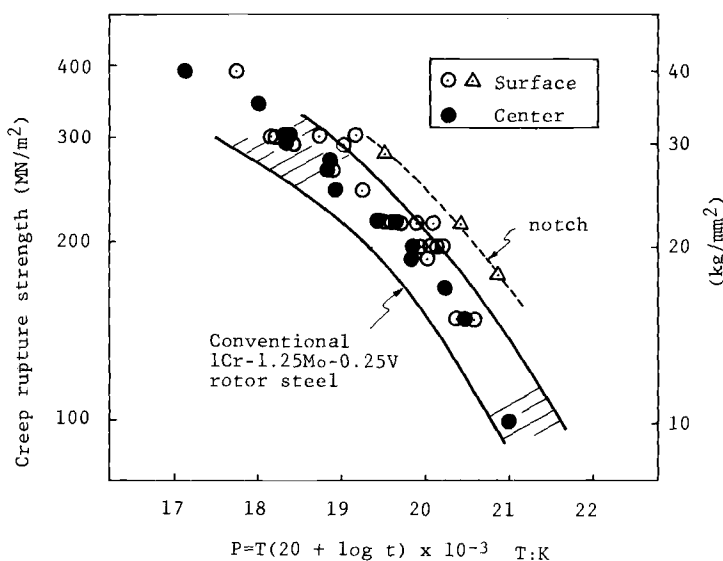


FIG. 9—Creep rupture strength of the HP zone of HLP rotors.

every rotor applied for several units. The results of creep rupture tests of rotors applied for several units (model rotor included) are shown in Fig. 9. The creep rupture strength in the HP zone is equivalent to or even better than that of conventional Cr-Mo-V steel forgings.

Conclusion

Integral HP-LP combination rotor forgings were developed which were satisfactory with regard to both creep rupture strength and toughness simultaneously. The important results obtained during the course of the development are as follows:

1. Addition of niobium and nickel, combined with differential heat treatment, is considered effective as a method for simultaneously satisfying both creep rupture strength and toughness.
2. Based upon the preliminary studies, an integral HP-LP combination model rotor was forged. As a result, it has clearly proved to be possible to manufacture this kind of rotor.
3. Rotors applied for several units satisfied the target characteristics and have been operated favorably.

It is suggested that this developed rotor can be adequately applied for the rotor of a HP-LP single-cylinder turbine such as medium/small rating fossil steam turbines and steam turbines of combined cycle power generation, etc.

References

- [1] Fukui, S., Yamada, S., and Tada, K., *Denki-Seiko (Electric Furnace Steel)*, Vol. 52, 1981, p. 99.
- [2] Curran, R. M., "Progress in the Development of Large Rotor Forging," *Convegno Internazionale Della Fucimatura*, May 1970, Terni, Italy.
- [3] Nakano, T., Yamamoto, S., Goto, T., and Suzuki, S., *Journal of the Iron and Steel Institute of Japan*, Vol. 49, 1963, p. 908.
- [4] Yukawa, S., ASME Annual Meeting, Los Angeles, CA, Vol. 17, 1969, p. 1, American Society of Mechanical Engineers, New York.

DISCUSSION

*K. H. Mayer*¹ (*written discussion*)—(1) Are all rotors performed with an axial bore (center bore)? (2) How is the time dependability of creep ductility? (3) Did you perform exposure tests to investigate the long-time toughness behavior?

M. Yamada, M. Miyazaki, O. Watanabe, and M. Kawai (*authors' closure*)—(1) All integral HP-LP rotor forgings have been performed with an axial bore (center bore) up to the present except one rotor. (2) Creep ductility is almost the same in the range of rupture time obtained in this investigation. (3) The long-time exposure test is being performed at present.

*V. P. Swaminathan*² (*written discussion*)—(1) For the laboratory specimen testing, austenitizing temperatures of 970 and 1020°C were reported. However, for the model forging, the temperatures were 945 and 980°C. What is the rationale for the selection of these lower austenitizing temperatures for the actual rotor forging? Was there any problem in obtaining good creep properties with high temperature austenitization? (2) What are the differences in grain sizes for these various austenitizing treatments? (3) Did the author conduct any long-term creep (10 000 h and above) tests? How does the creep ductility vary with rupture life? (4) Are there any specific reasons why the VCD process was used?

M. Yamada, M. Miyazaki, O. Watanabe, and M. Kawai (*authors' closure*)—(1) The austenitizing temperature for the sample forging was decided from 970°C, 1020°C laboratory test data and other internal test data, considering the balance of creep rupture strength, ductility, and toughness. (2) The differences in grain sizes are as follows:

Austenitizing Temperature	Grain Size (ASTM No.)
980°C	5.2
945°C	6.8

¹ MAN, Nuernberg, Dept. QF, West Germany.

² Westinghouse Electric Corp., Orlando, FLA 32817.

(3) We conducted long-term creep tests over 10 000 h. Creep ductility is almost the same in the range of rupture life obtained in this investigation. (4) The VCD process is effective in the reduction of the impurities and segregation and in the improvement of the toughness.

*R. M. Curran*³ (written discussion)—A Larson-Miller parameter extrapolation with a constant of 20 is used to predict high-temperature properties. Since this alloy is significantly different from 1Cr-1Mo-1/4V, this extrapolation may not be correct. Have long-time rupture tests been conducted to verify this extrapolation method?

M. Yamada, M. Miyazaki, O. Watanabe, and M. Kawai (authors' closure)—We conducted long-time rupture tests over 10 000 h, and we confirmed the validity of usage of this extrapolation method.

*N. S. Cheruvu*⁴ (written discussion)—This paper is very interesting. Mr. Yamada presented the effect of austenitizing temperature, cooling rates, and alloy modifications (addition of 0.04% niobium and 1.0% nickel) on the toughness of Cr-Mo-V steel.

It has been reported that the niobium addition to Cr-Mo-V and the high temperature austenitization treatment followed by forced air cooling improve the creep strength of the HP end of the rotor. High-temperature austenitization treatment is beneficial for creep strength because this treatment facilitates more alloying elements (carbide formers) to go into solution, which results in more carbide precipitation upon subsequent tempering. On the other hand, low-temperature austenitizing treatment followed by water spraying was used to improve the toughness of the LP end of the rotor.

However, the austenitizing temperature was varied from 940 to 980°C (from the LP to the HP end of the rotor) in the production rotors. It is necessary to austenitize low-alloy steels as high as 1100°C for complete dissolution of alloy carbides. Stone and Murray⁵ have observed undissolved carbides in standard Cr-Mo-V steel after 1050°C austenitizing treatment. Furthermore, niobium carbides or nitrides are more difficult to dissolve than chromium or molybdenum or vanadium carbides⁶. Therefore, the possibility exists for a significant amount of niobium to remain as undissolved niobium carbide in the production rotors. In this particular case, the addition of a small amount of niobium may not improve any creep strength. In other words, similar creep properties probably can be obtained without addition of niobium to Cr-Mo-V steel. It would have been nice if the author had compared creep properties of Cr-Mo-V steel (with and without the niobium addition) austenitized at 980°C. Furthermore, the effect of the austenitizing temperature on creep ductility was not addressed in the presentation.

³ General Electric Co., Schenectady, NY 12345.

⁴ Westinghouse Electric Corp., Orlando, FLA 32817.

⁵ *JISI*, 1965, p. 1096.

⁶ Honeycombe, R. W. K., "Structure and Strength of Alloy Steels," Climax Molybdenum publication.

The variation in austenitizing temperature between the LP and the HP of the rotor was 30°C. Is this small variation in austenitizing temperature necessary to achieve the properties reported?

M. Yamada, M. Miyazaki, O. Watanabe, and M. Kawai (authors' closure)—As we don't have the data of creep properties of Cr-Mo-V steel without the niobium addition austenitized at 980°C, we can't compare the data of the creep properties. But, as shown in Fig. 3, at the austenitizing temperature of 970°C, Cr-Mo-V steel with the niobium addition is superior to that without the niobium addition in the creep rupture strength.

From the test results, it is considered that the effect of the austenitizing temperature on creep ductility was not found in the range of the austenitizing temperature investigated.

Test results show that the small variation of 30 to 40°C in austenitizing temperature scarcely affects the tensile properties but affects the creep rupture strength and the toughness greatly.

Akira Suzuki,¹ Shushi Kinoshita,² and Hideo Kikuchi³

Manufacture of Differentially Heat-Treated Turbine Rotor Forgings

REFERENCE: Suzuki, A., Kinoshita, S., Kikuchi, H., “**Manufacture of Differentially Heat-Treated Turbine Rotor Forgings**,” *Steel Forgings*, ASTM STP 903, E. G. Nisbett and A. S. Melilli, Eds., American Society for Testing and Materials, Philadelphia, 1986, pp. 74–86.

ABSTRACT: Using modified Cr-Mo-V steel with small additions of nickel and niobium and reduced silicon, four integral high pressure (HP) and low pressure (LP) combination turbine rotor forgings with 1240-mm maximum barrel diameter were manufactured. To obtain improved toughness in the LP portion and sufficient creep strength in the HP portion, the rotor forgings were differentially heat-treated; HP portions were austenitized at high temperatures and LP portions at low temperatures, followed by forced air cooling in the HP portions and by water spray quenching in the LP portions. Evaluation of the manufactured rotor forgings revealed that the toughness and the creep strength were sufficient in the LP and HP portions, respectively, the residual stress was sufficiently low, and the heat indication testing results were satisfactory in spite of the differential heat treatment.

KEY WORDS: modified Cr-Mo-V steel, HP-LP combination turbine rotor forging, differential heat treatment, mechanical properties, toughness, creep strength

Single-cylinder steam turbines in which high-pressure (HP) and low-pressure (LP) turbines are integrated are being used increasingly in compact power generating units and require integral HP-LP combination rotor shafts. Single-cylinder steam turbines have been used so far for small power-generating systems under 100 MW, and combination rotor forgings were made of the conventional HP rotor of Cr-Mo-V steel, the toughness of which was improved in the LP portion at a slight expense of creep strength in the HP portion by applying a lower austenitizing temperature or higher cooling rate or both for its hardening. There is a trend for single-cylinder steam turbine systems to be used in as large a plant as around 150 MW, which requires a larger combination rotor forging, and thus

¹ Advisor to managing director, Kobe Steel, Ltd., Hyogo-ken, Japan 676.

² General manager, Technical Department, Steel Casting and Forging Division, Kobe Steel, Ltd., Hyogo-ken, Japan 676.

³ Manager, Forging Engineering Section, Steel Casting and Forging Division, Kobe Steel, Ltd., Hyogo-ken, Japan 676.

new technological development will be necessary for the manufacture of the combination rotor forging.

The present paper describes the study of heat treatment techniques on the manufacture of commercial integral HP-LP combination rotor forgings using modified Cr-Mo-V steel, to which this newly developed heat treatment technique has been applied.

Material

The metallurgical and mechanical characteristics required for a combination rotor forging are summarized in Table 1. To achieve them, modified Cr-Mo-V steel, which improves the toughness of conventional Cr-Mo-V HP rotor steel without sacrificing creep strength, was used. Table 2 indicates its chemical composition [1] in comparison with that of conventional Cr-Mo-V steel.

As can be seen, it is characterized by the additions of niobium and nickel and by the reduction of silicon, compared with conventional steel. Niobium is added to improve the toughness [2] of the steel through its grain-refining effect and also because it is considered to minimize decreasing creep strength resulting from the addition of nickel; 1% nickel is added to improve the toughness of the steel [1] and also to increase the hardenability of the steel, enabling the steel to be used for a larger rotor forging.

A reduced silicon content of under 0.10% favors reducing temper embrittlement susceptibility and allows the vacuum carbon deoxidation process to be applied at the steel ingot-making stage, which will have the advantage of increasing the cleanliness of the steel.

The reduction of the silicon content also will improve the toughness and the hardenability of the steel [3]. A slightly reduced carbon content will be favorable for toughness. Thus, modified Cr-Mo-V steel HP-LP combination rotor forgings will enable a combination rotor shaft to be manufactured with improved toughness in the LP portion, while the creep strength for the HP portion remains unvaried.

Preliminary Study

A preliminary study was carried out on the toughness and creep strength of the modified Cr-Mo-V steel.⁴

Figure 1 indicates variations of fracture appearance transition temperatures (FATT) as a function of austenitizing temperatures for hardening. The cooling rate of specimens during hardening is around 90°C/h (corresponding to the temperature at the center of a 1600-mm-diameter rotor forging when it is water spray-quenched). Tempering at 670°C followed the hardening to give approximately 815 MN/m² in tensile strength. The effect of normalizing temperature preceding hardening is indicated also. It can be seen that FATT decreases with a decreasing austenitizing temperature, and that a high austenitizing temperature

⁴ Study in cooperation with Toshiba Corp., Japan.

TABLE 1—Characteristic requirements for HP-LP combination rotor forgings.

	Required Properties	Microstructure		Heat Treatment Condition	
		Grain Size	Microstructure	Austenitizing Temperature	Cooling Rate
High-pressure portion	creep rupture strength	medium-grain size	bainitic	high	intermediate
Low-pressure portion	toughness	fine-grain size	bainitic	low	fast

TABLE 2—Comparison of chemical compositions between modified Cr-Mo-V and conventional Cr-Mo-V steels.

Steel	C	Si	Mn	P	S	Ni	Cr	Mo	V	Nb	Remarks
Modified Cr-Mo-V ^a	0.23/0.31	max 0.10	0.50/1.00	max 0.012	max 0.015	0.80/1.10	0.90/1.50	1.10/1.50	0.20/0.30	0.01/0.05	Ni and Nb added
Conventional Cr-Mo-V rotor	0.25/0.35	max 0.75	max 1.00	max 0.015	max 0.018	max 0.75	0.90/1.50	1.00/1.50	0.20/0.30	...	ASTM A 470 Class 8

^a Japanese patent of Toshiba Corp.

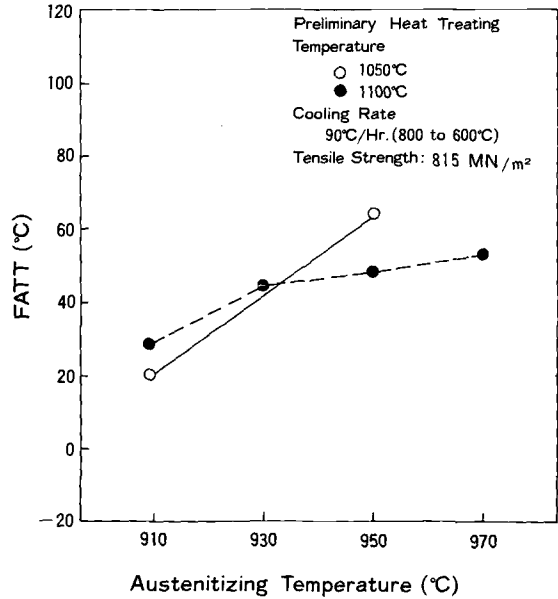


FIG. 1—The relation between FATT, preliminary heating temperature, and austenitizing temperature.

of 1100°C preceding normalizing temperature results in decreased FATT, whereas there is little effect of normalizing temperature on FATT. It is evident in Figure 1 that lower austenitizing temperatures for hardening are favorable for decreasing FATT.

Creep rupture strength with varied normalizing temperature preceding hardening was studied. Specimens were austenitized at 950°C and cooled at a rate of around 150°C/h (corresponding to the temperature of the surface of a 1300-

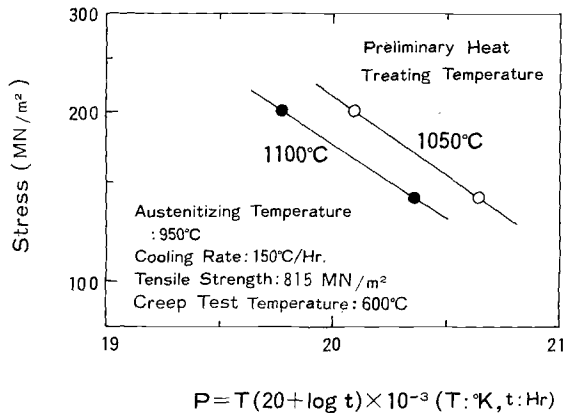


FIG. 2—The relation between rupture strength and preliminary heat treatment.

mm-diameter rotor forging when it is forced air-cooled). They were tempered at 670°C following hardening to obtain approximately 815 MN/m² in tensile strength. It can be seen in Figure 2 that the rupture strength is markedly affected by normalizing temperature.

Heat Treatment

In general, heat treatment favorable for toughness results in decreasing creep strength and vice versa. Increasing the austenitizing temperature in the hardening process will give rise to grain coarsening and increasing creep strength. However, it will result in reducing the toughness. To manufacture a rotor forging that has good toughness in the LP portion and good creep strength in the HP portion, it will be favorable if austenitizing temperatures can be varied from the HP to the LP portions, as can be seen in Figs. 1 and 2.

The cooling rate on quenching in the hardening process is known to affect toughness and the creep strength of steel. Increasing the cooling rate from the austenitizing temperature results in increasing toughness, whereas a medium cooling rate favors creep strength. Thus, an attempt was made to austenitize the LP portion of the combination at a low temperature followed by water spray quenching and the HP portion at a high temperature followed by forced air cooling to manufacture a combination rotor forging. Temperature measurements were made at several locations on a test rotor forging with a barrel diameter of 1660 mm in the LP portion and 1310 mm in the HP portion, and the thermal distribution in it was examined.⁴

To apply different heat treatments to the LP and HP portions, a thermal insulation plate of ceramic fiber, sandwiched between steel plates, was placed at the boundary of the LP and HP portions. The LP portion of the rotor forging with the thermal insulation plate then was austenitized at different temperatures from the HP portion in a cylindrical vertical furnace and cooled at different rates. This heat treatment is referred to as differential heat treatment. The calculated thermal distribution then was compared with the actual measured result to deduce the insulating ability of the insulation plate, which made it possible to calculate and establish the thermal distribution in manufacturing combination rotor forgings.

Manufacture of Commercial HP-LP Combination Rotor Forgings

Four commercial HP-LP combination rotor forgings were manufactured using modified Cr-Mo-V steel and this differential heat-treatment technique. Their chemical composition is given in Table 3. Four rotor forgings of similar dimensions were manufactured under the same specifications. A 50-ton ingot was made for each rotor forging by the vacuum carbon deoxidizing process. After heating at 1200 to 1240°C, the ingots were forged into rotor forgings of 1280-mm barrel diameter. After normalizing at 1050°C, the forgings were differentially heat-treated. An insulating plate of ceramic fiber sandwiched between steel plates was

TABLE 3—Chemical composition of commercial HP-LP combination rotor forgings, weight %.

Forging No.	C	Si	Mn	P	S	Ni	Cr	Mo	V	Nb
1	0.27	0.07	0.72	0.005	0.004	0.91	1.25	1.24	0.22	0.035
2	0.24	0.08	0.71	0.005	0.004	0.90	1.23	1.26	0.24	0.030
3	0.25	0.07	0.70	0.007	0.004	0.91	1.26	1.22	0.25	0.030
4	0.24	0.07	0.73	0.006	0.005	0.90	1.26	1.20	0.25	0.028

placed at the boundary of the LP and HP portions. The HP portion was austenitized at 970°C and the LP portion at 920°C. Calculated thermal distribution curves in the forgings are given in Fig. 3. The schematic shape and dimensions are shown also. It is noted that the transition zone is presumed to extend approximately 500 mm from the insulation plate in the axial direction on the rotor surface and approximately 1000 mm in the center, defining the transition zone to be 5°C different from the defined zone temperatures. Differentially austenitized rotor forgings were differentially cooled by water spraying in the LP portion and by forced air cooling in the HP portion down to a sufficiently low temperature. Tempering was performed at the uniform temperature of 670°C.

Evaluation of Manufactured Rotor Forgings

Typical examples of the microstructure and grain structure on the peripheries of the HP and LP portions and in the center core of the LP portion are shown

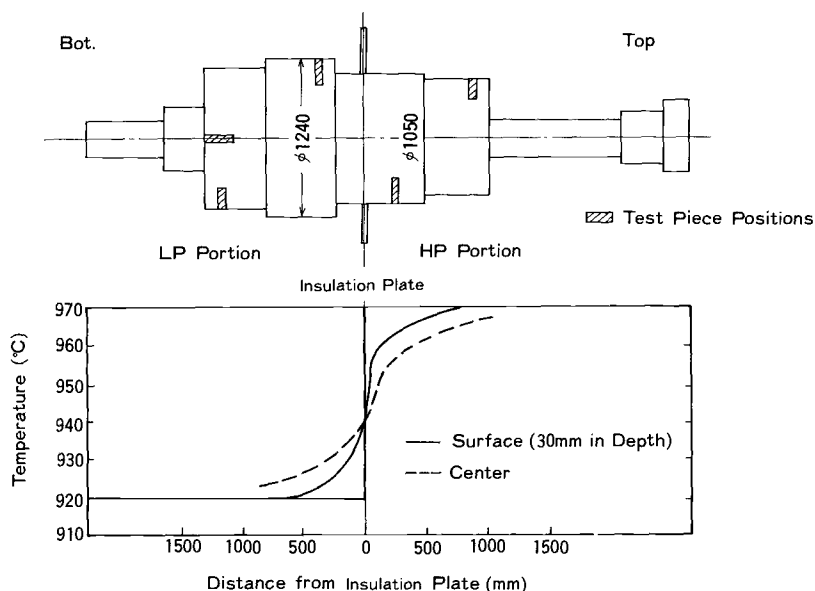


FIG. 3—The calculated thermal distribution around the insulation plate on heating for quenching.

in Fig. 4. It is evident that the microstructure in each portion is bainitic and that the grain size is 7.5 in the LP portion and 5.0 in the HP portion on the peripheries and 6.5 in the LP portion in the center core (in ASTM grain size number). Cylindrical specimen blocks with double the length of a specimen were taken out of several portions of the periphery of the rotor forgings in a radial direction. The only specimens from the center core of the rotor forging were obtained from the No. 1 rotor forging because it was the only rotor forging partially center-bored. Figures 5 and 6 summarize the results of tension and impact tests on the four rotor forgings in comparison with those on the test rotor⁴ manufactured in modified Cr-Mo-V steel and using the differential heat treatment just described. In Figure 5, "outer" means specimens taken from the surface side of the peripheral specimens, and "inner" means specimens taken from the inner side. Results obtained from the four rotors are consistent with those from the test rotor. Note that in the periphery are marked variations in impact properties across the HP-LP boundary where the heat treatment was differentiated, whereas a little

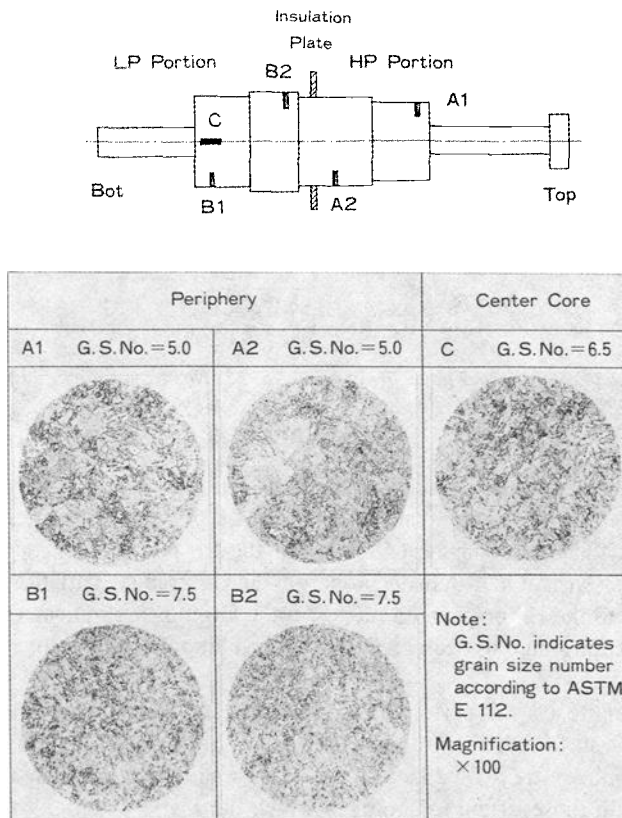


FIG. 4—The microstructure and austenite grain size of No. 1 rotor forging.

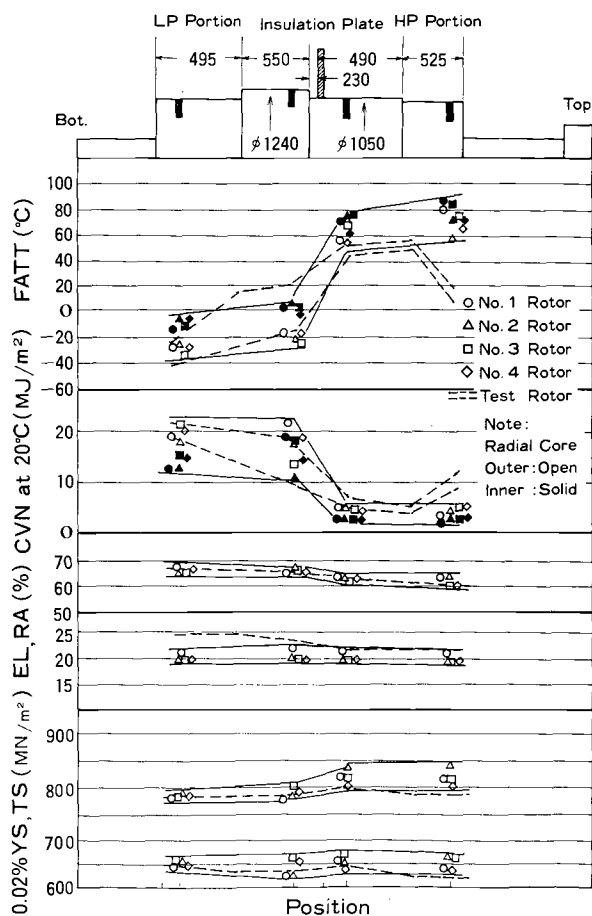


FIG. 5—Mechanical properties in the periphery of No. 1 to No. 4 rotor forgings compared with those of the test rotor.

variation in tensile properties such as strengths and ductilities is observed across the boundary. It is interesting that FATTs in the LP portions are sufficiently low; in particular, the FATTs in the LP center of the LP portion are approximately 25°C. A little variation in tensile properties and a gradual variation in FATT from the HP to the LP portions in the test rotor forgings are indicated in Fig. 6, which can be attributed to decreased thermal insulation in the center of the rotor forging.

A creep rupture test was performed on combined smooth and notched specimens taken from the surface of HP portions. The tests were conducted at 566°C (1050°F) under the applied stress of 295 MN/m². The results are given in Fig. 7 and compared with those of the test rotor in which the scatter band of conventional

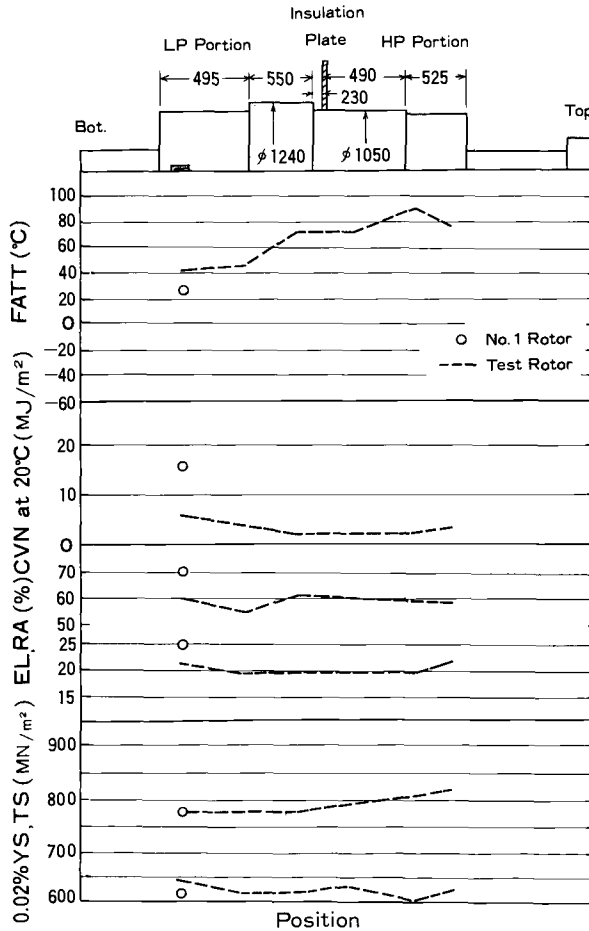


FIG. 6—Mechanical properties at the center of No. 1 rotor forging compared with those of the test rotor.

Cr-Mo-V HP rotor steel [4] is indicated also. The creep rupture strength of the HP portions is comparable to or slightly better than that of conventional Cr-Mo-V steel. No notch sensitivity was observed on the material examined.

Thermal stability, one of the important requirements for an HP rotor forging—in particular for the present differentially heat-treated combination rotor forging—was examined at 620°C in the heat indication tests of the rotor forgings, and the maximum deflection of the center axis was found to be 0.015 mm in the No. 2 rotor forging.

Residual stresses are also of primary interest and were measured on the surface of the rotor forging along the axial direction. Residual stress measurements were

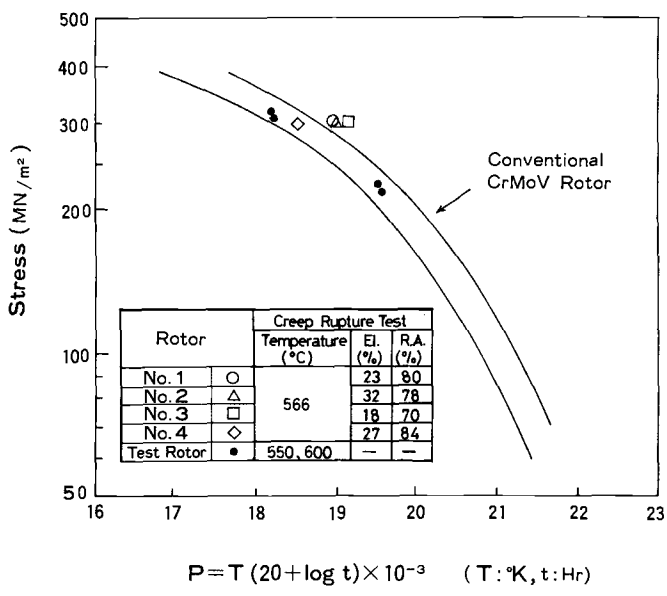
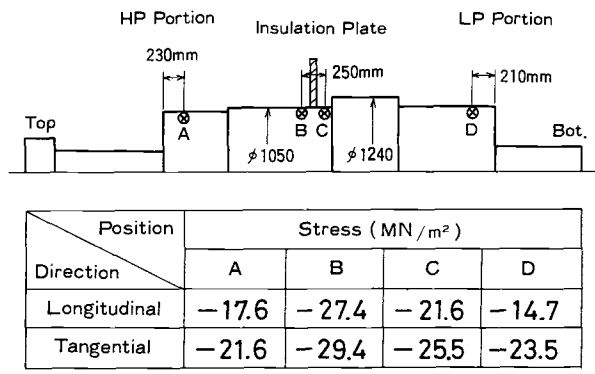


FIG. 7—Creep rupture strength of HP-LP combination rotor forgings.

made on the No. 1 rotor forging after differential heat treatment applying the Gunnert method with strain gage. The results obtained are indicated in Fig. 8. The maximum stress is 29.4 MN/m² in compression in the tangential direction, which is well below 60 MN/m² of the conventional allowable residual stress in a rotor forging.



Gunnert method with strain gauge

FIG. 8—Residual stress measurements of the No. 1 HP-LP combination rotor forging.

Conclusions

Four HP-LP combination rotor forgings were manufactured with the application of differential heat treatment to modified Cr-Mo-V steel and evaluated on their qualities:

1. Differential heat treatment was successfully applied to four commercial HP-LP combination rotor forgings and excellent toughness in the LP portions was obtained.
2. Creep rupture strength was comparable to or slightly higher in the rotor forgings manufactured than in the conventional Cr-Mo-V steel.
3. The width of the thermal transition zone was estimated to be approximately 500 mm on the rotor forging surface and 1000 mm at the center.
4. Maximum thermal deflection in the heat indication test was 0.015 mm at 620°C, which was satisfactorily low.
5. Maximum residual stress was 29.4 MN/m² in compression in the tangential direction, which is satisfactory.

Acknowledgments

The authors would like to express their great appreciation to M. Akiba, M. Miyazaki, and O. Watanabe of Toshiba Corp. for their cooperation and encouragement given to the developing stage of the rotor forging.

References

- [1] Kawaguchi, K., Miyazaki, M., and Watanabe, O., *Tetsu-to-Hagane*, Vol. 70, 1984, p. 1414.
- [2] Akiba, M., Watanabe, O., and Suzue, S., EPRI workshop "Rotor Forgings for Turbines and Generators," Electric Power Research Institute, Palo Alto, CA, 14–17 Sept. 1980.
- [3] Aaronson, H. I., Domian, H. A., and Pound, G. M., *Transactions of the Metallurgical Society of AIME*, Vol. 236, 1966, p. 768.
- [4] Newhouse, D. L., Boyle, C. J., and Curran, R. M., ASTM 68th Annual Meeting, American Society for Testing and Materials, 1965, p. 3.

DISCUSSION

V. P. Swaminathan¹ (*written discussion*)—(1) Are there any specific reasons why vacuum carbon deoxidation was employed? (2) How does the creep ductility (elongation and reduction of area) vary with the life of test? (3) What are the grain sizes for the HP and LP portions of the forging? (4) What is the effect of niobium on creep strength and ductility or FATT?

¹ Westinghouse Electric Corp., Orlando, Florida 32817.

A. Suzuki, S. Kinoshita, and H. Kikuchi (authors' closure)—(1) Reasons why vacuum carbon deoxidation was employed are to reduce the susceptibility to the temper embrittlement and to improve hardenability. (2) Not studied. (3) Please see Fig. 4. (4) Niobium has little effect on creep strength and ductility but has an effect of improving FATT through the reduction of grain size.

W. Meyer² (written discussion)—What's the lower temperature in the preliminary heat treatment?

A. Suzuki, S. Kinoshita, and H. Kikuchi (authors' closure)—200°C.

² Research and Development, VEW, Kaptenberg, Austria.

Jean Pisseloup,¹ Isabelle S. Poitrault,² Antoine de Badereau,²
and Pierre G. Bocquet¹

Manufacturing of Welded Polyblock Turbine Rotors for Pressurized Water Reactor Nuclear Plants; Optimization of the Steel Grade; Effect of Impurities

REFERENCE: Pisseloup, J., Poitrault, I. S., de Badereau, A., and Bocquet, P. G., "Manufacturing of Welded Polyblock Turbine Rotors for Pressurized Water Reactor Nuclear Plants; Optimization of the Steel Grade; Effect of Impurities," *Steel Forgings, ASTM STP 903*, E. G. Nisbett and A. S. Melilli, Eds., American Society for Testing and Materials, Philadelphia, 1986, pp. 87-103.

ABSTRACT: Le Creusot Heavy Forge has been manufacturing low-pressure (LP) disks and shaft ends for 1300-MW nuclear power plants. These forgings, in weldable 1.8Cr-1Ni-0.8Mo steel, are welded by Alstom Atlantique.

With the aim of improved quality, homogeneity of mechanical properties, hardenability, and weldability, this metallurgical research has been carried out:

1. Optimization of the steel grade (the effect of silicon, manganese, and molybdenum).
2. The influence of tempering and stress relief treatment parameters.
3. The effect of impurities.

These studies have led the Steel Melting Shop of Creusot-Loire Factory to invest in a high-performance process of steelmaking: the heating ladle refining process. This new process has had spectacular results that have been confirmed by investigations on cut-up industrial forgings.

KEY WORDS: welded polyblock rotor, 1.8Cr-1Ni-0.8Mo steel, mechanical properties, temper embrittlement, manufacturing

Le Creusot Heavy Forge has been manufacturing turbine rotors in two ways:

1. Monoblock rotors.

¹ Creusot-Loire Industrie, 56 rue Clémenceau B.P. 56, Le Creusot, France.

² Le Creusot Heavy Forge, Creusot-Loire Industrie, Le Creusot, France.

2. Polyblock rotors made up of:

- (a) Disks shrunk on a jack shaft [1].
- (b) Disks and shaft ends welded together [1].

The technique by welding assembly has been chosen for 1300-MW plants of the French Nuclear Program for which the turbine rotors are made by Alsthom Atlantique.³ An important preliminary metallurgical research program has been conducted to develop a convenient steel grade (1.8Cr-1Ni-0.8Mo). A large number of disks and shaft ends have been then manufactured (more than 400 in the last 10 years) with a close supervision of the manufacturing. So, this has allowed Le Creusot Heavy Forge to gain important experience in this area.

This paper, which concerns only the metallurgical point of view of manufactured forgings, deals with:

1. The main results of metallurgical studies that have led to an analytical precision close to the optimum of the steel grade. The purpose of the studies was to satisfy a hardening quality (a proper homogeneity of forgings) that matches weldability.
2. The statistical analysis of 400 plus delivered disks and shaft ends.
3. The investigations by cutting industrial parts for verification.

Information on Manufactured Forgings

Disks and Shafts Ends Design

The sketch in Fig. 1 gives a general view of the eight disks and two shaft ends which are forged separately by Le Creusot Heavy Forge and which compose the rotor.

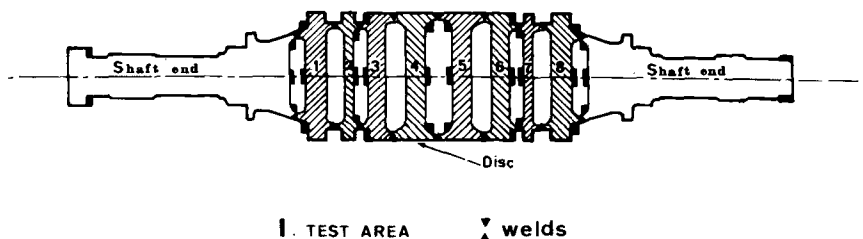


FIG. 1—Section through a welded polyblock turbine rotor.

³ Alsthom Atlantique, 55 Av. Jean Jaurés, 93 350 Le Bourget, France.

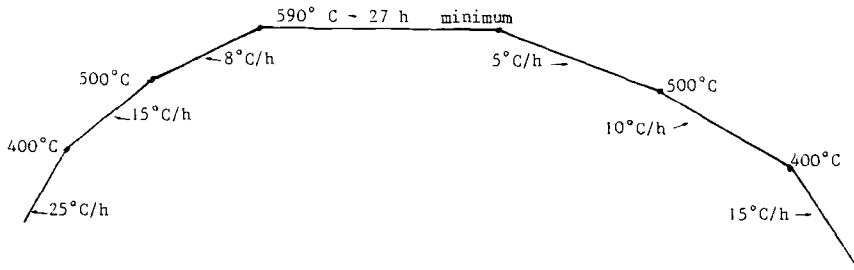


FIG. 2—Thermal cycle of postweld heat treatment.

Specification Requirements

The steel used (Cr-Ni-Mo) must lie in the following chemical range:

- %C = 0.18 to 0.25
- %Si = 0.10 to 0.40
- %Mn = 0.25 to 0.80
- %Cr = 1.20 to 2.00
- %Ni = 0.90 to 1.10
- %Mo = 0.50 to 0.80
- %S \leq 0.020
- %P \leq 0.020
- %V \leq 0.05

The thermal cycle of the postweld heat treatment (PWHT) is shown in Fig. 2.

Required mechanical properties after PWHT:

Yield strength (YS) (0.2%) at room temperature \geq 636 MPa.

Ultimate tensile strength (UTS) at room temperature = 735 to 882 MPa.

Charpy V-notch (CVN) at 0°C \geq 35 J/cm²—lowest result among the three specimens.

CVN at 0°C \geq 50 J/cm²—average of the three results.

Preliminary Research

To obtain the just-mentioned properties, it has been necessary to optimize steel composition and heat treatment in view:

1. To minimize the temper embrittlement effect (for impact properties after PWHT).
2. To have sufficient hardenability (for midthickness impact properties).

The research has been developed in different ways:

- 1. Study of the possibility to decrease the content of alloying elements (manganese, silicon, molybdenum) to increase impact properties.
- 2. Study of the effect of tempering and PWHT parameters on mechanical properties.
- 3. Study of the effect of impurities on impact properties.

Hardenability of 1.8Cr-1Ni-0.8Mo Steel Grade

Figure 3 shows the continuous cooling transformation (CCT) diagram for a steel grade lying in the higher parts of the chemical composition range. This type of steel obtains a homogeneous bainitic structure by water quenching all parts with a thickness up to 600 mm.

Decreasing the manganese and molybdenum contents (manganese and molybdenum are well-known for their deleterious effect on temper embrittlement) reduces noticeably the hardenability at the heart of thick forgings (Fig. 4). Such an arrangement of composition leads to a heterogeneous structure, therefore there is a more pronounced anisotropy of mechanical properties between the center and the surface of the parts.

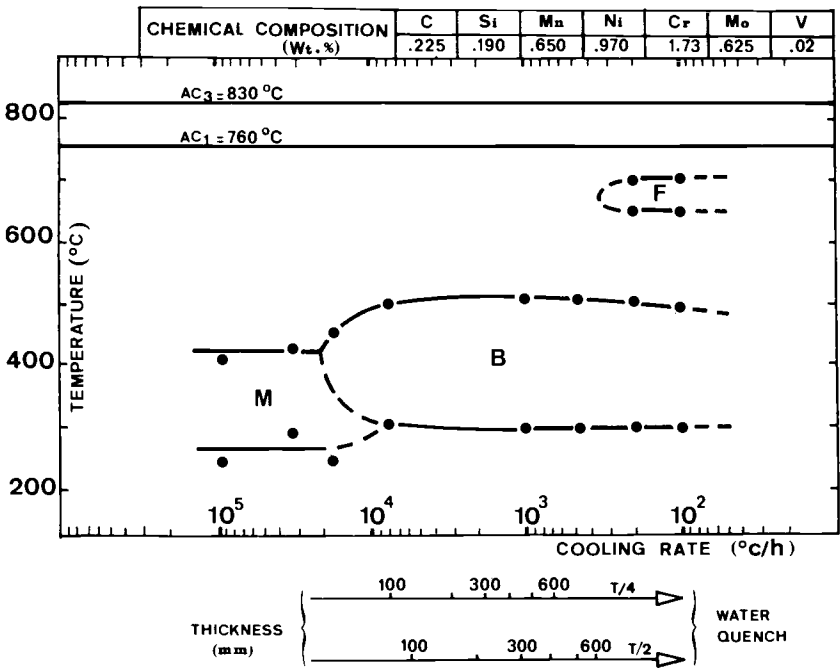


FIG. 3—Continuous cooling transformations diagram.

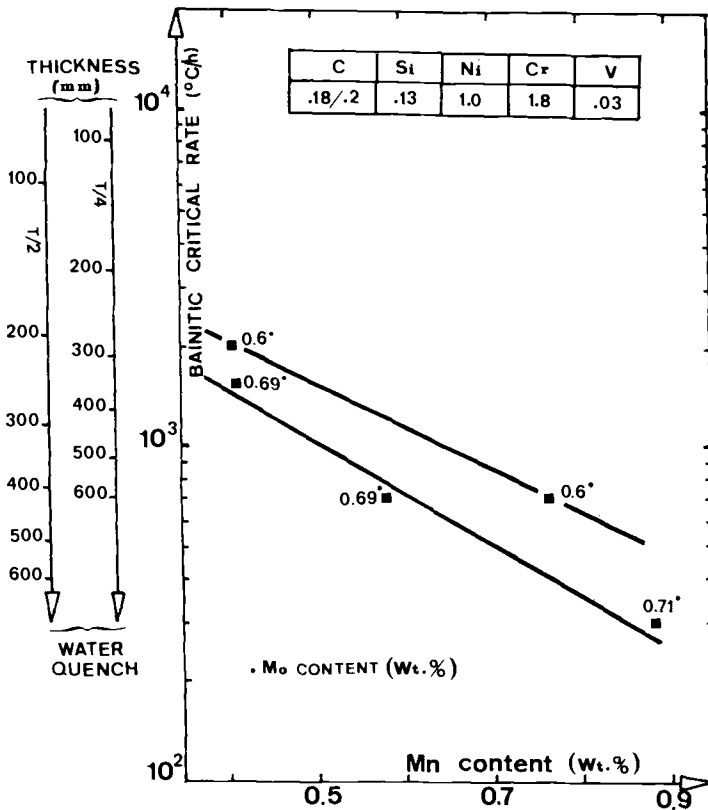


FIG. 4—Influence of manganese and molybdenum contents on the bainitic critical rate.

Effect of Tempering/PWHT Parameters on Mechanical Properties

With the aim of fixing the best heat treatment conditions of the steel, a study with simulated industrial conditions has been realized with:

1. Austenitization—875°C for 15 h.
2. Cooling rate (CR) 5000 and 850°C/h, respectively—cooling rate on the skin and midthickness of a 500-mm-thick disk.

Three heat treatment conditions are studied:

1. Quenched tempered (QT) condition.
2. Water-cooled tempering (WCT) condition to minimize the embrittlement.
3. PWHT condition.

Tension test results (room temperature YS 0.2% and UTS) and FATT obtained for each condition are given in parametrical [2] shape in Figs. 5 and 6.

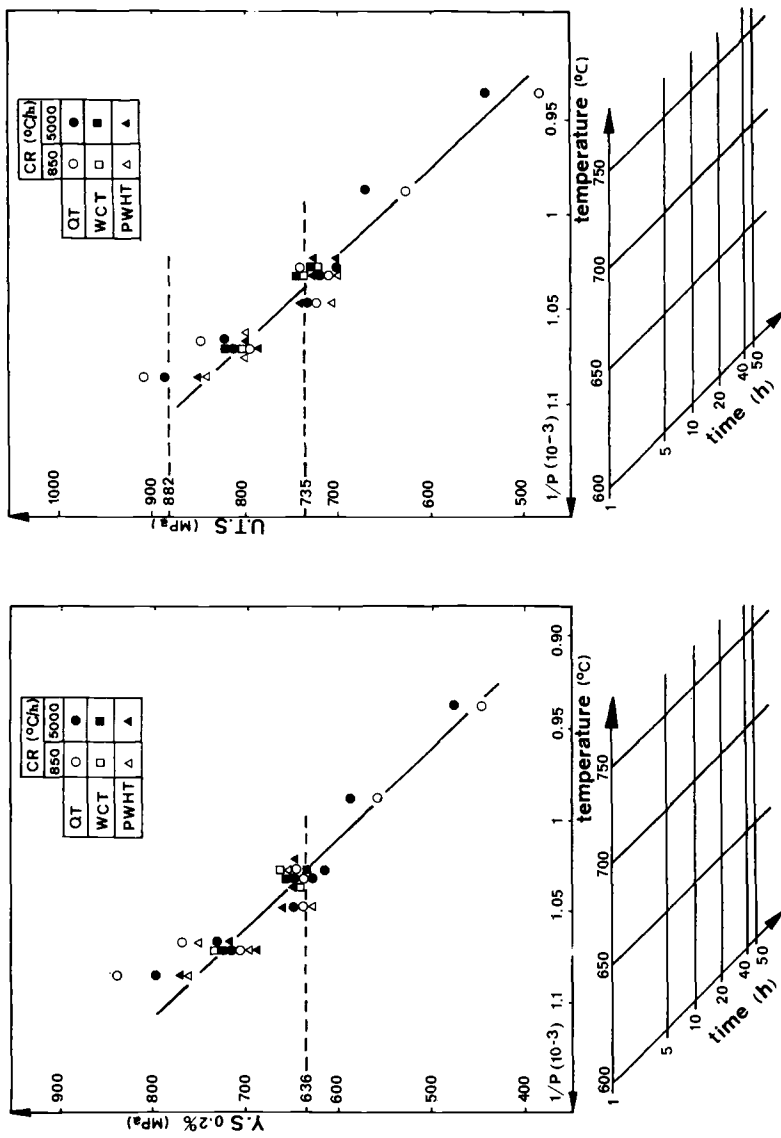


FIG. 5—Effects of tempering and PWHT on tensile properties.

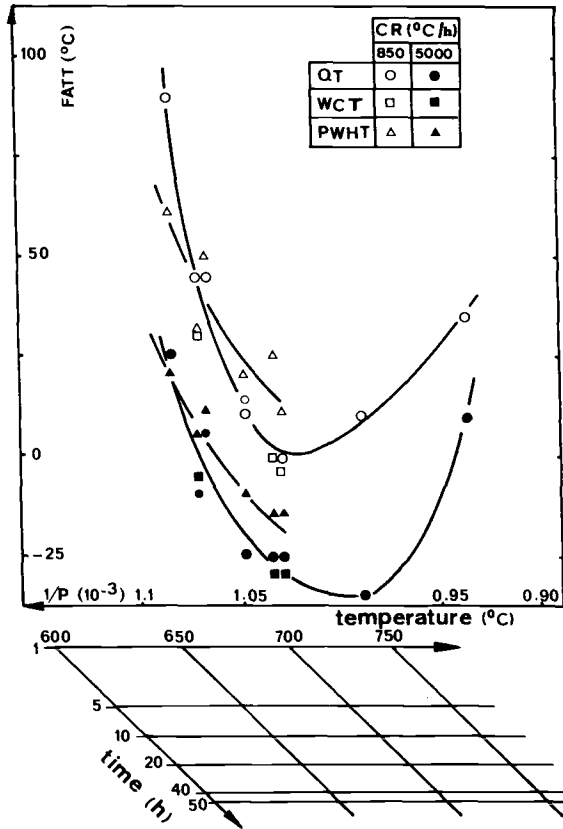


FIG. 6—Effects of tempering and PWHT on FATT.

With the same tempering parameter, each of the two cooling rates conduces to nearly identical tensile properties but to a higher FATT with the lower cooling rate (and this, for a bainitic structure in both conditions). This steel has very little susceptibility to reversible temper embrittlement; the FATT differences between QT and WCT conditions are very small. Only the PWHT condition exhibits a slight embrittlement at the highest temper temperatures. The irreversible embrittlement phenomenon becomes noticeable only for temperatures higher than 700°C.

Effect of Silicon on Tensile Properties

In the past, the decrease of silicon content by vacuum carbon deoxidization (VCD) has been proposed to reduce the temper embrittlement susceptibility. This, although interesting at the first sight, may result in insufficient tensile strength at room temperature. As shown in Fig. 7, lowering the silicon content decreases UTS about 50 MPa with the same tempering.

	C	S	P	Si	Mn	Ni	Cr	Mo	V	Cu	S _n	As
VCD	.215	.011	.010	.08	.625	.97	1.80	.71	.03	.04	.004	.015
Si.D	.200	.0031	.0058	.208	.67	.948	1.85	.709	.03	.05	.005	.008

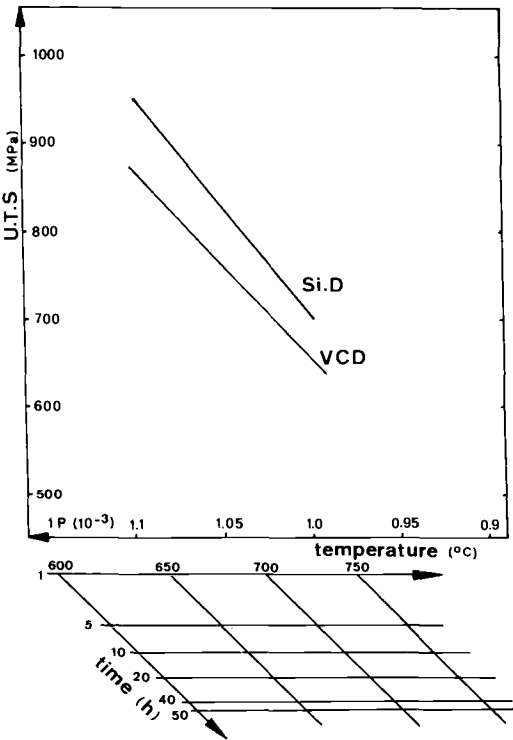


FIG. 7—Influence of silicon on ultimate tensile strength.

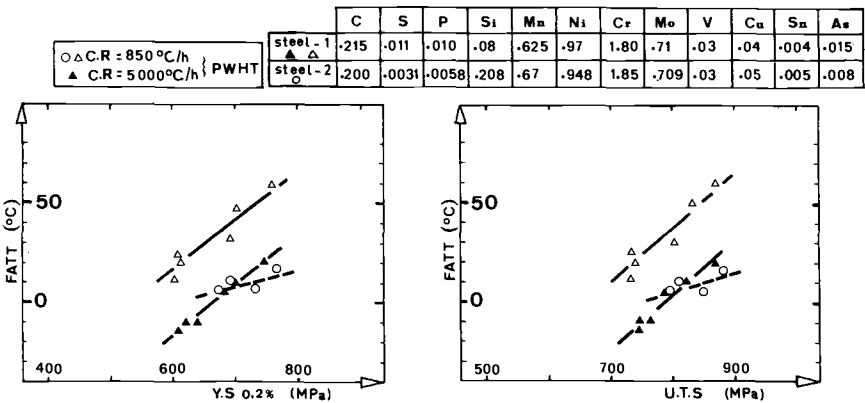


FIG. 8—Influence of impurities on FATT.

TABLE 1—*Influence of impurities on brittleness.*

	Steel 1	Steel 2
CR, °C/h	850	850
UTS, MPa	800	800
FATT, °C, QT	25	— 5
FATT, °C, PWHT	40	5
Δ FATT, PWHT—QT	15	10

Effect of Impurities on Impact Properties

It can be seen in Fig. 8 that a decrease of impurities such as phosphorus, sulfur, and arsenic leads to an important improvement of FATT for the same level of UTS or YS. The embrittlement due to PWHT is also reduced for the chosen UTS as shown in Table 1.

Comments on Preliminary Research

These studies have permitted:

1. On the one hand, fixing the best conditions of chemical composition and heat treatment for industrial forgings.
2. On the other hand, the great improvement due to low contents of impurities, this improvement very much more important than the one due to vacuum carbon deoxidization (low silicon).

Industrial Results

With the aim of improving quality, the industrial results have been collected and interpreted. The deleterious effect of a high level of trace elements (phosphorus, tin, and arsenic) on toughness has been clearly shown. These observations have led the Steel Melting Shop of Creusot-Loire Factory to invest in a high-performance process of steelmaking: the heating ladle refining process (HLRP). This new process allows the simultaneous obtaining of a low phosphorus content and a low sulfur content [3]. Hereafter, a statistical study of industrial forgings produced by the previous process and the new process is given.

Manufacturing

The main features of the fabrication of the forged parts are as follows.

1. Steelmaking

Two forgings are poured by ingot.

Two shaft ends—ingot weight 168.1 metric tons.

Disks 4 and 5—ingot weight 152.3 metric tons.

Disks 1 and 8—ingot weight 120.3 metric tons.

Disks 2 and 3—ingot weight 92.3 metric tons.

Disks 6 and 7—ingot weight 92.3 metric tons.

2. Forging

Forging is broken down into several operations, such as:

Cogging—cropping of top and bottom heads.

Upsetting between plates.

The forged contours are given in Fig. 9.

3. Rough machining for heat treatment

See contours and dimensions in Fig. 9.

4. Quality heat treatment.

Austenitization—water quenching by immersion—tempering.

5. Final machining

6. Expedition

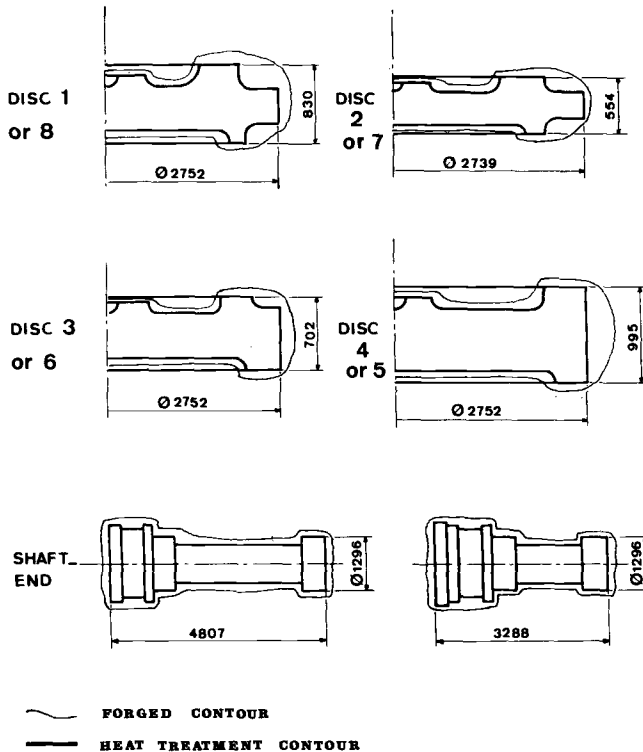


FIG. 9—Section through disks and shaft ends.

TABLE 2—Population under review; distribution of different forgings.

	Shaft ends		Disks							
			1	2	3	4	5	6	7	8
Previous process	17	18	21	17	19	22	20	22	20	20
New process, HLRP	20	20	22	22	20	20	23	22	18	19

Statistical Analysis

The population under review covers 196 forgings produced by the previous process and 206 forgings produced by HLRP (201 pourings or 50 190 metric tons of liquid steel). Table 2 shows that the population under review is quite homogeneous. The present statistics carried out with the aid of a computer include histograms, chronological evolution, determination of mean, minimal, maximal, and standard deviation values.

Chemical Analysis

Table 3 summarizes the statistical data of the elements of the ladle analysis. Figure 10 illustrates the chronological evolution of phosphorus and sulfur contents. It should be noted that HLRP:

1. Decreased considerably the trace elements, phosphorus and sulfur.
2. Obtained an analytical precision closer to the optimum of the steel grade (lowering of the standard deviation).

TABLE 3—Chemical analysis—statistical results.

Weight %	Previous Process, 196 Forgings				New Process, 206 Forgings			
	Mini	Average	Maxi	Standard Deviation	Mini	Average	Maxi	Standard Deviation
C	0.203	0.225	0.255	0.010	0.208	0.223	0.241	0.006
S	0.004	0.0100	0.0150	0.0028	0.0006	0.0035	0.0090	0.0019
P	0.006	0.0085	0.0150	0.0013	0.0025	0.0053	0.0100	0.0015
Si	0.060	0.183	0.350	0.059	0.165	0.196	0.242	0.014
Mn	0.580	0.677	0.760	0.029	0.615	0.691	0.830	0.030
Ni	0.950	1.001	1.150	0.030	0.945	0.994	1.147	0.024
Cr	1.500	1.855	2.000	0.070	1.724	1.807	1.900	0.035
Mo	0.585	0.697	0.775	0.024	0.650	0.686	0.795	0.021
V	0.019	0.032	0.045	0.004	0.023	0.028	0.034	0.002
Cu	0.047	0.068	0.125	0.015	0.029	0.058	0.091	0.011
As	0.006	0.012	0.037	0.005	0.005	0.010	0.018	0.002

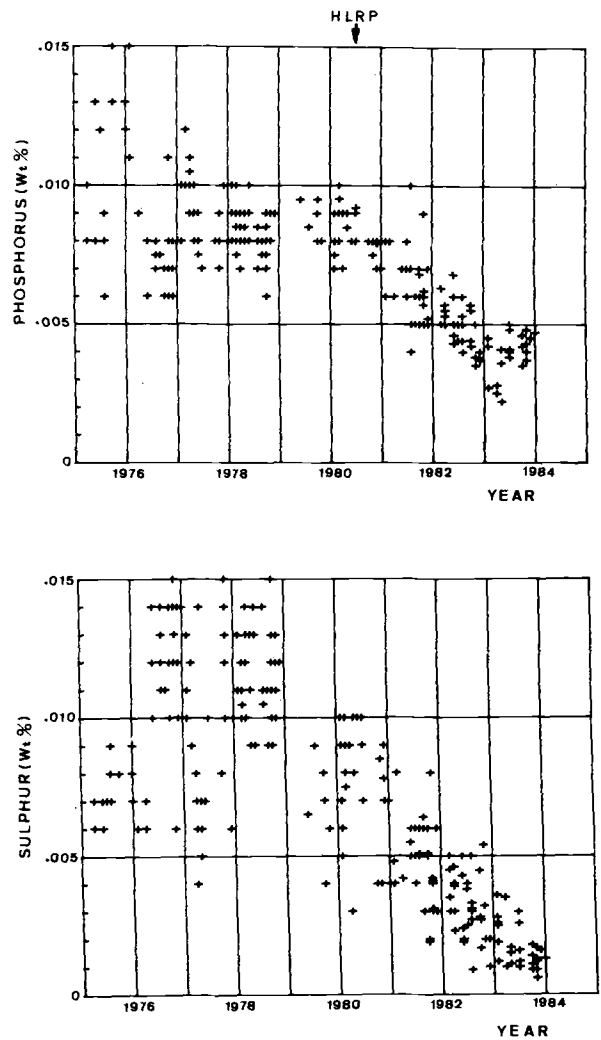


FIG. 10—Chronological evolution of sulfur and phosphorus contents.

Mechanical Properties

Table 4, a recapitulation of the mechanical values obtained, shows that for identical tensile properties, CVN and FATT values are decidedly improved. The minimal and mean values of CVN at 0°C have been multiplied by two, and the FATT has been decreased about 20°C. (See Fig. 11). The chronological evolution of those properties given in Fig. 12 is very significant.

TABLE 4—Mechanical properties after PWHT statistical results.

	Previous Process, 196 Forgings				New Process, 206 Forgings			
	Mini	Average	Maxi	Standard Deviation	Mini	Average	Maxi	Standard Deviation
Tensile test at 20°C, MPa, %								
Yield strength 0.2%	637	686	758	25	635	687	765	25
Tensile strength	742	801	881	27	748	804	865	26
Elongation	11.0	17.9	21.6	1.7	15.2	18.1	22.7	1.4
Reduction of area	17.6	55.0	77.5	10.9	37.5	64.1	75.5	8.3
CVN at 0°C, J/cm ²								
Lowest result	18	64	161	26	35	120	260	47
Average of three specimens	23	77	167	27	51	141	267	46
All results	18	77	175	31	35	142	285	51
FATT, °C	-46	-3	48	14	-51	-20	10	12

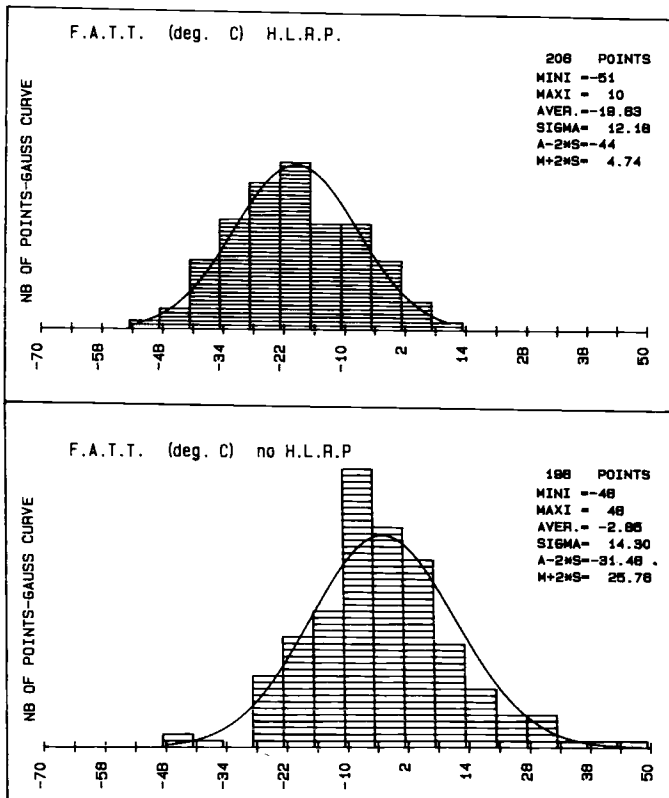


FIG. 11—Histograms of FATT after PWHT.

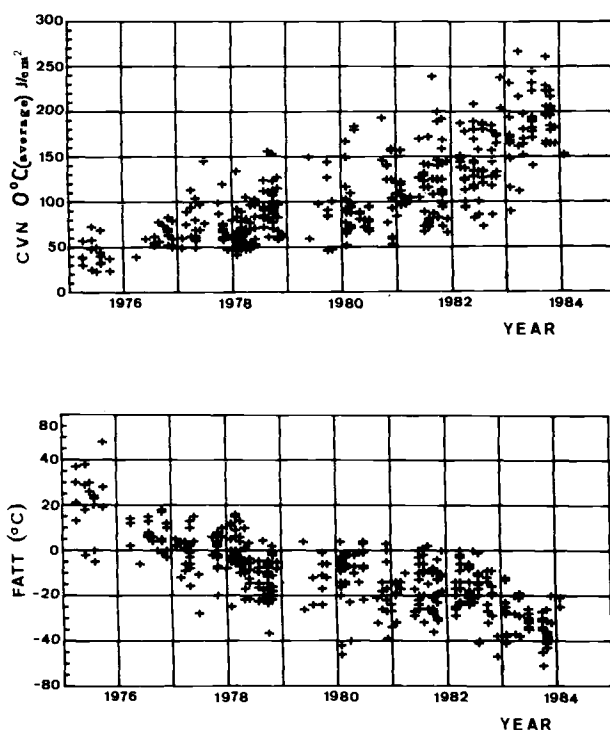


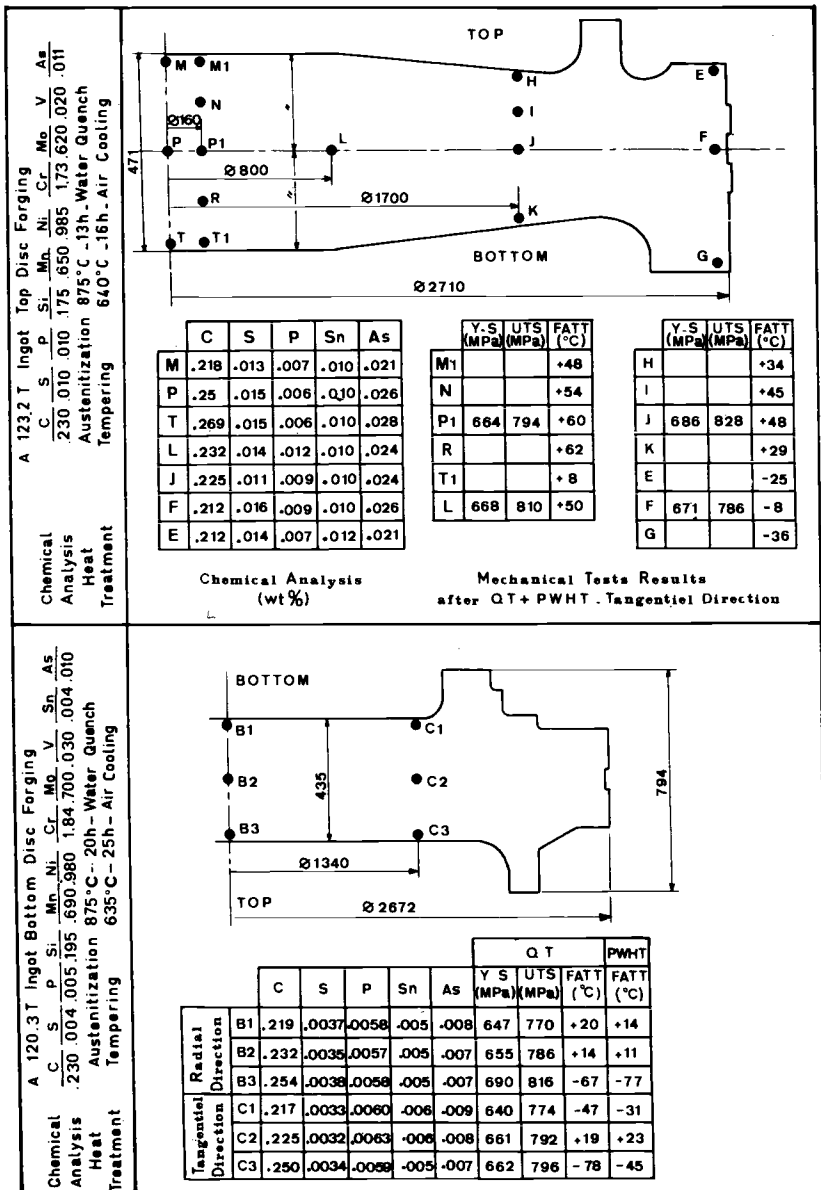
FIG. 12 —Chronological evolution of CVN at 0°C and FATT after PWHT.

Investigation of Industrial Parts

Two disks have been cut off to verify these results. One has been produced by the previous process [4] and the other by the new process. The mechanical properties in all parts (Fig. 13) confirm the preliminary studies as well as the statistical analysis on industrial forgings.

Conclusion

The preliminary and industrial research achieved has shown the chemical and metallurgical homogeneity of forgings. The research also permitted an optimization of the steel grade and a substantial increase of toughness connected with a reduction in the content of trace elements. Nowadays, we can easily obtain a phosphorus content less than 0.005% with a sulfur content less than 0.002%. We believe we can still improve the manufacturing of welded polyblock turbine rotors. Continuous effort is being applied to this scheme by Le Creusot Heavy Forge.



Dimensions in mm

FIG. 13—Chemical analysis and mechanical properties of two experimental disks.

References

- [1] Comon, J., "Production of rotor forgings," EPRI WS-79-235, Electric Power Research Institute, Palo Alto, CA, Sept. 1981.
- [2] Toitot, M. and Dor, P., "Equivalence du Temps et de la Température sur les Phénomènes de Diffusion. Formule Paramétrique Applicable aux Cycles Thermiques. Détermination des Temps de Maintien Équivalents," *Mémoires Scientifiques—Revue de Métallurgie* 63, No. 12, 1966.
- [3] Dor, P., Comon, J., "Conception et Réalisation d'une Installation d'Affinage en Poche—Application aux Lingots de Forge," 9th International Forging Conference, Dusseldorf, 1981.
- [4] Internal report, Electricité de France (unpublished), "Caractérisation d'un Disque en Acier 20 CND 8 de Creusot-Loire."

DISCUSSION

*W. J. Wiemann*¹ (*written discussion*)—In addition to the statistic regarding the results of shaft ends and disks for welded polyblock rotors, you presented the investigation results of two cut-off disks. The thickness of these disks was a maximum of 471 mm, and the difference in FATT between the rim and the midthickness of the specimen in the representative PWHT condition is about 70 to 80°C. You mentioned in the discussion that your largest disk thickness is 720 mm. What is the increase in FATT from rim to central position at this thickness, and what are the (to be expected) C_v energy values at these positions, at 0 and 20°C, respectively (minimum and mean values)? And, which values do you have in the upper shelf regime, and at what temperature are these values reached at the rim and the midthickness position, respectively.

J. Pisseloup, I. Poitault, A. de Badereau, and P. Bocquet (*authors' closure*)—It is clear that the difference in FATT between the rim and the midthickness is due to the difference in microstructure resulting from the cooling rate during quenching. The difference between the cooling rate at midthickness of a 470-mm-thick disk and a 720-mm-thick disk is lower than that existing between the rim and the core of a 470-mm disk. The CCT diagram shows that the increase of FATT is due to the presence of a small amount of ferrite (720 mm thick). So, the difference between the rim and the core of a 720-mm disk is slightly higher than this existing in a 470-mm disk, about 80 to 100°C expected.

The Charpy V notch energy values at these positions at 0 and 20°C depend on the relative position of these temperatures versus FATT. It is necessary to examine each particular case. The variation of the upper shelf depends on the hardness and on the nonmetallic inclusion content.

¹ Kraftwerk Union AG, D-4330 Muelheim a.d. Ruhr, Germany.

J. Ewald¹ (written discussion)—(1) You showed the development of FATT over the years. What position were the specimens removed from? (2) What was the largest disk thickness for the welded rotor type? (3) What microstructure do you expect in such disks? (4) Could you give us fracture toughness values (K_{Ic}) from inside and outside of the disks?

J. Pisseloup, I. Poitault, A. de Badereau, and P. Bocquet (authors' closure)—(1) The specimens were removed from the test coupon in the axial part of the forging at about 80 mm under the surface. The test coupon location can be seen in Fig. 1. (2) The largest disk thickness is 995 mm in the peripheral zone and 720 mm in the axial zone, including the test coupon. (3) The continuous cooling transformation diagram shows that a fully bainitic microstructure is obtained at the midthickness of a 600-mm-thick disk. For the largest disk (720 mm thick), the microstructure at midthickness is made from 90% bainite and 10% ferrite. (4) Some fracture toughness tests were performed by Electricité de France on a disk (470 mm thick) of the previous process. Three CT 150-mm specimens were taken at midthickness and fractured at room temperature. The K_{Ic} average value was 125 MPa \sqrt{m} .

R. Curran² (written discussion)—The paper describes the result of sectioning 400-mm disks, but indicates that bainitic microstructure can be achieved in 600-mm disks. Have any 600-mm disks been sectioned to determine the deep-seated FATT in 600-mm disks in the relatively lean alloy used?

J. Pisseloup, I. Poitault, A. de Badereau, and P. Bocquet (authors' closure)—The opportunities to cut parts for investigations concerned only 400-mm disks. We have not sectioned any 600-mm disks because we have not had an opportunity for this.

W. Meyer³ (written discussion)—What is the aluminum content of disks produced according to the new process?

J. Pisseloup, I. Poitault, A. de Badereau, and P. Bocquet (authors' closure)—The steel for producing these disks does not contain aluminum. This does not depend on the steelmaking process (new or previous).

² General Electric Co., Schenectady, NY 12345.

³ VEW, 8605 Kaptenberg, Postfach 10, Austria.

Turbine and Generator Forgings

Steels for Rotors

New 2Cr-Mo-Ni-W-V Steel for High-Pressure Rotors

REFERENCE: Finkler, H. and Potthast, E., "New 2Cr-Mo-Ni-W-V Steel for High-Pressure Rotors," *Steel Forgings*, ASTM STP 903, E. G. Nisbett and A. S. Melilli, Eds., American Society for Testing and Materials, Philadelphia, 1986, pp. 107–123.

ABSTRACT: In recent years, extensive research has been undertaken to improve the service properties of 1Cr-Mo-V steels with the aim of manufacturing high-pressure (HP) and medium-pressure (MP) turbine rotors having higher creep-rupture and toughness values. However, notched impact strength, fracture appearance transition temperature (FATT), and fracture toughness depend greatly on heat treatment. Oil quenching after austenitizing, which is common practice in Europe, gives higher values than air quenching, which is specified in the United States. A change in heat treatment, however, has little effect on the toughness in the core of turbine rotors. To improve this property, it is necessary to increase the alloy content of the steel. This has led to the development of a new 23Cr-Ni-Mo-W-V 8 8 steel for HP rotors. After testing this new steel at laboratory level, a 114-ton electroslag remelted (ESR) ingot was produced, from which a 42.5-ton turbine rotor with a 1370-mm maximum body diameter and a 1555-mm flange diameter was manufactured and extensively tested. Results obtained from transverse specimens showed an 0.2% yield strength of 650 N/mm², excellent elongation, reduction of area, and notched impact strength values, as well as a FATT of 273 K (0°C) at the surface, 293 K (20°C) at midradius, and 313 K (40°C) in the core. A modified production process will give a FATT of 293 K (20°C) in the core of the turbine rotor with excellent creep-rupture properties.

KEY WORDS: 1Cr-Mo-V steel, turbine rotor, creep-rupture properties, notched impact strength, fracture appearance transition temperature (FATT), influence of heat treatment, new high-pressure rotor steel with improved toughness

High-pressure (HP) and medium-pressure (MP) steam turbine rotors are made from 1Cr-Mo-V high-temperature steel and are operated at temperatures up to 825 K (550°C) worldwide. In recent years, intensive research was directed at improving the service properties of these steels with the aim of producing rotors with better creep-rupture strength and toughness within the analysis ranges of 1Cr-Mo-V steels, the properties of which are documented by long-term results [1].

¹ Chief engineer, Metals Research, ARBED Saarstahl, Völklingen, West Germany, 6620.

² Chief engineer, Quality and Materials Engineering, ARBED Saarstahl, Völklingen, West Germany 6620.

Metallurgical measures, such as lowering the content of trace elements; ladle treatment; the electroslag remelted (ESR) process; optimized forging technique; and heat treatment have resulted in an improvement of mechanical properties. Inhomogeneities such as segregations, which are an inevitable concomitant of conventional melting practices, have been eliminated to such a degree that they occur only locally and imbedded in a ductile matrix [1]. In this form they do not significantly affect the toughness properties over the cross section of a rotor.

The hardenability of these steels is sufficient to manufacture turbine rotors up to the current diameters with uniform 0.2% yield strength over the cross section and a high degree of freedom from ferrite in the core. Cooling from austenitizing temperatures between 1223 and 1250 K (950 and 975°C) has a predominant influence on the structure. Slow cooling in air, which is common practice in the United States, results in a structure of upper bainite in the rim zone and of upper bainite and perhaps some ferrite plus carbide in the core in areas of negative segregation, depending on rotor diameter and chemical composition. Cooling in oil, which is applied normally in Europe, gives lower bainite in the rim zone and upper bainite in the core.

Best creep-rupture properties of 1Cr-Mo-V steels are achieved with a structure consisting of tempered upper bainite, in which the vanadium carbides are uniformly and finely dispersed. Lower bainite gives lower creep-rupture strength. On the other hand, however, it augments the toughness at low temperatures. This relationship is illustrated in Fig. 1, where the creep rupture strength at 823 K (550°C) after 2500 h is plotted versus the fracture appearance transition temperature (FATT) [2]. This figure shows that the creep-rupture strength increases in proportion to the toughness, which is characterized by the FATT.

In the manufacture of turbine shafts, it has, therefore, to be considered whether a high-creep resistance at high temperatures or the resistance to brittle fracture

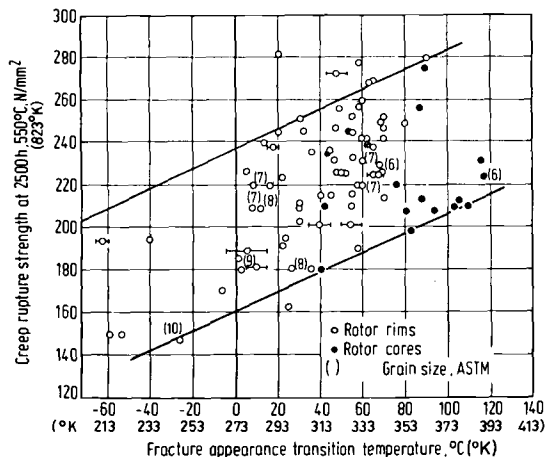


FIG. 1—Relationship between toughness and creep resistance for 1Cr-Mo-V turbine rotors [2].

at low temperatures shall be given priority. Whether the component shall be quenched in air or in a liquid medium depends on this decision.

In the literature [2-4], relatively wide scatterbands are given for the FATT and the impact energy (see Fig. 1). Values ranging from 213 to 363 K (-60 to $+90^{\circ}\text{C}$) for the FATT in the rim zone of turbine rotors cannot be explained only by different cooling rates from the austenitizing temperature and the dependence of both creep rupture strength and FATT on tensile strength and grain size. Batte, Murphy, Fischer, and Venkateswarlu [2] have determined the sharp drop in the quenching rate below the surface of a large forging as a possible source for this scatter. They have found that the absorbed energy decreases from 100 J at the surface to 50 J at a depth of 100 mm below the surface. This sharp drop in toughness suggests that the toughness in the core of a forging hardly can be improved under production conditions, even when higher quenching rates are employed.

We have proved this assumption by means of a special test method using a large end-quench specimen [5]. This test piece has a cross section of 70 by 120 mm and a height of 200 mm. It is sectioned into disks of 12-mm thickness after quenching and tempering. Each disk is examined for strength and toughness. In this way, the cooling conditions in the near surface zone of the rotor can be simulated and the mechanical properties can be determined up to a distance of 200 mm from the surface.

In Figs. 2 and 3, the test results obtained on a 30Cr-Mo-Ni-V 5 11 large end-quench specimen have been transferred to a turbine rotor having a 1200-mm diameter. Figure 2 shows the FATT curve for water, oil, and air quenching, and Fig. 3 shows the absorbed energy at room temperature at various distances from the surface.

These figures show the steep drop in absorbed energy and the rise of the FATT in the rim zone of liquid-quenched forgings. In practice, however, the toughness values in the zone immediately below the surface of oil-quenched turbine rotors will be somewhat lower than these test results. This is indicated in the illustrations by dashed lines.

The sharp toughness drop in the rim zone illustrates how important it is to know the exact sample location within the forging and its distance from the heat-treated surface in order to give a correct interpretation of the test results. This fact should be accounted for in specifications.

Furthermore, it becomes evident that the toughness gain due to oil quenching in comparison to air quenching is more marked in the rim zone of turbine rotors than in the core. This also is true for water quenching. Hence it follows that a significant toughness increase in the core of large turbine rotors cannot be achieved by a modified heat treatment. A decisive reduction of the FATT is only possible by increasing the alloy content.

On the basis of 150-kg experimental melts, we have developed a new high-pressure rotor steel which enables rotors with a 1500-mm diameter to be oil-quenched largely ferrite free through the bainitic range. With a 0.2% yield strength

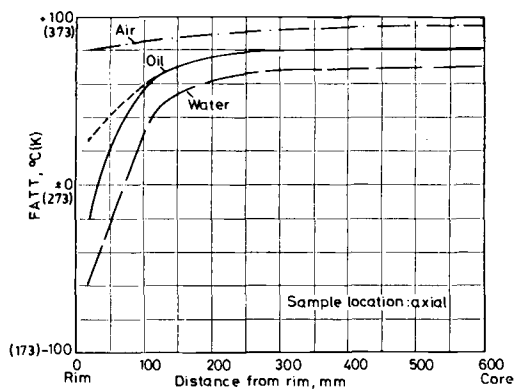


FIG. 2—Estimated FATT curves over the cross section of water-, oil-, or air-quenched rotors with a 1200-mm diameter. $C = 0.31$, $Si = 0.12$, $Mn = 0.72$, $P = 0.008$, $S = 0.003$, $Cr = 1.14$, $Mo = 1.25$, $Ni = 0.24$, $V = 0.24$, and $Al = 0.008$.

of approximately 650 N/mm^2 , a FATT of approximately 293 K (20°C) can be anticipated even in the core. At 823 K (550°C), the same creep-rupture strength as with Grade 30Cr-Mo-Ni-V 5 11 was determined.

This new 23Cr-Mo-Ni-W-V 8 8 steel has the following mean chemical analysis: 0.22% carbon, max 0.15% silicon, 0.70% manganese, max 0.010% phosphorus, max 0.010% sulfur, 2.1% chromium, 0.75% nickel, 0.85% molybdenum, 0.65% tungsten, 0.30% vanadium, and max 0.010% aluminum. Figure 4 shows the transformation diagram for continuous cooling for this steel.

After testing this new steel at the laboratory level, we manufactured a turbine rotor with a 1370-mm max body diameter, a 1555-mm flange diameter, and a 42.5-ton weight³ plus integral test material measuring 1350 mm in diameter. This

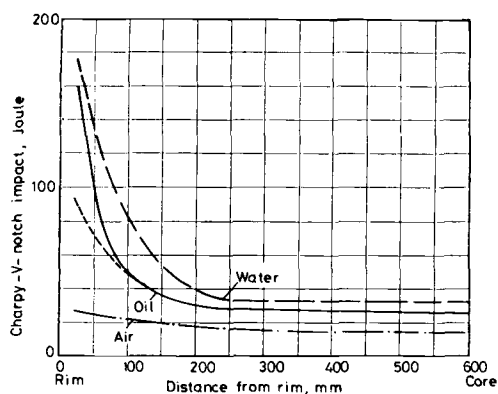


FIG. 3—Estimated impact energy curve over the cross section of water-, oil-, or air-quenched rotors with a 1200-mm diameter. $C = 0.31$, $Si = 0.12$, $Mn = 0.72$, $P = 0.008$, $S = 0.003$, $Cr = 1.14$, $Mo = 1.25$, $Ni = 0.50$, $V = 0.24$, and $Al = 0.008$.

³ All tons mentioned in this paper are metric tons.

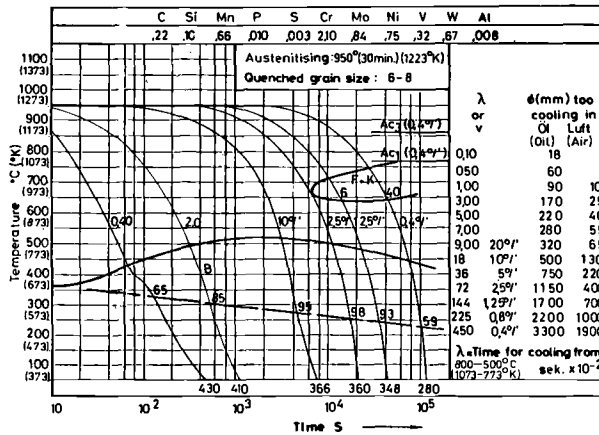


FIG. 4—Continuous-cooling transformation diagram for the 2Cr-Mo-Ni-W-V steel.

rotor was subjected to extensive testing in cooperation with Kraftwerk Union AG (KWU), Mülheim, West Germany. Test results were presented at the meeting of the Electric Power Research Institute's (EPRI) steering committee in Washington in December 1982.

This first turbine rotor was forged from a 114-ton ESR ingot having a diameter of 2300 mm. The chemical composition of ESR Melt No. 40 320 is given in Fig. 5 along with the check analysis of the rotor.

After equalization of temperature, the ESR ingot was heated to a 1553 K (1280°C) forging temperature. Rotor and integral test material were forged in seven heats (included cogging and upsetting) on our 40-MN press. The details of the forging sequence are given in Fig. 6. During subsequent preliminary heat treatment, the forging was austenitized at 1223 K (950°C) for 36 h, followed by furnace cooling down to 523 K (250°C) and tempering at 953 K (680°C) for 15 h.

After ultrasonic testing, the forging was machined to the dimensions shown in Fig. 7 and was subsequently oil-quenched from 1223 K (950°C) and tempered at 948 K (675°C) as shown in Fig. 8. During subsequent ultrasonic testing, no defects were revealed, defect detectability being good.

	C	Si	Mn	P	S	Cr	Mo	Ni	W	V	Al	As	Cu	Sn	Sb
	%	%	%	%	%	%	%	%	%	%	%	%	%	%	%
Guide Analysis	.21-.23	≤.20	.65-.75	≤.010	≤.005	2.05-2.15	.80-.90	.70-.80	.60-.70	.30-.35	≤.010	≤.025	≤.10	≤.010	≤.002
ESR-melt 40 320	.22	.10	.66	.010	.003	2.10	.84	.75	.67	.32	.008	.015	.06	.01	.0014
Turbine surface, top	.21	.12	.65	.010	.003	2.10	.83	.74	.66	.30	.006	.015	.06	.01	.0015
shaft axial, bottom	.22	.12	.67	.010	.003	2.07	.86	.74	.68	.29	.005	.014	.07	.01	.0015

FIG. 5—Chemical composition of the ESR Melt 40320 and of the 2Cr-Mo-Ni-W-V turbine shaft.

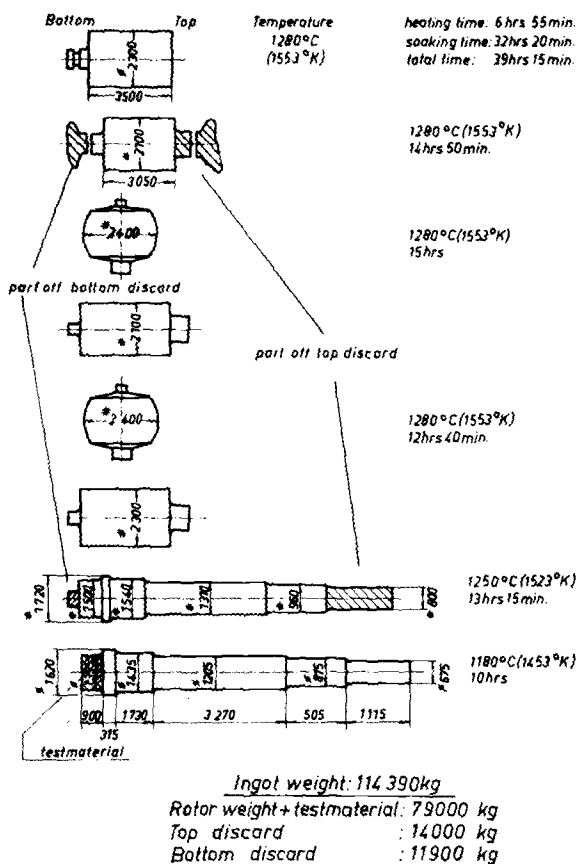


FIG. 6—Forging procedure of the ESR Ingot Melt No. 40320.

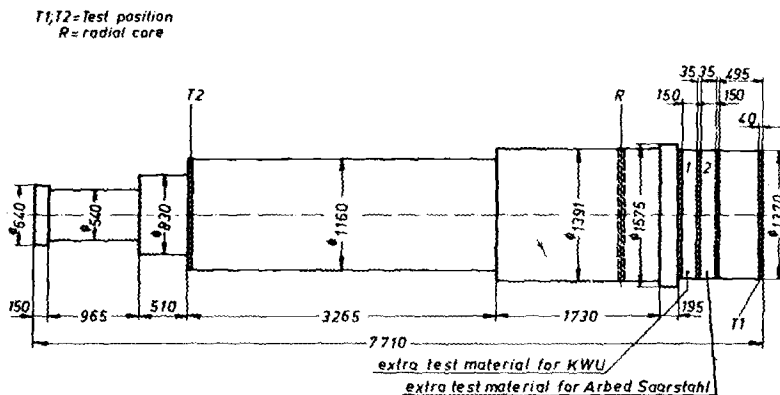


FIG. 7—Heat treatment contour of the 2Cr-Mo-Ni-W-V turbine shaft.

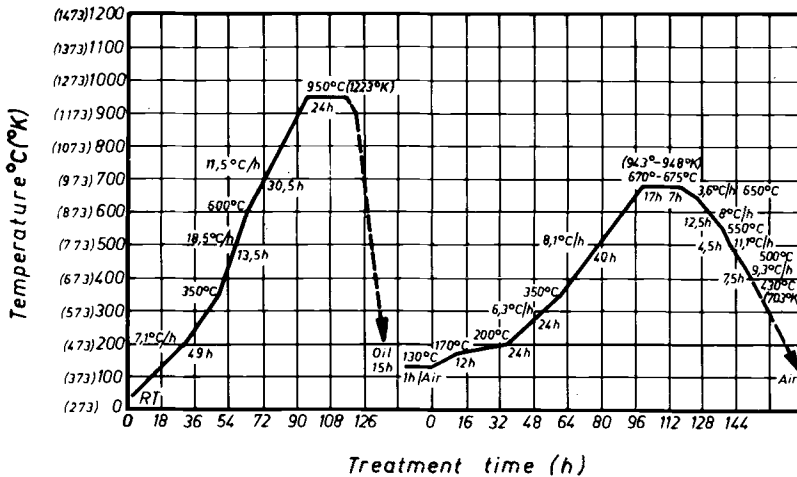


FIG. 8—Quality heat treatment of the 2Cr-Mo-Ni-W-V turbine shaft.

Excellent test results were obtained from tangential rim specimens in Test Locations T1 and T2 as well as from the radial core as shown in Fig. 9.

After these tests, the rotor was machined to as-delivered dimensions, and the additional test material (Fig. 7) was removed. From this material, a 1350-mm diameter by 150-mm disk was cut off at a distance of 530 to 680 mm from the end surface for testing in our works. A similar disk was taken at a distance of 715 to 865 mm from the end surface for testing by KWU.

The cross section of the disk was ground and etched with ammonium persulfate. The examination revealed no macroscopic segregation. Subsequently, a 220-mm-diameter bore core was removed from the center of the disk and four other cores at a distance of 475 mm from the center, as shown in Fig. 10, which also shows

Test position		$Rp0.2$ N/mm ²	Rm N/mm ²	A %	Z %	$ISO-Vbei+20^{\circ}C(293^{\circ}K)$ J	FATT °C(°K)
T1 (tang)		611	736	22	73	162 — 158 — 162	0 °C (273°K)
T2 (tang)		604	734	22	70,8	150 — 125 — 155	+5 °C (278°K)
Radial core checked by KWU	Distance from surface (mm)						
	90	642	750	20	71		
	165	648	759	21	68		
	270	648	754	21	70		
	475	648	766	19	66		
	650	652	765	19	65		

FIG. 9—Test results of the 2Cr-Mo-Ni-W-V turbine shaft.

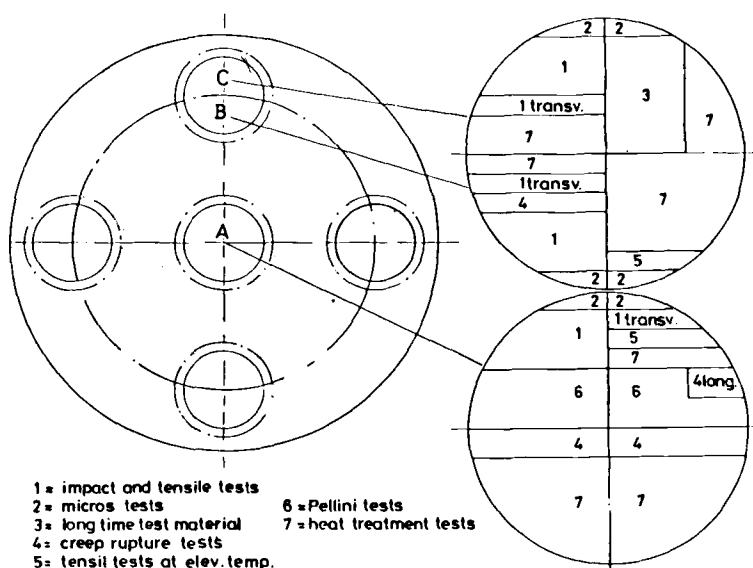


FIG. 10—Sample location in the test disk.

the specimen locations within the individual bore cores. As can be seen, the specimens from Location A are situated in the core of the shaft, while the B specimens are at a distance of approximately 400 mm from the core and the C specimens approximately 120 mm below the surface.

The tension and impact test results obtained from the three locations A, B, and C are shown in Fig. 11. As can be clearly seen from Figs. 12 and 13, the values for 0.2% yield strength, tensile strength, elongation, and reduction of area determined on longitudinal and transverse specimens at the respective distances from the rotor center are uniform over the cross section of the rotor.

Test position	Rp0,2 N/mm ²	Rm N/mm ²	A %	Z %	ISO-V in Joule					FATT (°K) °C
					(253) -20°C	(273) 0°C	(293) +20°C	(313) +40°C	(353) +80°C	
A (core) long.	650	766	18,7	71,4	14	40.	107	163	180	+30 (303)
"	650	762	17,8	71,7		41	73	114-135	180	
							87,55,85,48			
transv.	648	763	19,0	70,1	26		86	67	194	+40 (313)
"	651	759	19,0	70,6			117,69,40,	155-114	151	
B (400mm long. from core)	634	760	18,3	75,2	51	72	110	147	189	+20 (293)
"	635	757	18,7	72,8			136-134			
transv.	651	771	19,3	71,6		122	137	149		+20 (293)
"	649	761	19,3	71,6			109			
C (120mm long. from surface)	634	760	19,0	72,7	52	78	87	187	191	+20 (293)
"	632	757	18,3	73,7			123-135			
transv.	645	761	20,0	71,7		61	120	144		+25 (298)
"	648	758	18,3	70,5			94			

FIG. 11—Test results of the disk: diameter is 1350 by 150 mm.

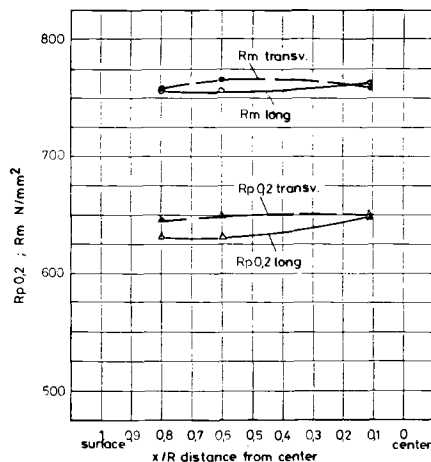


FIG. 12—The 0.2% yield and tensile strength results over the cross section, test disk diameter is 1350 by 150 mm.

Figure 14 shows the absorbed impact energy in the longitudinal and transverse directions as a function of the test temperature for the three just-mentioned specimen locations. Figure 15 shows the crystallinity of the fractured surface.

Impact testing of core material gave a FATT of 298 K (25°C) for longitudinal specimens and of 313 K (40°C) for transverse specimens, the absorbed energy (respectively, 120 and 115 J) being very high in relation to the FATT. However, there is a remarkably wide scatter of the absorbed energy at room temperature and at 313 K (40°C), as shown by the sharp drop of the absorbed energy curves in Fig. 14.

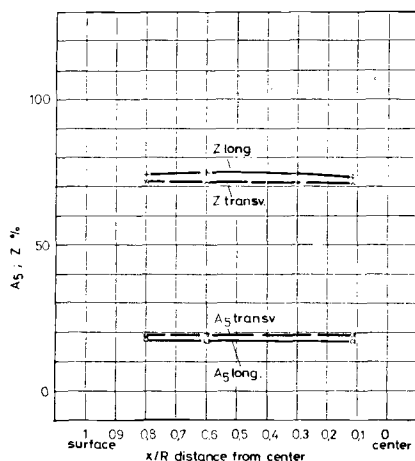


FIG. 13—Elongation and reduction of area results over cross section, test disk diameter is 1350 by 150 mm.

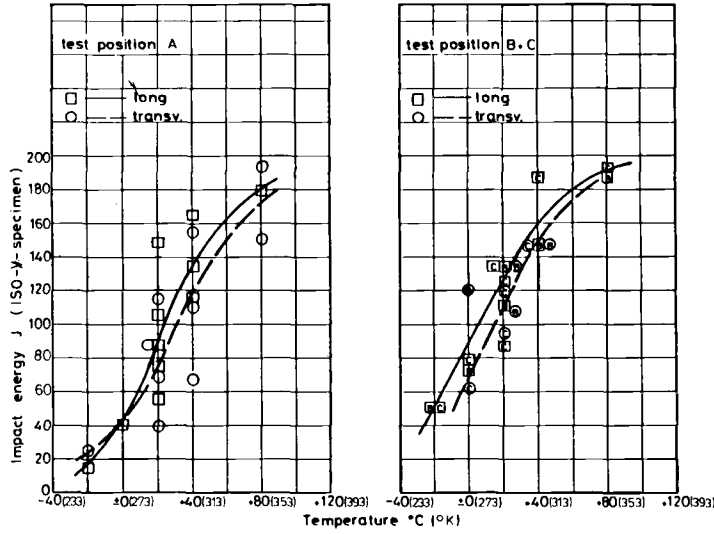


FIG. 14—Impact energy versus test temperature of the test disk.

In the B and C locations, which means approximately 400 mm from the core and 120 mm below the surface, a FATT of 293 K (20°C) was determined, the absorbed energy at FATT (115 J) being the same as in the core (Fig. 16).

Although we had expected a FATT of approximately 293 K (20°C) in the core, the values obtained are clearly lower than with the known 1Cr-Mo-Ni-V rotors. In Fig. 17, the results of the 2Cr-Mo-Ni-W-V rotors have been entered into the

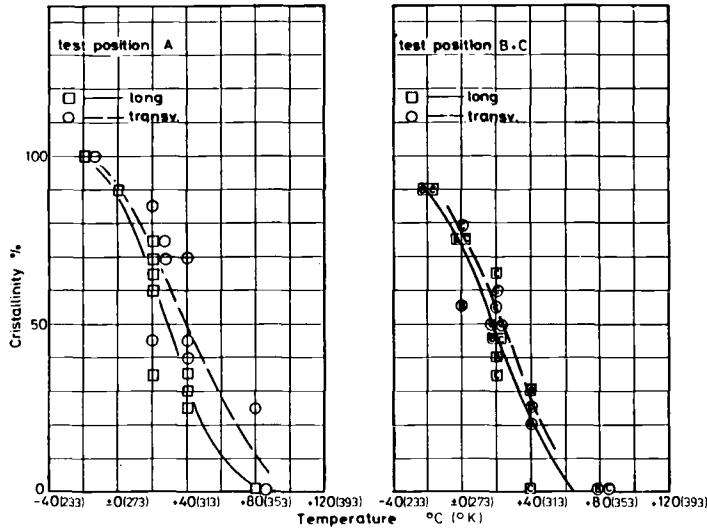


FIG. 15—Crystallinity versus temperature of the test disk.

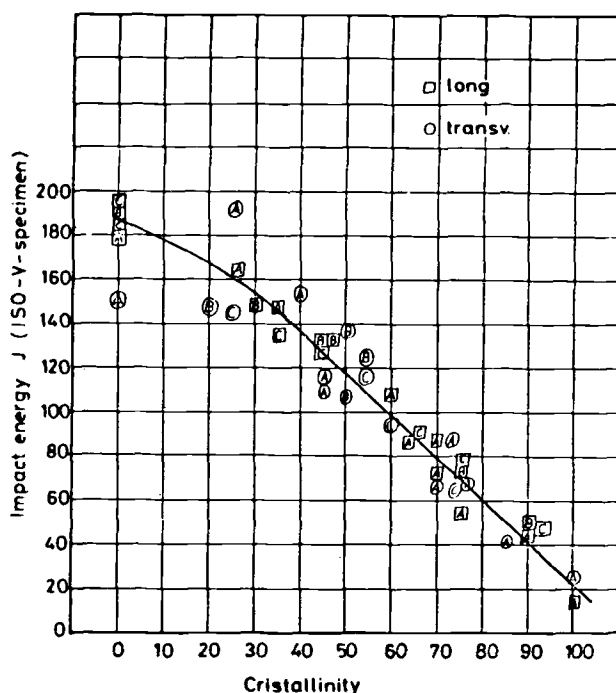


FIG. 16—Relationship between the impact energy and the crystallinity of the test disk.

graph for 1Cr-Mo-Ni-V rotors prepared by KWU [1]. The wide scatter of the absorbed energy at 293 K (20°C) and 313 K (40°C), and in particular the FATT in the core, which in our opinion is still too high for the new HP rotor steel, gave rise to further investigations starting with metallographic examinations. The structure was found to be composed of intermediate and upper bainite. However, there was a relatively high amount of mixed grain consisting of 50 to 70% coarse grain of ASTM Size 1–2 and a remainder of ASTM Size 3–5. It turned out that the impact specimens on which the lower values had been found contained a higher percentage of coarse grain.

In a second test series, the core material was examined in order to determine how the strength affects the FATT. These tests were conducted on core specimens that had been subjected to a second tempering treatment at 963 K (690°C) for 18 h. As a result, the 0.2% yield strength dropped from about 650 to 556 N/mm² in the longitudinal direction and to 571 N/mm² in the transverse direction. The FATT dropped by about 45 to 50° to 253 K (–20°C) in the longitudinal direction and to 268 K (–5°C) in the transverse direction.

As this considerable improvement of the FATT could not be explained by the strength reduction alone, there was reason to suspect temper embrittlement. The test material had been cooled in air, that is, at a much greater cooling rate than the core of the rotor. Therefore, other specimens were subjected to a step-cooling

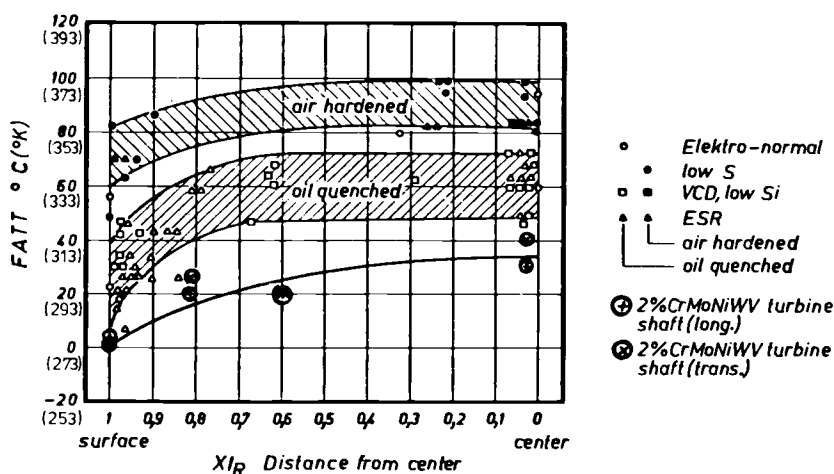


FIG. 17—FATT of the 2Cr-Mo-Ni-W-V turbine shaft compared with 1Cr-Mo-Ni-V turbine shafts [1].

treatment, according to Gould,⁴ following the additional tempering at 963 K (690°C) for 18 h. As a result, the FATT rose from 253 to 298 K (−20 to +25°C) in the longitudinal direction and from 268 to 298 K (−5 to +25°C) in the transverse direction, indicating that there was indeed temper embrittlement with a Δ -FATT of 30 to 45°.

As coarse grain has detrimental effects on the FATT as well as on the Δ -FATT, specimens were subjected to regenerative annealing in the pearlitic range [1253 K (980°C) for 2 h, furnace cooling to 893 K (620°C), heating with 5°/h to 973 K (700°C) for 12 h, furnace cooling] and to a simulated heat-treatment reflecting the heat-treatment conditions in the core of the turbine rotor [1223 K (950°C) for 12 h, with 150°/h to 773 K (500°C), with 50°/h to room temperature, plus 963 K (690°C) for 24 h—air cooling]. The resulting 0.2% limit was approximately 40 N/mm² lower than that of the rotor, as shown in the following table:

Specimen Location	$R_{p0.2}$, N/mm ²	R_m , N/mm ²	A_s , %	Z , %	Absorbed Energy, J			FATT, K
					0°C	293 K (+20°C)	313 K (+40°C)	
Longitudinal	595	725	20.0	73.6	124	133,164	175	278 (+5°C)

NOTE: $R_{p0.2}$ = 0.2% yield strength; R_m = tensile strength; A = elongation; Z = reduction of area.

The improvement of the FATT from 303 to 278 K (+30° to +5°C), however, is greater than could be expected from the lower 0.2% limit. It is mainly attrib-

⁴ See Temper Embrittlement in Steel, ASTM STP 407, p. 59.

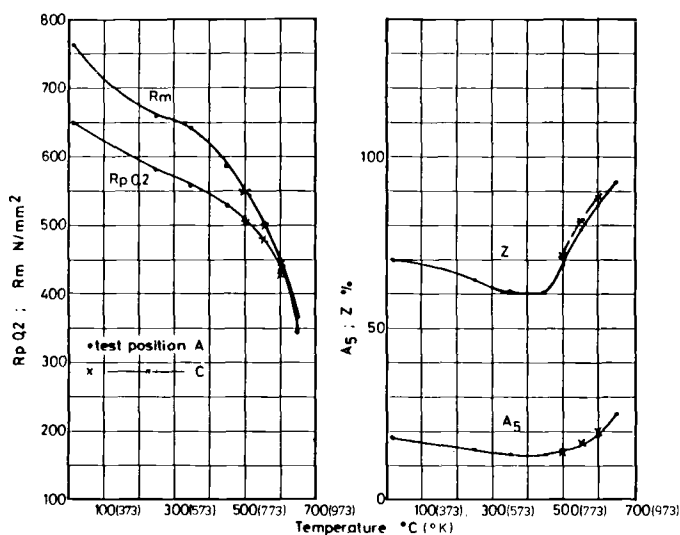


FIG. 18—Tensile properties at elevated temperatures of the 2Cr-Mo-Ni-W-V steel.

utable to the finer and uniform grain of ASTM Size 3 to 5. This grain refinement also suffices to eliminate the susceptibility to temper embrittlement, as evidenced by an additional step-cooling treatment, which gave the same FATT value: 278 K (+5°C).

The question of long-term embrittlement also was investigated. Specimens from Sample Locations B having a FATT of 293 K (+20°C) were subjected to a step-cooling treatment and were long-time annealed at 753 K (480°C) for 200 h, 500 h, and 1000 h. After 1000 h, a slight increase of the FATT to 313 K (+40°C) was determined. As this value also had been found after the step-cooling treatment, it was clear that the annealing for 1000 h had not caused a stronger embrittlement than step-cooling. Further tests confirmed that there is some long-term embrittlement at 753 K (480°C) but not at 803 K (530°C). Laboratory tests have shown that this embrittlement can be avoided in steel grade 23Cr-Mo-Ni-W-V 8 8 by lowering the content of trace elements, in particular of phosphorus to max 0.007% and of tin to max 0.008%.

High-temperature steels must exhibit not only toughness but also good strength at elevated temperatures as well as good creep-rupture properties.

In Fig. 18 the results of the elevated temperature tension tests are plotted versus the test temperature, which ranged from 523 to 923 K (250 to 650°C). While the 0.2% yield strength only drops by 100 N/mm^2 in the range from 523 to 823 K (250 to 550°C), it drops by 140 N/mm^2 in the range from 823 to 923 K (550 to 650°C). This shows that this steel loses strength above 823 K (550°C) like all other low-alloy high-temperature steels. Equally remarkable is the drop in elongation and reduction of area between 523 and 723 K (250 and 450°C), even though the absolute reduction of area value of min 60% is still relatively high. There is no significant difference between Specimen Locations A (core) and C

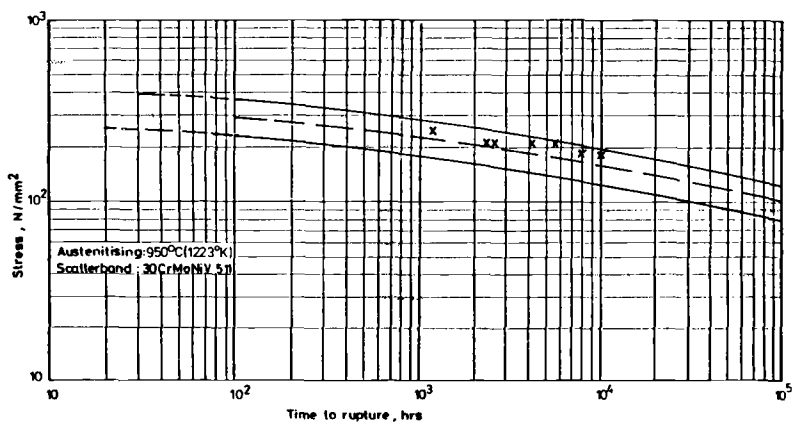


FIG. 19—Creep-rupture properties at 823 K (550°C) of the 2Cr-Mo-Ni-W-V steel compared with 30Cr-Mo-Ni-V 5 11.

(rim). At 723 K (450°C), 773 K (500°C), and 823 K (550°C), we also conducted notched impact tests. The ratio of notched tensile strength to tensile strength, which was found to be 1.7, shows that no significant notch sensitivity must be anticipated at elevated temperature. This assumption was confirmed by the creep-rupture tests.

Figure 19 shows the creep-rupture values up to 10 000 h obtained in current tests. The values are situated in the upper range of the scatter band known for 30Cr-Mo-Ni-V 5 11 high-temperature steel. They also agree with the results

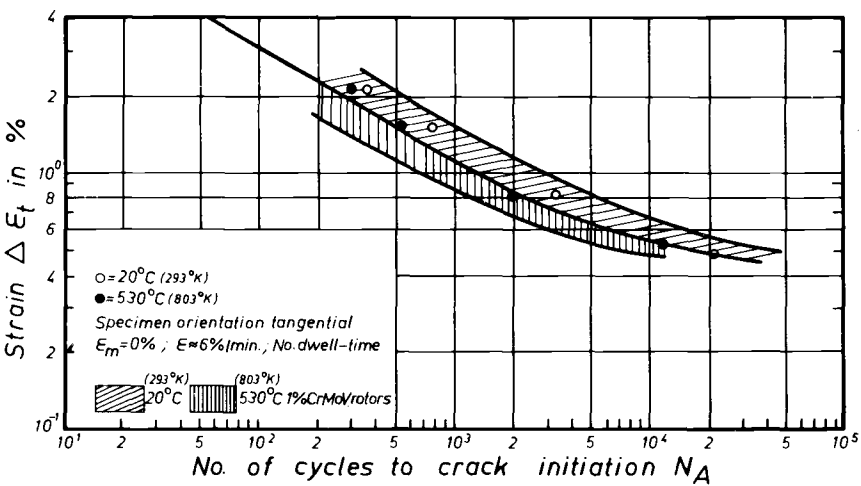


FIG. 20—Low-cycle fatigue of the 2Cr-Mo-Ni-W-V steel [7].

obtained on the experimental melts and show that 23Cr-Mo-Ni-W-V 8 8 steel has excellent creep-rupture properties in spite of its higher toughness.

At the meeting of the EPRI's steering committee in Washington in 1982, KWU had presented the first results of their investigations [7]. These investigations confirmed our results. Furthermore, the low-cycle fatigue tests showed that 23Cr-Ni-Mo-W-V 8 8 steel is comparable to 1Cr-Mo-V steel (Fig. 20). Among the physical properties it is the thermal conductivity and the thermal expansion coefficient which are of particular importance. In Fig. 21, these properties are compared with those of 1Cr-Mo-V and 12Cr-Mo-V steels. Again the values agree well with those of 1Cr-Mo-V steel.

Recent tests by KWU concerning fracture toughness and creep-rupture properties show the advantages of the new high-pressure rotor steels. These tests are not yet completed.

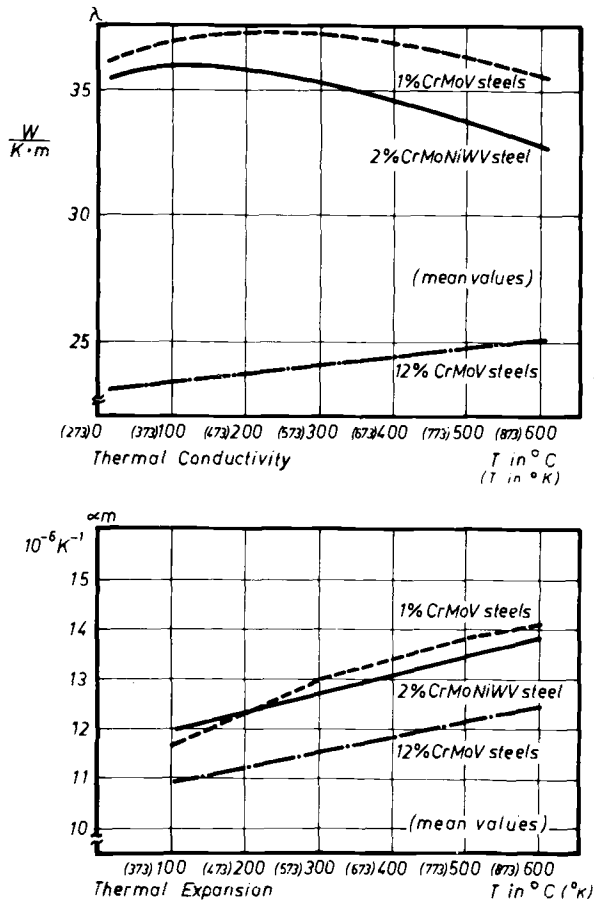


FIG. 21—Physical properties over temperature [7].

Summary

In recent years extensive research has been conducted in order to improve the service properties of 1Cr-Mo-V steels with the aim to produce HP and MP turbine rotors with better creep-rupture and toughness properties. However, impact strength, FATT, and fracture toughness are greatly dependent on heat treatment. Oil cooling after austenitizing, which is commonly employed in Europe, gives higher values than air cooling, which is specified in the United States. However, a significant improvement of the toughness in the core of turbine rotors cannot be achieved by a modified heat treatment. To achieve such an improvement, it is necessary to increase the alloy content.

This has led to the development of a new 23Cr-Ni-Mo-W-V 8 8 HP rotor steel. After testing this new steel at the laboratory level, we manufactured a 114-ton ESR ingot with a 2300-mm diameter, from which a 42.5-ton turbine rotor with 1370-mm max body diameter and 1555-mm flange diameter was manufactured. Integral test material measuring 1350 mm in diameter by 150 mm in length was thoroughly tested at ARBED Saarlust and KWU. The positive results obtained on the experimental melts generally were confirmed by these tests.

With an 0.2% yield strength of approximately 650 N/mm², excellent elongation, reduction of area, and impact strength, FATT values of 273 K (0°C) at the surface, 293 K (20°C) at midradius, and 313 K (40°C) in the core were determined on transverse specimens. Further tests have shown that there was some temper embrittlement due to mixed grain with a high percentage of coarse grain. By improving the grain size, which is possible by a modified forging practice and preliminary heat treatment, the FATT can be anticipated to be approximately 293 K (20°C), even in the core of the turbine rotor. There was a certain degree of long-time embrittlement at 753 K (480°C), which can be avoided by lowering the content of trace elements, particularly phosphorus and tin. Creep-rupture test results, up to 10 000 h available so far, also meet the expectations. They are in the upper range of the values known for 1Cr-Mo-V steels. Low-cycle fatigue, thermal expansion, and thermal conductivity values, too, are comparable to those of 1Cr-Mo-V steels. On the basis of these promising results, it seems to be justified to continue the development of this new steel and to confirm the expectations by new trial orders.

References

- [1] Ewald, J., Berger, C., Keienburg, K. H., and Wiemann, W., *Steel Research*, Vol. 57, 1986, pp. 83-92 and 172-177.
- [2] Batte, A. D., Murphy, H. C., Fischer, K., and Venkateswarlu, J., *Stahl und Eisen*, Vol. 98, 1978, pp. 941-949.
- [3] Schieferstein, U. and Wiemann, W., 8th International Forgemasters Meeting, Kyoto, Japan, 1977.
- [4] Wiemann, W., *VGB Kraftwerkstechnik*, Vol. 59, 1979, pp. 937-951.

- [5] Finkler, H. and Potthast, E., *Proceedings*, EPRI Workshop, Vol. WS-79-235, Electric Power Research Institute, Palo Alto, CA, 1981, pp. 83-104.
- [6] Finkler, H. and Potthast, E., meeting of the EPRI Steering Committee, Washington, DC, Dec. 1982, Electric Power Research Institute, Palo Alto, CA.
- [7] Ewald, J. and Wiemann, W., meeting of the EPRI Steering Committee, Washington, DC, Dec. 1982, Electric Power Research Institute, Palo Alto, CA.

Mechanical Properties of Advanced Technology 1Cr-Mo-V Steam Turbine Rotor Forgings

REFERENCE: Swaminathan, V. P., Jaffee, R. I., and Steiner, J. E., “**Mechanical Properties of Advanced Technology 1Cr-Mo-V Steam Turbine Rotor Forgings**,” *Steel Forgings, ASTM STP 903*, E. G. Nisbett and A. S. Melilli, Eds., American Society for Testing and Materials, Philadelphia, 1986, pp. 124–142.

ABSTRACT: Three advanced steel melting process—low-sulfur vacuum silicon deoxidation, electroslag remelting, and vacuum carbon deoxidation—were applied to produce three 1Cr-Mo-V [ASTM Specification for Vacuum-Treated Carbon and Alloy Steel Forgings for Turbine Rotors and Shafts A 470-82, Class 8] steel forgings for steam turbine application. A detailed evaluation of the tensile properties up to 565°C (1050°F), fracture toughness (K_{Ic} and J_{Ic}), high-cycle and low-cycle fatigue properties, and stress rupture (creep) properties were determined for the three forgings.

Compared to conventionally produced forgings, the advanced technology forgings show better tensile ductility and uniformity along the radial and longitudinal directions. Charpy upper-shelf energy shows about 40% improvement, and no temper embrittlement was found using a step-cooled and isothermal aging treatment. Significant improvement in fracture toughness (factors of two to three higher) is realized for these forgings. Low-cycle fatigue life is better at high temperatures due to the absence of nonmetallic inclusions. Creep strength shows slight improvement. However, creep ductility probably is improved due to low residual elements. Especially, the VCD forging shows excellent creep ductility even at long lives. Both the toughness and creep properties are better than those of oil-quenched rotors produced by European practice. These improvements are attributed to cleaner steel, low residual elements (especially very low sulfur content), and the associated reduction of nonmetallic inclusions.

KEY WORDS: advance melting, Cr-Mo-V steel, steam turbines, mechanical properties, tension, Charpy impact, fatigue (metals), fracture toughness, creep, stress rupture

Good center quality and uniform mechanical properties always have been two important requirements for steam turbine-generator rotor forgings to achieve prolonged rotor life, better reliability, and improved availability. In order to improve the life of the rotors, it is necessary that the cause of rotor cracking or degradation of properties be understood and eliminated. Inclusions, casting de-

¹ Senior engineer, Westinghouse Electric Corp., Orlando, FL 32826-2399.

² Senior technical advisor, Electric Power Research Institute, Palo Alto, CA 94303.

³ Consultant, Engineering Materials & Processes, Inc., Pittsburgh, PA 15217.

fects like porosity, and the segregation of impurity elements like sulfur and phosphorus can affect adversely the integrity and in-service life of turbine-generator rotors. The presence of hydrogen in the steel can cause hydrogen cracking in forgings [1]. Large amounts of residual elements like phosphorus and tin in the steel can cause temper embrittlement or the loss of toughness. Sulfur in the steel tends to segregate to cause high manganese-sulfide inclusion content in the "A" segregation bands. Inclusions of this type were found at the crack origin of the Gallatin No. 2 rotor [2].

Because of rotor failures during the mid-1950s, improved manufacturing techniques and inspection methods were introduced, and significant improvements were achieved in rotor forging manufacturing, particularly the introduction of vacuum casting to reduce hydrogen. Important advances have been made during the last few decades in the areas of steel refining, vacuum casting technology, hot topping methods, and the application of electroslag processes to the production of large ingots for turbine-generator rotor forgings [3-8].

Program Description

The subject project is a joint effort between the Electric Power Research Institute and the Westinghouse Electric Corp. The program was designed to apply three state-of-the-art steel melting and ingot production techniques to manufacture large 1Cr-1Mo-0.25V [ASTM (A 470-82) Class 8] steam turbine forgings. One of the objectives was to characterize thoroughly the metallurgical and mechanical properties of these forgings and to compare them with conventional rotor properties.

The advanced processes initially considered for this project were low-sulfur silicon deoxidation (low sulfur), vacuum carbon deoxidation (VCD), electroslag remelting (ESR), central zone remelting (CZR), and electroslag hot topping (ESHT). The first two processes (low sulfur and VCD) are modifications of the conventional process. Extra refining of the liquid steel is done in both cases to reduce the sulfur level. In the VCD process, deoxidation is achieved by carbon instead of silicon. The other three processes are electroslag processes in which the amount of the electroslag remelted steel varies depending on the process. It is nominally 100% for ESR, 10 to 15% for CZR, and 3 to 5% for the ESHT process. The low sulfur and VCD processes do not contain any electroslag remelted material. A schematic diagram of these processes is shown in Fig. 1. From these five processes, three were selected for the subject program. They were low sulfur, VCD, and ESR. A description of the steel melting and ingot production methods used in these three processes are given in Refs 9 and 10.

A Westinghouse rotor weighing approximately 30 tons finished and 40 to 50 tons as forged was selected for its large size and the availability of orders for the placement of the rotors in service. To obtain needed test material required for the extensive evaluation and testing, large test extensions 1070 mm (42 in.) in diameter by 915 mm (36 in.) long were provided on the top and bottom ends

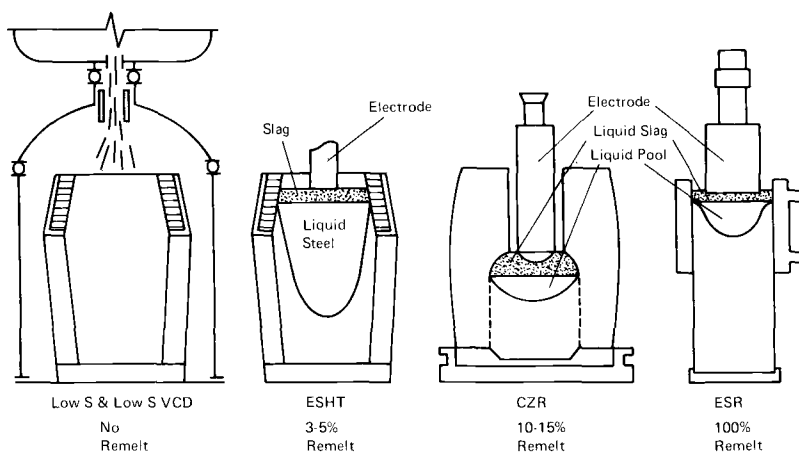


FIG. 1—Schematic diagram of the advanced ingot-making processes.

of each forging. These test ends were processed attached to the main rotor forging, so that the forging and heat-treatment procedures were the same as those for the rotor body. The low-sulfur forging was produced by the Japan Forging and Casting Corporation (JCFC), the VCD forging by the Japan Steel Works (JSW), and the ESR forging by Arbed Saarstahl, AG. The three ingots produced for this program had approximately the same body weight of 90 to 95 metric tons each.

Forging and Heat Treatment

The approximate configuration of the rotor forging and the size and locations of the test ends are schematically shown in Fig. 2. The test ends of the low-

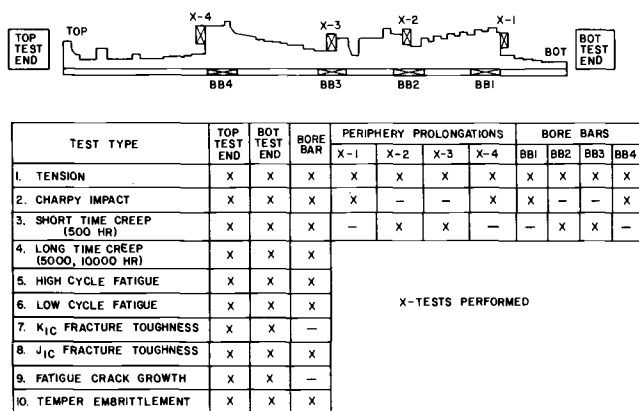


FIG. 2—Diagram of the rotor forging, the test material locations, and the type of mechanical tests.

sulfur and VCD forgings contained some material which would be normally considered as discard. Within the limitations of the standard operating practice of each producer, all of the forging and heat-treating variables were kept as uniform as possible for all three rotors. The low-sulfur and VCD forgings were single upset forged, while the ESR ingot was forged straight down without upsetting. The ESR forging received two quality heat treatments since it was necessary to reforge some small internal cracks formed due to unfavorable forging conditions in the bottom journal. These cracks were discovered during ultrasonic inspection. The test ends had only one quality heat treatment. The forgings were austenitized at 950°C (1740°F) and air cooled and tempered at 680°C (1255°F).

Material Evaluation Program

The characterization of the material was conducted under two categories. The first was the metallurgical characterization, which included chemical homogeneity, sulfur distribution and segregation distribution, and the internal material soundness as revealed by nondestructive testing, namely, ultrasonic and bore magnetic particle inspections. The second was the mechanical property determination. Tensile, Charpy impact, fracture toughness, low-cycle fatigue, high-cycle fatigue, fatigue crack growth, and stress rupture tests were conducted on samples taken from the top and bottom test ends and center locations along the length of these rotors. The results obtained from this program were compared with those of 29 Westinghouse rotor forgings produced by conventional processes during the period 1971 to 1977. Significant improvements in properties are observed for the three advanced technology forgings.

Results and Discussions

Chemical Composition

The chemical composition of the three forgings along with the mean composition of the 29 Westinghouse conventional rotors are presented in Table 1. The ESR ingot exhibited no axial segregation of sulfur and only about a 0.03% increase in carbon at the top discard. The low sulfur and VCD ingots exhibited a typical negative segregation of carbon at the bottom of the ingot and positive segregation at the top. The difference is about 0.12% through the main body and increases further in the sinkhead. Virtually no sulfur segregation from bottom to top is present in the low-sulfur and VCD ingots. These advanced refining and ingot production techniques have resulted in the significant reduction of potentially harmful elements like sulfur and phosphorus when compared to conventional methods as illustrated in Fig. 3. Gas content is also very low, especially hydrogen, which was kept below 2 ppm. Improvements in the cleanliness and nondestructive inspection results are presented in Ref 10.

The metallurgical soundness of the three advanced technology forgings is excellent in terms of freedom from axial centerline porosity or secondary piping

TABLE 1—Chemical composition from original melt.

Element	Conventional, Low S	VCD, Low S	ESR ^a	Conventional ^b , W	ASTM A 470-82, Class 8
Carbon	0.31	0.28	0.31	0.32	0.25 to 0.35
Manganese	0.78	0.76	0.78	0.83	1.0 max
Phosphorus	0.007	0.004	0.009	0.009	0.015 max
Sulfur	0.001	0.001	0.002	0.009	0.018 max
Silicon	0.23	0.05	0.19	0.27	0.15 to 0.35
Nickel	0.33	0.40	0.27	0.23	0.75 max
Chromium	1.13	1.18	1.18	1.07	0.9 to 1.5
Molybdenum	1.15	1.21	1.18	1.17	1.0 to 1.5
Vanadium	0.23	0.26	0.26	0.25	0.2 to 0.3
Tin	0.002	0.010	0.003	0.008	...
Antimony	0.0012	0.0015	0.001	0.001	...
Copper	0.04	0.04	0.04	0.09	...
Aluminum	0.004	0.005	0.009	0.003	...
Arsenic	0.003	0.006	0.011	0.010	...

^a Average of top and bottom analyses.^b Mean value from 29 Westinghouse conventional rotors (1971 to 1977).

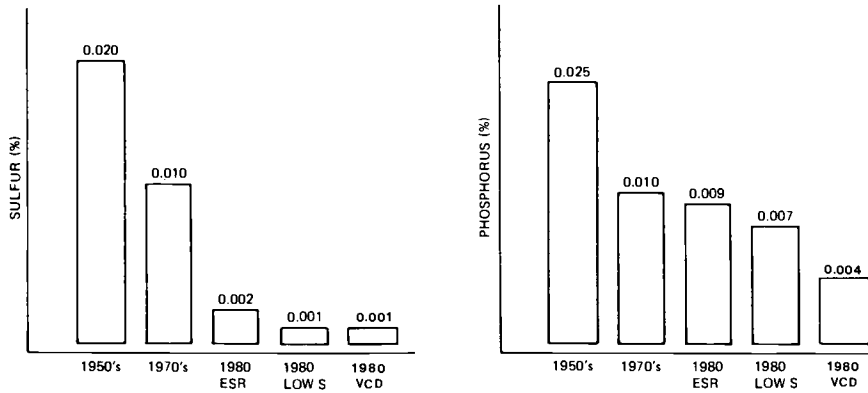


FIG. 3—Reduction of sulfur and phosphorus (1950–1980).

in the original ingots. Sulfur prints revealed that cleanliness was better even in the “A” segregate bands at the top of the low-sulfur and VCD forgings when compared to the conventionally produced forgings with average sulfur of about 0.010%. Because the detrimental effects of sulfur and sulfide concentration in segregation bands are many [2], this finding is important with respect to the axial center quality of large rotor forgings. Absence of such segregation bands in the ESR forging is positively an added improvement over the conventional technology. These improvements in the metallurgical properties are expected to result in prolonged life and reliable performance of these rotors.

Mechanical Property Evaluation

An extensive mechanical testing program was conducted to determine the tensile properties, Charpy impact properties, fracture toughness obtained by K_{Ic} testing, high-cycle and low-cycle properties, fatigue crack growth behavior, and creep (stress-rupture) properties at various locations of the forgings. These results are compared with the properties of conventionally produced forgings wherever available from 29 Westinghouse rotors of similar size. Significant improvements in the properties are found for the three advanced technology forgings.

Tensile and Impact Properties

Tension and impact test results showed good uniformity over the length and from the periphery to the centerline of the forgings. The results are summarized in Table 2. Both of these properties are equivalent to or superior to the average properties of the 29 conventional rotors. There is a slight anisotropy in the (radial versus longitudinal) ductility in the conventional rotors, whereas the advanced technology forgings show excellent ductility in both the transverse and the longitudinal directions. Typical distribution of the tensile properties at various locations of the forging is illustrated in Fig. 4. It should be noted that the periphery

TABLE 2—Tensile and impact test results from rotor forgings.

Property ^a	Prolongation				Bore Bar				ASTM A 470, Class 8
	Low S	VCD	ESR	^b Conventional, W	Low S	VCD	ESR	^b Conventional, W	
0.2% yield strength, ksi	90	94	96.3	TENSILE (75°C)					85 min
Tensile strength, ksi	113	114	118.2	90.6	91	91	96	90	105 to 125
Elongation, %	21	21.2	20.5	113.8	114	113	118	113	14
Reduction of area, %	62	63	60.7	19.3	20.5	22	20	20.6	38
				54.4	62	62.5	60	59.6	
Energy at 0°F, ft·lb	6	7	9	CHARPY IMPACT					6 min
Energy at 75°F, ft·lb	10	33	16	6	5	7	7	5	
Upper shelf energy, ft·lb	114	118	95	11	8	14	12	8	
FATT, °F	170	122	185	75	99	94	80	69	
				187	211	146	204	215	250 max

^a 1 ksi = 6.895 MPa; 1 ft·lb = 1.356 J; °C = (°F - 32)/1.8.^b Mean values from 29 Westinghouse rotors by conventional melting practice (1971-1977).

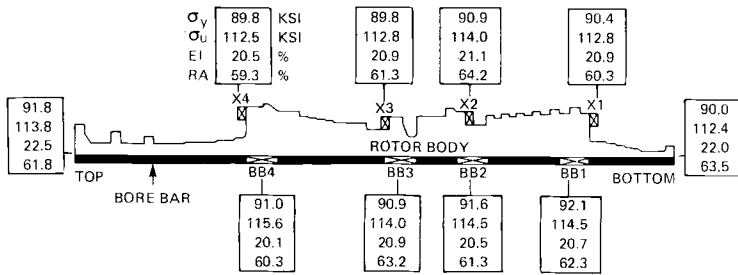


FIG. 4—Tensile properties (24°C) at various locations of the low-sulfur forging (1 ksi = 6.895 MPa).

specimens (X1 through X4) were radial, whereas the bore bar specimens (BB1 through BB4) were along the longitudinal direction.

Variation of yield strength, tensile strength, elongation, and reduction of area with temperature is as shown in Figs. 5 and 6. These properties are very similar for the three forgings. Compared to the conventional forging properties, the yield and tensile strengths are similar. This is expected since the heat-treatment parameters (temperature, time, cooling rate, etc.) were similar in both cases. Elongation values also are similar to those of the conventional forgings. However, the reduction of area shows consistent improvement. This is attributed to the improved cleanliness due to the very low sulfur level in these steels. The effect of sulfur content on the tensile reduction of area is illustrated in Fig. 7 [11].

Charpy impact test results show good uniformity over the length of the rotors. The impact energy values are higher at the periphery locations than at the centerline (bore bar), and FATT values are somewhat higher at the bore bar locations

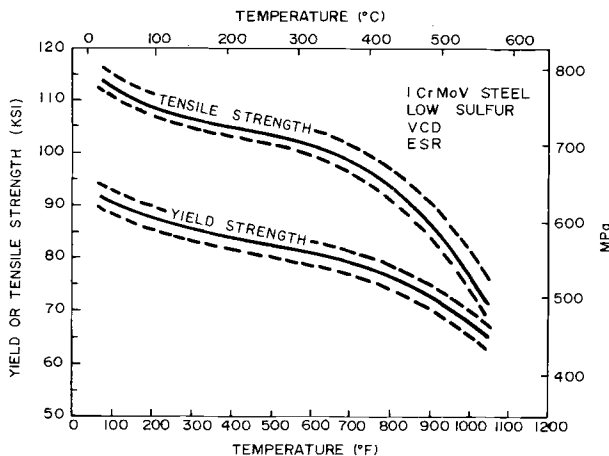


FIG. 5—Variation of yield and tensile strengths with temperature (dashed lines are 95% confidence bands).

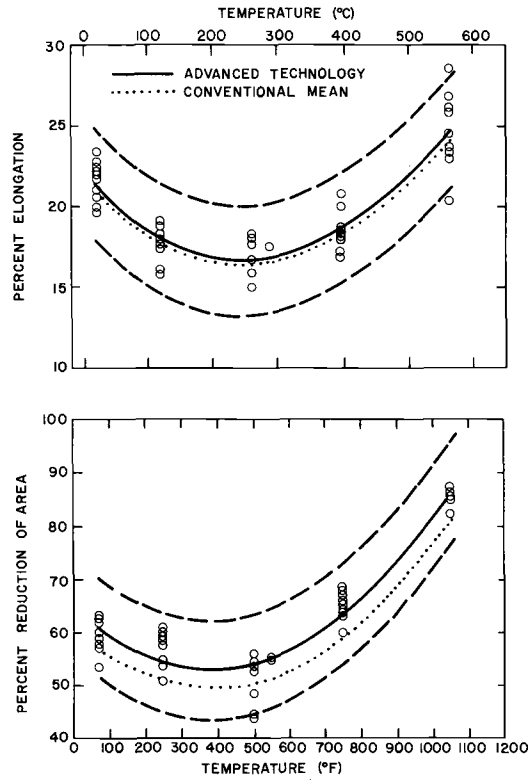


FIG. 6—Variation of tensile elongation and reduction of area with temperature (dashed lines are 95% confidence bands).

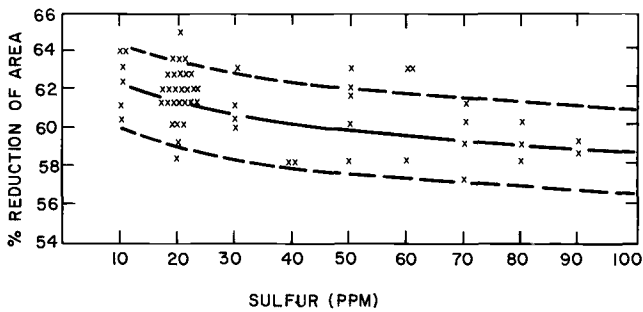


FIG. 7—Effect of sulfur content on the tensile reduction of area (courtesy: Japan Casting and Forging Corporation).

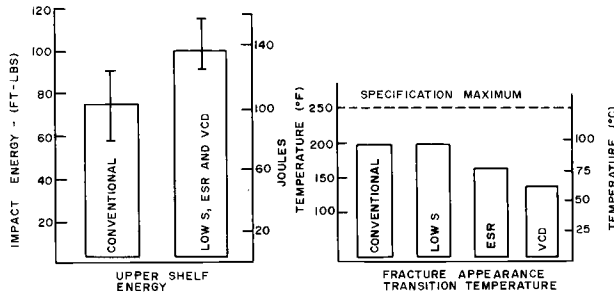


FIG. 8—Histograms of upper shelf energy and FATT.

(Table 2). These differences may be attributed to the differences in the cooling rates and temperatures between the periphery and the center during heat treatment. Compared to the conventional rotor properties, the current forgings show about 40% improvement in the upper-shelf energy values and somewhat lower FATT values. This may be due to the very low sulfur content in the present forgings, resulting in a large reduction in the number of nonmetallic inclusions, especially manganese sulfide, and improved cleanliness. The VCD rotor periphery prolongation shows unusually high Charpy impact energy of about 45 J at 24°C (33 ft-lb at 75°F) (Table 2). This may be due to the faster surface cooling rate from the final austenitizing temperature when compared to the cooling rates of the low sulfur and ESR rotors. It is believed that this increased cooling rate for the VCD forging was due to the use of air at subzero ambient temperature in the winter in northern Japan. The bore bar impact energy for the VCD rotor is only slightly higher than that of the other two rotors. The histogram shown in Fig. 8 illustrates the improvements in the upper-shelf impact energy and FATT of the advanced forgings. Figure 9 illustrates the significant improvement in the upper-shelf impact energy as the level of sulfur is reduced [11]. Higher Charpy impact energy implies

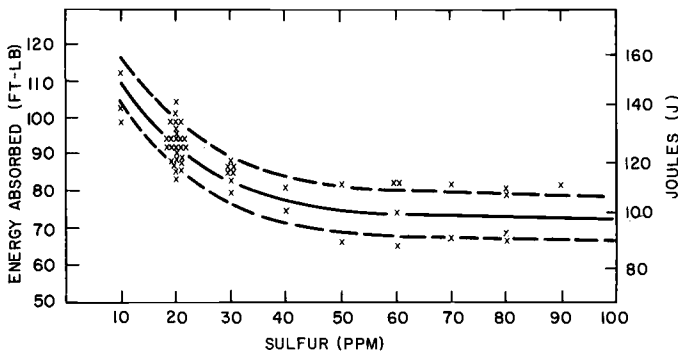


FIG. 9—Effect of sulfur content on Charpy upper-shelf energy. (Courtesy: JCFC.)

higher fracture toughness for these forgings. This yields better reliability and assurance against brittle fracture.

Relatively large amounts (greater than 0.020 weight %) of impurity elements like phosphorus, tin, and sulfur may lead to temper embrittlement. This condition leads to loss of toughness in rotor sections exposed to high temperatures [12]. In the current forgings, the impurity elements are very low. A limited temper embrittlement work was carried out in the current study. The following treatments were employed:

1. Step-Cooling Treatment

- (a) Charge into furnace at 538°C (1000°F), hold 15 h.
- (b) Furnace cool to 510°C (950°F), hold 15 h.
- (c) Furnace cool to 482°C (900°F), hold 24 h.
- (d) Furnace cool to 468°C (875°F), hold 72 h.
- (e) Furnace cool to 427°C (800°F), hold 100 h.
- (f) Furnace cool to 399°C (750°F), hold 168 h.
- (g) Furnace cool to room temperature.

2. Isothermal aging at 538°C (1000°F) for 2000 h.

The maximum shift in the FATT observed was 11°C (21°F) among the three forgings at the various test locations. This amount of change is insignificant, and essentially no embrittlement was found.

Fracture Toughness

Plane strain fracture toughness values (K_{Ic}) have been obtained from the forgings in the temperature range of 25 to 70°C (75 to 160°F) using specimens of 3T-CT and 2T-CT configurations. At the upper-shelf temperature of 150°C (300°F) and up to 427°C (800°F), the elastic plastic fracture toughness, J_{Ic} , was measured using smaller specimens [12]. The summary of the results is presented in Fig. 10. The J_{Ic} -values were converted to K_{Ic} -values using the relationship

$$K_{Ic}^2 = \frac{EJ_{Ic}}{1 - \nu^2} \quad (1)$$

where

ν = 0.3 (Poisson's ratio), and

E = Elastic modulus.

The advanced forgings show a definite improvement in the toughness values: low-sulfur rotor by 25%, the ESR rotor by about 50%, and the VCD rotor by 75% when compared to conventional rotor toughness at room temperature. Part of this toughness improvement for the VCD rotor may be attributed to the faster cooling rate from the austenitizing treatment as described previously. The J_{Ic} -

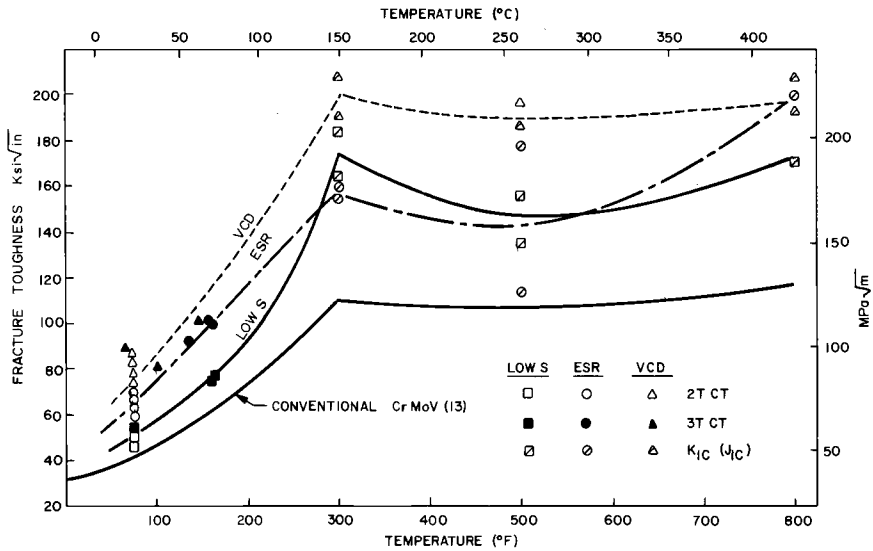


FIG. 10—Variation of fracture toughness with temperature.

values are a factor of two to three higher compared to conventional and vintage rotor forgings [13]. This level of improvement in toughness is very significant. These benefits are attributed to low sulfur levels, improved cleanliness, and controlled solidification in the original ingot. By increasing the fracture toughness of the steel, the chances of brittle fracture are reduced to a great extent since the material is more tolerant of flaws. By doubling the fracture toughness, the critical flaw size is increased fourfold. Thus, the life of the rotor will be increased significantly.

Comparison of the fracture toughness of the air-cooled Westinghouse conventional rotors, oil-quenched Kraftwerk Union (KWU) rotors [14], and the current air-cooled advanced technology rotors is shown in Fig. 11. The toughness of the current rotors is equal to or even better than that of the oil-quenched rotors produced by the European manufacturing practice.

High-Cycle and Low-Cycle Fatigue Properties

Rotating beam high-cycle fatigue tests on smooth specimens at room temperature yielded results comparable to those of the conventional forgings. The endurance limit at room temperature is about 414 MPa (60 ksi), which is about one half of the tensile strength.

Low-cycle fatigue testing under strain-controlled conditions was conducted at temperatures between 25 and 538°C (75 and 1000°F). Strain softening occurs in all cases. Room temperature strain-life behavior is similar to that of conventional steel (Fig. 12). At higher temperature, especially at 427°C (800°F), there is some

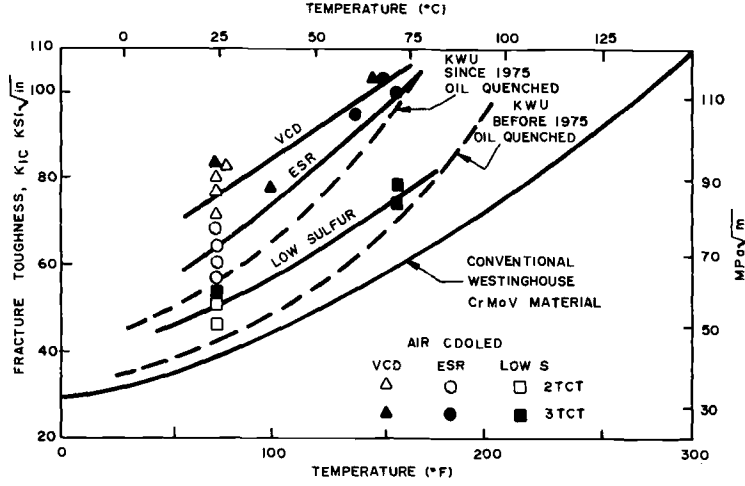


FIG. 11—Comparison of fracture toughness of low sulfur, VCD, and ESR rotors with oil-quenched rotors [14].

improvement in the strain life behavior of the advanced technology forgings. Compared to the Gallatin No. 2 material data at 427°C [2], low sulfur, ESR, and VCD material show significant improvement (Fig. 13). Since manganese-sulfide inclusions can act as crack initiation sites, especially at higher temperature [2], absence of this type of inclusions in the new forgings seems to improve the low-cycle fatigue life. At 538°C (1000°F) little improvement is noticed for the

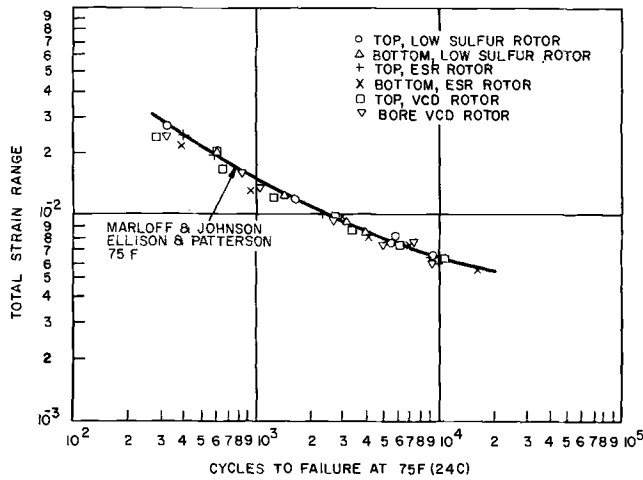


FIG. 12—Room temperature low-cycle fatigue curve.

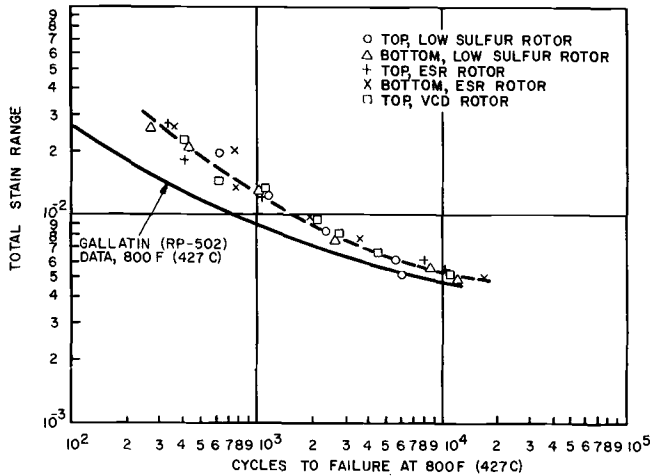


FIG. 13—Low-cycle fatigue curve at 427°C (800°F) showing improvement over vintage rotor material.

advanced technology rotor material when compared to the conventional rotor material produced in the 1970s.

Creep Properties

Creep tests were conducted using combination plain-notch bar specimens under constant load conditions. Tests were conducted at 510, 538, 565, and 593°C (950, 1000, 1050, and 1100°F). Creep lives were in the range 500 of 2000 h for various loading conditions for the three (low-sulfur, ESR, and VCD) forgings. The results are presented as stress versus Larson-Miller parameter (LMP) curves (Fig. 14). The three advanced forgings show improvement over the mean properties of the 29 conventional Westinghouse rotors. Even a small increase in creep strength will provide a significant improvement in creep life. At 538°C (1000°F) little improvement is noticed for the advanced technology rotor material produced in the 1970s.

Creep ductility is measured in terms of elongation and reduction of area from failed creep specimens. If the material is creep brittle or notch sensitive, failure may occur at the notch [15]. For creep ductile materials due to creep relaxation and the triaxial stress conditions at the notch, failure will tend to occur at the plain bar section. All of the creep specimens in the current study occurred at the plain bar section. Variation of elongation and reduction of area versus rupture life is illustrated in Figs. 15 and 16. In general, the ductility drops at longer creep lives. This drop is similar for the low sulfur and ESR forgings. However, the VCD material retains excellent ductility even at long lives. There seems to be a beneficial effect of the low silicon or low phosphorus or both on the long-

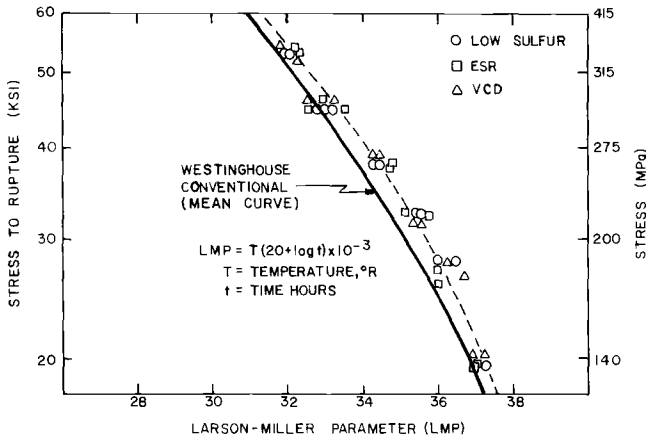


FIG. 14—Stress versus Larson-Miller parameter for the advanced technology forgings.

term creep ductility. The advanced technology rotors show much better creep ductility compared to oil-quenched rotors as illustrated in Fig. 17. The data for the oil-quenched rotors were taken from Ref 16. The tensile properties of the oil-quenched rotors are very similar to those of the current rotors. It is important to note that the data shown in this figure for the current rotors are for 565°C (1050°F), whereas for the oil-quench rotor the data are for 550°C (1022°F). The improvement in creep ductility for the current rotors may be attributed, in general, to the advanced steel melting processes. Due to the reduction of inclusions and other impurities, creep cavitation may be retarded in these steels.

It should be pointed out that modifications in the processing of the steel to

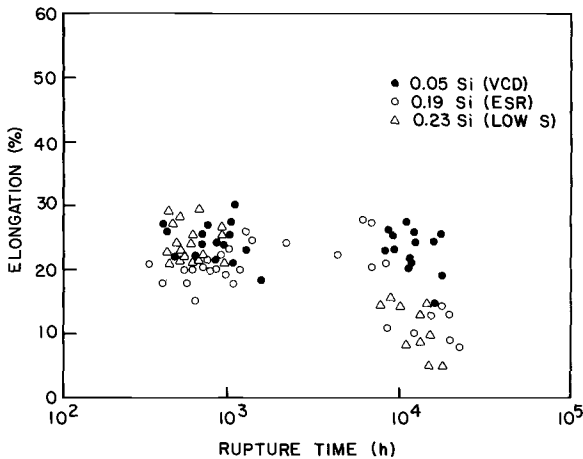


FIG. 15—Creep elongation versus rupture life.

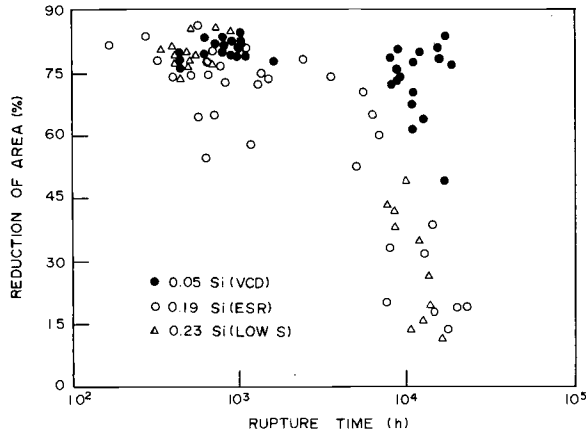


FIG. 16—Creep reduction of area versus rupture life.

improve toughness can adversely affect creep properties [17]. However, in the low-sulfur, VCD, and ESR forgings, toughness has been improved without any loss of creep strength. On the other hand, creep properties also show improvement. The VCD material, especially, shows the highest toughness and highest creep ductility.

Summary and Conclusions

The three advanced steel melting processes, namely, low-sulfur silicon deoxidation, VCD, and ESR were successful in producing three quality rotor forgings. All of these processes reduced sulfur to very low levels, to less than one tenth

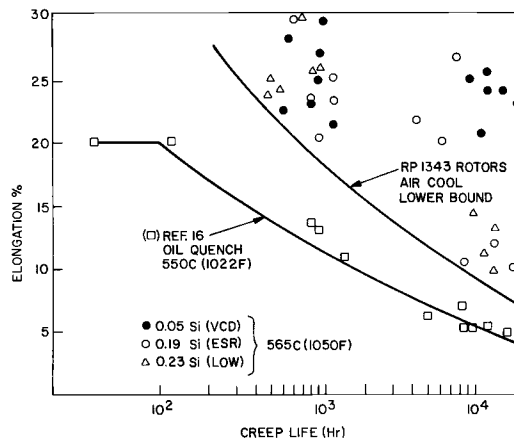


FIG. 17—Comparison of creep elongation for the air-cooled and oil-quenched rotor material.

of that in the conventionally produced steel. As a result, excellent centerline quality and cleanliness were obtained. Mechanical properties of the advanced technology rotor forgings are equal to or better than those of conventional rotors. Superiority is evident especially where the sulfur is influential, namely, tensile ductility, Charpy energy, fracture toughness, creep rupture ductility, and low-cycle fatigue life. The low-silicon VCD material has better creep ductility under long-term tests. These results prove that fracture toughness can be improved without any loss of creep properties. The toughness and creep ductility are better than or equal to those of oil-quenched rotors produced by European manufacturing practice.

Acknowledgment

The subject work was conducted under EPRI Contract RP1343-1. The authors acknowledge and thank the Electric Power Research Institute and the Westinghouse Electric Corporation for permission to publish this work. Participation in and the contribution of information to this project by the Japan Casting and Forging Corporation, Arbed Saarstahl, AG, and the Japan Steel Works are acknowledged.

References

- [1] Troiano, A. R., "General Keynote Lecture" in *Hydrogen in Metals*, Proceedings of the International Conference on the Effects of Hydrogen on Material Properties, Sept. 1973, I. M. Bernstein and A. W. Thompson, Eds., American Society for Metals, Ohio, 1974.
- [2] Kramer, L. D. and Randolph, D. D., "Analysis of the Tennessee Valley Authority Gallatin No. 2 Unit Turbine Rotor Burst, Part I: Metallurgical Considerations" in *Proceedings*, ASME-MPC symposium on Creep-Fatigue Interaction, New York, 1976, American Society of Mechanical Engineers, New York.
- [3] Kawaguchi, S. et al., "Challenge to Manufacture of Large Forgings from 500 Metric Ton Steel Ingots," *Proceedings*, International Forgemasters Meeting, Paris, France, April 1975.
- [4] Cooper, L. R., "Advanced Technology for Producing Large Forgings by Central Zone Remelting," *Proceedings*, International Forgemasters Meeting, Paris, France, April, 1975.
- [5] Jauch, R., Choudhury, A., Tince, F., and Lemor, W. R., "Present State of the Electroslag Remelting Process in Roehling-Burbach for Heavy Forging Ingots with 2300 mm Diameter," paper presented at the Third International Iron and Steel Congress, Chicago, April 1978.
- [6] Wood, R. A., "Status of Electroslag Processing for Production of Large Rotor Forgings," EPRI FP-799 final report, Electric Power Research Institute, Palo Alto, CA, July 1978.
- [7] "Forge Master Experience," in *Workshop Proceedings: Rotor Forgings for Turbine and Generators*, EPRI WS-79-235, Electric Power Research Institute, Palo Alto, CA, Sept. 1980.
- [8] Steiner, J. E., et al., "Advanced Steel Making Processes for Rotor Forgings," EPRI TPS 82-628 final report, Electric Power Research Institute, Palo Alto, CA, Dec. 1983.
- [9] Steiner, J. E., Swaminathan, V. P., and Jaffee, R. I., "Evaluation of Advanced Melting Technology for Large High Temperature Steam Turbine Rotor Forgings," *Proceedings*, Ninth International Forging Conference, Vol. 1, Duesseldorf, West Germany, May 1981, pp. 2.0.1-2.0.20.
- [10] Swaminathan, V. P., Steiner, J. E., and Jaffee, R. I., "High Temperature Steam Turbine Forgings by Advanced Steel Melting Technology," ASME Paper No. 82-JPGC-Pwr-24, Joint Power General Conference, Denver, CO, Oct. 1982, American Society of Mechanical Engineers, New York.

- [11] Sato, K. et al., "On the Properties of CrMoV Rotor Forging Produced by Low Sulfur Process," *Workshop Proceedings: Rotor Forgings for Turbines and Generators*, EPRI WS-79-235, Electric Power Research Institute, Palo Alto, CA, Sept. 1980, pp. 5-26 to 5-34.
- [12] Zhe, Q. et al., "Temper Embrittlement of CrMoV Turbine Rotor Steels," EPRI CS-2242, RP559, interim report, Electric Power Research Institute, Palo Alto, CA, Feb. 1982.
- [13] Swaminathan, V. P. and Landes, J. D., "Temperature Dependence of Fracture Toughness of Large Steam Turbine Rotor Forgings Produced by Advanced Steel Melting Processes" in *Fracture Mechanics: Fifteenth Symposium, ASTM STP 833*, R. J. Sanford, Ed., American Society for Testing and Materials, Philadelphia, 1984, pp. 315-332.
- [14] Berger, C., in discussions to "Evaluation of Advanced Melting Technology for Large High Temperature Steam Turbine Rotor Forgings" in *Proceedings, Ninth International Forging Conference*, 1981, Duesseldorf, West Germany, Vol. III, 1981, Verein Deutscher Eisenhuettenleute, Duesseldorf, West Germany, pp. 30-33.
- [15] Davis, E. A. and Manjoine, M. J., "Effect of Notch Geometry on Rupture Strength at Elevated Temperatures," in *Symposium on Strength and Ductility at Elevated Temperatures, ASTM STP 128*, American Society for Testing and Materials, Philadelphia, 1952, pp. 67-92.
- [16] Taylor, E. and Batte, A. D., "Creep Crack Formation in a 1% CrMoV Rotor Forging Steel" in *International Conference on Engineering Aspects of Creep*, Vol. 1, The Institute of Mechanical Engineering, London, 1980, pp. 225-232.
- [17] Viswanathan, R. and Jaffee, R. I., "Toughness of CrMoV Steels for Steam Turbine Rotors," EPRI RD-2357-SR, special report, Electric Power Research Institute, Palo Alto, CA, April 1982.

DISCUSSION

*J. Steiner*¹ (*written discussion*)—The copper content of the rotors in this project was typically 0.04%. Regarding Dr. Ewald's comment about his concern with copper as a residual, I agree with Dr. Jaffee that copper can be controlled through the use of "clean" basic oxygen steel scrap fed to the electric arc furnace. However, the modern heavy forge shop, with its relatively low raw steel tonnage requirements, usually does not have access to basic oxygen steel or basic oxygen steel scrap. Thus, the residual build-up problem, especially with regard to copper and tin, becomes a crucial economic problem for the heavy forgings producer and ultimately becomes a potential technical problem for the consumer.

*W. Wiemann*² (*written discussion*)—I would like to add some comments and hints to the excellent presentation of Dr. Swaminathan.

1. We did investigations on the test materials within the EPRI RP 1343, too, and found—within normal scatter from laboratory to laboratory—the same results.

2. The K_{Ic} - T curves cited from Kraftwerk Union were minimum curves in comparison to the mean curves of Dr. Swaminathan.

¹ Engineering Materials & Processes, Inc., Pittsburgh, PA 15217.

² Kraftwerk Union AG, D-4330 Muelheim a.d. Ruhr, West Germany.

3. The ductility after long-time creep tests up to about 20 000 h leads to rather low values in the case of ESR forging, too. We have investigated several ESR 1Cr-Mo-Ni-V forgings and up to now have found good ductility even in the transverse direction within these materials. Therefore, I would like to ask whether the aluminum content is unusually high in this specific RP 1343 ESR forging (see Table 1).

Answer to a discussion from floor—(Additional information to a question from the auditorium to FATT shift after long-time exposure at 538°C.) We have 1Cr-Mo-Ni-V oil-quenched core material at 530°C exposed for 90 000 h and generally found no variation in FATT.

Soft-Martensitic Stainless Cr-Ni-Mo Steel for Turbine Rotors in Geothermic Power Stations

REFERENCES: Schönfeld, K. and Potthast, E., “Soft-Martensitic Stainless Cr-Ni-Mo Steel for Turbine Rotors in Geothermic Power Stations,” *Steel Forgings, ASTM STP 903*, E. G. Nisbett and A. S. McIlilli, Eds., American Society for Testing and Materials, Philadelphia, 1986, pp. 143–154.

ABSTRACT: Steel Grade X5 Cr-Ni-Mo 12 6 containing 0.05% carbon, 12% chromium, 6% nickel, and 1.50% molybdenum is an advantageous material for turbine rotors in geothermic power stations because of its excellent strength and toughness properties in combination with good erosion and corrosion resistance.

In terms of the phase diagram, this soft-martensitic steel has its place at the martensite/austenite/ferrite interface. Therefore, its chemical composition must be chosen so as to have a completely martensitic structure after hardening. During tempering above 773 K (500°C), austenite is precipitated in finely dispersed form in the tempered martensite. This secondary austenite improves the toughness, is extremely stable, and does not transform even at temperatures down to approximately 73 K (–200°C).

The manufacture of and the mechanical properties of a turbine rotor 1200 mm in diameter by 5600 mm in length with a finished weight of approximately 21.5 tons are described in detail.

KEY WORDS: soft-martensitic stainless Cr-Ni-Mo steel, turbine rotor, geothermic, high toughness combined with good strength, austenite formation during tempering

In recent years, the search for alternative sources of energy has led to the development of methods to use geothermic heat for the generation of electrical power.

In 16 countries, power stations with a total of 2400 MW are already in operation [1], with a further 2000 MW being scheduled. This means that the utilization of geothermic energy is still at an early stage. In the future, however, this type of energy may reach a total capacity of 15 000 MW, according to forecasts [2,3].

Geothermic heat is used via water or steam. The water/steam mixture places high demands on the corrosion and erosion resistance of components because of its chemical composition, which includes carbon dioxide (CO₂), hydrogen sulfide

¹ Engineer and ²chief engineer, Quality and Materials Engineering, ARBED Saarstahl, Völklingen, Germany.

(H₂S), hydrogen (H₂), methane (CH₄), nitrogen (N₂), and ammonia (NH₃). Therefore, stainless steel may be the appropriate material for turbine rotors, depending on operating conditions.

Martensitic steels containing 13 to 17% chromium have sufficient corrosion resistance combined with high strength, but only limited toughness. Austenitic chromium-nickel steels, on the other hand, have good corrosion resistance, but insufficient strength, which limits their usability.

This is where soft-martensitic stainless steels come in. The importance of these steels has grown rapidly in recent years. They are frequently used in the form of shafts, disks, rings, blades, and valve components in the following applications: chemical engineering, food processing machines, pumps, centrifuges, paper machines, nuclear engineering, as well as in the form of turbine rotors in power stations.

Brenzina [4] has given a comprehensive description of soft-martensitic stainless steels. Their main characteristics are:

1. High yield strength.
2. High toughness.
3. Excellent through-hardening ability.
4. Good weldability, also of large cross sections.
5. Corrosion resistance.
6. Resistance to erosion.

Of the great number of soft-martensitic stainless steels that have become known, it is Grade X5 Cr-Ni-Mo 12 6 which is used in turbine rotors for geothermic power stations. This steel has the following mean chemical analysis: 0.05% carbon, 12% chromium, 6% nickel, and 1.6% molybdenum. In terms of the phase diagram, its place is at the martensite/austenite/ferrite interface. The transformation behavior of the usual martensitic chromium steels is characterized by a retarded transformation in the pearlitic range and the suppression of transformation in the bainitic range. As a result, transformation takes place mainly in the martensitic range. In the case of soft-martensitic steels, transformation in the pearlitic range is completely suppressed by the addition of nickel. As a result, the transformation of this steel takes place only in the martensitic range, even if it is cooled in air. The location of the transformation points is greatly influenced by alloying elements. Therefore, the chemical composition must be carefully chosen to ensure that the desired transformation in the martensitic range takes place above room temperature during hardening and to prevent the formation of austenite or ferrite. It is the low carbon content of 0.05%, in particular, which accounts for the formation of soft martensite. When the steel is tempered above 773 K (500°C), austenite is precipitated in finely dispersed form in the tempered martensite. This secondary austenite increases the toughness, is extremely stable, and does not transform, even at temperatures down to 73 K (–200°C). Because of the great effect of the chemical composition on the structure and, hence, on

the mechanical properties, analysis ranges must be very closely controlled and segregation must be largely eliminated, especially in heavy forgings [2].

Study of Experimental Melts

The manufacture of large forgings was preceded by small experimental melts, which were tested to determine how the mechanical properties are affected by chemical composition, forging reduction, and heat treatment.

Two ingots with a 190-mm mean diameter and a 150-kg weight were poured from two induction-melted heats.

The ingots could be assumed to be sufficiently segregation-free. Figure 1 shows the chemical composition of the experimental melts. The two melts were largely identical except for the chromium and nickel contents, which were varied within the range specified for turbine rotors.

The 150-kg ingots were forged without difficulty at temperatures between 1423 and 1123 K (1150 and 850°C) to sizes from 130 to 60-mm square, representing reduction ratios between 2/1 and 10/1.

To clarify the metallurgical context, dilatometer curves were established and the magnetic saturation was measured. The transformation temperatures for both melts are shown in Fig. 1. It can be seen that the slight change in chromium and nickel contents has an extraordinary effect on the transformation temperatures. For example, the lower chromium and nickel contents of Melt E 131 give a 55° higher temperature for the martensite formation. This is very important in connection with the requirement for transformation to be completed in the martensitic range. The beginning of austenite formation also is shifted towards a higher temperature. This is of importance for the tempering treatment, for which customer specifications require a minimum temperature of 853 K (580°C) in the first tempering cycle.

Chemical composition								
Melt	C	Si	Mn	P	S	Cr	Mo	Ni
E 130	0,034	0,13	0,50	0,007	0,005	12,4	1,48	6,87
E 131	0,030	0,15	0,47	0,005	0,004	11,8	1,43	5,74

Transformation temperatures				
Melt	A_{C1A}	A_{C1E}	M_S	M_F
E 130	808°K(535°C)	1023°K(750°C)	433°K(160°C)	≤ Rt
E 131	818°K(545°C)	1023°K(750°C)	488°K(215°C)	≥ Rt

FIG. 1—Chemical composition and transformation temperatures of experimental melts of X5 Cr-Ni-Mo 12 6 steel.

Melt	Tempering temperature				
		573°K (300°C)	773°K (500°C)	853°K+848°K (580°C+575°C)	873°K (600°C)
E 130	Percentage of austenite	0	1	35	45
E 131	"	0	0	16	26

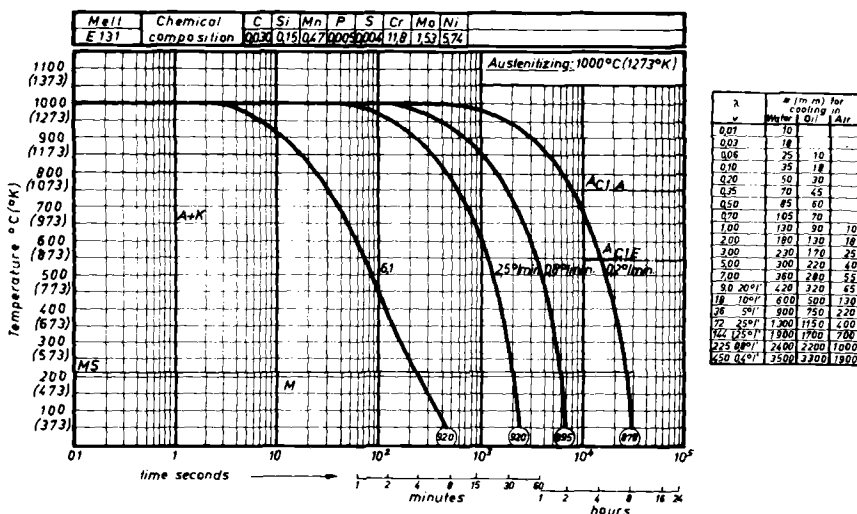
FIG. 2—Percentage of austenite after tempering of experimental melts of X5 Cr-Ni-Mo 12 6 steel (determined by saturation magnetization).

Tempering causes a partial retransformation of martensite into austenite, which was confirmed by magnetic saturation measurements. Specimens were hardened at 1273 K (1000°C) and subsequently double-tempered. Tempering temperatures and related martensite percentages are shown in Fig. 2.

The results of the dilatometer test were confirmed. Melt E 131 with the lower chromium and nickel contents shows the lower austenite percentages with increasing tempering temperatures.

Figure 3 shows the transformation behavior of Steel Grade X5 Cr-Ni-Mo 12 6. In the case of Melt E 131, the transformation of this steel takes place exclusively in the martensitic range with cooling rates up to $0.2^{\circ}/\text{min}$. This slow cooling rate also occurs in the core of forgings having over a 2000-mm diameter. Therefore, transformation cannot happen in the bainitic or pearlitic range in large turbine rotors, even if they are cooled in air.

The tempering diagrams shown in Figs. 4 and 5 apply to a hardening temperature of 1273 K (1000°C). Figure 4 shows the tensile strength and the 0.2%



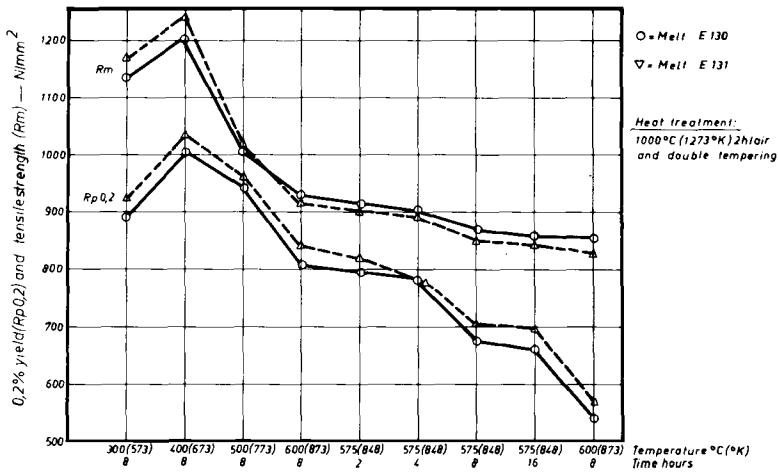


FIG. 4—0.2% yield and tensile strength versus tempering temperatures of X5 Cr-Ni-Mo 12 6 steel.

yield strength and Fig. 5 shows the elongation, reduction of area, and impact energy as functions of the tempering temperature. These results show that low-tempering temperatures can be used to achieve high-tensile properties combined with good toughness. With increasing tempering temperature, tensile strength and 0.2% yield strength are continuously decreasing, while elongation and reduction of area remain relatively unaffected.

The impact energy, however, is characterized by a steep increase from approximately 100 to approximately 170 J at 773 K ($500^{\circ}C$), as shown in Fig. 5.

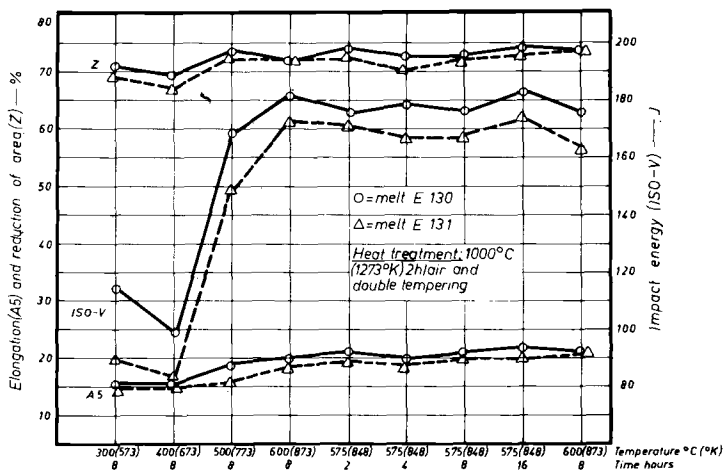


FIG. 5—Elongation, reduction of area, impact energy versus tempering temperature of X5 Cr-Ni-Mo 12 6 steel.

The percentage of secondary austenite decreases again above 873 K (600°C) tempering temperature due to diffusion, which has a destabilizing effect and finally causes the formation of transformable austenite. As a result, an increase in strength and a reduction in impact energy must be anticipated. Differences in mechanical properties between both experimental melts are small. However, Melt E 131 with the lower chromium and nickel contents shows a slightly higher 0.2% yield strength and a correspondingly lower toughness.

On the basis of the results available and in response to customer specifications, the following treatment was chosen for all other specimens:

- Hardening: 1273 K (1000°C)—2 h—air
 1. Tempering: 853 K (580°C)—8 h—air
 2. Tempering: 848 K (575°C)—8 h—air

Figure 6 gives the results of tension tests at elevated temperatures up to 673 K (400°C). These values, too, revealed no inconsistencies.

As in the manufacture of heavy forgings, the reduction ratio has a considerable effect on mechanical properties; the experimental ingots were forged with reduction ratios of 2, 3.5, 5, and 10/1 prior to heat treatment and mechanical testing. A significant influence of the reduction ratio was not found, as shown by the impact values in Fig. 7. In this figure impact energy is plotted versus temperature up to 77 K (−196°C) for reduction ratios of 2 and 10/1.

What has to be noted, apart from the insignificant effect of the reduction ratio, is the small difference between longitudinal and transverse values, which suggests a high homogeneity of the experimental steel. Figure 7 also shows that a noticeable decrease of impact energy only occurs when the temperature has dropped below 173 K (−100°C) and that there is no marked ductile-to-brittle transition.

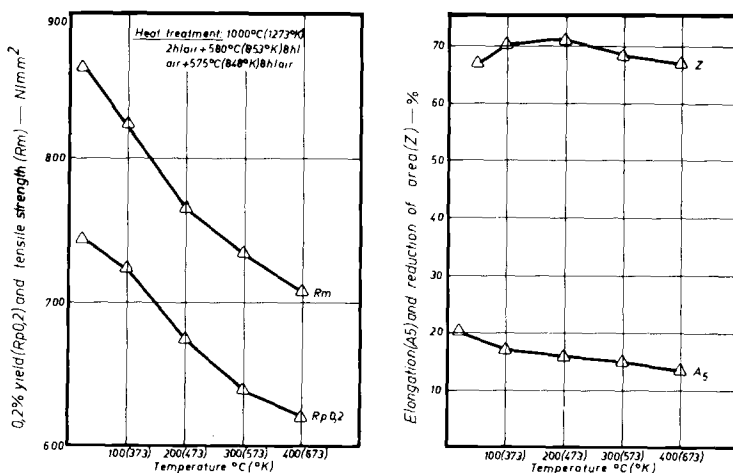


FIG. 6—Mechanical properties at elevated temperatures of X5 Cr-Ni-Mo 12 6 steel.

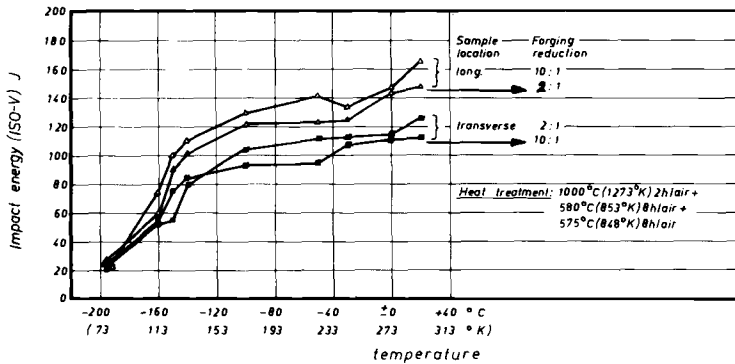


FIG. 7—Impact energy versus test temperature and forging reduction for Experimental Melt E 131 of X5 Cr-Ni-Mo 12 6.

The test results obtained on the two 150-kg experimental melts allow the following conclusions:

The transformation behavior of Soft-martensitic Steel X5 Cr-Ni-Mo 12 6 greatly depends on the chemical composition. As a result, the chemical composition must be kept within close tolerances. But this also means that macroscopic segregations, which are inevitable in large forging ingots, have a great influence on mechanical properties. To eliminate these segregations, conventional ingots must be subjected to a homogenizing treatment [2]. However, the best method to avoid these segregations is the electroslag remelting (ESR) process. In ingots produced by this method, transformation is completed in the martensitic range even in large cross sections of up to 2000 mm in diameter subjected to air quenching.

The advantage of the soft-martensitic steel over conventional stainless chromium and chromium-nickel steels is documented by its high tensile properties in combination with excellent toughness even at low temperatures. However, tempering must take place in the range between 823 and 873 K (550 and 600°C) in order to allow the formation of a finely dispersed secondary austenite.

In processing Steel Grade X5 Cr-Ni-Mo 12 6, no particular difficulties have to be expected.

Manufacture of a Turbine Rotor

A turbine rotor with a 1200-mm maximum body diameter, 5600-mm length, and 21.5 ton finished weight has been manufactured for a 105-MW power station in California. This rotor has the same chemical composition as the experimental steel.

	C	Si	Mn	P	S	Cr	Mo	Ni
ESR-melt 40 413	0,04	0,12	0,52	0,014	0,004	11,8	1,46	5,75
Turbine rotor								
Body	0,05	0,13	0,50	0,016	0,004	11,8	1,45	5,85
Journal	0,045	0,12	0,52	0,015	0,004	11,8	1,48	5,82
Axial core	0,05	0,13	0,52	0,017	0,003	11,6	1,46	5,80

FIG. 8—Chemical composition of X5 Cr-Ni-Mo 12 6 ESR melt and of turbine rotor.

The rotor was made from an 85-ton ESR ingot with a 2300-mm diameter. At present, a second rotor measuring 1200 mm in diameter by 4700 mm and weighing 16 tons in the finished condition is being manufactured from the same ingot.

The chemical composition of ESR Melt 40413 is given in Fig. 8 along with the check analysis values of the rotor. After equalization of temperature, the ESR ingot was heated to 1523 K (1250°C) forging temperature. The rotor was forged in six heats including cogging and upsetting on our 60-MN press. Final forging temperature was 1073 K (800°C). The forging sequence is illustrated in Fig. 9.

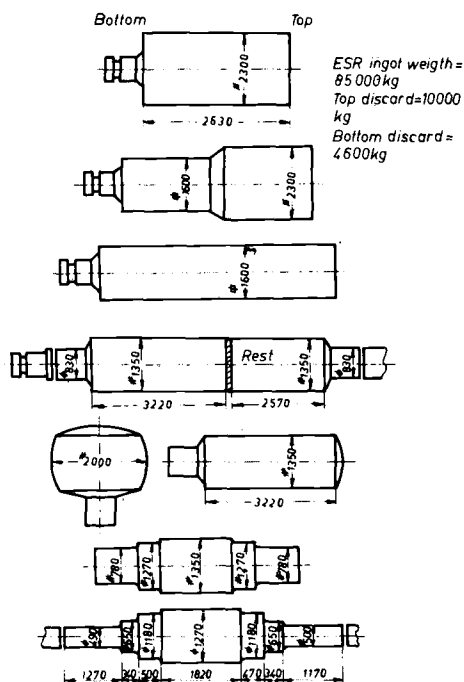


FIG. 9—Forging sequence of ESR Ingot 40413.

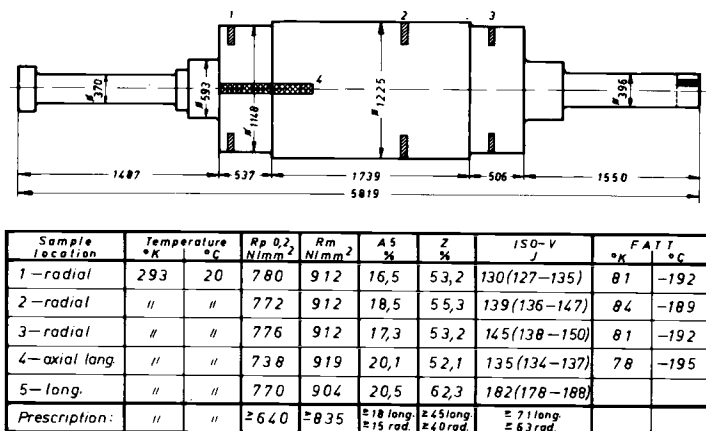


FIG. 10—Heat treatment contour and test results of ESR X5 Cr-Ni-Mo 12 6 turbine rotor.

After cooling in air, the rotor was subjected to ultrasonic examination and machined to the dimensions shown in Fig. 10. It was then austenitized at 1273 K (1000°C) for 23 h and cooled in air. Tempering took place at 853 K (580°C) for 20.5 h and at 848 K (575°C) for 18.5 h, followed by furnace cooling. During subsequent ultrasonic examination, no indications were found, the minimum detectable defect size being 1.8 mm Distance Gain Size (DGS).

Testing of the radial bore cores from Body Locations 1, 2, and 3 (Fig. 10) as well as from the journal (Sample Location 5) gave excellent results, which are shown in Fig. 10. The uniformity of the properties in the various locations is remarkable. Testing of the axial core (Sample Location 4) also revealed the good

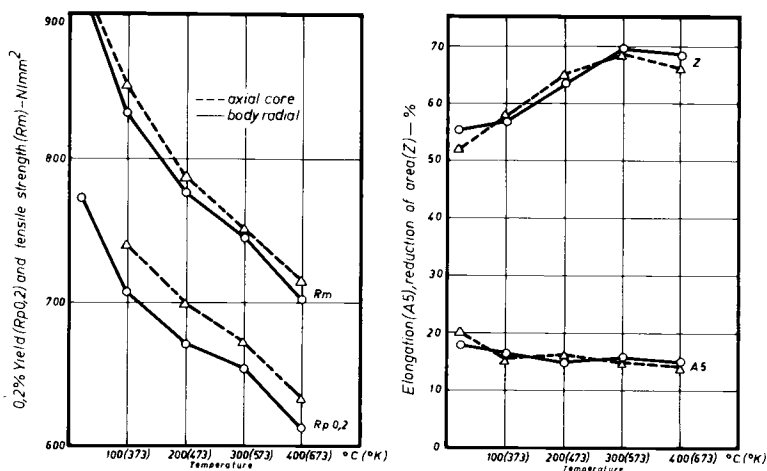


FIG. 11—Mechanical properties at elevated temperatures of ESR X5 Cr-Ni-Mo 12 6 turbine rotor.

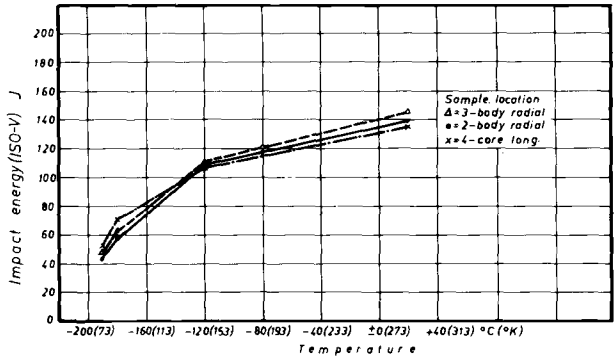


FIG. 12—Impact energy of ESR X5 Cr-Ni-Mo 12 6 turbine rotor.

through-hardenable of the forging with little scatter over the cross section. These results agree well with those obtained on the experimental melts. Apart from the high-impact energy, the fracture appearance transition temperature (FATT) also is remarkable [from 85 to 78 K (−188 to −195°C)] as determined on radial specimens from the rim and on axial specimens).

Tensile properties at elevated temperature (Fig. 11) and impact energy at low temperatures (Fig. 12) were determined on test material from the body and from the axial core. The uniformity of the properties in the various sample locations was again shown by these tests. This homogeneity also is confirmed by the check analysis given in Fig. 8.

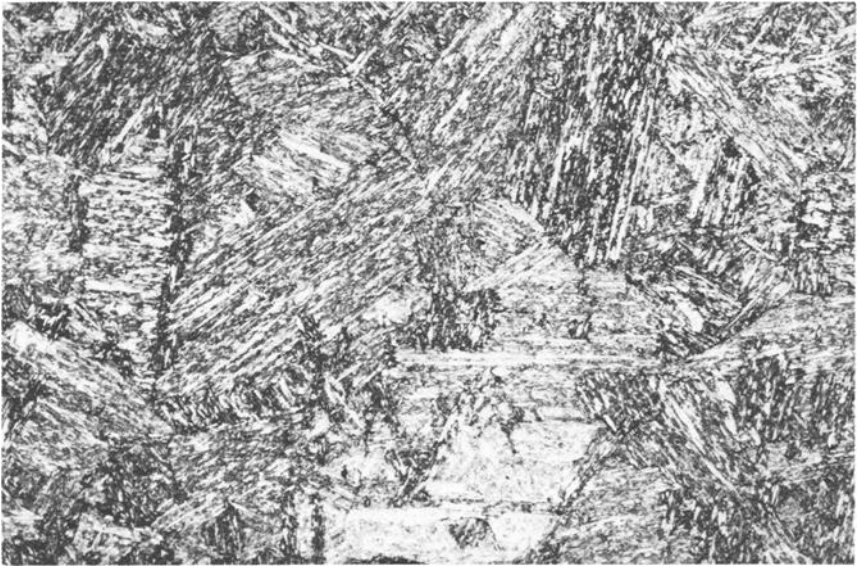


FIG. 13—Structure of soft-martensitic steel X5 Cr-Ni-Mo 12 6 (body of turbine rotor).

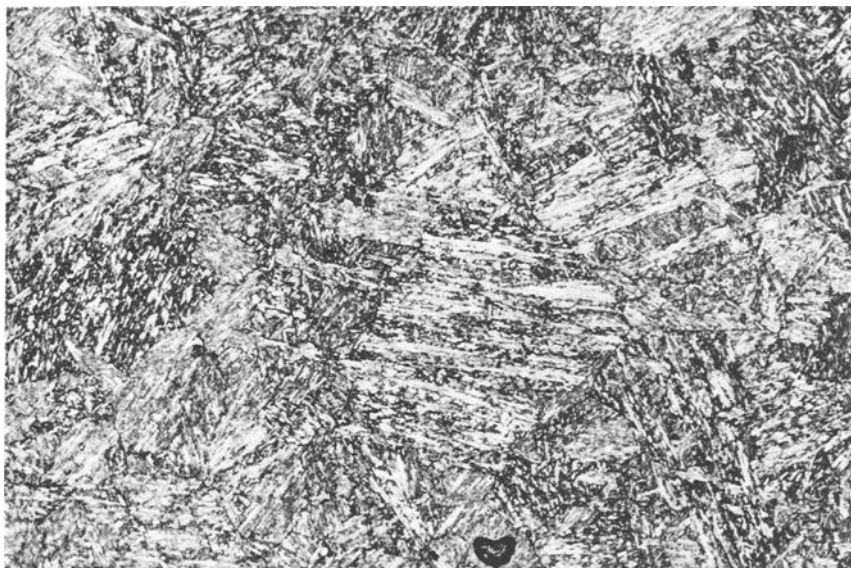


FIG. 14 · Structure of Soft-martensitic Steel X5 Cr-Ni-Mo 12 6 (journal of turbine rotor).

Figures 13 and 14 show the structure in the body and in the journal.

Summary

The transformation behavior and the mechanical properties of Steel Grade X5 Cr-Ni-Mo 12 6 were examined in extensive tests conducted on two 150-kg experimental melts. It was found that variations as small as from 11.8 to 12.4% in chromium and from 5.7 to 6.9% in nickel contents already cause a noticeable shift of the transition points. With chromium and nickel contents at the upper limit, transformation in the martensitic range is only completed below room temperature.

Therefore, the chemical composition must be very closely controlled and suitably matched to the transformation behavior so as to give a martensitic structure without austenite or ferrite after hardening. During tempering between 843 and 853 K (570 and 580°C) austenite is precipitated in finely dispersed form within the martensite. This secondary austenite accounts for the excellent toughness in combination with high strength.

Because of the great compositional effect on the properties, the steel—in particular heavy forgings—should be largely segregation free. This requirement is best fulfilled by electroslag remelting.

After completion of laboratory tests, we manufactured a turbine rotor 1200 mm in diameter by 5600 mm in length with a finished weight of approximately 21.5 tons. The rotor was forged from an 85-ton ESR ingot with a 2300-mm diameter on a 60-MN forging press. After machining, the rotor was austenitized

at 1273 K (1000°C), then cooled in air and double-tempered at 853 and 848 K (580 and 575°C), respectively. On radial specimens taken from the body as well as on longitudinal and axial specimens, the following average values were determined: strength—915 N/mm², 0.2% yield strength—740 N/mm², elongation—18.5%, reduction of area—53%, and impact energy ISO-V approximately 135 J.

Apart from the high-impact strength, the FATT is also remarkable [83 K (−190°C) as determined on radial specimens from the rim and on axial specimens]. Tension tests at elevated temperatures up to 673 K (400°C) revealed no inconsistencies in mechanical properties. Results show that the soft-martensitic stainless steel described in this paper retains its particular properties also in large turbine rotors.

References

- [1] Haenel, R., *Umschau*, 1982, pp. 53–55.
- [2] Priante, M. and Callegari, L., *Proceedings*, International Forging Conference, 1981, Düsseldorf, Germany.
- [3] Pasch, K. H., *Erdöl und Kohle-Erdgas-Petrochemie*, Vol. 35, pp. 483–486.
- [4] Brenzina, P., "Mitteilungen," Escher Wyss, 1980, Vol. 1/2, pp. 218–236.

DISCUSSION

*G. Oakes*¹ (*written discussion*)—The steel is susceptible to cracking during cooling due to high transformation stresses resulting from low M_s and M_f temperatures. In the manufacture of the turbine rotor, was it cooled to room temperature between austenitizing and tempering?

K. Schönfeld and E. Potthast (*authors' closure*)—Our experience shows that this steel is not susceptible to stress cracking during heat treatment. The turbine rotor was cooled to room temperature after austenitizing.

Question from Floor—Geothermal steam contains H₂S. What is experience with susceptibility to stress conversion cracking.

*Koren*² (*closure*)—Tests by Italian and Swedish turbine companies show better resistance of new steel as compared to low-alloyed rotor steel and 13Cr-4Ni steel. Maximum resistance, however, can be achieved by double intercritical heat treatment as practiced for compressor parts under NACE requirement HRC maximum 23. Yield strength is about 590 N/mm².

¹ Sheffield Forgemasters, England.

² VÖW (Böhler), Austria.

Turbine and Generator Forgings

Rotor Assessment

Metallurgical Analysis of Flaws in Carbon-Molybdenum and Nickel-Molybdenum-Vanadium Turbine Rotor Forgings

REFERENCE: Toney, S., Kim, W., Melilli, A. S., and Leone, S. G., “**Metallurgical Analysis of Flaws in Carbon-Molybdenum and Nickel-Molybdenum-Vanadium Turbine Rotor Forgings**,” *Steel Forgings, ASTM STP 903*, E. G. Nisbett and A. S. Melilli, Eds., American Society for Testing and Materials, Philadelphia, 1986, pp. 157–177.

ABSTRACT: The origins of metallurgical flaws in the vicinity of a 2.7Ni-0.5Mo-0.1V low-pressure (LP) rotor bore and on the bore surface of a 0.25C-0.5Mo high-pressure (HP) rotor, found after approximately 360 000 h of operation of a 50-MW tandem-compound, double-flow steam turbine, have been determined. LP rotor ultrasonic indications, the largest being equivalent to a 3.3-mm (0.13-in.)-diameter flat-bottom hole, were determined to be the result of void formation during ingot solidification shrinkage. Magnetic particle indications, maximum length of approximately 64 mm (2.5 in.) axially, on the HP rotor bore surface are a consequence of the intersection of a near-planar array of manganese-silicate inclusions by the bore hole. Evidence of service-induced transgranular growth of the HP-rotor flaw, predicted by the fracture mechanics analysis, is shown together with the actual-and-predicted flaw size and flaw location correlation for the LP and the HP rotors, respectively. The results of the metallurgical analysis, performed to characterize the nature of the LP and HP rotor flaws, and the low- and high-temperature tests, performed to determine whether the approximately 360 000 h of exposure of the 0.25C-0.5Mo HP rotor alloy to 722 K (449°C) adversely affected stress rupture strength or fracture toughness, are presented.

KEY WORDS: metallurgical analysis, low-alloy steels, forgings, rotor, steam turbine, flaws, inclusions, voids, crack propagation, stress rupture strength, temper embrittlement

A 50-MW tandem-compound, double-flow steam turbine was taken out of service for a planned inspection and rework. The general construction of the unit

¹ Manager—Metallurgical Engineering, General Electric Co., Lynn, MA 01910.

² Metallurgist, Engineer, General Electric Co., Lynn, MA 01910.

³ Manager, Materials and Process Engineering, General Electric Co., Lynn, MA 01910.

⁴ Technical leader, Mechanical Design, General Electric Co., Lynn, MA 01910.

is shown in Fig. 1. This steam turbine, which had a 2.7Ni-0.5Mo-0.1V low-pressure (LP) rotor and a 0.25C-0.5Mo high-pressure (HP) rotor, had been in service for more than 41 years. The rotor forgings were made from open hearth steels long before the advent of modern inspection methods. On the basis of available information, there had been no prior in-service inspection of the turbine rotors. Ultrasonic inspection of the near-bore zone of the LP rotor with the Dataq⁵ computerized system revealed approximately 13 000 indications. These flaw indications extended almost the full length of the rotor and were indicated to be concentrated within one quadrant of the rotor cross section. The size range of these ultrasonic indications was determined to be equivalent to flat-bottom hole diameters of 0.8 to 3.3 mm (0.03 to 0.13 in.). Visual examination of the HP-rotor bore surface revealed cracklike indications at a location corresponding to the seventh-stage wheel. Subsequent magnetic particle inspection confirmed the presence of two near diametrically opposite indications which extended approximately 64 mm (2.5 in.) axially on the 51-mm (2-in.)-diameter bore surface. On the basis of a 2.25-MHz ultrasonic inspection from the periphery of the HP rotor with a 13-mm (0.5-in.) transducer and the observation of cracklike indications on the bore surface in the vicinity of the ultrasonic indication, it was estimated that the maximum radial depth of these flaw indications was about 13 mm (0.5 in.) at a location 2311 mm (91 in.) from the coupling end. Since crack propagation from natural and service-induced flaws to a critical size has resulted in serious steam turbine and turbine-generator failures [1-4], it was essential that the nature of these flaw indications be determined and whether any service-induced growth

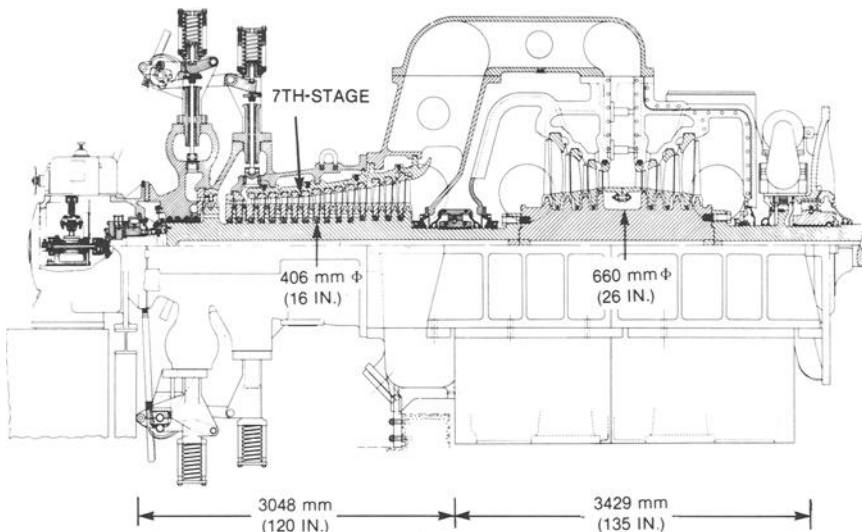


FIG. 1—General construction of 50-MW tandem-compound, double-flow steam turbine.

⁵ Trademark of the General Electric Co.

had occurred. It was also of interest to determine why the LP rotor ultrasonic indications were concentrated on one side of the bore hole.

Flaw indications found in utility and industrial steam turbine and generator rotors can be of major concern to both the user and equipment manufacturer. The opportunities to physically remove such flaws, particularly those in rotors which have been in service for a long time and subjected to cyclic loading conditions, and to perform a detailed metallurgical analysis and characterization of the actual flaws generally are rare. The information obtained in such investigations contributes toward more effective utilization of the flaw size and flaw location predictions made by nondestructive inspection of turbine and generator rotors. It should be noted that periodic in-service inspection of industrial and utility steam turbines has been recommended, particularly those made prior to modern steelmaking processes and nondestructive inspection techniques, to minimize the likelihood of field problems [5].

Fortunately, the location of the flaw indications made possible the removal of bore core samples containing ultrasonic indications possibly typical of those found along the length of the LP rotor. It also was possible to contain within a bore core sample the primary flaws corresponding to the magnetic particle indications (MPI) on the HP rotor bore surface. Since the steam-inlet end of the HP rotor was subjected to prolonged exposure at temperatures within the temper embrittlement range for alloy steels [6], attention was given to a determination of the occurrence, if any, of service-induced embrittlement. Charpy V-notch specimens obtained from the bore samples were used for transition temperature determinations, and the fracture surfaces were examined with a scanning electron microscope (SEM) for characterization of the low-temperature fracture mode. In addition to a determination of whether there was a significant shift in the 50% shear fracture appearance transition temperature (FATT) for the carbon-molybdenum HP rotor material exposed to 722 K (449°C) for 360 000 h, it was also of interest to determine whether there was a degradation of stress rupture strength. The comparison of data obtained for bore core samples taken from the relatively low-temperature coupling end and the high-temperature end of the HP rotor made it possible to determine whether the prolonged exposure at 722 K (449°C) affected stress rupture strength or microstructure.

A fracture mechanics analysis was performed to evaluate the significance of the HP rotor flaws on the bore surface. This analysis predicted that low-cycle fatigue flaw growth most likely had occurred, a prediction consistent with the metallurgical analysis of the bore surface flaw in the HP rotor.

Materials and Test Procedure

Materials

The test material used in this investigation included a bore core sample, designated BCS-GE, trepanned from the generator end of the 2.7Ni-0.5Mo-0.1V LP rotor and three bore core samples, designated BCS Nos. 1–3, trepanned from

the 0.25C-0.5Mo HP rotor. A single bore core sample was removed from the generator end of the LP rotor. This bore core sample had dimensions of 206 mm (8 $\frac{1}{8}$ in.) outside diameter by 127 mm (5 in.) length with a bore-hole diameter of approximately 96 mm (3.8 in.). The equivalent flat-bottom hole diameters corresponding to the ultrasonic indications found by the Dataq bore ultrasonic inspection system were determined to be 0.76 to 3.3 mm (0.03 to 0.13 in.). Contact ultrasonic inspection from the periphery surface of the bore core sample confirmed that the indications were concentrated within a 140° sector of the cross section on one side of the bore hole.

The three bore core samples, BCS Nos. 1–3, trepanned from the HP rotor, were located 330 mm (13 in.), 2286 mm (90 in.), and 2667 mm (105 in.), respectively, from the coupling flange. The maximum temperatures corresponding to BCS Nos. 1, 2, and 3 were estimated to be 344 K (71°C), 644 K (371°C), and 722 K (449°C), respectively. BCS No. 1 corresponded to HP-rotor material whose low- and high-temperature properties and microstructure are representative of the as-mill, heat-treated condition. The location of BCS No. 2 included the two near diametrically opposite bore surface indications. This sample permitted metallurgical analysis of the bore surface indications and a determination of their actual size. BCS No. 3 was obtained for determination of the effect of service exposure at 722 K (449°C) on low- and high-temperature properties and microstructure. The approximate dimensions of these bore core samples are 103 mm (4 $\frac{1}{16}$ in.) outside diameter by 51 mm (2 in.) inside diameter by 152 mm (6 in.) length; the outside diameter of BCS No. 3 was 106 mm (4 $\frac{3}{16}$ in.).

The chemical composition and mechanical properties of the LP and HP rotors, as reported on mill test certificates, are summarized in Table 1. The chemical composition of the LP rotor was intended to permit heat treatment to achieve the required mechanical properties. The HP rotor was made of a 0.40 to 0.60% molybdenum alloy steel. With respect to mill heat treatment of the forgings, it is only known that liquid-medium quenching was not allowed.

Test Procedure

The innermost end of the LP-rotor sample, BCS-GE, was surface ground and a sulfur print made to determine the uniformity of segregation with respect to the bore hole and the 140° sector of the cross section within which the ultrasonic indications were known to be concentrated. Macroscopically visible voids were apparent in the ground cross sections within the zone corresponding to the location of the ultrasonic indications. The nature of the voids corresponding to ultrasonic indications was determined by optical and scanning electron microscopy. Subsequent to the characterization of these voids, tangential and longitudinal tensile specimens were taken at locations within and outside the zone of the ultrasonic indications. Samples for determination of chemical composition were similarly located. Charpy V-notch specimens with axially oriented notches were machined only from a location outside the zone of ultrasonic indications. Brinell hardness

TABLE 1—Chemical composition of the low and high-pressure rotors.

Rotor	Data Source	Test Location	Weight %											ppm		
			C	Mn	P	S	Si	Cr	Ni	Mo	V	Al	Cu	Sn	As	Sb
LP	Mill TC		0.30	0.75	0.032	0.027	0.21	...	2.49	0.44	0.03
LP	BCS-GE	zone/UTI ^a	0.33	0.87	0.042	0.027	0.22	0.06	2.68	0.48	0.07	0.02	0.04	100	100	24
LP	BCS-GE	zone/No UTI	0.37	0.83	0.044	0.032	0.22	0.07	2.70	0.46	0.07	0.02	0.04	100	110	26
HP	Mill TC		0.27	0.75	0.029	0.031	0.24	0.60
HP	BCS No. 1	0.33 m from CF ^b	0.23	0.70	0.024	0.027	0.21	0.06	0.16	0.49	0.03	0.01	0.11	100	75	13
HP	BCS No. 2	2.29 m from CF	0.24	0.69	0.026	0.033	0.22	0.06	0.16	0.53	0.03	0.01	0.11	100	82	14
HP	BCS No. 3	2.67 m from CF	0.27	0.67	0.031	0.036	0.22	0.06	0.16	0.53	0.03	0.01	0.12	100	86	16

^a Test location within zone of ultrasonic indications.^b CF = designates coupling flange.

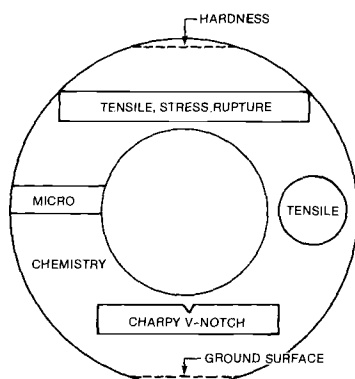


FIG. 2—Layout of specimens in HP rotor bore core samples machined from low- and high-temperature locations, BCS Nos. 1 and 3.

determinations were made at 25-mm (1.0-in.) intervals along the length of each bore core sample.

The low- and high-temperature specimen locations in the HP rotor, BCS Nos. 1 and 3, are shown in Fig. 2. Of particular interest in these tests was a determination of the effects of prolonged exposure at 722 K (449°C) on stress rupture strength and fracture toughness as measured by a shift, if any, in the FATT. Data obtained with specimens from BCS No. 1 correspond to the as-mill, heat-treated condition.

Similar tests were performed on the HP-rotor bore core sample, BCS No. 2, containing the bore surface flaws. An axial cut was first made to separate the portion of the sample containing the bore surface flaws. An isometric sketch showing the location of the bore surface indications, as determined by ultrasonic

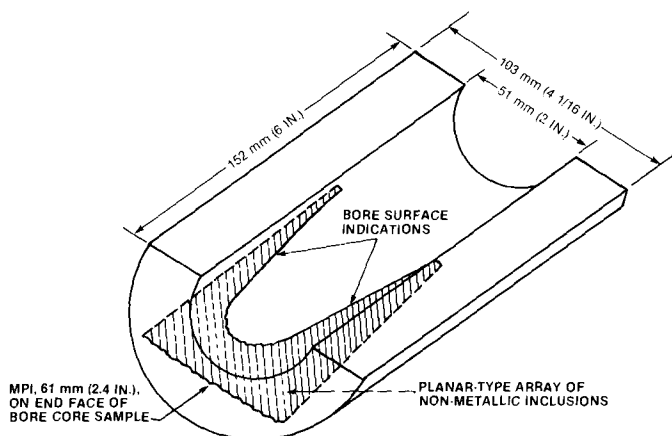


FIG. 3—Isometric sketch showing a flaw corresponding to bore surface indications under seventh-stage wheel of HP rotor, BCS No. 2.

inspection after removal of BCS No. 2 from the HP rotor, is shown in Fig. 3. The section removed to expose the bore surface indications was used to determine mechanical properties in the tangential and axial directions, hardness, and chemical composition. Several transverse cross sections were taken through the flaw for its metallurgical characterization by optical microscopy and determination of its actual size. Particular attention was given to a determination of service-induced flaw growth. It should be noted that it was necessary to remove 1.6 mm ($\frac{1}{16}$ in.) from the bore diameter in order to achieve the surface condition needed for visual and magnetic particle inspection of the bore. Microprobe analysis was performed to identify the nonmetallic inclusions which constituted the planar flaw shown in Fig. 3.

Results and Discussion

Low-Pressure Rotor

Table 1 lists the chemical composition of the LP and HP rotor forgings. The LP rotor was made of a silicon-deoxidized 2.7Ni-0.5Mo-0.1V steel with about 0.35% carbon at the generator end, somewhat higher than the heat analysis reported on the mill test certificate. As will be shown, the ultrasonic indications in the LP rotor BCS-GE were determined to be the result of void formation during solidification shrinkage. It was anticipated that carbon, phosphorus, and sulfur would tend to be higher within the 140° zone of the cross section within which the ultrasonic indications were concentrated. As shown by the data in Table 1, the amount of these elements was greater in the sample taken outside the zone of the ultrasonic indications. A second sample was taken from the location of the ultrasonic indications to check sulfur content; the 0.028% sulfur content was in agreement with the corresponding analysis shown in Table 1. The tin and arsenic contents shown in Table 1 are on the high side of the amount found in modern turbine forgings; the level of antimony is about two times that found in modern turbine forgings.

A sulfur print of the innermost end of BCS-GE is given in Fig. 4. The localized areas indicative of concentrations of sulfur are within the 140° zone corresponding to the ultrasonic indications. Contrary to the bulk chemical composition determined within and outside the zone of the ultrasonic indications, the sulfur print indicates the occurrence of sulfur segregation within the ultrasonic indication zone. Examination of microspecimens revealed that more numerous manganese-sulfide inclusions were associated with the ultrasonic indication zone and that the corresponding microsegregation zones are relatively coarse-grained.

Numerous irregularly shaped voids were observed during macroscopic examination of the innermost end of BCS-GE. On the surface examined, the size of the voids was determined to be in the range of about 0.25 to 5.1 mm (0.01 to 0.2 in.). The actual-to-predicted flaw-size ratio for the ultrasonic indications observed in BCS-GE is 0.3 to 1.5. The flaw size prediction made on the basis of the ultrasonic inspection results is considered to be excellent. There was no

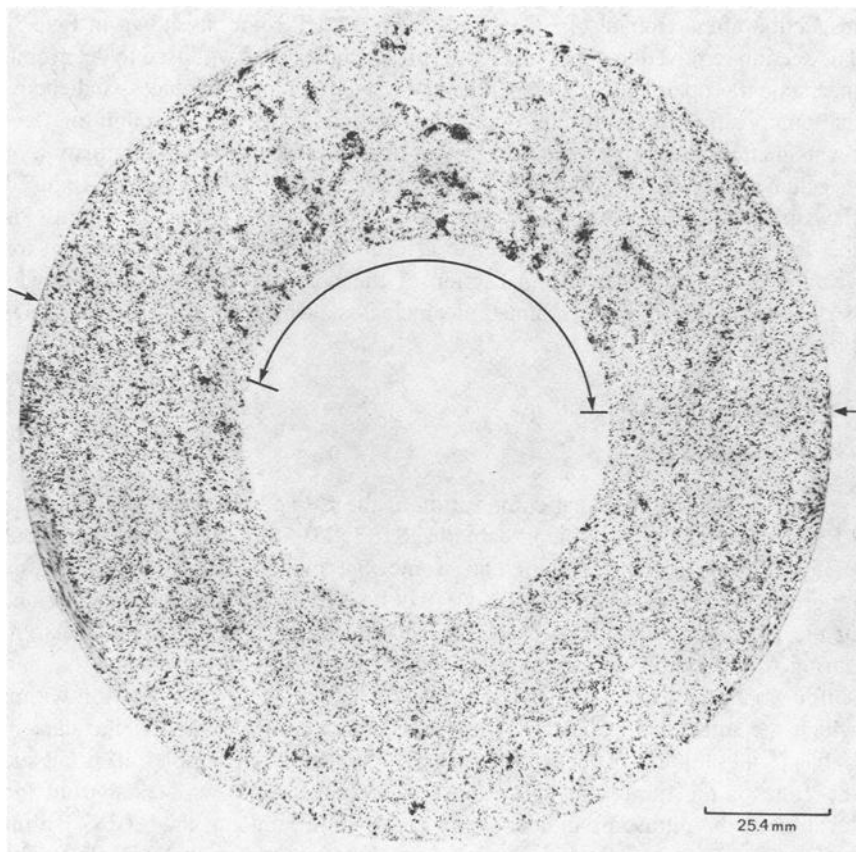


FIG. 4—Sulfur print of bore core sample from the generator end of the Ni-Mo-V LP rotor; zone of ultrasonic indications is shown.

evidence of linear, cracklike indications associated with any of the voids. An SEM micrograph showing the appearance of a void surface is given in Fig. 5. Dendrite growth from the surface of the void is evident. Clearly, the voids in the zone corresponding to the concentration of ultrasonic indications are a consequence of ingot solidification shrinkage. These solidification shrinkage voids remained unaffected by subsequent hot forging operations. The sulfur segregation pattern together with the determination that the ultrasonic indications correspond to voids formed as a consequence of solidification shrinkage suggests a possible explanation of the presence of ultrasonic indications on only one side of the bore hole; that is, the centerline of the turbine rotor was displaced with respect to the centerline of the ingot.

Tangential and axial mechanical property data are given in Table 2. The hardness across the bore core sample was uniform, 241 BHN. Both the standard 13-mm (0.505-in.)-diameter and 6.4-mm (0.252-in.)-diameter test-section tensile

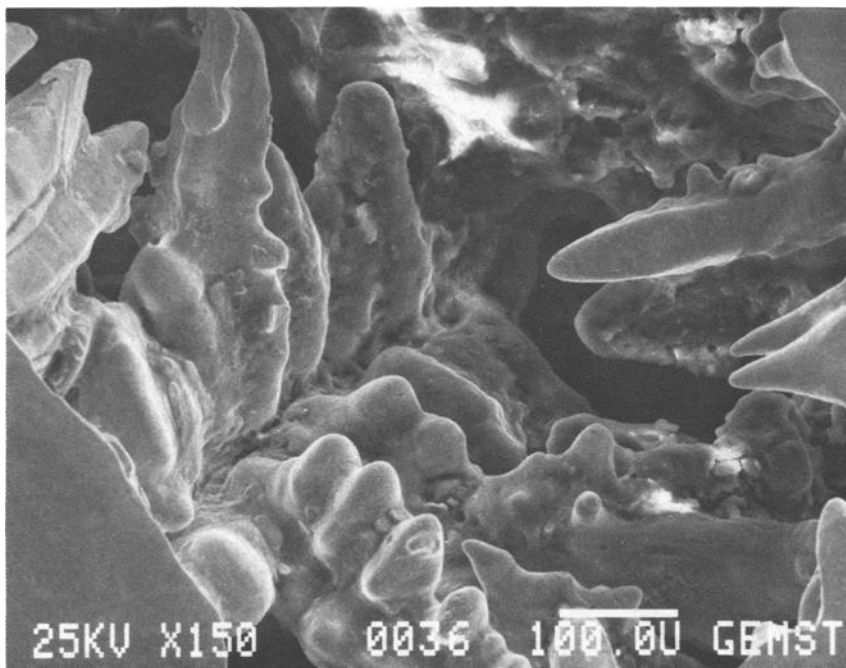


FIG. 5—SEM micrograph showing growth of dendrites from surface of solidification shrinkage voids corresponding to ultrasonic indication in a bore core sample from the Ni-Mo-V LP rotor.

specimens from the zone of the ultrasonic indications exhibited lower ductility. The subsize tangential tensile specimen located within the zone of the ultrasonic indications exhibited particularly low ductility, 2.5% elongation and 4.1% reduction of area. The low ductility value exhibited by the tangential tensile specimen through the ultrasonic indications zone was determined to be a consequence of a natural flaw, voids due to solidification shrinkage, within the test section of the specimen. The mechanical properties measured in the axial direction and outside the zone of the ultrasonic indications are comparable with those reported on the mill test certificate.

The transition temperature data are plotted in Fig. 6. These data indicate an FATT of 466 K (193°C) and a maximum shelf energy of 54 J (40 ft-lbs), values considered to be indicative of acceptable toughness for a rotor of this vintage.

High-Pressure Rotor

The chemical composition of the HP rotor is given in Table 1. These data for the silicon-deoxidized carbon-molybdenum HP rotor show evidence of carbon, phosphorus, and sulfur segregation during ingot solidification. The coupling end of the rotor most likely corresponds to the bottom of the ingot. Tramp elements, tin, antimony, and arsenic, are associated with the temper embrittlement sus-

TABLE 2—Mechanical properties of the low- and high-pressure rotors.

Rotor	Bore	Core Location	Specimen Orientation	Tensile Strength		0.02% Offset Yield Strength ^g		% EL ^h	% RA ^h	Charpy V-Notch, J at 297 K	FATT		Hardness BHN
				ksi	MPa	ksi	MPa				K	°C	
LP ^a	GE ^b		Axial ^d	111.6	769	77.5	534	12.5	17.2
			axial ^e	111.6	769	78.1	538	19.0	43.5
			tangential ^{d,f}	92.2	636	76.2	525	2.5	4.1
			tangential ^e	113.1	780	78.6	542	17.0	39.2	10.8	380	107	241
HP ^a	0.33 m (13 in.) ^c		axial	73.7	508	51.1	352	29.0	60.2
			tangential	72.1	497	36.3	250	25.0	47.9	12.2	352	79	159
			axial	76.2	525	44.3	305	27.5	54.7	159
			tangential	76.1	525	41.8	288	17.0	21.0
			axial	78.0	538	24.0	51.3
			tangential	78.1	538	42.2	291	17.0	21.7	6.1	377	104	167
Test Certificate													
LP	body		radial	108.0	745	75.0	517	19.0	47.7				
HP	body		radial	79.4	547	45.7	315	25.0	48.6				
HP	prolong		tangential	86.9	599	57.7	398	18.5	33.6				

^a LP = low pressure and HP = high pressure.^b GE = generator end.^c Distance from coupling flange.^d Specimen within zone of ultrasonic indications.^e Specimen outside zone of ultrasonic indications.^f Tangential specimens subsize, 6.4 mm (0.252 in.) diameter with 4D test section.^g Elastic limit given on mill test certificates.^h EL = elongation in area; RA = reduction in area.

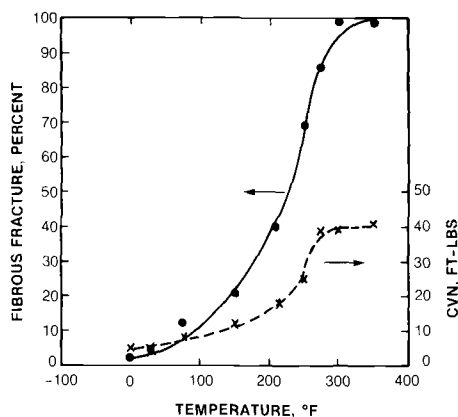


FIG. 6—Charpy V-notch transition temperature data for the Ni-Mo-V LP rotor ($1 \text{ ft} \cdot \text{lb} = 1.36 \text{ J}$; $K = [^{\circ}\text{F} + 460]/1.8$).

ceptibility of some alloy steels [6]. Compared with levels found in modern turbine forgings, the tin and arsenic in the HP rotor are on the high side, and antimony is present in about the same amount.

A sulfur print obtained on a BCS No. 2 cross section, approximately 114 mm (4.5 in.) from the end with the 61-mm (2.4-in.)-long magnetic particle indication shown in Fig. 3, is given in Fig. 7. Some sulfur segregation occurred at the location corresponding to the planar flaw.

Mechanical property data for the three HP rotor bore locations are given in Table 2. Compared with mill test certificate data, the mechanical properties of

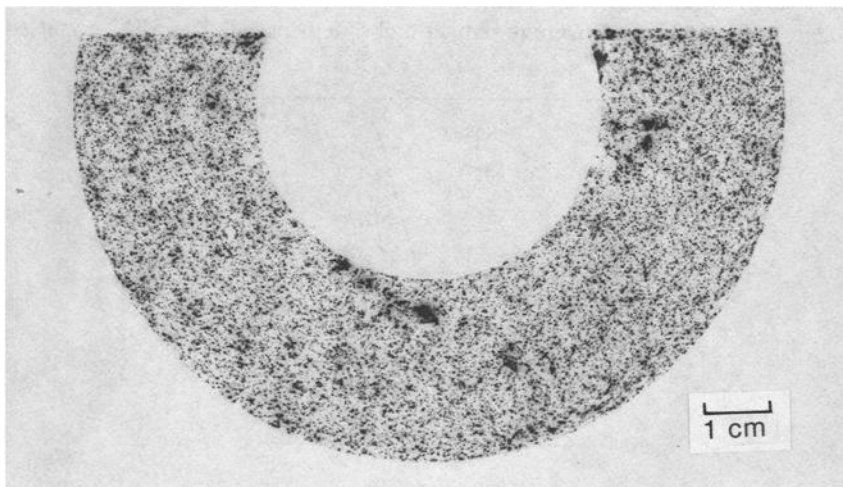


FIG. 7—Sulfur print of bore core sample from the C-Mo HP rotor at a location near the planar flaw.

the HP rotor at the bore locations are indicative of lower tensile and yield strengths. This difference is most likely the consequence of utilization of an alloy steel whose hardenability permitted austenite transformation to large amounts of proeutectoid ferrite during the relatively slow cooling rates achieved at the bore location. As would be expected for rotor forgings of this vintage, the tangential tensile ductility values are well below corresponding values in the axial direction. Macroscopic examination of the fracture surface of the lowest ductility tangential specimen from the HP rotor revealed the presence of light green-appearing non-metallic inclusions. Hardness at the three bore locations tested was uniform, 159 to 167 BHN.

Transition temperature data for the conditions corresponding to the as-mill heat-treated condition, BCS No. 1, and approximately 360 000 h at 722 K (449°C), BCS No. 3, are plotted in Fig. 8. These data, indicating a difference in the FATT of about 25 K (25°C), suggest the possibility of service-induced embrittlement. However, examination of the fracture surfaces of the impact specimens tested at 255 K (−18°C) revealed no evidence to suggest an intergranular fracture mode along prior austenite boundaries, a fracture mode associated with the loss of toughness in alloy steels due to a temper embrittlement phenomenon [7].

The typical appearance of the bainite-proeutectoid ferrite microstructure corresponding to the as-mill heat-treated condition, BCS No. 1, is shown in Fig. 9. On the basis of the line intercept method, it was estimated that the microstructure at the location of BCS No. 1 included approximately 67% proeutectoid ferrite, only a few percent less than that at the location of BCS No. 3. The austenite transformation which occurred during heat treatment of the carbon-molybdenum HP rotor resulted in the nucleation and growth of proeutectoid ferrite at prior austenite grain boundaries, a transformation product less susceptible than tempered martensite to temper embrittlement [8]. The SEM was used

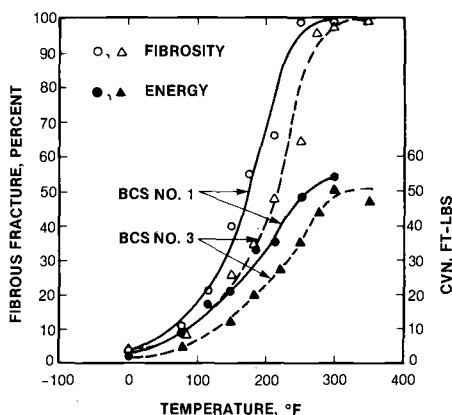


FIG. 8—Charpy V-notch transition temperature data for the C-Mo HP rotor ($1 \text{ ft} \cdot \text{lb} = 1.36 \text{ J}$; $K = [^{\circ}\text{F} + 460]/1.8$).

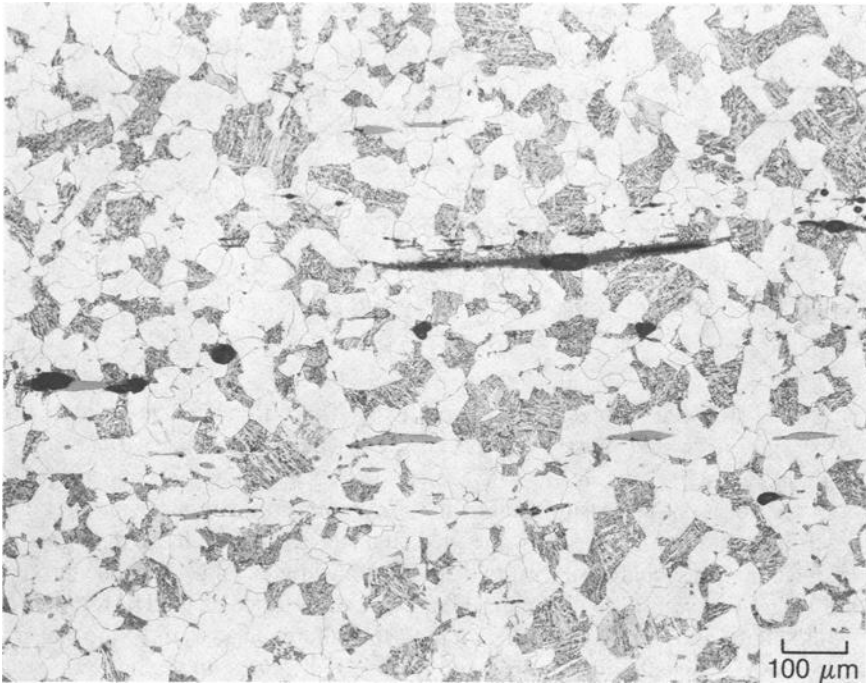


FIG. 9—Typical microstructure of HP rotor at location BCS No. 1 corresponding to as-mill, heat-treated condition.

to measure the mean length of cleavage facets in the brittle fractures of Charpy V-notch specimens from BCS Nos. 1 and 3. It has been shown that there is a good correlation between FATT and $d^{-1/2}$, where d is the mean length of the cleavage facets [9]. For brittle fractures in Charpy V-notch specimens from BCS Nos. 1 and 3, the mean length of the cleavage facets was determined to be approximately the same, 91.0 and 90.2 μm , respectively. The FATT difference of 25 K (25°C) for test locations corresponding to BCS Nos. 1 and 3 is not related to differences in embrittlement or the mean length of cleavage facets. The difference in toughness existed in the as-mill heat-treated condition and most likely is related to small differences in microstructure and hardness after mill heat treatment. The elongated nonmetallic inclusions apparent in Fig. 9 are responsible for the tensile ductility differences between specimens oriented in the axial and tangential directions.

Stress rupture data obtained for the carbon-molybdenum HP rotor at test locations BCS Nos. 1 and 3, corresponding to the as-mill heat-treated condition and 360 000 h at 722 K (449°C), respectively, are plotted in Fig. 10. The Larson-Miller parameter value corresponding to 360 000 h at 722 K (449°C) is 33 200. At this parameter value the stress rupture strength in the as-mill heat-treated condition and at the location corresponding to service exposure at 722 K (449°C)

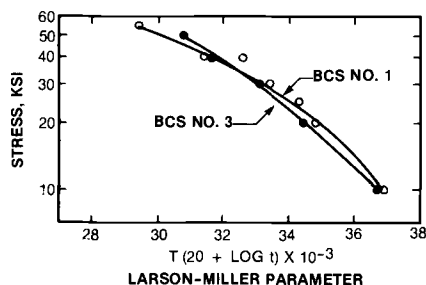


FIG. 10—Stress rupture strength of the C-Mo HP rotor for the low- and high-temperature locations, BCS Nos. 1 and 3, respectively (1 ksi = 6.89 MPa).

is 207 and 193 MPa (30 and 28 ksi), respectively. This difference is not considered to be significant and most likely is not a consequence of in-service material degradation; stress rupture ductility values for corresponding specimens from both test locations were similar. For the maximum bore stress, including both centrifugal and thermal stresses, the predicted stress rupture life on the basis of BCS No. 1 data would be at least two orders of magnitude longer than the turbine has been in service. Stress rupture initiation at the surface of the HP rotor bore would not be expected, and, as shown in the metallurgical analysis of the planar-type flaw associated with the magnetic particle indications on the bore surface, there was no evidence to suggest linkage between nonmetallic inclusions near the bore surface by an intergranular stress rupture mechanism.

Analysis of HP-Rotor Flaw Indication

The HP-rotor sample, BCS No. 2, was sectioned axially to expose the magnetic particle indications on the bore surface. As shown in Fig. 3, a U-shaped, cracklike indication was apparent on the bore surface. The maximum length of the axially oriented segments of the U-shaped indication was about 64 mm (2.5 in.) on the bore surface. As determined by ultrasonic inspection of BCS No. 2, the flaw indication extended into the body of the bore core sample in what appeared to be a planar configuration. The flaw manifested itself as a linear magnetic particle indication on one end of BCS No. 2. On the end face of this sample the flaw orientation was tangential with respect to the rotor bore and approximately 61 mm (2.4 in.) in length. Additional transverse sectioning of the bore sample confirmed that the U-shaped bore surface indication and the linear indication on the end face were on a single plane inclined approximately 30° with respect to the rotor axis. The isometric sketch shown in Fig. 3 depicts the planar distribution of the indication.

Metallographic observations of the cracklike indications are shown in Fig. 11. The flaw was determined to correspond to an array of nonmetallic inclusions with greater inclusion frequency in the area near the bore surface; towards the periphery of the flaw there was a decrease in the number of inclusions. These

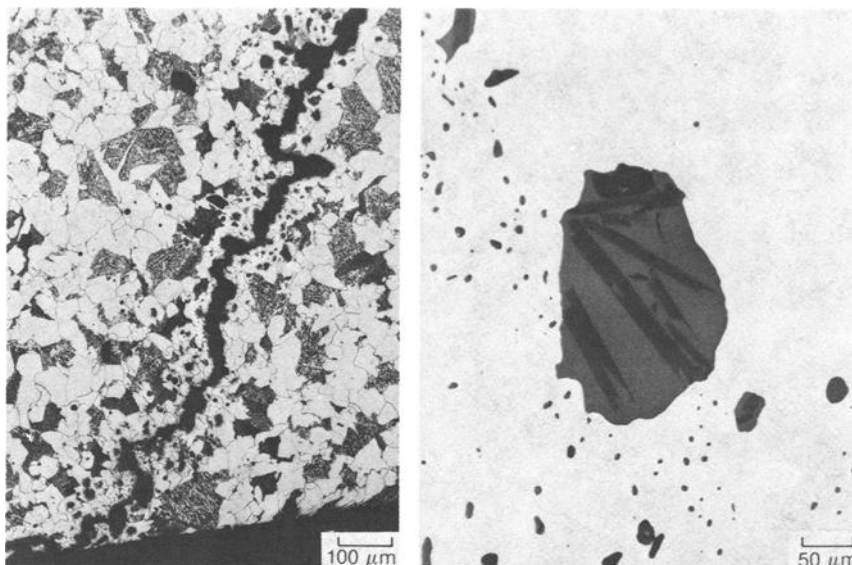


FIG. 11—Appearance of an HP-rotor flaw in a transverse cross section at the bore surface (left) and at a location near the flaw periphery.

nonmetallic inclusions are elongated in the direction of the rotor axis as typically observed in rotor forgings. On the basis of examination with the light microscope, the inclusions appeared to consist of two primary constituents shown in Fig. 11 (right). X-ray microprobe analysis of these nonmetallic inclusions indicated the light gray constituent to be composed of manganese and silicon with some sulfur. Silicon is the primary element in the darker gray, platelike constituent.

It was of interest to determine whether any service-induced crack growth had occurred in the region of the natural metallurgical flaw, a planar array of manganese silicate inclusions. In a cross section normal to the axis of the HP-rotor bore sample, shown in Fig. 12, it is evident that a transgranular crack of approximately 0.2 mm (0.008 in.) had grown at the periphery of the natural flaw. There was no evidence of nonmetallic inclusions present in the path of the transgranular crack. Shown in Fig. 13 is evidence of flaw growth by linking up of neighboring inclusions. The cracks in this region are also predominantly transgranular. The zigzag pattern of the crack path is in contrast to the straight path shown in Fig. 12 where the crack growth was not interrupted by the presence of nonmetallic inclusions.

As previously noted, ultrasonic inspection from the periphery of the HP-rotor surface revealed the presence of flaw indications up to 13 mm (0.5 in.) from the bore surface. Since the flaw extended under the seventh-stage wheel, it was not possible to ultrasonically determine its total length from the outer-diameter surface. A bore ultrasonic inspection was not performed since increasing the bore

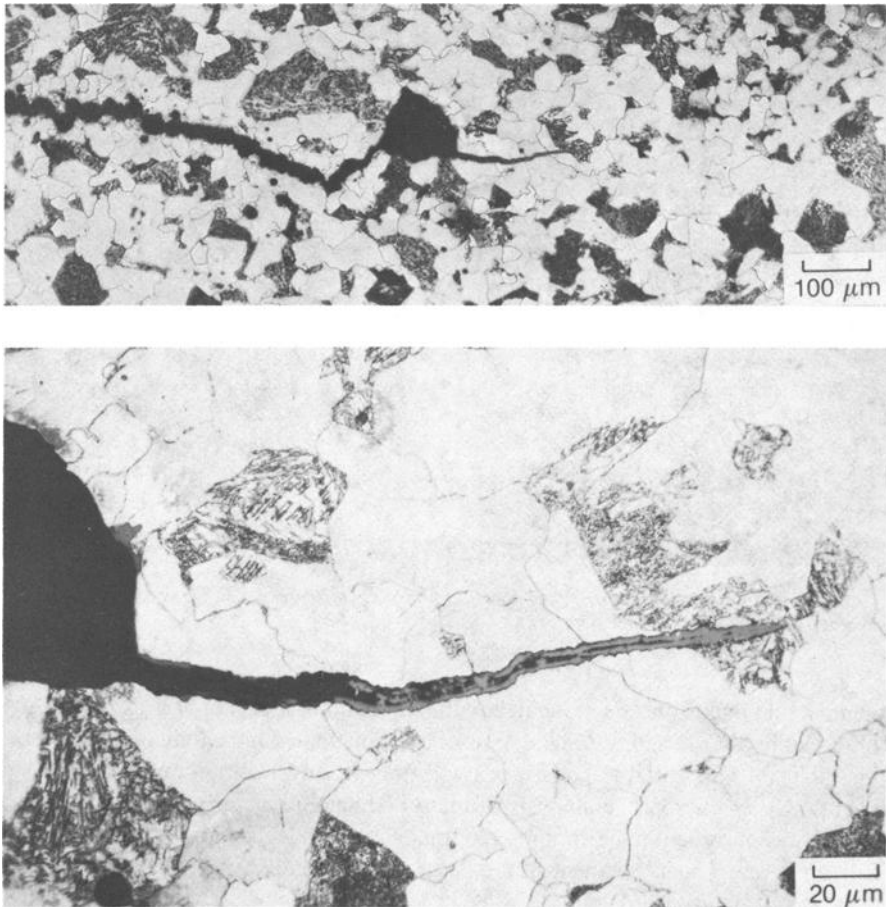


FIG. 12—Evidence of transgranular crack growth at the tip of an inclusion array in HP-rotor bore core sample.

diameter to the size required to physically accommodate the equipment would have entailed machining, and possibly removing, the bore surface indications. In addition, it initially appeared that the periphery ultrasonic indication corresponded to the cracklike indications on the bore surface. The actual size of the planar-type flaw in BCS No. 2 was determined to be approximately 61 mm (2.4 in.) wide and 95 mm (3.75 in.) long. The radial distance from the bore surface to the periphery location of the flaw corresponding to the ultrasonic indication was determined to be approximately 10 mm (0.4 in.). Given the limitations imposed on the ultrasonic inspection because of the interstage wheel spacing and the rotor surface configuration, the agreement between the actual and predicted location of the flaw with respect to the bore surface is considered to be good.

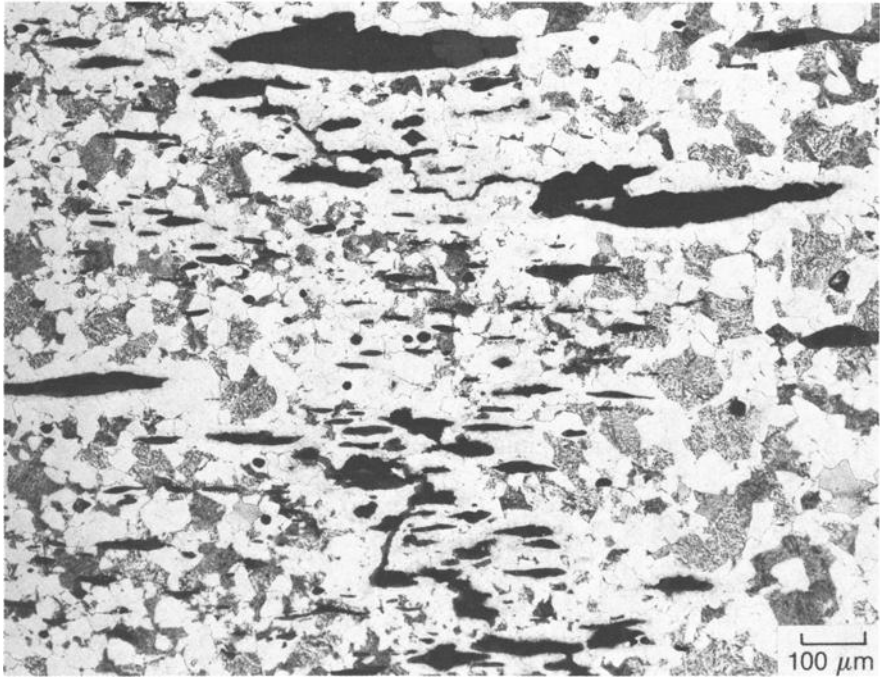


FIG. 13—Crack growth by linkup of nonmetallic inclusions in the HP-rotor bore core sample.

Fracture Mechanics of the HP-Rotor Flaw

A linear elastic fracture mechanics approach was utilized to evaluate the rotor integrity and crack growth potential of the flaw present in the HP rotor. To perform this analysis, the stress intensity factor must be calculated; this calculation includes the effects of applied cyclic stresses and defect crack size, shape, and orientation. This factor is combined with material crack growth properties to evaluate rotor integrity.

Among the stresses present at the cracks were centrifugal loads, proportional to the square of the rotational speed, due to the rotational pull of the rotor body and supported blading. Also present during turbine start-ups, shutdowns, and power output load swings are thermal stresses caused by temperature differences in the rotor body as it responds to steam flow changes. Because of the orientation of the flaw in the HP rotor with respect to the rotor axis, as shown in Fig. 3, those stresses which act to promote crack growth in the classical Mode I manner, where crack faces separate normal to one another, must be derived from the tangential and radial principal stresses. Estimates of the applied centrifugal and thermal stresses were made using design information describing the size and thermodynamic characteristics of the turbine. The components of stresses perpendicular to the crack plane were then added vectorially to produce the cyclic

loading which occurs with every start-up and shutdown and with every major power load change.

As shown in Fig. 3, the flaw can be quite closely modeled as semielliptical in shape, open to the bore surface, and of a size 64 mm (2.5 in.) long and 25 mm (1.0 in.) deep. The major axis of the crack was approximately parallel to the rotor longitudinal axis.

For this type of flaw, the stress intensity factor, including corrections for crack tip plasticity, becomes

$$\Delta K_I = \Delta \sigma \left[\frac{1.2\pi a}{Q} \right]^{1/2} \quad (1)$$

where

$\Delta \sigma$ = cyclic stress range normal to the crack plane,

a = crack depth,

$Q = \Phi^2 - 0.212(\sigma/\sigma_{ys})^2$,

$\Phi = \int_0^{\pi/2} [\sin^2 \phi + (a/c)^2 \cos^2 \phi]^{1/2} d\phi$,

c = $\frac{1}{2}$ crack length, and

σ_{ys} = 0.02% yield strength.

Crack growth rates as a function of stress intensity factor and temperature are a material property derived from laboratory testing over the past 15 years on actual rotor forging material. At normal operating temperature, 636 K (363°C), the crack growth rate per stress cycle in the HP rotor can be conservatively approximated by

$$da/dN = 1.724 \times 10^{-9} (\Delta K_I)^{2.7} \quad (2)$$

Similarly, estimates of the critical stress intensity factor, where rapid, uncontrollable crack growth occurs, also were determined for rotor forging steels. In estimating rotor integrity, rotor properties at room temperature, corresponding to the least ductile condition, are utilized in order to increase conservatism. For the HP rotor, the critical stress intensity at room temperature is estimated to be about 53 MPa \sqrt{m} (48 ksi $\sqrt{in.}$). Both of these properties were used in this analysis to predict the amount of crack growth expected and the closeness of the defect to its critical size.

Figure 14 shows estimates of crack depth versus the number of years of operation. The turbine in question has been used in an industrial application for approximately 40 years, during which the number of start-ups and shutdowns was kept at a minimum, probably less than 400 over the 40 years. More important are the load changes which can occur frequently during the turbine life. The plot in Fig. 14 shows the defect depth assuming ten start-ups per year and one major

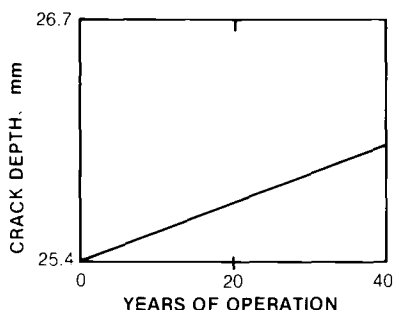


FIG. 14—Predicted crack growth in HP rotor as a function of service time.

load change per day. The defect increased beyond its original depth by about 2% over its lifetime, a small amount of growth for such a long period of time. Since crack propagation data can be very dependent on individual forging properties, environment, and testing inaccuracy, especially in the slow growth regime, the comparison of predicted-to-actual growth seems reasonable; that is, both indicate little growth.

The severity of the defect can be measured by comparing its actual size to the critical flaw size which would cause failure. Estimates of critical size are purposely very conservative and are made assuming an excessively fast start-up of the turbine at room temperature. The combination of centrifugal and thermal stresses thus present at running speed indicate that the defect would have to grow to a semicircular flaw having a radius of 117 mm (4.6 in.). This represents a flaw about 3.7 times the size of that found at the bore of the HP rotor. As previously noted, the service-induced growth of the flaw was small. On the basis of this fracture mechanics analysis, the actual flaw size was much smaller than the predicted critical size for the onset of a catastrophic failure of the HP rotor.

Conclusions

1. Ultrasonic indications in the 2.7Ni-0.5Mo-0.1V LP-rotor bore core sample were determined to correspond to voids due to ingot solidification shrinkage. Evidence of dendrite growth from the surface of the voids examined indicated that plastic deformation during the hot forging of the ingot was inadequate to consolidate the bore zone of the rotor.

2. The LP rotor exhibited extremely low tensile ductility in a direction tangential to the bore and within the zone of the ultrasonic indications corresponding to voids formed during ingot solidification.

3. Diametrically opposite magnetic particle indications, approximately 63.5 mm (2.5 in.) axially, were determined to correspond to the intersection of the 0.25C-0.5Mo HP-rotor bore hole with an array of manganese-silicate inclusions in a planar-type configuration oriented 30° with respect to the rotor axis. The

flaw intersected the end of the bore core sample to give the appearance of a cracklike indication in a tangential orientation with respect to the bore hole.

4. Evidence of service-induced, transgranular crack propagation linking the manganese-silicate inclusions was found; as expected on the basis of stress rupture strength determined for the HP-rotor material, there was no indication of flaw growth by an intergranular stress rupture mechanism.

5. As predicted by the fracture mechanics analysis, some flaw growth had occurred during the life of the turbine; low-cycle fatigue appears to be the mechanism responsible for flaw growth.

6. The correlations between the actual-and-predicted size of flaws in the 2.7Ni-0.5Mo-0.1V LP rotor and the actual-and-predicted location of the flaw in the 0.25C-0.5Mo HP rotor are considered to be good.

Acknowledgment

The authors would like to recognize the contributions made by D. J. Walls and D. R. Skinner in the planning stage of this investigation, the helpful discussions with A. Rotsko during the course of the investigation, and our associates who critically reviewed the paper. The scanning electron microscopy performed by S. M. Bishop and J. E. Kaippel is also greatly appreciated.

References

- [1] Schmerling, J. M. and Hammon, J. C., "Investigation of the Tennessee Valley Authority Gallatin Unit No. 2 Turbine Rotor Burst," presented at the American Power Conference, Chicago, IL, 20-22 April 1976.
- [2] Gray, J. L., "Investigation Into the Consequences of the Failure of a Turbine-Generator at Hinkley Point 'A' Power Station," *Institution of Mechanical Engineers, Proceedings*, Vol. 186, 1972, pp. 379-390.
- [3] Emmert, H. D., "Investigation of Large Steam-Turbine Spindle Failure," *Transactions of the American Society of Mechanical Engineers*, Vol. 78, 1956, pp. 1547-1565.
- [4] DeForest, D. R., Schabtach, C., Grobel, L. P., and Seguin, B. R., "Investigation of the Generator Rotor Burst at the Pittsburgh Station of the Pacific Gas and Electric Company," ASME Power Division Conference, 21-23 Oct. 1957, American Society of Mechanical Engineers, New York.
- [5] Timo, D. P., Bievenue, R. T., and Bullock, G. S., "In-Service Turbine Rotor Inspection and Evaluation," presented at the Southeastern Electric Exchange Conference, Atlanta, GA, 22-24 April 1981.
- [6] Newhouse, D. L., and Holtz, H. G., "Temper Embrittlement of Rotor Steels," in *Temper Embrittlement in Steel, STP 407*, American Society for Testing and Materials, Philadelphia, 1968, pp. 106-126.
- [7] Capus, J. M., "The Mechanism of Temper Brittleness," *Temper Embrittlement in Steel, STP 407*, American Society for Testing and Materials, Philadelphia, 1968, pp. 3-19.
- [8] McMahon, Jr., C. J., "Temper Brittleness—An Interpretive Review," *Temper Embrittlement in Steel, ASTM STP 407*, American Society for Testing and Materials, Philadelphia, 1968, pp. 127-167.
- [9] Karino, S. et al., "Applications of Low Si 2.7Ni-0.6Cr-0.5Mo-0.1V Steel to HP-LP Single Rotor Shaft," presented at the Ninth International Forgemasters Conference, Dusseldorf, 1981.

DISCUSSION

*J. H. Evans*¹ (*written discussion*)—It was reported by the speaker that the correlation between actual flaw size and that predicted by ultrasonic inspection was between 0.3 to 1.5. My question concerns how this correlation was established. How many flaws were examined? Since there were many inclusions, how was the area measurement made on the "flaw"?

I am quite surprised by the excellent correlation between actual and estimated flaw sizes. Tu and Seth² reported that sonic estimation underestimated by up to 6.6 times the actual flaw area. Do the authors have any comment about this large difference in the correlations?

S. Toney, W. Kim, A. S. Melilli and S. G. Leone (*authors' closure*)—The actual-to-predicted flaw-size ratios of 0.3 to 1.5 pertained to the ultrasonic indications in the carbon-molybdenum LP rotor. Use of the DATAQ computerized bore inspection system revealed a very large number of closely spaced indications near the bore surface. As typically shown in Fig. 5, those indications actually examined were voids, not inclusions, due to solidification shrinkage. A ground cross-section through the location of some of the ultrasonic indications intersected nine of them. Macroscopic examination of these irregularly-shaped voids at magnifications up to X30 was the basis for determination of their size; the diameter of the circle, which included the irregularly-shaped void, was taken as the "actual flaw diameter." Comparison of the extreme values of the actual and predicted flaw-size diameters, not areas, resulted in ratios of 0.3 to 1.5; had the comparison been made on the basis of areas corresponding to the actual and predicted flaw diameters, the actual-to-predicted flaw-size ratios would be 0.1 to 2.4.

With respect to the difference between the correlations found in this investigation and the work by Tu and Seth indicating ultrasonics underestimates by up to 6.6 times the actual flaw size, it can only be noted that the flaw sizes may not have been within the same range. The multiplying factor applied to ultrasonic indications is a function of the predicted flaw size; a larger multiplying factor is used for smaller flaw indications.

¹ Westinghouse Electric Corp., Orlando, FL 32817.

² Tu, L. K. L. and Seth, B. B., "Nondestructive/Destructive Test Correlations and Fracture Mechanics Analysis," *Journal of Testing and Evaluation (JTEVA)*, Vol. 5, No. 5, Sept. 1977, pp. 361-368.

The Fracture Toughness of Actual and Simulated Large Rotor Forgings Made from 3.5Ni Steel

REFERENCE: Albrecht, J., Bertilsson, J.-E., and Scarlin, B., "The Fracture Toughness of Actual and Simulated Large Rotor Forgings Made from 3.5Ni Steel," *Steel Forgings, ASTM STP 903*, E. G. Nisbett and A. S. McIlilli, Eds., American Society for Testing and Materials, Philadelphia, 1986, pp. 178-202.

ABSTRACT: The present work is aimed at determining the properties of 3.5Ni steels simulated to a condition in which they would be used for the manufacture of large turbine rotors. Samples were subjected to heat treatment schedules, particularly cooling rates, that would be experienced during manufacture. With increasing size, the cooling rate from the austenitizing temperature is reduced, leading to the formation of bainite with a coarse distribution of carbides. Since brittle fracture from the center of large forgings must be avoided, special emphasis has been placed on the fracture toughness and fracture mode and the way in which both are determined through the microstructure, particularly the carbide form and distribution.

KEY WORDS: quenched and tempered steel, 3.5Ni steel, rotor forgings, fracture toughness, yield strength, microstructure, fracture modes

This paper reports on part of a continuing basic investigation of the properties of large forgings used for the rotors of steam and gas turbines and generators. The size limits up to which a certain steel can be used without serious reduction of critical properties, such as yield strength, creep strength, or toughness, must be known in order to decide up to what sizes monoblock rotors can be employed and where other techniques, for example, welding, provide an alternative. The emphasis of the current investigation is on fracture toughness.

With the trend to larger steam-turbine output ratings, the necessity of increasing the diameter of half-speed low pressure (LP) rotors up towards 3 m (>100 in.) arose. When assessing different alternatives for steel for steam turbine rotors,

¹ Research metallurgist, Corporate Research Center (KLR), BBC Brown, Boveri & Co., Baden, Switzerland.

² Manager, Mechanics and Fluid Dynamics Development, Development of Steam Turbo Sets (TGE), BBC Brown, Boveri & Co., Baden, Switzerland.

³ Manager, Mechanical Testing, Central Metallurgical Laboratory (RLM), BBC Brown, Boveri & Co., Baden, Switzerland.

all relevant properties have to be considered. With regard to operational safety, the ability of a steel to tolerate defects is of utmost importance. Therefore, the toughness at the center of these rotors must be maintained at a high level. For nuclear power plants, the danger of damage to the radioactive system by turbine missiles resulting from brittle fracture has lead to stringent requirements from government authorities (Nuclear Regulatory Commission). The shrunk-on disks have encountered severe problems with stress-corrosion cracking at steeples, key ways, etc. This unexpected jeopardy of the operation safety has forced the utilities and the turbine manufacturers to look for alternative solutions.

One alternative is a monoblock rotor fabricated from a single large forging of huge dimensions. A 3.5Ni steel with good through-hardening properties is required for the monoblock.

It is well-known that the toughness of quenched and tempered steels is sensitive to the appearance of an upper bainitic microstructure with coarse carbide particles. For a certain steel, the occurrence of such a microstructure is dictated by the cooling rate on quenching, which in turn is determined by the forging size. The fracture toughness of an experimental forging with a diameter of 1200 mm was measured at various locations; to obtain information about the toughness in the center of even larger forgings having diameters as required for monoblock rotors, simulation tests were carried out. Microstructural investigations were performed to provide explanations of the observed behavior.

Experimental Program

Test Material

A 3.5Ni steel with the following chemical composition was used in the present work: 0.29C, 0.10Si, 0.30Mn, 0.008P, 0.008S, 3.62Ni, 1.70Cr, 0.40Mo, and 0.09V. The contents of major alloying elements and trace elements are typical for current large forgings.

The forging was made from a 94-ton basic electric arc ingot, upset (ratio 2.8) and normalized, followed by a preliminary heat treatment and the quality heat treatment (830°C/31 h, water quench, tempered 50 h at 600°C, followed by a controlled cooling).

In addition to the chemical composition, the extent of through forging is important since it affects the degree of microsegregation. Low-alloyed steels are susceptible to dendritic segregation of the alloying elements, especially of molybdenum and nickel. Therefore, using the electron microprobe and optical microscopy, it was checked to determine that both the extent of segregation and the appearance of the segregation bands are the same as occur in very large forgings.

Simulation of Large Diameters

Test material was taken from the center of a forging of 1200 mm (47 in.) in diameter [1]. Since no material was available from the centers of forgings with

diameters in excess of 2000 mm (78 in.), it was necessary to perform simulation tests. The cooling rate for large sizes was extrapolated from published cooling curves [2]. Figure 1 shows the cooling curves for 600, 1200, and 1800-mm-diameter forgings as solid curves, whereas the cooling curve obtained by extrapolation for 3000 mm is shown as a dashed line. The cooling curves are superimposed on the time-temperature-transformation (TTT) diagram for the 3.5Ni steel. According to information from forging manufacturers, the cooling rate of 27°C/h determined in this way for 3000-mm-diameter forgings is somewhat too high; a cooling rate of 21°C/h is given for this diameter.

A computer program for mathematical process modelling with which the cooling curves could be calculated for different locations within a forging was employed [3]. First estimates show satisfactory agreement with the graphic extrapolation of the published curves [2]. Based on the information available at the time when the measurements were made, simulation diameters of 1800, 2100, 2400, and 2700 mm were selected, the corresponding cooling rates being 35, 31, 27, and 24°C/h, respectively.

The simulation was performed in a tube furnace regulated by a programmer following the actual measured temperature. This permits close tolerances to be held on the temperature profile (about 2°C deviation of the specimen temperature from the intended value). The specimens were heat-treated in an inert atmosphere (argon) in the form of blanks with a size slightly larger than a compact tension (CT) specimen. One specimen per batch was instrumented with a control-thermocouple. The specimens were heated rapidly to the austenitizing temperature of 850°C and held there for 2 to 3.5 h, depending on the simulated diameter. They were then cooled at different rates to room temperature. The specimens were subsequently tempered at one of three temperatures (typically 590, 617, or 630°C). The tempering temperature determines the material yield strength whereby the dependence is very strong; that is, small differences in tempering temperature have a pronounced effect on the yield strength.

Determination of the Properties

The tension properties were determined for all conditions investigated (four different cooling rates, each with three different tempering temperatures). Typically, three specimens were tested for each condition, with the exception of the condition with the lowest cooling rate (27°C/h) and the lowest tempering temperature (590°C), where only one CT specimen was tested. The fracture toughness was of major interest. This was measured for each condition using 25-mm-thick CT specimens according to the partial-unloading method for determination of the critical J -integral value [ASTM Method for J_{Ic} , a Measure of Fracture Toughness (E 813-81)]. For brittle material behavior, the critical stress intensity factor was determined using a K -evaluation according to ASTM Method for Plane-Strain Fracture Toughness of Metallic Materials (E 399-83). Tension- and fracture toughness-testing were performed at room temperature.

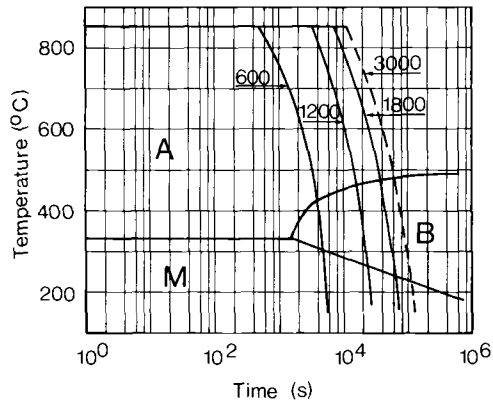


FIG. 1—TTT diagram for 3.5Ni steel with cooling curves for 600, 1200, 1800, and 3000-mm diameter forgings (from Ref 6). A = austenite, B = bainite, M = martensite.

Results

Tension Tests

The results of the tension tests are shown in Table 1. For the 1200-mm forging, tension data are given for the as-received condition (heat-treated, as just mentioned) for the surface and the center positions. Both strength and ductility are slightly lower for the center position.

TABLE 1—Mean values of tension tests for the conditions investigated: simulated diameter and cooling rate (or location in the 1200-mm forging, respectively), tempering temperature, yield strength, ultimate tensile strength, and elongation to failure.

Simulated Diameter, mm/Cooling Rate, °C/h	Annealing Temperature, °C	$\sigma_{0.2}$, MPa	Ultimate Tensile Strength, MPa	Elongation to Fracture, %
1800/35	590	871	1019	13.1
	617	718	853	16.8
	630	660	794	18.1
2100/31	590	886	1025	14.0
	617	722	862	17.9
	630	662	792	17.9
2400/27	590	810	947	16.3
	617	778	907	16.2
	630	659	801	19.3
2700/24	590	932	947	11.9
	610	784	921	16.0
	617	717	852	16.5
	630	614	770	18.8
1200 MM FORGING				
Surface	600	780	886	15.8
Center	600	745	860	14.8

The tension results for the simulated condition also are shown in Table 1. For a given tempering temperature, strength and ductility vary only slightly with the cooling rate, except for the tempering temperature of 590°C, where a noticeably higher yield strength (and lower ductility) is observed for the condition with the lowest cooling rate (simulated diameter—2700 mm).

Whereas the dependence of strength upon cooling rate is subtle, it is strongly dependent on tempering temperature. In this temperature range, the yield strength alters by about 5 MPa for each degree change of tempering temperature.

The tempering temperature of 590°C produces a yield strength of about 810 MPa, which is too high for applications in monoblock rotors where yield strength values of about 740 MPa would be more typical. For this reason, tempering treatments were performed at 617 and 630°C and, in addition, at 610°C for a diameter of 2700 mm.

Fracture Toughness and Fracture Mechanisms

The fracture toughness measurements provide the main aim of the program. The use of the partial-unloading method permits the scatter in the results for each of the conditions to be evaluated, since each specimen provides an individual toughness value.

The fracture toughness results for the 1200-mm forging are shown in Fig. 2, where K_{Ic} is plotted as a function of distance from the surface. The toughness is high over the cross section, and a slight decrease is noticed only towards the very center of the forging.

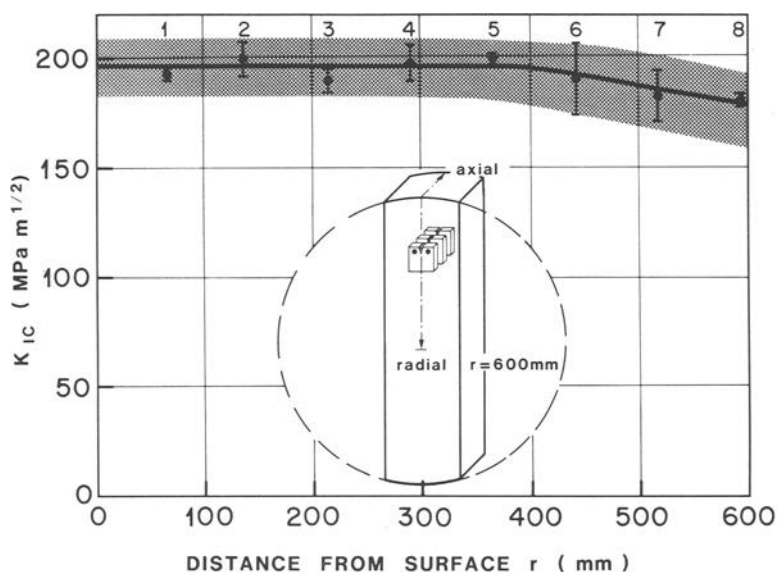


FIG. 2—Fracture toughness of the 1200-mm forging as a function of distance from the surface.

Investigation of the fracture surface confirmed that this decrease, small as it may be, is indeed real. One of the three specimens fractured at Position 7 (80 mm from the center) showed a small amount of unstable fracture. This behavior is shown schematically in Fig. 3*a*. Starting from the fatigue precrack, the crack began to propagate in a stable manner (ductile, dimpled fracture mode) until an instability occurred locally; in this instability zone, quasicleavage was observed (Fig. 3*b*). The crack was then arrested and propagated in a stable, ductile manner until the test was terminated.

It was, indeed, this observation that raised the question of the fracture toughness in the center of even larger forgings and that thus initiated the simulation test program.

The results for the simulation tests are shown in Fig. 4 (tempering temperature 590°C), Fig. 5 (tempering temperature 610 and 617°C), and Fig. 6 (tempering temperature 630°C). For all tempering temperatures, a reduction in the toughness is apparent with increasing forging section size.

At a yield strength of 614 MPa, the fracture toughness (mean values) falls from 200 MPa $\sqrt{\text{m}}$ at the 1800-mm diameter to 160 MPa $\sqrt{\text{m}}$ at the 2700-mm diameter. At a yield strength of 718 MPa, the fracture toughness at the 1800-mm diameter lies at 180 MPa $\sqrt{\text{m}}$ and reduces to 150 MPa $\sqrt{\text{m}}$ at a diameter of 2700 mm. The most extreme drop is observed at a yield strength level of about 810 MPa; here the fracture toughness at the 1800-mm diameter already lies at 120 MPa $\sqrt{\text{m}}$ and falls with increasing diameter rapidly to a value of 55 MPa $\sqrt{\text{m}}$ at 2700 mm (only one data point).

The results of the fracture toughness measurements are summarized in Fig. 7. The lowest measured values, which are relevant for safety analyses and design considerations, are illustrated as a function of the forging diameter for the three different yield strength values. In addition, the lowest measured toughness values are indicated as horizontal dashed lines. These values are used for the evaluation of defects in a fracture mechanics analysis.

From the point of view of safety, the fracture mechanism has an importance similar to that of the actual value of the fracture toughness. In the case of ductile failure, stable crack growth first occurs after the critical value of the stress intensity factor has been attained. Instability and rapid crack propagation only arise at much higher K -values. However, brittle failure unstable crack growth, that is, failure of the component, occurs as soon as the critical stress intensity, K_{Ic} , is reached. This means that stable crack growth provides an additional safety margin. For this reason, the broken specimens were fractographically examined. The results are summarized in Fig. 8. All measurements are shown once more but now designated according to the failure mechanism.

Specimens that fail predominantly in a brittle manner (cleavage and quasicleavage) are designated by open symbols, whereas the closed symbols represent specimens that failed in a ductile manner (ductile dimples, stable crack growth).

The fracture mechanisms observed are shown in Fig. 9. A typical ductile dimple fracture is illustrated in Fig. 9*a*, whereas Fig. 9*b* shows a mixed mode

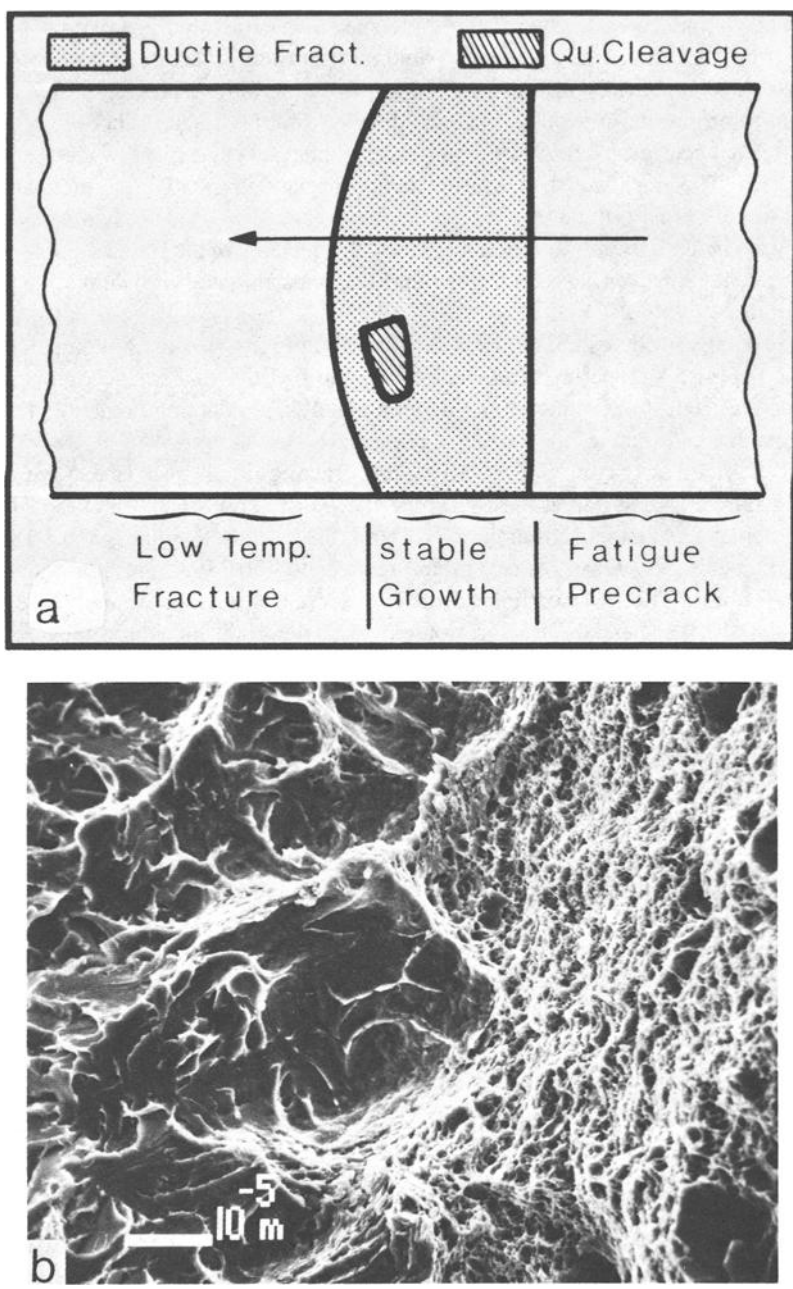


FIG. 3—Fracture surface (1200-mm forging); distance from surface 520 mm: instability zone. (a) fracture modes (schematically); (b) scanning electron micrograph of transition from regime of stable crack growth to quasicleavage.

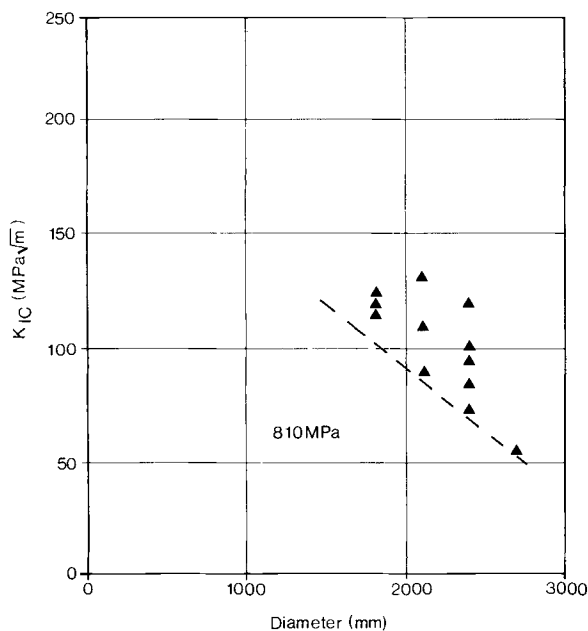


FIG. 4—Fracture toughness as a function of diameter for a yield strength of 810 MPa.

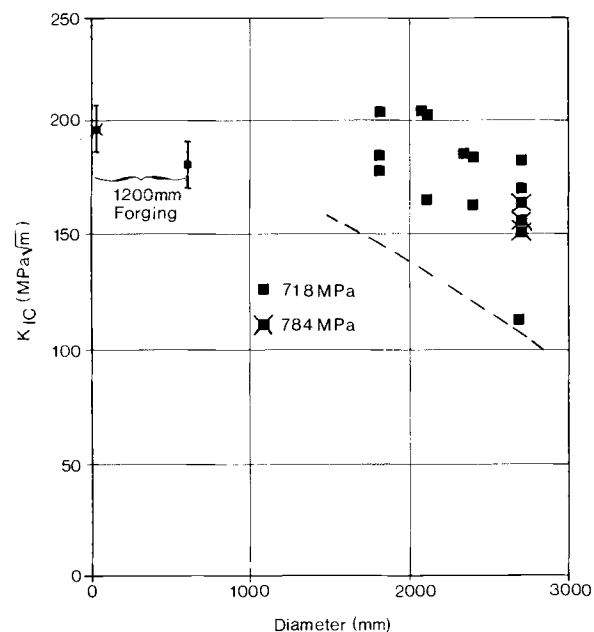


FIG. 5—Fracture toughness as a function of diameter for a yield strength of 718 and 784 MPa.

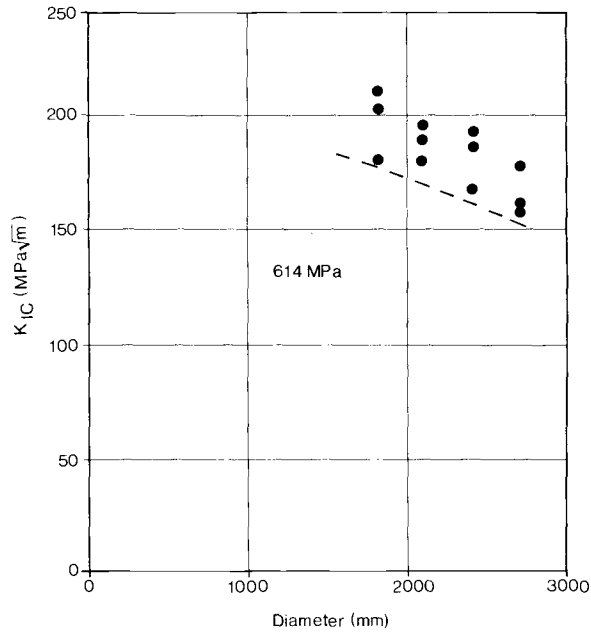


FIG. 6—Fracture toughness as a function of diameter for a yield strength of 614 MPa.

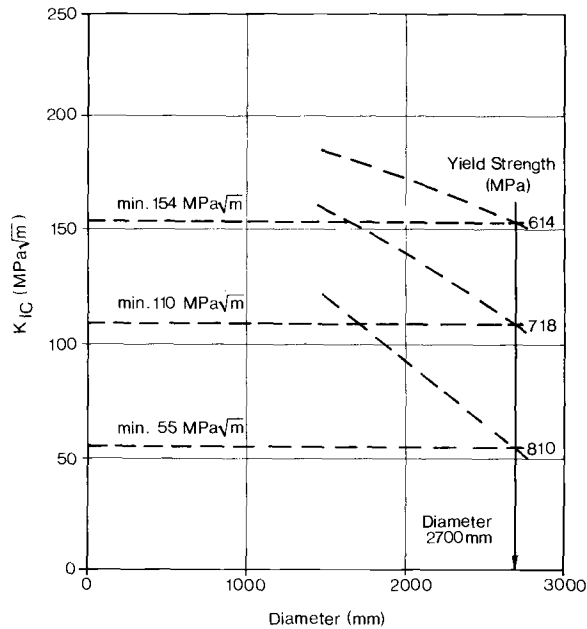


FIG. 7—Summary of the fracture toughness values: lower scatterband of the measured values; parameter: yield strength.

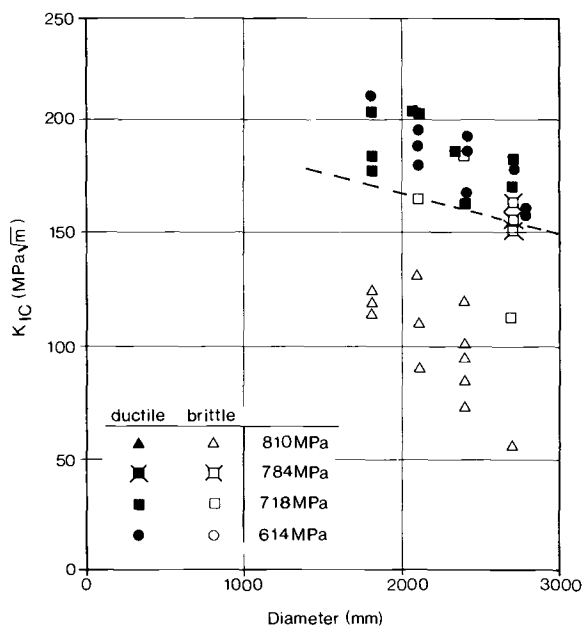


FIG. 8—Fracture mechanisms. Closed symbols = ductile dimple fracture; open symbols = brittle fracture.

fracture such as is generally found in the transition area between the upper and lower shelf regions. Finally, Fig. 9c exhibits a quasicleavage fracture (cleavage facets with ductile ridges).

It is apparent that brittle cleavage fracture occurs for all fracture toughness values below $150 \text{ MPa}\sqrt{\text{m}}$, that is, for all diameters investigated at a yield strength of 810 MPa.

At a yield strength of 718 MPa, as the diameter is increased, there is a transition from ductile failure (at 1800 and 2000 mm) to cleavage fracture (at 2400 and 2700 mm). In fact, at 2400 mm, two of the specimens tested broke in a ductile manner and one by cleavage, a behavior that is often observed if the test temperature is close to the transition temperature from the upper shelf toughness to the lower shelf toughness.

Microstructural Investigations

The microstructure of the 1200-mm forging was investigated at the surface and in the center, that of the material with the simulation treatment for a simulated diameter of 2100 mm and 2700 mm, using optical and electron microscopy. Except for the 1200-mm forging directly at the surface, where a homogeneous microstructure was found in the light microscope, the other conditions showed segregation bands consisting of light and dark zones. These bands are often

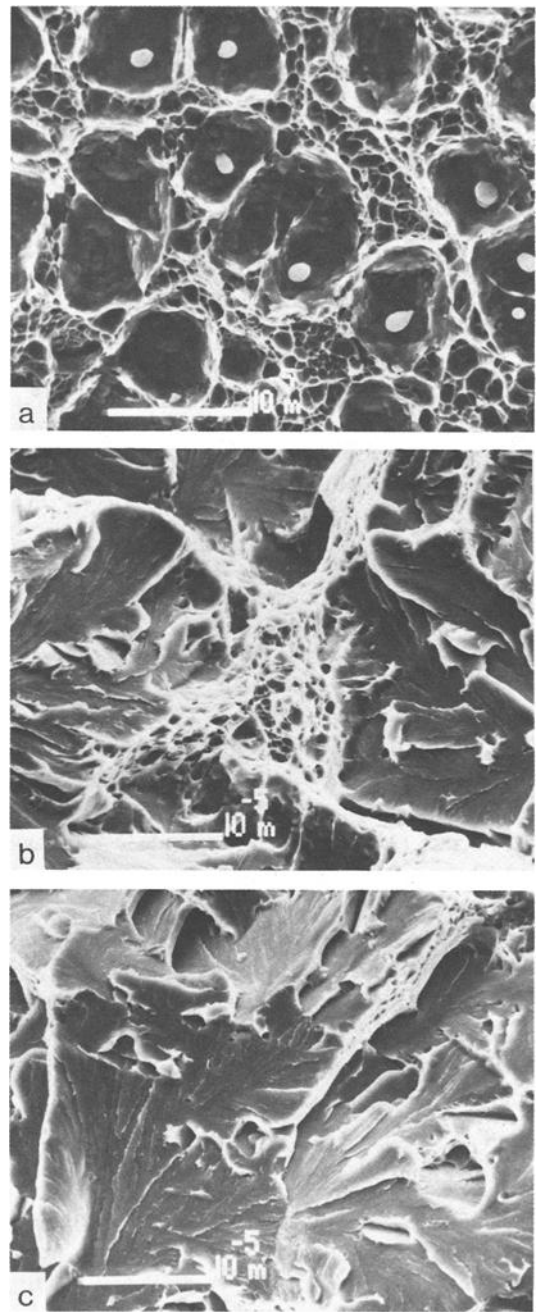


FIG. 9—Fracture mechanisms: (a) Ductile dimple fracture; (b) mixed mode: ductile dimple/quasicleavage fracture; (c) quasicleavage.

observed in forgings of low-alloyed steels; they are caused by areas of dendritic segregation, which are elongated to bands during the forging operation. The differences in contrast arise from the different constituents in the microstructure. Whereas the light bands consist predominantly of bainite, the dark bands are of tempered martensite. In this quenched and tempered condition, the two microstructural components differ in their carbide distributions, whereby it is also necessary to distinguish between upper and lower bainite.

A comparison of the two simulated diameters 2100 and 2700 mm shows (at the same yield strength) that the proportion of bainite, and in particular of upper bainite, increases with increasing diameter. The typical appearance of the microstructure is shown in Fig. 10. (Figures 10a and 10c are scanning electron micrographs of polished and etched sections; Fig. 10b is a transmission electron micrograph).

The upper bainite is coarser in comparison with lower bainite and tempered martensite; this applies to both the grain and lath sizes and to the carbide particles. In this phase, the carbides are large, often elongated, and precipitated preferentially on the grain and lath boundaries (Fig. 10a).

In comparison, the carbides in the lower bainite and in the tempered martensite are more homogeneously distributed. They are also smaller. The difference between these two microstructural components lies in the shape of the carbides. In lower bainite, the carbides are slightly elongated and oriented with their longer axes at an angle of about 60° to the lath axes, (Fig. 10b), whereas the carbides in tempered martensite have a rounded form (Fig. 10c).

The effect of the yield strength is visible in the shape of the carbides. The relationship is shown in Fig. 11. At higher yield strength levels (appropriate to low tempering temperature), the carbide shape in the upper bainite is unchanged (Fig. 11a). However, at lower yield strength values, rounded precipitates are found instead of the elongated, plate-shaped carbides; that is, the higher tempering temperature leads to a necking and rounding (spheroidizing) of the carbides (Fig. 11b).

The interrelationship between carbide distribution and carbide shape, on one hand, and between yield strength and fracture toughness, on the other, will be discussed further in the following paragraphs.

Discussion

Earlier experiments [4] already have shown that the fracture toughness of quenched and tempered steels is affected to a considerable extent by the distribution of the carbides.

Two dominant factors, which also are reflected in the present work, are the through hardening and the strength level. These factors can be traced back to more physical parameters: the cooling rate during quenching (austenitizing) and the tempering temperature.

These two factors will be considered separately.

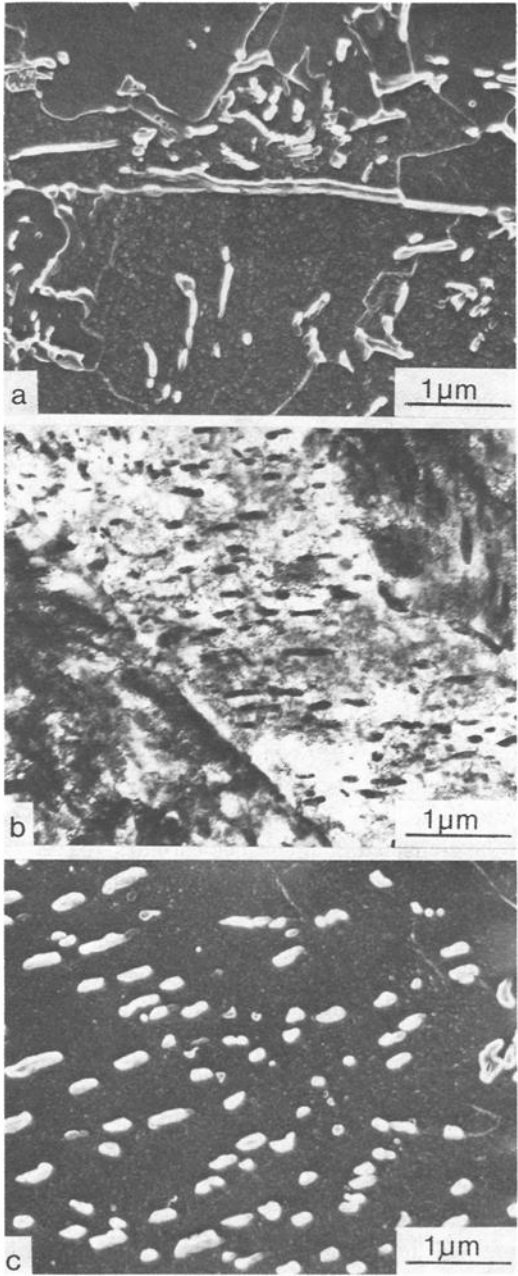


FIG. 10—Microstructural investigations: (a) upper bainite; (b) lower bainite; (c) tempered martensite.

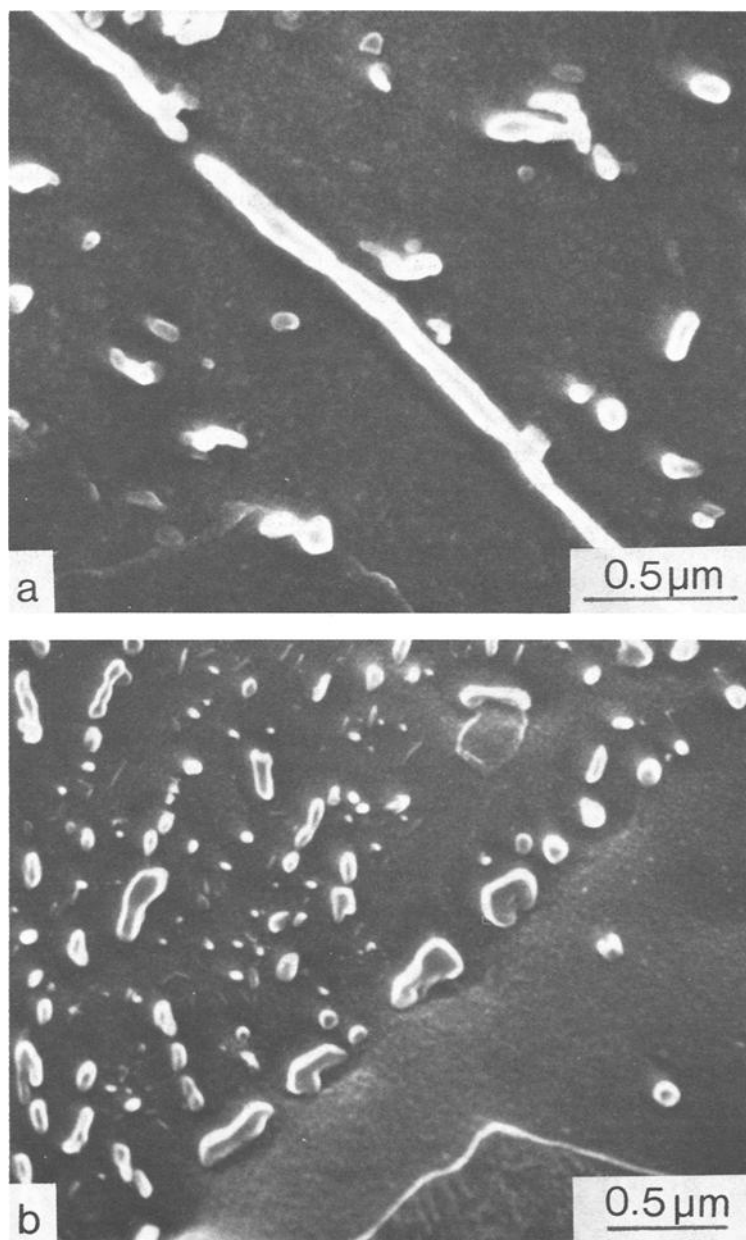


FIG. 11—The effect of tempering temperature on the carbide morphology: (a) tempering temperature 590°C; (b) tempering temperature 630°C.

Through Hardening

In the ideal condition, quenched and tempered steels consist of tempered martensite. A component is considered to be "through-hardened" if it consists of tempered martensite throughout its entire thickness. This assumes that the material is cooled sufficiently rapidly from the austenitizing temperature to below the temperature at which the martensite transformation occurs. Since this transformation takes place without diffusion, it depends only on the undercooling and not on the time; that is, a material cannot be transformed isothermally into martensite.

In contrast, all other transformations of austenite occur by diffusion processes or by nucleation and growth. The entire transformation behavior is represented using TTT diagrams. Figure 12 shows the TTT diagram for the steel investigated here.

For any steel, there is a critical cooling rate below which a complete transformation to martensite is no longer possible. On the TTT diagram, this critical cooling rate is defined by the point at which the martensite line (M_s line) meets the bainite field. This critical cooling curve is shown in Fig. 12 as a dashed line.

All slower cooling rates lead as a matter of course to the appearance of bainite in the microstructure. The transformation kinetics, that is, using the terminology of the TTT diagram, the position of the bainite curve, and later the pearlite curve,

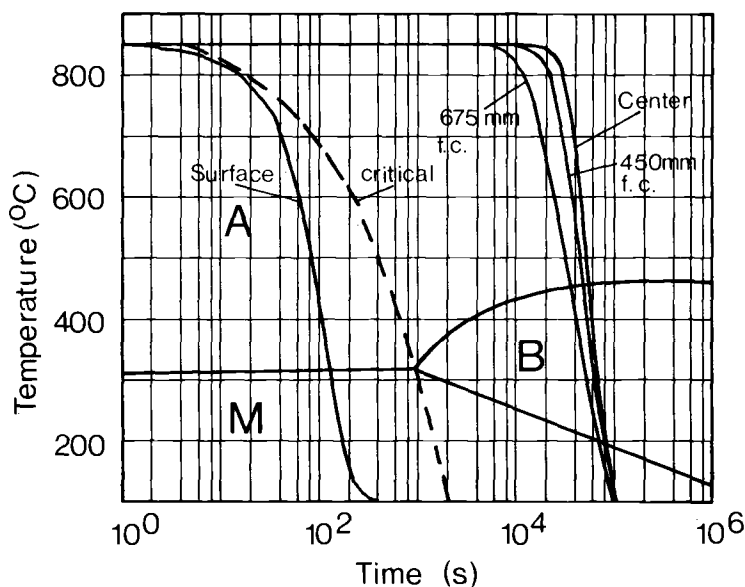


FIG. 12—TTT diagram for 3.5Ni steel with calculated cooling curves for a diameter of 2700 mm at various distances from the center (full lines) along with the "critical cooling curve" (dashed). A = austenite, B = bainite, M = martensite.

will be primarily determined by the presence of alloying elements. Nickel is an effective element in that even small amounts (a few percent) delay the transformation to bainite and thereby shift the position of the transformation curve to the right (longer times). In other words, nickel improves the hardenability.

The cooling rate of a forging is primarily a function of the physical quantities: thermal conductivity and specific heat, along with the thermal transport from the surface to the quenching medium, represented by the heat transfer coefficient.

It is instructive to note that for large sections the cooling rate at the center is mainly a function of the conduction of heat from the center, that is, from a physical quantity that, for a given steel, cannot be affected by external conditions such as the quenching medium, etc. Computer calculations showed that the cooling rate at the center of a cylinder with a diameter of 2700 mm is hardly affected by variations in the heat transfer coefficient; even a tenfold higher heat transfer coefficient does not affect the cooling rate in the center noticeably.

In Fig. 12, some cooling curves are shown appropriate to a forging with a diameter of 2700 mm and a body length of 5000 mm. The different curves apply to different distances from the center (for a fixed total diameter).

The cooling rate for the surface is higher than the critical rate; that is, the surface region is transformed completely into martensite. With the distance from the surface, the cooling rate decreases rapidly. From about 675 mm from the surface (half radius), the structure is practically fully bainitic with an increasing amount of upper bainite towards the center.

The temperature at which the bainite transformation commences determines the carbide morphology and distribution. This is precisely the difference between lower bainite and upper bainite. At high transformation temperatures, the diffusion rate is high, so that coarse carbides appear inhomogeneously distributed, particularly at locations with a low nucleation energy, such as grain boundaries, etc. At lower transformation temperatures, the nucleation rate is high, so that fine, homogeneously distributed carbides are formed.

Clearly the point at which the bainite curve is intersected by the cooling curve is of particular importance in determining the resulting carbide distribution: the higher the temperature, the coarser the carbides. In other words, the lower the cooling rate (larger diameter), the coarser the microstructure.

In turn, the distribution and shape of the carbides has a decisive effect upon the toughness of quenched and tempered steel [5]. Inhomogeneously distributed carbides lead to inhomogeneous distributions of dislocations and thereby to stress concentrations, which in turn lead to crack nucleation. The carbide shape also has a strong influence on crack nucleation in that elongated or even plate-shaped carbides crack at a lower stress level than rounded carbides.

The relationships mentioned so far explain the observed dependence of the toughness on the forging diameter. As the proportion of upper bainite increases, the toughness decreases. This is particularly clear at the highest yield strength level, that is, for the lowest tempering temperature.

Effect of the Tempering Temperature

The relationship between the tempering temperature and toughness is far less complicated than the effect of the cooling rate. After cooling from the austenitizing temperature, a certain carbide distribution has been attained within the bainite, which is little affected by the subsequent tempering treatment. However, the tempering treatment serves to determine the shape and size of the carbides. The observations lead to the conclusion that higher tempering temperatures lead to a rounding of the previously elongated or plate-shaped carbides.

Figure 11*b* illustrates this phenomenon: a chain of rounded carbides is visible on a grain boundary, and it is easy to imagine that before tempering the chain comprised a continuous carbide plate such as is shown in Fig. 11*a*. During tempering, the plate would have become necked at several points, leading finally to the appearance of isolated rounded carbides. With the relationships just mentioned between carbide shape and crack nucleation, the relationship between toughness and tempering temperature also becomes plausible. At lower tempering temperatures, the carbide shape is hardly affected.

The relationship between yield strength and toughness also is to be found in the tempering temperature since the yield strength is also dependent on the carbide distribution: growth of the carbides leads to a reduction of the yield strength. In addition, in a mixed microstructure of martensite and bainite, the carbon in the martensite phase remains in solution after cooling from the austenitizing temperature. The tempering treatment precipitates out this carbon in the form of carbides, resulting in a reduction in the yield strength.

It is apparent that the observed relationships between the fracture toughness on one side and both yield strength and forging diameter on the other can be explained on the basis of the carbide distributions, as illustrated schematically in Fig. 13.

Validity of the Simulation Technique

Finally, the simulation technique itself should be briefly discussed. The comparison of the cooling rates with values from the literature [2] shows that the cooling rates employed are realistic. However, the transformation microstructure is dependent not only on the cooling rate, but also on the internal stress state within the forging. Compressive internal stresses tend to suppress transformations that are accompanied by a volume increase, such as the face-centered cubic (FCC) \rightarrow body-centered cubic (BCC) transformation, whereas tensile stresses promote such transformations. In this case, this means that in the TTT diagram, the bainite curve will be displaced to longer times by the presence of compressive stresses and displaced in the opposite direction by tensile stresses.

On cooling from the austenitizing temperature, first compressive stresses arise in the center of a forging; however, recent finite-element calculations [6] have shown that if one properly takes into account the stresses which arise during transformation on cooling (volume increase for the transformation FCC \rightarrow BCC)

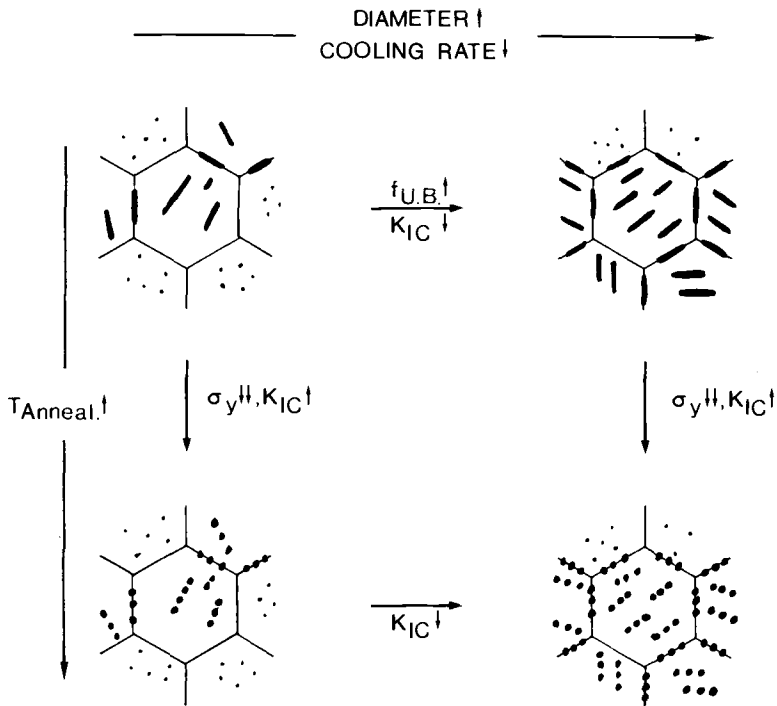


FIG. 13—Dependence of yield strength and toughness on the diameter and tempering temperature based on the carbide distribution (schematic).

in large forgings of over 1000-mm in diameter, then a stress reversal may occur in the center regions and tensile stresses will arise prior to transformation occurring at the point in question.

The calculation of the sign and magnitude of internal stresses during the quenching of large cylinders is only possible using finite-element computer models incorporating accurate material properties. The fact that internal stresses are not developed in simulation treatments may lead to slight differences in the measured properties as compared to actual forgings.

Conclusions

The fracture toughness of quenched and tempered steels is influenced by factors like alloy chemistry, grain size, and the concentration of impurity elements, but also by the parameters of the hot working and heat treatment.

This investigation focused on the influence of two parameters:

1. The cooling rate after austenitizing.
2. The tempering temperature which is employed to obtain the required yield strength.

Under the conditions considered here, the cooling rate at the center of a forging is mainly a function of the thermal conductivity, so that it cannot be influenced. Through the transformation kinetics, it determines both the spatial distribution of the carbides in the bainite phase as well as the volume fraction of bainite, thereby exerting a considerable effect on the material toughness.

The tempering temperature determines the yield strength of the material as a mechanical property through the carbide shape and size observed as microscopic features. In turn, they affect the fracture toughness through crack nucleation at carbides.

The effect that forging diameter and tempering temperature have on material strength and toughness are illustrated schematically in Fig. 13:

1. With increasing diameter, the cooling rate at the center is reduced. This results in an increase in the volume fraction of bainite, that is, in the quantity of elongated carbides. The toughness is correspondingly decreased.
2. With increasing tempering temperature, the carbides become spheroidized, resulting in a reduction of the yield strength and an increased toughness. The strong dependence of the yield strength on the tempering temperature requires precise temperature control.

The simulation experiments have shown that the fracture toughness at the center of forgings of the size required for the manufacture of large monoblock, low-pressure rotors may lie significantly lower than for forgings of smaller size.

References

- [1] Albrecht, J. and Wüthrich, C., *Zeitschrift Werkstofftechn.*, Vol. 13, 1982, pp. 96–103 (in German).
- [2] Forch, K., Fischer, K., and Piehl, K.-H., *Stahl und Eisen*, Vol. 101 No. 15, 1981, p. 1033.
- [3] Rebelo, N., "Temperature Distribution and Residual Stress Calculations of Quenched Impellers," BBC Report KLR 82-189 B, BBC Brown, Boveri & Co., Baden, Switzerland.
- [4] Albrecht, J., Bertilsson, J. E., and Scarlin, R. B., "Defect Tolerance of Different LP Rotor Materials and Designs," presented at EPRI seminar on Low Pressure Turbine Disc Integrity, 1–2 Dec. 1983, San Antonio, TX, Electric Power Research Institute, Palo Alto, CA.
- [5] Albrecht, J., *Material und Technik*, Vol. 10 No. 2, 1982, pp. 99–109 (in German).
- [6] Hougardy, H. and Wildau, M., *Härterei-Technische Mitteilungen*, Vol. 38 No. 3, 1983, p. 121.

DISCUSSION

*R. L. Novak*¹ (written discussion)—(1) You have related a simulated microstructure to material properties. What evidence do you have that the simulated microstructure is representative of the microstructure and properties of actual large forgings? (2) You said that the cooling rate and the tempering temperature are the two major factors which determine the fracture toughness of large forgings.

¹ Westinghouse Electric Corp., Orlando, FL 32817.

How can you neglect such major factors as chemistry (low residual impurities), cleanliness of the steel, forging practice, and grain size and refinement, which are known to affect fracture toughness? In light of this, why did you use centerline material for slow cooling simulation of the "large forgings" and surface material for the rapid quench?

J. Albrecht, J. Bertilsson, and B. Scarlin (authors' closure)—(1) Up until now, material has not been available for a comparison of actual and simulated centerline microstructures. Such material from the center of a large monoblock has been made available for testing by three different laboratories. Microstructure and fracture toughness data will be compared in coming months. It is hoped that the causes of the discrepancy will be clarified. (2) The chemical composition of the material used for the simulation is typical for current large forgings, including the concentration of tramp elements. The results of the tests mentioned will show if parameters like forging practice and grain refinement contribute to the discrepancy. Centerline material was used for the simulation tests, because it is this part of the forging that experiences the slow cooling rates.

G. S. Hartman² (written discussion)—The authors reported that by utilizing a simulation technique they computed the cooling rates of large forgings using a finite-element computer program. These cooling rates were then simulated in a programmable furnace with specimens removed from the 1194-mm (47-in.) diameter experimental test forging. The results obtained from these specimens yielded toughness values less than 55 MPa $\sqrt{\text{in.}}$ (50 ksi $\sqrt{\text{in.}}$) which, according to the authors, is less than safe and will result in a brittle-cleavage-mode-type failure.

Since it has been demonstrated time and again over the last 15 years that the actual fracture toughness values achieved from the center cores of large rotors [$>1524\text{-mm}$ (60 in.) in diameter] have very high levels of toughness [165 MPa $\sqrt{\text{in.}}$ (150 ksi $\sqrt{\text{in.}}$) or higher], this indicates that a ductile mode of failure should occur. Therefore, the question was asked, "What was the message that the author was trying to relate at this symposium and to the technical world?"

It has been well-known within the forging industry for the last 20 years that you cannot simulate in the laboratory what happens in the center of these very large Ni-Cr-Mo-V turbine generator rotors because of what we have called in ignorance "the mass effect."

Furthermore, the authors should be investigating why this "mass effect" phenomenon is occurring instead of reporting the simulation toughness values as newfound information on simulation techniques.

J. Albrecht, J. Bertilsson, and B. Scarlin (authors' closure)—If one compares the results of the simulation treatments with those obtained from real forgings at the same strength level and the same diameter, which is typically 700 to 740

² A. Finkl & Sons Co., Chicago, IL 60614.

MPa, the difference is not as great as the discussion remark implies. Also, specimens simulated to this condition failed in a ductile mode.

As to the validity of the simulation technique itself, there are several possible explanations for the discrepancy: the material, its thermomechanical treatment before the final heat treatment, and the lack of residual stresses in the simulation treatment.

It should be noted that it was not the intention of the investigation to find information on simulation techniques, but to use this tool to obtain information about the influence of the carbide distribution on fracture toughness.

J. Ewald³ (written discussion)—(1) You gave a contribution to 3.5Ni-Cr-Mo-V steel for large monoblock rotors, but it can be expected that your message was the comparison of welded polyblock rotors and monoblock rotors. For this it is necessary to know: (a) What is the chemical composition of the welded rotor material you use? Is it the same 2Cr-1Ni-Mo steel that was presented by Creusot-Loire⁴? (b) What are the toughness properties and K_{IC} -values for the welded rotor material? (2) During your heat treatment simulation, what was the lowest holding temperature after austenitization before reheating for tempering?

The background of my question is the TTT diagram. The cooling curve, referring to large diameters, shows a bainitic structure with remaining amounts of austenite at about 200°C. Therefore, it could occur as this austenite, unchanged to martensite, undergoes the tempering treatment. After that, these austenitic amounts are changed to untempered martensite and remain in a tempered bainitic structure. This untempered martensite could be one reason for the partial cleavage fracture appearance.

J. Albrecht, J. Bertilsson, and B. Scarlin (authors' closure)—(1) The properties of rotor steels of 2Cr-1Ni-Mo were discussed in the previous contribution of Creusot-Loire and are not subject of our presentation. (2) After austenitization, the specimens were cooled to a temperature below 80°C to prevent retention of austenite.

H. C. Argo⁵ (written discussion)—The authors' paper purports to show that 2500-mm (100-in.)-diameter, low-pressure turbine rotor forgings would have very low, unsafe fracture toughness properties. When material properties are measured for actual rotor forgings, the midradius and the axial centerline properties are verified to be much better than the data presented by the authors and are, in fact, the basis for a safe turbine rotor. To support these discussion points, the following data is presented.

³ Kraftwerk Union AG, D-4330 Muelheim a.d. Ruhr, Federal Republic of Germany.

⁴ Pisseloup, J., Poitault, I., Badereau, A. de, Bocquet, P., "Manufacturing of Welded Polyblock Turbine Rotors for PWR Nuclear Plants: Optimization of the Steel Grade; Effect of Impurities," this publication.

⁵ Westinghouse Electric Corp., Orlando, FL 32817.

The averaged chemistry for five fully integral low-pressure rotor forgings is:

C	Mn	P	S	Si	Ni	Cr	Mo	V
0.23	0.29	0.005	0.004	0.06	3.60	1.73	0.38	0.11

Mechanical property tests were taken at the locations shown in the rotor forging outline (Fig. 14). The results of these tests are shown in Fig. 15.

The properties of the axial bore core material are the centerline (Q_c) values. Midradius properties are the 625-mm (25-in.) radial position values. Fracture toughness values were calculated via Charpy V-notch results using the Rolfe-Novak correlation equation in *Review of Developments in Plane Strain Fracture Toughness Testing*, ASTM STP 463, published in 1970. Fully integral low-pressure turbine rotor forgings of 2500-mm (100-in.) diameter having greater than 200 MN/m^{3/2} (200 ksi $\sqrt{\text{in.}}$) fracture toughness for axial centerline material is the level of today's technology.

J. Albrecht, J. Bertilsson, and B. Scarlin (authors' closure)—The data presented in this discussion contribution support the results obtained from fracture toughness tests on core material of large forgings, which were published recently and acknowledged in the closing remarks of our presentation.

The average value of the results of the simulation tests from 2400-mm diameter forgings at a comparable strength level (compare Fig. 5) is 174 MPa $\sqrt{\text{m}}$, which is not considered very low or even unsafe.

Nevertheless, it is indeed lower than the values measured for actual forgings, which leaves open the question concerning possible reasons for this discrepancy. The discussor's results also show a reduction in *minimum* toughness of about 20% at the center as compared with the rim of the forging. (The SI unit scale for fracture toughness is incorrect.)

R. I. Jaffee⁶ (written discussion)—About one year prior to the presentation of this paper, a paper by Scarlin, Bertilsson, and Albrecht presented the same

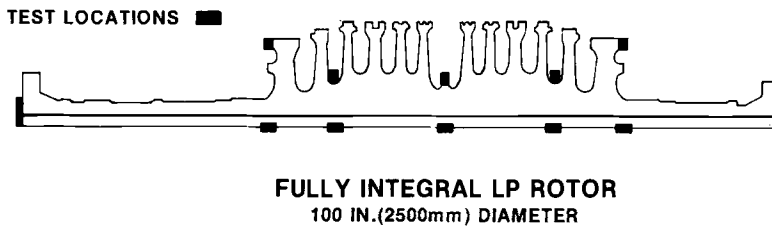


FIG. 14—Fully integral LP rotor, 2500-mm (100-in.) diameter.

⁶ Westinghouse Electric Corp., Orlando, FL 32817.

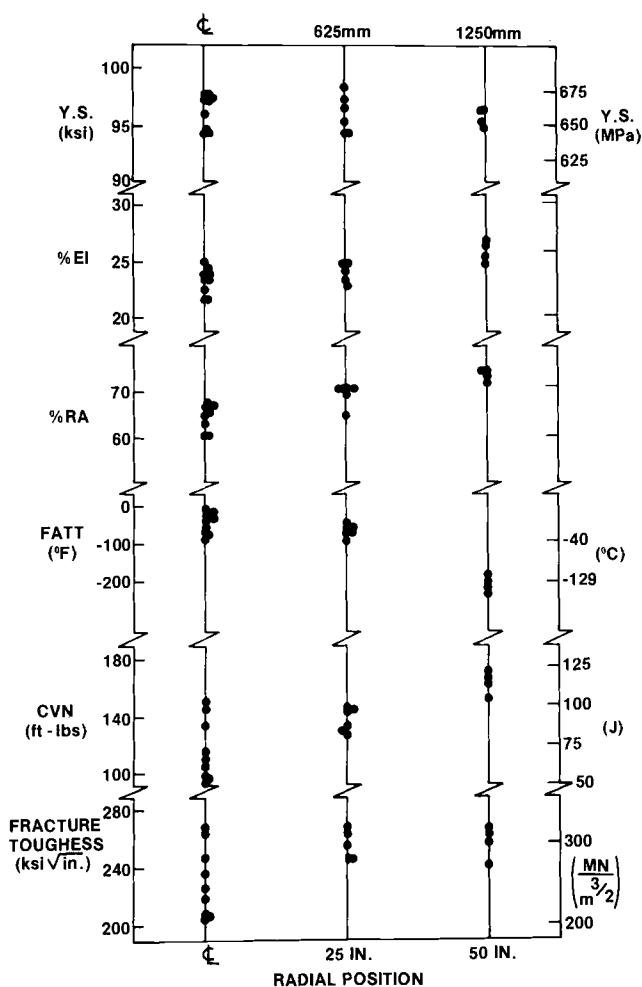


FIG. 15—Mechanical properties, fully integral LP rotors.

simulation data at an Electric Power Research Institute (EPRI) workshop in San Antonio. Scarlin et al. suggested that the fracture toughness at the center of large monoblocks might not be adequate to meet the requirements of the application in nuclear LP rotors. It is therefore most gratifying that, based upon data from actual monoblock forgings 2500-mm in diameter of 3.5Ni-Cr-Mo-V steel, that the authors now acknowledge that the center toughnesses of large monoblock forgings are high and adequate for the application. It is clear that simulated tests are not a satisfactory substitute to actual tests of the full component.

J. Albrecht, J. Bertilsson, and B. Scarlin (authors' closure)—At the time of our investigation very little data for fracture toughness of 3.5Ni forgings were available in the open literature; therefore, it was decided to perform simulation

tests. This method is well-known and has been applied in many laboratories for many years.

We agree that simulated tests are not a complete substitute for actual tests. They do, however, provide a fast and inexpensive tool—in some cases, as in alloy development, the only possible tool—for the identification of potential problem areas.

The limitations of simulation testing deserve future attention, for example, through comparison with data obtained from actual forgings.

*N. S. Cheruvu*⁷ (written discussion)—The speaker made a comment in his closing remarks that the toughness of the simulated rotor forging was inferior to that of actual large rotor forgings. It is well-known that toughness is strongly dependent upon steel melting practice and inclusions content, in addition to heat treatment and chemistry. What is the melting practice to make the experimental forging? When was this forging made? Does the forging have any inclusions? If so, what are they?

In discussing effects of tempering on microstructure, the speaker mentioned that the long platelet carbide on the grain boundaries breaks into small pieces upon tempering at higher temperatures. This creates new surfaces. Where is the energy coming from for the carbides to break and create new surfaces? Is there any reference or proof for this explanation?

It was reported by the speaker that the amounts of upper bainite, lower bainite, and martensite in the microstructure varied with the cooling rates. The lower bainite and martensite were differentiated by carbide *shape* (elongated versus spherical carbides). The shape of the carbide depends upon tempering temperature. One cannot distinguish between these two microstructural constituents based on the carbide shape; lower bainite exhibits the basic characteristics of shear transformation/martensitic transformation.

In order to distinguish these two microstructural constituents, one has to perform habit plane analysis. No such data was presented, and it is to be expected that additional analysis will be included in the paper.

These lower bainitic and martensitic transformations in the same steel differ in habit planes, shape deformation, and in their lattice invariant deformation.⁸

J. Albrecht, J. Bertilsson, and B. Scarlin (authors' closure)—(1) The forging was manufactured in 1979 in an electric arc furnace. A single melt was used to produce a 94-ton ingot that was used to fabricate two separate forgings. The degree of upsetting was 2.8. After preliminary heat treatments, the quality heat treatment was as follows: 830°C for 31 h, water cooling to 70 to 80°C, 600°C for 50 h, air cooling to 400°C for 30 h, cooling at 10°C/h to 200°C, and further cooling in air. The forging contains a number of small manganese-sulfide inclu-

⁷ Electric Power Research Institute, Palo Alto, CA.

⁸ Hehmann, R. F., "Transformation and Hardenability in Steels," Climax Molybdenum publication, 1967.

sions within the normal specified range. (2) Spheroidization of elongated precipitates is a well-known phenomenon during tempering. The driving force is the reduction of surface area, and the short-range diffusion necessary for the spheroidization is made possible by the high annealing temperature. Even pearlite can be spheroidized, yielding a microstructure called spheroidized cementite.⁹

Lower bainite can be distinguished from tempered martensite by the ellipsoidal shape of the carbides and the typical angle between the long axes of the carbides and the bainite lath axes.¹⁰ As far as fracture toughness is concerned, the appearance of lower bainite in the microstructure has a negligible effect. It is the inhomogeneous distribution and the coarseness of the carbides in upper bainite that have an adverse influence upon toughness.

⁹ Reed and Hill, *Physical Metallurgy Principles*, 2nd ed., Van Nostrand, New York, p. 749.

¹⁰ Reed and Hill, *Physical Metallurgy Principles*, 2nd ed., Van Nostrand, New York, p. 683.

Saburo Kawaguchi,¹ Noritaka Kanno,² Tadao Iwadate,³ and
Tateo Ohhashi³

Integrity of Full-Integral, Low-Pressure Nuclear Turbine Forgings

REFERENCE: Kawaguchi, S., Kanno, N., Iwadate, T., and Ohhashi, T., "Integrity of Full-Integral, Low-Pressure Nuclear Turbine Forgings," *Steel Forgings, ASTM STP 903*, E. G. Nisbett and A. S. McIlilli, Eds., American Society for Testing and Materials, Philadelphia, 1986, pp. 203–218.

ABSTRACT: Internal properties of disks from the body of a full-integral, low-pressure (LP) rotor forging were investigated. Segregation of alloying elements in forgings from 570-ton ingots is similar to that in forgings from 400-ton ingots, which have been used widely for the production of large rotors for more than 15 years. Distribution of tensile properties is quite uniform throughout the forging. Fracture Appearance Transition Temperature (FATT) is very low in the vicinity of the peripheral surface, increases with increasing depth into midradius, and remains almost constant from midradius to the center of the forging. Distribution of FATT along the length of the body was found. K_{Ic} -values converted from J_{Ic} are reported at several locations in the forging. Fracture toughness is in the upper shelf region even in the center of the rotor. The discrepancy between the K_{Ic} -value converted from valid J_{Ic} and valid K_{Ic} is discussed.

KEY WORDS: Ni-Cr-Mo-V rotor steel, very large ingots, large diameter forgings, fracture toughness, fatigue crack growth, crack initiation, mechanical properties, transition temperature, heat treatment

Low-pressure (LP) steam turbine shafts for modern nuclear power plants have been manufactured widely with the shrunk-on construction of disks and spindles because integral forgings large enough for such LP turbine shafts had not been available until recently. However, turbine manufacturers have begun to seek seriously the possibility of full-integral LP steam turbine forgings due to the problems associated with shrunk-on design, for example, stress corrosion cracking (SCC) at disk key ways.

The manufacture of full-integral, LP forgings requires very large ingots as

¹ Director, Steel Products and Fabrication Division, Tokyo Head Office, Japan Steel Works, Ltd., Muroran, Hokkaido, Japan.

² General manager, Forgings and Castings Department, Muroran Plant, Japan Steel Works, Ltd., Muroran, Hokkaido, Japan.

³ Deputy manager and senior metallurgist, respectively, Research Laboratory, Muroran Plant, Japan Steel Works, Ltd., Muroran, Hokkaido, Japan.

heavy as 570 tons, and the body diameter of a forging in the barrel shape could reach 2850 mm (112 in.). Experience with such a large diameter forging and the production results of ultra-heavy ingots have been reported already [1-4]. However, investigation results of internal properties of such large-sized LP turbine forgings is rare. Considering the importance of the component, it was decided to conduct an in-depth survey on the internal properties and the soundness of large LP turbine forgings for a half-speed machine. For this purpose, a full-integral LP shaft was sectioned and thoroughly studied. This paper presents the results of the investigation performed on the sectioned forging and data accumulated from the production of other integral LP forgings.

Experimental Procedure

Material and Sampling Location

The dimensions and weight of the sectioned forging are schematically shown in Fig. 1. The rotor shaft was manufactured conforming to a specification that is very similar to ASTM Specification for Vacuum-Treated Carbon and Alloy Steel Forgings for Turbine Rotors and Shafts (A 470-82), Class 6 except for the nickel content, which is approximately 3.1% in ladle analysis. Test Disks X and Y were cut out and used in this investigation. Material from two locations in Disk X were extensively investigated, namely, at 150 and 600-mm depths from the peripheral surface, each considered representative of the bucket or blade attachment area and the root of the machined disk, respectively.

The radial distribution of tensile properties, from the periphery to the center of the forging, were measured with specimens sampled from Disk X. In most cases, specimen direction was tangential, but radial and longitudinal specimens taken from several locations also were tested to evaluate the anisotropy of tensile properties.

Charpy impact specimens were taken radially through the full section of Disk X. Specimens taken from Disk Y at 600 mm from the surface and from the center of the disk were tested also.

Fracture toughness J_{Ic} was measured at 25°C with specimens taken from the center of both Disks X and Y. Specimen configuration was a 25.4-mm (1-in.)-thick compact specimen with 25% side grooves. The procedure conforms to the ASTM Test for J_{Ic} , a Measure of Fracture Toughness (E 813-81) unloading compliance method, and the specimen orientation is C-R according to ASTM Test for Plane-Strain Fracture Toughness of Metallic Materials (E 399-83). Measured J_{Ic} was converted to a K_{Ic} -value by the following equation.

$$K_{Ic}^2 = J_{Ic} \times E / (1 - \nu^2) \quad (1)$$

where

E = Young's modulus = 205 800 MPa, and
 ν = Poisson's ratio = 0.3.

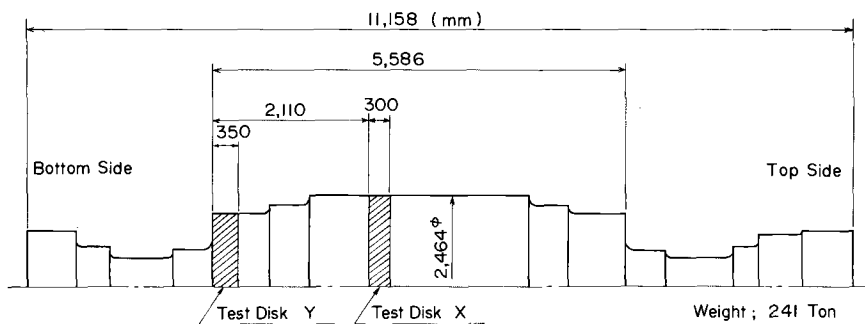


FIG. 1—The dimensions and location of test material of the investigated forging.

The fatigue crack growth rate (da/dN) was measured according to ASTM Test for Constant-Load-Amplitude Fatigue Crack Growth Rates Above 10^{-8} m/Cycle (E 647-83), using the samples taken from two locations, namely 150 and 600 mm from the peripheral surface of Disk X. Specimens from the location 150 mm from the surface were taken in C-R direction, and those 600 mm from the surface were oriented in C-L direction. Testing was done at room temperature in air with an R ratio of 0.05.

In order to measure the resistance of material in the center portion of the forging against crack initiation, the Japan Steel Works' Internal Pressure Bursting (JIB) test was performed. Its procedure has been reported in detail elsewhere [5,6]. Specimens with a 36-mm outer diameter with 3-mm wall thickness were taken longitudinally from the center of Disks X and Y and tested at room temperature.

Specimens for low-cycle fatigue (LCF) tests were taken radially from a 150-mm depth and tangentially from a 600-mm depth. Specimen configuration is the hour-glass type of 7-mm minimum gage diameter. Testing was done at room temperature, and sinusoidal waveform was used.

Results and Discussion

Segregation

Ingot-making plays an important role in manufacturing sound and homogeneous forgings. Therefore, in order to decide the optimum parameter of a 570-ton ingot, an extensive survey was conducted, including computer simulation of solidification and fundamental research on segregation. Figure 2 shows an example of the results of the survey.

To check the homogeneity at the approximate midbody of a rotor forging made from a 570-ton ingot, chemical analyses were conducted on material sampled from Disk X at radial locations of 120-mm increments from the surface to the center. Results are shown in Table 1. In order to evaluate the axial segregation of alloying elements in the ingot, the carbon content of the samples taken from

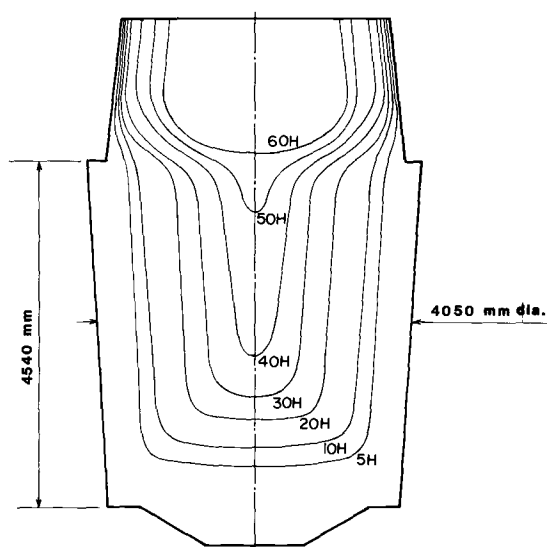


FIG. 2—The solidification front contour in a 570-ton ingot calculated as a function of time.

the center of Disks X and Y are compared with axial carbon segregation behavior of other monoblock LP shafts and large generator rotor forgings manufactured from 400-ton ingots. Carbon was used as an indication of segregation because it is most prone to segregation among alloying elements. The results are illustrated in Fig. 3. The *abscissa* is the axial location in a forging, and the *ordinate* is the ratio of checked carbon content to the ladle carbon content, which is averaged according to the weight and carbon content of each ladle. It is shown that axial carbon segregation in a 570-ton ingot is similar to that in a 400-ton ingot, which has been used for the production of approximately 100 specimens of large four-pole generator rotors for more than 15 years.

TABLE 1—Chemistry, weight %.

Distance from Surface, mm	C	Si	Mn	P	S	Ni	Cr	Mo	V
Ladle ^a	0.25	0.05	0.31	0.005	0.005	3.14	1.55	0.38	0.12
Surface	0.24	0.06	0.29	0.005	0.009	3.09	1.51	0.39	0.12
120	0.24	0.06	0.29	0.005	0.008	3.11	1.51	0.38	0.11
240	0.24	0.06	0.30	0.005	0.008	3.12	1.51	0.39	0.12
360	0.23	0.06	0.31	0.006	0.009	3.13	1.51	0.39	0.11
480	0.25	0.06	0.30	0.005	0.009	3.12	1.50	0.38	0.11
600	0.24	0.06	0.30	0.005	0.009	3.12	1.50	0.39	0.11
720	0.25	0.06	0.29	0.005	0.008	3.13	1.50	0.38	0.11
840	0.26	0.06	0.30	0.006	0.007	3.18	1.53	0.41	0.12
960	0.27	0.07	0.32	0.008	0.010	3.22	1.57	0.45	0.13
1080	0.28	0.07	0.32	0.007	0.010	3.24	1.58	0.44	0.13
Center	0.27	0.07	0.31	0.005	0.005	3.14	1.54	0.38	0.12

^a Weighted average of ladles.

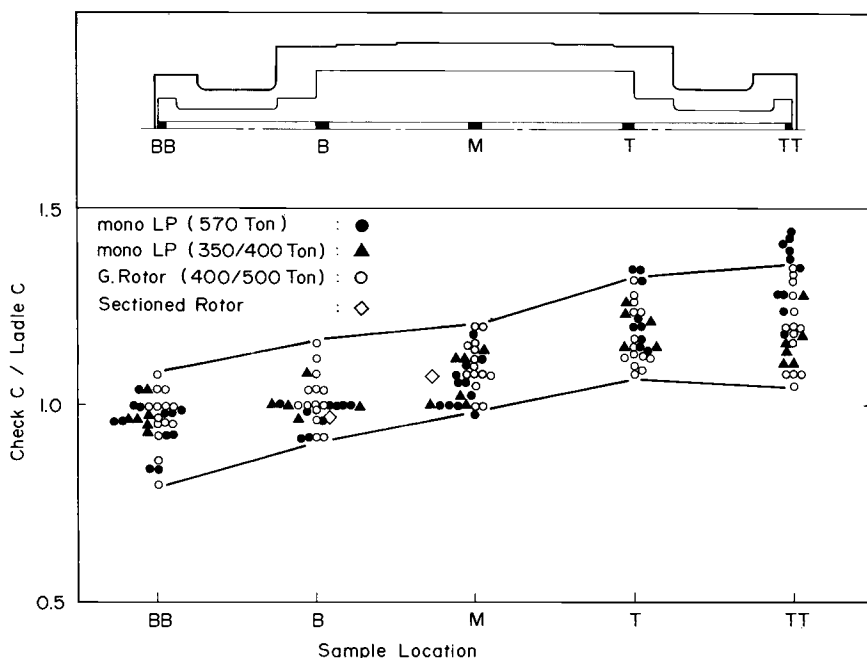


FIG. 3—Axial segregation of carbon in large rotor forgings.

Mechanical Properties

The distribution of mechanical properties from the periphery to the center of the forging was measured from material taken from Disk X. The tensile properties distribution, as shown in Fig. 4, is quite uniform throughout the full transverse section. Reduction of area exhibited a narrow scatter, but all values are high, with the minimum greater than 55%. This indicates that good solidification structure with little segregation was achieved at Disk X location in the 570-ton ingot and also that the material is clean and sound. Furthermore, the tension test results with specimens taken from Disk Y are almost the same as those from Disk X, showing good homogeneity of the forging at the X and Y disk locations.

The results of the Charpy impact test are shown in Fig. 5. For comparison, fracture appearance transition temperature (FATT) measured with material removed by long radial cores trepanned from body surface and center core bars of four other monoblock LP forgings (A, B, C, D) also are plotted in the same figure. It is clear from the figure that FATT measured with specimens taken from Disk X, which is approximately at the midlength of the body, is extremely low at the periphery and increases with increasing depth from the outside surface. Around midradius FATT reaches a plateau value that is well below ambient temperature and remains almost constant to the center of the forging. However, FATT of material removed from Disk Y is much lower than FATT of Disk X at

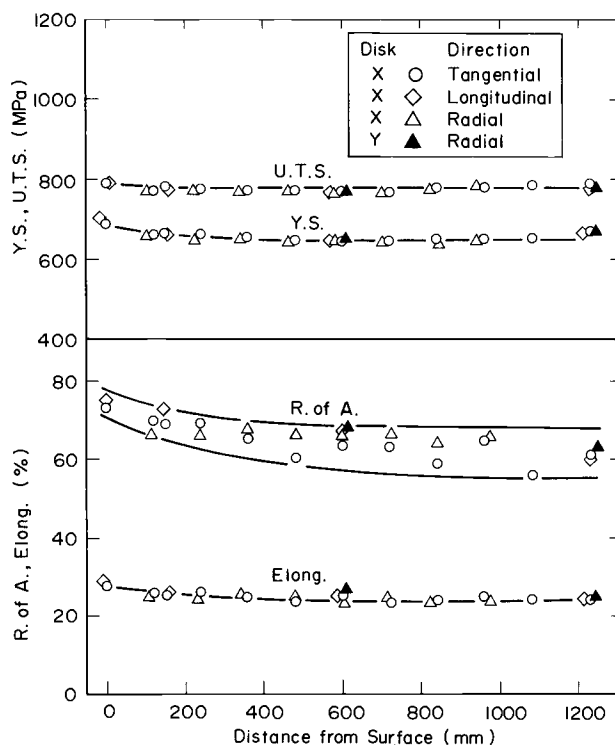


FIG. 4—Distribution of tensile properties from the periphery to the center of a monoblock LP rotor forging.

the same depth. This is due to the more effective cooling in the region of Disk Y during the quality heat-treatment cycle.

Rotor forgings A, B, C, and D differ from the sectioned rotor in chemistry, dimension, and strength level, and FATT distribution in each shaft is different accordingly. However, it is safe to conclude that the FATT of the center core bar material provides a conservative estimate of FATT of the full transverse section at the same axial location.

Since the LP turbine shaft is a highly stressed rotating component, it is of vital importance that the material has high resistance against brittle crack propagation. Therefore, fracture toughness was measured on the materials sampled from various locations of both Disks X and Y. Some of the results, namely, the relationship between the fracture toughness value and the test temperature of material taken from the center of Disks X and Y, are illustrated in Fig. 6 together with the K_{Ic} -value at room temperature of the center core bar material taken from other monoblock LP turbine forgings. At both locations, that is, the center of X and Y, fracture toughness is in the upper shelf region, and the fracture toughness value itself is sufficiently high. Other monoblock LP forgings, most of which have higher nickel content, exhibited even higher K_{Ic} -values.

Fracture toughness of material taken from these forgings was measured with

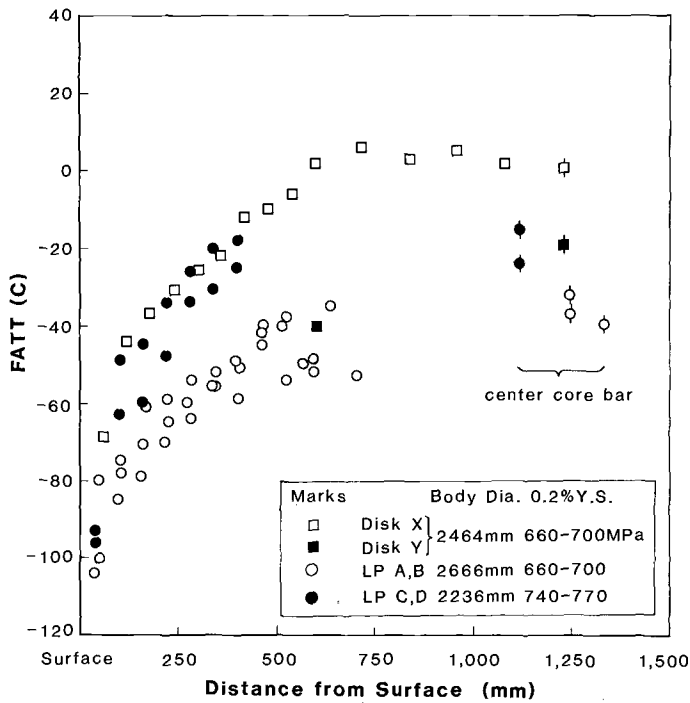


FIG. 5—Distribution of FATT from the periphery to the center of monoblock rotor forgings.

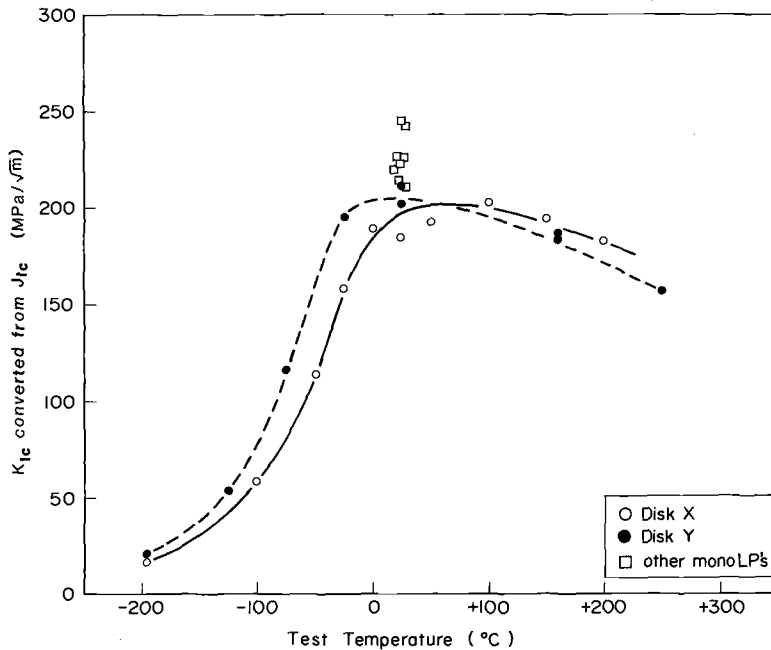


FIG. 6—Fracture toughness of material taken from the center of monoblock rotor forgings.

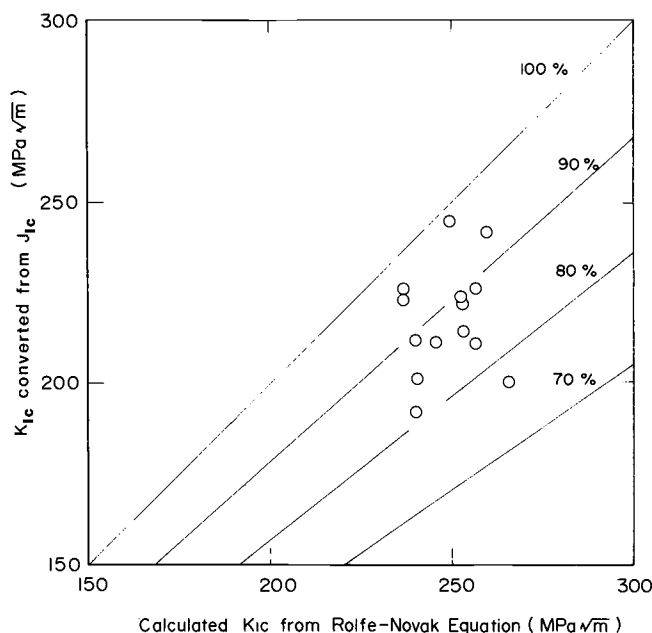


FIG. 7—Correlation between fracture toughness value K_{Ic} converted from J_{Ic} and calculated K_{Ic} from the Barsom-Rolfe equation.

the J_{Ic} method because a specimen of 250-mm (10-in.) width or larger would be needed to obtain valid K_{Ic} results. However, it has been reported that the K_{Ic} -value converted from the J_{Ic} method and valid K_{Ic} do not have close correlation to each other in the upper shelf region [5]. This discrepancy stems from the fact that while J_{Ic} is determined at the intersection of the blunting line and R curve, which represents the onset of a growing stable crack, K_{Ic} at the upper shelf is measured at the intersection of the loading line and cosecant line, allowing some extent of stable crack growth. Thus the K_{Ic} -value converted from J_{Ic} tends to yield lower value than a valid K_{Ic} . This effect was checked by comparing converted K_{Ic} from J_{Ic} and calculated K_{Ic} from the Barsom-Rolfe equation [7], whose results are shown in Fig. 7. It can be seen that K_{Ic} converted from J_{Ic} falls between 70 and 100% of calculated K_{Ic} . Therefore, when the fracture toughness value in the upper shelf region is to be discussed, the method of measurement is important and the results should be treated accordingly.

The fatigue crack growth rate was measured with samples taken from two locations of Disk X. In Fig. 8, the measured fatigue crack growth rate was compared with the results of the da/dN measurement on a conventional LP rotor forging in Refs 8 and 9, and it was found that da/dN of Disk X material locates at the bottom of the scatterband of da/dN of conventional LP.

Resistance against crack initiation was measured in two tests, namely the LCF test and the JIB test. The results of the LCF test performed on material taken

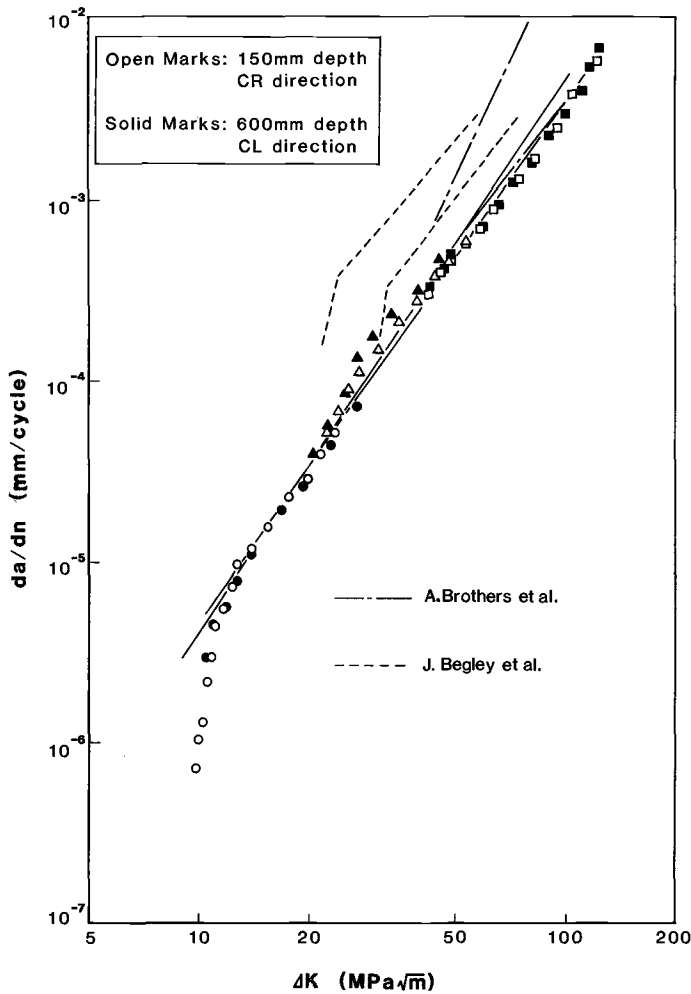


FIG. 8—Results of the fatigue crack growth rate measurement of specimens taken from Disk X.

from a location 600 mm from the peripheral surface of Disk X are shown in Fig. 9. The results are comparable to the LCF behavior of conventional rotor forging material.

JIB test results of material from the center of Disks X and Y are summarized in Fig. 10, together with the test results of other monoblock LP and conventional rotor materials. Results are generally regarded as good if the ultimate circumferential strain exceeds 3.5%. As shown in the figure, the ultimate circumferential strain of material taken from the center of monoblock LP forgings is greater than the 3.5% criterion.

Since monoblock LP rotor forgings have a very large body diameter, attainment

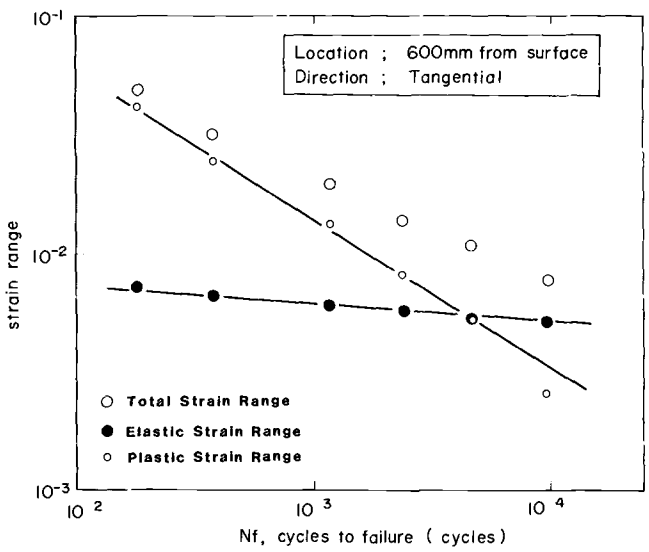


FIG. 9—Results of the low-cycle fatigue test performed on material taken from a 600-mm depth from the peripheral surface.

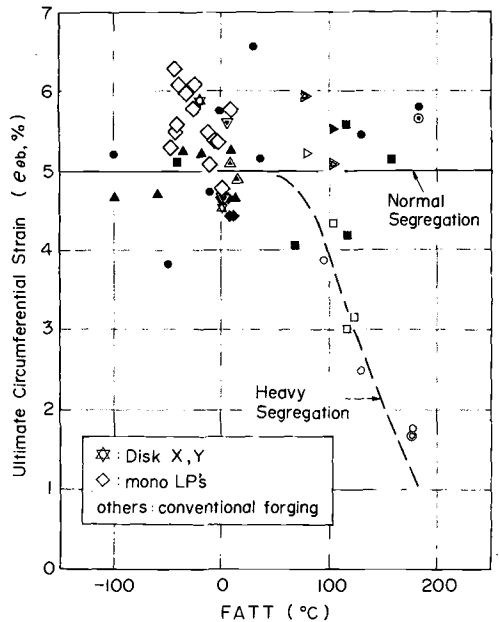


FIG. 10—Results of the JIB test on center core bars of monoblock LP forgings.

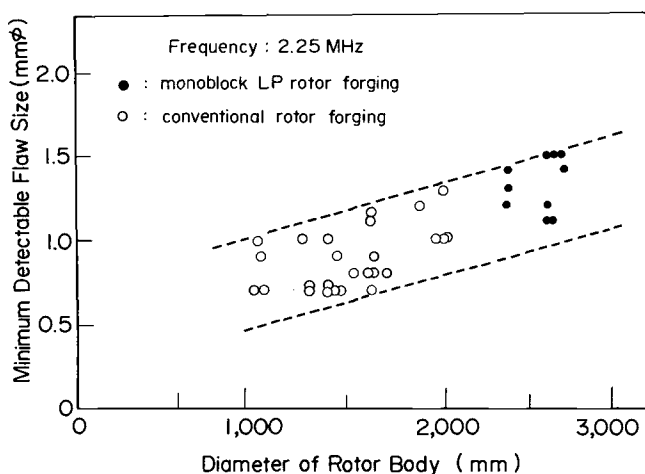


FIG. 11—The relationship between rotor body diameter and minimum detectable flaw size by ultrasonic test.

of good ultrasonic penetrability is extremely important from the viewpoint of reliability as a component. In order to achieve this, forgings receive lengthy heat-treatment cycles consisting of at least four separate austenitizations and temper cycles to obtain uniform fine-grain structure through the full section of the forgings. As a result, bainitic microstructure with ASTM Grain Size Number 5 to 6½ is consistently obtained in all monoblock LP forgings, and very small flaws can be detected in the center of forgings with the ultrasonic test, as shown in Fig. 11. The abscissa is the diameter of the rotor body, and the ordinate is the minimum detectable flaw size in the barrel shape condition, which is defined as a size of hypothetical flaw that gives twice the echo height of the noise echo at the center of the forgings. After trepanning the center bore, the bore sonic test can detect even smaller-sized flaws, if any, in the high-stressed region close to the bore surface.

Conclusions

In order to evaluate the reliability of large monoblock LP turbine forgings for a nuclear power plant, a full integral LP shaft forging was sectioned and investigated thoroughly. The results were compared with data generated from other monoblock LP shaft forgings as well as data from conventional rotor forgings such as LP shafts for fossil power plant or 4-pole generator rotor forgings. It was shown that internal properties of monoblock rotor forgings are excellent and exceed in all measured parameters the levels needed for safe operational performance. These results have been achieved in monoblock rotor forgings made to date despite their large diameters and the very heavy ingots from which they were produced.

References

- [1] Kashihara, M., Kawaguchi, S., Yanagimoto, R., Sawada, S., and Tsuchiya, K., "Development of Gigantic Forgings with Ultra-heavy Section Exceeding 2500-mm Diameter from Ingots Weighing over 400 Tons," presented at the Eighth International Forgemaster Meeting, Kyoto, Japan, Oct. 1977, Steel Castings and Forgings Association, Tokyo, Japan.
- [2] Kawaguchi, S., Nakagawa, Y., Watanabe, J., Shikano, S., Maeda, K., and Kanno, N., "Challenge to Manufacture of Large Forgings from 500 Metric Ton Steel Ingots," presented at Seventh International Forgemaster Meeting, Paris, France, Apr. 1975, Chambre Syndicale de la Grosse Forge Française, Paris.
- [3] Kawaguchi, S., and Sawada, S., "Workshop Proceedings: Rotor Forgings for Turbines and Generators," EPRI WS-79-235, Electric Power Research Institute, Palo Alto, CA, Sept. 1981.
- [4] Kawaguchi, S., Yanagimoto, Y., Sawada, S., and Ohhashi, T., "Historical View of Manufacturing Large Mono-Block Rotor Forgings and Future Outlook," presented at International Forging Conference 1981, Dusseldorf, West Germany, May 1981, VDEH and VDF, Düsseldorf.
- [5] Watanabe, J., Iwadate, T., and Karaushi, T., "Recent Development of the Strength Evaluation of Large Forgings," presented at the Eighth International Forgemaster Meeting, Kyoto, Japan, Oct. 1977, Steel Castings and Forgings Association, Tokyo, Japan.
- [6] Watanabe, J., Iwadate, T., and Saito, N., "A Study on Crack Initiation in Rotating Parts," presented at the Second International Conference on Mechanical Behavior of Materials, Boston, MA, 1976.
- [7] Barsom, J. M. and Rolfe, S. T. in *Impact Testing of Metals*, ASTM STP 466, American Society for Testing and Materials, Philadelphia, 1970, pp. 281-302.
- [8] Brothers, A. J. and Yukawa, S., *Journal of Basic Engineering*, March 1967, pp. 19-27.
- [9] Begley, J. A. and Toolin, P. R., *International Journal of Fracture*, Vol. 9, No. 3, Sept. 1973, pp. 243-253.

DISCUSSION

W. Wiemann¹ and J. Ewald¹ (written discussion)—Tateo Ohhashi showed with his clear and informative presentation results of mechanical and toughness properties over the cross section of very large LP monoblock rotors. It can be seen that the toughness of LP rotors of 3.5Ni-Cr-Mo-V steel made much more often today is distinctly greater than those made from 3Ni-Cr-Mo-V steel² (Fig. 12). The higher sensitivity against temper embrittlement with increasing nickel contents of these steels seems to be overcome by modern manufacturing processes. The danger of long-time embrittling is not at present due to low enough operational temperatures. Figure 12 also underlines the conclusion by J. Albrecht³ that the heat treatment simulation with even 3.5Ni-Cr-Mo-V steel distinctly underestimates the center toughness of 3Ni-Cr-Mo-V steel.

It should be noted that the feasibility of heavy rotors with diameters up to 107

¹ Kraftwerk Union AG, Muelheim a.d. Ruhr, Germany.

² Jaffee, R. I., "Letter on Fracture Toughness of Monoblock LP Forgings," compiled by Electric Power Research Institute (EPRI), Palo Alto, CA, 3 Aug. 1984.

³ Albrecht, J., Scarlin, R. B., and Bertilsson, J. E., "Fracture Toughness of Actual and Simulated Large Rotor Forgings made from 3.5% Nickel Steel," this publication.

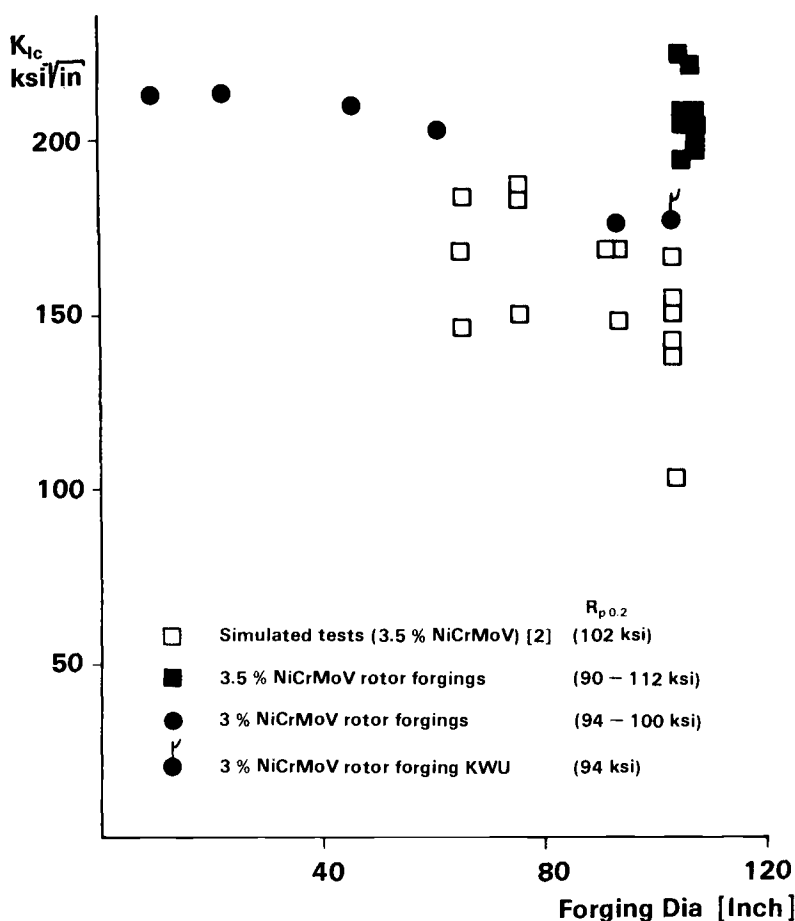


FIG. 12—Fracture toughness results for simulated specimens and rotor forgings of 3- and 3.5Ni-Cr-Mo-V steel, Kraftwerk Union AG.

in. has been proven since 1976.^{4,5} The fracture toughness—determined at room temperature—of center core material of such a rotor made by 3Ni-Cr-Mo-V steel is also included in Figure 12 and fits very well the results presented by T. Ohhashi. Figure 13 gives an impression of this rotor and summarizes the dimensions and chemical composition.

⁴ Kashihara, M., Kawaguchi, S., Yanagimoto, R., Sawada, S., and Tsuchiya, K., "Development of Gigantic Forgings with Ultra-Heavy Section over 2500 mm in Diameter from Ingot, Weighing over 400 Mg," Report No. 19, Eighth International Forgemasters Meeting, Kyoto, Japan, 1977.

⁵ Wiemann, W., "Requirements for Forgings for Turbine and Generator Rotors," VGB Kraftwerkstechnik, Dec. 1979, pp. 937–951.

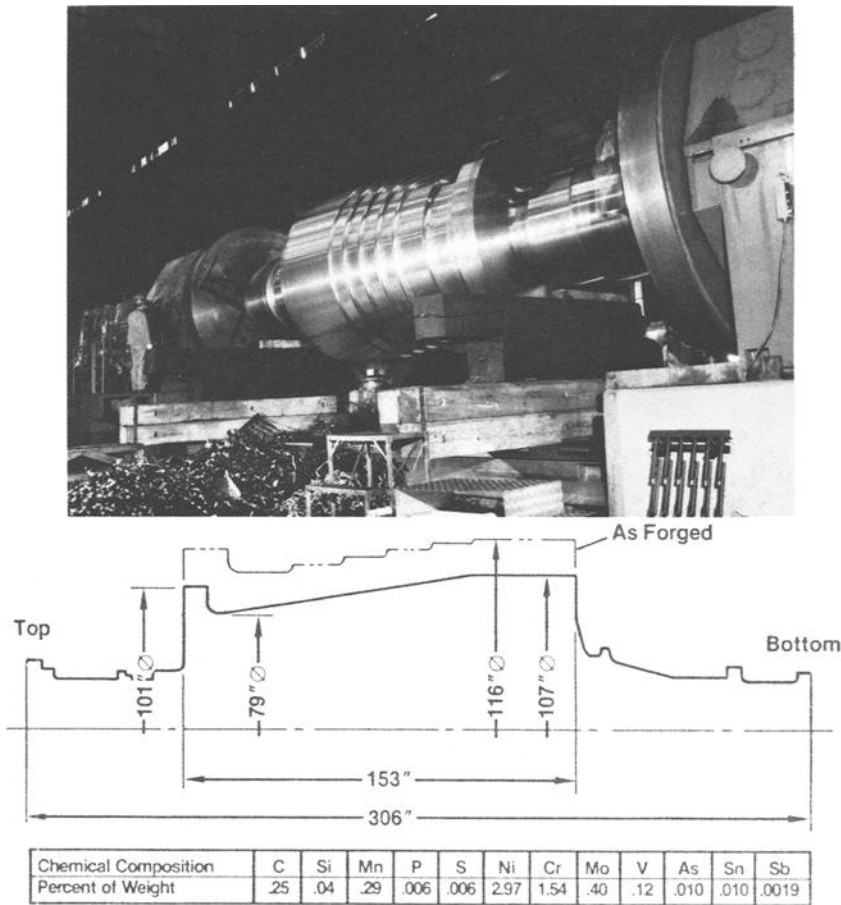


FIG. 13—A 190-ton LP rotor from vacuum-carbon-deoxidized 2.8Ni-Cr-Mo-V material, Japan Steel Works.

S. Kawaguchi, N. Kanno, T. Iwadate, and T. Ohhashi (authors' closure)—The discrepancy between the fracture toughness values obtained on the simulation heat-treated material and on the samples taken from the actual large forging has been widely discussed recently. The simulation heat-treatment technique will give a very good prediction of the strength level and a fairly good estimate of fracture appearance transition temperature of the large forgings, since both the strength level and also the FATT of a material are dependent on such factors as transformation products, grain size, and dislocation density, all of which can be easily reproduced by a simulation heat treatment. However, the fracture toughness value, especially in the uppershell region, is affected also by other factors like the distribution, size, and density of inclusions, etc., that are not controlled by heat treatments.

As the discussers pointed out, the sufficiently high toughness values were constantly achieved in a number of large monoblock LP rotors, which was illustrated in Fig. 12.

*G. Hartman*⁶ (*written discussion*)—You gave a ratio of check carbon/ladle carbon on one of your slides. What was the actual variation in carbon content along the centerline representing the bottom and the top of the ingot? Also, what was the ladle carbon content at these locations? Since phosphorus and sulfur do segregate and are very important in the Ni-Cr-Mo-V analysis, what segregation of these two elements occurred from top to bottom of the ingot along the axial centerline?

S. Kawaguchi, N. Kanno, T. Iwadata, and T. Ohhashi (*authors' closure*)—**Actual Variation in Carbon Content Along Centerline Representing the Bottom and Top of the Ingot**

In order to teem large ingots such as a 570-ton ingot, molten steel in multiple ladles from several basic electric furnaces is used. The carbon content of each ladle is varied to lessen the axial chemistry segregation, that is, heats with higher carbon content are poured to the bottom, and molten steel with leaner chemistry is filled toward the top of the ingot. However, the "ladle carbon" content used in the calculation of the check C%/ladle C% is weighted average value of each ladle, which is approximately 0.25% for most cases. The check C%/ladle C% values at BB and TT locations averaged over 22 monoblock rotor forgings and are 0.936 and 1.198, respectively. Therefore, the difference in carbon content between the bottom and the top of an ingot centerline is expected to be $0.25 \times (1.198 - 0.936)$ or 0.066%. As can be seen in Fig. 3, there is a wide scatter in the calculated ratio. However, the actual difference in carbon content

TABLE 2—Distribution of check analysis/ladle analysis value of phosphorus and sulfur from BB to TT locations.

Element	Location	Checked Value/Ladle Value	
		Average	Standard Deviation
P	TT	1.32	0.31
	T	1.25	0.20
	M	1.17	0.31
	B	1.05	0.23
	BB	1.01	0.26
S	TT	1.37	0.27
	T	1.32	0.25
	M	1.22	0.28
	B	1.18	0.30
	BB	1.09	0.27

⁶ A. Finkl & Sons Co., Chicago, IL 60614.

between TT and BB locations does not exceed 0.10% for most 3.5Ni-Cr-Mo-V monoblock rotor forgings.

Phosphorus and Sulfur Segregation

Axial segregation of phosphorus and sulfur is evaluated with the ratio of the check analysis value to the ladle analysis value at BB to TT locations. Results are summarized in Table 2.

In-Service Inspection Test and Evaluation Techniques for Large Generator Rotors

REFERENCE: Bellows, R. H., Zawoysky, R. J., and Walker, D. N., "In-Service Inspection Test and Evaluation Techniques for Large Generator Rotors," *Steel Forgings, ASTM STP 903*, E. G. Nisbett and A. S. Melilli, Eds., American Society for Testing and Materials, Philadelphia, 1986, pp. 219-234.

ABSTRACT: There is much interest on the part of utilities to pursue avenues for upgrading and for the life extension of electrical generating equipment. As an integral part of such an evaluation, the current condition of the generator rotor must be assessed fully to determine if the rotor can be expected to perform reliably for many additional years. A comprehensive nondestructive testing (NDT) and evaluation program has been developed by General Electric Co. to assess the condition of in-service generator rotors, to make predictions of remaining life, to set reasonable reinspection intervals, and, most importantly, to identify rotors that have a high probability of failure and to recommend that they be replaced or otherwise upgraded to minimize the chances of failure.

This paper will describe the inspection methods and analytical techniques that are used in the evaluation of in-service generator rotors and will provide a summary of recommendations that have been made to date.

KEY WORDS: in-service inspection, nondestructive tests, generator rotors, fracture mechanics

Large electrical generators manufactured by General Electric always have been designed for a long service life of high reliability and availability based upon the limits of existing technology at the time of manufacture. However, the service life of generator rotors manufactured with the same technology may vary significantly because of many factors. These factors include the operating conditions for a specific machine, misoperations that a unit might be subject to, and the material properties of the specific rotor that were developed during the original steel-mill processing from ingot to finished rotor forging. The use of modern steelmaking technology typically results in rotor forgings that are free of or nearly

¹ Metallurgical Engineer, Generator Mechanical Engineering, General Electric Co., Schenectady, NY 12345.

² Engineer, Generator Availability Engineering, General Electric Co., Schenectady, NY 12345.

³ Manager, Generator Mechanical Engineering, General Electric Co., Schenectady, NY 12345.

free or reportable indications; however, the best technology available at the time of production of some early generator rotor forgings resulted in some that contained material imperfections, such as forged-in laps and seams, large nonmetallic inclusions and stringers, and hydrogen flakes, to name a few.

In-service evaluations of generator rotors have been conducted for many years to assess the current condition of the rotor so that the outlook for future use could be established. The current program was initiated in 1974 with the goal to evaluate certain potentially high-risk rotors. These rotors fall in two basic categories: those manufactured prior to about 1959 when vacuum-treated steel was introduced into full production in the United States; and those rotors that are operated in a frequent start-stop duty mode (those that accumulate more than about 50 such cycles each year and may be subjected to the cumulative effect of low-cycle fatigue propagation of existing imperfections).

Historical Development of Testing Procedures

General Electric pioneered the development and application of nondestructive test techniques needed to evaluate the condition of turbine-generator rotors. New tests have been introduced for use in evaluating both turbine and generator rotors as shown in Table 1, which provides the approximate time of introduction of these tests. Bore visual and bore magnetic particle tests were introduced in the early 1930s, and the first periphery ultrasonic test was introduced in the late 1940s. The sensitivity of this test was very limited by comparison to the type of peripheral ultrasonic test employed today; however, it was capable of identifying rotor forgings with very serious internal defects.

Based upon this test, many forgings destined for service were terminated during production at the various steel mills and a replacement fabricated. Undoubtedly, the number of failed generator rotors would have been higher had this test not been implemented, because it was not much later that the average diameter of generator rotors began to increase significantly as did operating stresses in re-

TABLE 1—*History of generator rotor nondestructive tests.*

Year of First Significant Use	Nondestructive Test
Pre-1930	oil and whiting tests
1930	bore visual examination
1930	bore magnetic particle test
1949	periphery ultrasonic test
1959	bore ultrasonic test
1962	ultrasonic test of bottle bores
1974	high resolution periphery ultrasonic test
1976	DATAQ—automated boresonic test
1979	angle-beam boresonic test
1982	ABBOR—automated angle-beam boresonic test

sponse to utility demands for greater output per machine. Not all rotor forgings with harmful defects were identified because of the limited sensitivity of these early tests. Consequently, some such rotors that are still in service today may be nearing the end of their useful lives with their ability much reduced to survive the stresses associated with certain machine misoperations, such as overspeeding and high shaft torques due to electrical system disturbances.

Many generators have been manufactured with a borehole throughout the entire length of the forging because the poorest quality material in the rotor forging is usually located at and near the axial centerline and it is best to remove it. The earliest bore examinations were performed to determine by visual and magnetic particle techniques if the poor quality material had successfully been removed by the boring operation. These tests relied upon the observations of an operator as he viewed the bore through a long borescope but did not allow the examination of the critical internal material near the surface of the bore.

In the late 1950s, this situation was greatly improved by the introduction of an ultrasonic test conducted from the surface of the bore, which was closely followed by the ability to conduct the same type of test even in bottle-bored regions. These tests were not automated and required that the operator manually record any indications that were located, but they represented a major step forward in evaluating the material near the bore surface. This is of significance because the tangential stress at the bore surface is higher than at any other place in the rotor during normal operation, and unknown near-surface defects could initiate failure during overspeed conditions or as a result of start-stop cycling. The distribution of tangential bore stresses as a function of distance from the bore surface is shown in Fig. 1, where it can be seen that this stress drops off very rapidly with distance from the bore surface and emphasizes the need to know the metallurgical condition of the material that is close to the bore surface.

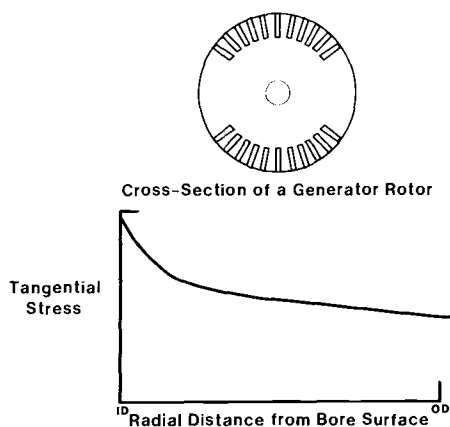


FIG. 1—Stress due to centrifugal loading.

Development of Automated Testing Procedures

From the first introduction of the peripheral and boresonic tests until the present time, many improvements have been made and implemented into the evaluation of new generator rotors. These same test techniques also are being applied to the in-service inspection of rotors so that the best possible information can be utilized in the evaluation of those rotors. The DATAQ⁴ computerized boresonic system is a fully automated *data acquisition* system. This automated system utilizes straight-beam transducers that are connected to a device that keeps the transducers in contact with the bore surface as the rotating head is fed into the bore of the rotor. All detected indications are automatically recorded and the minimum effective flat bottom hole (MEFBH) sizes calculated. The ABBOR⁴ computerized test system is a fully automated *angle beam boresonic* test that is used primarily to inspect for the existence of radial-axial cracks emanating from the bore surface.

Inspection Program

The objective of the inspection program is to inspect potentially high-risk rotors, defined by the time of manufacture and by the measured or estimated fracture appearance transition temperature (FATT), and to identify those rotors whose internal condition is such to present a significant operating risk of a rotor burst. When identified, such rotors would be recommended for corrective action or the frequency of reinspection identified so that the probability of a situation like that of the rotor bursts of the 1950s can be minimized [1]. Rotors that have been so identified either have been placed in a restricted operating mode, recommended for bore work to remove objectionable indications, or recommended for replacement.

A restricted operating mode might require that the rotor be used only for base-load power generation and be reinspected within a certain number of start-stop cycles or that the temperature of the rotor be prewarmed prior to reaching rated speed to increase the effective fracture toughness (namely, increase the critical crack size) or both. The use of bore work varies from the relatively easy removal of defects on or near the bore surface by local grinding and honing to much more difficult boring operations. Overboring is utilized when the entire length of the bore must be enlarged to correct unsatisfactory conditions, while bottle boring is employed when only a relatively short length of the bore diameter must be enlarged. Both overboring and bottle-boring have been employed in the same rotor; however, there are both stress and magnetic-flux-carrying criteria that must be satisfied when extensive bore work is being considered. The following list details the types of recommendations that have been made as a result of about

⁴ DATAQ and ABBOR are trademarks of the General Electric Co., Schenectady, NY 12345.

650 generator evaluations of about 475 different generator rotors:

1. Reinspect within a specified time.
2. Reinspect within a specified number of start-stop cycles.
3. Perform bore work and reinspect.
4. Replace the rotor.

Figure 2 illustrates the trends for those recommendations that have been made over the past ten years. The vertical axis represents the cumulative number of rotors in each of the major recommendation categories as a function of time. Subsequent retests of rotors are excluded from the statistics. The bore work category shown in Fig. 2 represents that population that was recommended for significant bore work prior to additional operation. Recently, the tendency for significant bore work to be required has diminished, and the percentage of rotors

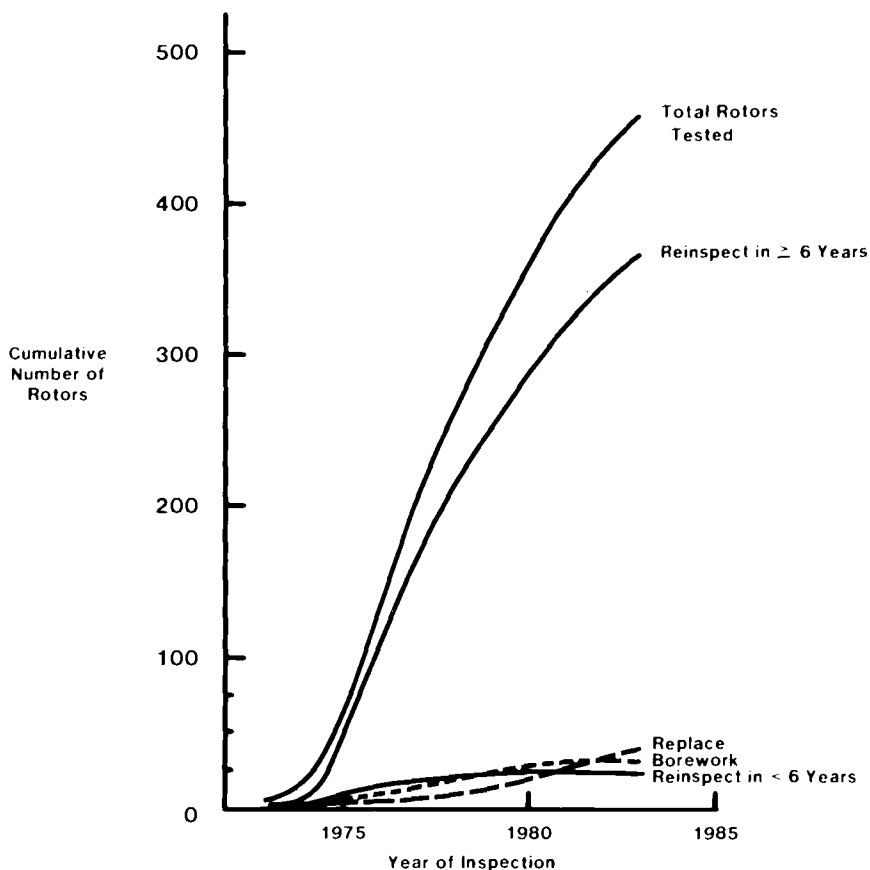


FIG. 2—In-service inspection trends for generator rotors.

with a 5-year-or-greater recommended inspection interval is on the increase. The standard inspection interval is now 6 years for most rotors, and the maximum suggested interval thus far has been 12 years. For some generators with relatively good test results and material properties, the reinspection interval has been set at 1000 start-stop cycles with no time limit. However, the percentage of rotors that have been recommended for replacement has shown a steady, although small, increase since 1974. This is because even though inspection priority lists were established based on the estimated fracture appearance transition temperature of each forging, it was not possible to predict which rotors would have the greatest probability of having serious defects.

Furthermore, some owners delayed having their generators inspected even though they were considered to be in the high risk population based on the FATT, and some such inspections have been conducted only quite recently. In addition, better definition of the pattern of imperfections as a result of using the automatic computerized DATAQ and ABBOR tests generally has resulted in lower predictions of rotor capability. However, there also have been several instances when the better definition of flaws has resulted in an improved prediction of rotor capability.

Test Procedures

In preparation for the normal in-service rotor inspection, the owner removes the rotor from the stator and places it in an appropriate location in the power station to provide sufficient access for nondestructive testing. Nondestructive testing (NDT) specialists of General Electric have the equipment and expertise to perform minor bore work, such as grinding and polishing of the bore surface in preparation for testing. Other operations such as oxide blasting, honing, and machining must be contracted for separately. The tests normally conducted as part of the in-service inspection program for generator rotors having a center bore hole are as follows:

1. *Bore visual inspection*—All visual surface indications and surface irregularities are described, and their axial and circumferential locations are recorded. Photographs of representative indications and conditions are taken for subsequent examination.

2. *Bore magnetic particle test*—All magnetic particle indications are described and the axial and circumferential locations on the bore surface recorded. Again, photographs representative of the more severe indications or conditions are taken for examination. Figure 3 shows examples of crack-like indications that were observed in the bore of a rotor by means of the magnetic particle test.

3. *Bore ultrasonic tests*—Two different ultrasonic tests are conducted from the bore surface. The computerized DATAQ straight-beam 2¼-MHz ultrasonic test is utilized to automatically identify and record the axial, radial, and circumferential location of all indications. Particular note is made of holding indications,

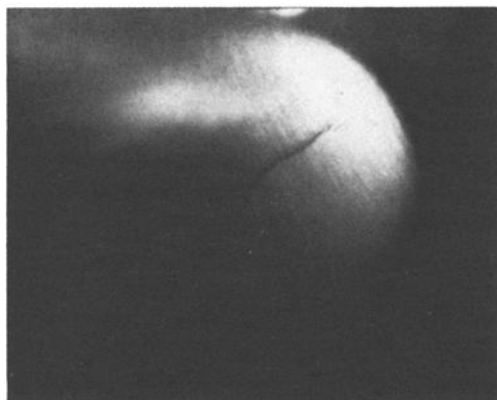
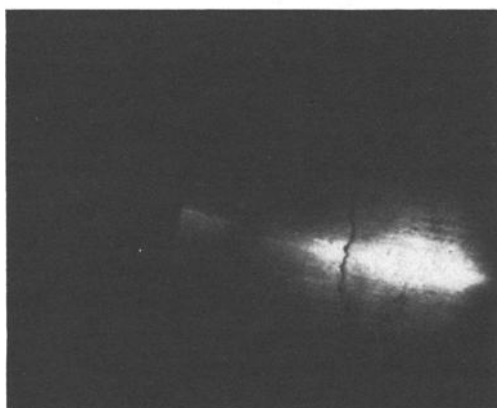
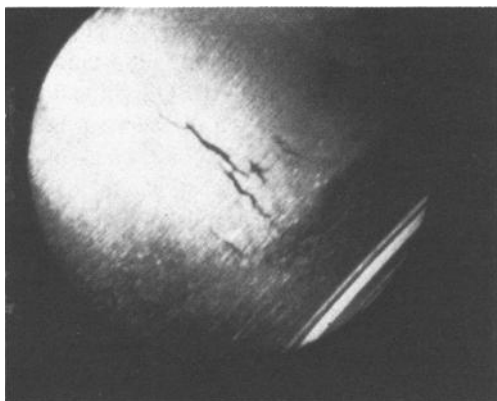


FIG. 3—Crack-like magnetic particle indications on bore surface.

that is, ones which continue to reflect ultrasonic energy beyond what would be expected of a point source reflector as the rotating ultrasonic test head is automatically fed into the bore of the rotor. The ABBOR computerized test system utilizes 2¼-MHz angle-beam probes to search the bore surface for radial-axial indications emanating from the bore surface that have crack-like characteristics.

Because some older rotors contain many indications, the data from these tests are plotted from a computer data file so that a visual representation of the data is available for analysis. Figure 4 is an example of a radial-axial computer plot of data from the DATAQ test of a rotor with many indications. These data are compressed into a single plane, and this type of presentation is helpful in assessing the success of a potential bottle bore that might be used to upgrade the rotor.

Another type of computer plot that is commonly constructed from DATAQ data for use in interpreting ultrasonic data is shown in Fig. 5. This relates the circumferential position of indications to the axial location and is helpful in identifying axially aligned defects and in deciding whether the most effective means of removing indications is by bottle boring or by local grinding.

By using visual presentations of data from the ABBOR test, an even better picture of the orientation, clustering tendencies, and planarity of any indications can be obtained. An example of a transverse plot covering a few inches of axial length is shown in Fig. 6. This indicates that the indications are in highly oriented clusters that emanate radially from the bore, like spokes from the hub of a wheel. The width of the radial bands suggests that they are composed of radial clusters of small indications rather than a single radial-axial crack that would appear much narrower, since any indications beyond a crack would not be seen because sound cannot propagate across a crack. Figure 7a shows a similar presentation of data

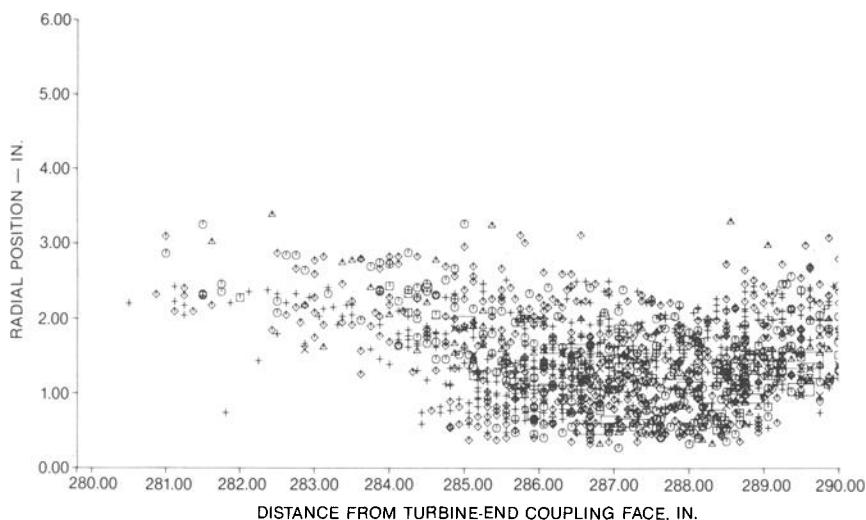


FIG. 4—Axial-radial boresonic data plot—DATAQ.

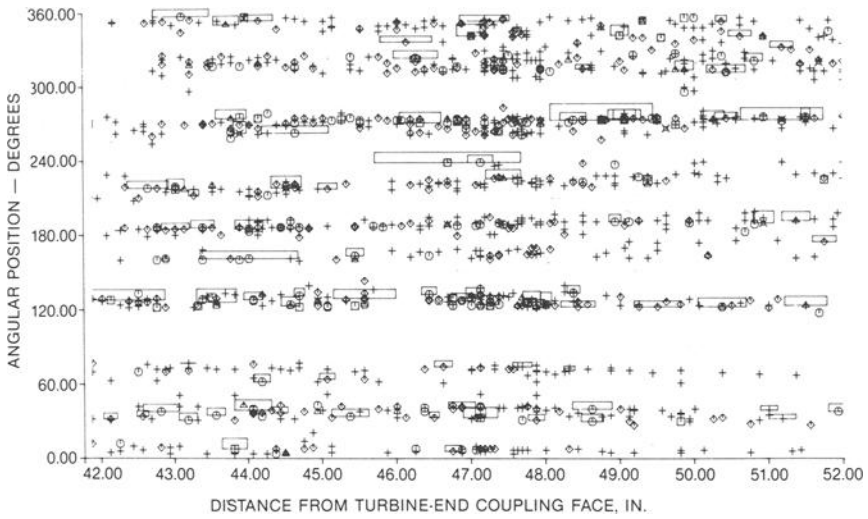


FIG. 5—Axial-circumferential boresonic data plot—DATAQ.

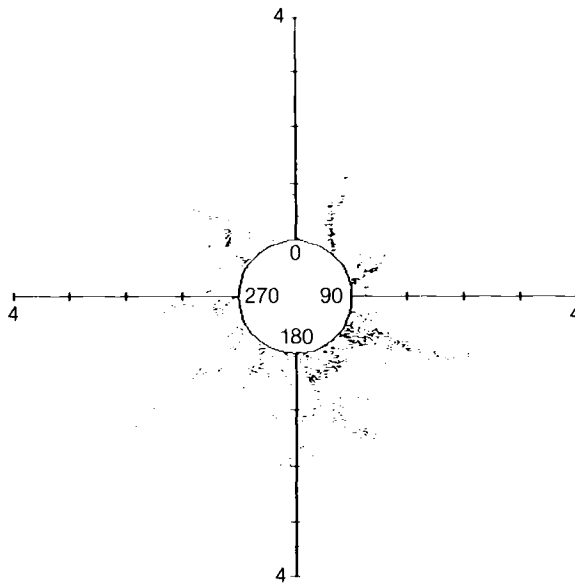


FIG. 6—Transverse section plot of angle-beam boresonic data—ABBOR.

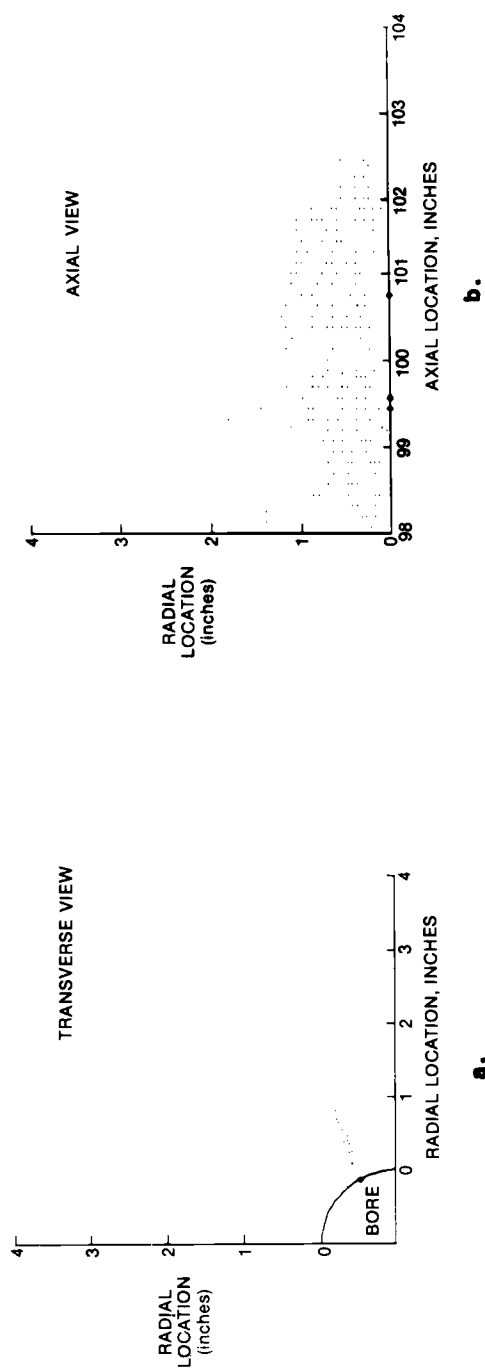


FIG. 7—Angle-beam boresonic data showing radial-axial flaws.

from an angle-beam boresonic test of a rotor. Here, the indication is revealed as a narrow, radial-axial planar cluster that would be indicative of a crack. The radial-axial plot of a similar man-made crack in Fig. 7*b* also suggests that the indication is a crack because the planar representation of the defect within a narrow angular band is characterized by a dense array of indications.

These examples demonstrate the powerful use of the computerized boresonic systems for gathering, displaying, and evaluating large numbers of indications (several thousand detected in some rotors).

4. *Periphery ultrasonic test*—Both 1.0 and 2.25-MHz longitudinal-beam transducers are used to perform tests from all accessible peripheral surfaces. Accessibility is especially hampered in the generator rotor main body locations because of the body grooves, slots, dovetails, and windings. The amplitude and axial, radial, and circumferential location of all indications are recorded. Special attention is paid to unusual indication patterns, to sizes, to orientation of clusters of indications, and to levels of indications.

The equipment utilized to perform all these tests is contained in three portable shipping containers that are transported to the job site. All ultrasonic test data are transmitted via telephone link directly to a data file where they are analyzed by the use of a main frame computer. Other information such as bore-visual and bore-magnetic particle test results are transmitted by means of a telecopier. In addition to the standard tests just listed, certain supplementary tests may be conducted in order to help clarify the results from the standard tests. For example, a high resolution (5-MHz) periphery test may be conducted to better define the sizes and spacing of indications within levels or those close to the outside diameter surface.

Evaluation of Test Results

The analytical technique is based on the use of all known information about the rotor to perform a linear elastic fracture mechanics analysis. This information is categorized as NDT data, material property information, and the knowledge of the design stress and operational history of the specific rotor. The use of all known information about the rotor, coupled with the extensive experience gained as a result of many years of performing these inspections and evaluations, allows for a realistic recommendation to be made. Use also has been made of information obtained by sectioning some rotors that were retired, correlating measured and actual defect sizes, and conducting fatigue tests on material samples containing known types of defects. For example, the photograph in Fig. 8 shows a large forged-in defect that was found near the bore of a retired generator rotor. It was identified by ultrasonic testing and removed from the rotor by means of a large diameter radial trepan and subsequently sectioned and broken open for examination.

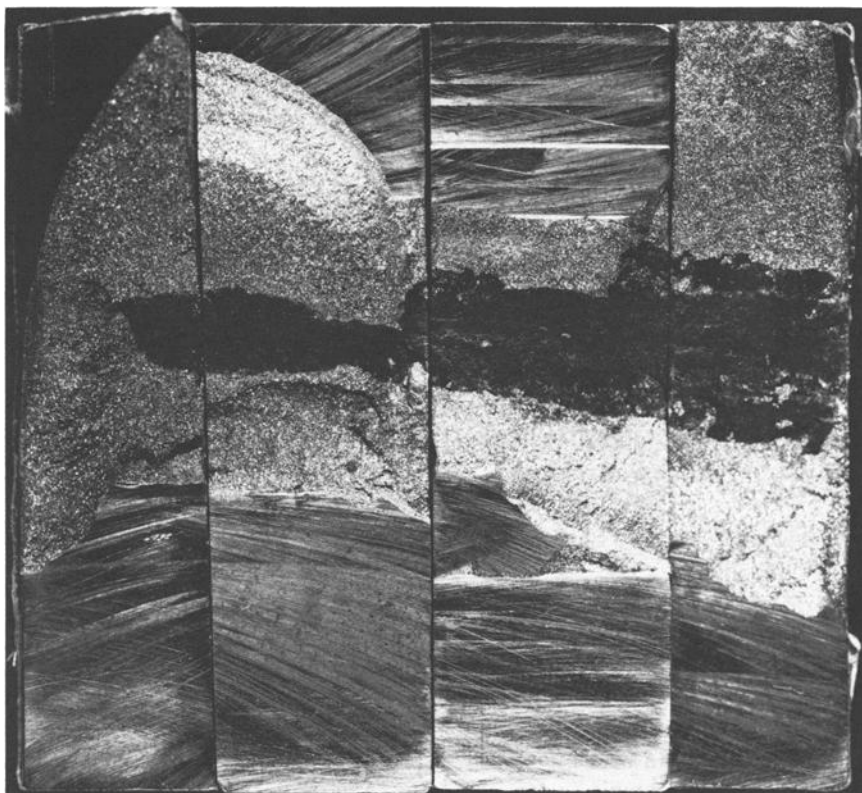


FIG. 8—*Defect removed from a generator rotor.*

Ultrasonic indications are reflections of acoustic energy that can come from many different types of discontinuities in the material. Porosity, large grains, nonmetallic inclusions, and cracks may all reflect ultrasonic energy in the same manner, and present ultrasonic methods cannot for the most part distinguish between small defects of these types, nor can the effects of these indications on the mechanical properties of the rotor be determined by the use of these techniques. Although many programs have been conducted in past years to relate the size of real and artificial defects to the reported ultrasonic test data and to determine the influence of these indications on the properties of the rotor, it is still not possible to distinguish cracks from other indications that can cause a similar reflection of ultrasonic energy. Furthermore, because indications that are not cracks can initiate cracks after repeated start-stop cycles and certain fault conditions, it is assumed in the analysis that all of the reported indications are cracks. Whereas this is a conservative assumption, it is the only one that can be justified recognizing the potential for a catastrophic rotor failure if an error in defect classification was made.

The stresses of most significance for fracture mechanics analysis of the generator rotor body are the tangential stresses due to the centrifugal loads. Thermal stresses are of second order significance in a generator rotor. The tangential stress is highest at the bore of the rotor, and it is magnified over what would be calculated for a uniform steel cylinder as a result of the difference in the centrifugal loading in the direction of the solid poles of the rotor and the quadrature axis in line with the rotor slots. In evaluating the relatively small-diameter generator rotor spindles, the magnitude of the torsional stresses due to worst-case electrical disturbances on the generator rotor must be considered. These stresses are highest at the outside diameter.

It was noted earlier that the vast majority of generator rotors manufactured by General Electric have been bored in the past because it is known that the poorest material in a large rotor forging is located at the centerline, being carried over from the original ingot. Because of the defects at the rotor centerline, it was considered good practice to remove this material even though the stress at the bore surface is nominally twice that which would occur if the rotor were solid. The stress drops off very rapidly as the distance from the bore surface increases, as shown in Fig. 1, and this behavior is modelled in our analysis of the stress intensity and critical flaw sizes. Consequently, the stress intensity and not the size of a defect is the determining factor in our analysis. Specifically, a large indication near the bore surface is of greater importance than one of the same size located several inches from the bore because the stress intensity will be higher.

Fracture Mechanics Evaluation

The early generator rotor forgings are known to contain various metallurgical defects that are readily detectable by current state-of-the-art, nondestructive test techniques. Destructive examinations have shown that these defects are predominantly nonmetallic inclusions and shrinkage porosity. It has been shown, however, for turbine rotors of a similar chemical composition and strength level that fatigue crack propagation through an area of such indications is much more rapid than in the base metal without these defects [2]. It also has been shown that the initially rounded extremities of these defects can form sharp cracks and grow as a result of the accumulation of start-stop cycles. Consequently, all NDT indications are assumed to be sharp cracks oriented normal to the maximum stress in the rotor for a conservative analysis. Once this assumption is made, it is possible to apply linear elastic, fracture mechanics analysis techniques to the evaluation of these rotors with the normal criterion that unstable crack growth will occur when the following condition is satisfied

$$K_I \geq K_{Ic} \quad (1)$$

where

$$K_I = \text{applied stress intensity} = \sigma(\pi a)^{1/2}F(\theta), \text{ and}$$

$$K_{Ic} = \text{critical stress intensity factor} = \sigma(\pi a_{cr})^{1/2}F(\theta).$$

The stress intensity is a function of the crack size, shape, and the stress in the rotor at the location of the defect. Consequently, the critical crack size of a rotor is not a single value but varies with location in the rotor.

The fracture mechanics evaluation of generator rotors involves an evaluation of the initial flaw sizes and then calculations of the predicted growth of those flaws as a result of start-stop cycles on the rotor, wherein one stress cycle is defined as starting the machine from standstill and running it up to a rotational speed of 3600 rpm and returning to standstill. Electrical load changes do not effect the generator stresses, nor do changes in the turbine steam supply conditions. The fatigue behavior of each individual generator rotor typically has not been measured; however, a compilation of determinations of several rotors has shown that the variability from rotor to rotor is small, so that compilation is used in the analysis of all rotors. The low-cycle fatigue (LCF) crack growth rate for generator rotor steels follows the familiar Paris equation where

$$da/dN = C(\Delta K_I)^m \quad (2)$$

where

$$a = \text{one half of the crack length,}$$

$$N = \text{number of cycles,}$$

$$\Delta K_I = \text{range of stress intensity factor, and}$$

$$C, m = \text{material constants.}$$

The material properties of each rotor under consideration are utilized to analyze the capability of that rotor for extended service. These are not minimum design requirements but the actual values that are taken from the material files on the rotor being evaluated that are maintained for the life of the machine. This always allows for a more liberal recommendation than could be made compared to a situation where design minimums were utilized.

The tensile properties of the rotor are used to compute maximum allowed overbore or bottle bore dimensions or both and to evaluate the possibility of locally grinding on the bore surface to remove defects. The impact energy and the FATT generally are not available for the older rotors, but the latter is needed to estimate the fracture toughness. This is not a significant problem because these values can be measured from specimens made from radial trepanns removed from the rotor surface in the pole region. Tests have shown that the FATT at the center of a rotor is approximately 20 C° (35 F°) higher than at the outer diameter (OD) surface, so this correction is made to obtain a more realistic value for the near bore material. The excess temperature is defined as the difference between the

rotor operating temperature and the measured FATT of the rotor, and the relationship between the fracture toughness and the excess temperature has been experimentally determined and supplemented by many investigators [3]. Hence, if the rotor operates above the FATT, then the excess temperature is positive and the K_{Ic} is relatively high, but if it operates below the FATT, then the excess temperature is negative and the K_{Ic} correspondingly low. Because of the wide variation in published test results, the lower bound values of the excess temperature to K_{Ic} scatter band are used to maintain a conservative analysis. The K_{Ic} is needed so that critical crack sizes in various parts of the rotor can be calculated and compared to defect sizes in the rotor after the effect of start-stop cycling has been accounted for on the growth of existing flaws.

Conclusion

Testing and evaluation procedures are available for making recommendations on repairs and the further operation of in-service generator rotors. The experience accumulated by General Electric during the past several years clearly indicates the desirability of conducting periodic in-service rotor inspections, particularly for that population of generator rotor forgings manufactured prior to the use of vacuum-poured steel. A number of rotors which were possible candidates for failure were discovered, and appropriate precautions were taken to prevent such failures. While effective in-service rotor inspection programs cannot absolutely guarantee the prevention of failure, the probability is substantially reduced.

There are various uncertainties associated with rotor evaluation. These uncertainties include the interpretation of ultrasonic test results, the variation of material properties from rotor to rotor and between different locations within the same rotor, and the great variability of in-service duty. As a result, recommendations for future operation not only are based on analytical results but also on the experience and judgment gained by our evaluation of nearly 650 generator rotors.

References

- [1] DeForest, D. R., et al., "Investigation of the Generator Rotor Burst at the Pittsburgh Station of the Pacific Gas and Electric Company," ASME Paper 57-PWR-12, ASME Power Division Conference, Allentown, PA, 21–23 Oct. 1957, American Society of Mechanical Engineers, New York.
- [2] Schwant, R. C. and Timo, D. P., "Life Assessment of General Electric Large Steam Turbine Rotors," EPRI Conference on Life Assessment and Improvement of Turbo-Generator Rotors for Fossil Plants, Raleigh, NC, 12–14 Sept. 1984, Electric Power Research Institute, Palo Alto, CA.
- [3] Newhouse, D. L. and DeForest, D. R., "Meeting Requirements for Larger Generator Rotors. . . A Metallurgical Challenge," International Forgemasters' meeting, Terni, Italy, 6–9 May 1970.

DISCUSSION

*V. P. Swaminathan*¹ (*written discussion*)—It was reported by the speaker that the axial centerline of the forging was shifted from the centerline of the ingot as revealed by sulfur prints. Also, a large density of ultrasonic indications were found in the near bore region. Are these indications due to inclusions in the centerline of the ingot or due to metallic segregation (“v” type)?

R. H. Bellows, R. J. Zawoysky, and D. N. Walker (*authors’ closure*)—The slide suggesting that the solidification centerline of the ingot was not coincident with the centerline of the rotor was not a sulfur print but a computer-generated plot of angle-beam boresonic indications. Since this plot is the result of a non-destructive examination, the cause of the indications can be only postulated.

¹ Westinghouse Electric Corp., Orlando, FL 32817.

Turbine and Generator Forgings

Generator Retaining Rings

The Development of New Materials for Nonmagnetizable Retaining Rings and Other Applications in the Power Generating Industry

REFERENCE: Stein, G., "The Development of New Materials for Nonmagnetizable Retaining Rings and Other Applications in the Power Generating Industry," *Steel Forgings, ASTM STP 903*, E. G. Nisbett and A. S. McLilli, Eds., American Society for Testing and Materials, Philadelphia, 1986, pp. 237-257.

ABSTRACT: Long before the first forged retaining rings were manufactured, our company, Schmiedewerke Krupp-Klöckner, was concerned with the development of nonmagnetizable steels for the manufacture of retaining rings. In addition to our company, only a few manufacturers are manufacturing rings that meet the requirements of present-day specifications.

As various steel brands developed beginning early in this century, the requirements of our customers concerning the mechanical properties and the corrosive environmental conditions became greater and greater. This led us in the late seventies to a material that meets present and future requirements regarding both mechanical properties and full corrosion-resistant behavior.

This paper will show the main steps in the development of retaining ring production by our company. Today we use as starting material for our retaining rings cast electrodes of electric furnace steel which are remelted in our electroslag remelting plant. The ingot undergoes several forging and reheating operations to produce a ring blank. The blanks are rough turned, solution heat-treated, and then work-hardened so as to obtain the desired 0.2% proof stress. This operation is followed by a stress-relieving heat treatment and a finish-machining operation. This production requires continuous monitoring of the production procedure as well as extensive in-process and final tests.

In the last 30 years, about 18 000 retaining rings have been manufactured from a material with 0.5% carbon, 18% manganese, 4.5% chromium, and 0.1% nitrogen. Physical and mechanical properties could be met with this material even in customers' advanced specifications. There is only one disadvantage: The material is susceptible to stress corrosion cracking. Some failures of retaining rings in recent years were due to the occurrence of stress corrosion cracking. The best way to avoid stress corrosion cracking is to use a nonsusceptible material. Such a material has been developed for the manufacture of retaining rings in our company. Up to now we have produced more than 400 rings with 0.2% proof stresses up to 1250 N/mm².

This paper will show the chemical analysis, mechanical properties, residual stresses, stress corrosion properties, susceptibility to hydrogen-induced cracking, fracture toughness properties, sensitization at elevated temperatures, and stress relaxation behavior.

¹ Manager, Head of Quality Dept. Essen/Hagen, Schmiedewerke Krupp-Klöckner, GMBH, Essen, Germany.

Even with this extraordinary material, we have not stopped the development of retaining ring material. Three years ago our company installed the only full-size pressure electroslag remelting equipment in the world. With this equipment we can increase the nitrogen content of any material above the normal solubility limit. This will lead to higher 0.2% proof stresses and more homogeneous mechanical properties without losing the corrosion-resistant behavior of the new retaining ring material.

KEY WORDS: nonmagnetizable generator retaining rings, high strength, stress corrosion resistant, fracture toughness properties, mechanical properties, stress relaxation behavior, pressure electroslag remelting, high nitrogen contents, high strength-high toughness nitrogen in ferritic steels, nitrogen solubility

In many sectors of industry, development is very frequently held back by the quality of the materials that can be produced on an industrial scale and by the costs involved in the use of superalloys. Even these superalloys, in many cases, cannot be used to produce components of the required size².

A new approach to materials development has become necessary, focusing above all on: (a) high strength, ductility, toughness, and resistance to corrosion; (b) large-scale production at viable cost. We have concerned ourselves with problems such as these for many years.

The aim of this paper is to report on the development of a corrosion-resistant, high-tensile austenitic material for generator retaining rings and the first step towards a new generation of materials.

Ever since turbogenerators have been used in power generation, it has been the retaining rings which, in the view of designers, have imposed restrictions on size. With the advent of a new material, future generators will no longer be subject to restrictions by the retaining rings, while today's generators, operating with retaining rings of this new material, will achieve a standard of reliability far superior to the level already achieved.

The Function of Retaining Rings and the Demands Placed on Them

Conventional generators are still the major means of producing electric power today. By far the greatest proportion of electric power supplied by generators comes from steam turbogenerators. In contrast to multipole water turbine-driven generators, two-pole generators operate at a speed of 3000 rpm when an alternating current of 50 Hz is generated. For an alternating current of 60 Hz, a speed of 3600 rpm is required. Four-pole machines operate at half the speed of two-pole machines, that is, at 1500 or 1800 rpm. Figure 1 shows a cutaway of a turbogenerator unit with a shrink-fitted retaining ring.

The retaining rings are shrunk onto the rotor body ends and have the function of securing the coils against the centrifugal force set up during operation at the point where they leave the longitudinal slots in the rotor body. In the majority of cases, the retaining rings are shrunk onto the rotor body ends and secured

² Personal discussions with P. J. Uggowitzer and M. O. Speidel.

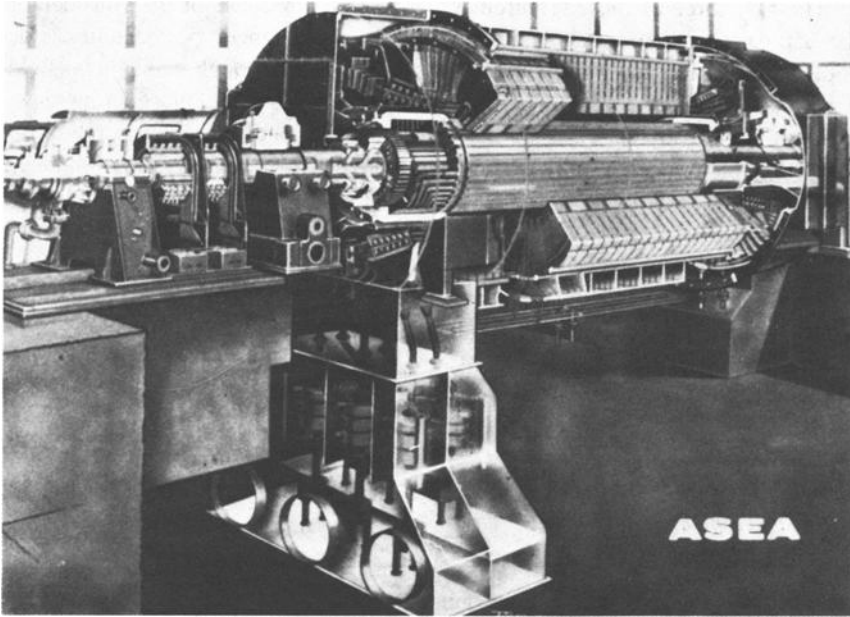


FIG. 1—Cutaway view of a water-cooled turbogenerator.

against rotational and axial movement by a kind of bayonet lock. In designing retaining rings the aim must be to achieve an optimal relationship between strength and wall thickness. This is because during operation not only the centrifugal force acting on the coil heads must be retained but also the mass of the retaining ring produced by the centrifugal force, which can amount to as much as 50% of the total forces acting. For example, in a four-pole 1320 MVA machine, these forces amount to 135 MN at test speed.

The retaining rings are, therefore, the most highly stressed components of a turbogenerator. When the machine is operating at rated speed, the retaining rings are loaded to about two thirds of their 0.2% proof stress and during overspeed testing up to about 80%. As generator units become larger, the retaining rings are subjected to increasing stresses from many causes. Very exacting demands, therefore, are placed on the rings and on the methods by which they are manufactured.

The material from which retaining rings are made must therefore meet the following requirements:

1. High 0.2% proof stress.
2. Adequate forming properties.
3. A not too low coefficient of thermal expansion.
4. In most cases, low magnetic permeability.

The first three of these requirements are needed because of the considerable centrifugal forces and for assembly reasons. Low magnetic permeability is desirable because when ferromagnetic materials move through a magnetic field, eddy currents are generated which result in power losses and place an increased load on the already complicated generator cooling system. The temperature rise occurring in a magnetizable retaining ring during operation must not endanger the shrink fit of the ring and must not cause damage to the insulation. These problems do not arise with nonmagnetizable retaining rings, and they, therefore, are used in most of today's high-capacity generators.

The dimensions of the retaining rings are governed both by the size and output of the generator and also by the design used. Retaining rings for modern machines usually have diameters from 500 to 2000 mm, wall thickness from 40 to 120 mm, and lengths up to 1250 mm.

Material Selection

Our Development

Long before the first forged retaining rings were manufactured, we were concerned with the development of nonmagnetizable steels for the manufacture of retaining rings. Our earliest records on such materials date back to the turn of the century.

Figure 2 shows some milestones in the development of nonmagnetizable steel by the Krupp Co. up to the present day. Records of 1910 appear to represent the material from which the first forged test ring was manufactured. Its dimensions were as follows: outside diameter—720 mm, inside diameter—520 mm, length—390 mm. Evidently, its properties in the as-forged condition were not considered satisfactory. The records indicate that comprehensive solution treatment tests were carried out.

Owing to its low 0.2% proof stress in the solution-treated condition, the material did not provide an acceptable alternative to the wire bandages used at

year	SKK steel brand	chemical composition in % b. wt.									
		C	Si	Mn	Ni	Cr	V	W	N	Mo	1/10
1901	BRUV	0.79	0.24	4.48	16.0						
1910	MBR 22 C	0.27	0.20	0.44	21.8	3.0					
1925	P 287			6.00	8.5	10.25					
1926	P 323	0.56	0.18	8.22	10.1	4.15					
1928	EFC 212 G	0.55	0.40	5.0	12.5	3.6					
1938	EFC 212 W	0.58	0.40	7.5	8.5	4.0		0.60			
1939	CF 87212	0.48	0.40	17.5		3.0					
1954	P 750 (UKR)	0.53	0.80	18.0		4.5	0.10				
1975	P 899	0.50	0.50	18.0	0.40	4.65	0.55		0.10		
1975	P 900	<0.12	0.30	18.5	0.80	18.5	0.10		0.5		
1980	UKR-N	0.50	0.50	18.0	0.40	4.6	0.10		0.60	0.10	
1981	P 900-N	<0.12	1.00	18.5	0.80	18.5	0.10		1.00	0.10	

FIG. 2—Development of retaining ring steels.

the time made of low-permeability materials, usually with a high nickel content. These records also indicate that the first retaining rings to be made from a steel containing 5% manganese, 12% nickel, and 4% chromium was made between 1924 and 1928. The rings were finished by a hammer-forging operation known as hot-cold forging at 500°C.

Tests showed widely varying mechanical properties over the circumference and height of the ring, the cause of which was found even at the time to be the inability to keep deformation uniform as temperature decreased. Nevertheless, it was realized that the approach was fundamentally sound and that the strength of the material used could be increased by cold working. Thus, the first step had been taken and the way paved for a production technique which is now so advanced that retaining rings can be made for the largest turbogenerators currently being built.

In the initial expansion tests, short conical wedges were forced through the ring. This involved considerable handling difficulties and was not without danger owing to the bullet-like expulsion of the wedges after being forced through the rings.

In the late 1920s, the first expanding device with internal segments and an "expanding mandrel" was devised and developed into the system that is still being used successfully today. The retaining rings manufactured in 1928 had a 0.2% proof stress of 700 N/mm². In the 1930s, customer requirements with respect to the 0.2% proof stress increased rapidly, and in 1939 900 N/mm² was the value specified. The worsening shortage of nickel in Germany after 1933 led to a continual decrease in the nickel content until finally nickel had to be entirely replaced by manganese. This led to a material containing approximately 0.5% carbon, 17.5% manganese, and 3% chromium, a forerunner of the nonmagnetizable retaining ring material (UKR) used up to today, which contains 0.55% carbon, 0.5% silicon, 18% manganese, and 4.5% chromium (nowadays + 55Mn-Cr 18/4 = 18Mn-4Cr steel).

While the substitution of manganese for nickel necessitated certain modifications to the manufacturing procedure, it did not hold up the further development of the nonmagnetizable retaining ring. By 1978 the continuing rapid increase in the size of generator units led to demands for ever higher 0.2% proof stresses being made at ever shorter intervals.

Apart from mechanical and magnetic properties, the material's resistance to stress corrosion cracking has in recent years become an increasingly important criterion. The failure, due to stress corrosion cracking, of a number of retaining rings during operation has underscored the importance of this. As a consequence, the further development of materials for retaining rings has had to proceed in a new direction.

At Krupp, the development of nonmagnetizable material variants for retaining ring manufacture began in 1975 with the production of X 10Cr-Mn-N 18/18 steel (18Cr-18Mn steel), which, after the completion of preliminary tests, was first used to manufacture rings in 1978. From this material, our company currently produces retaining rings with 0.2% proof stresses of up to 1300 N/mm².

Mechanical Properties

Steel containing 18% manganese and 4.5% chromium was for decades the standard material used in the production of retaining rings the world over. At the present time there are probably something like 16 000 to 18 000 retaining rings of 18Mn-4.5Cr steel in use around the world.

In recent years, for the reasons just outlined, more and more retaining rings have been manufactured from a material resistant to stress corrosion cracking containing 18% chromium and 18% manganese—to date about 900 rings of this alloy have been produced by us.

With these two materials, 0.2% proof stresses of approximately 1300 and 1250 N/mm², respectively, can be attained after cold expansion. At these 0.2% proof stresses, both steels display approximately 15% elongation.

The mechanical properties of the two steels at room temperature differ in two respects:

1. The absorbed energy value of 18/4 steel, at a 0.2% proof stress of 1,200 N/mm², is about 40 J; for 18/18 steel, at the same 0.2% proof stress, it is around the 130 J mark.
2. At the above 0.2% proof stresses, the ratio of yield point to tensile strength is around 0.90 for steel 18/4 and around 1.0 for the 18/18 steel. This high elastic ratio, however, does not detract from the serviceability of such retaining rings.

It also should be noted that much less cold working is required for 18/18 steel than for 18/4 steel to achieve a comparable 0.2% proof stress. Consequently, the anisotropy (tangential, radial, and axial) imparted to the ring during production is less in the 18/18 material than in the 18/4 material. The reason for this lies in the higher 0.2% proof stress of the 18/18 material in the solution-treated condition. The work-hardening exponents of the two materials are approximately equal.

In both steels, annealing temperatures in excess of 400°C cause irreversible damage to the material, which is reflected in reduced toughness. Therefore, the utmost care must be taken when *heat treating* the retaining rings at 400°C (the temperature often applied for shrink fitting and removing retaining rings). The 18/4 material is more sensitive than the 18/18 material. The drop in toughness is attributable to a change from transcrystalline to intercrystalline fracture induced by intergranular precipitations.

A further factor which has a bearing on the operational reliability of retaining rings is fracture toughness. Quantitative analysis of damage is dependent on knowledge of the fracture toughness since it permits the critical crack length to be calculated. In addition, fracture toughness is of major importance for determining inspection intervals and calculating the residual life of retaining rings in which subcritical crack growth has begun.

To date there have been very few cases in which the failure of retaining rings

has been attributable to spontaneous fracture as a result of inadequate toughness, that is, where the stress intensity K , defined by fracture mechanics, has reached the critical limit K_{Ic} . In the few cases that have been reported, the cause of the damage always was found to be related to some special feature of the manufacturing process (for example, hot-cold working).

A comparison of the fracture toughness diagrams of the two steels (Fig. 3) shows that at start-up and operating temperatures the 18/4 steel also displays adequate fracture toughness (approximately $140 \text{ MN m}^{-3/2}$) at a 0.2% proof stress of approximately 1150 N/mm^2 . Owing to the much higher fracture toughness of the 18/18 material (approximately $250 \text{ MN m}^{-3/2}$), which results in a greater critical crack length, this material is completely insensitive to the possible presence of minor material defects.

Resistance to Stress Corrosion Cracking, Corrosion Fatigue, and Hydrogen Embrittlement

One of the most common causes of failure in retaining rings is the occurrence of stress corrosion cracking. It is an established fact that stress corrosion cracking only occurs when three conditions are simultaneously fulfilled:

1. The material must be susceptible to stress corrosion cracking.
2. The mechanical tensile stresses must reach a certain level and maintain that level over a long period.
3. The environment must be specifically aggressive to the material.

To avoid stress corrosion cracking, it is sufficient either to use a nonsusceptible material, to remove the tensile stresses, or to eliminate the aggressive environment. For decades, however, it was only possible to avoid stress corrosion

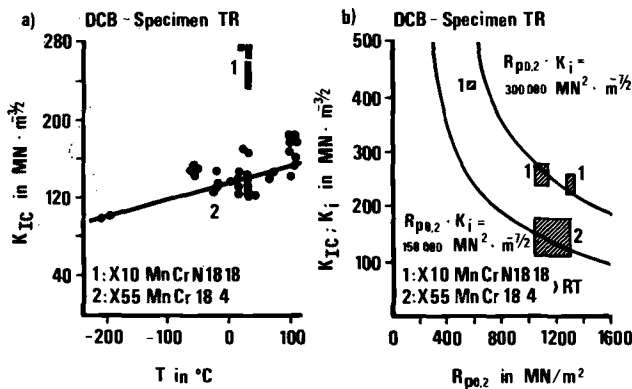


FIG. 3—(a) K_{Ic}/T ; (b) $K_{Ic}/R_{p0.2}$.

cracking in retaining rings by keeping aggressive media away from them. A material resistant to stress corrosion cracking was not available, and tensile stresses above a certain level were unavoidable.

These problems were largely solved by the development of the stress-corrosion-cracking-resistant retaining ring material 18/18. This does not rule out the possibility that this steel would display susceptibility to stress corrosion cracking in the presence of some theoretical academic medium. But tests carried out in laboratories all over the world using media only remotely related to practical operation have failed to produce an instance of failure caused by stress corrosion cracking (Fig. 4).

Manufacture of Cold-expanded Retaining Rings

Figure 5 is a schematic representation of the production procedure for cold-expanded retaining rings. On account of the stringent purity requirements, remelted material has to be used. Suitable electrodes are melted down in the electroslag remelting unit, forged, and divided up into blanks as required. They are then upset-forged and punched. In further heats the blank is finished-forged by the long-forging and rolling-up operation.

After forging and inspection, the rings are rough-machined, solution-treated, quenched, and then cold-expanded to obtain the requisite 0.2% proof stress. After expansion, the rings undergo stress-relieving heat treatment and are finish-machined and tested for compliance with customer specifications.

In our company, cold expansion is carried out on a hydraulic press using suitable tools. Every stage of production, from the melting down of the electrodes to the finish-machining of the ring, must be monitored in strict observance of the applicable quality assurance rules. Apart from numerous intermediate checks made during manufacture, the retaining rings also are tested for internal defects on a state-of-the-art immersion-type ultrasonic inspection unit. The results of ultrasonic inspection are recorded by plotters.

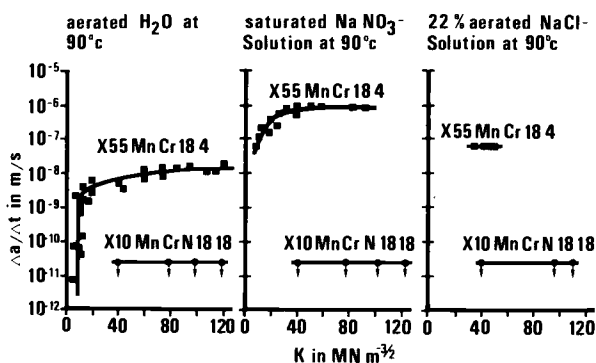


FIG. 4—Resistance to stress corrosion cracking (double cantilever beam specimen).



FIG. 5—Manufacturing procedure.

Future Retaining-Ring Steels

The aim of generator manufacturers to build more powerful turbogenerators only can be achieved with retaining rings having higher 0.2% proof stresses than are currently attainable. One of the authors [1] at the Electric Power Research Institute (EPRI) Workshop in 1980 said that the material quality for generator retaining rings so far attained fully meets the requirements of the generator manufacturers. But to satisfy future requirements, advances will be necessary primarily in the field of rotor retaining rings in regard to material quality, isotropy, resistance to corrosion, and further raising the 0.2% yield strength level. This point is illustrated by Fig. 6.

The requirements concerning isotropy and resistance to stress corrosion have since been fulfilled by the 18/18 steel. The problem up to now has been to achieve higher 0.2% yield strength levels in conjunction with sufficient ductility. Our present efforts to produce high-strength materials are focused on alloying tried and tested steels with nitrogen under high pressure in an electroslag remelting unit, the aim being to obtain a higher starting 0.2% proof stress in the solution-treated condition. Figure 7 shows the influence of nitrogen content on the 0.2% proof stress of retaining ring steels in the solution-treated condition as a function of the degree of cold expansion. Ingots with nitrogen contents above the normal solubility limit can only be remelted under increased pressure.

Nitrogen as an Alloying Element in Austenitic Steels

The improvement achieved in the strength properties of austenitic steels through the addition of nitrogen depends mainly on a widening of the austenite lattice.

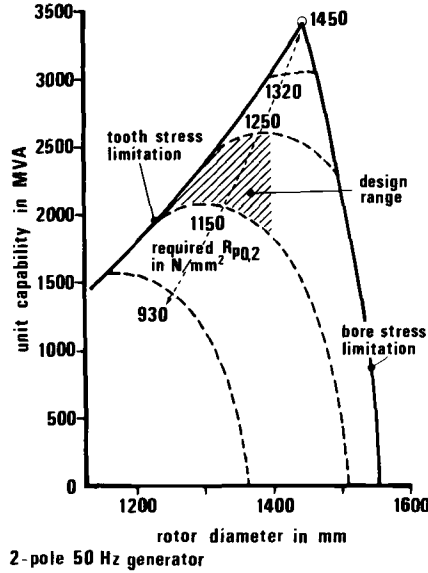


FIG. 6—Limitations imposed by shaft and retaining ring materials.

In low-carbon austenitic steels, nitrogen assumes the role normally played by carbon, which is also in interstitial solution. Nitrogen, however, offers the advantage of greater solid solubility. The microstructure of austenitic steels remains stable even during cold working. This is the reason why nitrogen-alloyed austenitic steels are “nonmagnetizable,” even after considerable amounts of cold work, continuous loading in the fatigue test, and stressing at elevated temperatures.

Nitrogen-alloyed austenitic steels, unlike steels without any addition of nitrogen, do not contain the ferrite which causes embrittlement and gives rise to

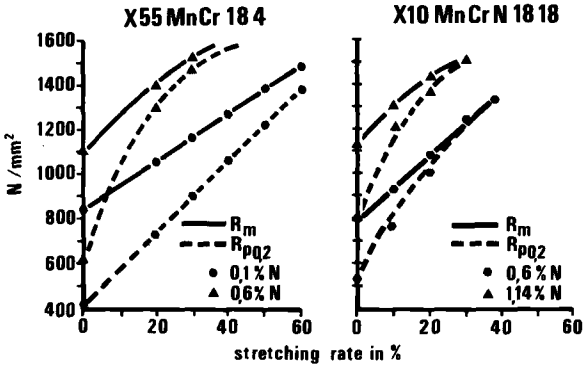


FIG. 7—Influence of nitrogen content.

difficulties in hot working. This is confirmed in the literature [2]. It is also reported [3] that nitrogen improves corrosion resistance.

In general, the required nitrogen content is obtained by adding high-nitrogen ferroalloys to the steel as it is being melted under atmospheric pressure in conventional melting furnaces. Nitrogen content in these cases is at or below the nitrogen solubility limit of the particular steel at atmospheric pressure.

In recent years a number of investigations have been carried out with the aim of increasing nitrogen levels beyond the solubility limit. Okamoto et al. [4] achieved nitrogen contents of 0.56% by melting austenitic steels containing 17% chromium, 12% nickel, and 2% molybdenum in a pressure induction furnace operating with a 1 MPa (10 bar) nitrogen atmosphere. The authors show that Sievert's square root law, already investigated in detail for nitrogen partial pressures up to 1 MPa (1 bar), is also valid for higher pressures. Frehser and Kubisch [5] achieved nitrogen contents of 0.76% in austenitic steels containing 18% chromium and 10% nickel by adding nitrogen in a pressure induction furnace operating at 2 MPa (20 bar). Melkumov and Klyuer [6] report on nitrogen alloying of austenitic steels in the plasma arc furnace, where a nitrogen content of 0.99% was obtained in steel containing 20% chromium, 8% manganese, and 7% nickel.

Particularly advantageous, however, in terms of technological effectiveness, flexibility, and attainable product quality, is the technique of electroslag remelting under pressure.

Solubility of Nitrogen in Steels

Solubility at Atmospheric Pressure

Nitrogen solubility is calculated from the equation

$$[\%N]_{Fe,X,Y} = \frac{[\%N]_{Fe}}{f_N} \quad (1)$$

where

- $[\%N]_{Fe,X,Y}$ = nitrogen solubility in multicomponent alloys,
- $[\%N]_{Fe}$ = nitrogen solubility in pure iron at 1600°C and $P_{N_2} = 0.1$ MPa (1 bar), and
- f_N = the interaction coefficient.

The solubility of nitrogen in pure iron at 1600°C and 0.1 MPa (1 bar) nitrogen pressure is 0.044%. Remelting in air is based on a nitrogen partial pressure of 0.08 MPa (0.8) bar, so that the value 0.0396 is used in calculating the nitrogen solubility for $[\%N]_{Fe}$.

The interaction coefficient f_N , also known as the activity coefficient, is a

measure of the effect of other alloying elements on nitrogen activity. The interaction coefficient is derived from the equation

$$\log f_N^{(X,Y,\dots)} = e_N^{(X,Y,\dots)} \cdot [\% X, Y, \dots] \quad (2)$$

where

$e_N^{(X,Y,\dots)}$ = the respective interaction parameters, and
 $[\% X, Y, \dots]$ = the percentages by weight of the various elements.

Elements with negative interaction parameters increase nitrogen solubility, while those with positive parameters reduce nitrogen pickup in steels. According to our own investigations, the following interaction parameters, as mentioned in the literature, should be used in calculating the nitrogen solubility of high-alloy steels at atmospheric pressure

$$\begin{aligned} e_N^{\text{Cr}} &= -0.045 \\ e_N^{\text{Mn}} &= -0.020 \\ e_N^{\text{V}} &= -0.10 \\ e_N^{\text{Mo}} &= -0.013 \\ e_N^{\text{Nb}} &= -0.061 \\ e_N^{\text{C}} &= 0.125 \\ e_N^{\text{Ni}} &= 0.010 \end{aligned}$$

The method of calculating the solubility limit of a steel with the following composition: 18.2% manganese, 4.7% chromium, 0.5% molybdenum, 0.2% vanadium, 0.6% carbon, 3% Ni, balance iron is as follows

$$\log f_N^{(X,Y,\dots)} = -0.02 \cdot [18.2] - 0.045 \cdot [4.7] - 0.013 \cdot [0.5] \quad (3)$$

$$-0.1 \cdot [0.2] + 0.125 \cdot [0.6] + 0.01 \cdot 3 = -0.4970$$

$$f_N^{(X,Y,\dots)} = 0.3184 \quad (4)$$

This value, inserted in Eq 1 = $0.0396/0.3184$, giving the just-mentioned steel a nitrogen solubility limit at an atmospheric pressure of 0.12%.

Solubility at Above-Atmospheric Pressure

Nitrogen solubility at pressures above atmospheric pressure follows Sievert's law, which to simplify understanding can be represented as follows

$$(\%N)_{\times \text{MPa}(\text{bar})} = L \cdot P_{\times \text{MPa}(\text{bar})} \quad (5)$$

where

L = solubility at atmospheric pressure.

If the system pressure is 3.6 MPa (36 bar), a nitrogen solubility limit of

$$(\% \text{ nitrogen})_{3.6 \text{ MPa (36 bar)}} = 0.12 \cdot 36 = 0.72\%$$

is obtained for the steel described under "Solubility of Nitrogen in Steels."

Results of Investigations from the Nitrogen Alloying of Retaining Ring Steels in Electroslag Remelting under Pressure

The aims of the tests were:

1. To obtain yield strength values greater than 1250 N/mm², with cold expansion less than 50%.
2. To guarantee the ratio of yield point to tensile strength at $R_{p0.2}$, $R_m > 0.95$, even at yield point values above 1250 N/mm².

The tests were carried out under pressure in a 100-kg electroslag remelting unit. The results are given in Figs. 8 and 9 for the 18/4 and 18/18 steels, respectively. Even in the solution-treated condition, the effect of raising the nitrogen content to values far above the solubility limit at atmospheric pressure can be observed in both steels. Worthy of note is that, in spite of the considerable increase in the strength values, there is hardly any decrease in the deformation

X55 Mn Cr N 18 4

N %	cold expan. %	mech. properties				
		$R_{p0.2}$ N/mm ²	R_m N/mm ²	A_5 %	Z %	$\frac{R_{p0.2}}{R_m}$
0.12	0	400	800	60	62	0.50
	20	740	1000	40	52	0.74
	30	900	1100	30	46	0.82
	40	1060	1230	24	42	0.86
	50	1250	1350	20	42	0.93
0.40	0	530	1055	53	45	0.50
	20	1030	1250	39	48	0.82
	30	1225	1350	27	45	0.91
	40	1385	1450	21	42	0.96

0 - solution treated

FIG. 8—Influence of cold expansion.

X 10 Mn Cr N 18 18

N %	cold expan. %	mech. properties				
		R _{p0.2} N/mm ²	R _m N/mm ²	A ₅ %	Z %	R _{p0.2} R _m
0,59	0	540	850	57	70	0,64
	10	750	960	35	68	0,78
	20	900	1020	28	65	0,88
0,79	0	600	1000	57	69	0,60
	10	920	1080	32	65	0,85
	20	1160	1220	26	63	0,95
	30	1360	1360	22	56	1,00
1,07	0	660	1060	54	70	0,62
	10	1080	1190	30	60	0,91
	20	1270	1330	27	58	0,95
	30	1530	1550	12	50	0,98

0 - solution treated

FIG. 9—Influence of cold expansion.

characteristics (elongation and reduction of area); the same is true for absorbed energy values.

The 18/4 steels with nitrogen contents of around 0.4% achieved yield point values of 1225 N/mm² after 30% cold working. The 18/18 steel reaches these yield point values after less than 20% cold working if the nitrogen content is greater than 1%. In this case the yield point to tensile strength ratio ($R_{p0.2}$; R_m) is also about 0.95.

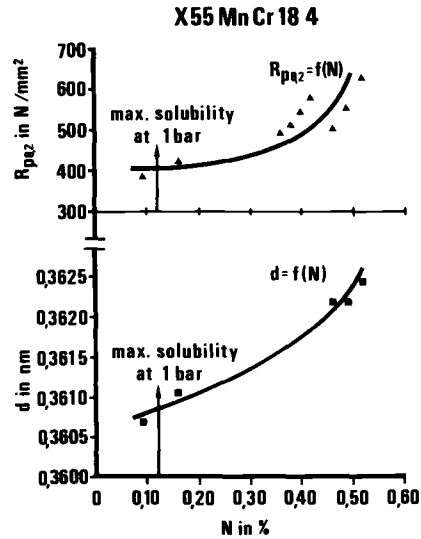
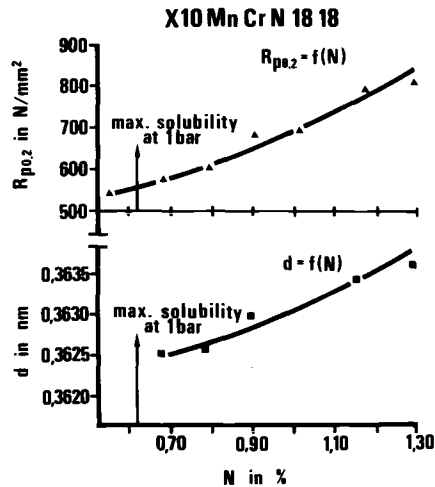
Fundamental investigations into the nitrogen alloying of austenitic generator retaining ring steels under pressure in the electroslag remelting unit revealed that the increase in the strength characteristics brought about by increasing the nitrogen content beyond the solubility limit at atmospheric pressure is attributable to a widening of the austenite lattice caused by the forced solution of nitrogen. This is shown clearly by Figs. 10 and 11, which plot yield point values and lattice parameters against the nitrogen contents of 18/4 and 18/18 steels, respectively.

Results of Investigations into the Nitrogen Alloying of Other Steel Grades

Nitrogen Alloying of Fe-, Cr-, Ni-, and Mo-Base Austenitic Steels

After austenitizing treatment (about 1100°C/H₂O), austenitic corrosion-resistant steels containing 16 to 20% chromium, 8 to 15% nickel, and 0 to 5% molybdenum display yield point values between 200 and 350 N/mm². In most cases, the steels with high yield point values contain up to 0.2% nitrogen.

The chemical compositions and mechanical properties of these steels are given in Fig. 12. In the D 17 steels, a large part of the nickel content was replaced by nitrogen 8. Figure 12 shows that the clear rise in strength does not coincide with

FIG. 10—Influence of nitrogen to $R_{p0.2}$ and lattice.FIG. 11—Influence of nitrogen to $R_{p0.2}$ and lattice.

N - alloyed austenitic steels, solution treated

steel	$R_{p0.2}$ N/mm ²	R_m N/mm ²	A_5 %	Z %	A_K iso-v J	chemical composition in %						
						C	Si	Mn	Cr	Ni	Mo	N
AISI-317	320	680	46	67	150	0.06	1.00	1.50	18.0	13.0	4.50	
D 15	560	970	45	65	100	0.03	1.73	0.84	18.5	13.5	4.58	0.55
D 16	630	1020	42	59	90	0.10	1.40	2.40	17.0	12.9	4.30	0.71
D 17	740	1100	46	65	106	0.06	1.60	5.30	20.8	3.0		0.85

FIG. 12—Influence of nitrogen content.

N - alloyed austenitic steels, solution treated					
steel	test temp.	mech. properties			
		R _{p0.2} N/mm ²	R _m N/mm ²	A ₅ %	Z %
AISI 317	400°C	170	530	40	57
	600°C	160	500	39	51
	800°C	150	310	57	72
D 15	400°C	370	770	50	62
	600°C	340	680	43	60
	800°C	330	510	33	40
D 16	400°C	410	830	40	55
	600°C	380	710	37	52
	800°C	310	530	36	48
D 17	400°C	360	710	48	64
	600°C	310	600	37	56
	800°C	200	400	32	32

FIG. 13—Mechanical properties at elevated temperatures.

a reduction in the deformation characteristics. The effect of a high degree of nitrogen alloying on the properties of austenitic chromium-nickel-molybdenum steels at temperatures up to 800°C becomes clear on examination of the results of high-temperature tension tests, as shown in Fig. 13. The yield points of the high-nitrogen D 15 to D 17 steels at 800°C were at roughly the same level as the room temperature values of AISI 317 steel to which no nitrogen had been added. Creep tests carried out to determine the stress rupture strength gave the following interim results for the just-mentioned steels after 1000 h

Steel	Temperature, °C	Load, N/mm ²	Elongation, %
D 15	600	200	0.06
D 16	600	200	0.038
D 17	600	200	0.058

Figure 14 shows the Wöhler curve of the nitrogen-alloyed D 17 steel. The figure shows that this steel has a fatigue strength of approximately ± 500 N/

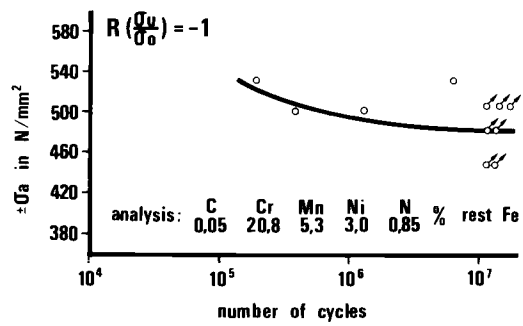


FIG. 14· Stress nitrogen graph.

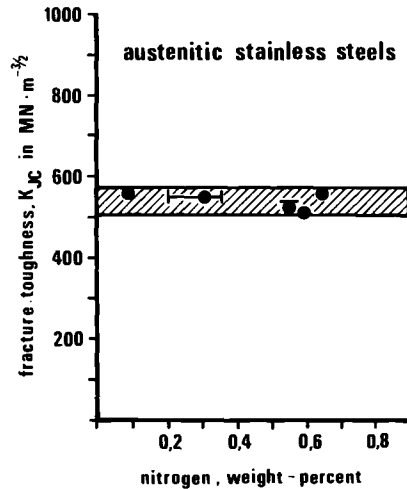


FIG. 15—Fracture toughness and nitrogen content.

mm². Values given in the literature for the fatigue strength of comparable steels with nitrogen contents below the solubility limit are below ± 300 N/mm².

Figure 15 shows that the fracture mechanics values are not impaired by nitrogen. Nitrogen alloying produces only slight grain refinement in austenitic steels, as can be seen in Fig. 16, which compares the microstructure of the conventional AISI 317 steel with that of the high-nitrogen D 17 steel.

Nitrogen Alloying of the Ferritic-Austenitic AISI 329 Steel

Nitrogen contents of 0.52% (Steel A) and 0.65% (Steel B) were obtained when ferritic-austenitic steels containing 0.05% carbon, 1.5% manganese, 25.5% chromium, 5% nickel, 1.7% molybdenum, 0.17% vanadium, and the balance iron were remelted under pressure in the electroslog remelting unit. Figure 17 shows the mechanical properties of the conventional AISI 329 steel containing 0.1%

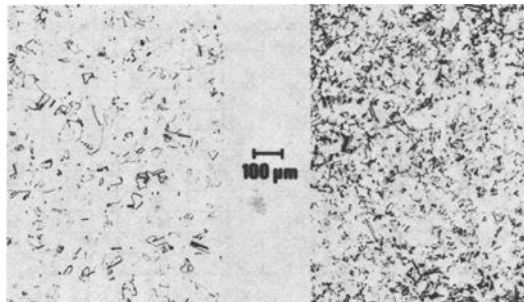


FIG. 16—(left) AISI 317; (right) 0.05C-20.8Cr-5.3Mn-3.0Ni-0.85N.

N - alloyed ferritic - austenitic steels, solution treated								
steel	chemical composition in %							
	C	N	Si	Mn	Cr	Ni	Mo	V
AISI 329	0.05	0.10	0.64	1.55	25.9	5.2	1.76	0.17
A	0.06	0.65	2.2	1.51	25.5	5.0	1.72	0.18
B	0.03	0.87	1.5	1.20	25.1	5.47	1.87	0.08

steel	test temp.	mech. properties				ultimate stress N/mm ² 10 000 h	creep stress N/mm ² 1% elongation in 10 000 h
		R _{p0.2} N/mm ²	R _m N/mm ²	A ₅ %	Z %		
AISI 329	RT	590	770	30	71		
	600 °C	320	460	33	69		
A	RT	710	1010	32	57		
	600 °C	400	620	35	64	130	70
B	RT	700	1090	39	64		
	600 °C	380	710	41	62	250	200

FIG. 17—Nitrogen content and high-temperature properties.

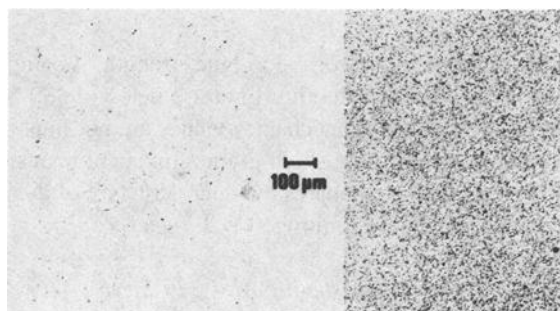


FIG. 18—(left) AISI 329, 0.1N; (right) AISI 329, 0.65N.

N - alloyed ferritic Cr-steels, solution treated								
steel	chemical composition in %							
	C	N	Si	Mn	Cr	Ni	Mo	Al
AISI 405	0.06	0.01	0.5	1	13	—	—	0.1
DE-28	0.06	0.51	1.3	1	13	—	—	0.1

steel	heat - treatment	test temp.	mech. properties			
			R _{p0.2} N/mm ²	R _m N/mm ²	A ₅ %	Z %
AISI 405	0.5h 800 °C/air	RT	250	600	20	
		400 °C	195			
DE-28	0.5h 800 °C/air	RT	530	790	23	61
		400 °C	608	820	22	70
	0.5h 950 °C/air + 3h 650 °C/air	RT	500	640	20	70
		400 °C	500	640	20	70
	0.5h 1050 °C/air + 3h 600 °C/air	RT	830	1060	17	56
		400 °C	720	870	15	60
		600 °C	630	750	14	42

FIG. 19—Mechanical properties at elevated temperatures.

nitrogen and of the nitrogen-alloyed Steels A and B at test temperatures of 20 and 600°C. Figure 18 shows the microstructures of AISI 329 steel and Steel A following heat treatment (1100°C/water). The effect of nitrogen content on grain refinement in austenitic steels clearly can be seen. Radiographic measurements revealed an austenite content of 30% in AISI 329 steel. In Steel A a rise in the austenite content to 60% was recorded. This also explains the fact that, as with the austenitic steels, there is no fall in the elongation values in spite of an increase in the strength values.

Nitrogen Alloying of Ferritic Chromium Steel 1.4002, AISI 405

The good results achieved with the just-mentioned steels also were obtained when nitrogen was added in large amounts to ferritic chromium steel, a material which plays a dominant role in modern turbine manufacture (shafts, blades, etc.). Figure 19 indicates what properties can be achieved by adding nitrogen to a pure ferritic chromium steel.

The technology of nitrogen alloying under pressure as described in the second part of this paper is without doubt a means of imparting mechanical and engineering properties which until now have been impossible to attain in the steels described here. We believe that a new generation of engineering materials has thus been developed. We realize that an important factor in all development work must be the amenability of the material to subsequent processing. A plant therefore has been built, as just described, in which we can produce ingots weighing up to 14 000 kg (14 tons).

References

- [1] Engelke, W., Joyce, J. S., Lambrecht, D., Mühle, E. E., and Wiemann, W., "Rotor Forgings for KWU-Designed Turbine Generators," EPRI Workshop, Turbine and Generator Rotor Forgings, Palo Alto, CA, 14-17 Sept. 1980, Electric Power Research Institute, Palo Alto, CA.
- [2] Thier, H., Bäuml, A., and Schmidtman, E., Einfluss von Stickstoff auf das Ausscheidungsverhalten des Stahles X 5Cr-Ni-Mo17 13, *Archiv f.d. Eisenhüttenwesen*, Vol. 40, No. 4, 1969, pp. 333-339.
- [3] Lennartz, G., and Kiesheyer, H., "Korrosionsverhalten eines seewasserbeständigen nichtmagnetisierbaren Cr-Ni-Mo-Stahles hoher Festigkeit," *Archiv f.d. Eisenhüttenwesen*, Vol. 43, No. 8, 1972, pp. 639-642.
- [4] Okamoto, M., Tanaka, R., Naito, T., and Fujimoto, R., "On the Manufacture of High-Chromium Steels in High-Pressure Nitrogen Atmosphere and Heat Resisting Properties of 316L-type Steels," *Tetsu-to Hagane Overseas*, Vol. 2, No. 1, 1962, pp. 25-27.
- [5] Frehser, J., and Kubisch, C., "Metallurgie und Eigenschaften unter hohem Druck erhitzter stickstoffhaltiger legierter Stähle," *Berg- und Hüttenmännische Monatshefte*, Vol. 108, No. 11, 1963, pp. 369-380.
- [6] Melkumov, I. N., and Klyuer, M. M., "Properties of Steels Alloyed with Above-Equilibrium Quantities of Nitrogen," *Steel in the USSR*, Aug. 1973, pp. 687-690.
- [7] Pant, P., "Massivaufstickung von austenitischen Stählen," 3rd BMFT status seminar, Eisen- und Stahlforschung, 3-5 Sept. 1984.

DISCUSSION

B. Jaffee¹ (written discussion)—The improvement in the room temperature yield strength of 13Cr steel by increased nitrogen is most impressive. Is the improved strength maintained in elevated temperatures, particularly 10⁵-h creep rupture strength at 500 to 600°C?

G. Stein (author's closure)—The improved strength at elevated temperatures is not the creep rupture strength at 500 to 600°C. Creep strength tests are still running at 650°C.

G. P. Simkins² (written discussion)—Were the various grades, compared to their corresponding nitrogen-bearing grades, electroslag remelted?

G. Stein (author's closure)—All material grades discussed in the paper are electroslag remelted.

E. G. Nisbett³ (written discussion)—The author is congratulated on the development of a method to pressurize and adapt the atmosphere above the slag in the electroslag remelt (ESR) process. Has an attempt been made to use the equipment to help control the hydrogen levels in ESR steels by means of reduced pressure or inert atmosphere?

G. Stein (author's closure)—The pressure ESR unit has been used to increase the nitrogen level in materials only. The unit may be capable of helping to control the hydrogen levels, but there was no attempt to do so.

D. L. Newhouse⁴ (written discussion)—Does welding present problems, such as porosity or reduced strength, in pressure-melted alloys in which the nitrogen content is well above the solubility of nitrogen at 1 atm?

G. Stein (author's closure)—In general, welding of pressure-remelted alloys causes welding problems, mainly porosity. But, by using suitable electrodes, welding is possible. A still running research program in our company shows excellent results: no porosity, no drop in strength.

O. Graham⁵ (written discussion)—In some of the steels discussed, the nitrogen contents recorded were in excess of the solubility of nitrogen at atmospheric

¹ Electric Power Research Institute, Palo Alto, CA.

² Westinghouse Electric Corp., Monroeville, PA 15146.

³ National Forge Co., Irvine, PA 16329.

⁴ Engineering Materials & Processes, Inc., Schenectady, NY 12306.

⁵ Sheffield Forgemasters, England.

pressure. Do the steels show any tendency to outgas during forging, heat treatment, etc.?

G. Stein (author's closure)—Up until now we have not seen any tendency to outgas during manufacture even after long-term heat treatment at high temperatures.

18–18 Corrosion-Resistant Retaining Rings for Nuclear Power Plant Generators

REFERENCE: Rambaud, J. B. and Cazenave, R. H., “18–18 Corrosion-Resistant Retaining Rings for Nuclear Power Plant Generators,” *Steel Forgings, ASTM STP 903*, E. G. Nisbett and A. S. McIlilli, Eds., American Society for Testing and Materials, Philadelphia, 1986, pp. 258–272.

ABSTRACT: Several years ago, the Pamiers Plant of the Compagnie Française de Forges et Fonderies (C3F) undertook a research program on the 18–18 corrosion-resistant grade for retaining rings.

An extensive testing program conducted in association with Electricité de France led to a decision to equip the 900- and 1300-MW generators of French nuclear power plants with NMF 18 retaining rings (NMF 18 is the C3F trademark for the 18–18 material).

To date, 20 rings have been manufactured in the following sizes:

1. Outer diameter: 1746 to 2040 mm (68.74 to 80.31 in.).
2. Thickness: 83 to 90 mm (3.27 to 3.74 in.).
3. Height: 700 to 775 mm (27.56 to 30.51 in.).
4. Weight: 2.5 to 3.5 metric tons.

The guaranteed yield strength at midwall is 750, 850, or 900 MPa (109, 123, or 130 ksi), depending on the type of ring.

After a review: (a) of the properties of the 18–18 grade and their comparison with the conventional 18–4 material and (b) of the principal results of the test program, we are describing the specifics of the manufacturing process and the facilities of these large rings.

KEY WORDS: Nonmagnetic rings, austenitic manganese steels, corrosion-resistant grades, stress corrosion

In a turbogenerator rotor, the field windings project from each end of the longitudinal slots machined in the rotor body periphery and form loops to complete the coil turns. These end windings are retained against the centrifugal force effect by a steel cylinder called a *retaining ring*.

Due to electromagnetic considerations and mainly to reduce the amount of power necessary to produce the rated magnetic field, the use of nonmagnetic retaining rings is preferable.

¹ Technical manager, Division Ateliers Forges et Fonderies, Usinor, Paris.

² Chief metallurgist, Pamiers Plant, Compagnie Française de Forges et Fonderies, Pamiers, France.

Service Conditions

Stressing

Retaining rings are highly stressed components, mainly in the circumferential direction. In operation, this stress is due to the density and rotation of the ring itself (for two thirds to three fourths of the stress) and to the load of the end winding on the ring.

In 20% overspeed conditions, the total hoop stress reaches up to about 70% of the material yield strength and to about 50% of the same yield strength under normal running conditions.

Stress Corrosion

In certain conditions, retaining rings may be exposed to corrosive agents like water, chlorides, or nitrates. The presence of water may be leakage from the rotor windings, in the case of water-cooled rotors, or moisture condensation from air or hydrogen, in the case of air- or hydrogen-cooled rotors.

Chlorides may be encountered in a marine atmosphere. Nitrates may be produced by the oxidation of nitrogen by ozone from the corona effect. Other corrosive agents may be encountered in particular cases, but plain water probably represents the most frequent risk of stress corrosion for a retaining ring.

Fatigue

Stressing is constant under normal operation, but the variable number of starts and stops to which some generators are subjected imposes fatigue conditions on rings. In some extreme cases, the start-stop cycle may occur daily.

Nonmagnetic Ring Material

Until now, the material most widely used for the manufacture of nonmagnetic retaining rings is the 18–4 alloy with a nominal composition of 18% manganese, 4.5% chromium, and 0.5% carbon. This austenitic alloy presents a low yield strength in the quench-annealed condition [340 MPa (50 ksi)], but, after cold working, it exhibits a yield strength which can go up to 1350 MPa (195 ksi).

At present, both forging suppliers and generator manufacturers have extensive production experience with 18–4 ring alloy, and this alloy certainly provides a good answer for service conditions in noncorrosive environments.

A yield strength of 1100 MPa (160 ksi) may be specified for two-pole generators and is achieved without difficulty. Yield strengths above 1200 MPa (175 ksi) also may be obtained for particular uses. At this level, the material exhibits K_{Ic} values above 110 MPa \sqrt{m} (100 ksi $\sqrt{in.}$), which means a good general level of toughness and a critical defect size well above the minimum detectable size.

In the presence of a corrosive agent, which can include plain water, these properties are not the same; in demineralized water, for example, the K_{Isc} of this

grade may be less than 10 MPa $\sqrt{\text{m}}$ (9 ksi $\sqrt{\text{in.}}$), which means a poor stress corrosion cracking resistance in this medium.

Furthermore, considering the known in-service failures of 18–4 rings, it should be pointed out that in most cases the failures involved a stress corrosion phenomenon, the cause of which was mainly exposure to water.

Therefore, there was a need for a material that would present a better stress corrosion behavior, while still retaining the same properties of nonmagnetism, strength capability, and toughness. Already having considerable experience as a supplier of 18–4 retaining rings under the trademark NMF 3, the C3F PAMIERS PLANT in 1969 undertook research on an alloy with an increased chromium content: 0.25C-12Mn-18Cr-0.3N.

It was found that high yield strengths with sufficient toughness could be achieved, but that stress corrosion resistance was somewhat inferior when compared to 18–4. Later, an alloy with 0.3C, 18Mn, 13Cr, and 0.25N also was studied, but it presented an insufficient toughness level. This lack of success probably resulted from a too high carbon content, which, together with a chromium content of 13 or 18%, promoted heavy carbide precipitations at grain boundaries, which were very difficult to put and keep in solution.

Logically, then, the next step consisted of lowering the carbon content, replacing it with nitrogen, and keeping a high chromium content of 18% in order to have a sufficient solubility of nitrogen and to enhance the corrosion resistance.

That led to the 18–18 alloy with 18Mn, 18Cr, and 0.5N. After preliminary investigations, the aim was to achieve a carbon content of less than 0.13%. Afterwards, it was lowered to a maximum value of 0.10%. Preliminary testing of this alloy revealed very interesting properties that deserved further investigation.

Primary Experiments on 18–18

The first experiments performed on laboratory melts showed that this alloy demonstrated remarkable characteristics of strength capability, ductility, and corrosion resistance. So, industrial melts were launched, and the results obtained on full-scale experimental retaining rings confirmed entirely what we found in the laboratory melts.

Yield Strength Capability and Ductility

By cold expansion, it was possible to achieve yield strengths of up to 1350 MPa (195 ksi). Moreover, the cold working ratio necessary to develop a given yield strength is less than that needed for the 18–4 material (Fig. 1). Besides, the ductility level is better than for 18–4 material. Figure 2 shows the relationship between impact energy and yield strength for the two materials.

Corrosion Resistance

In stress corrosion tests performed on flat specimens bent to develop a stress equal to 80% of the yield strength, the 18–18 specimens exhibited a much better

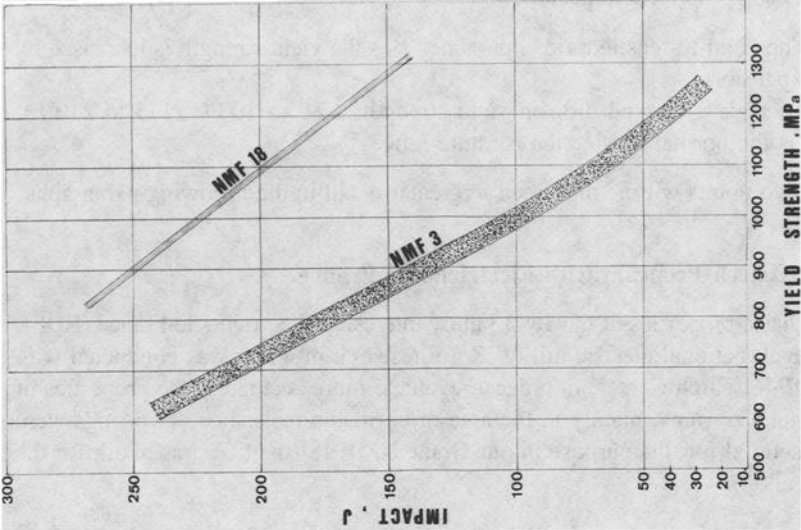


FIG. 2—Impact properties versus yield strength for experimental NMF 18 rings compared to NMF 3 rings population.

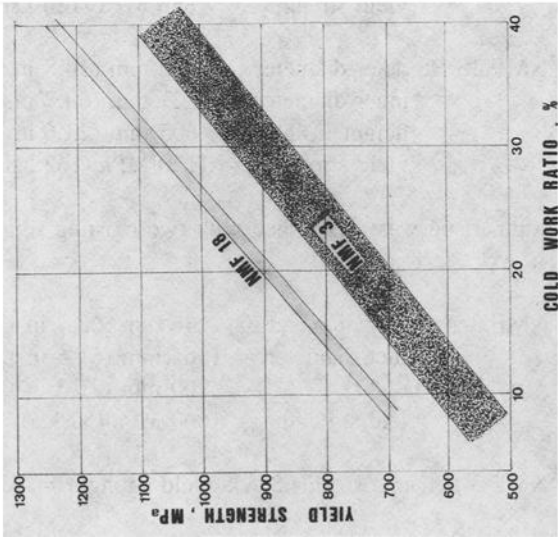


FIG. 1—Yield strength versus cold work ratio for NMF 3 and NMF 18.

behavior than the 18-4. In synthetic seawater, the 18-18 specimens lasted more than 2000 h without pitting or cracking. Under the same conditions, the cracking of 18-4 specimens occurred after only 200 to 300 h. Nevertheless, this alloy presents some noticeable peculiarities:

1. The yield-to-tensile ratio approaches 1 as the yield strength is increased by cold expansion.
2. There is a marked drop in yield strength at 80 to 100°C (175 to 210°F), which is the normal service temperature range.

These two points will be discussed in greater detail in the following paragraphs.

The Research Program with Electricite de France

The basic properties of the 18-18 alloy interested Electricite de France (EDF), the French national electric utility. So, a research program was conducted with the EDF Research Center³ in order to evaluate more accurately the properties of industrial size rings, mainly in the area of corrosion resistance. Two rings were manufactured for this purpose in our Grade NMF 18 (the C3F trademark for the 18-18 alloy):

NMF 18-A: outer diameter = 1000 mm (39.4 in.)
 inner diameter = 850 mm (33.4 in.)
 height = 650 mm (25.6 in.)
 yield strength = 880 MPa (128 ksi)

NMF 18-B: outer diameter = 986 mm (38.8 in.)
 inner diameter = 827 mm (68.7 in.)
 height = 605 mm (23.6 in.)
 yield strength = 1120 MPa (162 ksi)

The comparison was established with two existing rings in 18-4 (our Grade NMF 3).

NMF 3-A: outer diameter = 1746 mm (68.7 in.)
 inner diameter = 1565 mm (61.6 in.)
 height = 700 mm (27.6 in.)
 yield strength = 600 MPa (87 ksi)

NMF 3-B (same size as 3-A): yield strength = 955 MPa (138 ksi)

The chemical analysis of these four rings is given in Table 1.

³ EDF Research Center, Department Etude des Materiaux, Les Renardieres, Route de Sens, Euvelles, 77250 Moret sur Loing, France.

TABLE I—Analysis of the rings used for the EDF program (%).

	C	Si	Mn	S	P	Cr	Ni	Al	N2
NMF 18-A	0.126	0.53	18.6	0.001	0.031	17.6	0.45	<0.01	0.55
NMF 18-B	0.123	0.53	18.6	0.001	0.025	17.5	0.45	<0.01	0.56
NMF 3-A	0.46	0.50	18.4	0.003	0.025	4.1	0.17	<0.01	0.034
NMF 3-B	0.49	0.56	19.4	0.003	0.027	4.1	0.97	0.015	0.032

Mechanical Properties

Conventional mechanical tests confirmed what was already known about this material; that is, it possessed an excellent level of ductility. Attention was paid, however, to the drop in yield strength at service temperatures; the variation of yield strength as a function of temperature is given in Fig. 3 for Rings NMF 18-A, NMF 18-B, and NMF 3-B.

The influence of the temperature between 20 and 80°C (68 and 176°F) is greater for NMF 18 than for NMF 3, about 130 MPa (19 ksi) as opposed to 35 MPa (5 ksi). It should, however, be pointed out that the limit of proportionality is higher for NMF 18 at 20°C as well as at 80°C: the ratio yield strength (YS) 0.02/YS 0.2 is about 0.93 for NMF 18 but less than or equal to 0.85 for NMF 3 (Fig. 4).

Fracture Toughness

Fracture toughness tests have been conducted at room temperature on NMF 18-A and NMF 18-B rings and at 80°C (176°F) on the NMF 18-B ring. The specimens (CT50 and CT75 types) have been removed from Position C2 of Fig. 5, which corresponds to the preferential direction of the final rupture of a ring. The results are given in Fig. 6, which shows the energy parameter versus the cracking propagation.

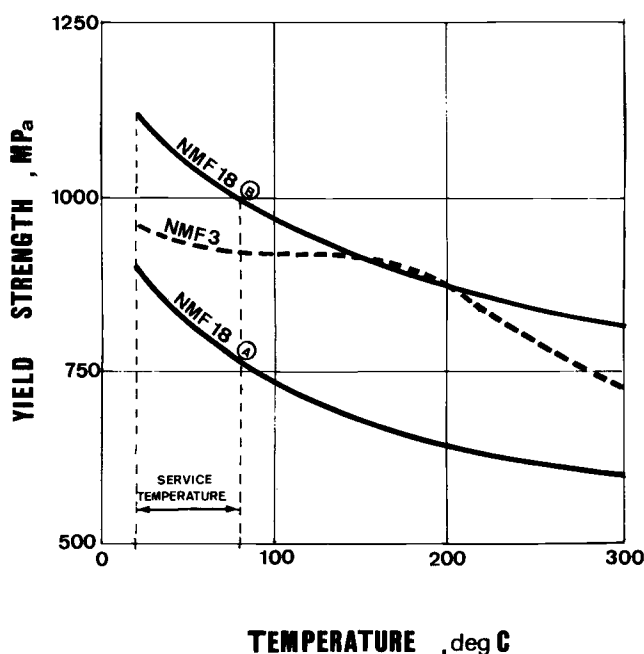


FIG. 3—Influence of temperature on yield strength.

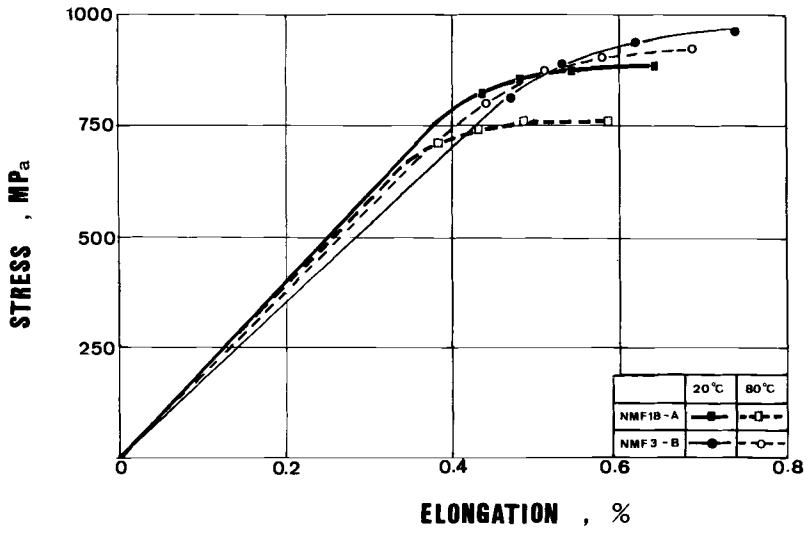
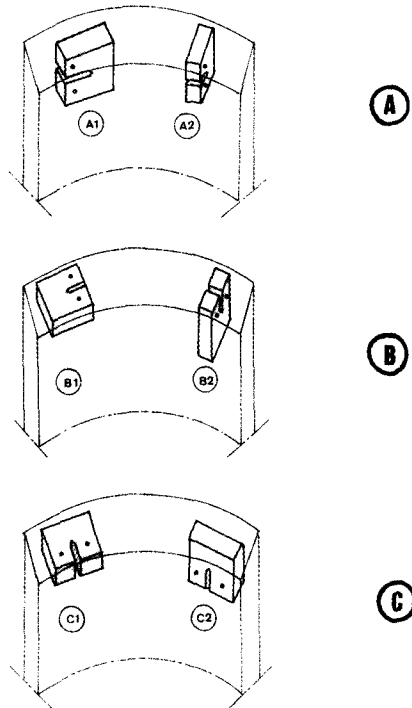


FIG. 4—Tensile curves at 20 and 80°C for NMF 3 and NMF 18.



CT SPECIMENS POSITION

FIG. 5—Position of CT specimens.

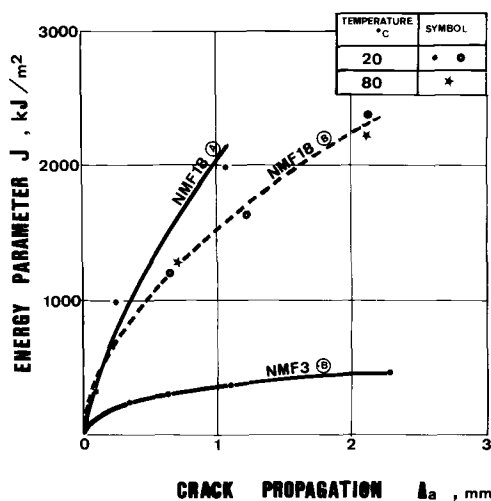


FIG. 6—Fracture toughness properties in air.

All the specimens present a completely ductile behavior, without instability. Under these conditions, it is not possible to determine a K_{Ic} -value, but this shows that the fracture toughness level of this grade is well above that of the 18-4. It is not possible to see an influence of the temperature.

Corrosion Behavior

Two aspects of corrosion behavior were studied: (1) crack propagation on precracked specimens and (2) cracking initiation on smooth specimens:

1. *Crack propagation on precracked specimens.* These tests were conducted on CT20 specimens positioned in the ring according to one of the positions in Fig. 5, with a sustained loading. Results in demineralized and deaerated water at 80°C (176°F) are given in Fig. 7, which represents the mean propagation speed versus the stress intensity factor. For NMF 18, with stress intensity factors as high as $100 \text{ MPa } \sqrt{\text{m}}$ (91 ksi $\sqrt{\text{in.}}$), no propagation was observed.

Tests are presently being conducted in a chloride environment (3% sodium chloride acidified to pH 3 at 80°C (176°F)), but the superiority of 18-18 is already well established.

2. *Cracking initiation:* These tests were conducted on smooth tension specimens with different loading up to yield strength, with demineralized, aerated, and deaerated water at 80°C (176°F). On NMF 3, intergranular cracking was observed in aerated and deaerated water for loading near the yield strength after less than 300 h. Also observed in aerated water were many pittings. On NMF 18, no cracking nor pitting was observed in aerated or deaerated water for loading equal to the yield strength after 2000 h of testing.

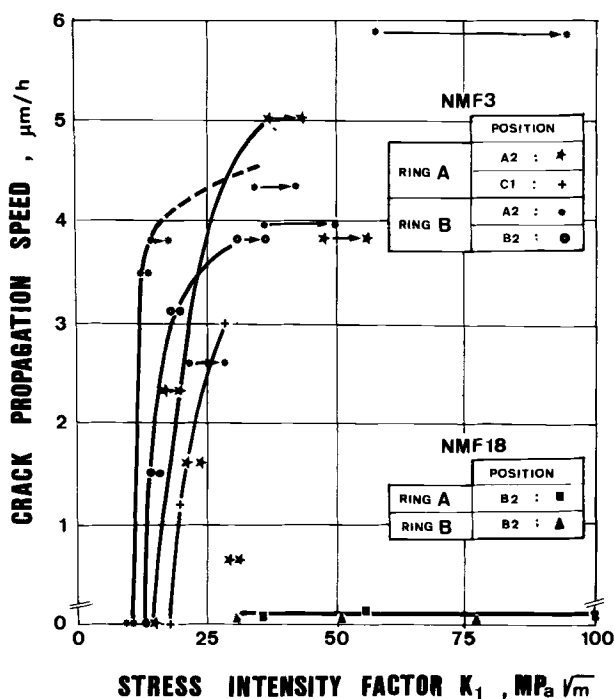


FIG. 7—Stress corrosion properties at 80°C in demineralized and deaerated water (CT 20 specimens).

Manufacture of Production Rings

Considering these results, EDF decided to progressively equip their generators with NMF 18 retaining rings, beginning with nuclear power stations, some of which were under construction. The four-pole generators used in French nuclear power plants were originally designed for a 900-MW output; today, the French nuclear plants are equipped with 1300-MW, four-pole generators. Depending on the type of generator, several sizes of rings are used (Table 2). To date, some 20 rings have been made, and it may be interesting to detail some particularities of the manufacturing sequence.

Melting

Melting is done in a basic electric furnace and completed by ladle refining. Mainly, the ladle refining gives more precise control of analysis and a better dephosphorization.

Electroslag Remelting

Electroslag remelting (ESR) has been a definite improvement for the 18-4 alloy in the areas of cleanliness, soundness, and mechanical properties. It was,

TABLE 2—*Characteristics of rings used in nuclear generators.*

Generator Power, MW	Outside Diameter, mm (in.)	Inside Diameter, mm (in.)	Height, mm (in.)	Required Yield Strength, MPa (ksi)
900	1746 (68.7)	1565 (61.6)	700 (27.6)	750 (109)
900	1657 (71.8)	1657 (65.2)	710 (27.9)	850 (123)
1300	2040 (80.3)	1850 (72.8)	775 (30.5)	850 (123)
1300	2040 (80.3)	1850 (72.8)	775 (30.5)	900 (130)

of course, adopted for 18–18. Our ESR furnace allows the remelting of ingots up to 1100 mm (43.3 in.) in diameter and 33 metric tons. This is the type of ingot which is used for the nuclear rings.

Hot Working

Control of grain size is an important factor in the quality of a retaining ring, especially in order to allow efficient ultrasonic inspection. In our case, this control is achieved by a carefully selected forging procedure concerning the heating and cooling cycles as well as the forging operations themselves. A systematic determination of ultrasonic attenuation is performed in the as-forged condition to check hot working efficiency.

Solution Treatment

Solution treatment at 1050°C (1922°F) is intended to put chromium carbides in solution and to keep them in solution by rapid water cooling. With 18–18, the risk of obtaining out of solution carbides is much less than with 18–4, but this precipitation must be avoided for better corrosion resistance. After solution treatment, another check of ultrasonic attenuation is performed.

Expansion

This operation is performed by our hydraulic process, using the Interforge 65 000-metric-ton press. For these types of rings, both the diameter and the strength necessary to maintain hydraulic pressure are well above the capacity of the Pamiers Plant's 20 000 metric-ton press. The cold working ratio is, however, moderate enough (less than 30%), due to the high yield strength capability of this alloy.

Stress Relieving

Stress relieving is quite similar for 18–18 and 18–4 and does not present any particularity. It is performed generally between 325 and 360°C (617 and 680°F). For 18–18, embrittlement occurs only if held above 400°C (725°F), which gives a good safety margin for stress relieving and shrinking onto the rotor.

Properties of Production Rings

The mechanical properties of nuclear rings supplied in NMF 18 up to the present time are given in Fig. 8. We paid particular attention to the drop of the yield strength at temperatures around service conditions. We perform tests on all the rings at 100°C (212°F). Results are given in Fig. 9. (NOTE: We added some results obtained on nonnuclear rings with yield strengths above the yield strength range of nuclear rings.)

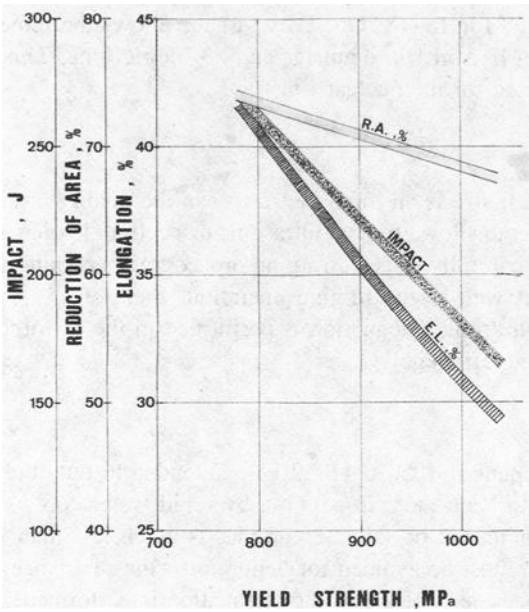


FIG. 8—Mechanical properties (at RT) of NMF 18 nuclear retaining rings.

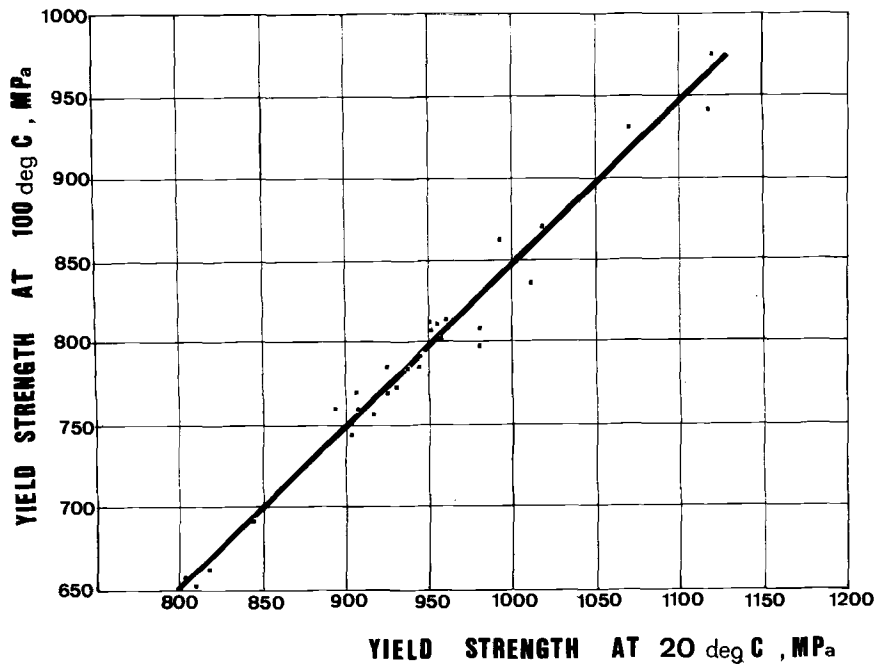


FIG. 9—Relationship between yield strength at 100°C and yield strength at 20°C for NMF 18 rings.

There is a good linear relationship between the yield strengths at 100°C (212°F) and at room temperature with a slope very close to 1, which means that the difference, rather than the ratio, remains constant, at least in this range of yield strength. This particularity of the 18-18 grade is, of course, to be taken into account when designing retaining rings.

Future Trends

The manufacturing of NMF 18 large rings is now well established, and the properties obtained are in full agreement with those which were expected. Of course, the use of this very interesting grade is not limited to medium yield strength rings, and rings with a yield strength around 1200 MPa (174 ksi) already have been manufactured and supplied. For investigation purposes, one experimental industrial size ring was expanded to a yield strength of 1350 MPa (195 ksi) at midwall with a very good level of ductility: 18% elongation, 63% reduction of area, and 171 J (126 ft·lb) impact energy. This shows the ability of this grade to reach high yield strength levels.

Under these conditions, however, the ratio of yield strength to ultimate tensile strength reaches values very close to 1 (0.99 in this particular case). Figure 10 shows the evolution of this ratio with the yield strength and confirms this tendency. These results, however, have been obtained with a tensile speed of 14 MPa/s (2000 psi/s), and it has been observed that this ratio decreases with the tensile speed. Furthermore, in spite of this elevated ratio, this material keeps a good deformation capability: for example, with a yield strength of 1190 MPa (172 ksi) and a ratio of 0.99, the uniform elongation (measured before the reduction of area) is still 50% of the total elongation. This ratio decreases at service temperatures as compared to room temperature.

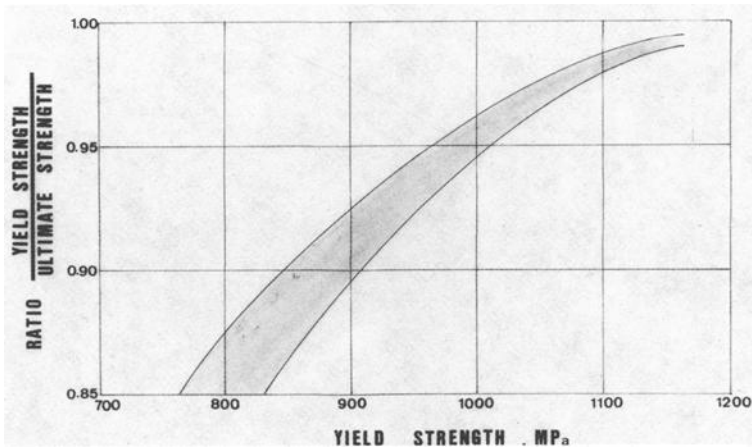


FIG. 10—Evolution of yield strength to ultimate strength ratio with the yield strength level (NMF 18 rings).

Consequently, we think that this material is fully usable for a large range of rings, including high and medium yield strengths. Nevertheless, we wish to point out that, in our opinion, this grade is not intended to completely replace the conventional 18-4. This latter grade, which bears a lower cost, has proved to be very well fitted to its function when the environment can be sufficiently controlled. Both grades can have their place in the retaining ring field.

DISCUSSION

R. H. Bellows¹ (written discussion)—Have you investigated the cause of the low-temperature strength reduction exhibited by this steel? If so, what is the cause and how might it be prevented?

J. B. Rambaud and R. H. Cazenave (authors' closure)—The low-temperature strength reduction seems to be a specific property of this steel, and it is probably in relation with the nitrogen strengthening mechanism. We think it cannot be prevented, and that the rings must be designed to take account of it.

¹ General Electric Co., Schenectady, NY 12345.

Pressure Vessel and Nuclear Forgings

Review

Seamless Shell Course Forgings for Heavy-Wall Reactor Vessels: A Forgemaster's Critical Review

REFERENCE: Bernabei, P., Callegari, L., Scepi, M., and Salinetti, T., "Seamless Shell Course Forgings for Heavy Wall Reactor Vessels: A Forgemaster's Critical Review," *Steel Forgings, ASTM STP 903*, E. G. Nisbett and A. S. Melilli, Eds., American Society for Testing and Materials, Philadelphia, 1986, pp. 275–300.

ABSTRACT: A review of current international specifications for forged pressure vessel (PV) components has shown that the steelmaking requirements are sometimes in conflict with the reality of worldwide installed facilities. A comparative investigation of three melts of SA-508 Class 3 steel has proven that vacuum carbon deoxidation offers toughness properties, even in the heat-affected zone, that are at least comparable with those obtained with the conventional fine-grain practice. Manufacturing experience with large hollow ingots, up to 181 metric tons, yielded quality results definitely comparable to those achieved with conventional hot pierced ingots. A review of specified post-weld heat treatments (PWHTs) has suggested that during PWHT some zones of a pressure vessel could undergo temperatures never reached either during the previous tempering treatments or during the simulated PWHT of acceptance test coupons. PWHTs at relatively high temperatures, therefore, should be avoided, especially for the 2.25Cr-1Mo steel.

KEY WORDS: pressure vessels, forged shell courses, basic electric furnace, ladle furnace, vacuum stream degassing, vacuum carbon deoxidation, fine-grain practice, 0.75Ni-0.5Mo-Cr-V steel (A-508 Class 3), hollow ingots, fabrication, post-weld heat treatments (PWHT), simulated PWHTs, 2.25Cr-1Mo steel (A-336 Grade F22), ultimate tensile strength, tempering parameter

Trying to regard chemical, petrochemical, and nuclear reactor vessels as a unique subject may be somewhat misleading, since service conditions, design criteria, and material requirements are significantly different. Nevertheless, from the forgemaster's standpoint, a rough attempt to discuss "the reactor pressure vessel" (RPV), forgetting for a little while hydrogen attack, creep embrittlement, Nelson curve, integrated neutron exposure, etc., makes sense.

To some extent, the awareness of the relative advantages of plates and forgings is based upon high-level advertising—for example, symposia papers, a pretty

¹ Customer Service, Metallurgy Dept., Forgings & Castings, TERNI Corp., Terni, Italy 05100.

² Quality supervisor, manager, and manager (retired), respectively, Metallurgy Dept., Forgings & Castings, Terni Corp., Terni, Italy 05100.

fine and sophisticated job. Unfortunately, vested interests may lead to exceed in critical aspects. Thus, forgemasters who claim out-of-roundness due to longitudinal seams, or plate producers who give an account of hot piercing as the forging operation that unfolds segregates on the inside surface of shell courses, are both a little unfair. The third position—a very secure one—is that of the plate *and* forging producers: high quality is high quality, so let us forget the type of intermediate product. To be honest, they are quite right. The soundness of large components depends mainly on steelmaking, ingot pouring, and ingot solidification; producers who have both adequate facilities and reliable practices are able to provide good ingots—rolling or forging, thereafter, is less important.

Melt shops for high-quality large ingots, however, have another problem to cope with: to find out the best balance between available capacity, daily production, and steel grade mix. Feeding large rolling mills *and* big presses requires a “fine tuning” approach: large production and large variety of ingot types and of steel grades are all disturbing factors. So we believe that the best heavy ingots for plates or forgings available today have an equivalent quality level; we just doubt that they are available everywhere and at all times.

The pressure vessel (PV) field is historically the kingdom of plates because the forged shells are more expensive. However, plates and forgings may become commercially competitive for very thick-walled PVs. It would be very complex to plot the two costs versus the thickness fairly on a graph since so many factors must be considered. We feel that in the range 125 to 250 mm (5 to 6 in.) purchase managers start to wonder whether their designers are going to exert pressure in favor of forged shells.

The purpose of this paper is to try to give a clear account of a few open questions relating to RPV shell courses in the forged version. Throughout this paper *heavy wall* means thicker than 125 mm (5 in.).

Steelmaking and Ingot Pouring

Specifications

Materials specified for forged shell courses are numerous. We believe Table 1 summarizes the most popular materials specified in the Western world.

HWPVs represent a more and more important percentage of the capital cost going from chemical to petrochemical to nuclear plants. So very often national standards—American Society of Mechanical Engineers (ASME), American Society for Testing and Materials (ASTM), Technischer Überwachungs-Verein (TUV), British Standards Institution (BSI), Electricité de France (EdF), etc.—are integrated by more stringent supplementary specifications written by the designer/user or by the PV manufacturer. Nonetheless, national standards are still of paramount importance since the public authorities in Western countries enforce design codes based upon materials acknowledged/specified by them. Furthermore, in the market of small-diameter PVs for applications of secondary impor-

tance, just the national standards are specified (quite often ASTM, even in Europe), without supplementary specifications. National standards have great influence on the philosophy of the supplementary specifications, especially in the paragraphs relative to manufacture. Almost all the specifications listed in Table 1, in fact, have a section dealing with the steelmaking process. This is very important because it means that RPV designers, manufacturers, and users also have knowledge of the process, or at least that they are aware of all the effects that the process may have on the final product beyond the acceptance criteria [for example, chemical requirements, mechanical requirements, nondestructive testing (NDT), etc.]. In our opinion, this area of the specifications needs some discipline.

Melting media do not seem to have much importance since they range from open-hearth to vacuum induction. Nonetheless, when nuclear components are involved (see SA-508 and M-2115 in Table 1), only basic electric furnace is spelled out. Separate refining (that is, ladle refining) is quite often an option, except for nuclear components. In fact, SA-508 envisages only electric furnace steel and the vacuum-treated basic oxygen steel, and M-2115 does not mention alternatives to electric furnace steel. While the SA-508 approach can be easily understood—vacuum *stream* degassing makes any previous degassing redundant or unnecessary—all other specifications prescribing a general vacuum degassing should mention separate refining, like A-182 and A-336 or, even better, A-350.

Another aspect of the specified steelmaking requirements is the so-called “fine-grain practice.” As can be seen in Table 1, American specifications, except A-350, do not mention it, whereas European specifications do very often. The fine-grain practice is, in short, a deoxidation technique in which killing with silicon is followed by further killing with aluminum. Fine-grain practices adopting other oxygen-bond elements such as vanadium, titanium, niobium, zirconium, or tellurium have been widely experimented, but unfortunately the presence of these elements may have an adverse effect on various properties of fine-grained steels [more difficult weldability (vanadium), too large carbonitrides—(titanium and zirconium), poor machinability, etc.]. In fact, disregarding the success achieved in the early seventies by steels fine-grained with vanadium, niobium, vanadium-niobium, or niobium-vanadium-nitrogen for small thickness plates [40 mm max (1½ in.)], present specifications for heavy-wall shell courses in low-alloy steels never mention deoxidizers or inhibitors other than aluminum. Advantages and limits of the aluminum additions are discussed in the next paragraph. As far as specifications are concerned, we have the following comments:

1. Whenever the fine-grain practice is specified, the aluminum content in check analysis should be specified as well (see question marks on Table 1—Al, % column). One should bear in mind that a Grain-size 3 ASTM can be achieved with about 100 ppm aluminum, that the classic requirement 5 or finer can be achieved with 180 to 280 ppm aluminum, that with 150 to 180 ppm or more aluminum, the forgeability of steel may become very poor (hot brittleness, surface

TABLE 1—Material specifications for pressure vessels, steelmaking requirements.

Specification	Year	Title	Steelgrades	Melting	Refining	Degassing	Si, %	Al, %
UNITED STATES								
ASME SA-182 (A182-81A)	1983	forged or rolled alloy-steel pipe flanges, forged fittings, and valves and parts for high-temperature service	low-alloy ferritic	open-hearth, electric-furnace, basic oxygen	separate degassing and refining optional.		yes	...
ASME SA-336 (A336-82)	1983	steel forgings, alloy, for pressure and high-temperature parts	ferritic grades	open-hearth, basic oxygen, electric furnace, vacuum induction	primary melting may incorporate separate degassing or refining.		yes	...
ASME SA-350 (A350-81A)	1983	forgings, carbon and low-alloy steel, requiring notch toughness testing for piping components	LF1, LF2, LF3, LF5	open-hearth, basic oxygen, electric furnace, vacuum induction	primary melting may incorporate separate degassing or refining. Optional esp or var to follow. The steel shall be fully killed, fine-grain practice.		yes	?
ASME SA-508 (A508-81)	1983	quenched and tempered vacuum-treated carbon and alloy steel forgings for pressure vessels	all classes	basic electric-furnace process (supplementary requirement S12: vacuum-treated basic oxygen furnace steel for Classes 1, 2, and 3 only)	vacuum stream degassing (... less than 1000 μ m ... within 2 min.)		yes	...

B.S. 1503	1980	steel forgings for pressure purposes	UNITED KINGDOM	(supplementary requirement S11: vacuum carbon deoxidized steel for all classes)	No, 0.12 max	...
			carbon-manganese and low alloy	open hearth, electric furnace, or basic oxygen	yes	0.018 min
				the steel shall be <i>fully killed</i>		
						if the steel is vacuum deoxidized the lower limit of the silicon range is not applicable. Aluminum treatment may be omitted. In both cases grain size shall be 6 or finer.
RCC-M M2115 (E.d.F.)	1984	Mn-Ni-Mo steel forgings for PWR steam generators tubesheets	FRANCE	LAFNOR 18MND5	0.10 0.30	0.040 max
					vacuum degassed	
VdTUV 354/3	1981	weldable steels with 355 N/mm ² min yield strength	WEST GERMANY	werkstoff No. 1.0562 1.0565 1.0566	yes	0.015 min
VdTUV 401/1	1980	fine grain quenched and tempered steel, 20Mn-Mo-Ni55, plates and forgings for high temperature service		werkstoff No. 1.6310	yes	0.010 0.040
VdTUV 404	1977	12Cr-Mo-910 steel, plates and forgings		werkstoff No. 1.7382	yes	0.010 0.030

TABLE 1—Continued.

Specification	Year	Title	Steelgrades	Melting	Refining	Degassing	Si, %	Al, %
TYPICAL EUROPEAN MATERIAL SPECIFICATIONS FOR HYDROGEN SERVICE REACTOR VESSELS								
1983	2.25Cr-1Mo	steel in quenched and tempered condition, plates and forgings	ASTM A387 Gr. 22 ASTM A182 Gr. F22 ASTM A336 Gr. F22		aluminum killed	vacuum degassed	yes	?
1984	2.25Cr-1Mo	material in thick wall shell	(material shall meet requirements of ASME viii, div. 1.)	Electric furnace or basic oxygen. <i>Fine grain practice</i> shall be used ... refining agents other than <i>aluminum</i> require written buyer approval. "J" factor less than 150.		vacuum degassed	0.20 max	?

cracks, etc.). Obviously, these figures will change with the type of refining, vacuum treatment, steel chemistry, mass, product type, heat treatments, etc.; we just want to emphasize the need for a correct attitude toward prescriptions. A rigorous prescription also should be concerned with soluble aluminum and soluble nitrogen, besides the total values, in product analysis.

2. The most critical specifications in Table 1 seem to favor the basic electric furnace (BEF). Aluminum additions during BEF refining are very difficult, especially when ultrasonic acceptance standards on the final product are stringent. The classic aluminum addition into the ladle after tapping does not yield cleaner steel, either. The various types of ladle furnaces (LF), on the other hand, may perform aluminum treatments during refining much more easily. So the German examples in Table 1 coherently prescribe the aluminum content for fine-grain steel and do not mention the refining facility, while the French example seems to force aluminum killing into the less suitable facility.

3. The British position in Table 1 is shared by several RPV manufacturers: fine-grain practice may be omitted providing that a very fine grain is achieved on the product. During the seventies important imaginative efforts led to grain refinement by means of cyclic rapid heating [1,2], thermomechanical processes with controlled deformations [2], and intercritical heat treatments [3,4]. Although these techniques are very attractive, especially the latter, none so far have ever been specified by RPV users or manufacturers. There are other methods of achieving grain refinement during forging, but, unfortunately, attaining Grain Size 6 or finer on huge shell courses without aluminum is extremely difficult. So the British alternative to aluminum killing indirectly applies to relatively small forgings only.

Vacuum carbon deoxidation (VCD) is another very important feature in Table 1. Since its invention [5] until the present day [6], VCD has been associated quite often with the vacuum stream degassing (VSD) process. As has already been said, the logic of A-508 with the sequence BEF, VSD by very low pressure/high extraction capacity facilities, VCD (S11), is very clear: that is, to be sure that optimum dehydrogenation takes place and that in the case of VCD the system is capable of taking out the extra gas (carbon monoxide plus lesser quantities of carbon dioxide, further hydrogen and nitrogen). It would seem, therefore, that VSD is the most reliable degassing process, although Supplementary Requirement S12 suggests that at least for Classes 1, 2, and 3 an unidentified vacuum treatment could suffice. It is well-known that many forgemasters have ladle furnaces besides the conventional BEF, and that heavy ingots for heavy-wall shell courses must be produced with the multiple melt technique. Japanese gigantic ingots (500 tons³), for instance, are produced by multipouring techniques [7] which use 4 BEFs in combination with 3 large LFs [8]. The variety of LF processes in use

³ Throughout this paper, tons refers to metric tons.

is so large that any further evaluation of them would go beyond the scope of this paper. A comparison between the following sequences, however, should be attempted:

	Melting	Refining	Pouring
1.	BEF	BEF	VSD, VCD
2.	BEF	LF	VSD, VCD
3.	BEF	LF, vacuum treatment, VCD	air or argon stream

Formally only No. 1 meets the requirements of A-508; No. 2 does not, but everybody knows that it is accepted. Could No. 3 be accepted too? Looking at published data on the performance of LFs [9], it seems that VCD is not only feasible but also that the results would be comparable to those obtained by conventional "stream" VCD.

Two more remarks on Table 1 and VCD:

1. Besides A-508, the BSI only mentions VCD, but with the penalty for 6 or finer.
2. The last line prescribes a rather low J factor for 2.25Cr-1Mo steel, and the lower the silicon the lower the J . Unfortunately, neither A-182, A-336 (F22), nor the numerous specifications for hydrogen service reactor vessels give the option for low-silicon VCD, in spite of the compelling evidence of the suitability of VCD for 2.25Cr-1Mo steel [10,11].

The conclusion of this critical and, we hope, positive review of the specifications is the following proposal. Forgemasters able to produce ingots for heavy-wall shell course forgings (large diameters and adequate lengths) are less than 20 in the Western world. Their facilities and their steelmaking practices have recently been reviewed by an excellent survey sponsored by the Electric Power Research Institute [12]. Future specifications should either eliminate steelmaking requirements or assess a thorough option matrix where the few reliable techniques/sequences would be correctly chosen by designers and RPV manufacturers (national standards) or by forgemasters (supplementary specifications).

Silicon Killing, Aluminum Treatment, Vacuum Carbon Deoxidation

As early as 1965, Mr. McQuaid suggested eliminating aluminum in high-quality steel for grain-size control, although "... in the mind of the user the term *fine grain* develops a much more attractive picture than the term *coarse grain* He . . . pictures the 'rock candy' fracture of greatly overheated cast iron . . . when he thinks of coarse grain" [13]. So we come to the crucial questions:

1. Do PVs actually need fine-grained steels?
2. Why can coarse-grained steel not be used?

Advantages and limits of aluminum additions (150 to 300 ppm) can be summarized as follows:

ADVANTAGES

1. After zirconium, aluminum is the strongest deoxidizer of molten steel.
2. After solidification, aluminum nitrides precipitate at the grain boundary. Aluminum-nitride inhibits grain growth during subsequent reheatings (forging/rolling, heat treatments, welding).
3. The presence of AlN in steel solves the problem of nitrogen diffusion, minimizing in turn the aging problem.

LIMITS

1. Aluminum affects the steel cleanliness. Due to their dendritic form, it is very difficult to eliminate alumina (Al_2O_3) inclusions from molten steel, especially when they are small in size. Furthermore, except for extra-low-sulfur steels, aluminum contributes to the formation of refractory oxide "galaxies" (Type II sulfides).
2. Unless molten steel undergoes a strong and effective degassing prior to or during pouring, aluminum increases the tendency of steel to flaking or micro-flaking, due to the fact that aluminum inclusions act naturally as gas concentrators.
3. Aluminum may decrease the grain-boundary cohesion, due to precipitation of microscopic alumina particles. An intergranular failure of an aluminum fine-grained steel is clearly shown in Fig. 1.

Thus, a general evaluation applicable to all grades is impossible. Aluminum treatment must be specified case by case, possibly when the pros outweigh the cons. The well-known A-508 Class 3 steel, widely used for nuclear RPVs, in our opinion is essentially affected by aluminum killing, with negligible advantages. Such an opinion is based upon the following evidence.

Material—Coupons cut from prolongation rings for official mechanical testing of three shell course forgings manufactured in 1983-1984 have been used for this evaluation. Production data are shown in Table 2. VCD of Heat A took place in a vacuum stream degassing facility whose extraction capacity is 340 000 m^3/h at pouring pressure. The theoretic principle of VCD rests on the influence of the carbon monoxide partial pressure on the carbon-oxygen equilibrium. Ladles should arrive at the VSD facility with a chemical composition aimed at a correct VCD. Such conditions may be summarized as follows:

1. Absence of deoxidizers which form solid deoxidation products silica [(SiO_2) , Al_2O_3 , etc.].
2. Oxygen activity in equilibrium with the carbon content at the pouring temperature.

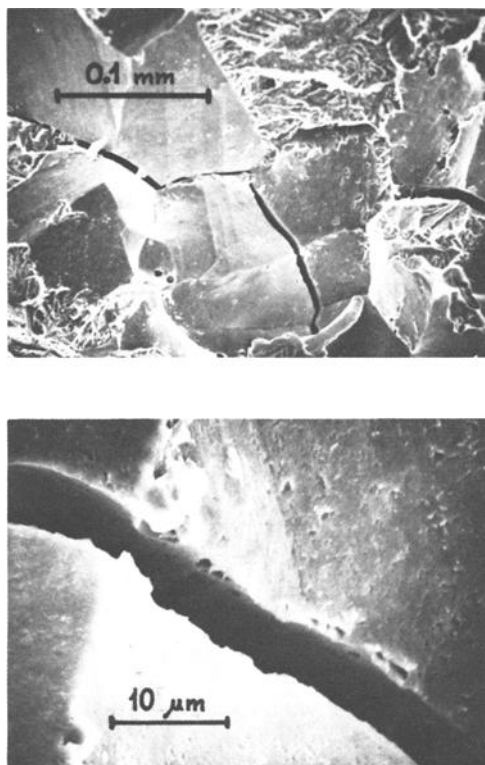


FIG. 1—Intergranular failure of SA-508 Class 3 steel. Appearance of a CVN specimen tested at 55°C (130°F). Heat B (aluminum killed).

Our practice is calibrated on these principles, by means of suitable argon stirring during refining and oxygen activity control with special oxygen probes. If the chemical conditions of the steel are close enough to the theoretical ones, when the molten steel stream opens out in the vacuum tank, a sudden drop of the carbon monoxide partial pressure occurs [from atmospheric pressure to 0.5 Torr (see Fig. 2)], allowing for the VCD chemical reaction



The deoxidation product is a gas; therefore, it can be completely eliminated by the vacuum system that expels large quantities of carbon monoxide, H_2 , N_2 , CO_2 . Clearly the extraction rate of this gas mixture must be quite high. Figure 2 shows the pressure evolution during VCD of a “TERNI” ingot of 240 tons in Ni-Cr-Mo-V steel. Good preliminary vacuum and a consistent low pressure during ingot body pouring should be appreciated.

Less powerful facilities may enable sufficient dehydrogenation to be performed, but a correct VCD could never be performed, since the pressure increase

TABLE 2—*Manufacturing data of evaluated materials (SA-508 Class 3 steel with different deoxidation techniques).*

Heat Code	Deoxidation Practice Code	TERNI Facilities Used			Ladle Analysis										Ingot Weight, tons	Forged Shell Dimensions (rough machined for Q and T)		
																Millimetres	Inches	
		Melting	Refining	Pouring	C, %w	Si, %w	S, ppm	P, ppm	Mn, %w	Cr, %w	Ni, %w	Mo, %w	V, ppm	Al, ppm				
A	VCD	UHP BEF 180 tons			VSD 5-stage steam ejectors	0.16	0.04	40	110	1.26	0.07	0.78	0.49	80	10	154 (1 × 1)	OD 2262 ID 1920 T 170 L 4546	... 6 3/4
B	Al killed	UHP BEF 40 tons			ASEA-SKF LF 42 to 50 tons	0.19	0.19	90	100	1.51	0.06	0.79	0.48	70	160	40 (1 × 3)	OD 1650 ID 1360 T 145 L 400 5 3/4 ...
C	Si-Al killed	BEF 80 tons			VSD 5-stage steam ejectors	0.14	0.26	60	100	1.35	0.17	0.88	0.47	140	150	52 (1 × 1)	OD 2450 ID 1950 T 250 L 2000 9 7/8 ...

NOTE: UHP BEF = ultra high power basic electric furnace; Q and T = quenching and tempering; OD = outside diameter; ID = inside diameter; T = wall thickness; L = length.

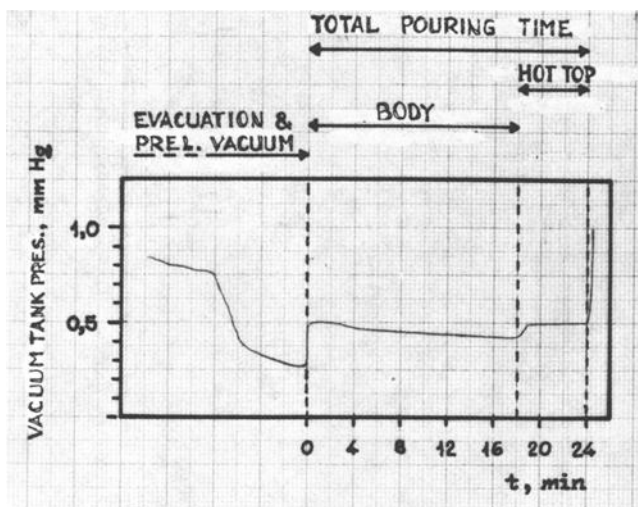


FIG. 2—Vacuum tank pressure during VCD of a 240-ton TERNI ingot in Ni-Cr-Mo-V steel.

inside the vacuum vessel would prevent the development of the VCD reactions.

Heat B was partially deoxidized by silicon and fully killed by aluminum addition after vacuum degassing in the ladle furnace. Heat C was melted and refined in a BEF with the classic two-slag process. Killing was performed during refining by silicon and aluminum additions. Further “star” aluminum was added in the ladle during tapping. The three coupons coming from Melts A, B, and C were in the as-quenched and tempered condition, without simulated post-weld heat treatment. The austenitizing temperature was always our standard 870°C (1598°F) for A-508 Class 3 steel.

Austenitic Grain Growth Kinetics—Specimens taken from the three coupons were reaustenitized in the range 850 to 1200°C (1560 to 2190°F) and soaked 2 to 10 h, in order to compare the growth sensitivities. Figure 3 shows the results. Obviously aluminum-bearing melts show a much better resistance to grain coarsening. The VCD melt, however, shows a decent grain size in the conventional heat treatment range (5 to 6 ASTM, circa 50 μm).

Influence of Grain Size on Toughness—Since the thicknesses of the three test ring sections were significantly different: 170 mm (circa 6¾ in.), 145 mm (circa 5¾ in.) and 250 mm (circa 9⅞ in.) (see Table 2), three equal blocks were machined out. They underwent simulated water quenches with a cooling rate relative to a nominal thickness of 220 mm (8⅝ in.). Austenitizing temperatures ranged from 850 to 1200°C (1560 to 2190°F) in order to have a wide range of grain sizes; minimum cooling rate between 850 and 300°C (1560 and 572°F) was 30°C/min. (circa 50°F/min.). Subsequent tempering was performed at temper-

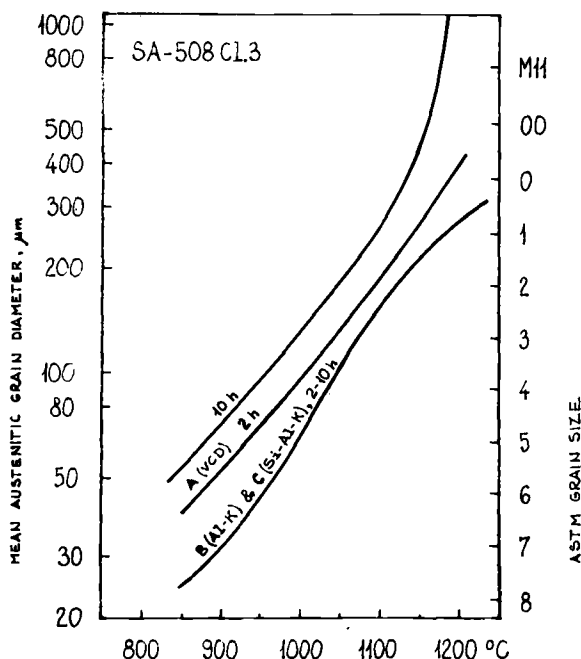


FIG. 3.—Influence of temperature and soaking time on the austenitic grain-size of the three heats.

ature suitable for attainment of yield strength (YS) 460 to 490 MPa (circa 65 to 70 ksi) and Ultimate Tensile Strength (UTS) 590 to 630 MPa (circa 83 to 89 ksi) under all the austenitizing conditions. Afterwards, impact-test specimens were machined out of the three blocks for transition curve plotting. Figure 4 shows the fracture appearance transition temperature (FATT) versus austenitic grain size. Figure 5 shows the absorbed energy at 4.4°C (40°F) versus austenitic grain size. It is extremely clear that for a given grain size, VCD steel yields markedly better values of FATT and energy than the conventionally killed melts.

Toughness Properties after Welding Simulation—A typical thermal cycle undergone by a 220-mm (8 $\frac{5}{8}$ -in.)-thick plate during submerged metal-arc welding in the heat affected zone (HAZ) is: preheating 200°C (410°F), 1350°C (2462°F) in 10 s with a heat input of 25 KJ/cm, and fast cooling with 11 s in the range 800 to 500°C (1472 to 932°F). This cycle has been simulated on several suitable test specimens coming from Coupons A, B, and C by means of the SMITWELD simulator shown in Fig. 6. The equipment is capable of simulating the cycle on a zone of the specimens circa 5 mm (circa $\frac{1}{4}$ in.) wide. Examples (Heat B) of the recorded cycles are shown in the same figure. Simulations were followed by tempering aiming at the same properties just mentioned.

Figure 7 shows the micrographic appearance of the specimens in the simulation sections (a), in the intermediate sections beyond the 6-mm band (b), and in the

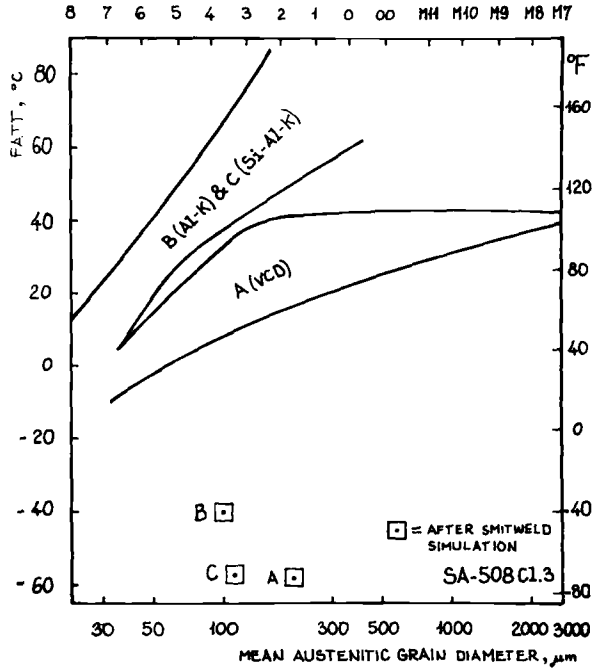


FIG. 4—Effect of austenite grain size on FATT of the three heats in the quenched-tempered condition and after welding simulation.

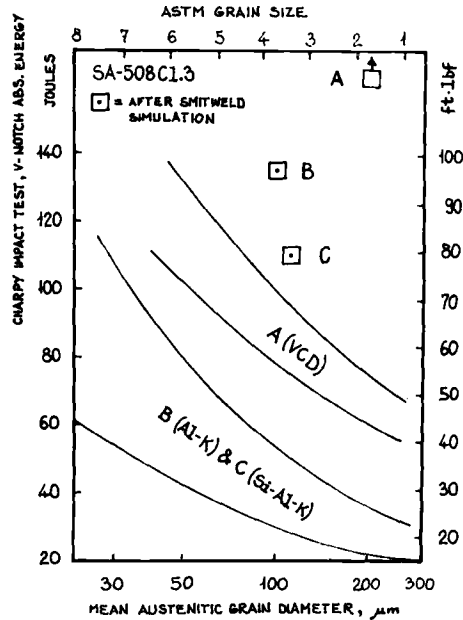


FIG. 5—Effect of austenite grain size on toughness [CVN absorbed energy at 4.4°C (40°F)] of the three heats in the Q + T condition and after welding simulation.

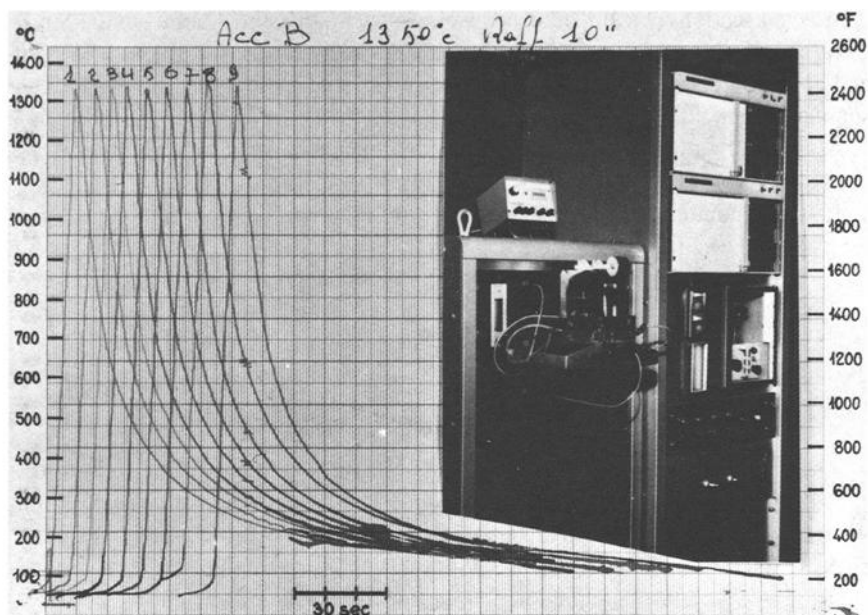


FIG. 6—The "Smitweld" simulator and the chart of nine thermal cycles (Heat B).

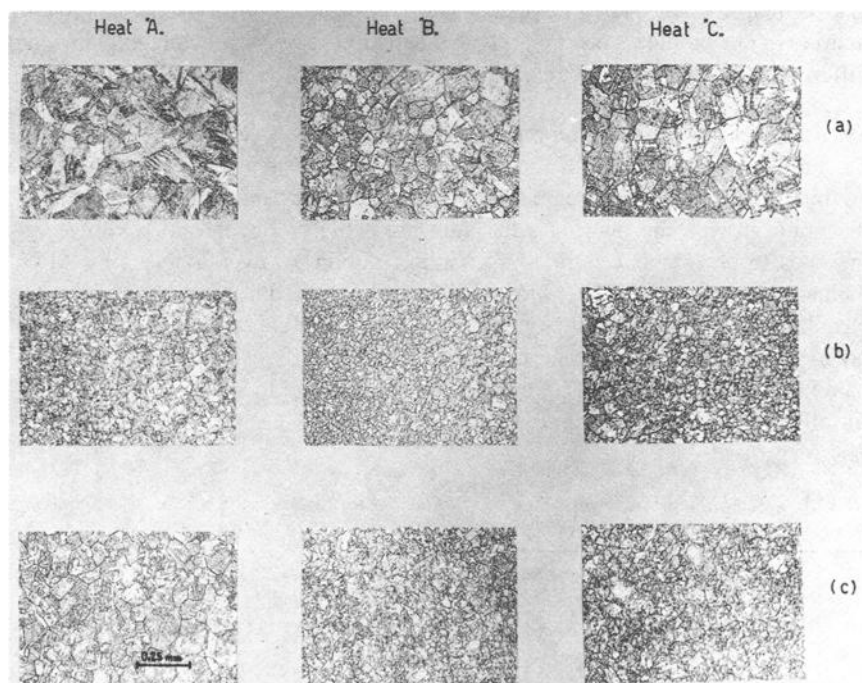


FIG. 7—Grain size of the three heats after Smitweld simulation: (a) maximum growth zones; (b) intermediate zones; (c) unaffected zones.

unaffected sections (c). Impact-test specimens were machined out from the Smit-weld specimens with the notches in the HAZs. The respective values of FATT and absorbed energy are summarized in Table 3 and plotted in Figs. 4 and 5 as supplementary points.

After review of these data, the following conclusions can be drawn:

1. Aluminum fine-grained heats (B,C) exhibit austenitic grain finer than VCD Heat A after welding simulation.

2. Regardless of the deoxidation practice, for a given grain size, absorbed energy at 4.4°C (40°F) after welding is always higher than in quenched and tempered condition. Comparing the three heats, however, the VCD heat A shows the best FATT and absorbed energy values, while Heats B and C show comparable values.

For a better understanding of the results obtained, sections of the impact-test specimens in the HAZs—that is, in the 6-mm band, but sufficiently remote from the fractured surface—and in the unaffected zones were observed with a scanning electron microscope (SEM). Figure 8 shows such micrographies for Heats A and B. The HAZ structures are predominantly fine martensite, while unaffected zones show coarser bainite with traces of pro eutectoid ferrite and martensite. The carbides at the bainitic grain boundaries of unaffected material are consistently coarser than the carbides precipitated during tempering in the HAZ martensitic matrix. In our opinion, this remarkable distinction in microstructure explains the different toughness in HAZs and unaffected zones of the two heats.

Recommendations—Aluminum treatment of molten steel is not very simple. Steel mills with suitable facilities and adequate practices may perform it correctly. Aluminum nitride may cause problems but on the other hand undoubtedly inhibits the grain growth and decreases the aging sensitivity. Beyond Al-N, however, the odds to bring about aluminum in solid solution or, even worse, tiny Al_2O_3 inclusions are high. VCD yields coarser grain, but due to a better inherent cleanliness of the grain boundary, and hence a stronger cohesion, this deoxidation practice offers toughness properties—even in the HAZ—which are at least comparable to the fine-grain practice ones. We recommend to specify optional VCD for all components in weldable low-alloy steel.

TABLE 3—FATT, absorbed energy at 4.4°C (40°F) and shelf energy values relative to Smitweld simulated materials.

Heat Code	FATT, °C	Absorbed Energy at 4.4°C (40°F), J	Shelf Energy, J	α Grain Size, μm
A	−63	215	215	200
B	−40	135	140	100
C	−57	110	115	110

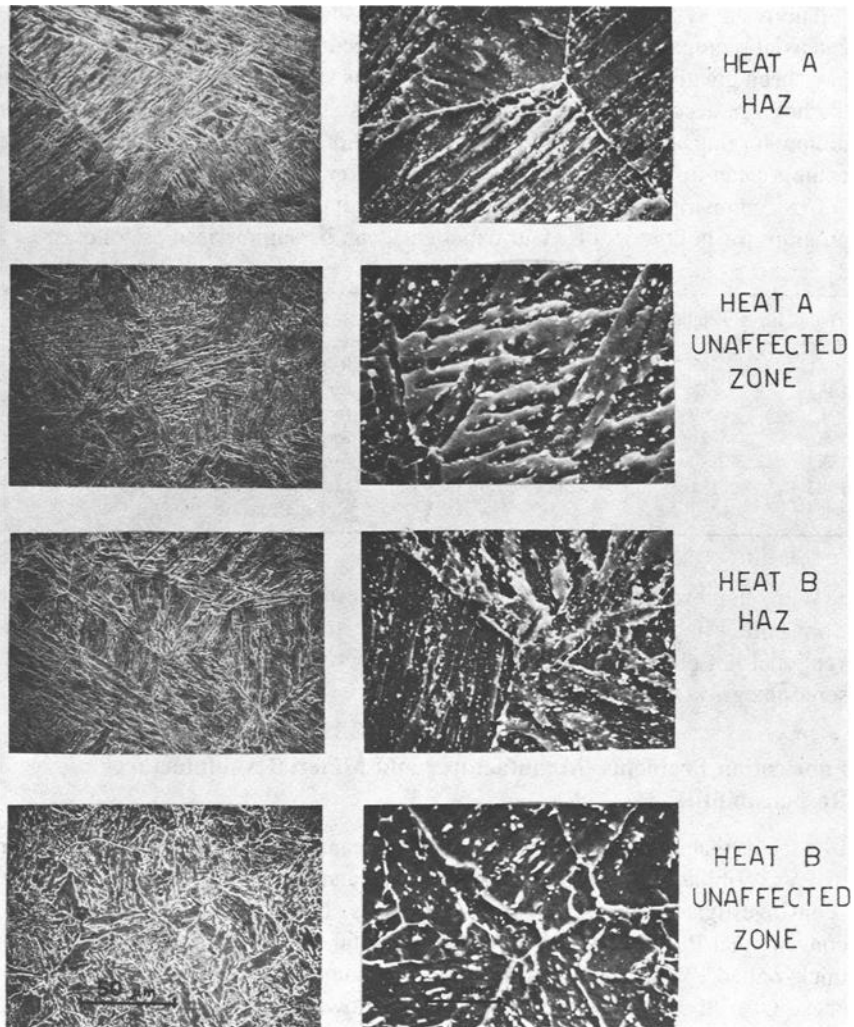


FIG. 8—Micrographic appearance of HAZ and unaffected zones after Smitweld simulation on SA-508 steel. Heats A (VCD) and B (aluminum killed).

Hollow ingots

Huge solid ingots for forgings suffer the phenomenon of macrosegregation. The technical literature on this subject is very massive (chiefly the proceedings of the various International Forgemasters' meetings).

After a deep study of the solidification phenomenon with different mould geometries and different hot top insulation practices by means of computer simulations supported by full-scale calibrations [20,21], we redesigned our mould series a few years ago.

The result is that in our solid ingots microshrinkage voids, microporositics, and axial segregations have been minimized; occurrence of nonmetallic inclusions have been greatly reduced; positive segregations are reduced and removed toward the hot top; accordingly, negative segregations also are reduced. Therefore, our hollow forgings manufactured with the classic hot piercing-mandrel forging cycle exhibit clean inside surfaces, as proven by several acceptance sulfur prints.

Cost comparisons and market conditions advised us to start a development program for hollow ingots. Our experience can be summarized as follows:

Year	Ingot weight, tons	Pouring Technique	Product Type
1981	57	bottom pouring	forged shells for centrifugal casting
1982	62	bottom pouring	forged shells for centrifugal casting
1982	59	bottom pouring	forged shells for centrifugal casting
1982	71	bottom pouring	forged shell course
1983	130	vacuum ^a stream degassing	forged shell course
1983	181	vacuum ^a stream degassing	prototype nozzle belt course (pressurized water reactor)

^aOptional VCD with the same facility/equipment.

With our present standard practices, quality results on hollow forgings produced from hollow ingots are definitely comparable to those achieved with the conventional hot pierced ingots (mechanical properties, inside surfaces cleanliness, sonic integrity, etc.).

Fabrication Problems: Manufacturer and Material Manufacturer Responsibilities

It seems that intermediate and final PWHTs cannot be avoided in the fabrication of PVs. Vibratory stress relieving, peening, and low-temperature PWHT have been investigated and proposed several times, but nobody is ready to replace conventional PWHT. Such treatments may total up to 100 to 120 h for huge or thick-walled PVs or both. Temperatures are dangerously close to the tempering ones. Over the last few years a tendency toward higher and higher PWHT temperatures for the 2.25Cr-1Mo steel has emerged. We believe this is due much more to the welding problems—availability of suitable welding materials, adequate welding techniques, etc.—than to the base metal properties. Effective tempering of HAZ; precipitation of suitable alloy carbides, their kinetics, and their influence on stress relief cracking sensitivity; and hydrogen concentration during welding and its reduction during PWHT are attractive and challenging subjects, but far beyond the purpose of this review.

Thus, among the acceptance criteria for plates and forgings, mechanical testing after simulated PWHT on test coupons is always specified. PWHT furnaces are not, usually, very precise in terms of temperature uniformity. Even the best furnaces, that is, those used for nuclear PVs, operate within temperature ranges wider than those of tempering furnaces used for single-shell course forgings. So,

PV manufacturers are forced to specify wide tolerances for the simulated PWHT on temperatures. Laboratory furnaces used for SPWHT, on the other hand, may operate with an even better uniformity than that of the tempering furnaces previously mentioned. The following table summarizes the possible situations:

Specified PWHT	Tolerance (690), $\pm 15^{\circ}\text{C}$	Performance (Actual Metal Temperature) (675) ————— (705)	Evaluation
Good tempering furnace for single shells	± 5	685 ——— 695 675 — 685	fair unfair
Poor tempering furnace	± 15	675 ————— 705	OK?
Good laboratory furnace for test coupons SPWHT	± 3	687 — 693 675 — 681 699 — 705	excellent fair unfair
Good PWHT furnace	± 15	675 ————— 705	OK?
Poor PWHT furnace	± 25	665 ————— 715 675 ————— 725	dangerous dangerous

In this example, the nominal tempering temperature is the same range as the SPWHT temperature. For many low-alloy steels, this would not be correct since tempering should be performed 30 to 50°C higher than stress relief. Nevertheless, for chromium-molybdenum steels, PWHT temperatures have become so high that the material manufacturer is forced to temper in the same range. Several producers have put forward an alternative cycle where the tempering is delayed at the time of the final PWHT. This is usually applied to quenched and tempered grades, with a low-temperature tempering (650°C for the 2.25Cr-1Mo) after water quenching. The advantage in terms of tempering parameter is evident, but unfortunately this cycle can be resorted to only when the forgemaster and PV manufacturer belong to the same company. Official acceptance of the forged shell, in fact, cannot take place before the final tempering.

If the example in the just-mentioned table is correct, when contractual requirements are not well-defined, during PWHT some zones of a PV could undergo temperatures never reached either during tempering or during SPWHT of test coupons. Can this be tolerated? Is there enough allowance in mechanical properties? It is our opinion that at least for the 2.25Cr-1Mo steel, it should be worthwhile to reconsider either the tensile strength or the PWHT temperature.

In Table 4 we have tried to summarize from the literature all available data. Approximation is unavoidable when working out tempering parameters; but we believe that the overall averages are rather meaningful: in the worst conditions (maximum thickness, chemical analysis toward the minima, VCD steel, etc.)

TABLE 4—Possible strength deterioration of quenched and tempered 2.25Cr-1Mo steel (ASTM A-387 Grade 22 Class 2, A-336 Class F22) caused by excessive PWHT during fabrication of heavy-wall pressure vessels.

Authors	Ref./ Year	Affiliation/ Country	Product/Thickness	Tensile Specimens Location	PWHT Time to Reach the Specified Min UTS 515 MPa (75 ksi), Hours				Explanations
					At 690°C (1274°F)	At 700°C (1292°F)	At 710°C (1310°F)	At 720°C (1328°F)	
W. E. Erwin J. G. Kerr	[14] 1982	Standard Oil Co., USA	plate and forging (23 heats)	variety	109 18	47 10	38 6	24 4	MC LC 95% scatter band lower confidence limit (LC) and master curve (MC); 2 data points forgings, 170 data points plates. Source: Chevron Materials Laboratory, Babcock & Wilcox, Combustion Engineering, and Foster Wheeler.
S. Ueda M. Ishikawa S. Sato S. Matsui T. Enami T. Tobi	[15] 1981	Kawasaki Steel Corp., Japan	50 and 100 kg ingots, rolled or forged into plates 20 mm ($\frac{3}{4}$ in.) thick, "not boron added," data only.	Simulated centerline of 200-mm (8-in.) thick plate Simulated centerline of 500-mm (20- in.) thick plate	(166)	(96)	(59)	(35)	— direct reading >> extrapolation of original master curve direct reading

R. A. Swift	[16] 1980	Lukens Steel, USA	Plate 260 to 300 mm 10¼ to 11¾ in. (8 heats, low-Si ones, Al-fine grained ones, Ca-treated ones)	quarterline transverse	(48)	(29)	(18)	(10)	—	master tempering curve drawn with data points relative to tempering at 655 and 690°C, and to PWHT at 690°C; time 5 to 36 h
J. A. Berthet	[17] 1980	Creusot-Loire, France	Plate 200 mm (8 in.)	¼ thickness	(65)	(34)	MC	extrapolation of original master straight line.
D. Catelin										
A. Cheviet										
J. H. Roux										
Y. Murakami	[18] 1980	The Japan Steel Works, Japan	500 mm (20 in.) Forging and plate 108 to 450 mm (4¼ to 17¾ in), 10 heats, low-Si VCD Steel	variety	50 40	28 24	16 15	10 9	MC LC	Direct reading scatter band, upper and lower limits, without master curve.
T. Monura										
J. Watanabe										
G. F. Frassoni	[19] 1983	Soc. A. T. B., Italy	Plate	variety	125 20	70 12	43 7	27 5	MC LC	Direct reading scatter band; more than 120 data points. Direct reading
A. Somigli										
R. Federighini										
overall average, master curves, and intermediate thicknesses					112	61	45	26		
overall average, lower confidence limits, maximum thicknesses and VCD steels					29	17	10	6		
This paper		Soc. TERNI, Italy	Hollow forging 180 to 300 mm (7 to 12 in.), 18 heats, VCD steel	Centerline, tangential, ½ T by T, prolongations or thermal buffers	17	9	5	3	MC	95% scatter band, master curve

Warning: "Direct reading" means that the tempering parameter has been read on original graphs (intersection between min specified UTS and curves) and computed out for this table. Extrapolations of original straight lines [17] or, even worse, of curves [18], as well as plotting curves with data listed by others [16], shall be regarded as our arbitrary initiative. By no means, figures within brackets shall be considered commitment, statement, or opinion of the relative authors.

PWHT must be performed at temperatures lower than 690°C. Our master curve is lower than the average. This depends on the location of test specimens, always at centerline and always with at least one thickness buffering in longitudinal direction. Twenty-seven shells were forged out of the 18 ingots, and only two shells were buffered by welded rings—all the others had forged prolongations. The second reason is the low silicon content: it was all VCD steel with silicon ranging from 0.03 to 0.09%. Carefully reading Table 4, one can realize the large differences between master curves and lower confidence curves. We believe this is due to the “weight” of data points relative to the small thickness components. The minimum tensile strength of PV components manufactured to the requirements of A-541 Classes 6 and 6A (forgings) or A-542 Classes 1 and 2 (plates), for instance, range from 720 to 790 MPa (105 to 115 ksi). This is all liquid-quenched and tempered 2.25Cr-1Mo steel with martensitic microstructure and low toughness. Undoubtedly, tempering parameter scatter bands are pushed upward by data points relative to the steel grades just mentioned. In our experience, VCD has a minor influence on hardenability for a given thickness. So the large differences in Table 4 could be better explained in terms of “mass effect” than deoxidation practice. We do not need to claim here the advantages of VCD 2.25Cr-1Mo steel: improvements in temper embrittlement sensitivity as well as in creep behavior have been widely proven and advertised by Japanese producers, also for the HAZ. We can only confirm that the VCD 2.25Cr-1Mo we produce exhibits very low transition temperatures and negligible shifts of the transition curves after step cooling or after long-term embrittlement. Obviously it is not just the low silicon which causes this; other elements like phosphorus, arsenic, antimony, and tin must be kept as low as possible. Nonetheless, large VCD ingots for huge shells offer other advantages such as better segregation pattern and better cleanliness. But silicon has some influence on the tensile strength of steel; 2.25Cr-1Mo steel must have also a relatively low carbon content (lower than 0.15% both in American and European specifications, and the minimum German ultimate tensile strength (UTS) is 540 MPa against the more popular 515). Since the carbon segregation in large forging ingots is unavoidable, lower ends of huge forged shells corresponding to the bottom of such ingots may have 0.10 to 0.11% carbon or even less. Thus, sometimes a relatively slight drop in silicon content (0.25 to 0.30% silicon killed to 0.04 to 0.08% VCD), that under normal circumstances (for example, large turbine rotor forgings in Ni-Cr-Mo-V steel with a nominal carbon = 0.30%) would have an undetectable effect, may push the material tensile strength toward the minimum.

On the other hand, Table 4 points out that commercial “high-silicon/mean carbon/intermediate thickness” material (master curves) would resist one day only at 720°C. This is a rather high PWHT temperature but not unreal: recently we have been asked to perform SPWHT on test coupons cut from production forged shells at 725°C (1337°F). Over the last few years, other PV manufacturers in Europe have been asking for 710, 705, 700°C (1310, 1301, 1292°F). It may be useful to recall that the minimum holding temperature specified by ASME

TABLE 5—Specification requirements and allowable stress values for 2.25Cr-1Mo steel, plates and forgings.

	Min Specified UTS at RT		Max Specified Carbon		Specified Heat Treatment ^a	Min Specified Tempering		Most Used Heat Treatment for Heavy Thickness Components, ^a		ASME VIII, Div. 1, USC-23, 1/4 of UTS				ASME VIII, Div. 2, ACS-1, 1/2 UTS			
										Room Temperature		317°C (700°F)		Room Temperature		375°C (710°F)	
	ksi	MPa	Ladle, %	Product, %		°C	(°F)			ksi	MPa	ksi	MPa	ksi	MPa	ksi	MPa
SA-387 Grade 22 Class 1	60	415	0.15	0.17	A NT QT	675	(1250)	NT	15	103	15	103	20	137	17.8	123	
Class 2	75	515	0.15	0.17	(NT) QT	675	(1250)	QT	18.8	129	17.2	118	25	172	23.3	161	
SA-182 Grade F22	75	515	0.15	0.16	A NT QT	677	(1250)	QT	18.8	129	17.2	118	25	172	23.3	161	
F22a	60	415	0.15	0.16	A NT QT	677	(1250)	NT	15	103	15	103	20	137	not		
SA-336 Class F22	75	515	0.15	0.20	NT (QT)	595	(1100)	QT	18.8	129	25	172	23.3	161	acknowledged
F22a	60	415	0.15	0.20	NT (QT)	675	(1250)	NT	15	103	15	103	20	137	17.8	123	
(F22 Norm & Temp)	17.2	118
VdTCV 404, 12Cr-Mo9 10	78	540	0.15	0.17	QT NT	680	(1255)	QT	(3/4) YS at T and UTS > 1.25 YS
						(Max 710)	(Max 1310)					Min YS at 450 = 275 MPa; 1/2 = 183 MPa					

NOTE: YS = yield strength; T = design temperature; RT = room temperature.

^aHeat treatments code: A = annealed; NT = normalized and tempered; QT = quenched and tempered.

VIII, Div. 2 is 677°C (1250°F) (Table UCS-56, P-No. 5). If the fabricators confirm the need for long and high temperature PWHTs, something should be done about the tensile requirements. YS does not seem to suffer significantly the PWHT “weakness,” at least for quenched and tempered grades. The problem concerns the UTS.

Maximum allowable tension stresses used by PV designers are obviously related to the tensile properties of the material. Forgemasters are not supposed to consult design codes, nonetheless, since the PWHT of 2.25Cr-1Mo steel is becoming so critical, we tried to summarize specified requirements and allowable stresses at 370°C (700°F) in Table 5. Simple considerations on the design criteria of ASME VIII, Divs. 1 and 2 enable us to conclude that the thickness of quenched and tempered 2.25Cr-1Mo PVs is dictated, below the creep range, by UTS *at design temperature*. UTS at room temperature (RT-UTS) divided by 4 (Div. 1) or by 3 (Div. 2) is never the least. Is this simple and naive consideration sufficient to propose a slight lowering of the minimum specified RT-UTS? Are there other considerations that make “untouchable” the RT-UTS? Divisions 1 and 2 unfortunately introduce the allowable stress at the test temperature (that is, almost always RT) for establishing the test pressure in the standard hydrostatic tests. So a slightly lower RT-UTS could be afforded, in principle, only by PVs designed by a relatively low maximum allowable working pressure. And this is very rare for 2.25Cr-1Mo PVs. Obviously all this is pure speculation. Our conclusion, then, is that high temperature PWHT should be avoided.

Two more remarks about Table 5:

1. Permissible variations on product analysis penalize the largest forgings manufactured with the requirements of A-182 (carbon = 0.16% max), while the large variation provided by A-336 (carbon = 0.20% max) in our experience is never tolerated by fabricators.

2. We have intentionally reported the little misunderstanding introduced by ASME VIII, Div. 1, Table UCS-23, page 262, Summer 83 Addenda (F-22, F22A, F22 Norm & Temp), as the best evidence of the “name complexity” of 2.25Cr-1Mo steel; only the number 22 is clear: the supplementary digits around it have different meanings; F22 is QT forging, 22 alone is plate, P22 is pipe, F22A is NT forging, 22 Class 1 is QT plate, 22 Class 2 is NT plate. Thus it is not surprising at all that Table UCS-23 is somewhat misleading when it lists an F22 Norm & Temp besides the F22A. Other misunderstandings such as F22 Class 1, Grade 22A Class F, or “is the forging Class 1 or Class 2?” are rather frequent, especially in Europe.

Conclusions

Specifications

A review of current international specifications for forged PV components has showed that the steelmaking requirements are sometimes in conflict with the

reality of the different facilities installed in the Western world. Since a survey report on such facilities [12] is already available, it could be useful to assess a "thorough option matrix" where the correct steelmaking requirements could be chosen by PV designers and manufacturers.

Deoxidation Techniques

Although widely experimented by several forgemasters and emphasized by the Japanese producers with several high-level papers, vacuum carbon deoxidation is still very rarely required or acknowledged for forged PV components. A comparative investigation of three heats of SA-508 Class 3 production forgings has proven that VCD offers toughness properties—even in the HAZ—that are at least comparable with those obtained with the fine-grain practice.

Possible combinations of VCD with aluminum treatment have been investigated, and 2 years ago two ingots were produced. The technique consisted of a first VSD (ladle-to-pony ladle) followed by a second VSD (pony ladle-to-mould) including a gradual aluminum addition. The results were good, but the technique turned out too complex with the present facilities layout.

Hollow Ingots

Six hollow ingots ranging from 57 to 181 tons were produced over the last 3 years. The last two ingots were vacuum stream degassed. VCD is possible with the same facility and equipment. Quality results were definitely comparable to those achieved with the conventional hot pierced ingots.

Fabrication Problems

A review of specified PWHTs has suggested that during PWHT some zones of a PV could undergo temperatures never reached either during the previous tempering treatments or during simulated PWHTs of acceptance test coupons. The present tendency toward high temperature PWHTs for the 2.25Cr-1Mo heavy-wall PV has been verified against several tempering parameter curves available in the literature, as well as against the authors' own curve relative to heavy-wall VCD shell forgings, at midthickness. The need to reconsider critically either the minimum specified UTS or the PWHT temperatures has been evident. A rather rough speculation on the possibility to lower slightly the minimum specified RT-UTS of 2.25Cr-1Mo steel, on the ground of design criteria, has failed. The conclusion is that high temperature PWHT should be avoided. Assuming that such high temperatures are deemed necessary for weld joint problems, the authors recommend to consider VCD weld metal.

References

- [1] Mahajan, S. W. et al., "Grain Refinement of Steel by Cyclic Rapid Heating," *Metallography*, No. 6, 1973.

- [2] Grange, R. A., "Strengthening Steel by Austenite Grain Refinement," *Transactions, American Society of Mechanical Engineers*, New York, Vol. 59, 1966.
- [3] Hrivnak, I., "General Theory of Heat Treatment in the A_1 - A_3 Range," Italian translation, *Rivista Italiana Della Saldatura*, No. 6, 1973.
- [4] Nisbett, E. G., et al., "Improving the Notch Toughness of Nuclear Forgings in Carbon and Low-Alloy Steels by Intercritical Heat Treatment," *Proceedings*, 8th International Forgemasters meeting, Kyoto, Japan, 1977.
- [5] Danner, G. E. et al., "Deoxidizing Steel by Vacuum," *Metal Progress*, May 1961.
- [6] Sawada, S. et al., "The Beneficial Effect of Vacuum Carbon Deoxidation on Rotor Forging Properties," *Proceedings*, EPRI Rotor Forgings Workshop, Electric Power Research Institute, Palo Alto, CA, 1980.
- [7] Onodera, S. et al., "Mono-block Vessel Flange Forging for PW RPV 1000 MWE," *Proceedings*, International Forgemasters meeting, Kyoto, Japan, 1977.
- [8] Kawaguchi, S. et al., "Production Capability of a Large Mono-Block Rotor Forging," *Proceedings*, EPRI Rotor Forgings Workshop, Electric Power Research Institute, Palo Alto, CA, 1980.
- [9] "ASEA-SKF Ladle Furnace for Steel Refining," Pamphlet AU20-106E, Ed. 1, ASEA-SKF, Västerås, Sweden.
- [10] Murakami, Y. et al., "Heavy Section Cr-Mo Steels for Hydrogenation Services," *Proceedings*, 17th CIM Conference, Canadian Institute of Mining and Metallurgy, Montreal, Canada, 1978.
- [11] Kohno, M. et al. in *Application of 2 1/4Cr-1Mo Steel for Thick-Wall Pressure Vessels*, ASTM STP 755, Philadelphia, 1980, pp. 208-227.
- [12] "Advanced Steelmaking Processes for Rotor Forgings," Final Report, *Engineering Materials & Processes, Inc.*, Dec. 1983.
- [13] McQuaid, H. W., "The Importance of Aluminum and Vanadium in High Quality Carbon and Alloy Steel," *Iron and Steel*, June 1965.
- [14] Erwin, W. E. and Kerr, J. G., "The Use of Quenched and Tempered 2.25Cr-1Mo Steel for Thick Wall Reactor Vessels in Petroleum Refinery Processes: An Interpretive Review of 25 Years of Research and Application," WRC Bulletin 275, Welding Research Council, N.Y., Feb. 1982.
- [15] Ueda, S. et al., "Improvement in Strength and Toughness of 2.25Cr-1Mo Heavy Section Steel Plate and Forging," KAWASAKI Steel Corp. Report, April 1982.
- [16] Swift, R. A. in *Application of 2 1/4Cr-1Mo Steel for Thick-Wall Pressure Vessels*, ASTM STP 755, American Society for Testing and Materials, Philadelphia, May 1980, pp. 166-188.
- [17] Berthet, J. A. et al. *Application of 2 1/4Cr-1Mo Steel for Thick-Wall Pressure Vessels*, ASTM STP 755, May 1980, pp. 148-165.
- [18] Murakami, Y. et al. *Application of 2 1/4Cr-1Mo Steel for Thick-Wall Pressure Vessels*, ASTM STP 755, May 1980, pp. 383-417.
- [19] Frassoni et al., "Condizioni e Modalità Esecutive dei Trattamenti Termici per Recipienti a Pressione," *Rivista Italiana Della Saldatura*, No. 2, March-April 1983.
- [20] Scepi, M. et al., "Thermal and Metallurgical Control of Forging Ingot Mould Efficiency" in *Proceedings*, International Forging Conference, Düsseldorf, Vol. 1, 1981.
- [21] Scepi, M. et al., "Modello Matematico di Solidificazione di Lingotti da Forgia," *Bollettino Technico Finsider*, No. 391, 1981.

Pressure Vessel and Nuclear Forgings

Steels for Pressure Retaining Components

Evaluation of Modified 9Cr-1Mo Steel Forging

REFERENCE: Khare, A. K. and Sikka, V. K., "Evaluation of Modified 9Cr-1Mo Steel Forging," *Steel Forgings, ASTM STP 903*, E. G. Nisbett and A. S. Melilli, Eds., American Society for Testing and Materials, Philadelphia, 1986, pp. 303–327.

ABSTRACT: A new 9Cr-1Mo steel with significant improvement in elevated-temperature mechanical properties and toughness over 2 1/4Cr-1Mo and standard grade 9Cr-1Mo steel has been developed jointly by Oak Ridge National Laboratory and Combustion Engineering³. The new alloy obtains its elevated-temperature strength from small additions of niobium, vanadium, and nitrogen. The alloy has been melted commercially in the United States and Japan. It also has been fabricated into tubes, pipes, plates, bars, and forgings.

National Forge saddle-forged a heavy-walled cylinder from a billet produced from an electroslog remelted ingot of this modified alloy. The 781-mm-outside diameter by 67-mm-thick wall by 762-mm-long cylinder was normalized at 1050°C and tempered at 760°C.

The production of the saddle forging and its mechanical properties and microstructure are described. A comparison between the mechanical properties of this forging with the results on plates, bars, and tubes fabricated from the same alloy is presented. Data show the forging to be highly isotropic in its properties and a strong promise for the use of modified 9Cr-1Mo alloy in hydrocrackers for operation at 500°C and higher temperatures.

KEY WORDS: 9Cr-1Mo; heavy-walled forging; elevated temperature properties; creep strength; argon-oxygen deoxidation (AOD); electroslog remelted (ESR); impact transition temperature; fatigue crack propagation (da/dN); J_{IC}

Modified 9Cr-1Mo steel, currently approved in ASTM Specification for Pressure Vessel Plates, Alloy Steel, Chromium-Molybdenum (A 387/A 387M-83) for plate and ASTM Specification for Seamless Ferritic and Austenitic Alloy-Steel Boiler, Superheater, and Heat-Exchanger Tubes (A 213-83) for tube and also approved for ASTM Specification for Forged or Rolled Alloy-Steel Pipe Flanges, Forged or Rolled Alloy-Steel Pipe Flanges, Forged Fittings, and Valves and Parts for High-Temperature Service (A 182-82a) for forgings and ASTM Specification for Seamless Ferritic and Austenitic Alloy-Steel Boiler, Superheater, and Heat-Exchanger Tubes (A 335-81a) for extruded pipe as Grade 91

¹ Senior Developmental metallurgist, Research and Development Dept., National Forge Co., Irvine, PA 16329.

² Metallurgist, Research Staff, Metals and Ceramics, Oak Ridge National Laboratory, Oak Ridge, TN 37830.

³ Combustion Engineering, Chattanooga, TN.

TABLE 1—*Chemical analysis of saddle forging of modified 9Cr-1Mo steel (Heat 14361).*

Elements	Specifications	Weight %	
		Ladle Analysis ^a	Forging ^b
Carbon	0.08 to 0.12	0.12	0.11
Manganese	0.30 to 0.60	0.48	0.58
Phosphorus	0.020 max	0.014	0.010
Sulfur	0.010 max	0.009	0.001
Silicon	0.20 to 0.50	0.33	0.30
Nickel	0.40 max	0.12	0.12
Chromium	8.00 to 9.50	8.62	8.83
Molybdenum	0.85 to 1.05	0.96	0.97
Vanadium	0.18 to 0.25	0.22	0.21
Niobium	0.06 to 0.10	0.09	0.064
Titanium	0.002
Cobalt	...	0.02	0.017
Copper	0.10
Aluminum	0.04 max	0.02	0.016
Boron	<0.001
Tungsten	0.02
Arsenic	0.006
Tin	...	0.004	0.004
Zirconium	<0.001
Nitrogen	0.03 to 0.07	0.038	0.041
Oxygen	0.003

^a AOD material.^b ESR material.

(Table 1), offers significantly improved elevated-temperature strength properties over those of 2 1/4Cr-1Mo (Grade 22) and the standard 9Cr-1Mo (Grade 9) [1,2]. The alloy also has higher creep strength than Type 304 stainless steel for temperatures up to 600°C [1,2]. Code Case 1943 also has been issued for the use of this alloy for the American Society of Mechanical Engineers (ASME) Code Section I construction. The use of this alloy for pressure vessel construction according to ASME Code Section VIII was approved as Code Case 1973.

Operating experience on this alloy is being obtained by the installation of tubes in various boilers. The current status of testing of modified 9Cr-1Mo steel tubes in the United States and foreign steam plants is presented in Table 2. Use of this alloy for pressure vessels required the experience in the fabrication of large, thick forgings and their properties. The purpose of this paper is to describe the fabrication of a saddle forging of Grade 91 at National Forge Co., its mechanical properties (hardness, Charpy impact, tensile, creep, and fracture toughness), and microstructure. Data on saddle forging will be compared with data obtained previously on tube, plate, bar, and forgings of commercial heats of this alloy. Except for creep and limited microstructural observations, all testing was conducted by National Forge.

TABLE 2—Current status of testing of modified 9Cr-1Mo steel tubes in U.S. and foreign steam power plants.

Utility	Plant	Tube Location	Operating Temperature, °C	Tubes Being Replaced	Number of Tubes	Date Installed	Status
Tennessee Valley Authority	Kingston Steam Plant, Unit 5	superheater	593	Type 321	8	May 1980	operating
American Electric Power	Tanners Creek Unit 3	secondary superheater	593	Type 304	10	Apr. 1981	operating
Detroit Edison	St. Clair Unit 2	reheater	538	Type 347	2	Feb. 1981	operating
Central Electric Generating Board (United Kingdom)	Agcroft Power Station	superheater	590–620	2 1/4Cr-1Mo	6	Apr. 1982	operating
Ontario Hydro (Canada)	Lambton Thermal Generating Station	reheater	538	Type 304H	9	May 1983	operating
Ontario Hydro (Canada)	Nanticoke TGS	secondary superheater	538	Standard 9Cr-1Mo 2 1/4Cr-1Mo	9 11	Oct. 1984	operating planned

Material Background

The primary heat of this material was made at Electralloy Corp.⁴ by the argon-oxygen-deoxidation (AOD) process and bottom-poured into a 533-mm round electrode. The ladle analysis of the AOD material is compared with the specifications in Table 1. The AOD electrode was subsequently electroslag remelted (ESR) into a 762-mm-diameter ingot at National Forge Co. This ESR ingot was used in the saddle forging and will be discussed in more detail later. The chemical analysis of the forging made from the ESR material also is included for comparison in Table 1. The ESR process produced significant reductions in sulfur content with some reductions in phosphorus, silicon, and niobium content. The product check chemistry of the forging meets the requirements for all elements in the specification.

Fabrication

A section of the 762-mm-diameter ESR ingot was straight-forged on an open die press to 559 mm in diameter and 1372 mm in length. This piece then was

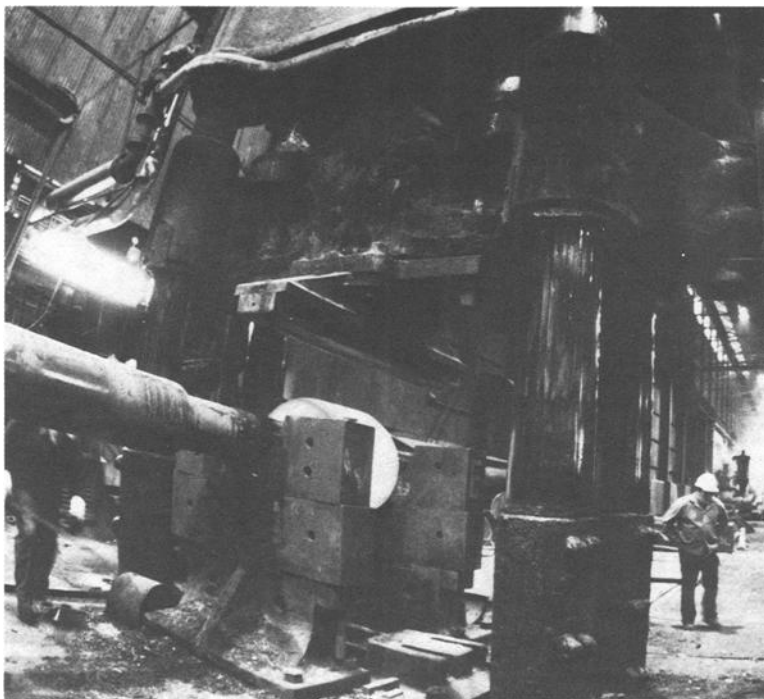


FIG. 1—Saddle forging setup.

⁴ Electralloy Corp., Oil City, PA.

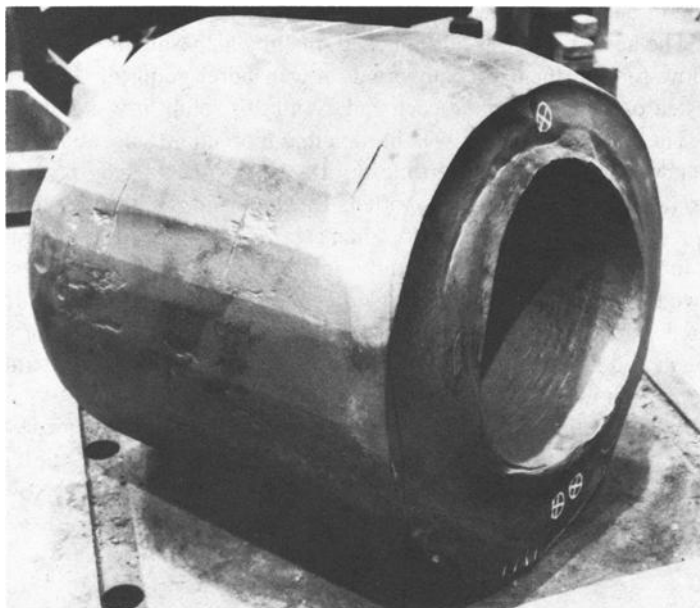


FIG. 2—Saddle forging after completing the final heat treatment. Circle on the end shows location of core holes for tension and Charpy-impact tests performed at room temperature.

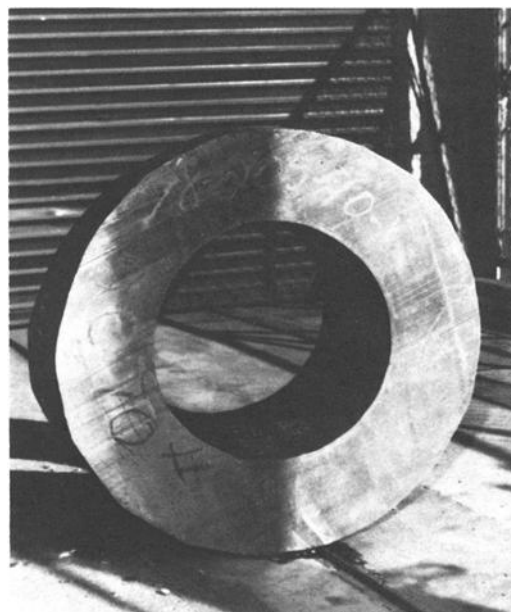


FIG. 3—Saddle forging section received by ORNL.

stood on end and upset between the two flat dies to an approximate length of 914 mm. The upset piece was hot-punched, making a 254-mm hole in the center. This hollow forging then was supported on a mandrel going through the hole, which rested on end supports at each end. With this setup, it was saddle forged (Fig. 1). The metal movement was in the circumferential (tangential) direction. The metal was squeezed between the top flat die of the forging press and the mandrel on which the piece was supported. The dimensions of the finished forging were approximately 781-mm outside diameter by 448-mm inside diameter by 762-mm long. The forging temperature range was 1230 to 815°C. The forging was allowed to air cool to about 320°C after the forging operation and then was heat treated. The heat treatment consisted of normalizing at 1050°C for 6 h and tempering at 760°C for 6 h. Air cooling to room temperature was used after each step. Figure 2 shows the final saddle forging after heat treatment.

This saddle forging was sectioned to provide a 305-mm-long piece to Oak Ridge National Laboratory (ORNL) (Fig. 3), a 150-mm-long piece for testing at National Forge, and half of the 150-mm-long piece for testing at Novatome, France.

Mechanical Properties

Various properties of the saddle forging are described under various categories.

Hardness Data

Brinell hardness traverses across the wall thickness of the saddle forging are shown in Fig. 4. The indentations were made at 19 mm from the outer and inner diameter of the forging and through the wall; indentations were spaced at 25-mm intervals. The hardness is uniform across the wall and at various locations of the forging. The hardness value of 217 Brinell Hardness Number (BHN) confirms the proper tempering of the forging. A typical value obtained for tube, plate, and bar products is 220 BHN.

Charpy-Impact Data

Charpy-impact tests were conducted on longitudinal and tangential specimens from the quarter thickness of the forging (Table 3) and on longitudinal, tangential, and radial specimens from the half thickness of the forging (Table 4). Charpy-impact energy values versus test temperature plots for specimens of various orientations from 1/4 and 1/2-thickness sections of the saddle forging are shown in Figs. 5 and 6. Curves for the longitudinal and transverse specimens from the 1/4 and 1/2-thickness sections of a forged plate from another electroslag remelted heat of this alloy are included in these figures for comparisons. Similar plots of fracture appearance versus test temperature are shown in Figs. 7 and 8. These figures show the following:

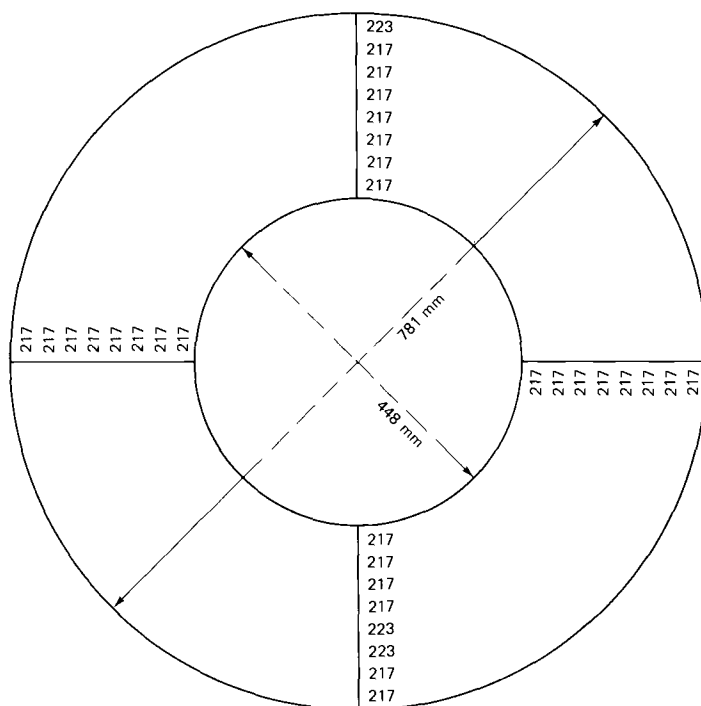


FIG. 4—Brinell hardness traverses across the wall thickness of the saddle forging.

TABLE 3—Impact properties of LC and CR specimens from the 1/4-thickness section of modified 9Cr-1Mo steel saddle forging (781-mm OD by 167-mm wall by 763-mm long). (All tests were conducted at National Forge Co.).

Temperature, °C	Impact Energy, J	Fracture Shear, %	Lateral Expansion, mm
LONGITUDINAL			
204	267	100	2.29
135	246	100	2.29
79	242	100	2.34
24	212	77	2.49
−18	109	43	1.35
−59	39	20	0.41
−101	14	11	0.20
−129	5	0	0.25
TANGENTIAL			
204	302	100	1.78
135	253	100	2.34
79	241	100	2.21
24	218	94	2.34
−18	98	42	1.24
−59	39	16	0.48
−101	14	9	0.18
−129	7	0	0.10

TABLE 4—Impact properties of LC, CR, and RC specimens from the midwall section of modified 9Cr-1Mo steel saddle forging (781-mm OD by 167-mm wall by 762-mm long). (All tests were conducted at National Forge Co.).

Temperature, °C	Impact Energy, J	Fracture Shear, %	Lateral Expansion, mm
LONGITUDINAL			
204	249	100	2.06
135	231	100	2.39
79	226	100	2.18
24	203	77	2.29
–18	121	51	1.60
–59	29	14	0.25
–101	11	9	0.18
–129	3	0	0.15
TANGENTIAL			
204	261	100	2.08
135	239	100	2.36
79	239	100	2.26
24	178	79	2.21
–18	98	23	1.27
–59	37	18	0.61
–101	5	6	0.08
–129	4	0	0.05
RADIAL			
204	250	100	2.26
135	233	100	2.21
79	229	100	2.31
24	184	81	2.11
–18	105	56	1.27
–59	84	29	1.04
–101	10	9	0.15
–129	3	0	0.03

1. The impact energy values and the fracture appearance for specimens of longitudinal and tangential orientations from the quarter thickness are virtually identical. They are virtually identical for specimens of longitudinal, tangential, and radial orientations from the half thickness. These results imply that the saddle forging is highly isotropic. Furthermore, there appeared to be no difference in the properties of the 1/4 and 1/2-thickness sections, implying that the properties are uniform across the wall thickness of the forging.

2. The forged plate from another heat of this alloy showed a much larger variation in Charpy-impact energy values between the longitudinal and transverse specimens. The fracture appearance values also showed more scatter for the forged plate than saddle forging.

3. The Charpy-impact energy values of the saddle forging were near the average values expected for the longitudinal and transverse specimens of the forged plate. The fracture appearance results for the saddle forging were very similar to the curve observed for the transverse specimen of the forged plate.

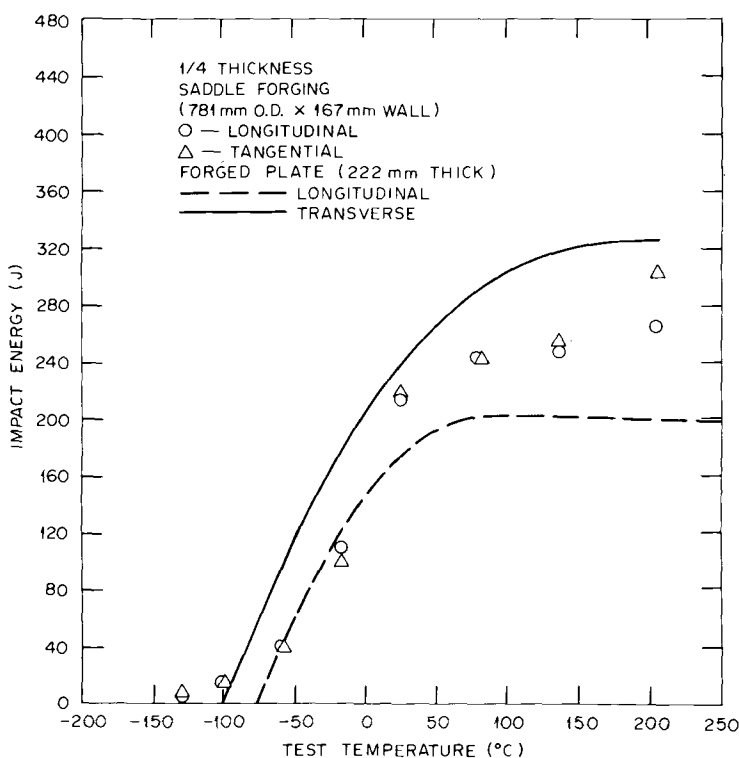


FIG. 5—Charpy-impact energy versus the test temperature of LC and CR specimens from the 1/4-thickness section of the saddle forging. Curves for the LC and RC specimens from the 1/4-thickness section of a forged plate from another heat are included for comparison.

4. The 50% shear-impact transition temperature for 1/4-thickness specimens ranged from -9 to -12°C and for 1/2-thickness specimens ranged from 0 to -24°C . The 68-J (50 ft · lb) transition temperature values for the 1/4 and 1/2-thickness sections were -36 and -37°C , respectively.

Tensile Data

Tension tests were conducted at room temperature to determine the property variation across the forging wall. Specimens of longitudinal and tangential orientations were tested from the outside and inside regions of the wall and of longitudinal, tangential, and radial orientation from the midwall section (Table 5). Tensile data at room temperature are plotted in Fig. 9. This figure shows that the strength and ductility properties are nearly the same for various orientations and locations in the wall. These results are similar to those observed for hardness data in Fig. 4, and they indicate that the forging wall is very isotropic in tensile properties.

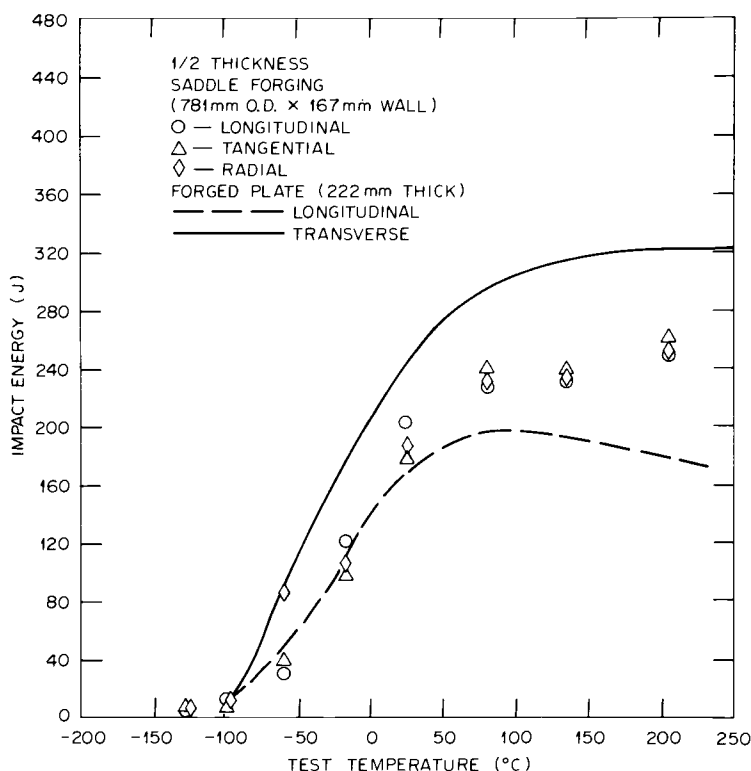


FIG. 6—Charpy-impact energy versus test temperature of LC, CR, and RC specimens from the 1/2-thickness section of the saddle forging. Curves for the longitudinal and transverse specimens from the 1/2-thickness section of a forged plate from another heat are included for comparison.

A complete set of tension tests from room temperature to 649°C were conducted on longitudinal, tangential, and radial specimens from the middle wall section of the forging (Table 6). Tensile properties are plotted as a function of test temperature in Figs. 10 through 13. The average and average ± 1.65 standard error of estimates (SEE) curves for various product forms of several commercial heats are included in these figures for comparison. These figures show the following:

1. Both the strength and ductility properties for all three specimen orientations are nearly the same at all test temperatures. This suggests that the forging properties are isotropic at both room temperature and elevated temperatures.
2. Both the yield and ultimate tensile strength of the saddle forging are within the average and average ± 1.65 SEE curves for various product forms (tube, plate, and bar) of several commercial heats of this alloy. This implies that the fabrication technique used in this study can result in forging properties of levels

similar to those observed in products made by hot-forging/hot-rolling and hot-forging/hot-extrusion processes.

3. Total-elongation and reduction-of-area values also are well-defined by the average and average ± 1.65 SEE curves for various product forms. Slightly lower total-elongation values of the forging may be a result of use of 51-mm gage length specimens versus 25-mm gage length specimens used for most of the other product forms. The small gage length will result in higher elongation values due to obvious geometrical reasons.

Creep Data

Creep testing of the saddle forging is in progress at 538, 593, and 649°C. All specimens in the test are of tangential orientation from the midwall section. Two tests have ruptured thus far and five are currently in progress. The average creep-

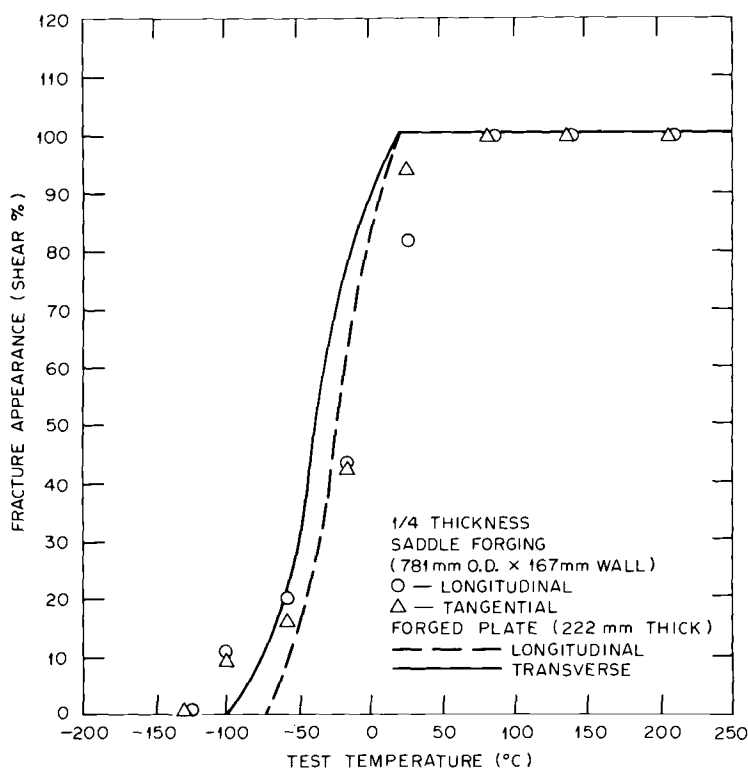


FIG. 7—Fracture appearance versus test temperature of LC and CR specimens from the 1/4-thickness section of the saddle forging. Curves for the LC and RC specimens from the 1/4-thickness section of a forged plate from another heat are included for comparison.

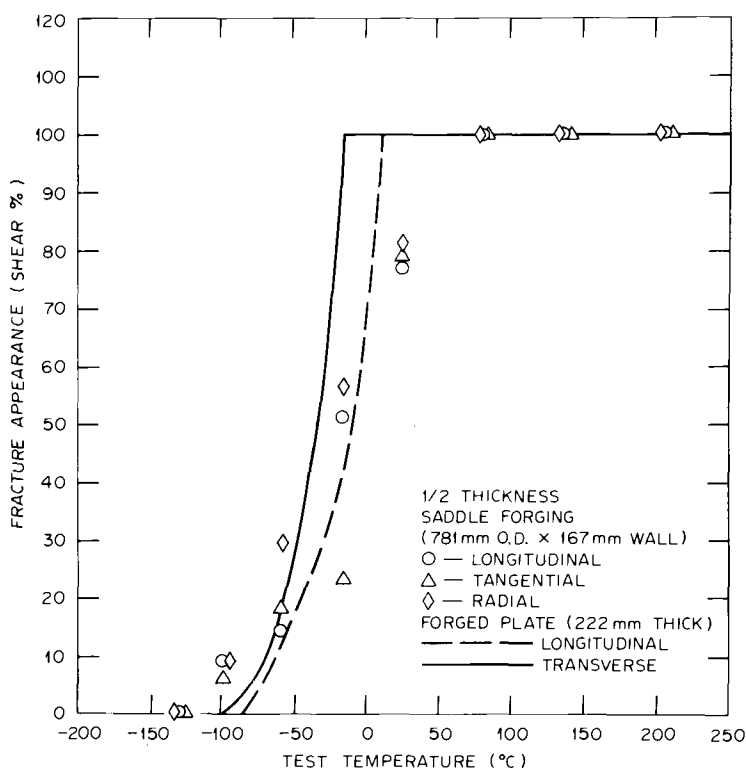


FIG. 8—Fracture appearance versus test temperature of LC, CR, and RC specimens from the 1/2-thickness section of the saddle forging. Curves for the LC and CR specimens from the 1/2-thickness section of a forged plate from another heat are included for comparison.

rupture behavior of various product forms of several commercial heats of modified 9Cr-1Mo steel has been described [3] by the following model

$$\log t_r = -24.244 - 0.02374\sigma - 2.4871 \log \sigma + 31\,876/T \quad (1)$$

where

- t_r = time to rupture, h,
- σ = applied stress, MPa, and
- T = test temperature, K.

Creep-rupture data on the saddle forging are compared with the average behavior of various products for several commercial heats in Fig. 14. This figure shows that the creep properties of the saddle forging are exceeding or expected to exceed (based on tests in progress) the average curve for various product forms. This implies that the fabrication technique used in this study results in forging of the same rupture properties as observed for products made by other fabrication tech-

TABLE 5—Room-temperature tensile properties of modified 9Cr-1Mo steel saddle forging (781-mm OD by 167-mm wall by 762-mm long).

Specimen Orientation	Strength, MPa		Elongation, %	Reduction of Area, %
	0.2% Yield	Ultimate Tensile		
OUTSIDE				
LC	548	690	23.5	68.8
LC	552	690	24.0	65.6
CR	545	686	22.5	62.9
CR	539	683	22.5	71.7
MIDWALL				
LC	545	686	22.0	64.9
LC	545	683	22.0	64.0
CR	539	683	22.0	64.8
CR	541	683	22.0	65.2
RC	544	683	22.5	64.2
RC	544	690	23.0	66.8
INSIDE				
LC	541	683	24.0	67.7
LC	542	683	23.0	68.5
CR	569	703	22.0	64.1
CR	562	693	23.0	67.0

niques. The maximum allowable design stress curve from ASME Code Case 1943 for Grade 91 is included in Fig. 14 to show its relative position with respect to the average curve. The fact that creep-rupture values on the saddle forging exceed the average curve for the plate, bar, and tubing that went into the computation of maximum allowable design stresses suggests that the design stresses for the plate, bar, and tubing also could be used for forgings.

Fatigue Crack Propagation Data

Fatigue crack growth tests were conducted at room temperature on longitudinal (LC), tangential (CR), and radial (RC) specimens (Fig. 15). This figure shows that the crack growth rate for all three orientations is identical.

The crack growth equation (Eq 2) constants at room temperature for the saddle forging are

$$da/dN = C(\Delta K)^n \quad (2)$$

Specimen Orientation	C	n
Longitudinal	2.04 E10	3.04
Tangential	1.90 E10	3.06
Radial	1.80 E10	3.08

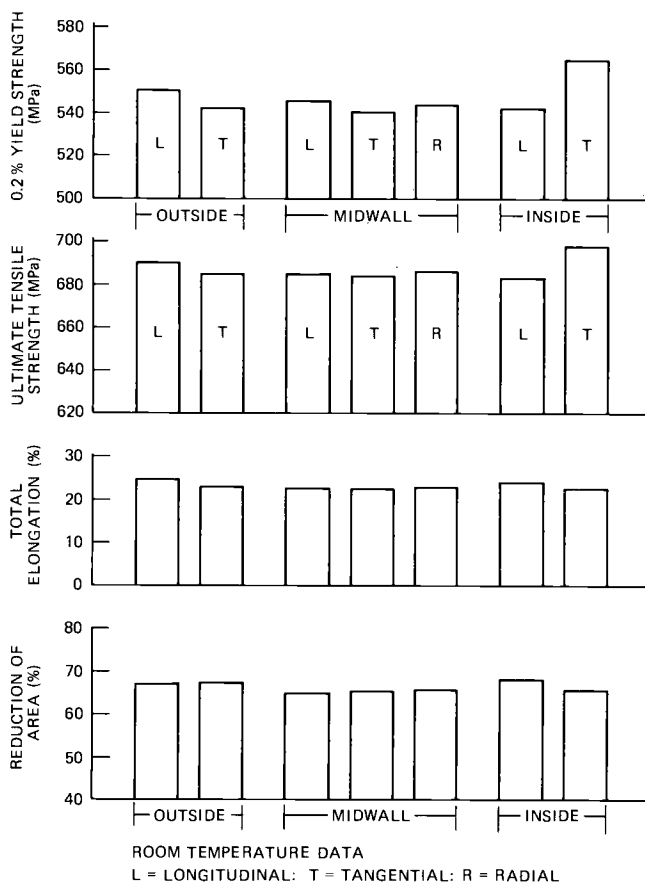


FIG. 9—Room-temperature tensile data across the wall thickness of the saddle forging. Note that the properties are nearly the same for all orientations and locations in the wall.

where $da/dN = \text{in./cycle}$, $\Delta K = \text{ksi} \sqrt{\text{in.}}$, and conversion to the international system (SI) units are $(\text{in./cycle}) (25.4) = \text{mm/cycle}$; $\text{ksi} \sqrt{\text{in.}} = 1.099 \text{ MPa} \sqrt{\text{m}}$. Note that the constants C and n are nearly the same for specimens from all three orientations. Figure 16 shows that the fatigue crack growth rate of the saddle forging at room temperature is near the average behavior observed for the hot-forged/hot-rolled plates of the commercial heats.

J-Integral Fracture Toughness Data

Single specimen J -integral testing procedures in accordance with ASTM Test Method for J_{Ic} , a Measure of Fracture Toughness (E 813-81) were used to evaluate the fracture toughness of three orientations of the saddle forging at room temperature. Toughness expressed in terms of J ($\text{in.} \cdot \text{lb/in.}^2$) and K ($\text{ksi} \sqrt{\text{in.}}$) was

TABLE 6—Tensile properties of LC, CR, and RC specimens from the midwall section of modified 9Cr-1Mo steel saddle forging (781-mm OD by 167-mm wall by 762-mm long).
(All tests were conducted at National Forge Co.).

Temperature, °C	Strength, MPa		Total Elongation, %	Reduction of Area, %
	0.2% Yield	Ultimate		
LONGITUDINAL				
RT	545	686	22.0	64.9
RT	545	683	22.0	64.0
93	514	638	22.0	68.7
149	497	617	22.0	65.5
204	480	596	19.5	64.1
260	470	576	20.0	66.9
316	470	572	19.5	68.5
371	459	559	20.0	67.5
427	441	524	18.0	64.0
482	431	483	19.5	74.9
538	386	421	22.0	87.1
593	338	345	24.0	92.8
649	272	279	29.0	95.0
TANGENTIAL				
RT	539	683	22.0	64.8
RT	541	683	22.0	65.2
93	514	638	21.5	65.8
149	496	614	21.0	67.0
204	483	596	21.0	68.7
260	469	579	20.5	68.8
316	463	569	20.0	65.7
371	455	552	19.5	60.8
427	441	528	19.0	64.0
482	417	476	21.0	76.1
538	386	417	23.5	86.8
593	330	343	25.0	90.1
649	262	272	32.5	95.2
RADIAL				
RT	544	683	22.5	64.2
RT	544	690	23.0	66.8
93	514	638	21.5	64.1
149	497	614	21.0	66.2
204	474	587	21.0	67.0
260	469	583	21.0	67.9
316	462	565	20.0	66.9
371	452	559	19.0	63.2
427	431	514	19.0	70.1
482	417	472	20.5	73.9
538	386	410	22.5	87.0
593	334	345	25.0	92.3
649	265	279	27.0	94.2

NOTE: RT = room temperature.

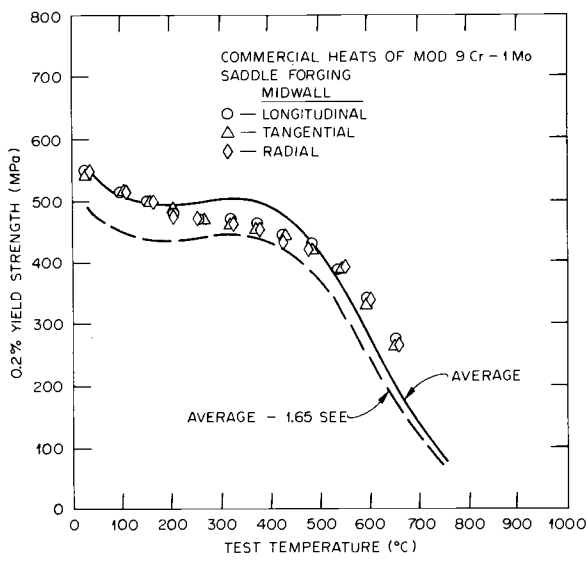


FIG. 10—Yield strength versus test temperature for the LC, CR, and RC specimens from the midwall section of the saddle forging. The average and average - 1.65 SEE curves for various products forms of several commercial heats are included for comparison.

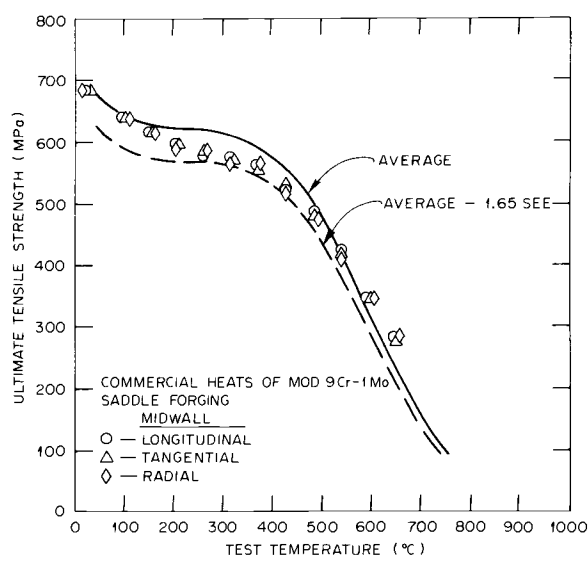


FIG. 11—Ultimate tensile strength versus test temperature for the LC, CR, and RC specimens from the midwall section of the saddle forging. The average and average - 1.65 SEE curves for various products forms of several commercial heats are included for comparison.

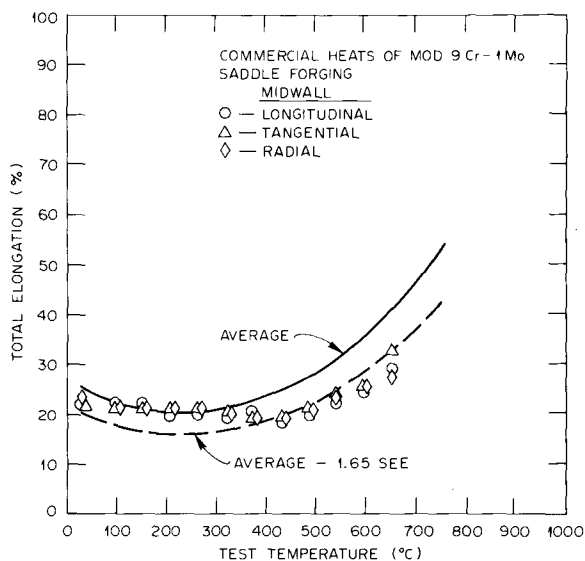


FIG. 12—Total elongation versus test temperature for the LC, CR, and RC specimens from the midwall section of the saddle forging. The average and average ± 1.65 SEE curves for various products forms of several commercial heats are included for comparison.

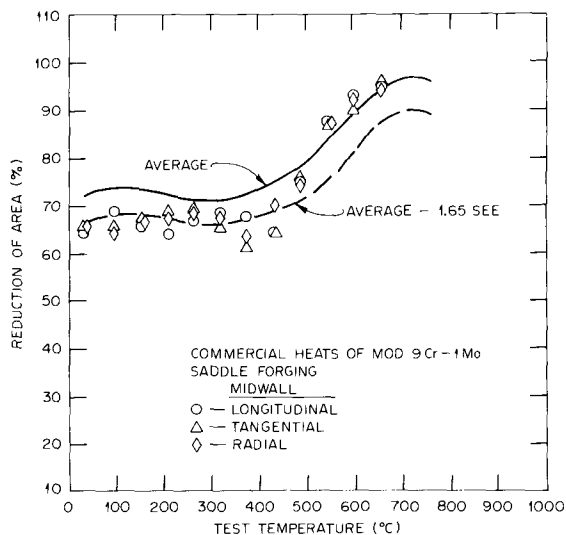


FIG. 13—Reduction of area versus test temperature for the LC, CR, and RC specimens from the midwall section of the saddle forging. The average and average ± 1.65 SEE curves for various product forms of several commercial heats are included for comparison.

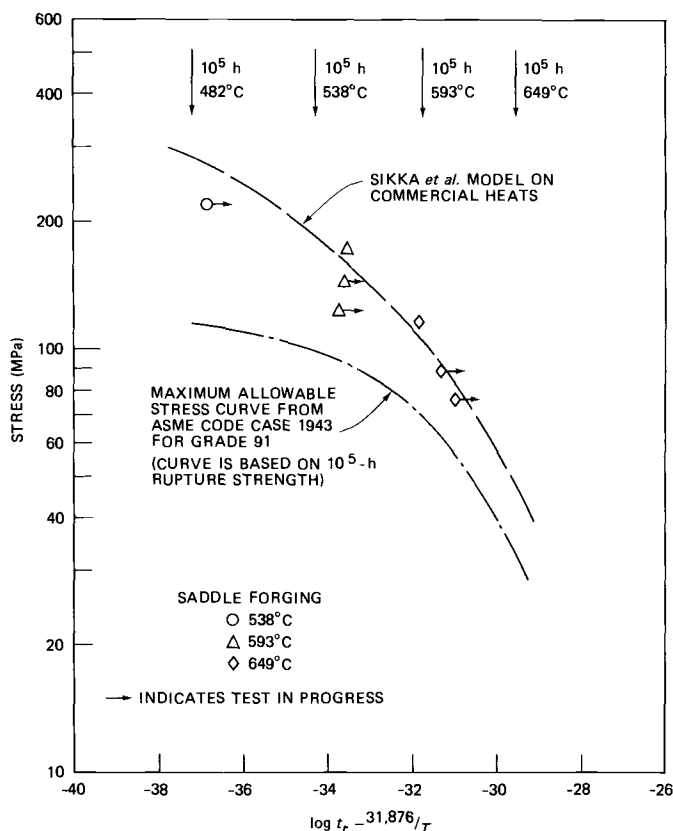


FIG. 14—Comparison of creep rupture data on saddle forging with the average curve developed from the model for various product forms of several commercial heats. Maximum allowable design stress curve from ASME Code Case 1943 for Grade 91 is also included for comparison.

determined for the compact tension specimens. Specimens from three orientations, LC, CR, and RC, exhibited entirely stable crack extension during testing. Sufficient data were generated in each case to construct an R -curve (Fig. 17) and determine J_{Ic} -values according to the requirements of ASTM (E 813-81). Examination of Fig. 17 reveals that the R -curves for RC and LC orientations are virtually identical. The J_{Ic} -values for these two tests are the same. The CR orientation possessed a slightly higher R -curve, and, correspondingly, a higher value of J_{Ic} . The plane strain fracture toughness K_{Ic} and J_{Ic} used in its determination is

$$K_{Ic} = \text{sq rt}(J_{Ic} * E) \quad (3)$$

where

E = modulus of elasticity.

Specimen Orientation	J_{Ic}		Calculated K_{Ic}	
	in. · lb/in. ²	kJ/m ²	Ksi $\sqrt{\text{in.}}$	MPa $\sqrt{\text{m}}$
Longitudinal	1701	299	226	248
Tangential	1999	351	245	269
Radial	1701	299	226	248

No J -integral toughness data are available at present to compare with the data on the saddle forging.

Macrostructure and Microstructure

Figure 18 shows a typical macroetched section of the saddle forging. Some indication exists of large-grain irregular structure near the inner diameter of the forging. This irregular structure is in the area of the wall thickness which will be machined out during finish machining, which is standard practice for forgings.

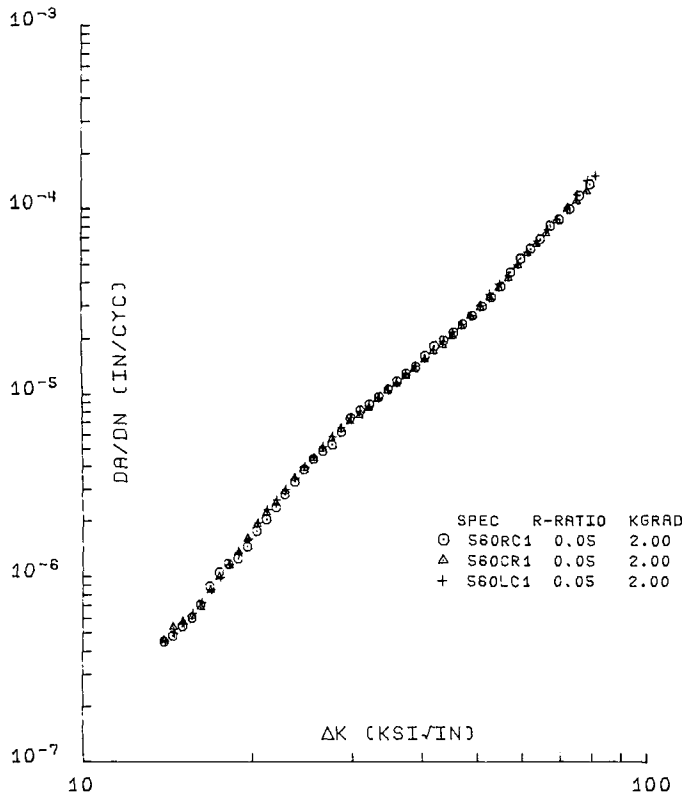


FIG. 15—Fatigue crack growth versus stress intensity values at room temperature for LC, CR, and RC specimens from the saddle forging. See text for conversion of units.

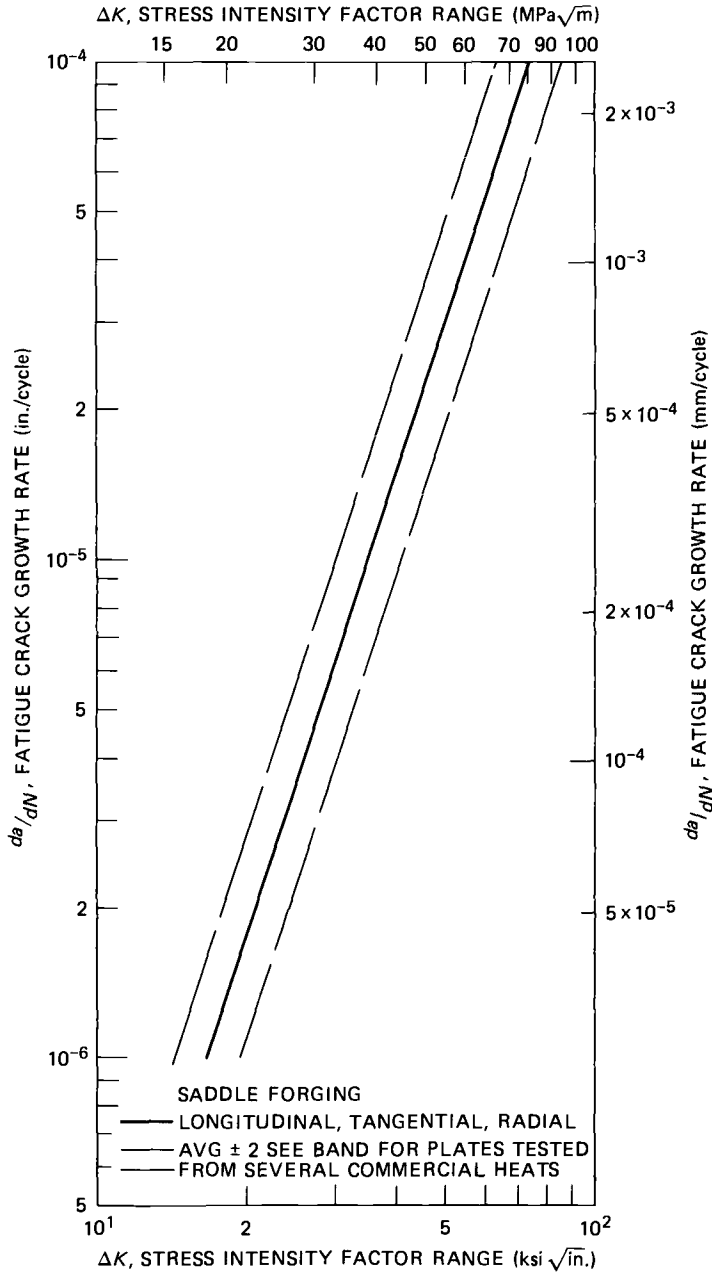


FIG. 16—Comparison of fatigue crack growth rate of the saddle forging at room temperature with the average ± 2 SEE band for plates tested from several commercial heats.

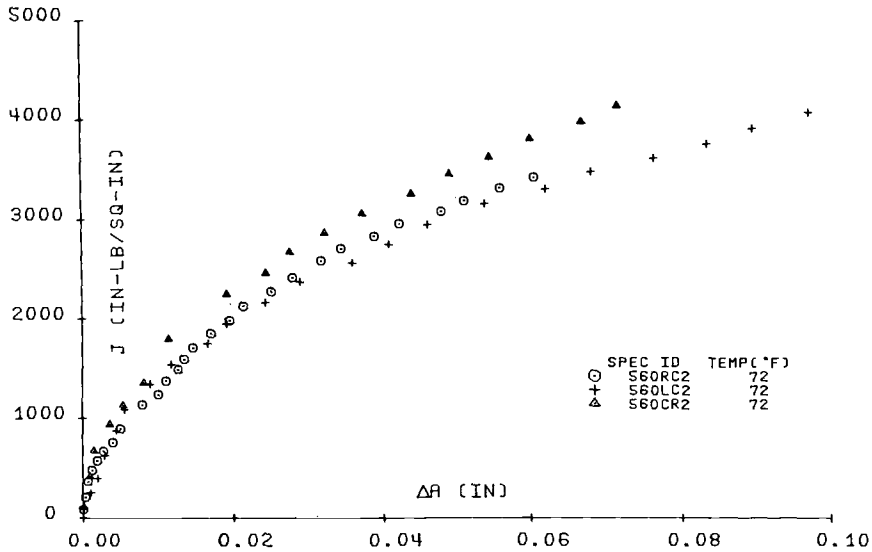


FIG. 17—Single specimen J-integral R-curves for LC, CR, and RC specimens from the saddle forging at room temperature.

However, the hardness, Charpy-impact, and the tensile data reported in the previous section was found to be unaffected by such a macrostructure. Low- and high-magnification (100 and 1500 times) photomicrographs of the outer edge, midwall, and inner edge of the forging are presented in Figs. 19 and 20, respectively. Both figures show the existence of fine-grain microstructure at the

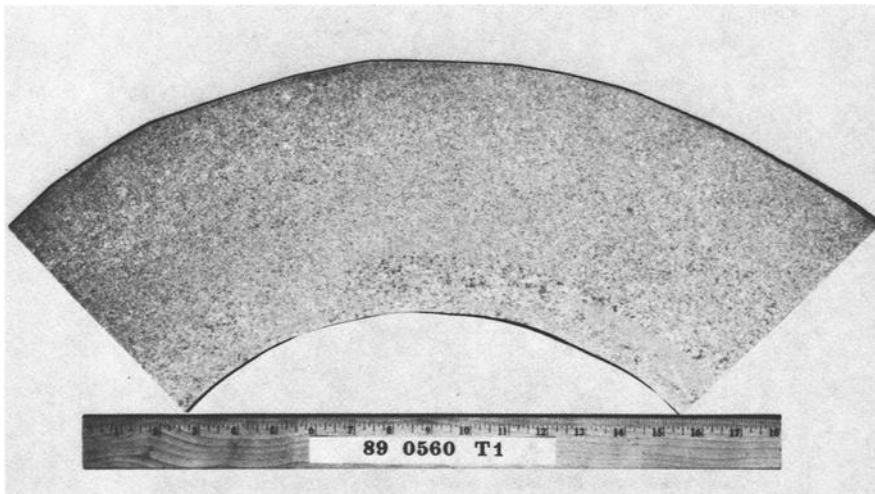


FIG. 18—Photograph showing macroetched section of the saddle forging.

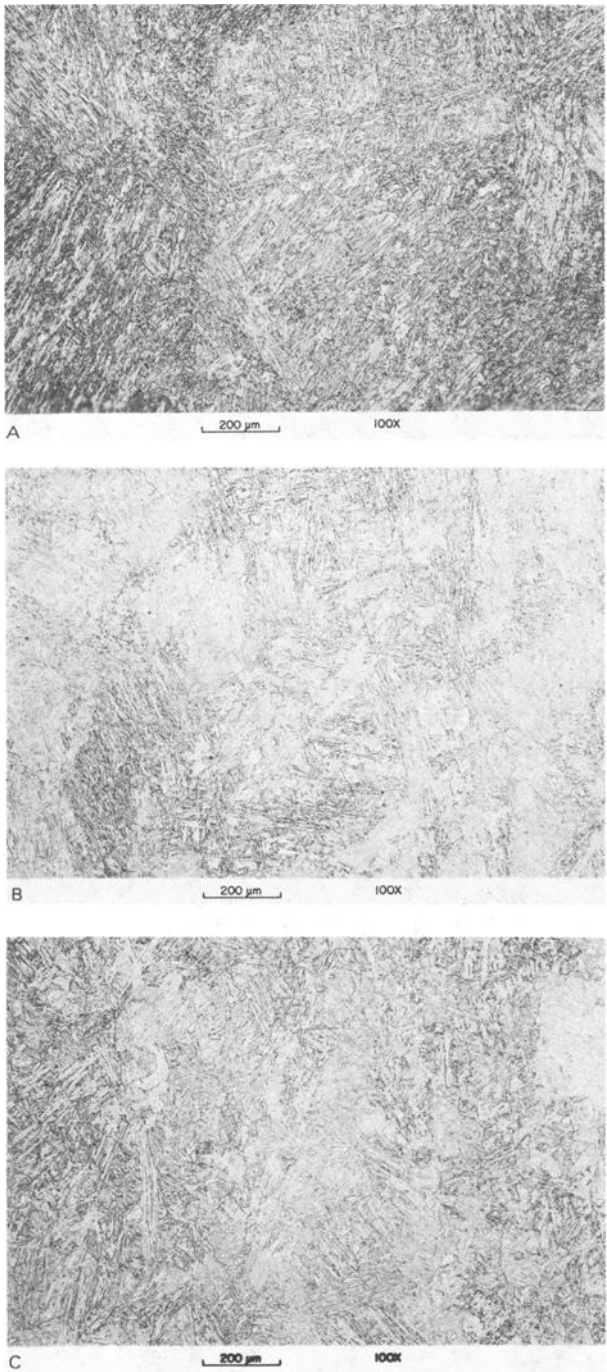


FIG. 19—Low magnification photomicrographs of the (a) outer-edge, (b) midwall, and (c) inner-edge sections of the saddle forging.

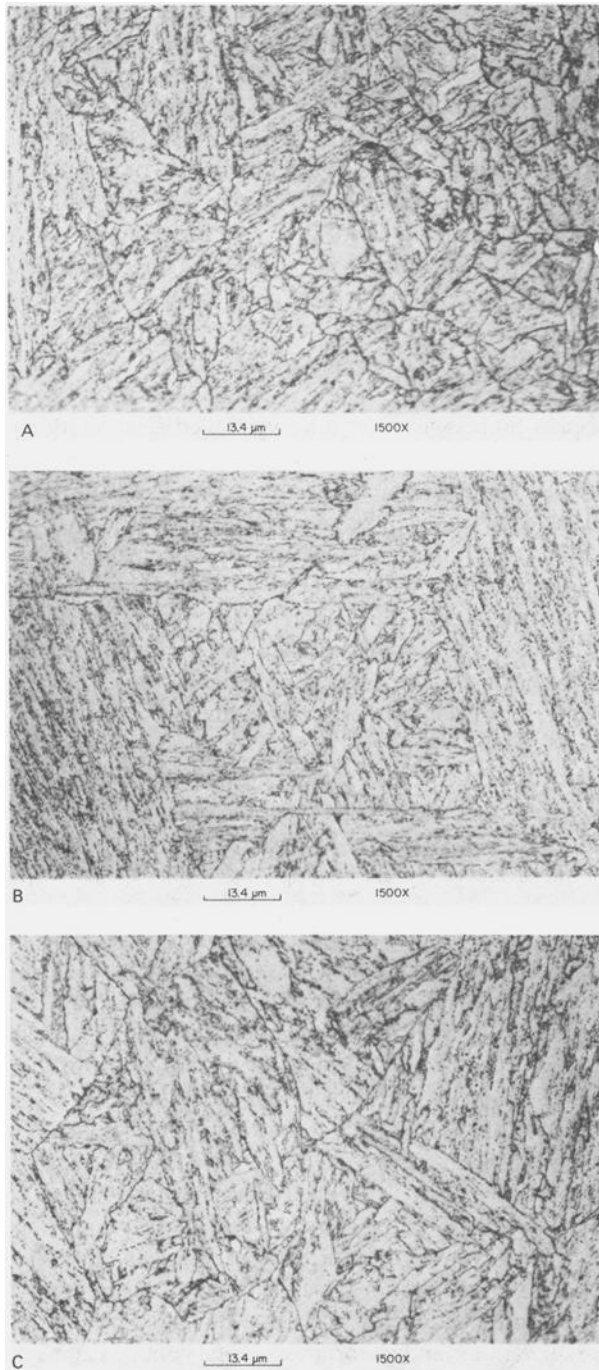


FIG. 20—High magnification photomicrographs of the (a) outer-edge, (b) midwall, and (c) inner-edge sections of the saddle forging.

outer edge, intermediate-grain in the midwall, and coarse-grain at the inner edge. This variation in microstructure is believed to have arisen from the variation in the forging temperature from the outer to the inner edge. However, regardless of the variation in grain size, all of the mechanical properties measured here showed the forging to be quite isotropic. We believe that the mechanical properties in this alloy are derived from the size and distribution of carbides, which is quite uniform across the forging thickness. The size and distribution of carbides is determined by the normalized and tempering treatment, whereas grain size depends on the forging temperature and time and temperature of normalization treatment.

Summary and Conclusions

The fabrication process used for a heavy-walled saddle forging from a billet of modified 9Cr-1Mo (ASTM Grade 91) steel is presented. The forging was fabricated at National Forge Co. and sectioned into pieces for testing at National Forge, ORNL, and Novatome in France. Test results on the forging from National Forge and ORNL were presented. The forging was evaluated for its hardness, Charpy-impact, tensile, creep, fatigue crack growth, and *J*-integral fracture toughness. A limited microstructural evaluation across the forging thickness also was conducted. The mechanical properties data on the forging were compared with the result on various product forms of several commercial heats.

The following conclusions are drawn from this work:

1. The fabrication procedures for the saddle forging from a billet of modified 9Cr-1Mo steel were normal for Cr-Mo steels.
2. Hardness data across the forging wall were nearly the same, indicating uniform material produced by the forging process and the subsequent heat treatment.
3. The Charpy-impact energy values and fracture appearance for the specimens of longitudinal and transverse orientations from the quarter thickness section were nearly identical. They were nearly identical for specimens of LC, CR, and RC orientations from the 1/2-thickness section of the forging. Furthermore, there appeared to be no appreciable difference in the properties of the 1/4 and 1/2-thickness sections, implying the saddle forging to be highly isotropic and uniform in Charpy-impact properties. The 68-J transition temperature values for the 1/4 and 1/2-thickness sections were -36 and -37°C , respectively.
4. Tensile properties of LC, CR, and RC specimens from the midwall section were nearly identical at both room-temperature and elevated temperatures up to 649°C . Tensile properties of this forging fall within the average and average -1.65 SEE curves for several commercial heats of this alloy.
5. Time-to-rupture data at 538, 593, and 649°C of the forging exceeds the average curve for various product forms of several commercial heats of this alloy.
6. The fatigue crack growth heats of the LC, CR, and RC specimens of the forging were the same at room temperature. The crack growth curve for all three

orientations matched the average value curve observed for hot-forged/hot-rolled plates of several commercial heats.

7. The variation in grain size from the outer to inner edge of the forging wall did not effect the mechanical properties, which were observed to be very uniform. Properties are believed to be controlled by the size and distribution of carbides, which were nearly the same across the forging wall.

References

- [1] Booker, M. K., Sikka, V. K., and Booker, B. L. P., "Comparison of the Mechanical Strength Properties of Several High-Chromium Ferritic Steels" in *Ferrite Steels for High-Temperature Applications*, Warren, PA, 6-8 Oct. 1981, A. K. Khare, Ed., American Society for Metals, Metals Park, Ohio, 1983, pp. 257-73.
- [2] Sikka, V. K., "Development of Modified 9Cr-1Mo Steel for Elevated-Temperature Service" in *Proceedings, Topical Conference Ferritic Alloys for Use in Nuclear Energy Technologies*, Snowbird, Utah, 19-23 June 1983, Metallurgical Society—American Institute of Mining, Metallurgical, and Petroleum Engineers, New York, Sept. 1984, pp. 317-328.
- [3] Sikka, V. K., Cowgill, M. G., and Roberts, B. W., "Creep Properties of Modified 9Cr-1Mo Steel" in *Proceedings, Topical Conference Ferritic Alloys for Use in Nuclear Energy Technologies*, Snowbird, Utah, 19-23 June 1983, Metallurgical Society—American Institute of Mining, Metallurgical, and Petroleum Engineers, New York, Sept. 1984, pp. 412-24.

DISCUSSION

*W. J. Wiemann*¹ (*written discussion*)—You showed results of a thick-walled 9Cr-1Mo forged cylinder, and at first sight the properties of this steel seem to be better than these of the competitive 12Cr-Mo-V pipe steel (Grade 20Cr-Mo-V 12 1). Is there any information about the results inside of solid forgings of an outer diameter similar to your investigated forging or of solid cylindrical forgings up to about 1200-mm outer diameter? Are these results or the to-be-expected results of such pieces also better than those of 12Cr-Mo-V (Grade 22 Cr-Mo-V 12 1, SEW 555 draft, March 1984) rotor forgings? Most decisive would be the comparison of real long-time tested creep results (more than 30 000 h) and in addition to this the comparison of (fracture) toughness results and their variation after long-time high temperature exposure at 480°C to 565°C.

A. K. Khare and V. K. Sikka (authors' closure)—There is no information available at present on the results inside a solid forging of up to about 1200-mm outer diameter. We expect the results of such forgings also to be better than 12Cr-Mo-V rotor forgings. Creep data of more than 30 000-h duration are available on several product forms (tubing, plate, and bar) of modified 9Cr-1Mo steel. Results of these tests are still in agreement with our previous extrapolations. Thermal aging for 25 000 h at 482, 538, and 593°C produced Charpy impact energy values of 60, 38, and 54 J, respectively, at room temperature. These values are considered satisfactory.

¹ Kraftwerk Union AG, D-4330 Muelheim a.d. Ruhr, Germany.

Evaluation of the Modified 9Cr-1Mo Steel Forging by French Laboratories

REFERENCE: Gelpi, A., "Evaluation of the Modified 9Cr-1Mo Steel Forging by French Laboratories," *Steel Forgings, ASTM STP 903*, E. G. Nisbett and A. S. McIlilli, Eds., American Society for Testing and Materials, Philadelphia, 1986, pp. 328–345.

ABSTRACT: The use of Oak Ridge National Laboratory's (ORNL) modified 9Cr-1Mo steel in liquid metal fast breeder reactor (LMFBR) steam generators (SGs) could present significant advantages as compared with the other ferritic steels envisaged or used for this application.

Novatome (France) received from ORNL a specimen of this steel obtained from a National Forge Co. (NF) saddle forging.

The evaluation of this specimen by French laboratories covers the topics deemed the most significant to confirm the advantages of this steel for a LMFBR-SG application. Namely: tensile, creep, impact properties, tensile and impact behavior after heat treatment performed to simulate very thick forgings, fatigue, stress corrosion cracking, fracture mechanics, and aging behavior.

Our results confirm that the impact properties of modified 9Cr-1Mo steel are excellent, at least up to a simulated thickness of 300 mm (12 in.), even after step cooling. They also confirm that this steel has among the highest mechanical properties and creep resistance, as compared with other ferritic steels envisaged or used for LMFBR-SG applications.

On the basis of these first satisfactory results, we are encouraged to continue the characterization of this steel in France. This work is proceeding, on the one hand, on the NF forging and, on the other hand, on a forged-rolled thick plate manufactured in France. This characterization program will last 5 years.

KEY WORDS: forgings, chromium molybdenum steels, mechanical properties, microstructure, heat treatment, fast nuclear reactors, breeder reactors, boiler plate

The results of the characterization work undertaken in the United States [1,2] on the Oak Ridge National Laboratory's (ORNL) modified 9Cr-1Mo steel show that the use of this steel in liquid metal fast breeder reactor (LMFBR) steam generators (SGs) could present significant advantages as compared with the other ferritic steels envisaged or used for this application.

The advantages would be:

1. Better mechanical properties and creep resistance than 2¼Cr-1Mo, 2¼Cr-1Mo-Nb, or 9Cr-1Mo steels.

¹ Consulting engineer, Department of Metallurgy, Framatome, Paris-La Défense, France.

2. Better impact properties than EM12 steel².
3. Better weldability than 12Cr-1Mo steel.

Moreover, the stress corrosion cracking resistance of this steel in various environments would appear to be satisfactory as is its decarburization behavior in sodium.

These properties were deemed sufficiently advantageous to justify undertaking the characterization of this steel in France, with a view to confirming its interest for LMFBR-SG applications. In the present paper, we shall discuss the results we have obtained to date on this steel.

This work has been performed on the specimen represented in Fig. 1. It is part of the same National Forge Co. (NF) forging as discussed in the paper entitled "Evaluation of Modified 9Cr-1Mo Steel Forging" by A. Khare and V. K. Sikka in this publication.

Study of the As-Received State

Chemical Composition

Table 1 shows the results obtained at different depths in the forging. The chemical composition is in accordance with the specification published by ORNL for this steel [2]. Particularly noteworthy is the low sulfur content of this steel. Moreover, as the phosphorus, tin, and antimony contents are also very low, we can expect no serious temper embrittlement problems. However, the outer surface appears to be significantly depleted in carbon. This decarburization affects a depth of less than 10 mm (0.39 in).

According to our chemical analyses and to the formula given in Fig. 2 taken from Ref 3, the chromium equivalent is 10.5, which, considering the carbon plus nitrogen contents, situates this steel in the optimum area of the diagram established during the development of the grade (Fig. 2) [3].

Transformation Points

In order to perform studies to simulate a very thick forging (see Thick Plate Simulation Heat Treatment), we have determined the transformation points for this steel. Points Ac_1 and Ac_3 , determined by means of a Chevenard differential dilatometer, are situated at 835 and 905°C (1535 and 1661°F), respectively. The continuous cooling transformation test performed under welding conditions [after fast heating to 1350°C (2462°F), held for 3 s] shows that this steel is martensitic

² The chemical composition of EM12 steel is: carbon = 0.08 to 0.12%, silicon = 0.30 to 0.50%, manganese = 0.90 to 1.20%, phosphorus = 0.020% max, nickel = 0.30% max, chromium = 9.00 to 10.00%, molybdenum = 1.90 to 2.10%, vanadium = 0.25 to 0.35%, niobium = 0.35 to 0.45%, aluminum = 0.020% max, sulfur = 0.010% max, nitrogen = 0.050% max, and copper = 0.20% max.

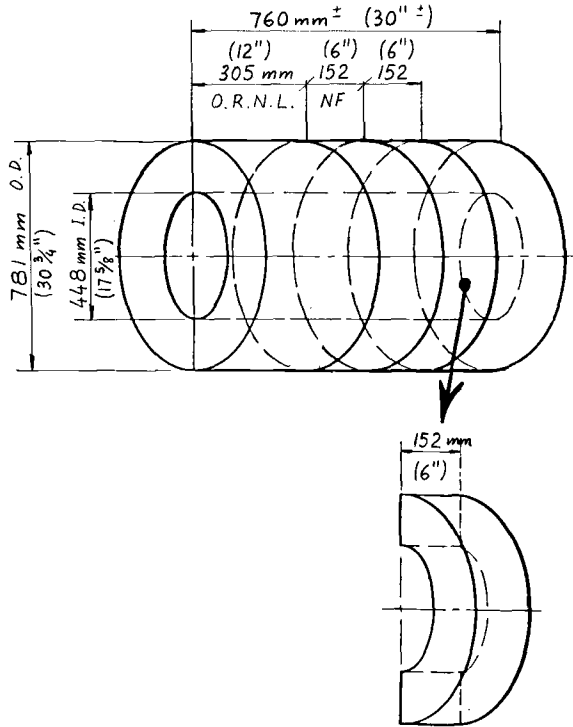


FIG. 1—Sketch of the layout of our specimen as located in the saddle forging (received from National Forge Co.).

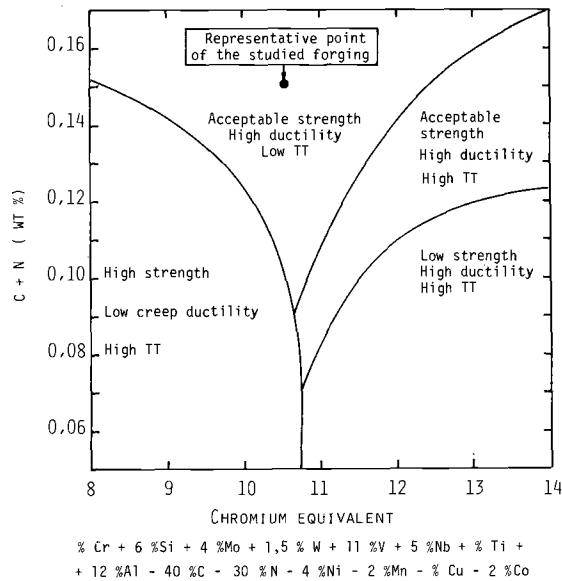


FIG. 2—Diagram relating the alloy properties to the specimen's chemical composition (Ref 3).

TABLE 1—Chemical analysis (weight %).

	Inner Surface		Midthickness		LABORATORY			10 mm Under		Outer Surface		ORNL Specification	
	Les Renardieres		Lcs Renardieres		Usinor			Marcel Chateaufneuf		Les Renardieres		Limits (Ref 2)	
	EDF		EDF		Dunkerque			Creusot		EDF			
C	0.082		0.11		0.11			0.11		0.054		0.08 to 0.12	
Mn	0.54		0.55		0.54			0.56		0.52		0.30 to 0.50	
P	0.007		0.007		0.011			0.011		0.007		0.02 max	
S	0.001		0.001		...			0.002		0.001		0.01 max	
Si	0.31		0.34		0.33			0.30		0.32		0.2 to 0.5	
Ni								0.14		0.12		0.4 max	
Cr	9.40		9.45		...			8.80		9.00		8 to 9.5	
Mo	0.94		0.93		1.01			0.95		0.96		0.85 to 1.05	
V	0.21		0.21		...			0.20		0.21		0.18 to 0.25	
Nb	0.05		0.05		...			0.08		0.05		0.06 to 0.10	
Ti	<0.005		<0.005			<0.005		...	
Co								0.016		
Cu	0.07		0.07		...			0.075		0.06		0.1 max	
Al	0.011		0.011		...			0.009		0.011		0.04 max	
Sn, ppm	50		50		...			50		50		...	
N						0.03 to 0.07	
Sb, ppm	<20		<20			<20		...	
Pb, ppm	<30		<30			<30		...	
As, ppm	90		90		...			90		90		...	

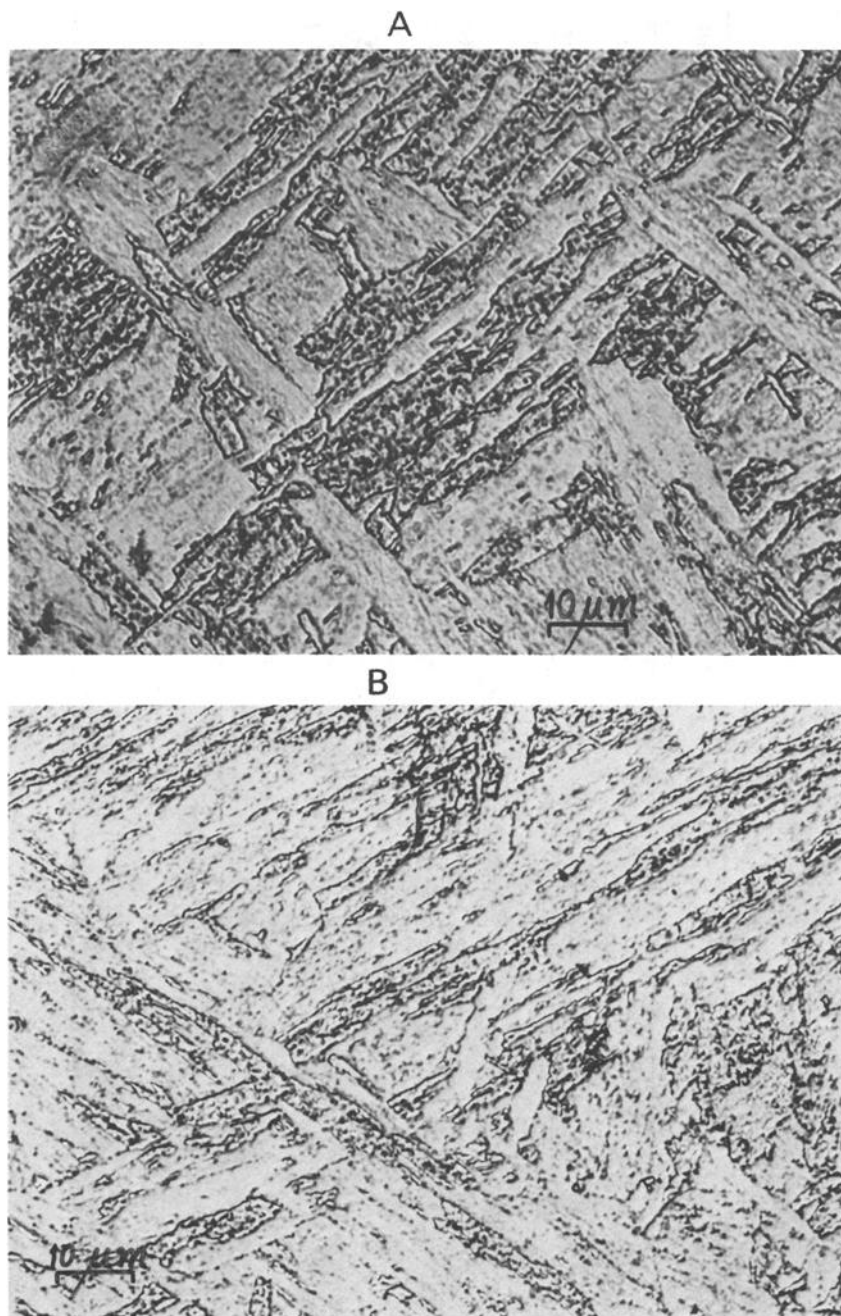


FIG. 3—(A) Optical microstructure of the as-received state at inner surface; (B) optical microstructure of the as-received state in the midthickness.

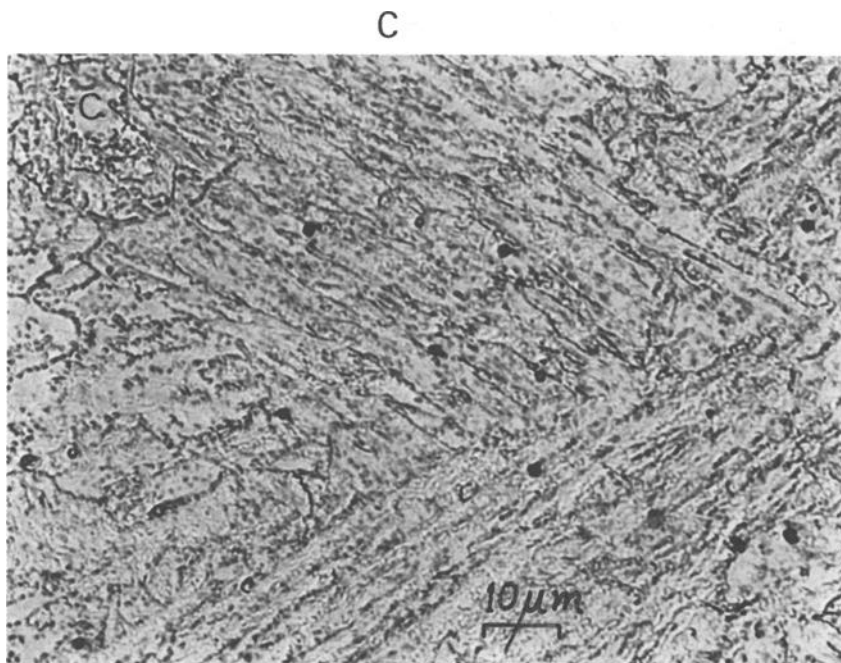


FIG. 3 (continued)—(C) optical microstructure of the as-received state at the outer surface.

down to very low cooling rates [below 5°C (9°F) per min]. The M_s point is situated at 360°C (680°F).

Microstructure and Inclusions Examination

Optical Microscopy—As we were led to expect by the continuous cooling transformation results on this product, its structure is entirely martensitic. Moreover, it is homogeneous from inner to outer surfaces (Fig. 3), but its grain size would appear to be relatively coarse.

Analysis of Inclusions—We undertook inclusion counting through a cross section of the product. According to their morphology, the inclusions are of the D type (oxides). Their size varies between 2 and 20 μm, the average value being 5 μm, which corresponds to thin inclusions. They are often clustered. Figure 4 shows the inclusion counting results. The inclusion content is seen to be fairly low and constant through the greater part of the product. However, it increases in the vicinity of the outer surface.

Figure 5A shows several of these inclusions as observed on X-ray microanalyzer Camebax. X-ray microanalysis of these particles by energy dispersion and wavelength dispersion indicates the presence of oxygen, aluminum, calcium, zircon-

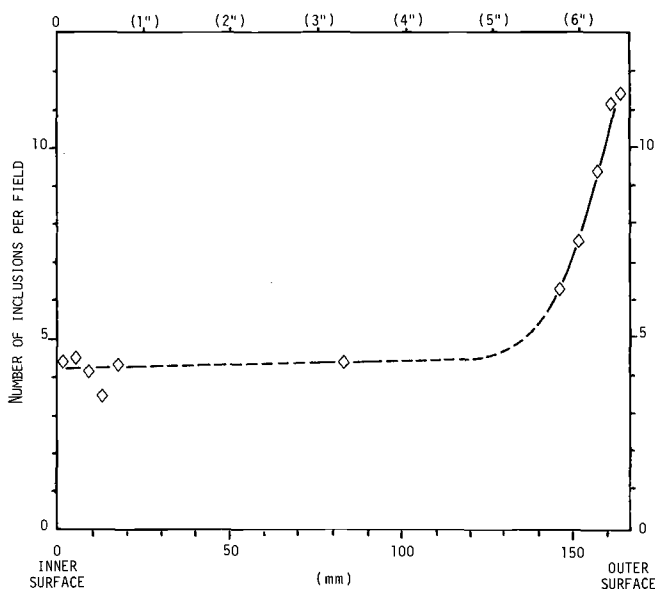


FIG. 4—Number of inclusions per 0.8-mm-diameter field (average over ten fields) versus the distance from the inner surface.

ium, and cerium (Fig. 5B), which confirms that the inclusions are of the oxide type as their morphology appeared to indicate.

Electron Microscopy on Thin Foils—Examination of thin foils of the metal with a Philips EM430 electron microscope revealed with some detail the tempered martensite and the carbide precipitation. Figure 6A shows the presence of dislocation cells inside the martensite laths. The very small size of the cells (smaller than in the case of EM12 steel) together with their morphology (certain walls are not completely formed) indicate that the martensite tempering is incomplete, which tends to imply the possibility of further softening if the tempering continues and also perhaps under high-temperature operating conditions. This impression of an incompletely tempered structure is reinforced by the presence of carbides inside the laths on dislocations in the process of recovery (Fig. 6B). These carbides are unstable and will probably go into solution when the metal is held at high temperature, while the lath boundary carbides will coarsen.

Electron Microscopy on Extractive Carbon Replicas—After extraction (Fig. 7A), the carbides were identified by electron diffraction and by energy-dispersive X-ray (EDAX) microanalysis. In all the cases examined, the carbides encountered were of the $M_{23}C_6$ type (Fig. 7B), where M represents statistically: 64Cr, 27Fe, 7Mo, 1V, 1Mn. We encountered no niobium carbonitrides. However, we assume that their existence is practically certain, owing to the presence of significant quantities of nitrogen and niobium elements in the chemical composition of the steel examined.

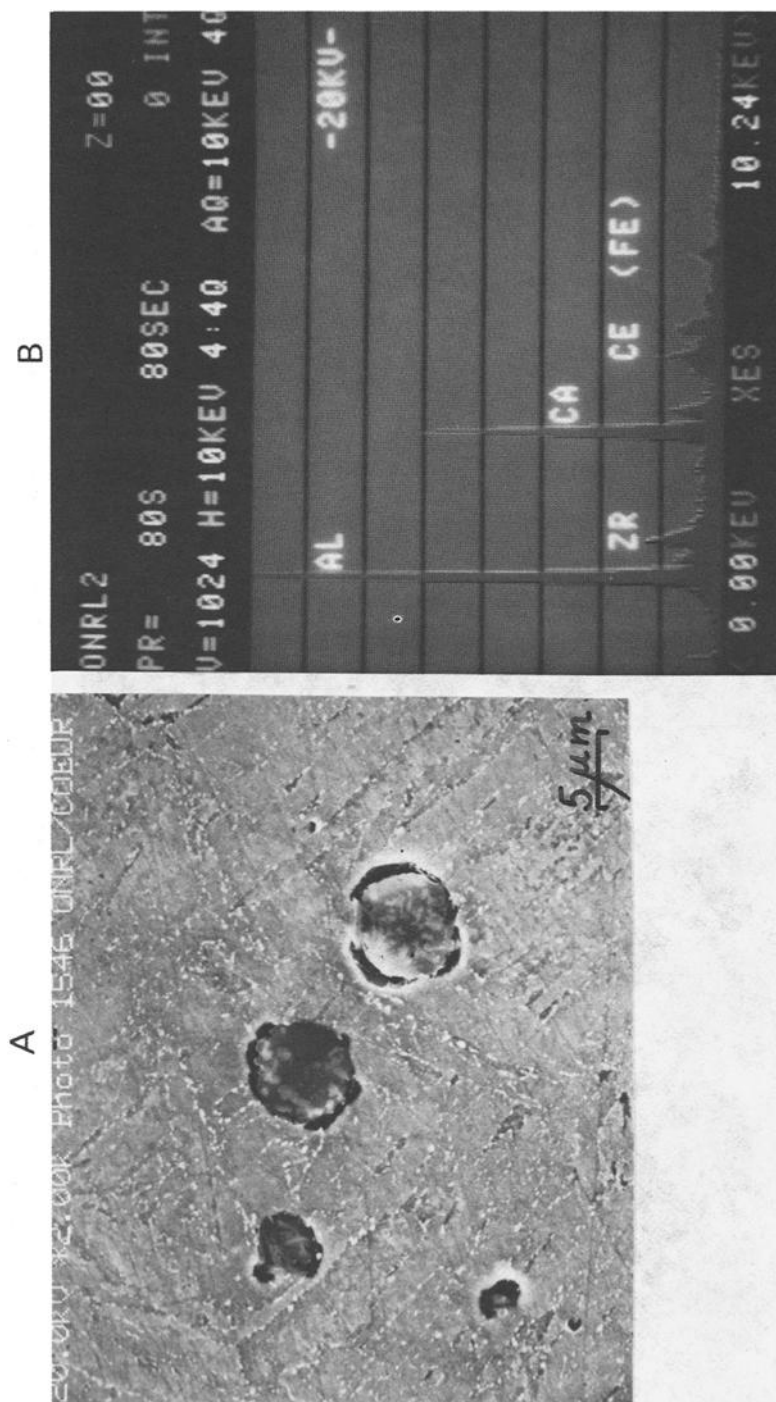


FIG. 5—(A) Micrograph of inclusions; (B) result of the energy dispersion X-ray microanalysis performed on Inclusion A.

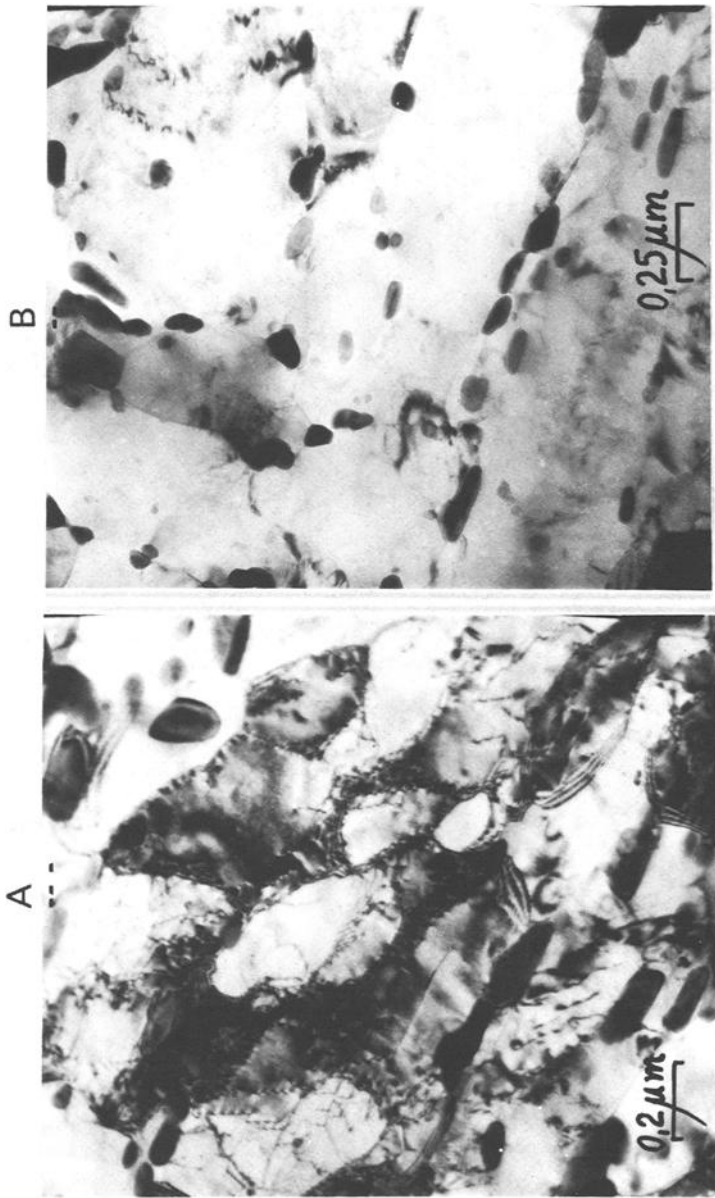


FIG. 6—Thin foil electron micrographs showing: (A) dislocation cells in the martensite laths; (B) carbides inside the laths and in the lath boundaries.

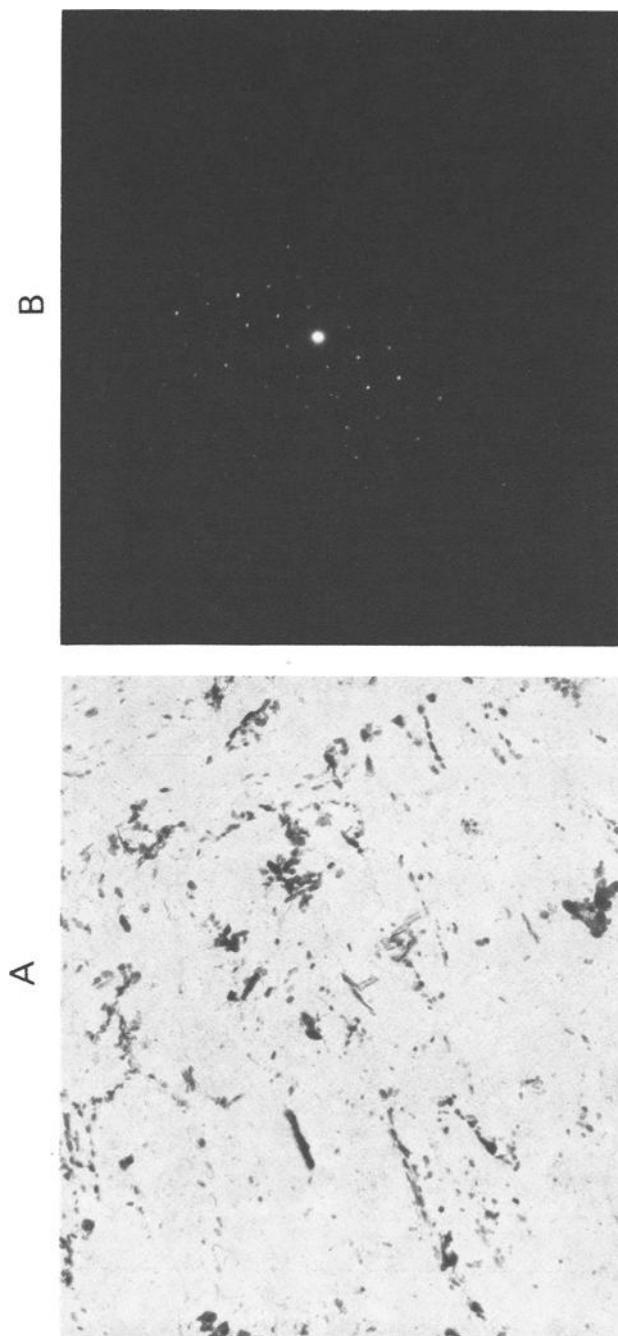


FIG. 7—Examination of carbides on extractive replica: (A) transmission electron micrograph; (B) diffraction pattern corresponding to $M_{23}C_6$.

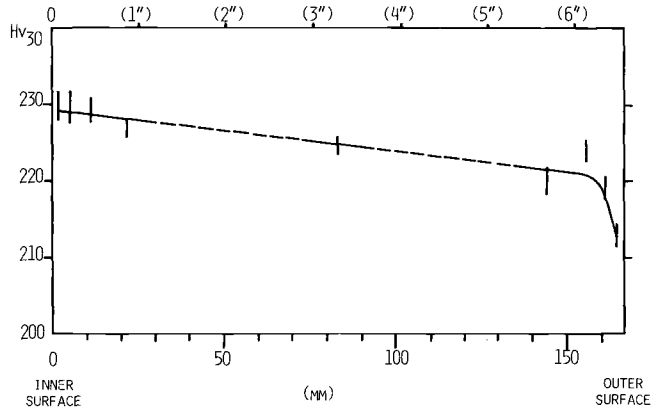


FIG. 8—Vickers Hv30 hardness versus the distance from the inner surface. The hardness drops sharply near the outer surface of the forging.

Hardness

Figure 8 shows the hardness values measured in the forging. We note its regular evolution between the inner surface and a distance of about 5 mm (0.20 in.) from the outer surface, after which it drops sharply in the vicinity of the

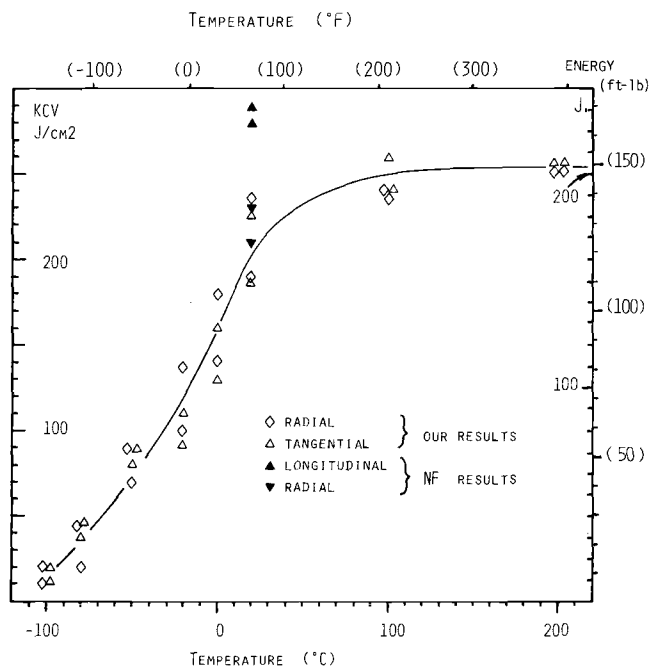


FIG. 9—Impact properties in the as-received state.

outer surface. The lesser hardness in this area is probably connected with the decarburization detected by the chemical analysis.

Mechanical Properties

Impact Properties—Figure 9 shows the as-received transition curve for radial and tangential samples, obtained with an ISO/AFNOR Charpy pendulum. At the 68 J level (50 ft·lb), we found a temperature of about -40°C (-40°F), the upper shelf energy being about 200 J (148 ft·lb). The room temperature impact properties are in agreement with the NF values for this product, under equivalent sampling conditions. These impact properties are excellent for a forging of this size and correspond to the values announced for the grade [1].

Tensile Properties—Figure 10 shows the evolution with temperature of yield strength and ultimate tensile strength between room temperature and 600°C (1112°F), while the true stress-strain curves are given in Fig. 11. Our results on tensile properties are close to the mean values established by ORNL for the grade [2]. The monotonic evolution of the temperature-dependent values obtained [without

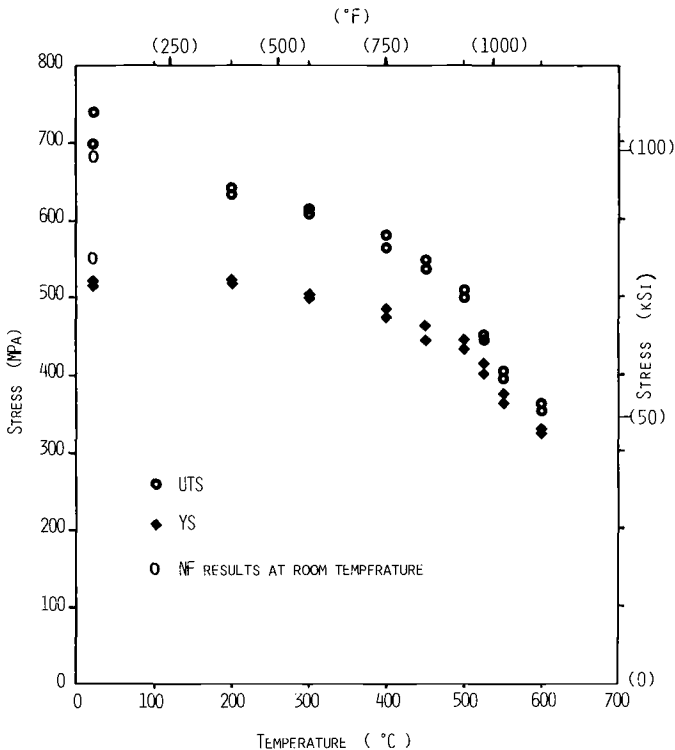


FIG. 10—Yield strength (YS) and ultimate tensile strength (UTS) versus test temperature.

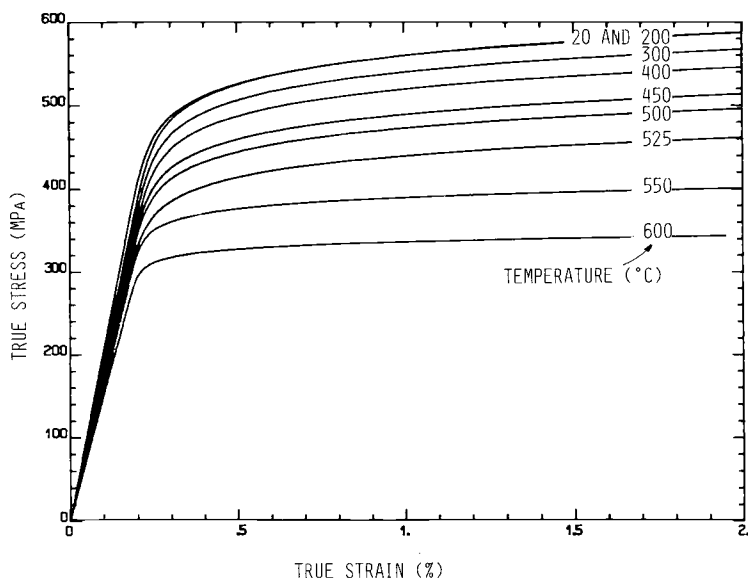


FIG. 11—True stress—strain curves between room temperature and 600°C.

a strength peak around 300°C (572°F)] is probably related to the low free interstitial content of this steel.

As regards the room temperature values, they are in agreement with the NF values for this product. However, it should be noted that one of the ultimate tensile strength values we obtained exceeds 700 MPa (102 ksi). This value corresponds to the upper limit imposed by the French regulations for the as-received state of steels intended for nuclear power plant primary system pressure vessel applications. The use in France of this forging for such an application would consequently necessitate:

1. Either a heat treatment differing from that used by NF and designed to lower the ultimate tensile strength (UTS).
2. Or the compilation of exhaustive justifications, mainly evidencing the weldability of the steel and its toughness.

Creep Properties—Figure 12 shows the creep-rupture results that we have obtained to date on this product at 550°C (1022°F), which is the temperature for which the most exhaustive creep data is available for our LMFBR materials. These results are below average for this steel grade [2]. They are nevertheless well above the minimum stress curve determined at 80% of the mean curve. As the duration of these tests is not sufficient to permit the determination of the creep properties of the product studied, testing will continue. For the tests presently proceeding under 210 MPa (30.46 ksi), the time to rupture expected should

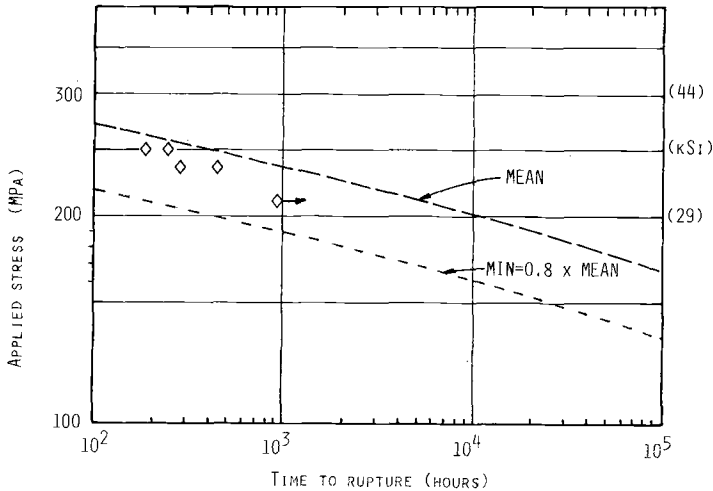


FIG. 12—Creep-rupture properties at 550°C. The mean values for the grade (upper dotted line) are taken from Ref 2.

be about 3000 h. These tests will be followed by others, where the time to rupture target will be 10 000 h.

Fatigue Properties—We have determined the endurance limit at 450°C (842°F) up to 10^7 cycles for this steel, using a Vibrophore machine at a frequency of 100 Hz. We applied stress cycles with $R = -1$ and the staircase method on 10 specimens with $K_t = 1.035$. The value obtained was $\sigma_e = \pm 270$ MPa (39 ksi) at 10^7 cycles. We found this value satisfactory.

Thick Plate Simulation Heat Treatment

Since we envisage using this steel for thick steam generator tube plates, we have tried to determine the structure and properties which could be obtained in this kind of product. For this purpose, blanks sampled from the NF forging were heat treated, with heating and cooling rates equivalent to those found at midthickness of a 300-mm (12-in.)-thick plate air-cooled (normalized). Furthermore, with a view to obtaining a fine structure, we fixed the austenitization temperature at $A_{c3} + 55^\circ\text{C}$ (99°F). The simulation heat treatment applied was consequently as follows:

1. Starting from 300°C (572°F), heating to 960°C (1760°F) at a rate of 100°C (180°F) per hour. After holding this temperature for 2 h, cooling between 800°C (1472°F) and 500°C (932°F) at a rate of 130°C (234°F) per hour.

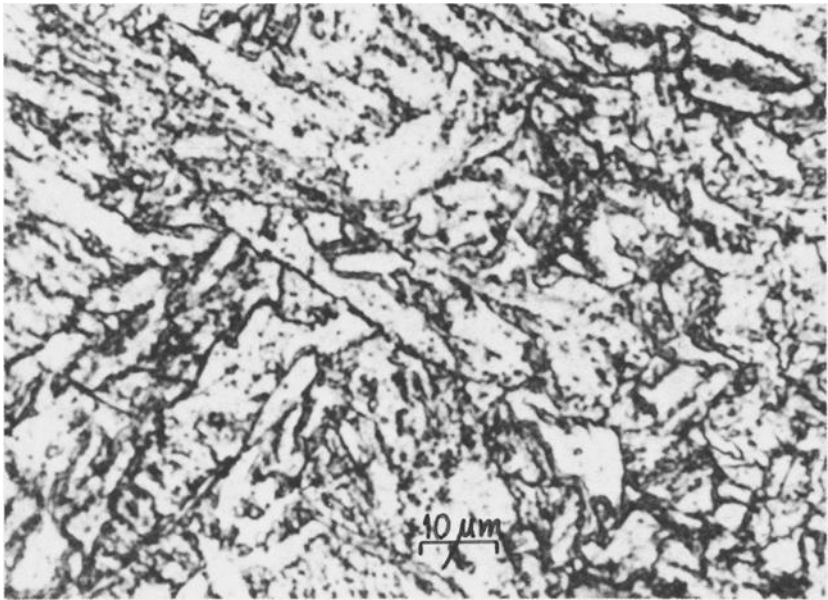


FIG. 13—Optical micrograph of the structure obtained after a heat treatment simulating a 300-mm-thick plate. It is martensitic, like the as-received state, but finer.

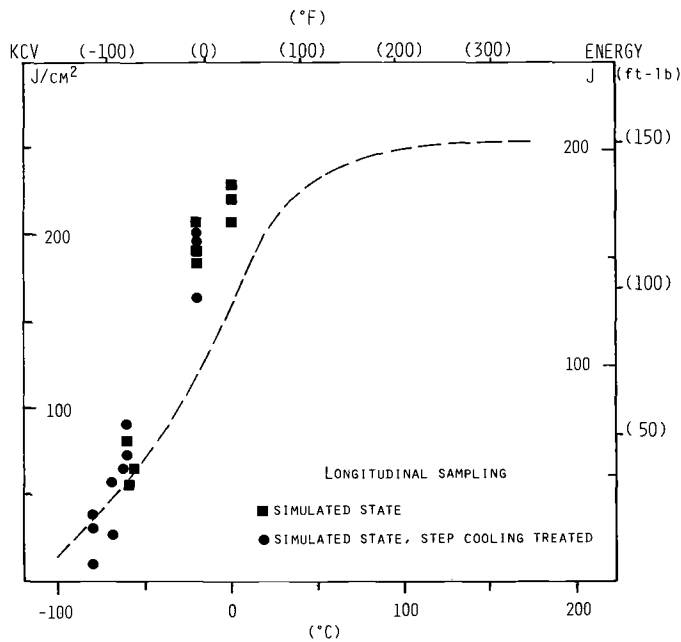


FIG. 14—Impact properties after heat treatment simulating a 300-mm-thick plate. The dotted line corresponds to the as-received state. Note that sampling is different in these cases.

This simulated normalization treatment was followed by a tempering/stress-relief treatment:

1. Heating to 760°C (1400°F) at a rate of 50°C (90°F) per hour, 18 h holding time and cooling at a rate of 50°C (90°F) per hour. This holding time includes several intermediate stress-relievings and the final Post Weld Heat Treatment (PWHT) necessary in the fabrication of a vessel.

Figure 13 shows that the microstructure obtained, still entirely martensitic, is, as wished, finer than that of the as-received product. The impact properties obtained after this simulation heat treatment are excellent (Fig. 14). The same figure shows that the level of the impact properties remains unimpaired by a step-cooling treatment, which tends to indicate that this steel is not liable to temper embrittlement. This was foreseeable, given the low residual element content revealed by the chemical analysis. The tensile properties obtained at room temperature and at 500°C (932°F) after the simulation heat treatment are lower

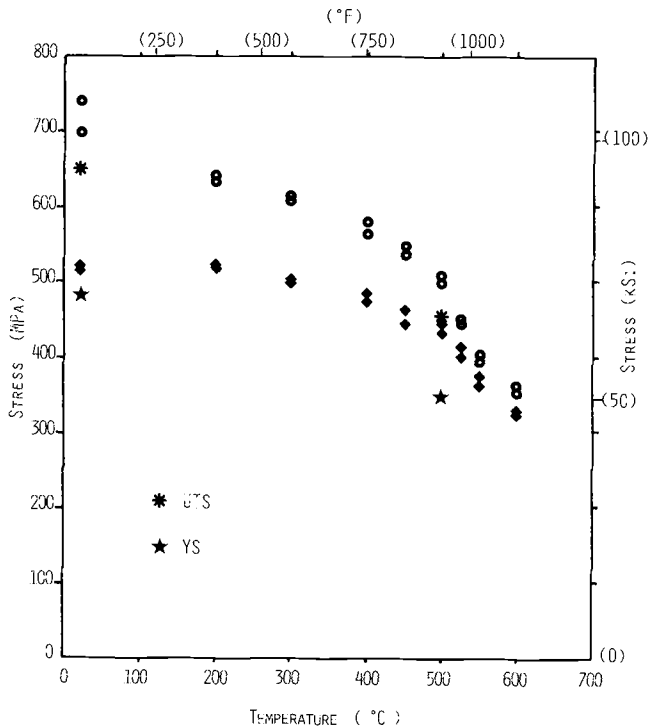


FIG. 15.—Tensile properties YS and UTS at room temperature and 500°C after heat treatment simulating a 300-mm-thick plate as compared to those of the as-received state.

than those obtained on the as-received product (Fig. 15). However, this result is, at least partly, related to the long tempering/stress-relief treatment applied in this case.

Conclusions

The results that we have obtained on the NF forging evidence the homogeneous martensitic structure and satisfactory inclusion content of the product and show that the mechanical properties identified for this product are in agreement with values previously published for the grade. Our results confirm that the impact properties of modified 9Cr-1Mo steel are excellent, at least up to a thickness of 300 mm (12 in.), even after step cooling. They also confirm that this steel has among the highest mechanical properties and creep resistance as compared with other ferritic steels envisaged or used for LMFBR-SG applications.

On the basis of these first satisfactory results, we are encouraged to continue the characterization of this steel in France. This work is proceeding, on the one hand, on the NF forging and, on the other hand, on a product manufactured in France. So, aging, creep, and long-term stress corrosion cracking (SCC) tests are in progress of the NF forging together with J_{Ic} determination. We also plan to perform welding tests on this product. As regards the French product, it is a 300-mm (12-in.)-thick, forged-rolled experimental tube plate which has just been manufactured. Its characterization will last about 5 years.

Acknowledgements

Oak Ridge National Laboratory and the National Forge Co. supplied the modified 9Cr-1Mo forging. I should like to express my most sincere thanks to P. Patriarca and V. K. Sikka (ORNL) and to A. Khare and A. Laporte (NF), without whom this work would not have been possible. I also wish to thank D. Guttman and J. C. Van Duysen (EDF les Renardières), M. F. Felsen (CEA-SRMA), A. Cheviet and J. Burlat (Creusot-Marrel Chateaufort), and L. Sabatier (UNIREC) for their lively interest in this work and for having been kind enough to make their results available to me in time for inclusion in the present paper.

References

- [1] Patriarca, P., "Modified 9Cr-1Mo Steel," a technical program and data package for use in ASME Sections I and VIII--Design Analysis, 2nd printing June 1982, ORNL technology transfer meeting, Knoxville, April 1982, American Society of Mechanical Engineers, New York.
- [2] Sikka, V. K. and Patriarca, P., "Data package for modified 9Cr-1Mo alloy," Oak Ridge National Laboratory, Oak Ridge, TN, Dec. 1983.
- [3] Irving, R. R., *Iron Age*, 25 June 1982.

DISCUSSION

E. Juergen¹ (written discussion)—From the presentation of Dr. Sikka², we saw a specified chemical composition of the 9Cr-1Mo steel with, for example, phosphorus = 0.010%. The test forging investigated here, having no susceptibility to temper embrittlement, had rather low phosphorus and impurity contents. To guarantee this nonsusceptibility, it could be necessary to specify generally similar low phosphorus and impurity elements. Did you do this?

A. Gelpi (author's closure)—One of the main experimental products used in France for the study of modified 9Cr-1Mo steel is a 300-mm (12-in.)-thick, forged-rolled plate. Its phosphorus content is lower than 0.010%. However, our purchase specifications for the commercial products (tube plates, tubes, sheets) will be established only when the French studies regarding this steel are more advanced.

¹ Kraftwerk Union AG, Muelheim a.d. Ruhr, Federal Republic of Germany.

² "Evaluation of Modified 9Cr-1Mo Steel Forging," by A. K. Khare and V. K. Sikka, this publication.

G. W. Kuhlman,¹ R. Pishko,² W. S. Darden,³ and W. L. Krubsack⁴

Optimizing Mechanical Properties of Specialty, Stainless, and Heat-Resistant Alloy Steel Forgings by Thermomechanical Processing

REFERENCE: Kuhlman, G. W., Pishko, R., Darden, W. S., and Krubsack, W. L., "Optimizing Mechanical Properties of Specialty, Stainless, and Heat-Resistant Alloy Steel Forgings by Thermomechanical Processing," *Steel Forgings, ASTM STP 903*, E. G. Nisbett and A. S. Melilli, Eds., American Society for Testing and Materials, Philadelphia, 1986, pp. 346–364.

ABSTRACT: Ferrous alloy forgings typically are used at the critical points in any given application, and thus it is incumbent upon the forger to select optimum melting technology and design processing techniques to provide specialty, stainless, and heat-resistant steels that possess the full extent of the grade's mechanical properties. Thermomechanical processing techniques can be employed to achieve such goals. In specialty steels such as HP310, HP9Ni-4Co-0.20C, and AF1410, combinations of working practices and thermal treatments have been examined to maximize the ductility and/or fracture toughness of these ultra-high strength steels. In stainless steel Grades 15-5PH and PH13-8Mo in forgings, critical fracture-toughness requirements can be enhanced by careful selection of forging parameters. Finally, for heat- and corrosion-resistant materials, including A286 and Inconel 625, relationships between forging and thermal treatments have been studied that optimize grain size, strength, and toughness.

KEY WORDS: specialty steels, ultra-high strength low-alloy steels, precipitation-hardening stainless steels, heat/corrosion-resistant alloy steels, superalloys, thermomechanical processing, mechanical properties

Aerospace, power generation, chemical process, and oil field applications of ferrous alloy forgings place stringent demands upon the performance of these materials, particularly in large, heavy-section forgings that are typical of these critical applications. It is therefore incumbent upon the forging producer to combine the selection of optimum melting technologies for the basic material with

¹ Manager—Advanced Technology, Alcoa Forging Division, Cleveland, Ohio 44105.

² Senior engineer, Alcoa Forging Division, Vernon, CA 90058.

³ Senior metallurgist, Alcoa Forging Division, Cleveland, Ohio 44105.

⁴ Division metallurgist, Alcoa Forging Division, Cleveland, Ohio 44105.

carefully designed forging processing techniques in order to provide specialty, stainless, and heat-resistant alloy steel forgings that demonstrate the full extent of the mechanical properties that any given grade of steel can offer.

Thermomechanical processing is a technique of combining working procedures with subsequent thermal treatments in order to achieve specific mechanical property goals. It is a technology that manipulates the microstructure of the material in such a manner as to yield optimized properties for critical applications. In this work, thermomechanical processing technology is explored for several types of alloy steels. Nominal compositions of the alloy steels used in this study are outlined in the Appendix.

Procedure

Specialty Steels

Tempering Study HP310—A large flap track forging was fabricated from a 16-in. round cornered square (RCS) billet produced using argon-oxygen decarburization (AOD) first melt and vacuum arc remelting (VAR). Short transverse tension specimens were excised from this forging and heat-treated using the practice outlined in Table 1. Double tempering at temperatures from 177 to 399°C, with the second temper at or slightly below the first temper, was then accomplished. Prior to tension testing, specimens were stress relieved at least 10°C below the final temper. Specimens were tested by Methods of Tension Testing of Metallic Materials (ASTM E8-85) and examined metallographically.

Fabrication of HP9Ni-4Co-0.20C Forgings—A series of B-1B forgings, depicted in Fig. 1, were manufactured under production conditions. Selected forgings were destructively tested for mechanical properties using the heat treatment required by current material specifications: Normalize at 899°C, 1 h/in.; austenize at 843°C, 1 h/in; quench in oil; refrigerate at -73°C, 1 h minimum, air warm; temper at 522 to 579°C, 4 to 8 hours, air cool. The billet used to manufacture these forgings had been AOD-VAR refined.

Thermal Treatment Study AF1410—A series of B-1 attachment fitting forgings were manufactured under production conditions. Selected forgings were heat-treated with two approaches, shown in Table 2. Heat Treatment A is a process designed to minimize machining distortion, and Heat Treatment B is a process designed to maximize properties, particularly fracture toughness. The forging billet had been vacuum induction melted (VIM)—VAR refined.

Stainless Steels

The interactions of forging and thermal treatments were studied on two alloys, 15-5PH and PH13-8Mo. For 15-5PH, AOD-VAR-refined bar was employed and given hot forging work using the temperatures outlined in Table 3. Resulting

TABLE 1—Tempering study of Alloy HP310.

Temper Temperature, °C	Test Direction	Ultimate Tensile Strength, MPa	Yield Strength, MPa	Elongation, %	Reduction in Area, %	R _c
177	ST	2337	1993	2.7	11.9	58
204	ST	2330	1979	7.5	12.2	56
232	ST	2303	1979	6.5	8.6	57
260	ST	2310	1979	6.0	6.5	57
287	ST	2303	1986	5.5	9.9	57
302	ST	2289	1993	5.0	11.8	57
316	ST	2282	2006	7.5	14.9	58
329	ST	2227	1986	6.0	16.4	57
343	ST	2241	1986	7.0	12.7	57
357	ST	2220	1986	7.0	13.3	56
371	ST	2193	1979	7.0	16.0	55
385	ST	2165	1965	7.0	12.3	56
399	ST	2151	1944	7.0	19.2	54
MINIMUM PROPERTIES						
	ST	2137	1862	...	12	...

NOTE 1: Composition: HP310 (weight %): C-0.44, Mn-0.70, P-0.009, S-0.001, Si-2.49, Cu-0.18, Ni-1.76, Cr-0.86, Mo-0.45, V-0.22, Fe-balance.

NOTE 2: Heat Treatment:

- Normalize 927°C, 1 h, air cool.
- Austenize 871°C, 871°C, 1 h, oil quench.
- Cool - 73°C, 1 h, air warm.
- Temper double, 2 + 2 h.

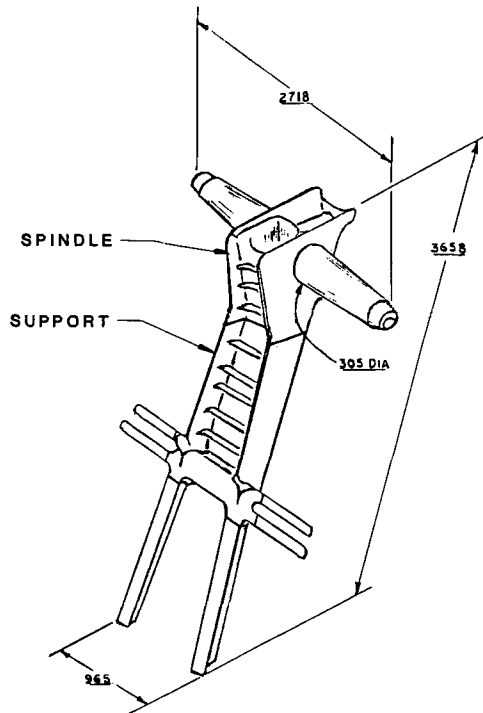


FIG. 1—HP-9Ni-4Co-0.20C B1B Spindle and support forgings, dimensions in millimetres.

forgings were thermally treated to the H900 temper per current specifications (Table 3) and tested for tensile properties per ASTM B 557-84 and fracture toughness per Method for Plane-Strain Fracture Toughness of Metallic Materials (ASTM E 399-83). A series of B-1B flap track forgings were manufactured under production conditions in alloy PH13-8Mo, using VIM-VAR-refined billet in accord with current specifications. Forgings were destructively tested with specimens heat-treated according to the specification practice shown in Table 4.

Heat/Corrosion-Resistant Materials

Thermomechanical Processing A286—VIM-VAR-refined A286 bar was submitted to forging hot work using the temperatures outlined in Table 5. Resultant forgings were tested for tensile properties per ASTM E 8-85 and fracture toughness per ASTM E 399.

Thermomechanical Processing of Inconel 625—Bar stock was procured that had been AOD-VAR refined. Forging was accomplished using two routes: (1) hot working only, with total reduction of 75%, and (2) a combination of hot and “warm” working with a similar level of total reduction. Resultant forgings were

TABLE 2—*Thermomechanical processing specialty steel alloys: heat treatment study AF1410.*

Heat Treatment ^a	Test Direction	Section Thickness, mm	Ultimate Tensile Strength, ^b MPa	Yield Strength, ^b MPa	Elongation, ^b %	Reduction in Area, ^b %	K_{IC} , ^b MPa \sqrt{m}
A	L	100	1765	1634	18	40	166
	T	100	1737	1600	15	36	...
B	L	50	1620	1510	20	44	169
	T	50	1675	1530	19	41	...
	L	100	1765	1648	19	42	196
	T	100	1682	1572	16	39	...
	L	50	1710	1600	21	47	216
	T	50	1696	1579	18	41	...
	TENTATIVE MINIMUM PROPERTIES						
	L		1585	1517	15	30	143
	T		1585	1517	12	25	...

NOTE: Composition AF1410 (Nominal Weight %): C-0.16, Mn-0.10, Si-0.10, S-0.005, P-0.008, Cr-2.0, Ni-10.0, Co-14.0, Mo-1.0, Fe-balance.

^a Heat Treatments:

A: 899°C, 1 h, air cool, plus
 816°C, 1 h, air cool, plus
 -73°C, 1 h, air warm, plus
 510°C, 5 h, air cool (minimum machining distortion).

B: 899°C, 1 h air cool, plus
 899°C, 1 h, water quench, plus
 816°C, 1 h, water quench, plus
 510°C, 5 h, air cool (maximum properties).

^b Average properties.

TABLE 3—Thermomechanical processing, stainless steel alloys: mechanical properties—15.5PH H900.

Forge Temperature, °C	Heat Treatment	Ultimate Tensile Strength, ^b MPA	Yield Strength, ^b MPA	Elongation, ^b %	Reduction in Area, ^b %	K _{IC} , ^b MPA \sqrt{m}
980	H900	1358	1213	20	62	76
1035	H900	1379	1282	20	60	81
1095	H900	1400	1282	18	54	77
1150	H900	1379	1331	18	60	78
1175	H900	1365	1275	18	56	74
1205	H900	1365	1262	19	57	76
1230	H900	1372	1234	18	56	73
MINIMUM PROPERTIES						
		1310	1172	10	35	...

NOTE 1: H900: 1035°C-1 h, air cool to below 32°C, 482°C-2 hours, air cool.

NOTE 2: Composition 15.5PH (weight %): C-0.03, Si-0.31, Mn-0.49, P-0.24, S-0.003, Ni-4.30, Cr-14.95, Mo-0.04, Cu-3.37, CD + TA-0.028, Fe-balance.

^a Final forge temperature, reduction 40%.^b Average properties.

TABLE 4—*Thermomechanical processing stainless steel alloys: mechanical properties PH13-8Mo H1000 B-1B, "Flap Track Forgings."*

Test Direction	Section Thickness, mm	Ultimate Tensile Strength, ^a MPa	Yield Strength, ^a MPa	Elongation, ^a %	Reduction in Area, ^a %	K_{Ic} , ^a MPa \sqrt{m}
			INBOARD TRACK			
L	100	1469	1413	13	58	102
T	152	1482	1427	13	60	98
			INTERMEDIATE TRACK			
L	127	1517	1462	17	60	94
T	100	1510	1455	16	59	95
			OUTBOARD TRACK			
L	152	1406	1365	17	63	125
T	100	1400	1372	15	62	124
			MINIMUM PROPERTIES			
L		1379	1310	10	50	82
T		1379	1310	10	40	82

NOTE 1: Composition: PH13-8Mo (nominal weight %): C-0.03, Mn-0.01, P-0.002, S-0.003, Si-0.02, Cr-12.60, Ni-8.24, Mo-2.10, Al-1.00, Fe-balance.

NOTE 2: Heat Treatment: 927°C, 3 h, air cool, to below 16°C; 538°C, 4 h, air cool.

^a Average properties.

TABLE 5—*Thermomechanical processing heat resistant alloys: mechanical properties A-286.*

Forge ^b Temperature, °C	Heat Treatment	Ultimate Tensile Strength, ^a MPa	Yield Strength, ^a MPa	Elongation, ^a %	Reduction in Area, ^a %	K_{Ic} , ^a MPa \sqrt{m}
980	STA	1124	648	26	44	47
1035	STA	1096	614	26	47	45
1095	STA	1082	579	28	47	85
1120	STA	1069	620	27	46	94
1150	STA	1069	745	27	43	91
1175	STA	1034	669	25	44	83
MINIMUM PROPERTIES						
		896	586	15	20	...

NOTE 1: Composition A-286 (Weight %): C-0.04, Mn-1.59, Si-0.63, Cr-15.11, Ni-25.89, Mo-1.31, Ti-2.01, Al-0.19, V-0.38, B-0.006, Fe-balance.

NOTE 2: STA: 899°C, 1 h, oil quench plus 704°C, 12 h, air cool.

^a Average properties.^b Final forging temperature, reduction approximately 40%.

given single-step anneals or two-step anneal plus aging treatments with practices as outlined in Table 6. Resultant forgings were tested for mechanical properties per ASTM B 557 and grain size.

Results and Discussion

Specialty Steels

Tempering Study of HP310—HP310 is a further silicon modification of 300 M/4340 Modified developed by LTV (Republic) Steel in the 1970s [1]. HP310, with a minimum ultimate strength capability of 2137 MPa, is feasible as an engineering material primarily because of the impact of first melting via AOD on key compositional elements. AOD has been shown [2] to provide extremely low sulfur contents, sulfide shape control, and low residual gas contents (hydrogen, oxygen, and nitrogen), all of which are keys to the development of adequate fracture-related properties in a low-alloy steel capable of this strength level. Previously, in the manufacture of initial HP310 steel forgings for the aerospace industry, difficulty had been encountered with the development of required short transverse reduction in area (ductility) properties. At that time, specifications required tempering the alloy at 302°C, a practice widely used for other ultra-high strength, low-alloy steels to develop desired strengths and ductility. With the 302°C tempering practice, marginal ductility had been encountered with HP310.

Thus, alternate tempering temperatures were explored with the results of this tempering study for HP310 presented in Table 1 and graphically in Fig. 2. The data in Fig. 2 suggest that ultimate and yield strength criteria can be met with tempering temperatures considerably above 302°C, and that yield strength is essentially independent of tempering temperature in the range studied. Reduction of area on the other hand undergoes a minimum at temperatures less than 302°C, in fact at this temperature reduction of area has just started to increase. These data then suggest that optimum tempering practice for HP310 is in the 315 to 343°C range in order to achieve current ductility requirements with the desired high-strength levels. This tempering practice subsequently has been confirmed on other forging shapes produced in this alloy. In these tests, ultimate strengths achieved on specimens removed from forgings and heat-treated with a double temper at 329°C provided ultimate strengths over 2200 MPa, yield strengths over 1970 MPa, reduction in area of 15 to 22%, and fracture toughness of 50 to 60 MPa $\sqrt{\text{m}}$.

Forging Evaluation of HP9Ni-4Co-0.20C—HP9-4-20 was also developed by LTV (Republic) Steel [3] for applications requiring high strength with superior fracture toughness. The manufacture of the very large B-1B support and spindle forgings shown in Fig. 1 provided a challenge to develop required high strengths and high toughness in very heavy section parts up to 254-mm thick. In addressing this challenge, current specifications require control of forging processing on

TABLE 6—*Thermomechanical processing heat resistant alloys: mechanical properties Inconel 625.*

Forging Method	Heat Treatment	Ultimate Tensile Strength, MPa	Yield Strength, MPa	Elongation, % in 4D	R_c	ASTM Grain Size
HOT WORKED ONLY	A	864	448	55	14	6
	B	1068	689	42	28	6
	C	931	489	51	17	7
	D	1120	710	39	30	7
	E	1310	1054	13	46	9
HOT/WARM WORKED	A	930	496	49	16	8
	B	1117	751	39	30	8
	C	965	524	45	21	8.5
	D	1160	810	33	32	8.5
	E	1340	1160	11	48	10
GOAL	413	4-6

NOTE 1: Composition Inconel 625 (Weight %): C-0.04, Mn-0.19, Fe-4.10, S-0.001, Si-0.39, Ni-60.91, Cr-21.83, Al-0.15, Ti-0.21, Mo-8.51, CB + TA-3.66, P-0.011.

NOTE 2: Heat Treatments:

A—980°C, 4 h, air cool (anneal).

B—980°C, 4 h, air cool (anneal), plus 650°C, 48 h, air cool (age).

C—870°C, 4 h, air cool (anneal).

D—870°C, 4 h, air cool (anneal), plus 650°C, 48 h, air cool (age).

E—785°C, 24 h, air cool (age).

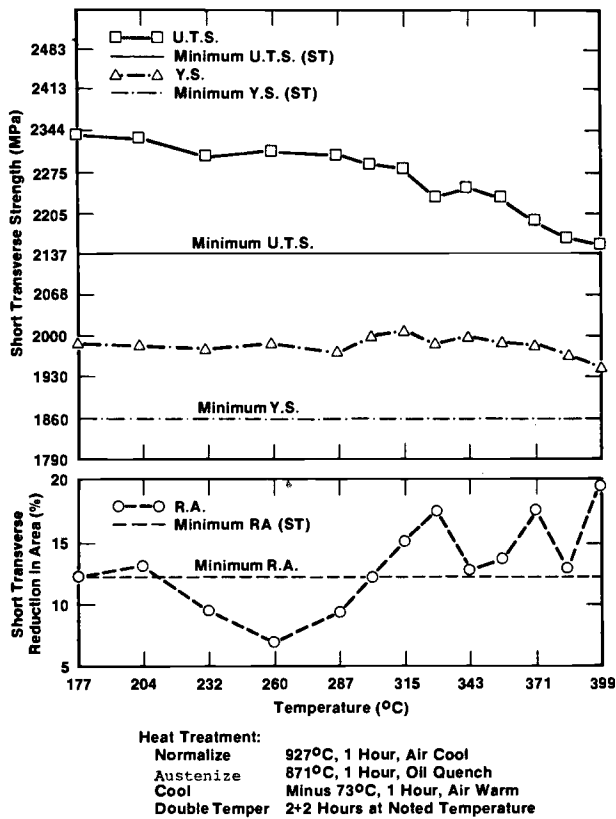


FIG. 2—Tempering curve, Alloy HP310.

fracture critical HP9-4-20 parts such that final forging is to be accomplished from relatively low temperatures, making it difficult to achieve adequate die fill on forgings this large in this alloy. For these parts, a forging process was designed to meet these specification criteria, and destructive test results on the two forgings are outlined in Table 7.

The forging producer is allowed to temper test material in the range of 551 to 579°C, with selection of the final temper to be based upon the response of the forgings in question. The ultimate user of the parts then uses the suggested tempering practice in hardening the final machined parts. In this work with HP-9-4-20, the full range of tempering temperatures was explored on test material removed from these large forgings in order to establish an optimum practice. The combination of forging practices employed, heavy sections of the part, and total deformation imparted suggested that tempering at the low end of this range was required. The properties shown in Table 7, the result of tempering optimization, were achieved with final tempering temperatures in the range of 551 to 565°C.

TABLE 7—*Thermomechanical processing specialty steel alloys: mechanical properties HP9Ni-4Co-0.20C, B-1B "Jolly Green Giant Forging."*

Test Direction	Section Thickness, mm	Ultimate Tensile Strength, ^a MPa	Yield Strength, ^a MPa	Elongation, ^a %	Reduction in Area, ^a %	K_d^a MPa \sqrt{m}
			SPINDLE			
L	254	1400	1289	20	70	189
T	254	1393	1276	19	68	190
T	178	1400	1289	18	67	...
			SUPPORT			
L	178	1386	1282	21	71	223
T	178	1372	1276	20	70	222
L	127	1372	1269	20	73	...
L	100	1393	1276	20	70	...
L	75	1379	1269	20	73	...
			MINIMUM PROPERTIES			
		1310	1241	12	45	121

NOTE 1: Composition: HP9Ni-4 Co-0.20C (nominal weight %): C-0.20, Mn-0.30, P-0.010, S-0.010, Si-0.20, Ni-9.0, Cr-0.75, Mo-1.0, V-0.08, Co-4.5, Fe-balance.

^a Average of two to six tests.

Heat Treatment Study AF1410—AF1410 is a modified HY180 developed by Cytemp under a contract with the U.S. Air Force [4]. The cobalt modification employed serves to increase the strength of the alloy with only modest reduction in fracture toughness and provides an alloy with minimum ultimate strength of 1585 MPa and minimum fracture toughness of 143 MPa $\sqrt{\text{m}}$. With these mechanical properties, AF1410 is competitive with titanium alloys on specific property (corrected for density) and critical crack length bases. AF1410 is an alloy that is forged at relatively low temperatures, approximately 980°C [4], in order to develop desired starting structures, and hardening is achieved through a combination of martensitic and precipitation reactions. Thermal treatments employed in the development of the alloy were double austenize and water quench followed by age in order to develop optimum strength and toughness properties.

With such double austenizing and quenching treatments, distortion of machined parts is highly probable, thus an alternate heat treatment of double austenizing with air cools and a subzero treatment followed by aging also was explored in order to minimize part distortion. Results for these two heat treatment approaches are outlined in Table 2.

The tensile and toughness data presented suggest that current minimum property criteria can be met with the alternate air cool process (Heat Treatment B), but that there is some sacrifice in both strength and fracture toughness properties. Microstructural evaluations of the two heat treatment methods suggest that the lower strengths and toughnesses of the slower cooling rate process result from slight modifications of the lath martensite morphology and slightly coarser precipitates.

Stainless Steels

Forging Process Study of 15-5PH—15-5PH is a precipitation hardening steel [5] that is used in aerospace and other applications requiring high strength and good corrosion resistance; however, fracture toughness minima are not typically specified for this grade. The forging process study conducted was to explore the optimum forging process conditions for 15-5PH in the high strength H900 temper required to develop maximum fracture toughness. These procedures then could be applied to production forgings, if necessary, or translated to similar alloys where fracture toughness is a specification requirement.

The results of tensile and fracture toughness properties as a function of final forging temperature are shown in Table 3 and graphically in Fig. 3. This alloy displays a modest dependence of strength/toughness on forging process conditions. Interestingly, both strength and toughness reach optimum levels with forging in the 1050 to 1150°C range and are somewhat depressed with lower or higher forging reheat practices or both. The structural explanation for the strength and toughness behavior at higher forging temperatures is clear: austenite grain size is coarsened with high metal temperatures and such an effect carries through the final heat treatment. The explanation for similar behavior at lower forging temperature is not yet understood.

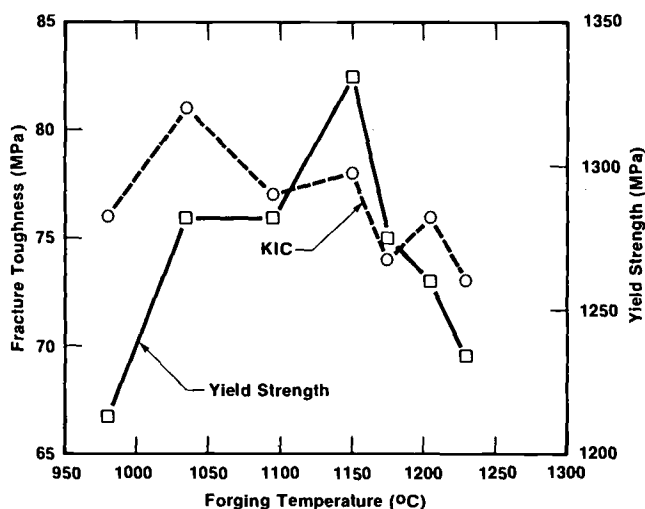


FIG. 3—Yield strength and fracture toughness versus forging temperature, alloy 15-5PH H900.

The results of this study suggest that a minimum fracture toughness guarantee for 15-5PH H900 of $60 \text{ MPa} \sqrt{\text{m}}$ is supportable should aerospace or other users desire to have such a guarantee on this alloy and temper.

Forging Evaluation of PH13-8Mo—PH13-8Mo is also a precipitation hardening grade developed by Armco Steel [6] that is higher in strength than 15-5PH and capable of excellent fracture toughness. In this work, a series of B-1B flap track forgings were manufactured, using the forging practice guidelines developed for 15-5PH as mentioned, with destructive specimens from these forgings heat treated per specifications to the H1000 temper. Results of these tests are outlined in Table 4.

These data suggest that the strength and fracture toughness of these relatively heavy section forgings have been optimized and readily meet minimum specification criteria. In developing final aging temperatures to employ for the test material and therefore the resultant machined parts, it was found that temperatures in the 538 to 549°C range (within heat treatment specification allowances) provided optimum final property combinations.

Heat/Corrosion-Resistant Alloys

Thermomechanical Processing of A286—Table 5 summarizes the tensile and fracture toughness results achieved with the forging process study of A286. This alloy is widely used in energy and gas turbine applications where optimum combinations of strength, toughness, corrosion resistance, and creep are sought. Thus, processes which optimize strength and toughness can be exploited. Graphical presentation of properties achieved in the solution treated and aged (STA) condition (a practice contained in current specifications), Fig. 4, suggests that

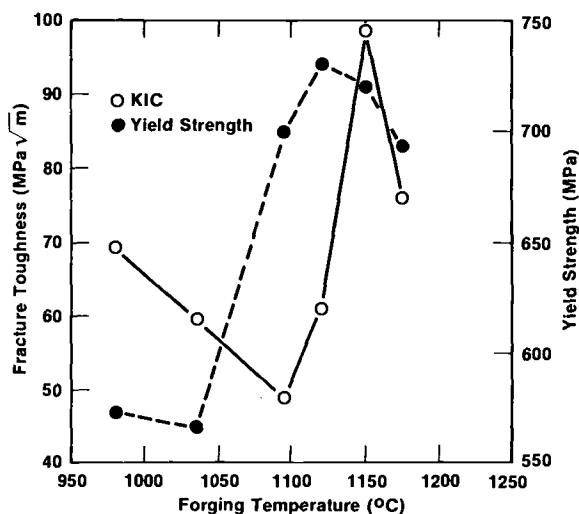


FIG. 4—Yield strength and fracture toughness versus forging temperature, alloy A-286STA.

strength and toughness can be optimized concurrently with forging in the 1125 to 1175°C range, a rather narrow forging processing range.

Structural evaluations of forgings processed under these conditions indicate that forging temperatures in the 980 to 1100°C range produce a very fine grain size, considerable substructure, and little discernible precipitate. As the forging temperature reached the 1100 to 1175°C range, grain size coarsened, substructure lessened, and precipitate size became larger. Finally, at temperatures over 1175°C, grain size did not coarsen significantly, substructure was, however, absent, and grain boundary precipitates were now in evidence. It thus appears that the moderate grain size, substructure, and precipitates found with forging in the 1100 to 1175°C region explain the good combinations of strength and fracture toughness and can be postulated to provide adequate creep and corrosion resistance. Tests on the latter are in progress.

Thermomechanical Processing of Inconel 625—Large Inconel 625 forgings have become of interest for power generation and nuclear applications where the higher strength of this alloy can provide lower weight and/or improved performance over Monel or other alloys in use. The challenge present in these forgings is to develop forging thermomechanical processes that provide minimum yield strength of 413 MPa in very heavy sections.

Hot-warm working of nickel base superalloys has been studied by others [7], in particular for Inconel 718, to develop fine-grained, high-strength materials with superior fatigue resistance. Other workers [8] have studied alternative annealing or aging treatment or both for Inconel 625. This alloy derives its strength from two mechanisms, solid solution strengthening from molybdenum and co-

lumbium additions, and, to a much lesser extent, γ' precipitation with low-temperature aging. Typically, single-step annealing treatments are employed to develop final properties and to maintain the facility to weld-machined components.

Table 6 summarizes the results of thermomechanical processing studies conducted with this alloy where both hot working and hot/warm working forging practices were employed, followed by single-step anneals and two-step anneal plus aging practices. Recognizing that the latter method is likely not to be desirable for components that will be welded, the data in Table 6 and Ref 8 suggest that significant strength improvements can be obtained with two-step treatments. Further, it also is evident from these tests that forging procedures which involve hot/warm working cycles will optimize final properties, but offer a significant challenge to the forger, for such warm working is conducted at considerably higher flow stresses and thus results in difficulty in achieving die fill on very large components.

Considering the opposing demands of forgeability, weldability, and strength, the results of this program indicate that the goal properties of 413 MPa minimum yield strength can be met by several routes, either hot-worked or hot/warm-worked and single-step annealing treatments in the 870 to 980°C range. These practices are currently being verified on production scale forging products.

Conclusions

1. In order to optimize ductility of ultra-high strength alloy steel HP310 forgings, tempering temperatures in the range of 315 to 343°C appear justifiable without sacrifice in high-strength criteria.

2. Alloy HP9Ni-4Co-0.20C forgings can be successfully thermomechanically processed to achieve excellent combinations of strength and fracture toughness in very heavy sections. Optimum tempering temperature appears to be in the range of 551 to 565°C for such heavy section parts.

3. Forgings manufactured in AF1410 may be successfully heat-treated by two cooling rates to achieve minimum ultimate strength of 1585 MPa and minimum fracture toughness of 143 MPa $\sqrt{\text{m}}$. While the slower air cooling rate meets properties and minimizes distortion, it does result in slightly lower mechanical properties.

4. Strength and fracture toughness of 15-5PH H900 does vary modestly with forging practice with the optimum achieved in the range of 1050 to 1150°C. A minimum fracture toughness of 60 MPa $\sqrt{\text{m}}$ appears supportable for 15-5PH H900 forgings.

5. Using forging process guidance developed on 15-5PH, large PH13-8Mo flap track forgings were successfully fabricated and met all property criteria. Optimum aging temperature for test material/final parts was found to be in the range of 538 to 549°C.

6. Strength and fracture toughness, and possibly creep, of A286 in the STA condition may be optimized with forging in the narrow range of 1125 to 1175°C.

7. In order to meet a minimum yield strength of 413 MPa in alloy Inconel 625, either hot-working or hot/warm-working procedures may be employed with single-step anneals in the 870 to 980°C range. Two-step anneal plus aging treatments increase yield strength by up to 50% over a single-step anneal but may not be practical for forgings that will be welded into final components.

APPENDIX

Nominal Compositions (Weight Percent) Alloys Used in This Study

1. HP310: C-0.42, Mn-0.75, Si-2.50, Cr-0.78, Ni-1.82, Mo-0.40, V-0.20, Fe-balance.
2. HP9Ni-4Co-0.20C: C-0.19, Mn-0.30, Ni-9.0, Cr-0.75, Mo-1.0, V-0.08, Co-4.50, Fe-balance.
3. AF1410: C-0.16, Cr-2.0, Ni-10.0, Co-14.0, Mo-1.0, Fe-balance.
4. 15-5PH: C-0.07 (Max), Mn-1.0 (Max), Si-1.0 (Max), Cr-14.75, Ni-4.50, Cu-3.50, Cb + Ta-0.30, Fe-balance.
5. PH13-8Mo: C-0.05 (Max), Cr-12.75, Ni-8.0, Al-1.12, Mo-2.25, Fe-balance.
6. A286: C-0.08 (Max), Mn-2.0 (Max), Si-1.0 (Max), Cr-14.75, Ni-25.5, Mo-1.25, Ti-2.12, Al-0.35 (Max), V-0.30, Fe-balance.
7. Inconel 625: C-0.10 (Max), Mn-0.50 (Max), Si-0.50 (Max), Cr-21.5, Mo-9.0, Fe-5.0 (Max), Co-1.0 (Max), Cb + Ta-3.65, Ni-balance.

References

- [1] Ault, R. T., "Development of an Improved Ultra-High Strength Steel for Forged Aircraft Components," Final Report, Contract F33615-69-C-1638, LVT (Republic) Steel, Cleveland, OH, Jan. 1971.
- [2] Kuhlman, G. W., Gurganus, T. B., and Perry, T. E., "Argon-Oxygen Refining Steelmaking Practice: The Pass-Through Effect on VAR Remelted Alloy Steel Forgings," *Electric Furnace Proceedings*, Vol. 38, ISS-AIME, 1980, 148.
- [3] "Technical Data Sheet HP9-4-20 Alloy Steel," 2369R-5M-574-G, LTV (Republic) Steel, Cleveland, OH, undated.
- [4] Black, H. L., Shiring, D., and Milavec, C., "Production Melting and Thermomechanical Processing of AF1410 Steel," Final Report Contract F33615-76-C-5026, Cytcomp, Bridgewater, PA, 1978 June.
- [5] "Armco 15-5PH Precipitation Hardening Stainless Steel Bar and Wire," Bulletin S-21a, Armco Steel Corp., Baltimore, MD, undated.
- [6] "Armco PH13-8Mo Precipitation Hardening Stainless Steel Bar, Wire and Forging Stock," Bulletin S-33d, Armco Steel Corp., Baltimore, MD, undated.
- [7] Brown, E. E. and Boettner, R. C., "Processing of Nickel-Base Alloys for Improved Fatigue Properties," U.S. Patent No. 3,660,177, May 1972.
- [8] "The Effect of Intermediate Aging on the Final Aging Response of Inconel Alloy 625," Huntington Alloys, Inc., Huntington, WV, undated.

DISCUSSION

*E. G. Nisbett*¹ (written discussion)—In dealing with the HP310 forging which was double-tempered, you mention stress relieving the tension specimen at least

¹ National Forge Co., Irvine, PA 16329.

10°C (18°F) below the final tempering temperature. Is this a simulation of a stress-relieving cycle which the component would be given after machining and prior to use? If so, since the stress-relieving temperature could be close to the final tempering temperature, and bearing in mind the temperature tolerance on a production furnace, is a control tension test sample normally run with the part?

G. W. Kuhlman (author's closure)—This question refers to stress relieving of HP310 tension specimens at least 10°C (18°F) below the final tempering temperature and whether it was a simulation of the stress-relieving cycle that might be applied to a component. The post-machining stress relieving employed on tension specimens was not necessarily in simulation of processing components but was employed instead to ensure that all stresses that might have been induced during specimen preparation were removed and had no influence on mechanical properties measured. HP310 forgings are normally supplied in a premachining normalized/subcritical annealed condition, and we understand that our customers, who then machine the forgings and heat-treat them to their final hardness, do process with each lot or each part in the case of critical parts tension test samples excised from forging prolongations in order to assure that parts have been properly heat-treated, including, if necessary, stress-relieving of finish-machined parts after all machining is complete.

W. Childs² (written discussion)—The author mentioned that an extensive grain boundary precipitate was present in alloy A286 forged at temperatures in excess of 1175°C, and that some lesser amount was present in material forged in the 1125 to 1150°C range.

I would like to know how extensive the precipitate was and what form it took. Film? Solid or discontinuous? Or a chain of globular precipitates? Also how was the evaluation done? Optically? Scanning electron microscope (SEM)? Etched or unetched?

G. W. Kuhlman (author's closure)—This question has to do with the extent and form of grain boundary precipitate found in A286 as a function of the forging process conditions and methods used to evaluate the nature of the precipitate. On the latter, both optimal and SEM techniques were employed, predominately etched, but some unetched. The etchant employed was 30 mL hydrochloric acid (HCl), 20 mL nitric acid (HNO₃), and 20 mL acetic acid. Predominately, the precipitate was globular in form and discontinuous in nature; however, at very high forging temperatures, the precipitate tended to become continuous and even filmlike in nature. Frequently, the globular precipitate at the grain boundary would suggest a chainlike structure; however, this condition was certainly not prevalent. Subsequently, we have completed some creep and stress rupture testing of A286 forged under the conditions noted in the paper, and our findings are

² Turbodyne Division, Dresser Industries, Inc., Wellsville, NY 14895.

that some grain boundary precipitate, globular in form, as was noted with forging in the 1125 to 1175°C range, yielded the optimum elevated temperature properties. We found inadequate stress-rupture when the grain boundary precipitates became excessive, that is, chainlike or films, as noted with forging temperatures over 1175°C. We also found a tendency for marginal creep results when grain boundary precipitates were totally absent, as was noted with very low forging temperatures.

Pressure Vessel and Nuclear Forgings

*Forging Processing for Pressure Vessel
and Nuclear Application*

Application of New Types of Ingots to the Manufacturing of Heavy Pressure Vessel Forgings

REFERENCE: Bocquet, P. G., Saint-Ignan, J. C., and Blondeau, R. P., “Application of New Types of Ingots to the Manufacturing of Heavy Pressure Vessel Forgings,” *Steel Forgings, ASTM STP 903*, E. G. Nisbett, and A. S. Melilli, Eds., American Society for Testing and Materials, Philadelphia, 1986, pp. 367–384.

ABSTRACT: Forging components for pressure vessels issued from conventional ingots may present some inconveniences, such as an important waste of metal and metallurgical problems induced by segregation.

Le Creusot Heavy Forge has developed three new types of ingots specially adapted to these components:

Type 1. Ingots with vertical-oriented solidification and low height/diameter ratio for manufacturing flat components.

Type 2. Ingots with horizontal-oriented solidification for manufacturing hollow forgings with a noncladded inner surface.

Type 3. Cylindrical hollow ingots for hollow forgings, the inner face of which has to be cladded.

The mode of solidification and the location of macrosegregation areas of each new ingot type are described.

Three examples of components manufactured from these new ingot types are presented:

1. A head for a 1300-MW pressurized water reactor (PWR) pressure vessel forged from a Type 1 ingot.
2. A prototype shell forging in 2¼Cr-1Mo steel for the petrochemical industry issued from a Type 2 ingot.
3. A B shell for a 1400-MW French nuclear reactor issued from a hollow ingot.

KEY WORDS: low-alloyed steel, solidification, segregation, mechanical properties, ingot, forging, pressure vessel, nuclear material

¹ Metallurgical engineer, Le Creusot Materials Research Center, Creusot-Loire Industrie, Le Creusot, France.

² Production manager, Le Creusot Heavy Forge, Creusot-Loire Industrie, Le Creusot, France.

Pressure vessels are principally made from hollow cylindrical components (like shells, nozzles, rings, flanges, etc.), flat parts (like the tube sheet of heat exchangers), and hot-formed parts (that is, top and bottom heads).

The 1300-MW pressurized water reactor (PWR) pressure vessel used in the French nuclear program is a typical example in which all components are forged parts.

The internal surface of the components is clad in two layers by stainless steel. Parts then are joined together by submerged arc welding.

In this case, the reason for the choice of forgings for shells is for the avoidance of longitudinal welds because they are more sensitive than the base metal to radiation embrittlement and also because welds need a costly in-service inspection.

Manufacturing of Forgings with Conventional Ingots

The distribution of segregation areas of a core shell made from a conventional 152-metric ton ingot, with a typical forging sequence like: (a) cogging and cutting extremities, (b) upsetting and hot piercing, (c) drawing on mandrel, and (d) expanding on mandrel, is illustrated in Fig. 1.

Areas with major carbon segregation (positive and negative) and an important number of Type A segregates can be noted on the internal surface.

Such a manufacturing sequence presents some inconveniences:

1. Their shape and geometry lead to an important waste of material and to complex forging sequences, increasing the cost.
2. The location of segregation areas can eventually lead to welding defects (that is, underclad cracking [1]) or to insufficient quality during service life (that is, the disbonding phenomenon of hydrocrackers [2]).

Development of New Ingots

Le Creusot Heavy Forge has studied and developed new ingots with shapes specially adapted to flat (and hot-formed) components and to hollow cylindrical forgings.

The aim of these studies was to achieve:

1. The elimination or the reduction of segregation areas or their location in less critical zones in order to improve welding facilities.
2. A better material quality (cleanness, homogeneity).
3. A simplified forging sequence.
4. A reduction of metal loss.

The solidification conditions have been simulated with a computer; pouring parameters have been optimized from tests on liquid steel fluid flow (simulated

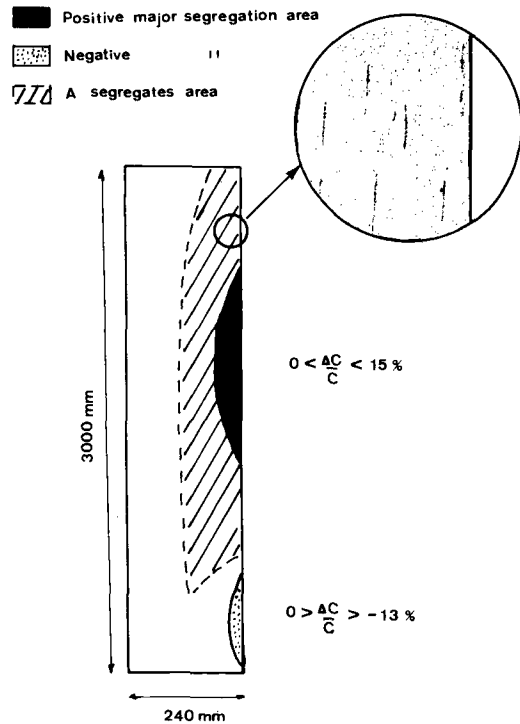


FIG. 1—Location of segregated areas in a shell made from a conventional ingot.

with an hydraulic model); and small-scale and full-scale ingots have been poured and investigated.

This work has allowed the selection of three new types of ingots:

1. Ingots with vertical-oriented solidification and very low height/diameter ratio for manufacturing flat components.
2. Ingots with horizontal-oriented solidification and "high" height/diameter ratio for manufacturing hollow forgings with a noncladded inner surface.
3. Cylindrical hollow ingots for hollow forgings, the internal surface of which has to be cladded.

Each type of ingot is patented [3–5].

For simplification, the ingots will be called:

1. Short LSD, for the first type.
2. Long LSD, for the second type.
3. Hollow ingot, for the third type.

LSD is from the French *Lingot à Solidification Dirigée*, whose meaning is oriented solidification ingot.

Solidification Modes of New Ingots

Short LSD

As shown in Fig. 2, the mode of solidification of "short LSD" is to get the maximum of heat extraction through the bottom cast-iron plate and the better thermal insulation of the top of the ingot. On this figure, arrows indicate the solidification direction. With our system, these conditions are obtained for H/D ratios up to 0.8.

The positive macrosegregation area is located on the upper surface. Near the axis of the ingot, the depth of the segregation zone where $\Delta C/C$ exceeds 20% is about 20% of the total height of the ingot.

Type A segregates show a little extension.

Long LSD

The device for "long LSD" is quite similar, but, in this case, the heat extraction is made mainly through the cylindrical wall of the cast-iron mold. So, the solidification direction is essentially horizontal (see arrows on Fig. 3). H/D is between 0.8 and 1.3.

In the axial part of the ingot, an important shrinkage cavity develops, with a V-shaped area of positive macrosegregation. The extension of Type A segregates

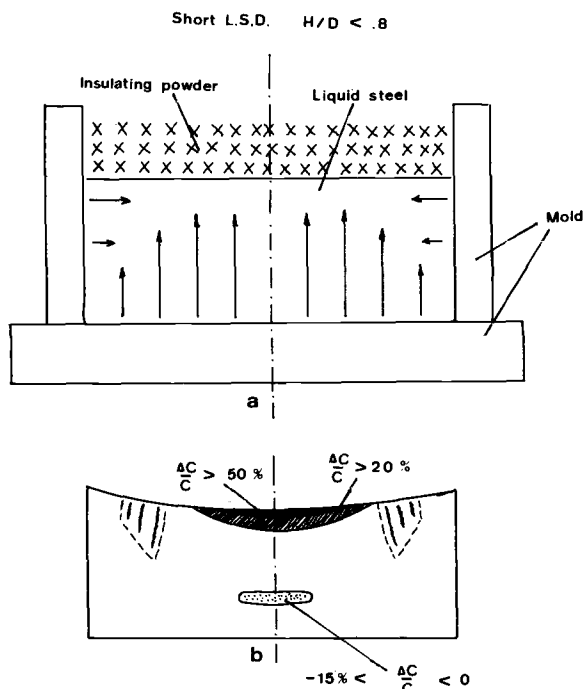


FIG. 2—Short LSD ingot type: (a) mode of solidification; (b) location of segregated areas.

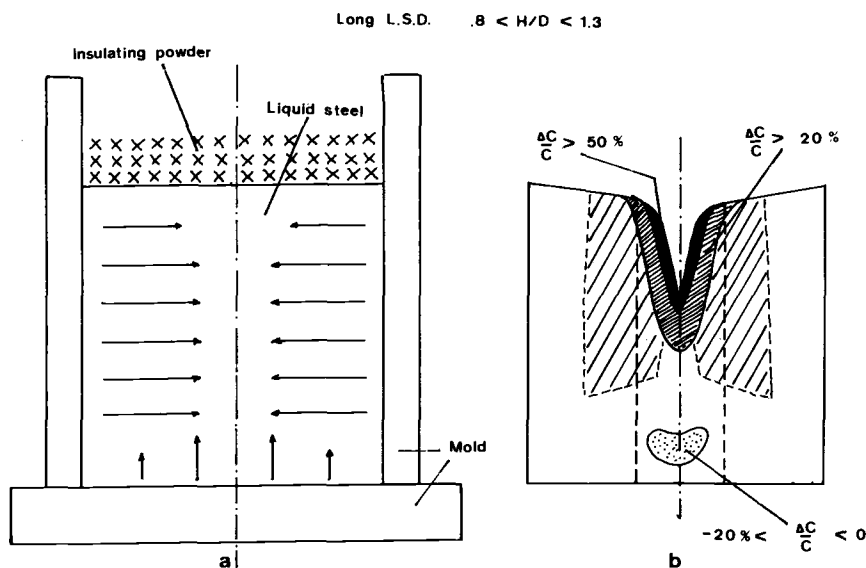


FIG. 3—Long LSD ingot type: (a) mode of solidification; (b) location of segregated areas.

appears quite similar to that of a conventional ingot. Most of macrosegregation is eliminated by piercing.

Hollow Ingot

To obtain solidification very close to the midthickness of a hollow ingot (Fig. 4), a system has been designed and realized giving a symmetric extraction of heat through the outside cast-iron mold and through the inside mandrel.

Hollow ingots made by this process weigh up to 186 metric tons, with 3460 mm of external diameter and 1300 mm of internal diameter.

The distribution of segregation areas in a cross section is very similar to a similar cross section from parallelepipedic ingots used to make heavy plates.

Manufacturing of Nuclear Reactor Heads from Short LSD Ingots

The fabrication of heads (cover dome and bottom dome) for the 1300-MW PWR pressure vessel is an example of components made with the short LSD ingot.

All forgings of French nuclear reactors are made of 16 MND5 steel grade according to A 508 Class 3.

The manufacturing sequence of these parts is as follows:

1. Melting in an electric arc furnace.
2. Refining and degassing in a heating ladle (vacuum arc degassing process).
3. Bottom pouring of a 63-ton short LSD ingot: $H = 1200$ mm; $D = 3100$ mm; and $H/D = 0.4$.

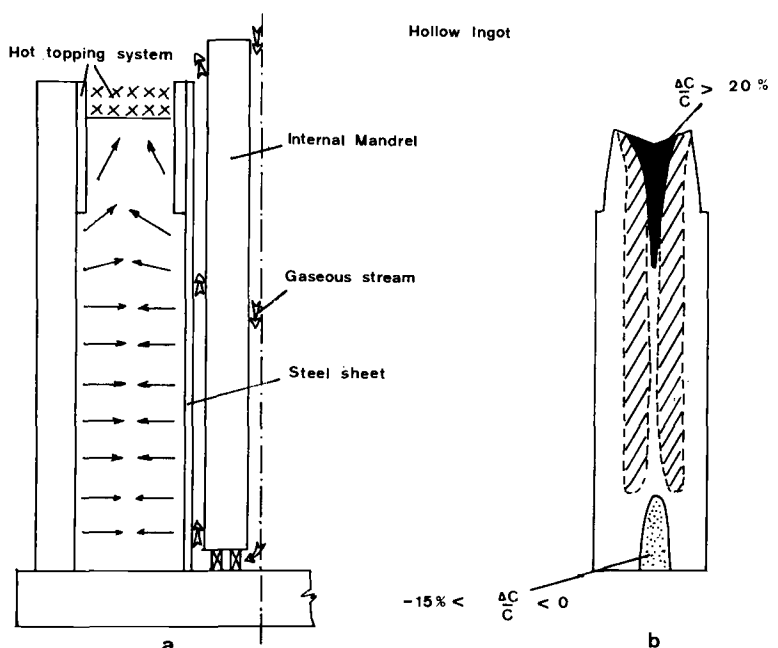


FIG. 4—Cylindrical hollow ingot: (a) mode of solidification; (b) location of segregated areas.

4. Forging by direct upsetting of the ingot to get a disk: $H = 295$ mm and $D = 5380$ mm.
5. Dehydrogenation heat treatment and nondestructive testing.
6. Rough machining.
7. Hot forming to a spherical shape: $D = 4600$ mm; thickness = 235 mm.
8. Quality heat treatment (875°C ; water quenching and tempering at 645°C air cooling).
9. Mechanical testing.
10. Final machining.
11. Final nondestructive testing.

It will be noted that the manufacturing of such forgings from a conventional ingot would need a 90-metric ton ingot. Short LSD saves about 30% of metal weight in this application.

In view of the qualification for nuclear applications, metallurgical investigations have been performed on a full-scale prototype forging.

Heat composition is as follows (weight percent):

C	S	P	Si	Mn	Ni	Cr	Mo	Cu	Sn	Al
0.16	0.004	0.011	0.21	1.31	0.73	0.20	0.48	0.06	0.005	0.018

Chemical analyses and macroscopic investigations show that most macrosegregation areas have been removed from the part by forging. Location and intensity of major segregation are shown in Fig. 5.

Except in the top zone of the external surface—corresponding to the top axial zone of the ingot—where macrosegregation gives higher strength and lower toughness, a very good mechanical homogeneity can be noted. All values satisfy the specification.

Up to now, Le Creusot Heavy Forge has delivered 30 heads (top and bottom) for 1300-MW nuclear reactors.

With this type of ingot, other forgings like tubesheets for heat exchangers and channel heads for steam generators, etc. have been successfully manufactured.

Manufacturing a Prototype Shell of SA 336 F22 Steel Grade from Long LSD Ingot

For the petrochemical industry, forging suppliers have to provide thick-wall shells with an excellent combination of strength and toughness and a low susceptibility to temper embrittlement. In order to give better information on 2¼Cr-1Mo steel performances, an important study has been conducted on a prototype shell manufactured from a long LSD ingot.

The manufacturing sequence is:

1. Melting in an electric arc furnace.
2. Refining and degassing in a heating ladle [Vacuum Arc Degassing (VAD) process].

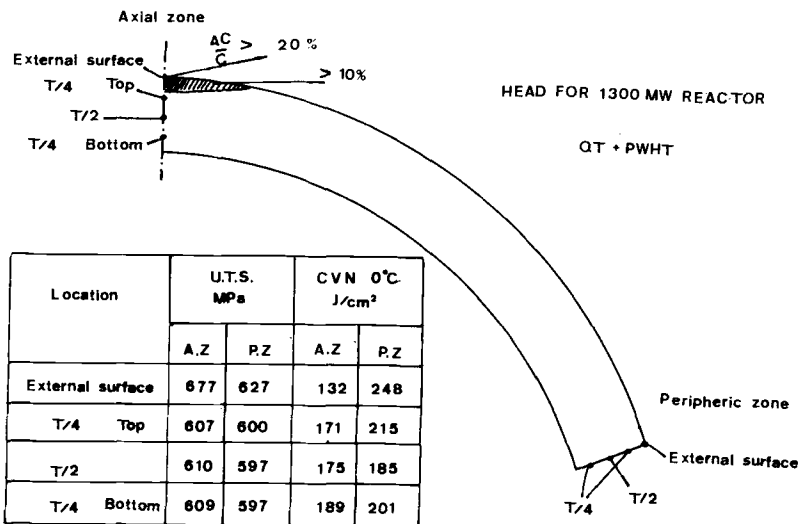


FIG. 5—Head for 1300-MW reactor (short LSD): location of segregated areas and mechanical properties.

3. Bottom pouring of a 60 ton, long LSD ingot: $H = 2350$ mm; $D = 2100$ mm; and $H/D = 1.1$.

4. Heat analysis (weight percent):

C	S	P	Si	Mn	Ni	Cr	Mo	Cu	Sn	As	Sb, ppm
0.13	0.005	0.006	0.13	0.61	0.22	2.30	0.93	0.095	0.006	0.011	5

5. The prototype shell has been forged at the top extremity of a thinner tube with the following simplified sequence:

- (a) hot piercing of the ingot
- (b) drawing on mandrel
- (c) expanding on mandrel

The rough forging dimensions are:

	Prototype Shell	Tube
Length, mm	1000	9140
Inner diameter, mm	980	980
Outer diameter, mm	1790	1250
Thickness, mm	405	135

- 6. Dehydrogenation heat treatment.
- 7. Nondestructive testing.
- 8. Cutting the prototype shell.
- 9. Quality heat treatment: 950°C ; water quenching and tempering at 650°C /12 h air cooling.
- 10. Cutting a test ring (Fig. 6).

The chemical homogeneity of the test ring at three locations (inner and outer $T/4$ – $T/2$) is very good (Table 1).

The microstructure (Fig. 7) is composed mainly of bainite, with some grains of ferrite at $T/4$ and about 10% ferrite at $T/2$. The austenitic grain size is $G = 5$.

Mechanical properties (Table 2) have been determined after simulated post weld heat treatment (PWHT) of 12 h at 690°C with cooling at $10^{\circ}\text{C}/\text{h}$. Charpy V-notch impact tests have been performed after PWHT and after PWHT plus step cooling heat treatment ($593^{\circ}\text{C}/1$ h + $538^{\circ}\text{C}/15$ h + $524^{\circ}\text{C}/24$ h + $496^{\circ}\text{C}/48$ h + $468^{\circ}\text{C}/72$ h).

Tensile properties present a very good homogeneity. The little amount of ferrite

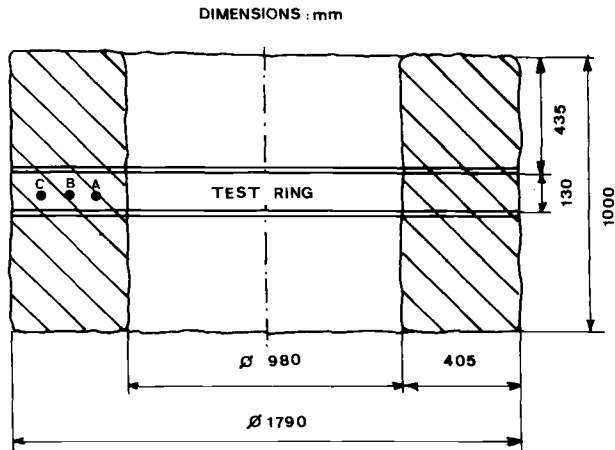


FIG. 6—Prototype shell forging in $2\frac{1}{4}\text{Cr}-1\text{Mo}$ steel (long LSD): forging dimensions and testing location.

at T/2 induces a slight decrease of Charpy V-notch impact properties versus T/4.

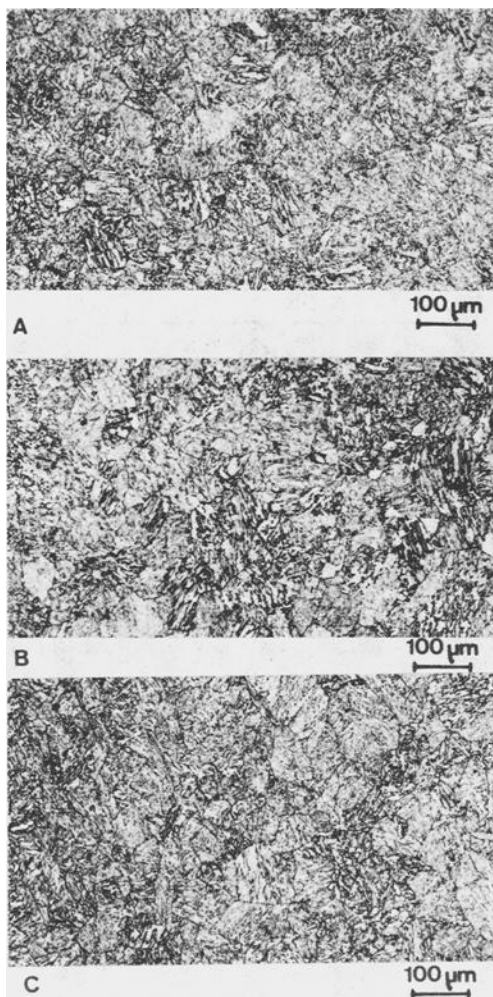
The very low impurities level of steel induces a very low embrittlement after step cooling:

1. Bruscato's parameter is $X = (10 P + 5 \text{ Sb} + 4 \text{ Sn} + \text{As})/100 = 9.75$.
2. J factor is $J = (\text{Mn} + \text{Si}) (P + \text{Sn}) \cdot 10^4 = 89$.

The metal savings comparatively for a conventional ingot is about 10%.

TABLE 1—Prototype shell in SA 336 F22 steel (chemical analysis, weight %).

	Location		
	A. T/4 Inside	B. T/2	C. T/4 Outside
C	0.135	0.132	0.136
S	0.005	0.005	0.006
P	0.006	0.006	0.007
Si	0.115	0.112	0.135
Mn	0.640	0.630	0.610
Ni	0.231	0.229	0.220
Cr	2.352	2.240	2.240
Mo	0.961	0.958	0.940
Cu	0.107	0.105	0.105
Sn	0.010	0.009	0.009
As	0.011	0.011	0.011
Sb, ppm	8	5	4



T/4 INSIDE

G.S = 5

FERRITE : 2/3 %

T/2

G.S = 5

FERRITE : 10 %

T/4 OUTSIDE

G.S = 5

FERRITE : < 1 %

FIG. 7—Prototype shell forging in 2 1/4Cr-1Mo steel: microstructure at different location.

TABLE 2.—*2 1/4Cr-1Mo steel prototype shell forging, tensile and Charpy V-notch impact properties.*

Location	Axial Direction					Tangential Direction				
	YS, MPa	TS, MPa	EL, %	RA, %	CVN, -7°C, J	CVN, -40°C, J	CVN, 0°C, J	FATT, °C	TK 40 ft.lb, °C	
T/4 INNER	476	610	23.2	79	247	148	226	-38 (SC -34)	-54 (SC -48)	
T/2	477	607	22.7	79	269	123	188	-29 (SC -21)	-54 (SC -48)	

NOTE: All results after PWHT except SC = PWHT plus step cooling. YS = tensile strength; TS = tensile strength; EL = elongation; RA = reduction in area; CVN = Charpy V-notch; FATT = fracture appearance transition temperature; TK = temperature at which impact energy is 54 J (40 ft.lb); SC = step cooling. Conversion factor: 1 ft.lb = 1.356 J.

Manufacturing a Shell for a Nuclear Reactor from a Hollow Ingot

The qualification of the hollow ingot for manufacturing the shells of French new 1400-MW PWR pressure vessels has led to the manufacture of a full-size B shell and two test rings of SA 508 Class 3 steel grade.

The manufacturing sequence has been:

1. Melting in an electric arc furnace.
2. Refining and degassing in a heating ladle (VAD).
3. Bottom pouring of a 186-ton, hollow ingot type:
 - (a) outer diameter = 3460 mm
 - (b) inner diameter = 1300 mm
 - (c) height of body = 2790 mm
4. Forging by drawing and expanding on the mandrel to the rough forging size:
 - (a) outer diameter = 5100 mm
 - (b) inner diameter = 4340 mm
 - (c) thickness = 380 mm
 - (d) height = 2870 mm
5. Dehydrogenation heat treatment.
6. Nondestructive testing.
7. Quality heat treatment: 875°C; water quenching and tempering at 640°C air cooling.
8. Nondestructive testing.
9. Cutting test rings.
10. Determination of mechanical properties.
11. Final machining.

The manufacturing of such forgings from a conventional ingot would need a 205-ton ingot. The metal savings from a hollow ingot is slightly lower than 10%.

Investigations have been conducted in test rings (located at the top and bottom extremities of the ingot) and in the nozzle cutout (Fig. 8). Some sulfur prints have been performed on the delivered part itself.

Chemical Properties

Heat analysis (weight percent):

C	S	P	Si	Mn	Ni	Cr	Mo	Cu	Sn	Al
0.154	0.0016	0.0047	0.203	1.380	0.731	0.164	0.502	0.061	0.006	0.013

Chemical analyses and sulfur prints have been made in different locations in order to evaluate the chemical homogeneity of the forging.

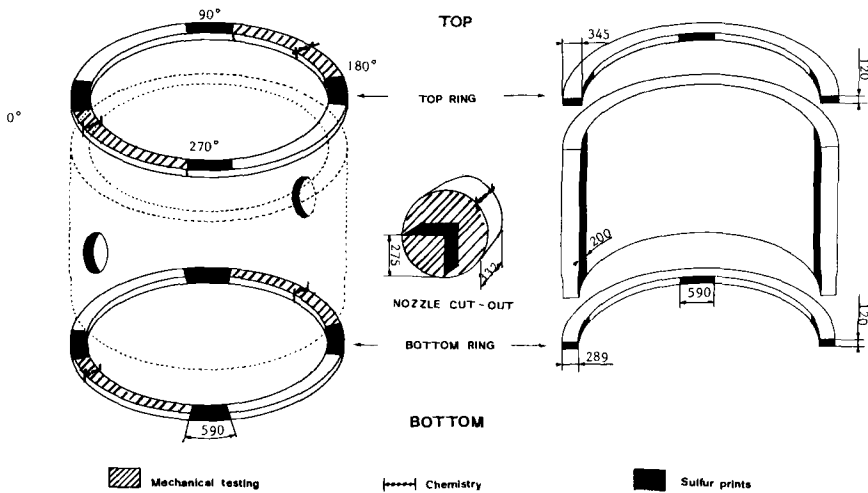


FIG. 8—Shell and test rings manufactured from hollow ingot: location of investigated zones.

An example of a sulfur print realized on the upper test ring cross section (Fig. 9) shows the location of Type A segregates in the wall. No Type A segregates have been observed on the sulfur prints performed on the inner face of the shell.

Another illustration of the location of Type A segregates is given by the macroetching of the cross section of a nozzle cutout (Fig. 10). It is clear that Type A segregates do not affect the inner face of the shell.

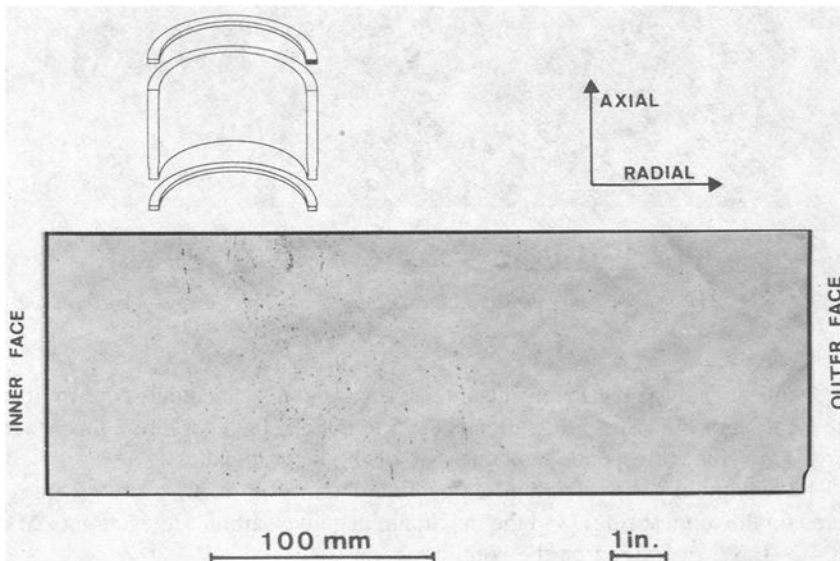


FIG. 9—Shell made from hollow ingot. Sulfur print on top test ring cross section.

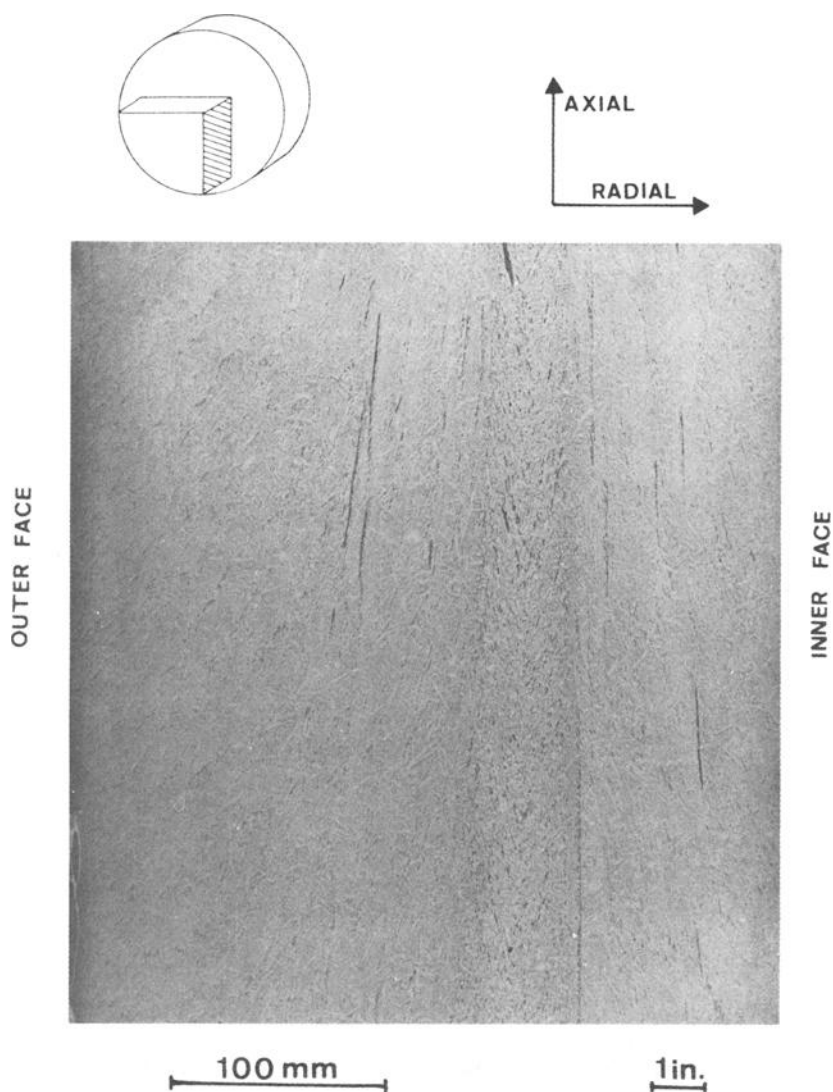


FIG. 10—Shell made from hollow ingot. Macroscopic aspect of a cross section of nozzle cutout.

Chemical analysis measurements on test rings and nozzle cutouts confirm that the location of the last solidification is at 25 to 30% of thickness from inner face (Fig. 11). This corresponds to about 47% of the ingot thickness.

The maximum positive carbon segregation obtained is $\Delta C/C = 29.9\%$ (measured on the top test ring), and the maximum negative carbon segregation is $\Delta C/C = -6.5\%$ (measured on the bottom test ring).

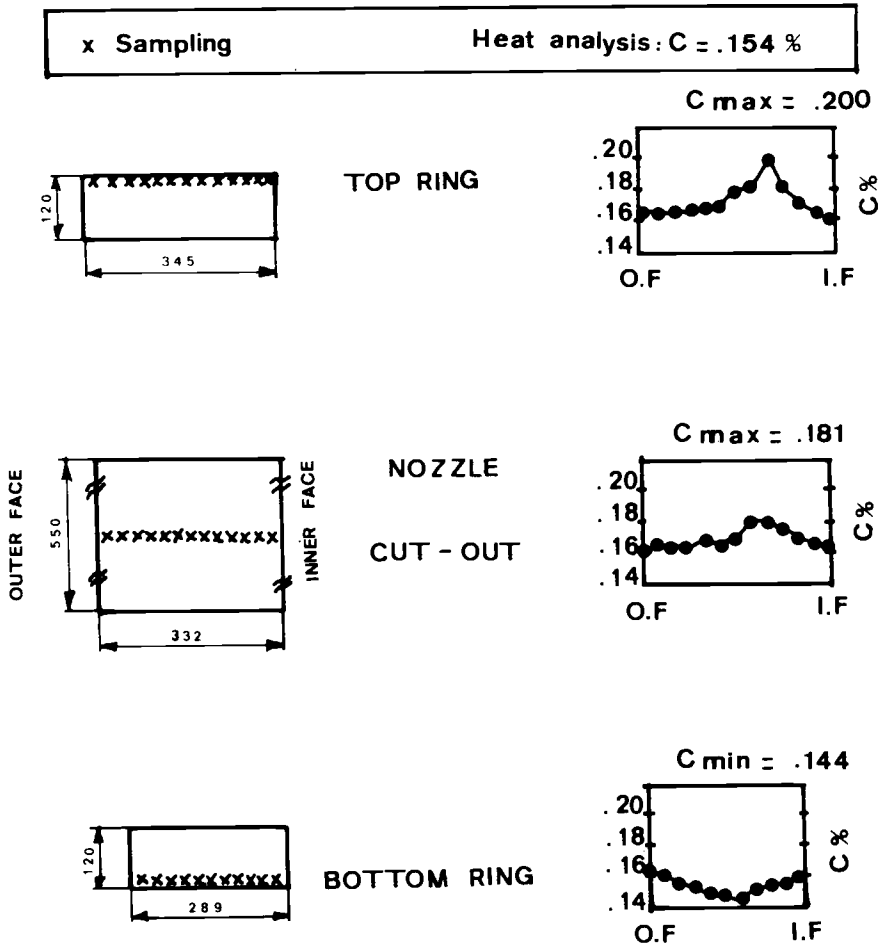


FIG. 11—Chemical analyses in rings and shell made from hollow ingot (SA 508 Class 3 steel).

Mechanical Testing

Mechanical tests (tensile and Charpy V-notch impact) have been performed on test samples in the as-quenched and tempered mode (QT) and as QT + PWHT conditions (PWHT = 615°C/16 h, cooling at 30°C/h). Samples have been taken in different regions (inner and outer surfaces T/4-T/2 of the test rings and the nozzle cutout) and orientations (tangential, axial, and radial).

The results of tensile and Charpy V-notch impact tests are given in Figs. 12 and 13.

All values satisfy the specifications of the French Nuclear Code (RCC.M).

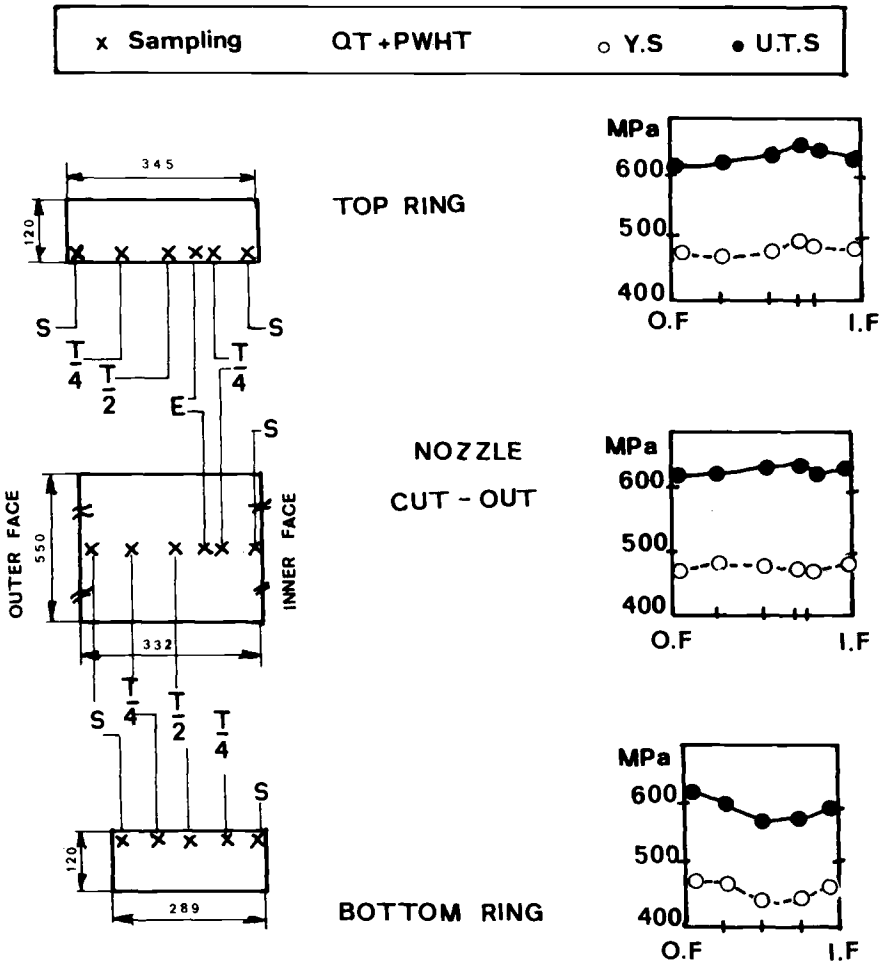


FIG. 12—Tension tests in rings and shell made from hollow ingot (SA 508 Class 3 steel).

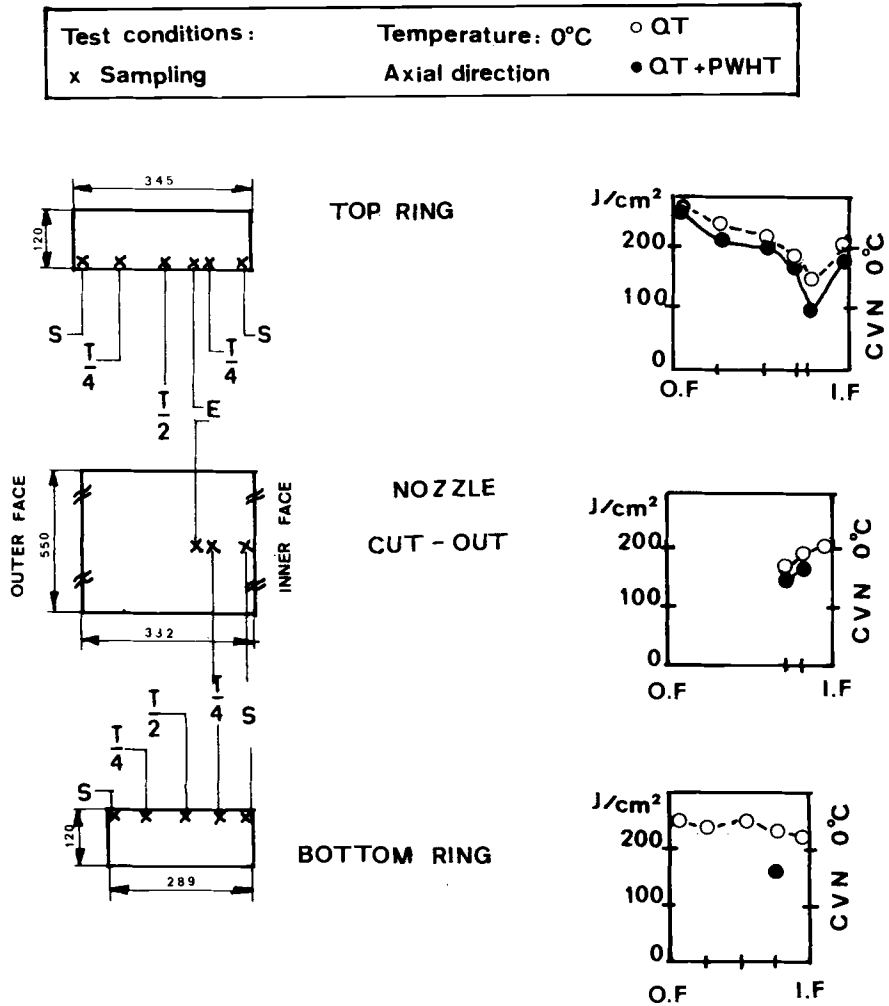


FIG. 13—Charpy V-notch impact tests in rings and shell made from hollow ingot (SA 508 Class 3 steel).

Conclusion

The examples show that the main purposes of the development of new ingots have been reached.

On many points (chemical segregation, mechanical properties, weldability), the components forged from these types of ingots have a better, or at least equivalent, quality than that of conventional forgings.

The forging sequences generally are simplified, and the waste of metal is, in many cases, reduced.

The experience of Le Creusot Heavy Forge with these new ingots is now very large.

Since the beginning of the development to April 1984, the number of forgings made from these ingots is:

1. Two hundred and ninety-five components issued from 239 LSD (short or long) ingots, which provide 14 470 tons of liquid steel or more.
2. Twenty components issued from 17 hollow ingots, corresponding to 2105 tons.

The possibilities offered by these ingots are very large, and the choice of the ingot type for a component may be optimized according to the requirements of the user and the manufacturer.

References

- [1] Fondeviole, M. and Vignes, A., "Technology of Joining the Dissimilar Metals Austenitic Stainless Steel or Ni.Cr.Fe Alloy to 20 M5M or 16 MND5 Steel," Report No. 75, *Welding in Nuclear Engineering*, German Welding Institute, Aachen, Germany, Nov. 1982, pp. 182-189.
- [2] Blondeau, R., Pressouyre, G. M., Cheviet, A., Berthet, J. A., Duranseaude, J. M., "Contribution to a solution to the Disbonding Problem in 2¼Cr-1Mo Heavy Wall Reactors," in *Proceedings*, First International Conference on Current Solutions to Hydrogen Problems in Steels, Washington, DC, Nov. 1982, American Society for Metals, Metals Park, Ohio, p. 356-360.
- [3] French patent—78-23063, 4 Aug. 1978.
- [4] French patent—79-09985, 20 April 1979.
- [5] French patent—82.06475, 15 April 1982.

Integral Forged Pump Casing for the Primary Coolant Circuit of a Nuclear Reactor: Development in Design, Forging Technology, and Material

REFERENCE: Austel, W. and Körbe, H., "Integral Forged Pump Casing for the Primary Coolant Circuit of a Nuclear Reactor: Development in Design, Forging Technology, and Material," *Steel Forgings, ASTM STP 903*, E. G. Nisbett and A. S. McIlilli, Eds., American Society for Testing and Materials, Philadelphia, 1986, pp. 385–397.

ABSTRACT: Developments in the forging of large casings for primary circuit coolant pumps for light water reactors in Germany are demonstrated beginning with the multiple forging fabricated version and ending with the integral forged type. This version is the result of the joint efforts of the pump manufacturer and the forgemaster after a cost-gain evaluation and represents an optimum solution in view of its functional and economical performance and also considering the high requirements for mechanical-technological properties, including homogeneity of the material. The development from 22 NiMoCr 3 7/A 508 Class 2 to 20 MnMoNi 5 5/A 508 Class 3 and their optimization will be demonstrated. This development is based mainly on minimizing the sulfur content and on vacuum carbon deoxidation (VCD), which results in a reduction of the A-segregations, in improving fracture toughness and isotropy, and in the desired fine-grain structure.

KEY WORDS: castings for reactor primary coolant pumps; forged/welded version; integral forged version; reactor pressure vessel steels; segregations; vacuum carbon deoxidation (VCD); fracture toughness; mechanical properties; isotropy

Primary coolant pumps are located in the primary coolant circuit of light water or heavy water reactors, providing for a forced circulation of the coolant. Placed either inside or outside the reactor pressure vessel, they are subject to quite the same rigorous design criteria as applicable to the reactor pressure vessel itself.

Initially, large pump casings for light water reactors were made from austenitic steel castings in Germany. However, the calculated load limited their application to the boiling water reactor type; high design pressures in the range found in pressurized water reactors would lead to wall thicknesses, conflicting with the physical properties of the austenitic structure. Moreover, the 100% volumetric

¹ Managers, Schmiedewerke, Krupp-Klöckner, GMBH, 4500 Osnabrück, West Germany.

radiographic examination raised considerable problems with wall thicknesses up to 500 mm.

In 1964, pump casings for the Obrigheim and Stade nuclear power stations were designed from the forging material 22 NiMoCr 3 7, which is similar to ASTM A 508 Class 2, and manufactured by Klöckner-Werke in Osnabrück. The inner surface of these casings was protected by a corrosion-resisting austenitic weld cladding. The casings were cup-shaped and joined by welding from five separately forged items (Fig. 1). This method was introduced, among others, during the International Forging Symposium in Terni, Italy in 1970.

Whereas for Obrigheim and Stade the discharge output of a coolant pump was some 15 000 m³/h at an engine performance of about 2400 kW, the primary coolant pumps for the Biblis A power station, a 1150 megawatt electrical plant, were designed for a discharge output of 24 000 m³/h, requiring an engine performance of 8000 kW. A ball-shaped casing, made from four separate forgings, was chosen to solve the task.

The demand of the power plant manufacturers and inspection authorities for a periodic ultrasonic in-service inspection of all weldments within the primary circuit led to an initial reduction of the number of weld seams and then to a total abolition of weldments later.

The two-part casing without discharge nozzle was manufactured by our company by the so-called "tandem method." A hollow cylinder of ample size, made from a 250-ton rough ingot, was reduced by forging centrally and at its ends, thus forming two casings in one. A total of eight pump casings were forged by this method in 1977–1978.

During very intense and repeated discussions between the pump manufacturer and forging experts, including a cost-gain evaluation, the pump casing, especially its outer contour, was optimized, so in 1980 we started the production of the one-part casing with an integrally forged discharge nozzle, intended for service in several German nuclear power stations. This type of casing will be reviewed

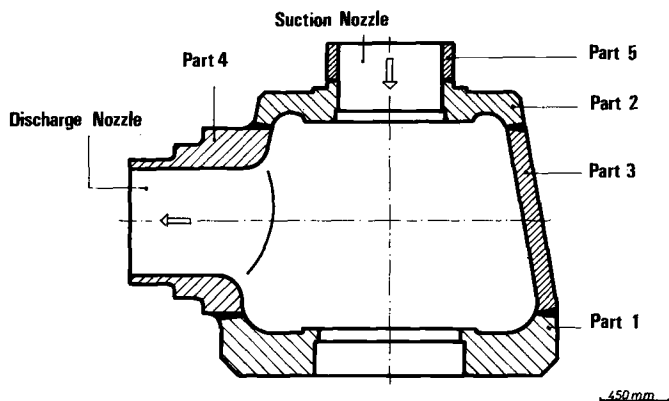


FIG. 1—A five-part primary circuit coolant pump casing (RCP).

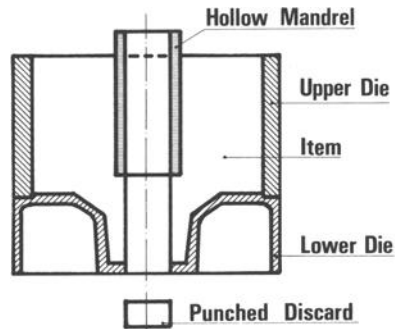


FIG. 2—A two-part forging die.

in detail in following paragraphs. The number of sampling locations and the amount of testing material were reduced to an economical, however acceptable, level. The outer contour of this casing was approved by power plant manufacturers and inspection authorities.

In order to create an as-forged shape as near as possible to the final shape, a special tool is used, consisting of an upper and a lower part (Fig. 2). The forging is made from an 135-ton octagonal rough ingot (Fig. 3a).

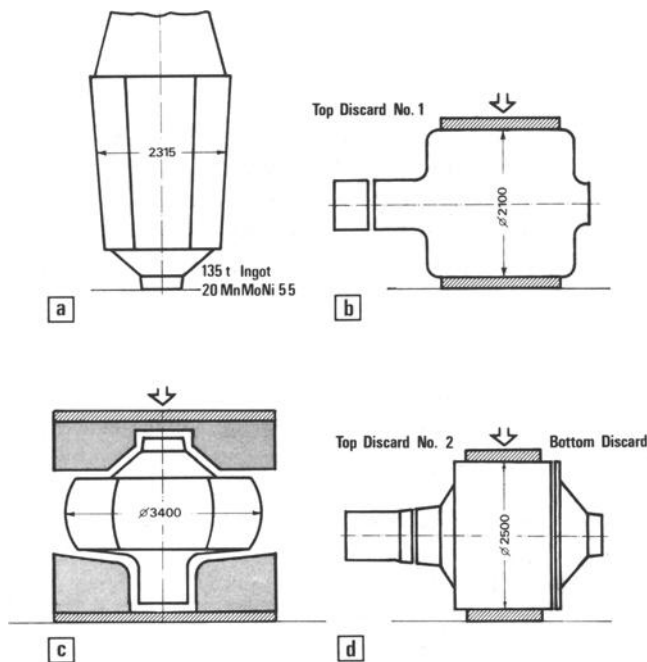


FIG. 3.—The stages of an open die forging: (a) 135-ton rough ingot; (b) forging to cylindrical shape; (c) upsetting operation; and (d) forging to shape prior to die forging.

At a temperature of about 650°C, the rough ingot is transferred from the electric steel plant to the forging shop, where it is equalized in a natural-gas-fired bogie hearth furnace at a temperature of about 600°C for 12 h, followed by a heating-up period to a temperature of approximately 1250°C, that is, to forging temperature. After a soaking time of another 24 h, the ingot is forged to a cylindrical shape, with the ingot top formed into a plug, necessary for the following upsetting operation. Surplus material, the so-called Top Discard No. 1, is discarded (Fig. 3*b*).

After that, the ingot is reheated and, after another soaking period of about 24 h, upset as a solid piece (Fig. 3*c*). Forging to shape commences after a third reheating. During this operation, the remainder of the ingot top, the Top Discard No. 2, is cut off along with the bottom discard (Fig. 3*d*). The final shape is reached by die-forging the blank into the two-part die, mentioned previously. Finally, a central core is punched out, using a hollow mandrel, while the pump casing is still in the die (Fig. 2).

All forging operations are performed on a 75/90-MN water hydraulic, three-cylinder press. Figure 4 shows the ready forging when it is removed from the lower die prior to the diffusion and soft annealing treatment.

This so-called “post-forge annealing” is intended to diminish the residual hydrogen content by diffusion to a degree that avoids the formation of flakes and segregation-induced cracks; it is also intended to create a favorable structure for the forthcoming machining operations and quenching and tempering treatment.

In Fig. 5, one can see the cooled down forging on the marking table, being prepared for the following machining process. The outer and inner contour is cut on a vertical boring mill, while the discharge nozzle is faced on using a boring and milling machine. However, the discharge nozzle core is not trepanned out at that time, since after quenching and tempering this core delivers the material for the production of weld test plates required for each pump casing.

The quenching and tempering treatment is performed in the prefinal-machined state. For the material 20 MnMoNi 5 5, which is similar to ASTM A 508 Class 3, the heat treatment consists of water quenching from a furnace temperature range of approximately 900 through 920°C, followed by a tempering treatment at approximately 640 through 660°C.

The attainment of the required mechanical properties and their uniformity, especially of the tensile strength and fracture toughness, is proved by using test material removed from the area of the suction nozzle and from the engine flange at locations 180° from each other prior to finish machining and establishing the final shape, as shown in Fig. 6.

In order to protect all inner surfaces of the pump from corrosion attack, these areas are weld-cladded using a stabilized austenitic steel of the chromium-nickel-type (4551 steel). The cladding is applied by the two-layer strip submerged arc process. After final stress relieving and final ultrasonic and surface crack examination, the pump casing is ready for the assembly at the facilities of the pump manufacturer.

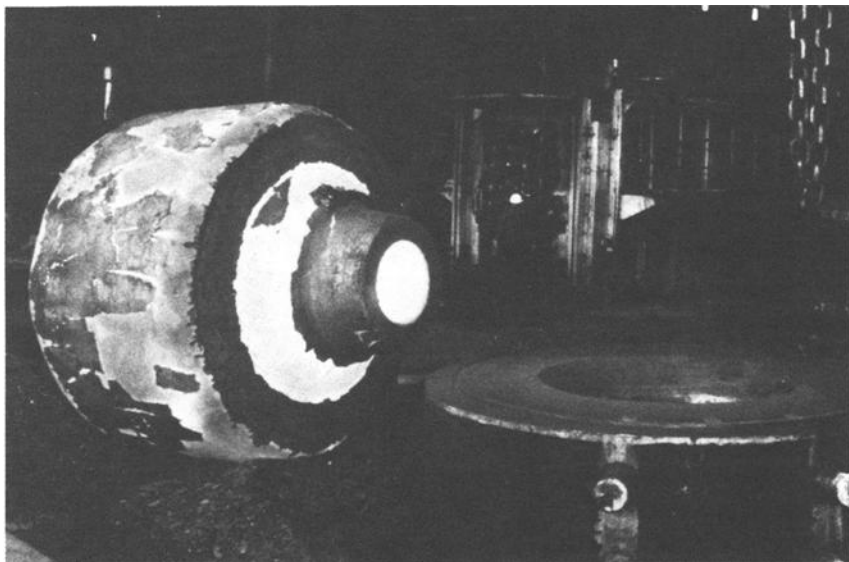


FIG. 4—A pump casing RCP, forged to contour.

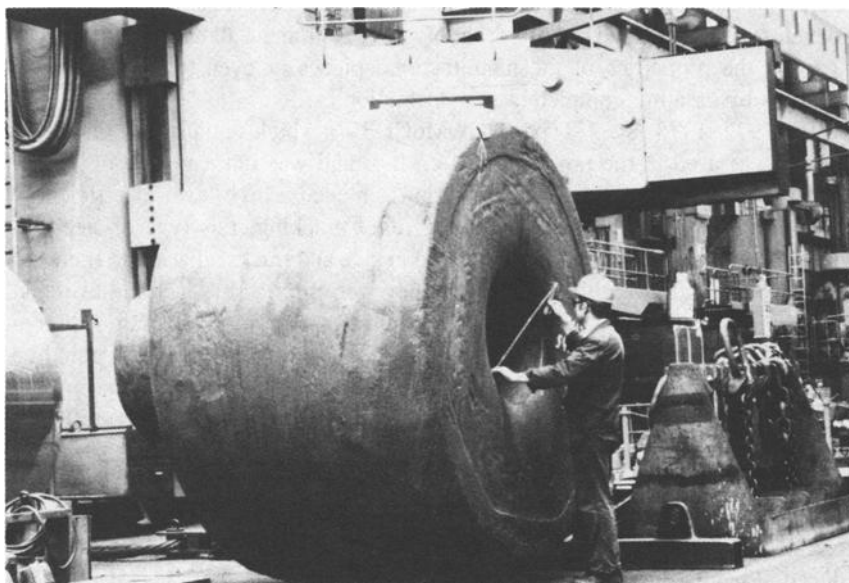


FIG. 5—A pump casing RCP, forging contour.

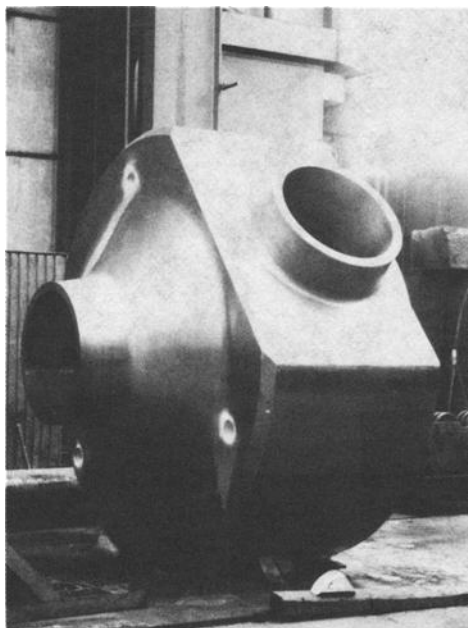


FIG. 6—A pump casing RCP, machined state.

Along with the development of the forging technology, comprehensive work has been done in optimizing materials, resulting eventually in an alteration of the steel type in use. At the same time, the steel plants have made great endeavors in developing melting and pouring technologies to eliminate all harmful influences impairing the properties of the manufactured pieces or even to improve these properties by creating completely new technologies.

Until 1977–1978, steel Type 22 NiMoCr 3 7, which equals ASTM A 508 Class 2, was used in the production of casings and was fabricated from several single parts. Manufacturing and fabrication achieved a high level of efficiency. However, because of the so-called stress relief cracking, this type of steel exhibited a certain susceptibility to underclad cracks and tracks adjacent to the weld seam. Such defects were tolerated when they were limited to a certain level and were compensated for by sophisticated manufacturing and examination procedures. A certain reduction of the susceptibility to stress relief cracking could be obtained after studying the effects of trace elements and impurities and by the determination of their maximum contents (copper = 0.11%; tin = 0.011%; phosphorus = 0.007%; sulfur = 0.008%; molybdenum = 0.60%).

Manufacturing problems found with steel Type 22 NiMoCr 3 7, resulting from its susceptibility to stress relief cracking, might be solved by the use of a material providing the same features in properties on one hand, along with a reduced susceptibility to relaxation embrittlement on the other. It is deemed to

be favorable to select steel Type 20 MnMoNi 5 5, equal to ASTM A 508 Class 3, the properties of which have been improved continuously during past years, especially in view of its fracture toughness and isotropy. On the basis of thorough research work, including weldability, optimum requirements for the chemical composition were established in the code of the German Nuclear Committee (KTA).

For pump casings fabricated from several individual forgings, a rough ingot of 30 tons is required for the heaviest forging. For a one-part casing, as used in the 1200-MW power station Isar II, a rough ingot of 135 tons is necessary to come up with a 34-ton finished pump casing. In other words, the calculated gain from the 135-ton ingot is about 25%.

It is a fact that, as opposed to the multiple-part casing, the forgemaster faces increased difficulties in reaching the contour of the final casing with one-part integrally forged casings. In addition to very comprehensive machining operations, this leads to cutting into ingot regions that are, from the metallurgical point of view, very unfavorable, particularly if a weld cladding is applied later on. So a high integrity of the rough ingot is of utmost significance. This means that, in addition to the prevention of a second center of solidification in the ingot center, the technically relevant and quality-degrading effects of A-segregation and manganese sulfides have to be reduced significantly or even suppressed entirely.

In the center of the ingot, a second center of solidification may arise, if, due to accelerated vertical heat flow, solid material bridges are formed below the feedhead, preventing the residual liquid melt from flowing down into the ingot. This causes the formation of cavities in the center of the ingot, accompanied by shrinkage cracking. At the same time, the desired rising of nonmetallic phases into the feedhead region is disrupted; even with unfavorable shaped molds, when constrained to use such, a second center of solidification may be avoided by application of exothermic feeder head mixture instead of insulating mixture, thus reducing the vertical heat flow and shifting the residual solidification into the feeder head area.

The A-segregation is generated within the heterogeneous and pasty area of the solidification front line, containing dendrites and residual melt simultaneously. It is brought about by interdendritic flow, which may result in a local tubular rising of the residual melt. A-segregated areas are characterized by a higher content of alloying elements and considerable nonmetallic inclusions. This type of macrosegregation is the primary cause for inhomogeneous properties, for example, in tensile strength or fracture toughness of a large forging.

Generally, the injurious effects of A-segregation can be eased or even avoided by reducing the sulfur or the silicon content or both. However, the action of these two elements is different. Whereas sulfur and carbon are of general influence on macrosegregation and cause sulfide formation, a low silicon content is responsible for small dendrite branching distances during the process of solidification, which reduces the amount of A-segregation by affecting the interdendritic flow.

The first step in the improvement of fracture toughness and in reducing the anisotropy during the manufacture of pump casings and other large forgings was a drastic reduction of the sulfur content by implementing special procedures for the secondary ladle metallurgy. In the authors' company, the reduction of sulfur, occasionally below 0.002%, was achieved in such a way that, during the predegassing phase in the ladle, the desulfurization was affected by the use of a calcium oxide-containing, desulfurizing slag and by supporting the slag-steel reaction by argon stream agitation. After that, the main degassing was performed by stream degassing. A prerequisite for this process is a basic lining of the ladles.

The results of this practice may become most distinct in fracture toughness. The upper shelf energy is increased and the transition temperature tends to lower values. At the same time, a reduction of the anisotropy can be observed; that is, the difference between longitudinal and transverse test values, as well as the scattering around the mean value, is becoming less.

A further step to improve the properties of the material used for the pump casings was made by melting steel with a very low silicon content, using vacuum carbon deoxidation (VCD) instead of deoxidation by silicon and aluminum as usual.

Steel made by the VCD process exhibits the following advantages:

1. Favorable formation of micro- and macrosegregation, particularly of the A-segregation.
2. Low anisotropy of the mechanical properties.
3. Improved fracture toughness.

Due to the lack of aluminum, this steel cannot be referred to as fine-grain steel. Since the material for the pump casings had to be made to the fine-grain practice, a special method was developed enabling the addition of aluminum to the liquid steel in the mold.

Metallurgically, the following procedure was applied:

1. Melting without silicon in the electric arc furnace.
2. Predegassing in the ladle, accompanied by desulfurization.
3. VCD treatment with the addition of aluminum for grain refining.

As becoming evident by sulfur prints and macroetching, pump casings manufactured by this method are practically free of A-segregation bands, which may be observed even in forgings containing 0.004% sulfur.

Moreover, microsegregation also is less evident. This can be determined by the segregation factor for molybdenum, which is approximately 1.60 for material made by silicon-aluminum deoxidation and 1.3 for VCD-treated material.

There is no difference in structure and secondary grain size between steel deoxidized to one of these processes: by definite addition of aluminum during the VCD treatment, the fine-grain structure required for 20 MnMoNi 5 5 can be adjusted (Fig. 7).

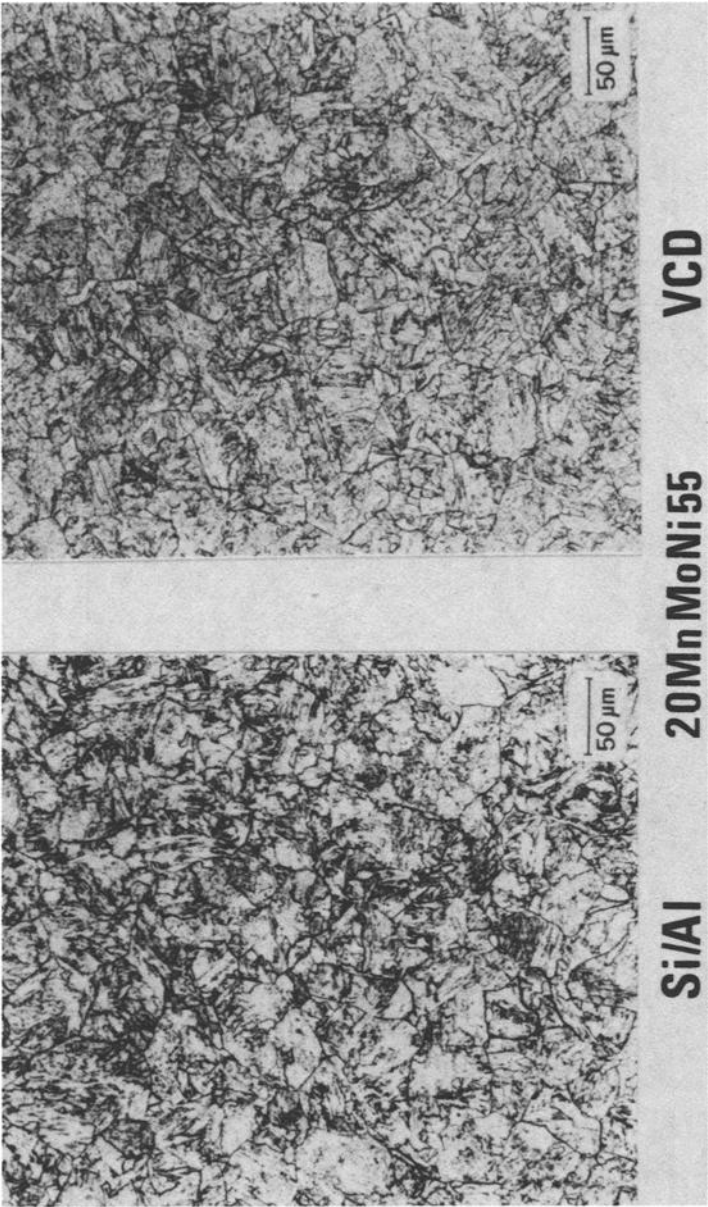


FIG. 7—Pump casings, microstructure.

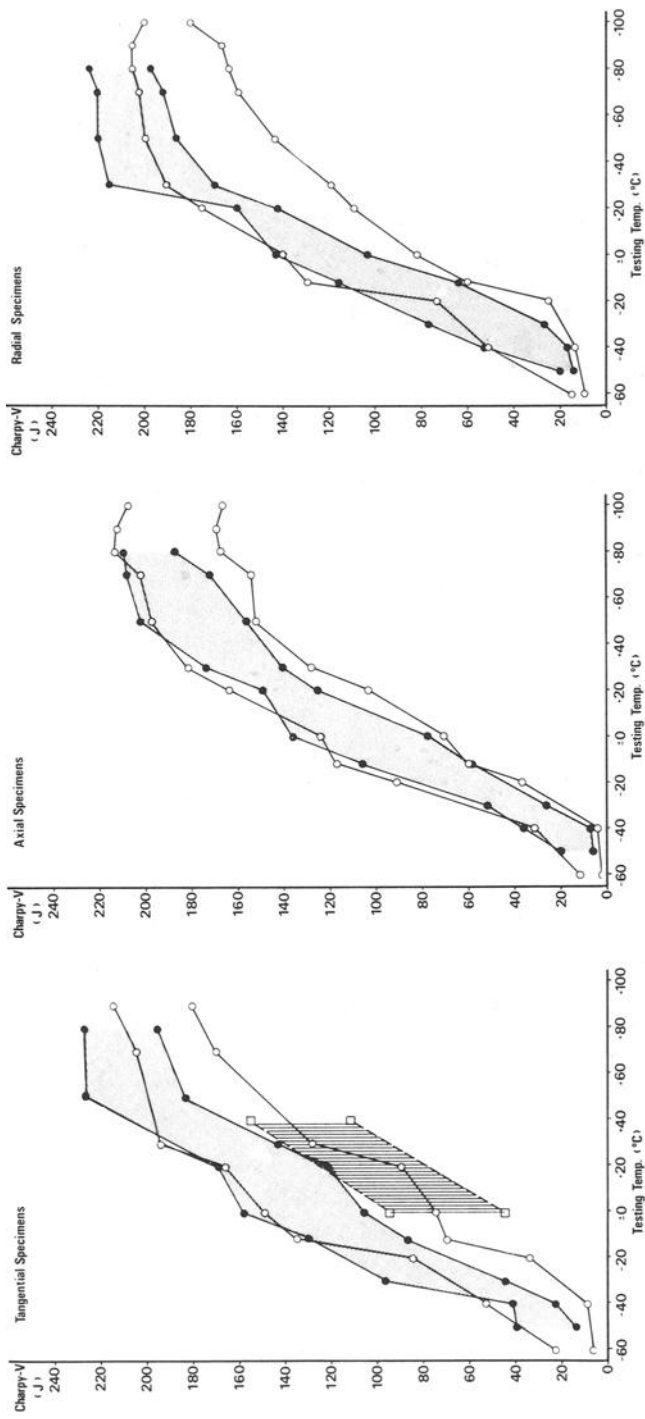


FIG. 8—Fracture toughness: influence of deoxidation and sulfur content.

As one would expect, VCD-treated steel with a definite aluminum addition exhibits a better fracture toughness when compared with silicon-aluminum deoxidized steel. This can be taken from the improved fracture appearance transition temperature (FATT), determined for each of three specimen orientations (tangential, axial, and radial) and from the scatter around the mean value, figured out as the scatter range for the standard deviation of the single value from the mean value (Fig. 8).

The improved fracture toughness also can be noticed in tension testing, especially by regarding the figures for the reduction of area. An analysis of the integrated frequency very distinctly shows the favorable location of the 50% value for the VCD material at smallest scatter of the single values. The integrated frequency curve of the steel containing $>0.005\%$ sulfur is clearly set off against the curves of the low sulfur material (Fig. 9).

The difference between VCD steel and silicon-aluminum-deoxidized material containing 0.005% sulfur becomes most evident by review of the reduction of area values of radial specimens. The absence of macrosegregation lines, which occur on non-VCD material even at sulfur contents of $<0.005\%$, is of decisive influence (Fig. 10).

Nevertheless, a comparison shows that VCD material, molten to the fine-grain practice, exhibits a somewhat lower tensile strength; however, the demands are met in any case. To counteract this tendency, carbon and manganese are adjusted near the upper limit of the analysis range.

Compared with heats only desulfurized and silicon-aluminum-deoxidized, VCD heats have approximately 0.0015% higher content of sulfur, which is still a very

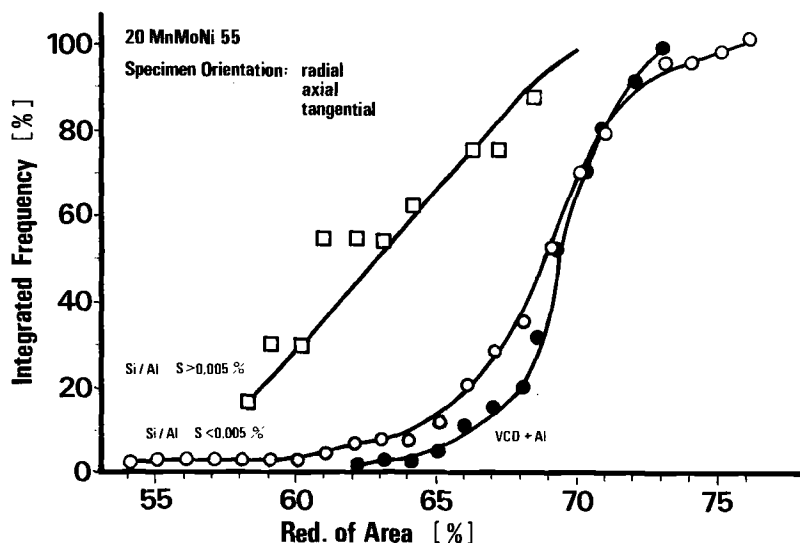


FIG. 9—Integrated frequency reduction of area; influence of deoxidation and sulfur content.

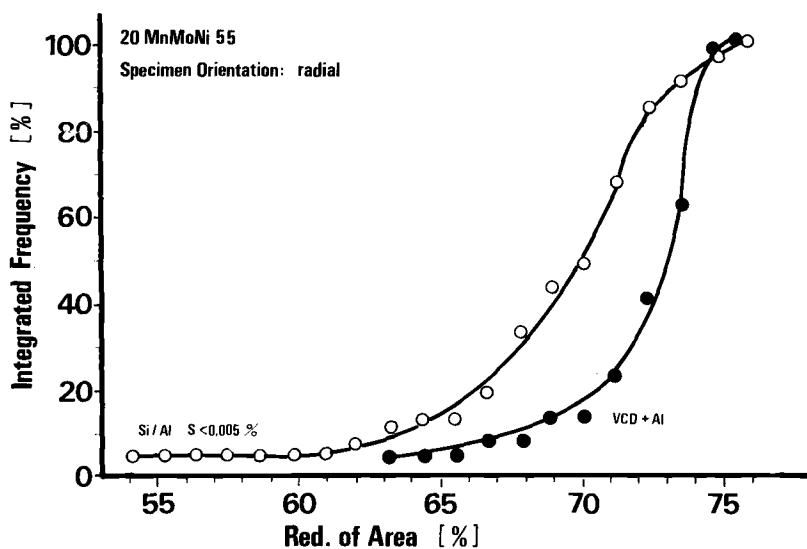


FIG. 10—Integrated frequency reduction of area: influence of deoxidation.

low level. This is brought about by a certain minimum content of oxygen, needed for an optimum VCD treatment but impairing prior desulfurization since desulfurization is decreased with a rising oxidation potential or with a dropping reduction potential.

Meanwhile, the authors' company has developed a procedure enabling a desulfurization under the same reducing environment as available when no VCD treatment is intended. However, the VCD treatment takes place with the necessary content of oxygen in the melt. In this way, lowest sulfur contents may be obtained during VCD treatment, even after addition of a definite quantity of aluminum. The results of this technology are evaluated now.

As supported by weld simulation tests, steel Type 20 MnMoNi 5 5, produced to the VCD process with definite addition of aluminum, shows no symptoms of susceptibility to strain, to temperature-induced embrittlement, or to stress relief cracking in the heat affected zone (HAZ).

Bibliography

- Austel, W., Körbe, H., and Weisser, E., "Fortschritte in der Herstellung von Schmiedeerzeugnissen unter besonderer Berücksichtigung der Schweißtechnik," Internationale Schmiedetagung, Terni, 1970.
- Cerjak, H., Debray, W., and Papouschek, F., "Eigenschaften des Stahls 20Mn-Mo-Ni 5 5 für Kernreaktorkomponenten," VGB-Konferenz "Werkstoffe und Schweißtechnik im Kernkraftwerk 1976," Düsseldorf, 1976.
- Grote, G., and Schneider, W., "Die Entwicklung geschmiedeter Gehäuse für Primärumschlepppumpen von Kernkraftwerken," *Atomkernenergie-Kerntechnik*, No. 34, 1979, pp. 94-100.
- Hochstein, F. and Maidorn, C., "Seigerungen in schweren Schmiedeblocken," 4. MPA-Seminar, Stuttgart, 1978.

Hochstein, F., Austel, W., and Maidorn, C., "Herstellung von Schmiedestücken aus schweren und schwersten Rohblöcken mittels verbesserter Technologien," DVM-Tag, Stuttgart, 1979.

Hochstein, F., Austel, W., and Maidorn, C., "Application of a New Processing Procedure for the Further Improvement of Nuclear Grade Structural VCD Steel," International Atomic Energy Agency, Wien, 1983.

Maidorn, C., "Erstarrungsablauf und Seigerung in schweren Schmiedeblocken unter besonderer Berücksichtigung des Stahls 20 MnMoNi 5 5," Dr.-Ing.-Dissertation, Techn.-wiss. Ber. MPA Stuttgart, 1983, Heft 83-04.

Maidorn, C. and Blind, D., "Erstarrungsablauf und Seigerungen in schweren Schmiedeblocken," 9, MPA-Seminar, Stuttgart, 1983.

Onodera, S., "Fortschritte in den Verfahren der Stahlerzeugung," 5. MPA-Seminar, Stuttgart, 1979.

Schellhammer, W., "Über die Ursachen von Relaxations- und Heißrißbildung in der Wärmeeinflußzone der Feinkornbaustähle 22 NiMoCr 3 7 und 20 MnMoNi 5 5," Techn.-wiss. Ber. MPA Stuttgart, 1978, Heft 78-01.

Saburo Kawaguchi,¹ Hisashi Tsukada,² Komei Suzuki,³
Ikuro Sato,⁴ and Shinsaku Onodera⁵

Manufacturing of Large and Integral-Type Steel Forgings for Nuclear Steam Supply System Components

REFERENCE: Kawaguchi, S., Tsukada, H., Suzuki, K., Sato, I., and Onodera, S., "Manufacturing of Large and Integral-Type Steel Forgings for Nuclear Steam Supply System Components," *Steel Forgings, ASTM STP 903*, E. G. Nisbett and A. S. Melilli, Eds., American Society for Testing and Materials, Philadelphia, 1986, pp. 398-409.

ABSTRACT: Forgings for the reactor pressure vessel (RPV) of the pressurized heavy water reactor (PHWR) 700 MWe, which is composed of seven major parts and nozzles totaling about 965 tons, were successfully developed. These forgings are:

1. Flanges: an outside diameter of 8440 mm and a weight of 238 tons max, requiring an ingot of 570 tons.
2. Shells and torus: an outside diameter of about 8000 mm with large height.
3. Cover dome: a diameter of 6800 mm and a thickness of 460 mm, requiring a blank forging before forming of 8000 mm in diameter and 550 mm thick.

The material designation is 20Mn-Mo-Ni 5 5 (equivalent to SA508, Class 3).

Even with greater dimensions and weight than the current largest forgings, the manufacture and the qualities achieved were satisfactory. These successful results were obtained by recent developments in the manufacturing technology of steels, such as steel making, metal-working processes, and heat treatment, which are vital to the quality of large-sized and heavy-walled steel forgings.

In this paper, the manufacturing of and the properties of such large and integral forgings are discussed, including an overview of manufacturing processes for ultralarge-sized forgings over the last two decades.

KEY WORDS: forging, reactor pressure vessel (RPV), pressurized heavy water reactor (PHWR), flange, shell, torus, cover dome, ingot, forming, 20Mn-Mo-Ni 5 5, SA508—Class 3, manufacture, qualities, steel, steel making, metal working, heat treatment

The requirements for the reliability of a nuclear power station and the structural safety of its components are becoming severer with the increased intention of

¹ Managing director, Japan Steel Works, Tokyo, Japan.

² General manager, Research Laboratory, Japan Steel Works, Muroran Plant, Hokkaido, Japan.

³ Manager, Atomic Energy Dept., Japan Steel Works, Muroran Plant, Hokkaido, Japan.

⁴ Senior engineer, Atomic Energy Dept., Japan Steel Works, Muroran Plant, Hokkaido, Japan.

⁵ Associate director, Japan Steel Works, Tokyo, Japan.

making the execution of the in-service inspection (ISI) easier. The components of the light water reactor (LWR) are attracting particular attention on this behalf, in the minimization of weld seams and in the use of the large-size and more integral-type materials. Use of steel forgings for pressure vessels extremely enhances their structural integrity over those fabricated from plate materials, especially for the pressure vessels used in high-temperature and high-pressure application such as reactor vessels in the core of nuclear power plants.

Following the trend of seeking scale merit of economy of the LWR system, the unit capacity of the nuclear power plant raised to the level of 1300 MWe. This requires a large ring forging of 5800-mm outside diameter for pressurized water reactor pressure vessel (PWRPV) and 7400-mm outside diameter for boiling water reactor pressure vessel (BWRPV) with the integral design of individual forging, which was initiated by Kraftwerk Union (KWU), ASEA-ATOM, and Cockerill Mechanical Industries and was jointly developed by the Japan Steel Works (JSW). Details of these reports were in several papers and reviews [1–5].

Larger units of 6-loop pressurized water reactor (PWR) are reportedly planned by European plant contractors, for which the manufacture of required steel forgings foresees no essential difficulties.

Another current problem of the nuclear power plant is the integrity of turbine rotors. The use of huge-size, monoblock-type rotor shaft forgings were developed by JSW [6] as a definite countermeasure to exclude the possibility of stress corrosion cracking (SCC) at the shrinkage assembly of the rotor shaft.

These two potential requirements have led JSW to a larger ingot of 570 tons.

Coincidentally, KWU planned a pressurized heavy water reactor (PHWR) of 700 MWe where the ring forgings of over 8000-mm outer diameter are required. JSW could fulfill the request. These forgings have been successfully delivered.

The present paper describes briefly the manufacturing and the properties of the ultralarge-diameter 20Mn-Mo-Ni 5 5 steel forgings for the PHWR.

Reactor Pressure Vessel of Pressurized Heavy Water Reactor 700 MWe

The layout of forgings in the RPV of PHWR 700 MWe is shown in Fig. 1 and is composed of seven major parts and nozzles totaling about 965 tons.

In dimensions and weight, the component forgings are:

1. Flanges: an outside diameter of 8440 mm and weight of 238 tons max, requiring an ingot of about 600 tons.
2. Shells and torus: an outside diameter of about 8000 mm with large height.
3. Cover dome: a diameter of 6800 mm and a thickness of 460 mm, requiring a blank forging before forming of 8000 mm in diameter and 550 mm thick.

The material designation is 20Mn-Mo-Ni 5 5 steel, and the chemical compositions for seven major parts are shown in Table 1. Particular effort was made to minimize tramp elements.

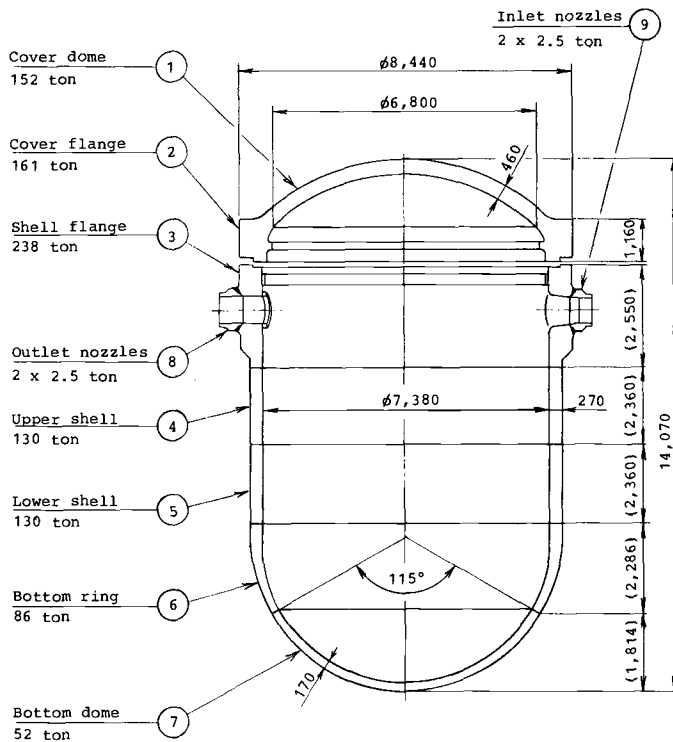


FIG. 1—Layout of forgings in RPV.

Manufacturing of Forgings

Manufacturing Sequence

The manufacturing sequence for the component forgings is basically identical with those established for the forgings of KWU 1300-MWe PWRPV.

Taking one part as an example, the manufacturing sequence of shell flange is given in Fig. 2.

Steel and Ingot Making

Figure 3 shows the developments of steel-making and ingot-making methods and of ingot sizes in the last two decades.

The 1300-MWe PWR shell flange forging manufactured from a 400-ton ingot in 1972 was the very first use of large-sized, integral forgings. The first two pieces from a 570-ton ingot of 20Mn-Mo-Ni 5 5 formed the shell and cover flanges of the RPV of the PHWR 700 MWe shown in Fig. 1. Nevertheless, the ingot making and the quality of ingots were highly satisfactory.

TABLE 1—Chemical composition (ladle analysis), weight %.

Part	C	Si	Mn	P	S	Ni	Cr	Mo	V	Al	As	Cu	N	Sb	Sn	Co	Ta
Cover dome	0.21	0.27	1.41	0.005	0.004	0.73	0.12	0.50	≤0.01	0.026	0.007	0.04	0.0081	0.0014	0.006	0.008	≤0.005
Cover flange	0.21	0.24	1.39	0.004	0.004	0.75	0.10	0.50	≤0.01	0.027	0.005	0.04	0.0082	0.0012	0.005	0.008	≤0.005
Shell flange	0.21	0.25	1.44	0.007	0.006	0.77	0.11	0.50	≤0.01	0.028	0.006	0.04	0.0099	0.0017	0.006	0.005	≤0.005
Upper shell	0.19	0.23	1.39	0.005	0.005	0.74	0.13	0.50	≤0.01	0.029	0.004	0.03	0.0103	0.0011	0.005	0.008	≤0.005
Lower shell	0.20	0.25	1.38	0.006	0.005	0.73	0.11	0.49	≤0.01	0.029	0.005	0.03	0.0103	0.0012	0.005	0.008	≤0.005
Bottom ring	0.20	0.25	1.41	0.005	0.005	0.75	0.11	0.50	≤0.01	0.027	0.005	0.03	0.0121	0.0011	0.005	0.008	≤0.005
Bottom dome	0.20	0.21	1.37	0.006	0.005	0.72	0.11	0.50	≤0.01	0.030	0.004	0.03	0.0097	0.0010	0.004	0.011	≤0.005

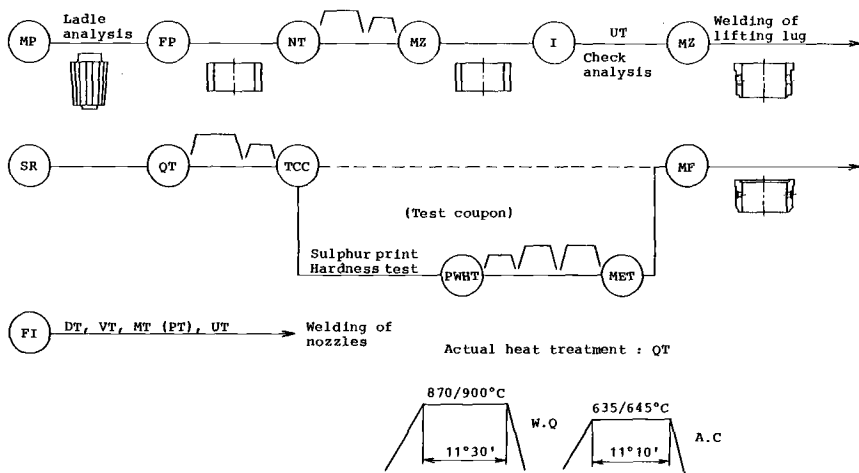


FIG. 2—Manufacturing sequence of shell flange made from 570-ton ingot.

In the steel making, combined refining and degassing in ladle was successfully developed and fully utilized, aiming at cleanest possible steels. The pouring sequence and the appearance of a 570-ton ingot are given in Figs. 4 and 5.

Forging

As shown in Fig. 6, Process 1 is the most common forging process. It is employed for ring forging less than 5 m in outer diameter. Process 2 (outside press process) was developed for large flange forgings over 5 m in outer diameter (for example, 251-in. BWRPV flanges). However, Process 2 has a serious weak point in the pressing force and a limitation on ring height. To improve Process 2, the unique forging process (Process 3) has been developed. This process was first adopted for the manufacture of a shell flange for a 1300-MWe PWR vessel

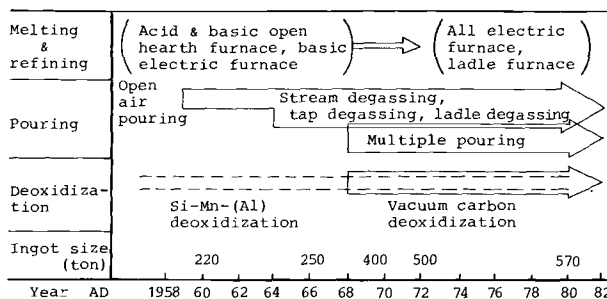


FIG. 3—Development of steel-making and ingot-making methods and of ingot size in two decades.

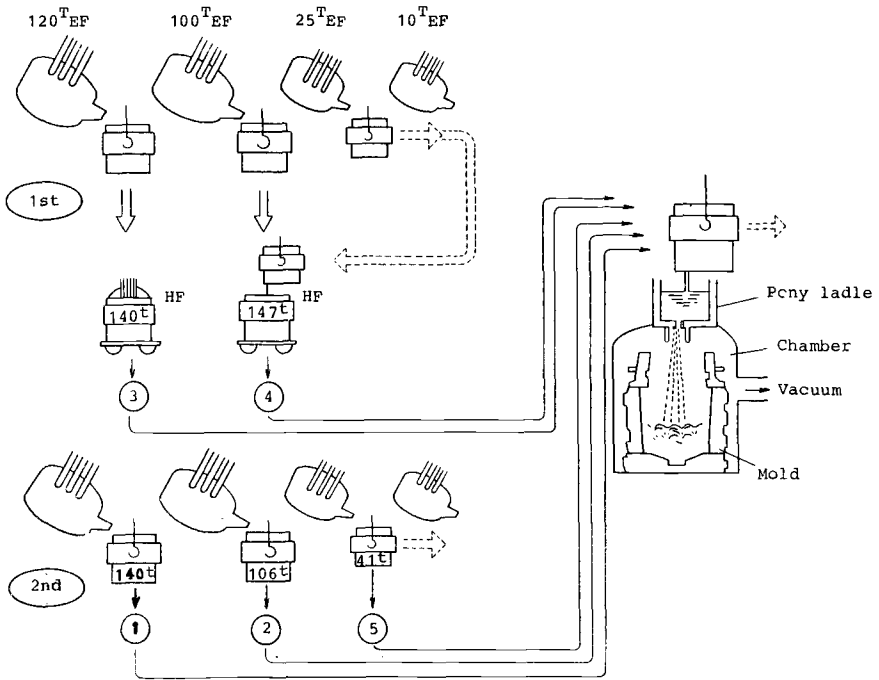


FIG. 4—Pouring sequence of 570-ton ingot.

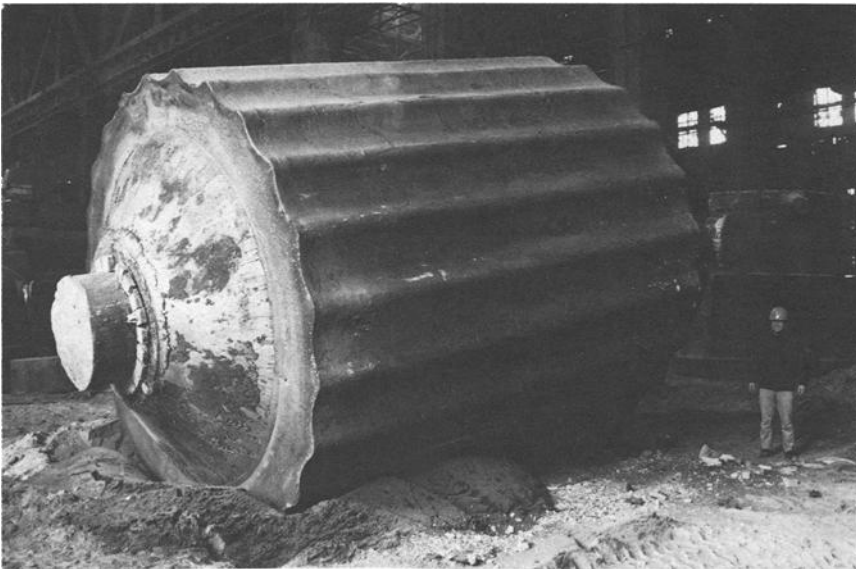


FIG. 5—570-ton ingot.

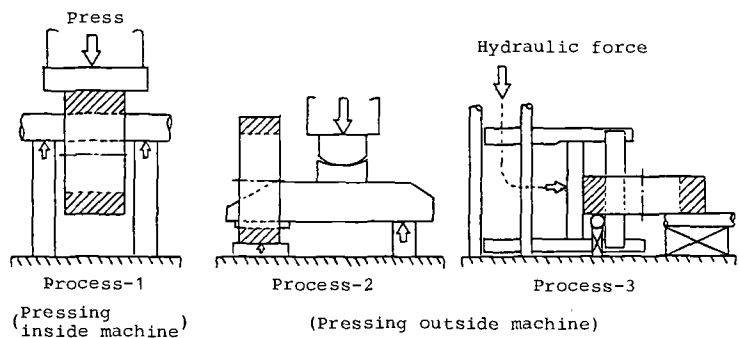
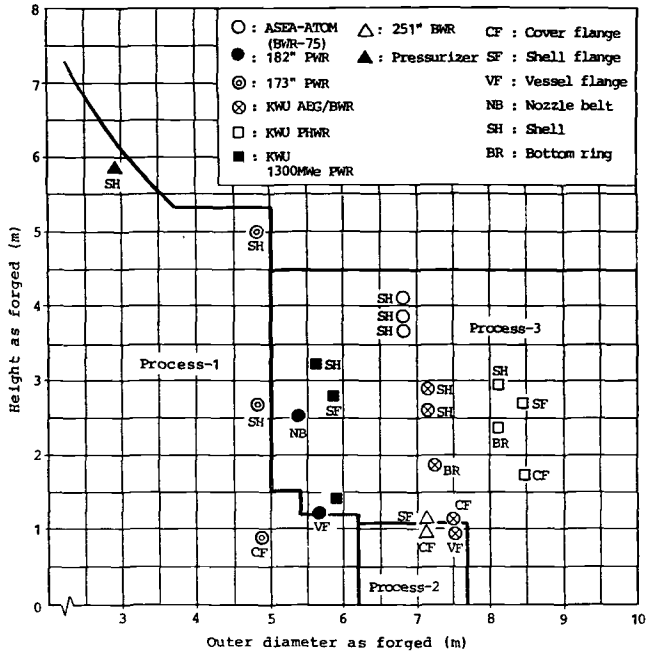


FIG. 6—Ring-forging processes and capacity in Japan Steel Works using 10 000-ton press and typical experiences.

in 1972. Included in Fig. 6 are the manufacturing experiences of JSW for typical ring forgings.

Figure 7 shows the forging sequence for shell flange. Referring to Fig. 6, the later steps of forging operation for shell flange are performed by Process 3.

Heat Treatment

Figure 8 shows the quenching operation of the shell flange. The handling of huge pieces is the first concern in the heat treatment operation. In addition to

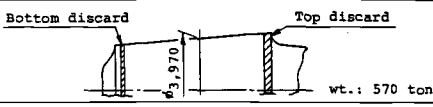
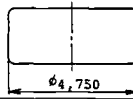
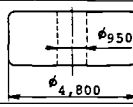
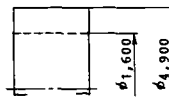
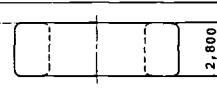
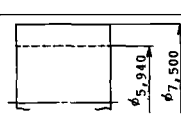
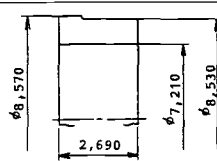
	Forging process	Sketch
1	Ingot T. & B. discard by flame cutting	 <p>Bottom discard Top discard</p> <p>wt.: 570 ton</p>
2	Upsetting	 <p>$\phi 4,750$</p>
3	Piercing	 <p>$\phi 950$</p> <p>$\phi 4,800$</p>
4	Enlarging	 <p>$\phi 1,600$</p> <p>$\phi 4,900$</p>
5	Upsetting	 <p>$\phi 2,800$</p>
6	Enlarging	 <p>$\phi 3,940$</p> <p>$\phi 7,500$</p>
7	Finish forging	 <p>$\phi 8,570$</p> <p>$\phi 7,210$</p> <p>2,690</p> <p>$\phi 8,530$</p>

FIG. 7—Forging sequence of shell flange made from 570-ton ingot.

and in order to assure uniform and good mechanical properties, the following methods were considered:

1. Uniformity of heating temperature.
2. Rapid immersion operation for quenching the forging.
3. Vigorous agitation of the water in the quenching bath.

Properties of Forging

Quality of Ingots

Uniformity of Carbon Distribution—Figure 9 shows the carbon distribution in shell flange. The carbon distribution for shell flange is well-controlled within a small range even for a 570-ton ingot.

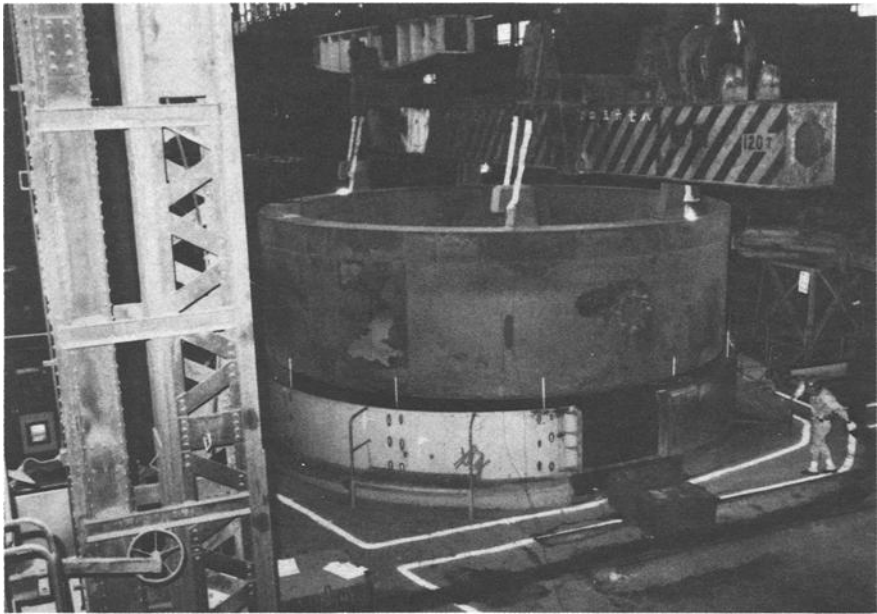


FIG. 8—Quenching operation of shell flange made from 570-ton ingot.

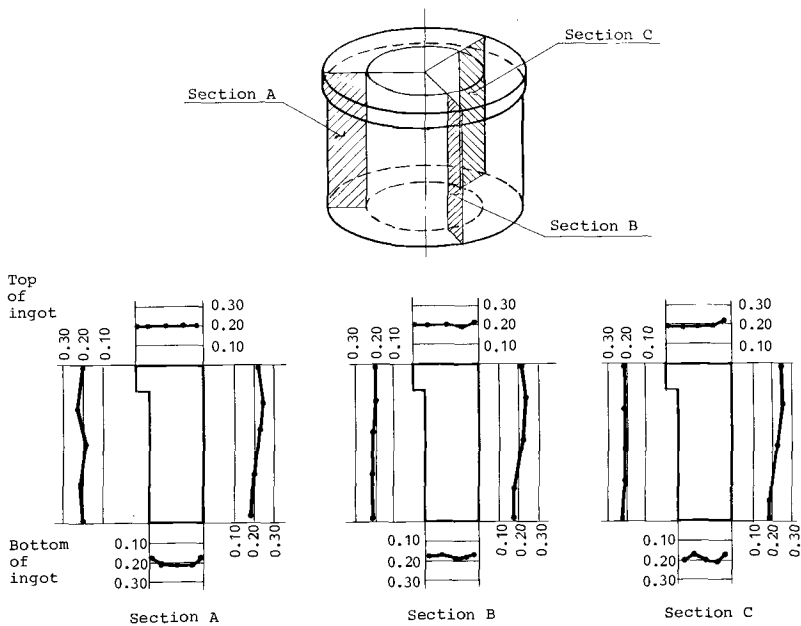


FIG. 9—Carbon distribution in shell flange (weight %).

Hydrogen and Nonmetallic Inclusions—In Fig. 10, the results of determinations of hydrogen and nonmetallic inclusions made on top, bottom, and core discards are plotted. A low level of these impurities is evident.

Mechanical Properties

Homogeneity and isotropy of mechanical properties of huge forgings are achieved by decreasing the nonmetallic inclusions in the steel and ingot-making process, by reducing microsegregation in the forging process, and by the accurate control of temperature during the quenching and tempering operations.

Figure 11 shows the mechanical properties of the shell flange at room temperature and 350°C including the Charpy V-notch impact properties. The high levels of uniformity and isotropy of mechanical properties are clearly demonstrated for this massive forging.

Internal Quality

In evaluating the quality of the forgings, the level of internal defects is another factor. Based on past experience, forge masters were aware that a steel forging sometimes contains miscellaneous types of detrimental internal defects. However, progress in steel making has eliminated most of these defects. Two types were of special concern:

1. Nonmetallic inclusions, particularly in clusters.
2. Hydrogen-induced, small flake cracks at depth in a steel forging.

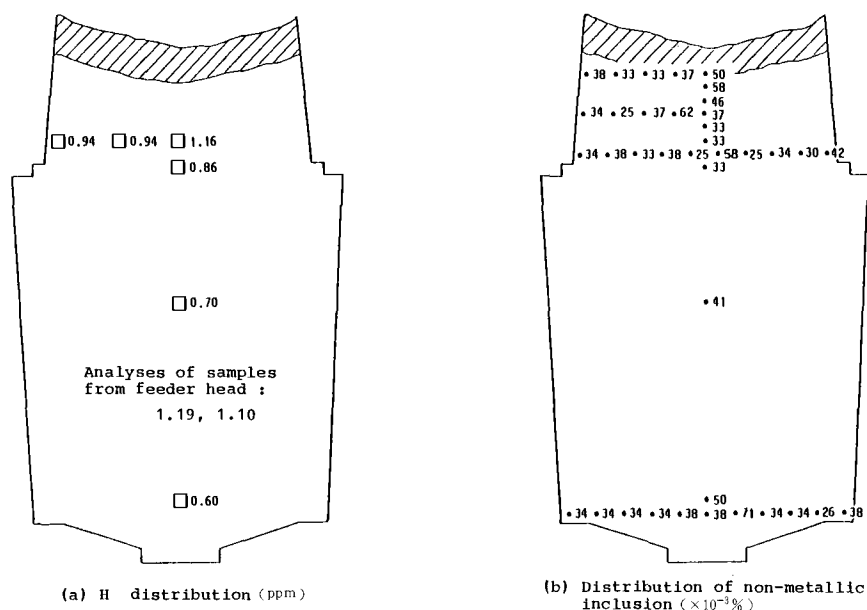
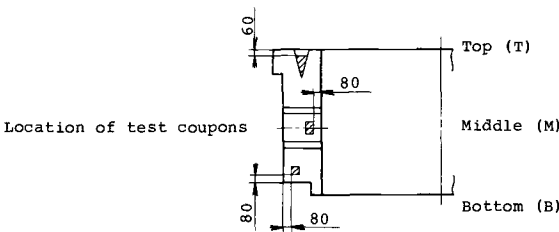


FIG. 10—Hydrogen and nonmetallic inclusions in a 570-ton ingot.



Properties	Test at		Room temperature		350 °C	
	Location					
Yield strength (N/mm ²)	T			441		397
	M			475		412
	B			462		405
Tensile strength (N/mm ²)	T			600		552
	M			627		571
	B			617		560
Elongation (%)	T			24.1		20.6
	M			24.0		22.7
	B			24.2		22.8
Reduction of area (%)	T			73.0		70.8
	M			74.0		74.5
	B			70.6		74.5
Impact value at 0 °C (J)	T			62		
	M			92		
	B			111		

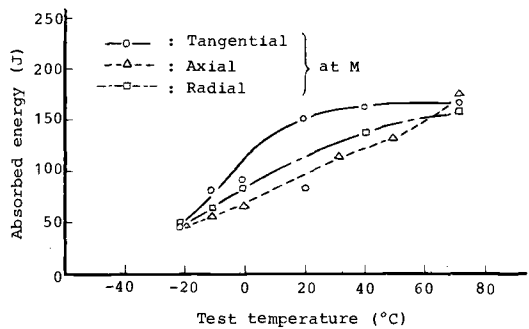


FIG. 11—Mechanical properties of shell flange.

In the ultrasonic examination of the forgings, no indications were found over the recordable size of equivalent flaw size, that is, 6-mm diameter by straight beam technique at the depth of the forgings. For example, in the shell flange, only several spots of 1 to 2-mm diameter were detected.

Summary and Conclusions

A set of component material for PHWR RPV, including the largest forgings ever manufactured so far such as flanges (8440 mm outer diameter), shells, and torus (7960 mm outer diameter) and dome (6800 mm diameter in chord, 460 mm thick), was presented in the outline of manufacturing and properties.

Even with greater dimensions and weight than the current largest forgings, the manufacture and the qualities achieved were satisfactory.

These results encourage us in further developing PWRs and PHWRs with increased capacity.

Acknowledgments

The authors wish to express their appreciation to the management of JSW for their permission to submit the paper. Gratitude also is due for the cooperation extended by KWU through this development work.

References

- [1] Onodera, S., Fujioka, K., Tsukada, H., and Suzuki, K., "Advantages in Application of Integral Flange Forgings for Reactor Vessels," 3rd Materialprüfungsanstalt-Seminar, Stuttgart, Sept. 1977.
- [2] Onodera, S., Moritani, H., Tsuchiya, K., Tsukada, H., Widart, J., and Scailteur, A., "Mono-block Vessel Flange Forging for PWRPV 1,000 MWe," 8th International Forgemasters Meeting, Kyoto, Japan, Oct. 1977, Steel Castings and Forgings Association of Japan.
- [3] Onodera, S. and Suzuki, K., "Progress in the Methods of Steel-Production," 5th Materialprüfungsanstalt-Seminar, Stuttgart, Oct. 1979.
- [4] Onodera, S., "Current Steels for Nuclear Pressure Vessels," Tetsu to Hagane, *Journal of the Iron and Steel Institute of Japan*, No. 167, 1981, p. 880.
- [5] Onodera, S., "Improved quality of heavy steels and their welds as related to the integrity of RPC," IAEA-SM-269/116, International Atomic Energy Commission symposium, Vienna, March 1983.
- [6] Kawaguchi, S., Yanagimoto, R., Sawada, S., Ohhashi, T., "Historical View of Manufacturing Large Mono-Block Rotor Forgings and Future Outlook (Topic: E)," 9th International Forging Conference, Düsseldorf, May 1981.

Advanced Technology of Heavy-Section Tube Sheets for Nuclear Power Generation

REFERENCE: Skamletz, T. A. and Grimm, W. W., “Advanced Technology of Heavy-Section Tube Sheets for Nuclear Power Generation,” *Steel Forgings*, ASTM STP 903, E. G. Nisbett and A. S. McIlilli, Eds., American Society for Testing and Materials, Philadelphia, pp. 410–424.

ABSTRACT: Considered in particular were the toughness requirements at low temperatures, the safe weldability, and the minimum sensitivity against temper embrittlement at stress-relieving temperatures of Steel 20 MnMoNi 5 5, corresponding to ASTM A 508 Class 3. High-temperature tensile and creep properties up to 450°C had to be met.

These targets were achieved by applying the production steps as follows:

1. The steelmaking was done according to the Buderus calcium-argon blowing (CAB) process. The low sulfur contents of 0.002% and lower and the special pouring technology to achieve low segregation rates are the basic reasons for the outstanding toughness and the isotropy of the material properties.
2. The forging technology, in particular the temperature range and the deformation rate, was designed to produce fine-grain structure already in the as-forged condition.
3. A newly developed, three-step, quality heat treatment is most important for the hardening through and the toughness level of the heavy section.
4. The report submits a discussion of the dimensional limits for 20 MnMoNi 5 5 forgings produced according to different technologies.

KEY WORDS: properties of steel 20 MnMoNi 5 5, corresponding to ASTM A 508 Class 3, when used for heavy-section tube sheets; influence of structure, grain size, sulfur content, and three-step heat treatment on the toughness and the isotropy of tube sheets as a function of the cross section

The West German specialty steel producers, Edelstahlwerke Buderus AG, received an order from Kraftwerk Union (KWU) to supply tube sheets for the nuclear power stations under construction in Emsland, Neckar (Neckar-Westheim) and Ohu (Isar II) in West Germany.

The order covered tube sheets for the heat exchangers in the condenser and in the preheating section of the water-steam circuit (shown as a schematic in Fig. 1). One of the preliminary conditions for acceptance of the order was an As-

¹ Manager—Technical Services, and manager—Quality Assurance, respectively, Edelstahlwerke Buderus AG, Wetzlar, Germany.

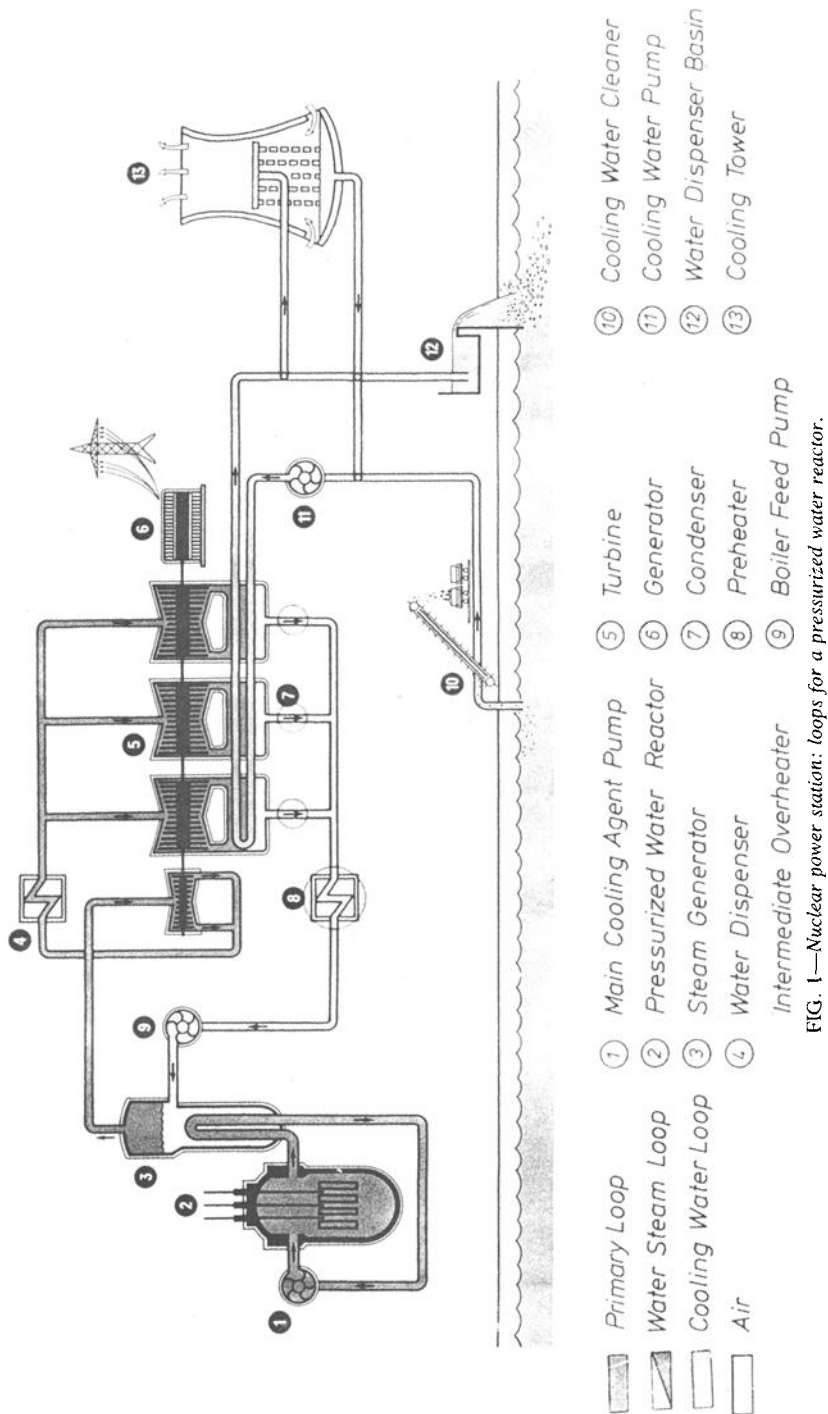


FIG. 1—Nuclear power station: loops for a pressurized water reactor.

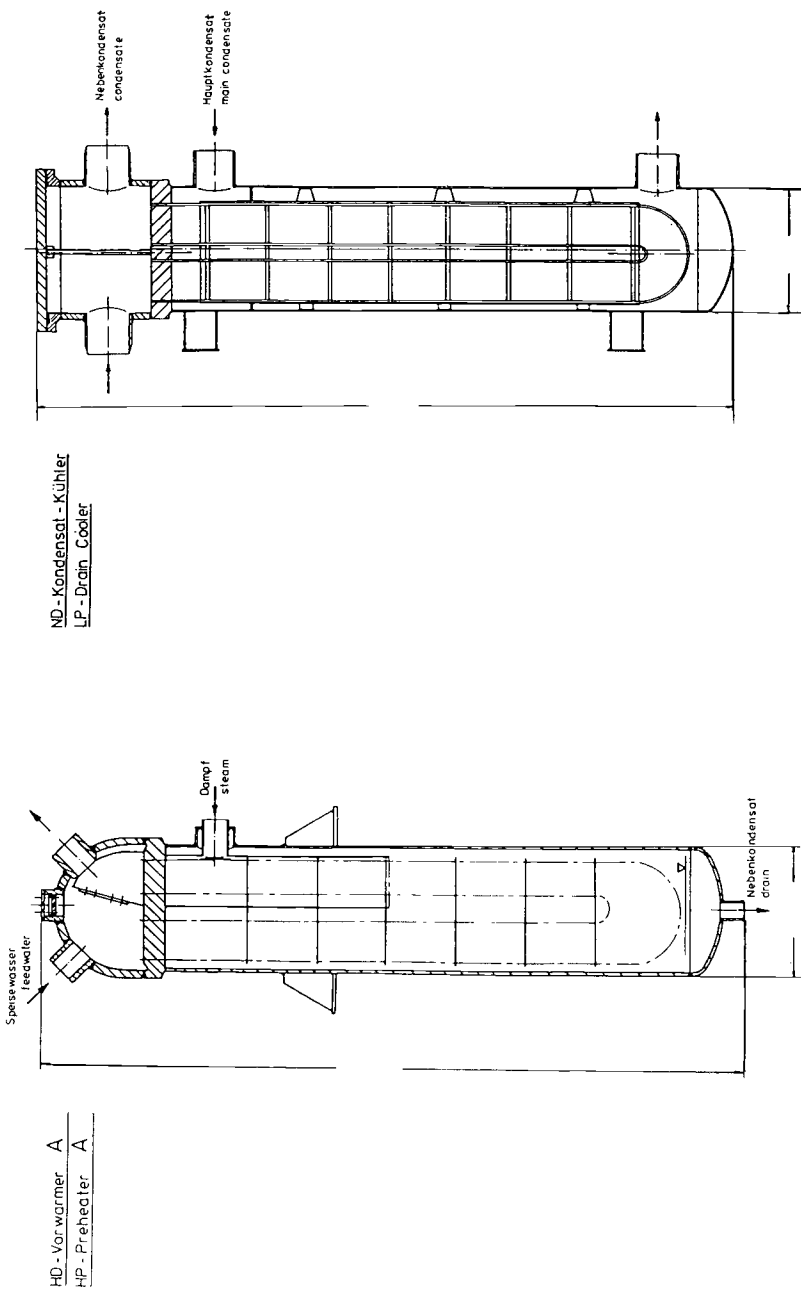


FIG. 2—Position of tube sheets in the low pressure (LP) cooler and in the high pressure (HP) preheater of a pressurized water reactor.

sociation of Technical Supervisory Bodies (TÜV) inspectorate license for the production of quenched and tempered (QT) forgings of the specified steels and dimensions.

The layout of the tube sheets in the low-pressure coolers and high-pressure preheaters is shown in Fig. 2. All tube sheets thicker than 300 mm were produced from the heat-resistant QT steel 20 MnMoNi 5 5. Figure 3 shows the range of dimensions as well as the position of the forgings in the ingot together with the sample position. The maximum ingot weight for the biggest tube sheets, diameter 2623 by 535.5 mm, was 110 tons.

The mechanical qualities aimed for compliance with the KWU specification, analogous to VdTÜV Werkstoffblatt (Table of Materials issued by the Association of Technical Supervisory Bodies), are shown in Fig. 4 together with the prescribed chemical analysis.

Specified Analysis of 20 Mn Mo Ni 5 5 steel, %.

C	Si	Mn	Cr	Ni	Mo
0.17	max	1.00	max	0.40	0.45
0.23	0.35	1.50	0.30	0.80	0.60

Experience has shown that the homogeneity of the forgings in respect to segregations and nonmetallic inclusions can be regarded as the critical factor for industrial production to obtain an ultrasonic image without indication. To solve this problem, the use of specially developed metallurgical procedures is indispensable.

In respect of the mechanical properties, problems are encountered in achieving a sufficiently high notch toughness transverse to the direction of deformation, particularly in the upper dimension range of the material 20 MnMoNi 5 5, and requires the application of suitable technology.

The Buderus specialty steelworks routinely use a specially designed computer program to check whether the specific mechanical properties in the components can be maintained. Depending on the chemical analysis of the steel, the dimensions of the specimen, and the quenching medium, the structure can be predicted over the cross section with sufficient accuracy. These relationships have been clearly defined and require no further explanation [1-3].

Knowledge of the transformation structure in the envisioned test zone enables determination of the strength and toughness characteristics in a second step after tempering. For steels with a carbon content of 0.2%, the toughness parameters elongation (A_5), reduction in area (necking) (Z), notch impact toughness at ambient temperature (A_v), and the fracture appearance transition temperature ($FATT$) for the transformation structures ferrite and pearlite, bainite, and martensite are plotted over the yield strength (R_p) in the following illustrations (Figs. 5-8). Here, the dark field represents the specification range for tube sheets of the steel 20 MnMoNi 5 5.

Dimensions of Tube Sheets 20MnMoNi 55
(ASTM A 508 Cl.3) :

$\phi 2403 \times 355,0 \text{ mm}$

$\phi 1803 \times 385,5 \text{ mm}$

$\phi 1603 \times 412,5 \text{ mm}$

$\phi 2003 \times 436,0 \text{ mm}$

$\phi 2623 \times 535,5 \text{ mm}$

Test sampling for Tube Sheets and blind covers
 for $s > 320 \text{ mm}$

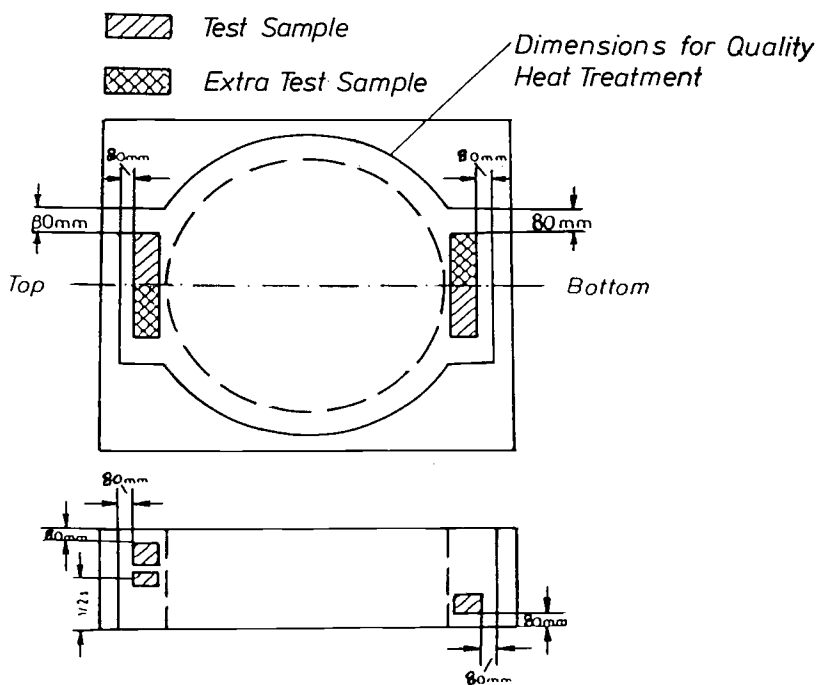


FIG. 3—Tube sheet dimensions and test sampling.

Testing Temp.	Yield Strength $R_p 0,2$	Ult. Strength R_m	Elongation A_5	Red. of Area Z	Impact A_v (ISO-V)	Lateral Expansion
$^{\circ}\text{C}$	N/mm^2	N/mm^2	%	%	J	mm
0	-	-	-	-	41	-
+33	-	-	-	-	68	0,9
+20	390	560/700	19	45	-	-
+80	-	-	-	-	100	1,3
+100	370	520	16	-	-	-
+200	350	505	16	-	-	-
+300	330	505	14	-	-	-
+350	315	505	14	-	-	-
+375	300	505	14	-	-	-
+400	290	490	14	-	-	-

20MnMoNi55
acc. A 508 Cl. 3

in %:

C=0,25max

Mn=1,35

Si=0,275

Ni=0,70

Cr=0,25max

Mo=0,525

Minimum values acc. Vd TÜV-Werkstoffblatt 401/3 after
Post weld Heat Treatment, transverse

FIG. 4—Specification for the mechanical properties of steel 20 MnMoNi 5 5, according to ASTM A 508 Class 3.

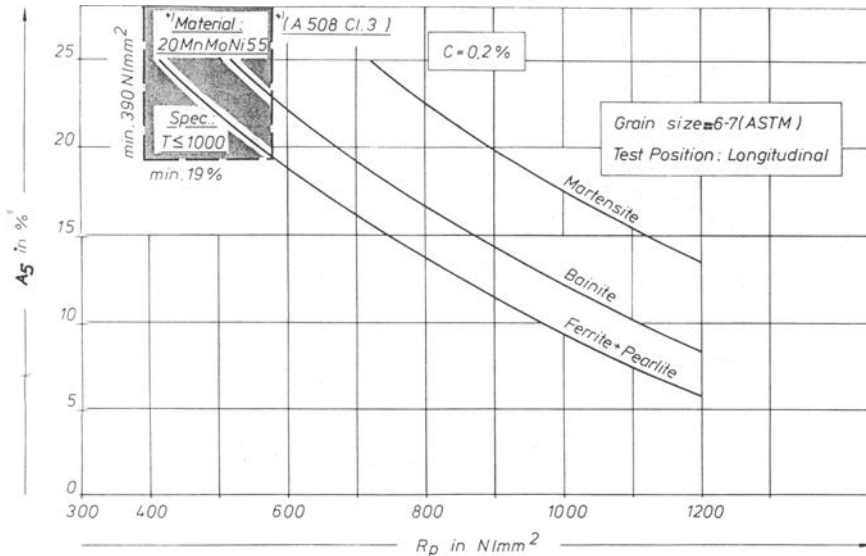


FIG. 5—Elongation A_5 as a function of yield strength R_p and structure.

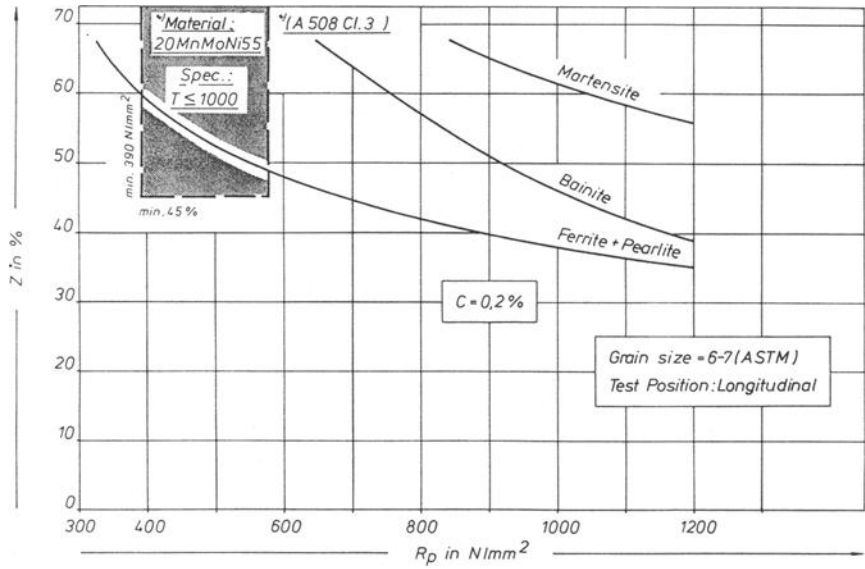


FIG. 6—Reduction of area Z as a function of yield strength R_p and structure.

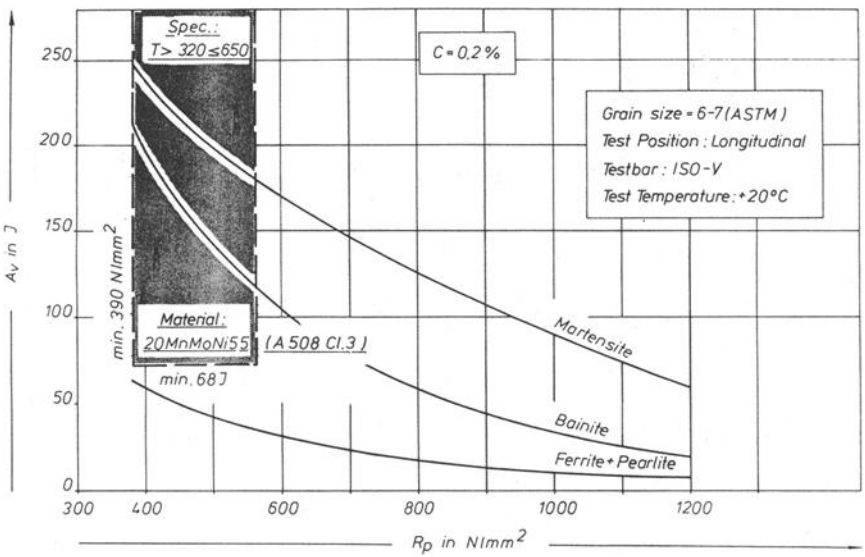


FIG. 7—Impact A_v as a function of yield strength R_p and structure.

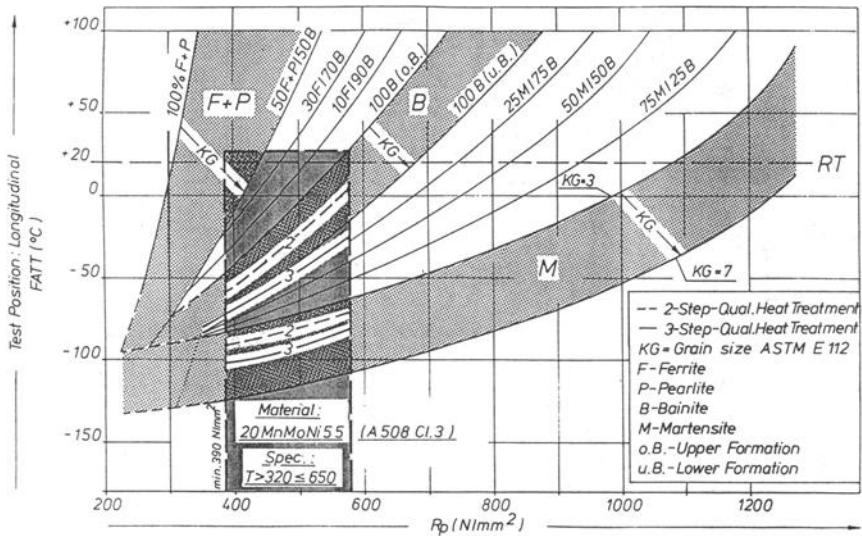


FIG. 8—FATT as a function of yield strength R_p and structure.

The diagrams in Figs. 5–8 are developed on the basis of a few hundred test results from tube sheets and similar size forgings. The curves represent the mean values of all test results.

Making use of the various nomograms based on longitudinal samples, the structure required to meet the specification values can now be determined for a steel with little segregation and a low level of inclusions because longitudinal and transverse values are located at the same level for the quasi-isotropic material condition.

With respect to elongation (A_5), Fig. 5 shows that the minimum value of 19% can be maintained with certainty and can even be attained with purely ferritic-pearlitic structures. The same relationship is represented for the reduction in cross-section parameter (minimum 45%) in accordance with Fig. 6.

With regard to the notch impact toughness, it can be seen from Fig. 7 that the structure has to be predominantly bainitic or martensitic to meet the notch impact toughness. Figure 8 shows the same relationship for the FATT. By this means, the toughness parameter at the desired transformation structure can be read off as a function of the grain size and is independent of dimension. The rise in FATT as a function of the yield strength and structure is particularly visible. The operating results obtained on various tube sheets and after various heat treatments (two-step and three-step heat treatments) are plotted in this graph and show good agreement with the theoretical curves of the nomogram.

The structure attainable in Test Position T/2 with water quench on bars and disks of 20 MnMoNi 55 is shown in Fig. 9 as a function of the wall thickness T or the diameter. The FATTs belonging to the various structures also are plotted in the graph, showing the limit value to VdTÜV specification. As a result, it

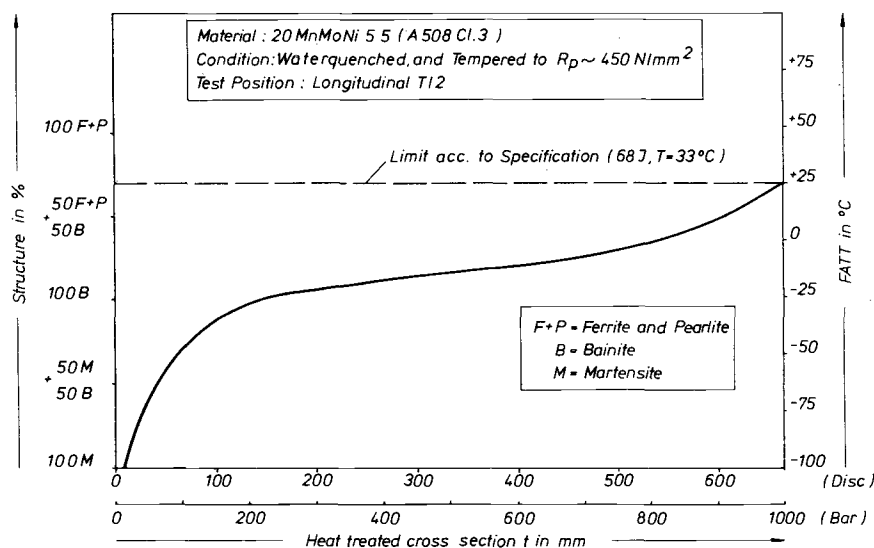


FIG. 9—Structure and FATT as a function of dimensions.

can be stated that the maximum theoretical wall thickness of tube sheets is approximately 650 mm, and the maximum theoretical diameter for round bars is 1000 mm, based on the minimum notch impact toughness in accordance with the VdTÜV specification.

Up to now, we have been discussing the effects of the structure on the toughness values. This, however, ignored a drop-in toughness which can be expected in the transverse direction as a result of deformed sulfides in the structure.

Figure 10 shows the considerable influence of the increasing sulfur content on the notch impact toughness in the transverse direction expressed as the isotropy factor A_v transverse over longitudinal.

To ensure the avoidance of critical sulfide concentrations, particularly in the zones of positive segregations on large forging ingots, melts must be provided with sulfur contents of approximately 0.001 to 0.002%.

The Buderus calcium-argon blowing (CAB) process is a good method of achieving this state. In this process, maximum desulfurization of the steel bath in the ladle is obtained by lance injection of powders containing calcium [4,5]. The remaining sulfides then are bound into globular form as nondeformable oxysulfides [scanning electron microscope (SEM) photomicrograph], as shown in Fig. 11.

In general, it is a characteristic feature of steels with a high level of cleanliness to show an increased inclination towards grain growth at elevated temperatures as a result of heating to forging temperature (Fig. 12). These results have been developed from labor tests and were found to conform to the characteristic grain growth in the tested tube sheets 20 MnMoNi 5 5. The mechanism is due to the

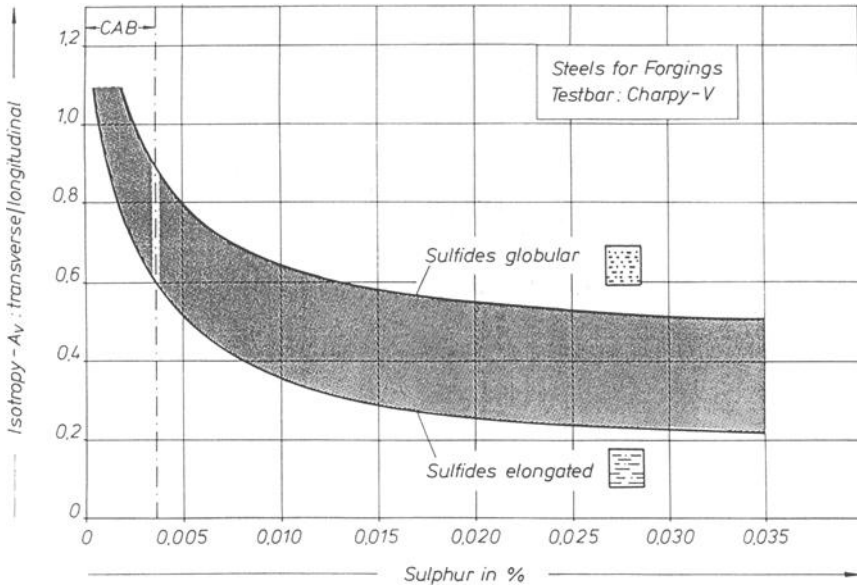


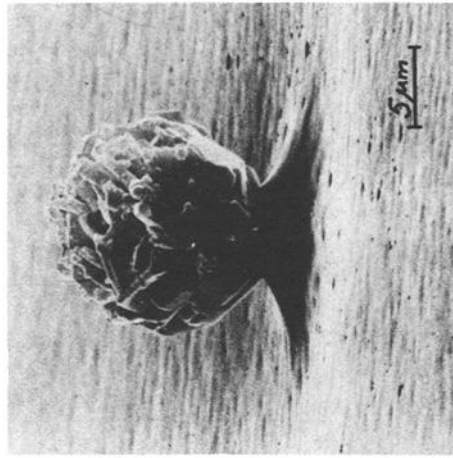
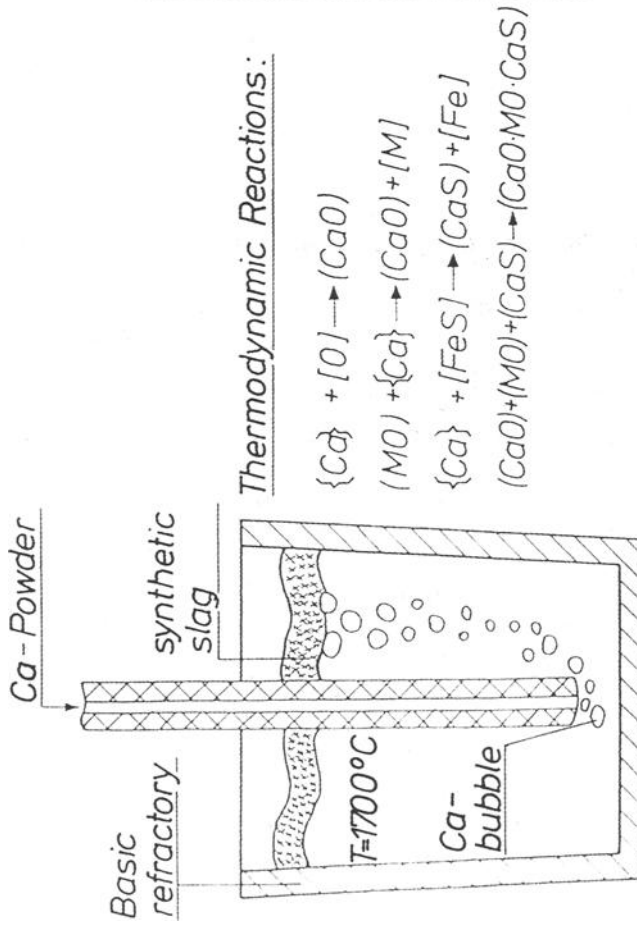
FIG. 10—Isotropy of impact energy A_v as a function of sulfur.

well-known controlling effect of phases in solid solution onto grain growth at forging temperatures.

To provide the fine-grain structure necessary to meet the toughness specifications, the tube sheets must, without fail, be subjected to suitable heat treatment after forging. Figure 13 shows the change in grain size as a function of the alpha-gamma transformations for the steel 20 MnMoNi 5 5.

The ideal fine-grain structure is obtained by using three-step QT heat treatment. Compared with the conventional two-step treatment involving austenitizing above AC_3 , the QT three-step heat treatment includes a second austenitizing step with quenching from the double phase range between AC_1 (720°C) and AC_3 (860°C) or steel 20 MnMoNi 5 5 (Fig. 14).

The result is a considerable refining effect on the grain size without major changes in the transformation structure of the material as per specification. Numerous test results from laboratory and production made evident that the optimum temperature for the solution treatment in the gamma-alpha double phase area is approximately 50°C above AC_1 ; the share of rebuilt structure is then approximately 40% [6]. For steel 20 MnMoNi 5 5, the structure of both phases consists of upper bainite after tempering. The primary structure is characterized by a higher intensity of tempering effect. In view of the distinctly improved mechanical properties, the TÜV has issued Edelstahlwerke Buderus with a license to produce heavy-section tube sheets up to 600 mm in thickness, including a three-step heat treatment.



SEM 3000:1
complex globular
Calcium sulfide inclusion

FIG. 11—Key plan of CAB lancing.

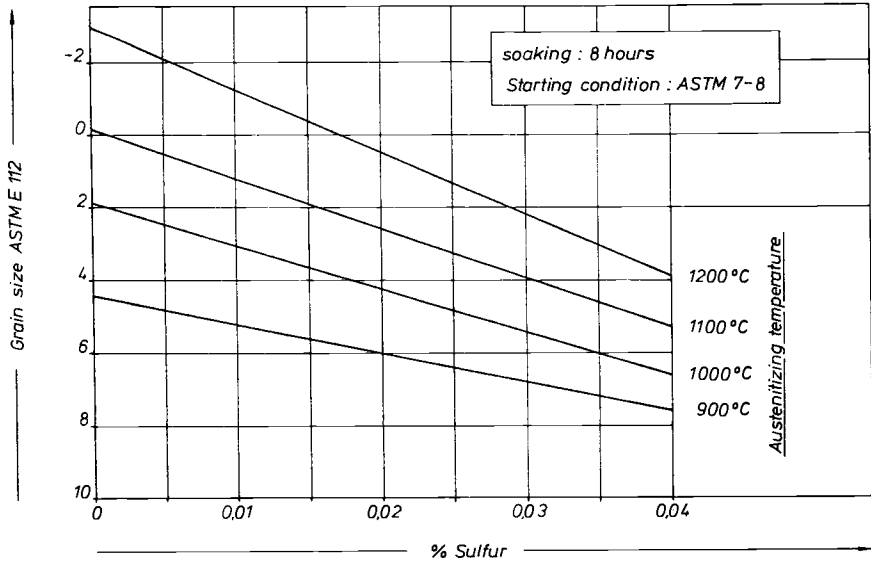


FIG. 12—Grain growth as a function of the sulfur content of heat-treatable steels.

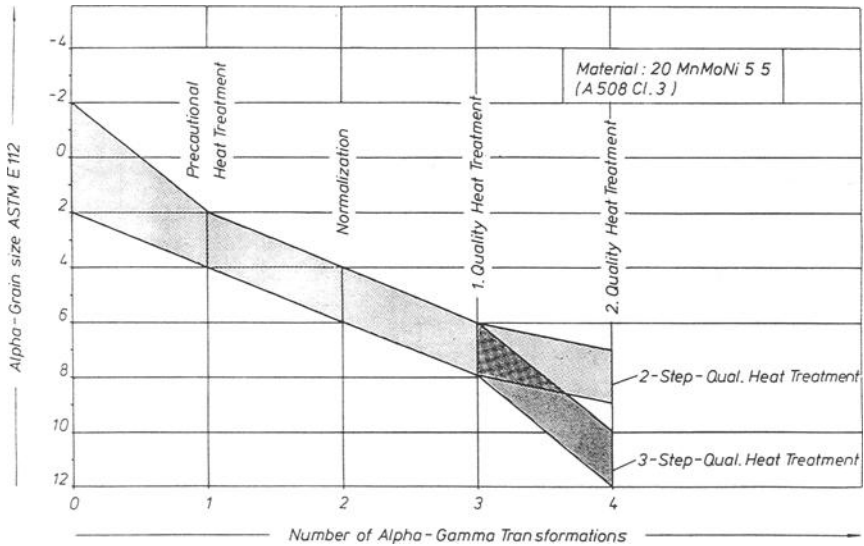


FIG. 13—Influence on the alpha grain size after alpha-gamma transformation.

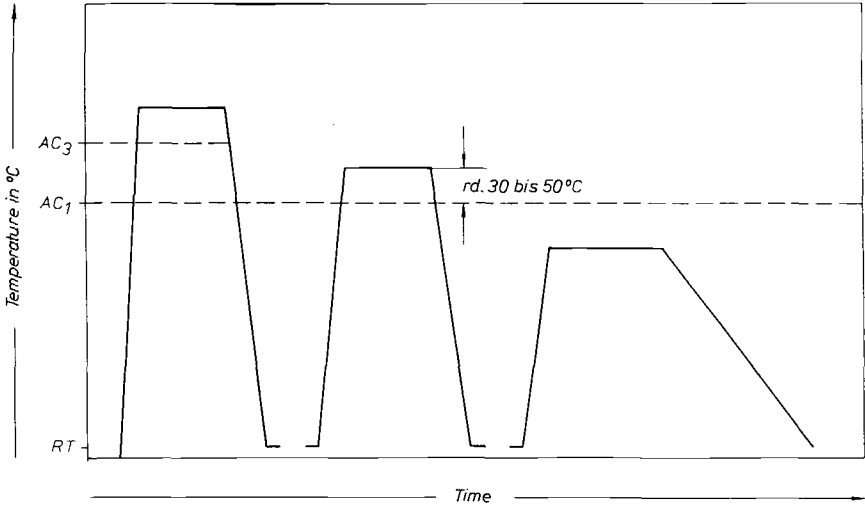


FIG. 14—Key plan of the three-step quality heat-treatment.

Figure 15 shows a comparison of the scatter bands of *FATT* values for disk-shaped forgings of 20 MnMoNi 5 5 from various production mills analogous to the results of TÜV documentation [7–9]. All the individual results can be collated into three scatter bands as a function of sulfur content and heat-treatment technology.

At a constant specimen dimension, the best toughness values together with the lowest scatter are obtained on heats with sulfur contents below 0.003%, where three-step heat treatment has been applied.

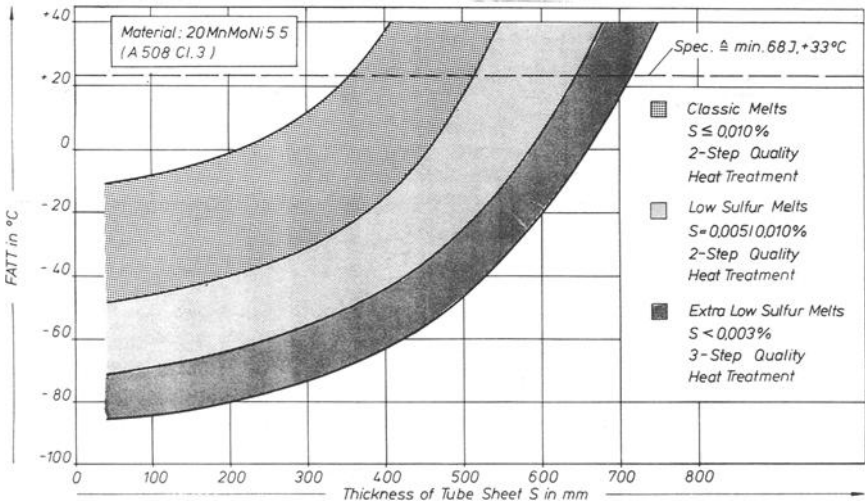


FIG. 15—TÜV statistics of tube sheet test results from different producers.

The maximum wall thickness for tube sheets produced by this method is approximately 680 mm. By comparison, tube sheets up to approximately 580 mm can be produced from heats with reduced sulfur contents between 0.005 and 0.010% with the two-step heat treatment.

Tube sheets produced by conventional means with sulfur contents higher than 0.010% exhibit the widest *FATT* value scatter. The maximum production dimensions here are limited to approximately 450 mm.

In connection with ensuring an adequate level of toughness, temper embrittlement can be excluded after simulated stress-relieving. This is proven by the test results after simulated post-weld heat treatment. Nor was it difficult to provide evidence of the required creep resistance values at 200°C.

Summary

This report deals with a new metallurgical and technological concept for the production of heavy-section tube sheets of 20 MnMoNi 5 5 for nuclear power stations within the KWU Konvoi project.

To meet the notch impact toughness specification in the upper dimension range for the tube sheets, a particularly fine-grain size is essential in addition to minimum sulfur contents. The CAB process combined with a three-step heat treatment has proven to be a suitable method.

Comparison with the toughness values attained by this method on conventionally produced tube sheets of 20 MnMoNi 5 5 proves the distinct qualitative advantages of the new technology.

References

- [1] Bandel, G. and Haumer, H.-Ch., *Stahl u. Eisen*, No. 84, 1964, pp. 932–46.
- [2] Kulmburg, A., "Beitrag zur Berechnung von ZTU-Schaubildern," in *Fortschritte in der Metallographie*, Vol. 10, 1979, Dr. Ruderer-Verlag, Stuttgart, Ed., pp. 285–99.
- [3] Blondeau R., et al., "Heat Treatment 76," The Metals Society, London, 1976, pp. 186–200.
- [4] Grimm, W., et al. *Stahl u. Eisen*, No. 101, 1981, pp. 569–72.
- [5] Grimm, W., and Feller, J., *Radex-Rundschau*, 1981, pp. 455–65.
- [6] Forch, K., et al. *Stahl u. Eisen*, No. 100, 1980, pp. 1329–38.
- [7] "Bericht über den Stand der Begutachtung des Werkstoffes 20 Mn Mo Ni 5 5," VdTÜV, 15 Nov. 1976.
- [8] "Ergänzungsbericht," VdTÜV, 28 Nov. 1982.
- [9] Technical Report No. W 5383, TÜV-Hessen, 18 April 1983.

DISCUSSION

*E. G. Nisbett*¹ (written discussion)—I was most interested to hear of the success of your three-step heat-treatment procedure for the forged ASTM A 508 Class 3

¹ National Forge Co., Irvine, PA 16329.

type of material. Was vanadium or aluminum used for grain-size control in these heats?

At National Forge Co. we did have success in using this type of heat treatment for heavy-walled A 508 Class 3 nozzle forgings when no deliberate additions of either aluminum or vanadium were made to the steel.

T. Skamletz and W. Grimm (authors' closure)—The final grain size was achieved by the multiple gamma-alfa transformation as demonstrated in Fig. 13. Extra additions of aluminum or vanadium have not been used to control grain size.

Jean P. Badeau,¹ Isabelle S. Poitrault,² Antoine de Badereau,²
and Regis P. Blondeau¹

Best Possible Heat Treatment of Steel SA 336 F22 for the Production of Forged Shells with Heavy Walls

REFERENCE: Badeau, J. P., Poitrault, I., de Badereau, A., and Blondeau, R., "Best Possible Heat Treatment of Steel SA 336 F22 for the Production of Forged Shells with Heavy Walls," *Steel Forgings, ASTM STP 903*, E. G. Nisbett and A. S. Melilli, Eds., American Society for Testing and Materials, Philadelphia, 1986, pp. 425–438.

ABSTRACT: The manufacturing of thick-wall components, such as shells, for petrochemical reactors normally requires the 2.25Cr-1Mo (SA 336 F22) steel. This paper deals with:

1. Experienced difficulties in producing thick-wall forgings up to a thickness of 500 mm with standard 2.25Cr-1Mo steel.
2. The solutions offered by Le Creusot Heavy Forge.

The studies discussed are: (1) the effect of the structure; (2) the effect of the chemical composition on hardenability and temper embrittlement in steel making; and (3) the effect of austenitization conditions.

Some examples concerning industrial forgings are presented, among them:

1. The manufacturing of shells for the petrochemical industry.
2. A thick-wall shell from a 146-metric ton hollow ingot.

KEY WORDS: chromium-molybdenum steel, metallographic structures, chemical composition, residual elements, hardenability, temper embrittlement, heat treatment, manufacturing

Components of petrochemical reactors usually are manufactured either with ring-rolled and welded plates or with forged shells. Important developments in the oil refining and coal liquefaction industries have led engineers to ask frequently for thicker walls for reactor vessels and for a minimum of welds, particularly with regard to longitudinal welds. Only forgings can easily satisfy these requirements.

The technical literature shows that many studies have been undertaken to

¹ Metallurgist engineer, Creusot-Loire, Le Creusot Material Research Center, Le Creusot, France.

² Metallurgist engineer, Creusot-Loire, Le Creusot Heavy Forge, Le Creusot, France.

improve steel by modification of chemical composition (addition of nickel, vanadium, boron, etc.) [1–5]. Those studies on modified 2.25Cr-1Mo steel aim at the manufacturing of thick-wall forgings.

Although Le Creusot Heavy Forge also has studied modified steel, we have tried to improve standard 2.25Cr-1Mo steel for heavy section (up to 500 mm) parts because the standard steel is still mainly used today. This paper presents the obtained results.

Parameters Influencing Hardenability and Temper Embrittlement

Several properties can be carried as quality index:

1. Mechanical properties (tensile, toughness, and creep properties after post-welded heat treatment) tightly related to hardenability.
2. Behavior during service life related to the temper embrittlement rate due to long holding times at service temperatures.

This is why the effects of structure, chemical composition, and austenitization conditions on these properties (hardenability, temper embrittlement) have been studied.

Effect of Microstructure

It is well known that standard 2.25Cr-1Mo steel has not sufficient hardenability to obtain a wholly bainitic microstructure in thick-wall forgings.

Experimental Procedures—Material tested: steel from an industrial heat (chemical analysis in Table 1). Heat treatment: austenitization 950°C for 5 h; four cooling rates: 100, 250, 550, and 5000°C/h; tempering; postwelded heat treatment (PWHT) 690°C for 12 h; step cooling (Fig. 1).

Results—Table 2 summarizes the results. The 100% bainitic microstructure gives the best mechanical properties. This has been noted already by Blondeau and Berthet [6] and Sato et al. [7]. But a given ferrite percentage does not necessarily have the same influence on the different properties. As shown in Fig. 2, ductility properties (elongation and reduction of area) are not affected by a high ferrite percent, while ultimate tensile strength (UTS), yield strength (YS), and the YS/UTS ratio decreases sharply when the ferrite percentage increases over 10%. The usual requirement, the minimum room temperature yield strength

TABLE 1—Chemical composition of material used for the study of the effect of ferrite content (weight %).

C	S	P	Si	Mn	Ni	Cr	Mo	Cu	Sn	Al
0.125	0.0022	0.0056	0.211	0.519	0.080	2.44	0.939	0.088	0.006	0.005

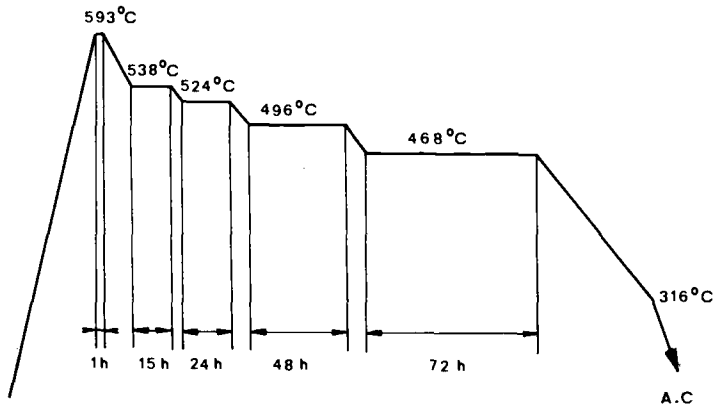


FIG. 1—Step cooling cycle.

of 310 MPa, cannot be obtained (after a PWHT of 690°C) with a microstructure with more than 40% ferrite.

Figure 3 exhibits the effect of ferrite content on toughness. Increasing the ferrite percentage by 10% increases the fracture appearance transition temperature (FATT) by 10°C. The hardest requirement nowadays [54 J (40 ft · lb) at -40°C] can be obtained only with a microstructure containing less than 25% ferrite.

The step-cooling heat treatment has little effect on properties, however, irrespective of the ferrite percentage. Besides, as seen in Table 3, the relation Charpy V transition (VTR) $54 \text{ J} + 1.5\Delta(\text{VTR } 54 \text{ J}) \leq -10^\circ\text{C}$ is right for each type of microstructure studied.

All these results suggest that the structure at midthickness of the parts has to have a maximum of 25% ferrite insider to guarantee the usual requirements.

Chemical Composition

Hardenability—In any case, the delivered chemical composition has to be in the range of the ASTM A 336 F22 specification. As chromium has a light effect [8,9] and molybdenum a narrow range, only carbon and manganese may be used to improve hardenability [15].

Figure 4—the evolution of the bainitic critical cooling rate depending on carbon and manganese content—shows that carbon and manganese are very efficient, but the ASTM limits do not allow enough increase to obtain a wholly bainitic structure for higher than 300-mm, thick-wall forgings.

Temper Embrittlement—Two formulas have been proposed as temper embrittlement index:

1. Bruscato factor [10]: $\bar{X} = (10 \text{ P} + 5 \text{ Sb} + 4 \text{ Sn} + \text{As})/100$ (in ppm).
2. J [11]: $J = (\text{Mn} + \text{Si}) \cdot (\text{P} + \text{Sn}) \cdot 10^4$ (in %).

TABLE 2—Results of mechanical tests of the study of the effect of ferrite content.

CR, °C/h	Ferrite, %	Condition ^a	Tension Test				CVN, J/cm ²				FATT, °C	VTR 54 J ^b , °C
			YS 0.2%, MPa	UTS, MPa	EL, %	RA, %	0°C	-7°C	-20°C	-40°C		
100	60	1	263	516	30.4	80	170	21	9	7	5	0
		2	267	516	30.2	78	248	102	44	8	0	-10
250	35	1	350	553	25.4	79	331	322	290	18	-27	-32
		2	355	551	26.8	80	289	248	263	36	-30	-37
550	10	1	456	585	26.5	80	369	307	324	278	-60	-65
		2	454	580	25.6	80	327	315	282	265	-55	-67
5000	0	1	477	608	25.6	81	307	299	256	229	-60	-60
		2	476	609	26.0	80	351	301	331	272	-60	-77

NOTE: CVN = Charpy V-notch; CR = cooling rate; EL = elongation; UTS = ultimate tensile strength; FATT = fracture appearance transition temperature; RA = reduction in area; YS = yield strength; VTR = Charpy V-transition; PWHT = postweld heat treatment; SC = step cooling; QT = quality treatment.

^a1 = QT + PWHT; 2 = QT + PWHT + SC.

^bVTR 54 J = temperature at which CVN = 54 J (67.5 J/cm²) 40 ft · lb.

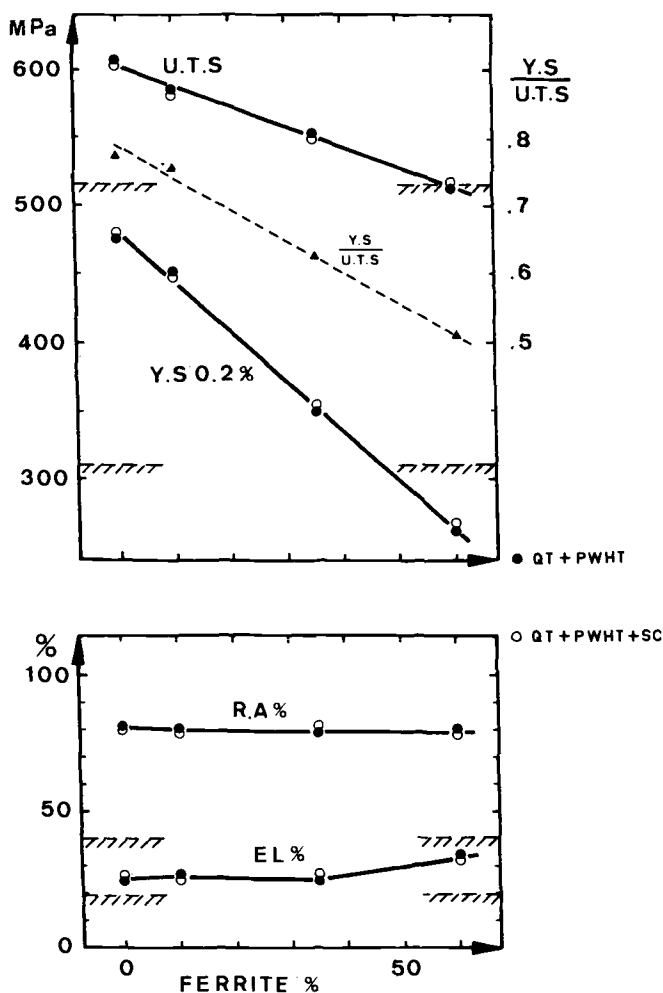


FIG. 2—Effect of ferrite content on tensile properties.

It is now known that the main element leading to temper embrittlement is phosphorous [12–14], elements such as arsenium, tin, and antimony exhibiting only a slight degradation of toughness; manganese and silicon increase temper embrittlement susceptibility [7,10–12]. Also, there is a multiplicative effect of $Mn \times P$ [6]; but the manganese range has to be aimed near the maximum to lower the ferrite percentage.

The low silicon solution due to vacuum silicon deoxidization appears, at first sight, interesting. However Blondeau and Berthet [6] have noted clearly that reducing this element produces a very deleterious effect on room- and high-

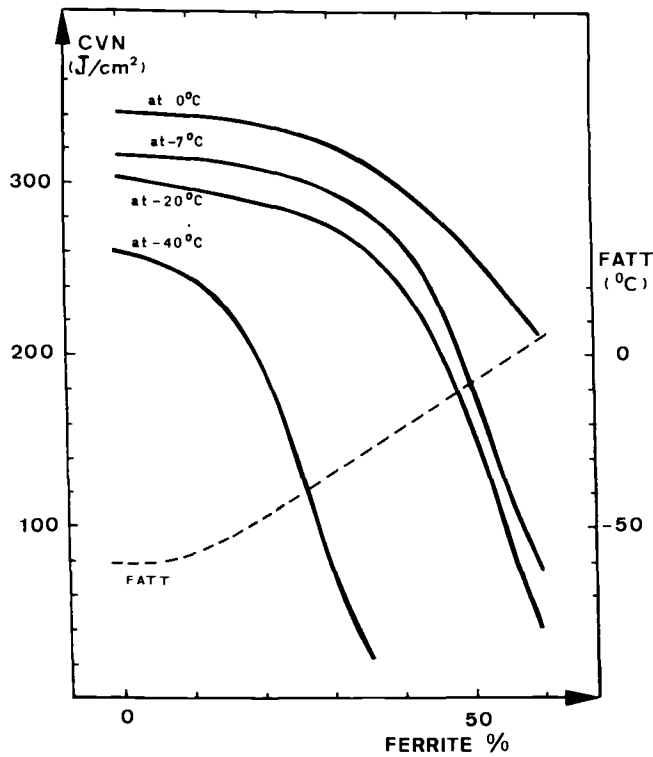


FIG. 3—Effect of ferrite content on toughness (Charpy V-notch impact properties).

temperature UTS. So, Le Creusot Heavy Forge has chosen the following parameters:

1. Carbon and manganese content according to the thickness (between the limits of the ASTM specification) to obtain a wholly bainitic structure at mid-thickness.
2. Silicon dcoxidization.

TABLE 3—Effect of ferrite content on embrittlement after step cooling.

Ferrite, %	VTR 54 J + 1.5Δ (VTR 54 J), °C
60	– 15
35	– 40
10	– 68
0	85

NOTE: VTR = Charpy V-transition.

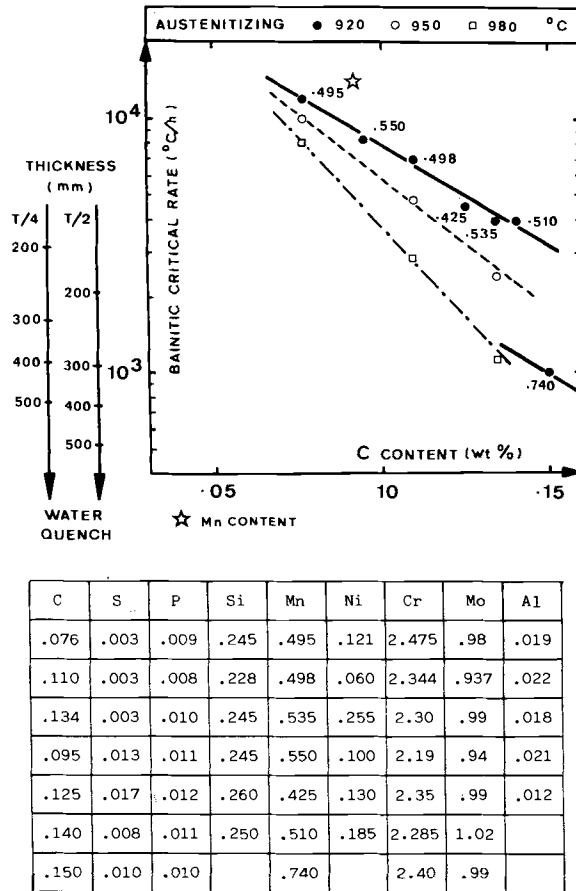


FIG. 4—Effect of carbon and manganese contents and austenitizing temperature on the bainitic critical cooling rate.

3. Very low phosphorus and sulfur contents. (Guarantees phosphorous percent to be < 0.005 with sulfur percent, < 0.002). These percents can be easily obtained with the heating ladle refining process (HLRP) and low tin, arsenium, and antimony contents by a close scrutiny of the selection of scrap iron.

Based upon these conditions, Le Creusot Heavy Forge can guarantee $\bar{X} \leq 10$ and $J \leq 100$.

Austenitization Conditions

Increasing the austenitization temperature always increases hardenability as shown by Sato et al. [7] and Creusot-Loire studies (Fig. 4). But the hardenability

TABLE 4—Effect of austenitizing temperature on mechanical properties of SA 336 F21 steel grade.

		QT + PWHT						QT + PWHT + SC									
		CR, °C/h	YS 0.2%, MPa	UTS, MPa	EL, %	RA, %	CVN 0°C, J/cm ²	CVN -40°C, J/cm ²	FATT, °C	YS 0.2%, MPa	UTS, MPa	EL, %	RA, %	CVN 0°C, J/cm ²	CVN -40°C, J/cm ²	FATT, °C	Δ FATT, °C
Austenitizing	950°C, 5 h	2400	404	557	31.8	76	212	112	-13	395	562	29.8	77	199	85	-6	7
	1400	2400	393	559	29.8	77	225	115	-20	394	563	28.1	76	199	59	-7	13
	2400	2400	407	567	30.8	77	190	44	-10	409	571	28.8	75	170	79	3	13
	5 h	1400	397	563	29.1	74	193	42	-10	413	572	29.7	75	142	42	5	15
	2400	2400	419	575	29.7	75	182	22	-2	425	581	29.1	74	122	13	10	12
	1050°C, 5 h	1400	413	570	29.4	75	195	60	-18	428	579	27.7	75	150	35	4	22
	900	416	572	29.0	75	191	57	-10

Note: CR = cooling rate; QT = quality treatment; YS = yield strength; CVN = Charpy V-notch; FATT = fracture appearance transition temperature; RA = reduction in area; EL = elongation; RA = reduction in area; SC = step cooling; UTS = ultimate tensile strength; PWHT = postweld heat treatment.

TABLE 5—Effects of austenitizing temperature on mechanical properties. Industrial study.^a

Austenitizing	Grain Size	Direction-Axial				Direction-Tangential				
		YS 20°C, MPa	UTS 20°C, MPa	EL 20°C, %	RA 20°C, %	CVN -7°C, J/cm ²	CVN 0°C J/cm ²	CVN -40°C, J/cm ²	FATT, °C	TT54 J ^b °C
950°C	5	466	593	22.4	82	348-358-360	306-314-320	120-240-298	-46	-77
1000°C	4	462	596	22.6	82					
		466	590	23.4	82	297-309-339	275-293-319	164-194-226	-43	-69
1050°C	1	466	590	23.4	82					
		479	601	21.4	81	283-289-304	239-275-303	66-91-208	-27	-61
		479	599	22.6	80					

NOTE: QT = quality treatment; YS = yield strength; UTS = ultimate tensile strength; EL = elongation; CVN = Charpy V-Notch; RA = reduction in area; FATT = fracture appearance transition temperature.

^aLocation = T/4 inside; condition: QT + PWHT (690°C - 12 h).

^bTT40 = temperature at which CVN = 54 J (67.5 J/cm²) 40 ft · lb.

TABLE 6—*Chemical composition of hollow ingot (weight %).*

C	S	P	Si	Mn	Ni	Cr	Mo	V	Cu	Sn	Al	As	Sb
0.139	0.004	0.004	0.218	0.530	0.162	2.43	1.07	0.007	0.045	0.005	0.015	0.008	0.001

NOTE: $\bar{x} = 7.3$; $J = 67.3$.

increase must not induce other unfavorable phenomena for toughness such as coarse-grain structure.

A laboratory study on SA 336 F21 steel with different austenitization temperatures (950°C, 1000°C, 1050°C), results reported in Table 4, has shown that austenitization temperature increasing from 950 to 1050°C with a 100% bainitic microstructure increases tensile properties without any important change in temper embrittlement.

An industrial study on 400-mm, thick-wall shells has been realized to confirm these results, after PWHT and after step-cooling heat treatment (Table 5). But the fast increase of grain size with an austenitization temperature higher than 1000°C led to an industrial austenitization temperature limited to 1000°C.

Some Examples of Industrial Manufacturing

Shell from a Hollow Ingot

This shell was forged by drawing and expanding on mandrel from a 146-metric-ton hollow ingot. Chemical analysis is given in Table 6. The dimensions for quality heat treatment were:

1. Outer diameter = 5075 mm.
2. Inner diameter = 4355 mm.
3. Thickness = 360 mm.
4. Height = 2725 mm.

After the heat treatment—980°C, water quenching by immersion and tempering, 660°C—test rings have been removed and postwelded heat-treated at 690°C for 30 h and step cooled.

As shown in Figs. 5 and 6, the shell showed a high level and a very good homogeneity of properties in the entire forging (through thickness and through height). The step cooling led to a very slight temper embrittlement, so the imposed requirement $VTR\ 54\ J + 2.5\Delta(VTR\ 54\ J) \leq 21^\circ C$ has been satisfied. (Obtained results: -49 to $-110^\circ C$.)

Shells from a Cylindrical Ingot with Horizontal-Oriented Solidification (LSD)

Twenty-five shells were forged by drawing and expanding on mandrel from different types of “long LSD” ingot types [16]. This manufacturing included shells with two thicknesses, 230 and 500 mm, before quality heat treatment.

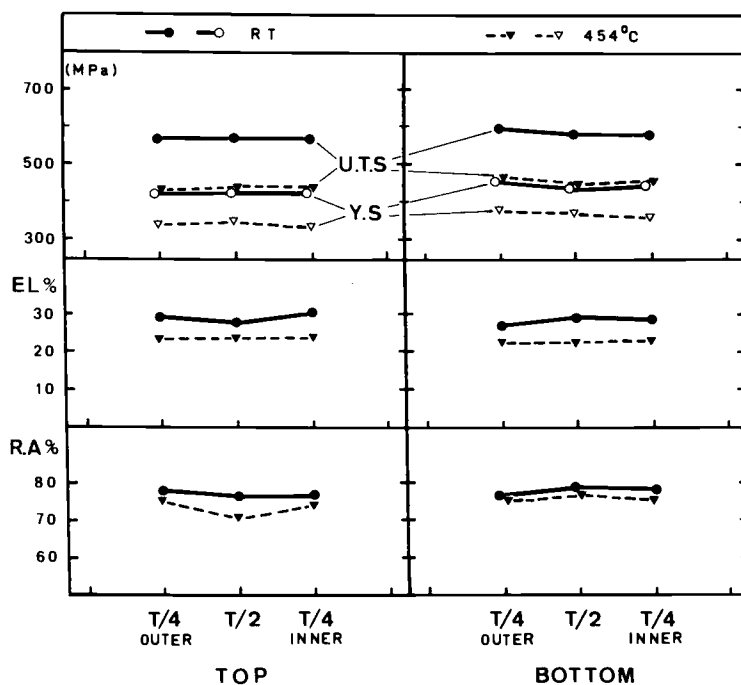


FIG. 5—Hollow ingot. Variation of tensile properties through thickness. Tangential direction. QT + PWHT (690°C - 12 h).

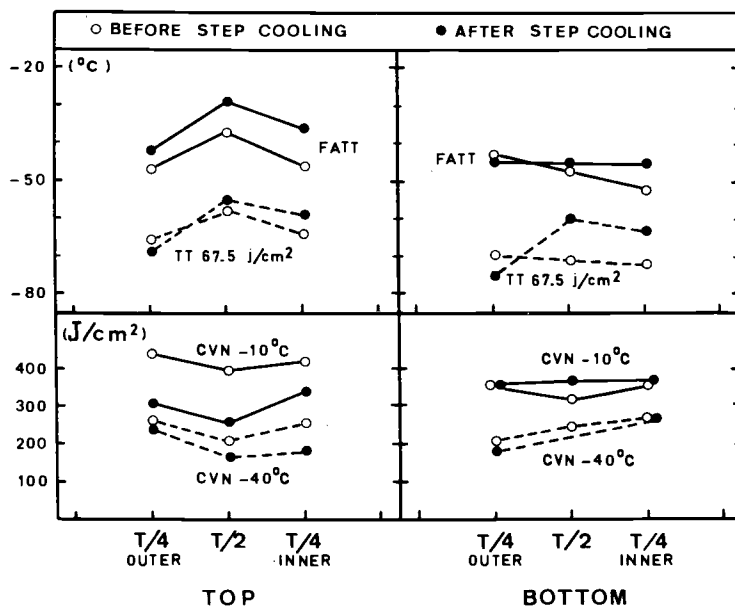


FIG. 6—Hollow ingot. Variation of impact properties through thickness. Tangential direction. QT + PWHT (690°C - 12 h).

TABLE 7—Mechanical properties on industrial forging.

Location = T - T/2

Population	Thickness, mm	Austenitizing, °C	Condition ^a	Tensile Properties						Impact Properties					
				YS 20°C, MPa		UTS 20°C, MPa		YS 454°C, MPa		CVN - 20°C, J/cm ²		CVN - 40°C, J/cm ²		FATT, °C	
				Min	Max	Min	Max	Min	Max	Min	Max	Min	Max	Min	Max
14	500	1000	1	443	465	580	606	383	409	224	360	176	332	-29	-53
			2	145	365	75	277	-27	-47
11	230	950	1	404	422	557	573	344	369	377	>445	150	>446	-44	-49
			2	142	>445	70	>446	-15	-36

NOTE: YS = tensile strength; UTS = ultimate tensile strength; CVN = Charpy V-Notch; FATT = fracture appearance transition temperature.
^a1 = QT + PWHT; 2 = QT + PWHT + SC.

The previous studies on this steel grade have permitted the optimization of the quality heat-treatment conditions:

1. Austenitization: 950°C for 230-mm, thick-wall vessels; 1000°C for 500-mm, thick-wall vessels.
2. Quenching by water immersion.
3. Tempering at 660°C.

For each part, after the heat treatment, two test rings (top and bottom) were removed after discarding overlenghts of 230 or 500 mm at each end equal to the thickness. PWHT and step cooling were applied to specimens.

Table 7 summarizes the results of tension and impact tests obtained in the midthickness location related to thickness. It appears that:

1. Mechanical properties are very good and quite homogeneous.
2. The optimization of austenitization temperature permits a sufficient hardenability combined with a very slight temper embrittlement.

Conclusion

We have optimized chemical composition (carbon, manganese, silicon, and impurities) and heat treatment conditions of the standard 2.25Cr-1Mo steel with the view of guaranteeing the higher possible mechanical properties to thicknesses up to 500 mm. However, we believe that nowadays we have obtained the maximum mechanical properties of this steel grade.

For again improving mechanical properties, in particular for higher in-service temperatures, Le Creusot Materials Research Center and Heavy Forge are studying standard and modified 9Cr-1Mo (SA 182 F9) steel grades. We believe that in the future there will be a significant increase of requirements, particularly for mechanical properties at high temperatures, and that 9Cr-1Mo will have these requirements.

References

- [1] Nieuwland, H. C. D. et al., "Development of Thick-Wall 2.25Cr-1Mo-Ni-Nb Steel Forgings for Steam Generators of Fast Breeder Reactors," Ninth MPa Seminar, 13-14 Oct. 1983, Stuttgart.
- [2] Prescott, G. R. and Braun, C. F., "Update on Modified 2.25Cr-1Mo and 3Cr-Mo Alloys," the Metal Properties Council, Inc., Ann Arbor, MI, 1983.
- [3] Wada, T., "2.25Cr-1Mo Steel Modified with Vanadium Addition," Report RP 32 75 03, Climax Molybdenum Co., Ann Arbor, MI, 22 Feb. 1977.
- [4] Wada, T., "SSC Resistance of 2.25Cr-1Mo Steels for Oil Wellhead Components," Report J 4518, Climax Molybdenum Co., Ann Arbor, MI, 26 Nov. 1979.
- [5] Wada, T., "Modified 2.25Cr-1Mo Steels Containing 0.5% Nickel and Microalloys," Report L294-10, Climax Molybdenum Co., Ann Arbor, MI, 21 Apr. 1983.
- [6] Blondcau, R. and Berthet, J. A., "Heavy Section 2.25Cr-1Mo Steel Plates with Good Resistance Embrittlement."
- [7] Sato, S., et al., "Strength and Temper Embrittlement of Heavy Section 2.25Cr-1Mo Steel," Kawasaki Steel Co., Kurashiki 712, Japan.

- [8] Wada, T. and Eldis, G. T., "Transformation Characteristics of 2.25Cr-1Mo Steel," MPC/ASTM Symposium, Denver, May 1980, American Society for Testing and Materials, Philadelphia.
- [9] Blondeau R. et al., "Metallurgical Properties of 3Cr-1Mo Steel Used on High Temperature Petrochemical Reactors," 4th International Conference on Pressure Vessel Technology, May 1980, London.
- [10] Bruscatto R., "Temper Embrittlement and Creep Embrittlement of 2.25Cr-1Mo Shielded Metal Arc Weld Deposits," *Welding Research Supplement*, April 1970.
- [11] Marakami, Y. et al., "Heavy Section Cr-Mo steels for Hydrogenation Service," 17th Annual Conference of Metallurgists, Montreal, Canada, Aug. 1978.
- [12] Jinyu and McMahon, C. I., "The Effects of Composition and Carbide Precipitation on Temper Embrittlement of 2.25Cr-1Mo Steel. Effects of P, Sn, Mn, and Si," *Metallurgical Transactions A*, Vol. 11A, Feb. 1980.
- [13] Swift, R. A., "The Effects of Phosphorus on the Temper Embrittlement Susceptibility of 2.25Cr-1Mo Steel," *Chrome Poly in 1976*, ASME MPC 4, American Society of Mechanical Engineers, New York.
- [14] Takamatsu, T. et al., "Temper Embrittlement Characteristics of 2.25Cr-1Mo Steels," *Transactions ISIJ*, Vol. 22, 1982.
- [15] Blondeau R. et al., "Mathematical Model for the Calculation of Mechanical Properties of Low Alloy Steel Metallurgical Products," *Heat Treatment* 76, May 1976.
- [16] Bocquet P. et al., "Application of New Types of Ingots to the Manufacturing of Heavy Pressure Vessel Forgings," this publication.

DISCUSSION

*H. Nishiyama*¹ (*written discussion*)—In Table 7, what is the reason that the FATT value of 500 mm is better than the FATT value of 230 mm?

J. P. Badeau, I. Poitraul, A. DeBadereau, and R. Blondeau (authors' closure)—The question is judicious. Other things being equal, the FATT values of 230 mm were expected to be better than the FATT values of 500 mm. The principal reason arises due to a better quench structure on the 500-mm products. Referring to 230-mm products, the blank of hardenability is to provide with: (1) higher carbon content; (2) austenitization at higher temperature.

¹ Japan Casting & Forging Corp., Kitakyushu City, Japan.

Production of a 304 Stainless Steel Nuclear Reactor Forging from a Very Large Electroslag Refined Ingot

REFERENCE: Watkins, E. J. and Tihansky, E. L., "Production of a 304 Stainless Steel Nuclear Reactor Forging from a Very Large Electroslag Refined Ingot," *Steel Forgings*, ASTM STP 903, E. G. Nisbett and A. S. McIlilli, Eds., American Society for Testing and Materials, Philadelphia, 1986, pp. 439–449.

ABSTRACT: A four-loop, upper barrel flange forging for a nuclear reactor was produced from what the authors believe to be the largest 304H grade stainless steel electroslag refined (ESR) ingot ever refined. The ingot was refined in a 1524-mm-diameter, ingot withdrawal-type ESR furnace using a lime-bearing slag, low-frequency a-c power, and dry air protection. Five electrodes were remelted in order to produce the desired ingot weight. The ingot was subsequently forged in a five-step operation on a 6800-metric-ton press to produce the desired barrel flange configuration. Testing of the finished machined forging revealed excellent tensile ductility, excellent ultrasonic penetrability, and good chemical uniformity with no macrosegregation. Overall quality was judged to be superior to previously produced, conventionally melted forgings.

KEY WORDS: barrel flange forging, nuclear reactor, 304H stainless steel, ESR ingot, slag, ingot withdrawal furnace, tensile properties, ultrasonic penetrability, chemical uniformity, macrosegregation

Forgings used in nuclear reactors must be of high quality and must meet stringent metallurgical and mechanical property requirements. Electroslag refining (ESR) has the capability to produce ultra clean, homogeneous, high-quality ingots that are eminently suitable to the production of nuclear reactor forgings. This paper deals with the production of a four-loop, upper barrel flange forging of 304H stainless steel (ASME SA-182, Grade 304H) that was processed from what the authors believe to be the largest 304 grade ESR ingot ever refined.

ESR Process and Equipment

The ESR process involves the melting of a consumable electrode through a molten flux in a water-cooled mold or crucible. The flux is electrically heated

¹ Melting metallurgist, and general foreman, Electroslag Remelting, Bethlehem Steel Corp., Bethlehem, PA 18016.

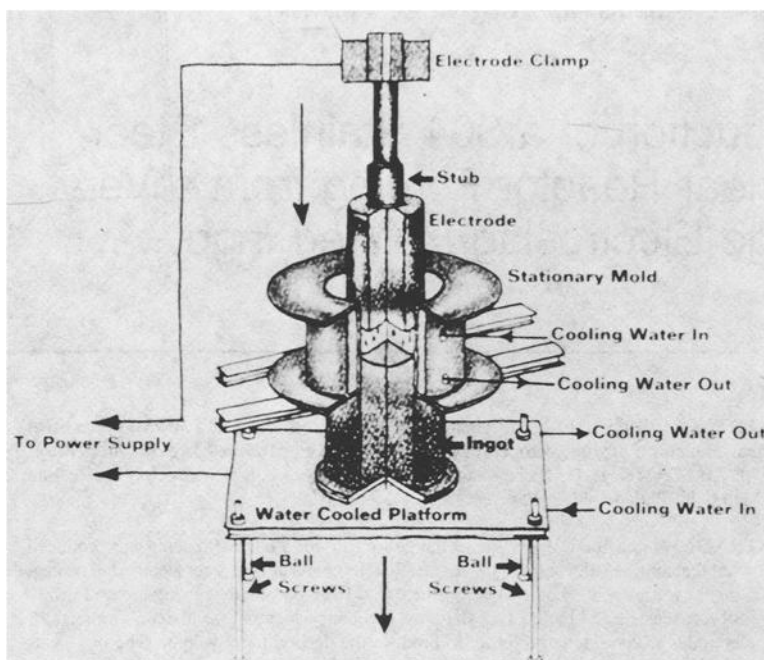


FIG. 1—ESR ingot withdrawal furnace.

by resistance to a temperature above the melting point of the electrode. As the tip of the electrode melts, a film of molten metal is formed. Droplets are developed in the film, detach, and pass through the molten slag where refining reactions occur. The refined metal is collected in the mold and solidification takes place by heat extraction through the water-cooled mold and baseplate. By careful matching of the electrode melting rate with the ingot freezing rate, sound segregation-free ingot structures can be obtained.

There are several types of ESR furnaces in common use. The Bethlehem installation has four melting stations which are all of the ingot withdrawal type. In this type of ESR furnace, the desired ingot length is produced by withdrawing the solidified ingot from the bottom of the mold as melting progresses. A cross-sectional drawing of an ingot withdrawal furnace is presented in Fig. 1. The water-cooled baseplate (on which the ingot initially forms) is withdrawn from the mold using ball screws.

Furnace sizes at Bethlehem range from 660 to 1524 mm in diameter and all are powered by thyristor-controlled, low-frequency a-c power supplies. The 304H grade stainless steel ingot was refined in the 1524-mm furnace using two coupled 27.5 kA, 100-V power supplies.

ESR Electrodes

The steel used for electrodes was melted in an electric arc furnace, vacuum degassed, and then bottom poured into four round electrode molds. A fifth,

TABLE 1—*Electrode chemical analysis, weight %.*

	C	Mn	P	S	Si	Ni	Cr	Co
Requirements	0.04	1.50	0.30	9.25	18.50	...
ASME SA-182 304H	0.08	2.00	0.025 max	0.025 max	0.70	10.25	19.50	0.20 max
Electrodes	0.07	1.55	0.009	0.020	0.55	9.95	19.20	0.13

smaller diameter electrode also was poured to provide a hot topping electrode for the ESR process. The chemical requirements of ASME SA-182 Grade 304H and the electrode chemistry are presented in Table 1.

No special efforts were made to produce a low-sulfur content because of the excellent desulfurization that can be obtained in the ESR process. All other elements were at desired levels before ESR melting.

ESR Ingot Production

Following electrode cleaning, current carrying stubs were electrosag-welded to the electrodes, and the 1524-mm furnace was set up to begin melting. A thin-gage, mild steel starter can packed with steel chips and welded to a steel plate was clamped to the withdrawal table baseplate before the mold was swung into the melting position. The chips used for production of the 304H grade ingot were also 304 stainless steel in order to minimize oxidation and dilution losses that can occur during the furnace start-up period. Approximately one third of the total slag weight was charged into the furnace before start-up. The slag used to produce this ingot was prefused and had a nominal composition of 60% calcium fluoride (CaF_2), 20% calcium oxide (CaO), 20% aluminum oxide (Al_2O_3). This slag (60/20/20) provides good melting characteristics, moderate resistivity, and excellent desulfurization because of the 20% CaO content.

The initial stages of melting were conducted using d-c power to provide a stable arc to melt the starter can and initial flux charge. One-half hour after start-up, power was switched to 2 Hz a-c for the remainder of the refining period. During refining, the slag was continuously deoxidized using aluminum shot in order to keep the slag ferrous oxide (FeO) content as low as possible. Low slag FeO contents (generally less than 0.5 weight %) are necessary in order to provide maximum ingot cleanliness and efficient desulfurization. A plot of slag FeO content versus refining time is presented in Fig. 2, and the consistent, low values are readily apparent.

During refining, the molten slag was shielded from the ambient atmosphere by a blanket of dry air. The dry air, supplied by a refrigerant dryer, is introduced into the melt zone of the furnace through a combination exhaust-dry air hood. This hood is constructed in such a fashion to extract efficiently exhaust fumes generated in the ESR process, while at the same time blanketing the slag with a protective cover of dry air. Continuous monitoring of the melt zone dew point just above the slag bath was conducted during refining. Melt zone dew points for this ingot were in the range of -18 to -20°C . Experience has shown that dew points of this level prevent any atmospheric moisture pickup by the molten slag. This is especially important when a highly basic slag such as 60/20/20 is used because any significant slag moisture content is readily transferred as elemental hydrogen to the molten metal as it passes through the slag.

Four electrode changes were made during refining. Each electrode change was accomplished in under 1 min, thus insuring minimal disruption to the process.

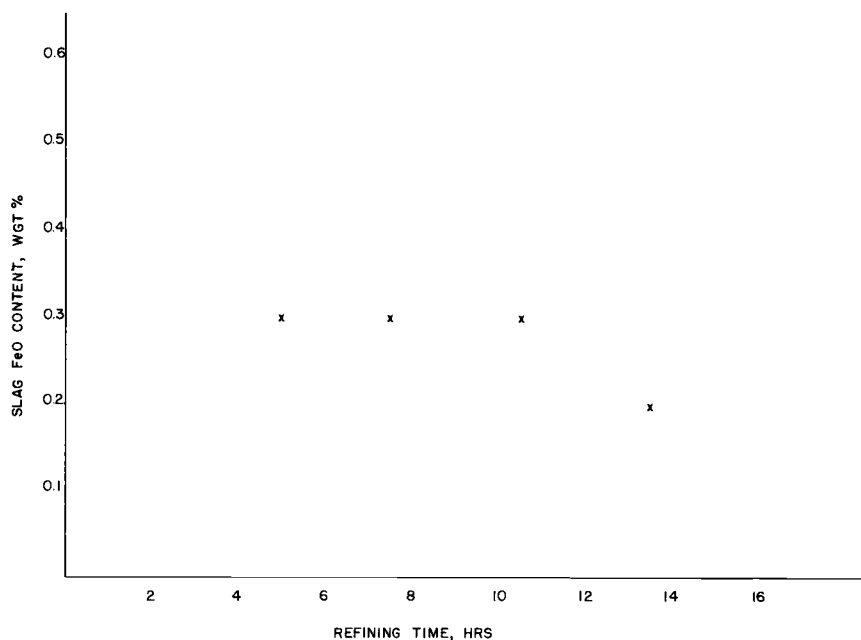


FIG. 2—Slag FeO content versus refining time.

The final electrode change was made to a smaller diameter electrode that was used for hot topping the ingot. Hot topping ESR ingots involves planned reductions in energy input over specified time intervals. Careful control of the hot topping process is necessary to avoid shrinkage defects and minimize the amount of top ingot discard.

Following the hot topping process, the ingot was allowed to cool in the furnace until the slag cap solidified. After removal of the slag cap, the ingot was stripped and sent to the forge shop. A photograph of the ingot as it was being stripped from the furnace is shown in Fig. 3. Ingot surface quality was rated as fair due to the presence of several minor surface runouts and a slightly rough surface condition on the withdrawal portion. Overall dimensions of the ingot were 1524 mm diameter by 3023 mm long. The weight was 43 002 kg. This ingot is believed to be the largest 304H grade ingot ever produced by the ESR process.

Forging Operations and Thermal Treatment

All forging operations were conducted on a 6800-metric-ton steam hydraulic press. A schematic of the forging sequence is shown in Fig. 4. After careful heating to 1204°C, the ingot was draw forged to 1372 mm diameter using V dies. Ingot discards were removed at this time. Subsequent forging operations, which were conducted at lower temperatures, included upsetting under flat dies, spreading using flat dies, punching out the center core using a hollow punch,



FIG. 3—*Finished ESR ingot.*

and enlarging over a mandrel. Care was taken to ensure that the entire forging was worked uniformly in the final enlarging operation. After this operation, the forging was air-cooled to room temperature. The finished barrel flange forging dimensions were 4572 mm outside diameter (OD) by 3658 mm inside diameter (ID) by 559 mm long.

Subsequent to forging, the barrel flange was heat-treated to an annealed condition per specification. The treatment consisted of heating to 1052°C, holding until the forging achieved temperature equilibrium, and then water quenching to cold.

Nondestructive Testing

After thermal treatment, the barrel flange forging was machined to the finished size of 4394 mm OD by 3734 mm ID by 470 mm long and subjected to both

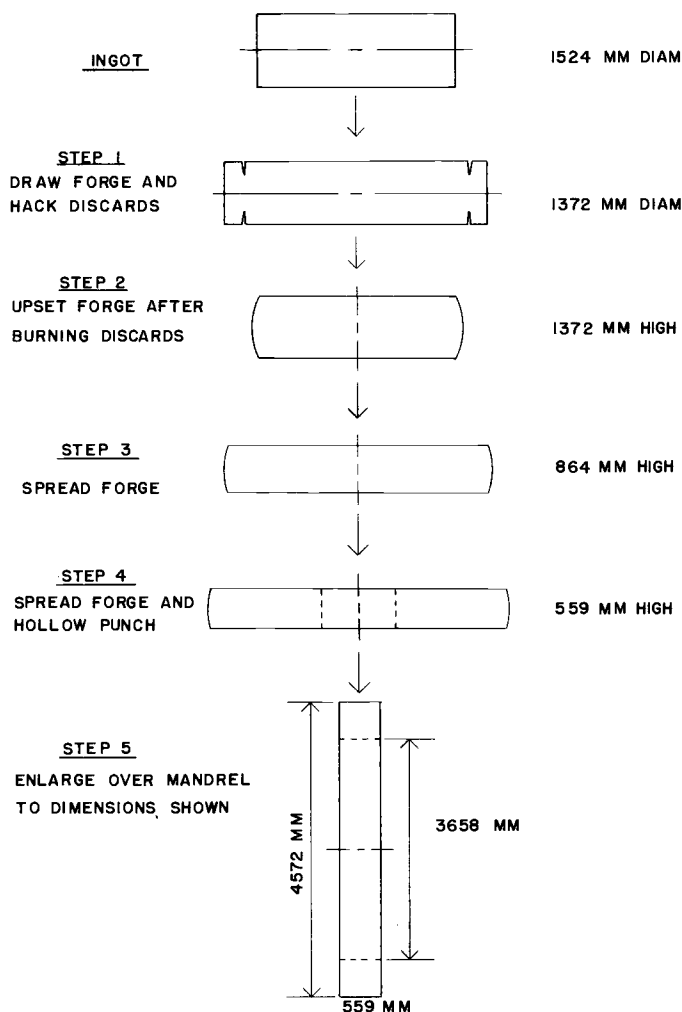


FIG. 4—Forging sequence.

ultrasonic and dye penetrant examinations. Ultrasonic testing was conducted using a 1 MHz transducer and a 0.4 MHz 45° angle shear wave transducer. Reference defect size was a 9.52 mm diameter flat bottom hole. No indications were found in either the longitudinal or shear wave testing modes. Ultrasonic penetrability, which had historically been a problem with conventionally melted (that is, electric-arc furnace) 304H grade forgings, was considered excellent with no variation in back reflection and slightly lower than usual noise levels. Liquid penetrant testing was conducted to ASME Boiler and Pressure Vessel Code Section III, Div. 1 NG2546.3 (D) (1). No indications were found.

TABLE 2—*Tensile properties.*

	Yield Strength, kPa	Tensile Strength, kPa	Elongation, %	Reduction of Area, %
ASME SA-182 Gr 304H	206 850	482 650	45 min	50 min
Barrel Flange	251 668	503 335	68	81.2
Forging	253 736	506 782	67.5	80.9

Forging Properties

Two tangential tension test coupons—180° apart—were removed from the barrel flange forging near the periphery. Tensile properties are reported in Table 2.

Both tension tests easily met the required properties and exhibited excellent ductility. Two intergranular corrosion tests were conducted to ASTM Recommended Practices for Detecting Susceptibility to Intergranular Attack in Austenitic Stainless Steels (A 262) Practice E using test material removed from the forging adjacent to the tension tests. Both specimens met the requirements of ASTM A 262.

Test material for chemical analysis also was removed adjacent to the above-mentioned tests. The official chemical analysis of the barrel flange forging is presented in Table 3 along with the electrode chemical analysis for comparison.

The differences apparent in electrode/ingot manganese, phosphorus, nickel, and chromium contents are attributable to normal analytical variations. The difference in electrode/ingot silicon content is due to the normal oxidation of silicon that occurs during the ESR process. Desulfurization at 70% was excellent. This is attributed to the use of the highly basic lime-bearing slag and the low-slag FeO contents experienced during refining.

Supplemental Testing of Forging Center Core

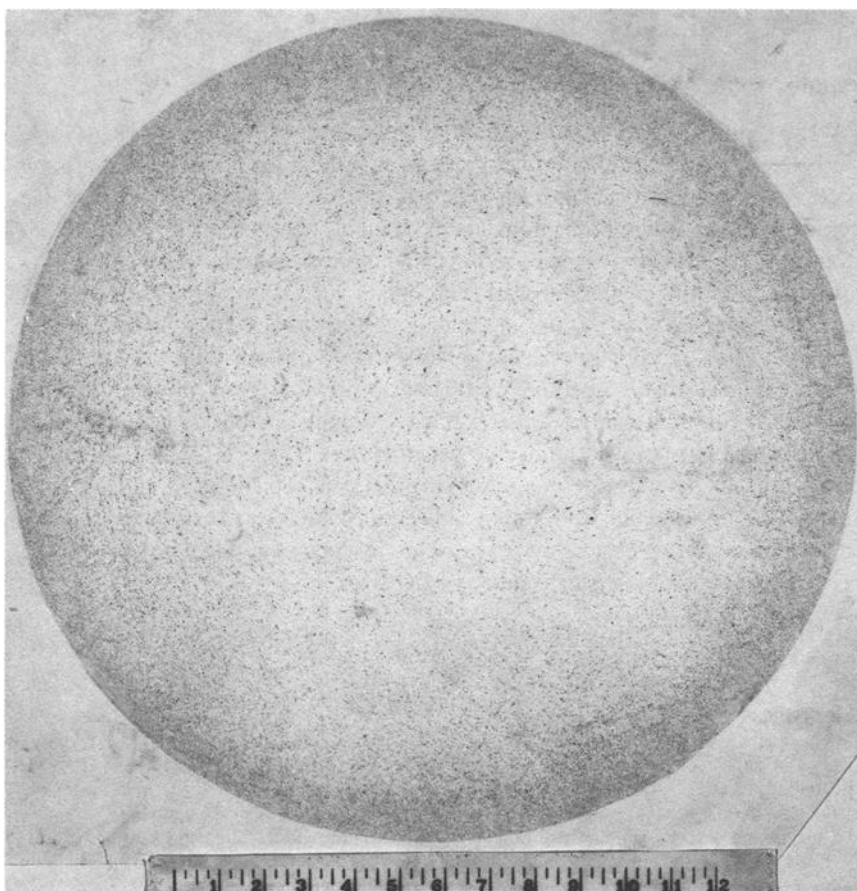
The center core (508 mm diameter by 749 mm long) of the barrel flange forging, which had been removed during the forging sequence by hollow punching and then air-cooled, was ultrasonic tested using a 25.4-mm transducer at 2.25

TABLE 3—*Electrode and barrel flange chemical analyses, weight %.*

	C	Mn	P	S	Si	Ni	Cr	Co
Electrodes	0.07	1.55	0.009	0.020	0.55	9.95	19.20	0.13
Barrel flange	0.06	1.62	0.011	0.006	0.49	10.11	19.10	0.13

TABLE 4—*Center core ultrasonic axial test results.*

Forging Core	2.25 MHz Regular Gain	1 MHz Regular Gain	1 MHz High Gain
ESR center core	moderate structure pattern—no indications	no structure pattern; no indications	insignificant structure pattern—no indications
Conventional center core	could not penetrate	could not penetrate 152 mm diameter center section; 5% structure pattern at other locations	not tested

FIG. 5—*Center core sulfur print.*

and 1 MHz in the axial direction. The 1-MHz test was conducted at both regular and high-gain levels. These ultrasonic results along with results from a center core test of a conventionally melted 304 grade forging are presented in Table 4.

The test results shown confirm the previously reported excellent ultrasonic penetrability of the actual forging and demonstrate the ability of the ESR process to produce segregation-free products of uniform grain size.

Following ultrasonic testing, a 25-mm-thick disk was cut from the center core section and smooth ground. The disk was then sulfur printed. A photograph of the sulfur print is presented in Fig. 5. The sulfur distribution was uniform but somewhat finer near the edge of the disk. It is postulated that the finer sulfur distribution may have resulted from additional forge work in this region during the hollow punching operation. The disk was then cold-etched in a 10% ferric chloride solution. No "bright spots" or regions of segregation were observed.

Summary and Discussion

A 1524-mm-diameter by 3023-mm-long ESR ingot of ASME SA-182, Grade 304H steel was successfully refined in an ingot withdrawal furnace. The refining process was conducted using a highly basic lime-bearing slag, aluminum slag deoxidation, and dry air protection. The ESR ingot was subsequently forged into a four-loop, upper barrel flange forging using a five-step forging operation. The barrel flange forging met all mechanical property and chemical requirements and passed all nondestructive tests. Additional testing of the forging center core section revealed excellent ultrasonic penetrability, a uniform sulfur distribution, and no evidence of segregation. Compared to previous conventionally melted 304H grade forgings, the ESR barrel flange forging as well as the center core section exhibited improved ultrasonic penetrability.

These results demonstrate that the ESR process is capable of producing large ingots of superior quality and homogeneity. Such ingots are eminently suitable for the production of critical nuclear reactor forgings and other forgings in the energy production and power generation fields.

References

- [1] Duckworth, W. E. and Hoyle, G., *Electroslag Refining*, Chapman and Hall, London, 1969.
- [2] Niimi, T. et al., "An Evaluation of the Electroslag Remelted Large Ingot: II," *Proceedings of the Fourth International Symposium on Electroslag Melting Processes*, Tokyo, 1973, p. 322.
- [3] Holzgruber, W., "Possibilities and Limitations to Influence the Structure and Properties of ESR Ingots and Properties of ESR Products," *Proceedings of the Fifth International Symposium on Electroslag and Other Special Melting Technologies*, Pittsburgh, PA, 1974, p. 70.
- [4] Choudhury, A. et al., "Application of Electroslag Process for the Production of Heavy Turbine Rotors from 12% Cr Steel," *Proceedings of the Fifth International Conference on Vacuum Metallurgy and Electroslag Remelting Processes*, Munich, Germany, 1976, p. 237.

DISCUSSION

*J. Ewald*¹ (*written discussion*)—What was the lowest detectable ultrasonic test—effective flat bottom hole achieved in the 304 stainless steel forgings?

E. J. Watkins and E. L. Tihansky (*authors' closure*)—The minimum detectable flaw size was 3.2 mm diameter.

*K. Handerhan*² (*written discussion*)—Reduced grain size is probably responsible for the improved ultrasonic penetrability of the ESR forging. What was the difference in grain size between the electric furnace melted conventional ingot cast product and the ESR product?

E. J. Watkins and E. L. Tihansky (*authors' closure*)—The authors believe that a more uniform grain size was responsible for the improved ultrasonic penetrability. Unfortunately, material is no longer available from either forging to allow for a grain size determination.

¹ Kraftwerk Union, Muelheim, Germany.

² Ellwood City Forge Corp., Ellwood City, PA 16117.

General Industrial Forgings

Equipment and Forging Process

Survey of New Developments in Forging Techniques and Equipment

REFERENCE: Kramarow, N. M., "Survey of New Developments in Forging Techniques and Equipment," *Steel Forgings, ASTM STP 903*, E. G. Nisbett and A. S. Melilli, Eds., American Society for Testing and Materials, Philadelphia, 1986, pp. 453–475.

ABSTRACT: This paper discusses the introduction into commercial practice of a number of new forging press and control technologies developed by press builders for the forging of high-temperature alloys and special stainless steels.

The paper categorizes forging technologies by forging characteristics and press characteristics. A number of specific fields are then surveyed:

1. Warm die forging to produce finished gear profiles without further machining.
2. Isothermal and hot die forging, in which the die temperature and the billet temperature are identical or very close, for forging high-temperature materials used in gas turbine engines and similar applications. The presses and controls required for these different applications are described in some detail.
3. Precision forging, also known as draftless forging in the aircraft industry, is described. The sophisticated controls needed for this type of forging are discussed.
4. Multiaxis forging, not a new technique, used for the production of items weighing several tons for severe duty. Again, modern controls and press design make these forging technologies commercial practice.
5. Automation is now moving into the forge shop; items such as the ring preforms for ring mills, which formerly were hammered to shape, are now produced at high speeds on automatic ring preform presses.
6. Computer controls have now been applied to preform forging to eliminate the open die in the hand shaping of preforms before finishing. This operation now can be fully programmed at great savings in labor and energy.

The paper concludes with a discussion of a very large installation for the production of thick-walled forged tubes and a new mechanical screw press which can deliver very large amounts of energy on each blow.

KEY WORDS: forging, precision forging, isothermal forging, computer-controlled forging, warm die forging, multiaxis forging, screw press

The forging industry has been the beneficiary in the last two decades of the introduction into commercial practice of a number of new forging technologies. A substantial number of these technologies are associated with the production of high-temperature alloys, special stainless steels, and similar hard-to-work ma-

¹ Manager, Metalworking Presses, Siempelkamp Corp., Marietta, GA 30067.

terials. The metallurgical technologists, in developing new techniques for the forging of these difficult alloys, have worked with press builders to attain the needed developments in press design and techniques for control of hydraulic and electric circuits.

The temperature, pressure, and envelope tolerances required for proper forging techniques with these materials were unattainable approximately 25 years ago. New instrumentation and control technologies, together with computer-aided design techniques, have been instrumental in these developments.

This paper will outline the major new hot forging technologies and their accompanying improvements in equipment which have made these processes commercially feasible.

Impression Die Forgings—Classification by Process Technology and Forging Press Characteristics

There is considerable overlap and common use of many of the terms associated with these techniques. Tables 1 and 2 summarize the relationship of the various forging processes by their operating characteristics and by the types of hydraulic forging presses used for each process.

The main characteristic of the forging processes (other than conventional) summarized in these tables is their attempt to bring the forging to “near net shape.” This phrase has become the rallying cry for all technologies associated with expensive materials since the extremely high cost of the basic ingot material, to \$100 and over per kilo for exotic alloys, requires minimum process material loss.

This paper will not touch upon advances in the billet preparation, such as: rotating electrode furnaces, hot and cold isostatic pressing, various plasma powder preparation schemes, and other technologies used for the refinement of the basic alloys. These metallurgical advances are the necessary prerequisite for bringing a suitable quality ingot to the forging press for final shaping to a wrought product.

Warm Die Forging

The technology of warm die forging of gear profiles has attained great commercial success in the last 10 years. The main technique is forging at a temperature that permits work hardening but is not below the recrystallization temperature [1,2].

The major application is the forging of gears for high-volume commercial applications, such as automobile and truck transmissions. The gear profile is formed to final size by the forging die without any further machining of the gear profile. Warm-forged gears require only minimum subsequent machining—usually only boring of the shaft hole and facing (and heat treating, if specified) prior to final usage. A typical part is shown in Fig. 1.

TABLE 1—*Characteristics of forging processes.*

Type of Forging Process	Tooling Complexity	Temperatures			Flash	Billet Accuracy
		Tool	Workpiece			
Conventional	simple dies	warm	warm to hot		large	nominal
Warm	simple dies (usually with registry)	warm	warm		small as practicable to none	close
Precision	split multipart dies	warm	cold to hot		small as practicable to none ^a	close to very close
Isothermal (or hot die)	simple dies to split multipart dies	hot	hot		little to none	close to very close

^a Usually requires intermediate flash trim.

TABLE 2—*Hydraulic press characteristics for various forging processes.*

Type of Forging Process	Press Design	Pressing Tonnage	Pressing Speeds
Conventional	one cylinder or multi-cylinder	moderate	normal
Warm	one cylinder or multi-cylinder	moderate to high	normal
Precision	one cylinder (usually)	high	creep
Isothermal (or hot die)	Four cylinder	low to very low	slow

Production applications are usually for bevel gears; however, spur gears now are being formed in limited quantities, and research is underway now for the commercial, high-volume forging of spiral bevel gears.

It is to be noted that this development has come about through die engineering, close control of furnace temperatures, and the control of the volume of the stock being processed. Since the dies finish to a closed part, weight control to a few ounces per slug is very important. Machining is used where necessary.

There has been no basic change in the characteristics of the presses used for forging. Conventional crank-type forging presses or the new high-energy, clutch-type screw press are used. Press cycling and speeds as used for conventional closed die forgings in carbon and alloy steels are followed for warm die forging.

Isothermal and Hot Die Forging

In the last 30 years, these processes have played an important part in the success of the high-temperature gas turbine engine, as well as in many other developments using hard-to-form alloys and refractory alloys.

Isothermal forging is defined as a forging process in which the die temperature and workpiece temperature are almost identical. Hot die forging usually is defined as a near-isothermal forging process in which the dies are 110 to 167°C (200 to 300°F) below the billet workpiece temperature. Both processes are designed for forging with minimum loss of heat and maximized flow stress [3,4].

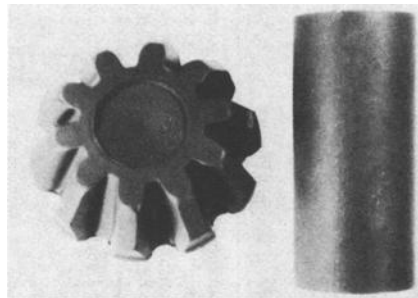


FIG. 1—Warm-forged gear. (Courtesy of *Precision Metal* magazine.)

A main characteristic of presses for isothermal and hot die forging involves provisions for heating the dies and billets continually throughout the forging process. Induction, infrared, and resistance heating, sometimes in combination, are used. This requires adequate die space within the press and suitable insulation of press components from the heat loading. A typical hot die forging setup is shown in Fig. 2.

A variation of the isothermal forging process developed for high nickel alloys such as IN-100 is the Pratt & Whitney "Gatorizing" process used by that company and licensed to other forges. The entire process is conducted in a vacuum or inert gas chamber to protect the high-temperature, molybdenum-based alloy dies (and the workpiece), which would deteriorate in atmospheric conditions. A typical installation is shown on Fig. 3.

The effects of this process on the forging press design are:

1. The press daylight must be very large to accommodate the chamber enclosing the die area.
2. The moving crosshead or slide is fitted with a secondary main pressing ram which transmits the pressing force to the upper die through seals in the top of the die chamber.
3. The chamber must be large enough to accommodate the heating arrangements for the die and billet.
4. The press frame must accommodate the manipulation chambers for incoming hot billet and finished forging. These chambers, with suitably interlocked doors, maintain the atmosphere in the die area.

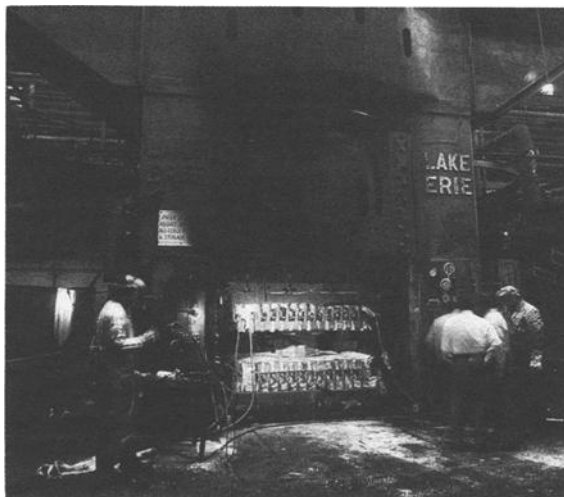


FIG. 2—Hot die forging setup. (Courtesy of Wyman-Gordon Co.)

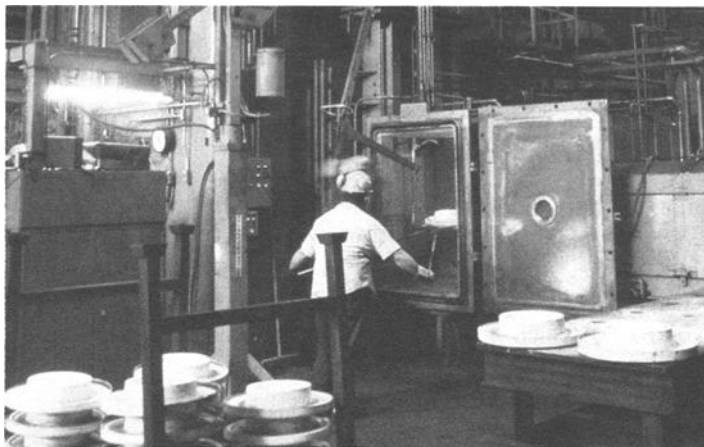
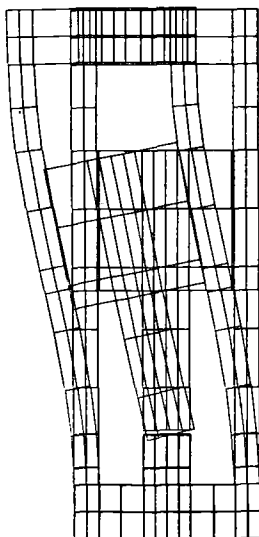


FIG. 3—*Isothermal forging setup.* (Courtesy of Wyman-Gordon Co.)



Finite-Element Calculation Plot No. PM06400S
Scale 1:100 vertical, 1:5 horizontal
Siempelkamp—Plotter drawing 15/10/80

FIG. 4—*Computer displacement drawing of single-cylinder press under eccentric load.* (Courtesy of Schirmer-Plate-Siempelkamp Hydraulic Presses.)

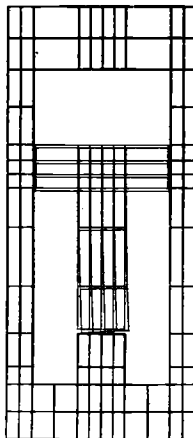
Previous installations have consisted of conventional hydraulic forging presses converted for "Gatorizing." Recently, a number of presses with ratings to 100 MN (10 000 metric tons) have been installed in the United States specifically for this process.

Almost all of the presses specified for "Gatorizing" or isothermal work to date have been of the single-cylinder design, designed to forge parts of concentric shape with minimum off-center loadings. The mechanical accuracy available from the guiding system dictates the off-center capability of the press.

To enable the press to isothermally forge with large off-center loads—for example, a large turbine blade with heavy stock at one end and accurate varying thicknesses of airfoil contour at the blade section, the press must be able to react to a great range of eccentric loads in all directions. Figures 4 and 5 show computer displacement drawings of a large press in single-cylinder and multicylinder design after finite-element analysis of the distortion and mismatch at the die plane under eccentric loads.

A German forge is now operating an isothermal forging press for large non-concentric parts. This press is shown in Fig. 6. It is rated at 50 MN (5000 metric tons) with a bolster size of 2500 by 2000 mm (100 by 80 in.). The control of this machine involves continual accurate monitoring of the four corners of the press to detect and almost instantaneously provide corrective force so that the moving crosshead remains within very close parallelism tolerances.

The computer-controlled system provides for a displacement error of ± 0.1 mm (± 0.004 in.) at the corners of the press during the forging operation and ± 0.05 mm (± 0.002 in.) at the corners at die close. Figure 7 shows the operator



Finite-Element Calculation Plot No. PM06400S (Controlled Forcing = -400)
 Scale 1:100 vertical, 1:5 horizontal
 Siempelkamp—Plotter drawing 15/10/80

FIG. 5—Computer displacement drawing of multicylinder press under eccentric load. (Courtesy of Schirmer-Plate-Siempelkamp Hydraulic Presses.)



FIG. 6—A 50-MN (5000 metric ton) isothermal/hot die forging press. (Courtesy of Schirmer-Plate-Siempelkamp Hydraulic Presses.)

control station with cathode tube display, keyboard entry, and force monitors, in addition to the conventional press-running controls. Figure 8 shows the complete computer in the control cabinet. The operator control in Fig. 7 has digital set point and actual readings of corner settings, as well as actual tonnage display.

The control system works as follows: A digital counter is actuated by the computer at a counting frequency, whose rate is set in proportion to the pressing speeds desired at different portions of the cycle. Differential calculating circuits evaluate the error between programmed and desired corner settings and the desired counting rate (proportional to speed) and actual press speed. Digital error signals thus generated are changed into analog signals to actuate the very accurate servo-valving controlling the press-forcing cylinders.

Another useful feature built into the controls is a "pretilt" setting, where the moving crosshead can be programmed to move in a tilted manner to provide additional loading in one or two quadrants of the die area. An obvious use is the desired increased load necessary to form the airfoil shape of a blade as contrasted to the conventional forging load needed for the root section. The "tilt" direction is preset into the computer on an azimuth basis (0 to 360°) to provide a tilt plane in the direction desired.

These controls provide:

1. Easy presetting by keyboard dialogue of all functions at the press or control cabinet.

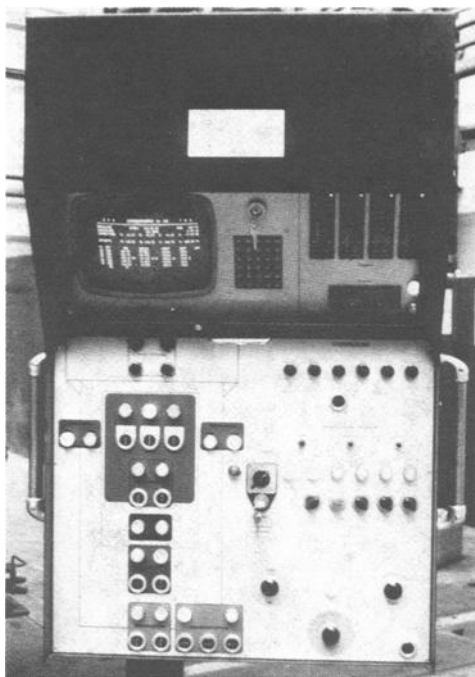


FIG. 7— *Operator station of computer-controlled press.* (Courtesy of Schirmer-Plate-Siempelkamp Hydraulic Presses.)

2. Storage of successful forging programs for reuse.
3. Ability to extract and store press forging data (strain rate, tilt, etc.) for further technical analysis of the forging procedure.

A word about press safety controls. The main press safety device is the differential circuitry which will shut down the forging stroke when excessive eccentric displacement is encountered. In addition, maximum pressure regulators are installed in each quadrant of cylinders, since the maximum eccentric forging tonnage could be reached in a quadrant without excessive local displacement of the slide. Again, the forging cycle is stopped.

An accurate tilting device independently and simultaneously monitors the out-of-plane tilt of the moving crosshead and will shut down the cycle on reaching a preprogrammed maximum setting.

Speed control of isothermal presses is very important. Servohydraulic circuits provide for an adjustable pressing speed up to 4 mm/s (9.5 in./min) to half tonnage 25 MN (2500 metric tons) with 2 mm/s (4.25 in./min) maximum available up to full tonnage of 50 MN (5000 metric tons).

As an indication of the capabilities of new servoelectronic controls, Schirmer-Plate-Siempelkamp is supplying circuitry with speeds as low as 0.004 mm/s

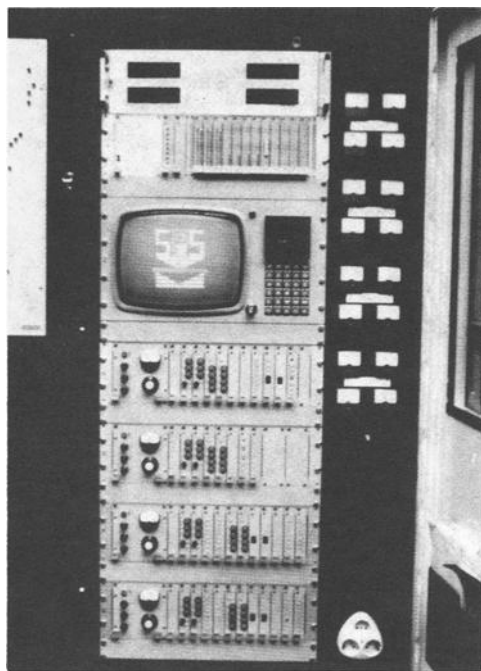


FIG. 8—*Computer section of press control.* (Courtesy of Schirmer-Plate-Siempelkamp Hydraulic Presses.)

(0.01 in./min) for precision forging. These “super-slow” circuits are used for precision forging installations (discussed later in this paper).

Auxiliaries

Isothermal forging presses are usually equipped with bottom ejectors. Other features sometimes incorporated are knockouts in the moving crosshead, rotating die devices in the bed to enable the forging of spiral elements, moving tables to assist setup of dies and heaters, etc.

Precision Forging

Although the term “precision forging” has been used for many years to describe close tolerance impression die forging, it now generally is used to describe the process of forging aluminum and titanium parts, used mostly by the aerospace industry, with the following characteristics [5]:

1. Draft angles between 0 and 1°.
2. Very thin webs, walls, and flanges, as low as 1 mm (0.040 in.).

3. Small radii at intersections of webs and walls.
4. Reentrant corners and pockets which cannot be forged with conventional tools.
5. Excellent as-forged surface conditions.
6. Minimum post-forging machining, eliminating five-axis milling, etc.

These forgings require very slow pressing and breakaway speeds. Typical parts are shown in Fig. 9.

There are three types of dies usually employed:

1. A through die allowing vertical part removal, albeit with a very small draft angle.
2. Segmented dies. The die is designed with multiple segments held together by a ring or similar device during the forging stroke. The holding ring must be loaded to lock up the die prior to the forging stroke and released to remove the part and die segments during intermediate lubrications. Segmented dies are required to produce parts with reentrant pockets and protrusions which prevent vertical part removal.
3. Flashless or seamless dies: This is a variation of a segmented die, usually used together with a side-pressing ram to eliminate end grain in valve bodies, etc.

A major advantage of the precision forging method is the excellent flow-line characteristic of the finished forging, providing high strength in thin sections of the part.

Hydraulic presses used for precision forging have been, until recently, con-

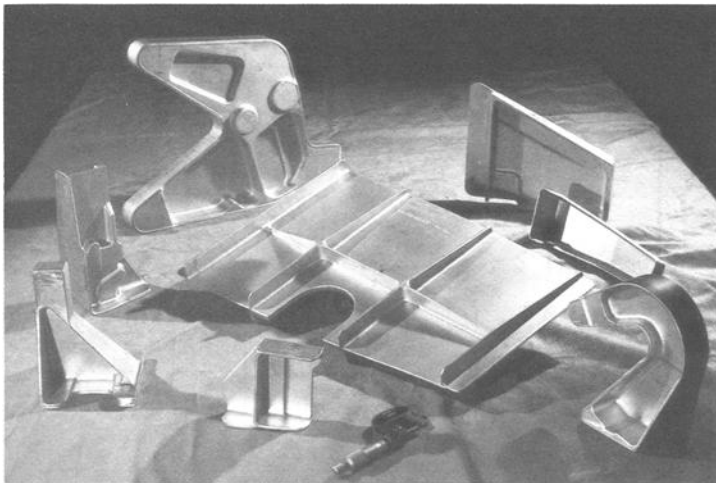


FIG. 9—*Precision forged parts.* (Courtesy of Martin-Marietta Aluminum.)

ventional single-cylinder machines to 35-MN (3500-metric ton) rating. Some of these presses have been retrofitted with slow-speed controls.

There are now considerable efforts underway to produce large plan area parts. Large forging presses with higher ratings are now being adapted for this process. A part of 2600 cm² (400 in.²) recently has been made on a 100-MN (10 000-metric ton) press.

Pressing speeds as low as 0.004 mm/s (0.01 in./min) are now being specified for this process. A special servocontrol must be used for this low speed; conventional press servocontrols only are effective down to press speeds of approximately 0.4 mm/s (1 in./min).

The adaptation of these very low speeds to large hydraulic presses of 150 MN (15 000 metric tons) and upward poses a difficult hydraulic/electronic control problem, since these presses are usually driven by large water hydraulic central accumulator stations. The use of oil hydraulic servocircuitry driving special water control valves under computer control has solved this problem.

These large presses [150 to 500 MN (15 000 to 50 000 metric tons)] have big beds and multiple cylinders. For example, a 500-MN (50 000-ton) press has eight main cylinders and a table size of 10 by 3 m (33 by 10 ft). The techniques of multiple cylinder parallelism control described in the preceding section (Isothermal/Hot Die Forging) are used in conjunction with the slow-speed control to provide proper regulation of the press.

Multiaxis Forging

Forgings which require penetration by tooling in the vertical and horizontal planes are represented by Fig. 10.

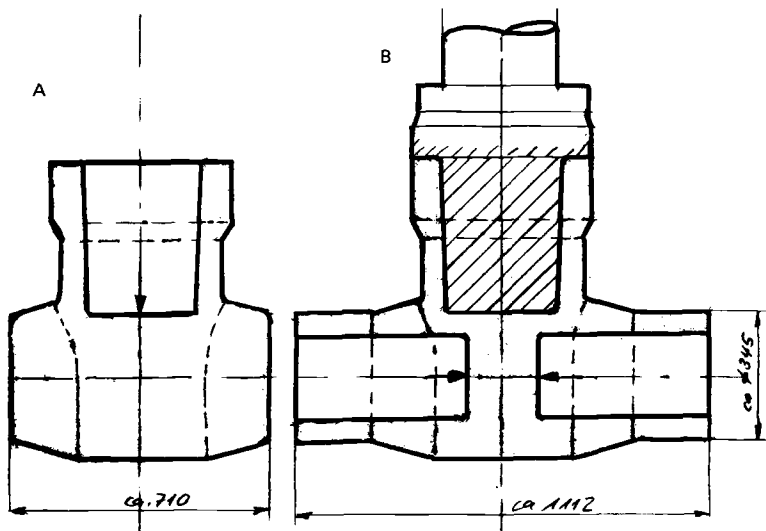


FIG. 10—Multiaxis forging: (A) Piercing Stroke I vertical; (B) Piercing Stroke II horizontal.

The forging technology uses split dies. In practice, the heated billet is inserted into the cavity and upset by the vertical ram, which upsets the part, closes the vertical chamber of the die, and locks up the die.

Depending upon the forging needs, typically the side rams then pierce the billet, advancing to the center or as close as practicable. Multi-action backflow around the rams fills the die cavities and recesses to fill out the forging, provide flanges, bosses, etc.

Oil field valve bodies and fittings are typical products. Large multi-axis presses have been built specifically for this forging process. Typical press tonnage ratings are 70 to 80 MN (7000 to 8000 metric tons) in the downward vertical direction and two opposed horizontal rams of 20 to 40-MN (2000 to 4000-metric ton) rating each.

Since multi-axis presses are very expensive and are designed to forge specialty products, a leading press builder now will supply adaptations to enable hydraulic forge presses of 80 MN (8000 tons) and up to be used as a multi-axis press. These presses, which have large moving tables, can be equipped with a self-contained package consisting of two 20 to 30-MN (2000 or 3000-ton) cylinders coupled both mechanically and hydraulically and integrated with the existing press control to provide multi-axis forging capability. The horizontal pressing unit is easily dismantled to allow the press to function conventionally.

It should be noted that modern servohydraulic press controls now overcome previous control difficulties in which the side rams would not move in synchronization, or, even worse, one side ram would not function.

Automatic Ring Preform Forging

Most forged rings, whether of rectangular or contour cross section, are rolled out on ring rolling mills using a ring preform or "doughnut" as the starting workpiece for the mill. (See Fig. 11 for the general process.) The billet is upset, pierced, and flattened, and the slug is sheared through.

The ring preform can be prepared by hammers or by presses. Hammers are used in many shops for the upsetting, piercing, flattening, and holing through operations. Conventional presses with hand-placed tooling also are used; both methods are comparatively expensive because of the large crew needed and the slow cycle time.

A more efficient application is to equip the press with automatic equipment for ingot and tool movement. Most presses supplied for production ring and wheel mills are of the "swing-arm" type in which the pierce tool is swung into the press centerline.

An improved design is shown in Fig. 12. It contains multiple tool slides. The top slide is equipped with upsetting plate and piercing punch stations. The lower slide contains upsetting plate and hole through stations. Many presses keep the hole through station outside of the press bed.

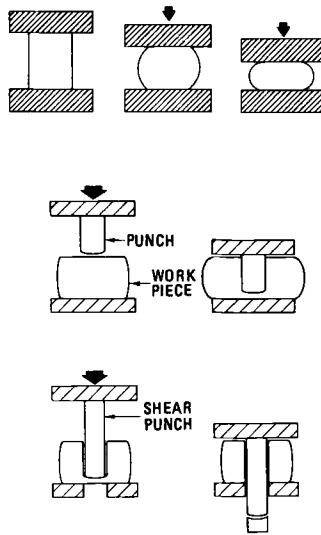


FIG. 11—Forging of ring preforms. (Courtesy of the Forging Industry Association.)

A new design of ring preform forging presses has greatly improved the time cycle and has improved concentricity of the pierced hole. The general design is shown in Fig. 13. The press has a heavy piercing cylinder located within the main pressing ram. Centering and lifting cylinders for manipulating the workpiece are built into the press frame, thus avoiding the use of the fork lift truck to recenter the billet several times during the cycle.

The use of a central piercer press allows continual upsetting, piercing without reflattening. In addition, there is a substantial material savings in a minimum-

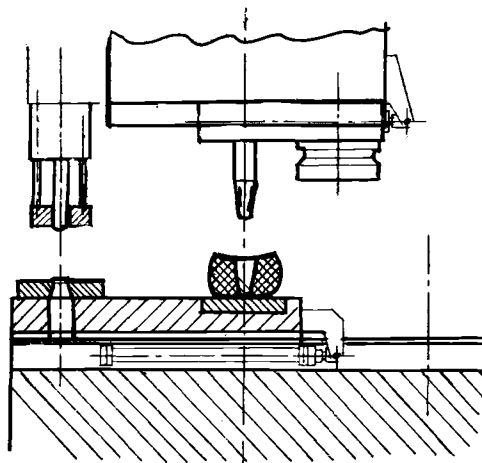


FIG. 12—Ring preform with tool slides.

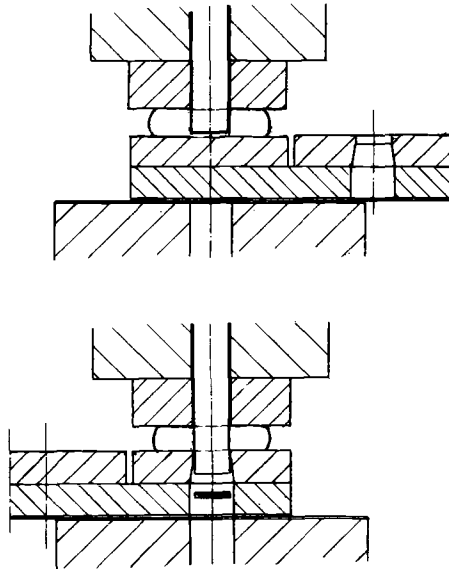


FIG. 13—Central piercing ring preform press.

pierced slug. Savings of up to 40% in process time and 500% in slug size are reported. Presses of this size are being built to 70-MN (7000-metric ton) upsetting capacity.

Forge Drawing of Heavy-Walled Tubes

Heavy forged tubes, larger in diameter and wall thickness than those produced by seamless tube mills—say over (14 in.), are produced by the Erhardt process (see Fig. 14 for a schematic representation). The main usage of these tubes is

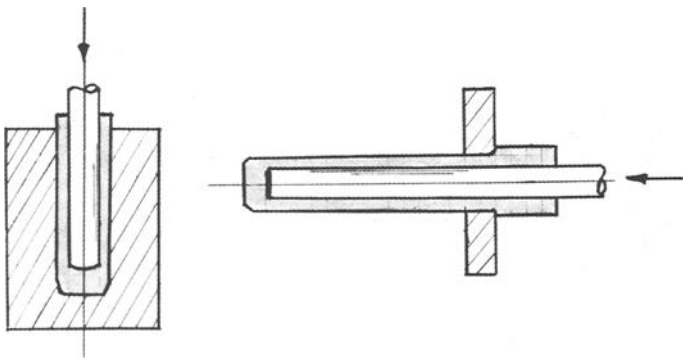


FIG. 14—Erhardt process—heavy-walled tubes. (Courtesy of Schirmer-Plate-Siempelkamp Hydraulic Presses.)

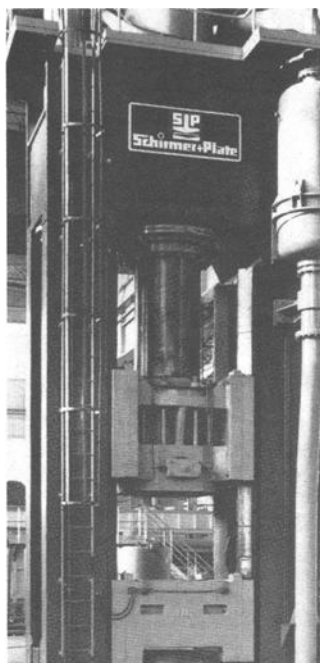


FIG. 15—A 40-MN (4000 metric ton) piercing press for forged tubes. (Courtesy of Schirmer-Plate-Siempelkamp Hydraulic Presses.)

power plant piping to a 1219-mm-diameter by 152-mm (a 48-in.-diameter by 6-in.) wall maximum in chrome alloys and stainless steel.

A very large installation is shown in Figs. 15 and 16. The 40-MN (4000-metric ton) piercing press with 4-m (13-ft) stroke handles ingots to 20 000 kg (22 tons). After reheat, the pierced ingot is drawn out through ring dies in the horizontal push bench.



FIG. 16—A 15-MN (1500 metric ton) horizontal push bench for forged tubes. (Courtesy of Schirmer-Plate-Siempelkamp Hydraulic Presses.)

This process produces heavy-walled piping of better quality than piping which is only pierced and back extruded. It is more cost-effective than forging sleeves or rings on a mandrel or forging solid ingots and boring to size.

Computer-Controlled Preform Forging

With the exception of high-volume automotive and similar applications, most impression die forgings are produced in small lot sizes. This usually precludes the installation of preforming rolls or upsetters which must be tooled for each part. At present, most preforms are prepared for final blocking and finishing dies by skilled hammermen (a disappearing breed).

Automatic cogging presses for the production of bar from ingot or bloom have been in production approximately 10 to 15 years, due to development of control integration of the forging press and manipulator. Only bars or simple-shouldered shafts have been produced automatically by these automatic cogging installations.

Recently a press/robot manipulator has been installed in a German forge to automatically form preforms on the equipment shown in Fig. 17. Typical preform shapes are shown in Fig. 18 (single-sided forgings) and Fig. 19 (forgings worked from both sides). A turning device is included in the press.

The main technical advance is the development of software and servocontrols which enable the press/manipulator to function completely automatically. The programming is done by the forge operator in dialogue with the machine.

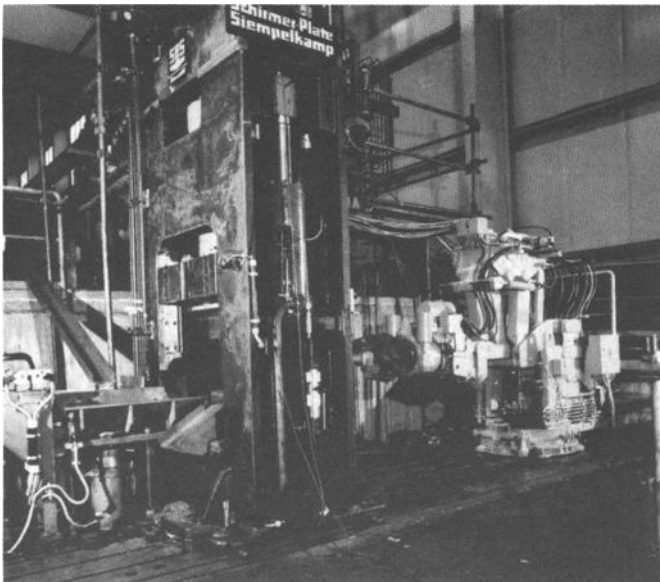


FIG. 17—Automatic preform forging press. (Courtesy of Schirmer-Plate-Siempelkamp Hydraulic Presses.)

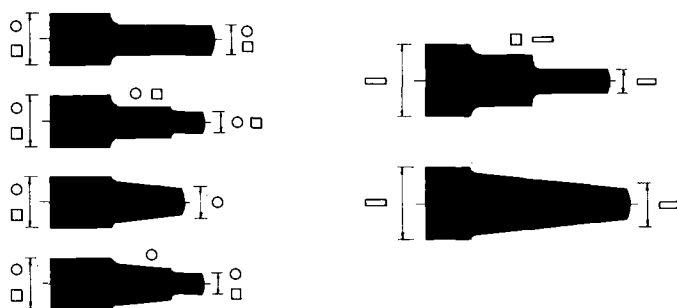


FIG. 18—Preforms forged from one side. (Courtesy of Schirmer-Plate-Siempelkamp Hydraulic Presses.)

After each part is successfully forged, the program is stored for future use. The program for a particular part can be modified or improved at any time. The floor-to-floor times are very dramatic; cycle times of 40 s are reported for 90-kg (200-lb) preforms with three diameters and a taper.

Figure 20 shows a heated bar being pushed into the die area to be received by the manipulator; Fig. 21 shows the forging in process. One key to the success of the machine is the rapid movement of the part by the manipulator between the fixed tools.

A new development for presses/robots which will handle complicated preforms and parts bigger than 150 kg (330 lb) is the introduction of movable tool slides and upsetting tools. Fig. 22 shows some of the possibilities for different tool saddles in the press.

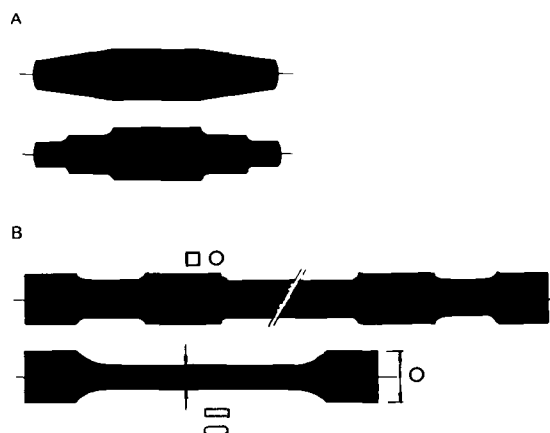


FIG. 19—Preforms forged from both sides: (A) double-sided, forged on ends only; (B) double-sided, forged between the ends. (Courtesy of Schirmer-Plate-Siempelkamp Hydraulic Presses.)

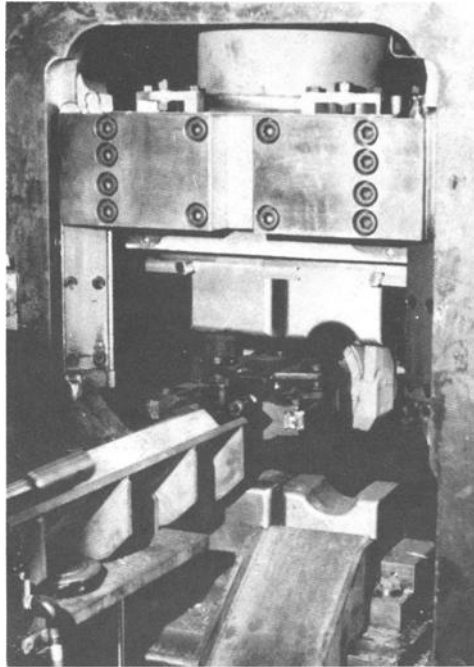


FIG. 20—*Billet entering automatic preform press.* (Courtesy of Schirmer-Plate-Siempelkamp Hydraulic Presses.)

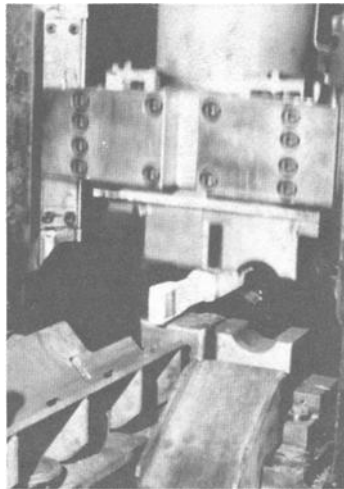


FIG. 21—*Automatic preform forging press in operation.* (Courtesy of Schirmer-Plate-Siempelkamp Hydraulic Presses.)

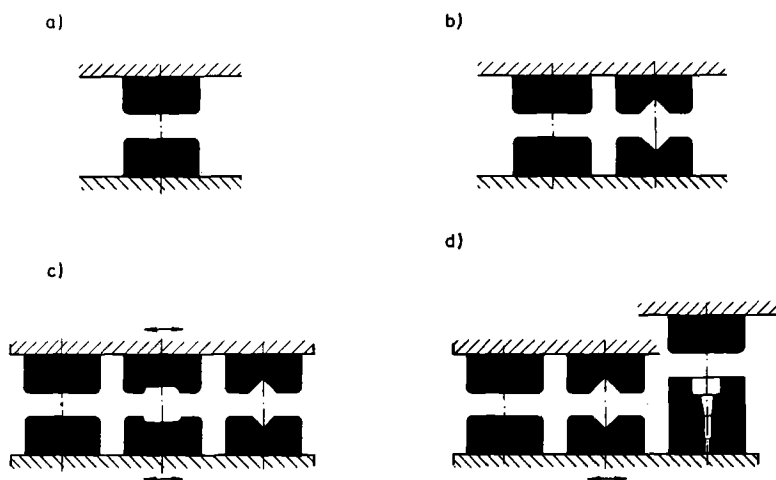


FIG. 22—Various tool saddles for automatic preform forging press: (a) flat tool saddle, without tool shift; (b) flat and profile tool saddles, without tool shift; (c) flat calibrating and profile tool saddles, with tool shift top and bottom; (d) flat and profile tool saddles with bottom tool shift, for upsetting operations.

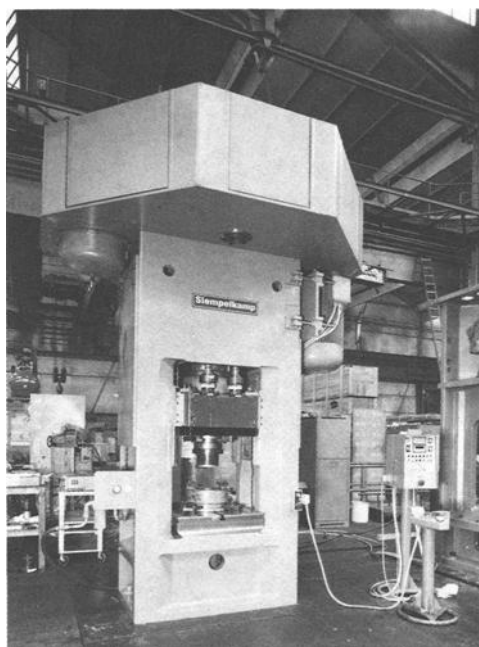


FIG. 23—High-energy, fast-acting screw forging press. (Courtesy of Schirmer-Plate-Siempelkamp Hydraulic Presses.)

High-Speed Energy Screw-Type Forging Press

Used for many years in European forges, screw presses now are entering U.S. forges as another manufacturing tool for impression die forgings. Conventional screw presses use the time-honored principle of the screw thread translating the ram, taking energy from motors driving a flywheel rigidly affixed to the threaded spindle.

The difficulty that arises with this design—which has been built to very large press ratings—is that the press must be slowed down or braked as it approaches the die close position to prevent self-destruction of the machine frame. This means that energy transfer, which is proportional to velocity, drops to zero as the ram slows to zero, which usually is converse to the needs of the forging.

A new design, high-energy screw press has been introduced in the last few years. This machine features a large flywheel connected to the drivescrew by a very fast-acting clutch which can load or unload the spindle in fractions of a second. Production forgings from this press require less heats than those made on hammers or other presses. The use of the fast-acting clutch gives this machine

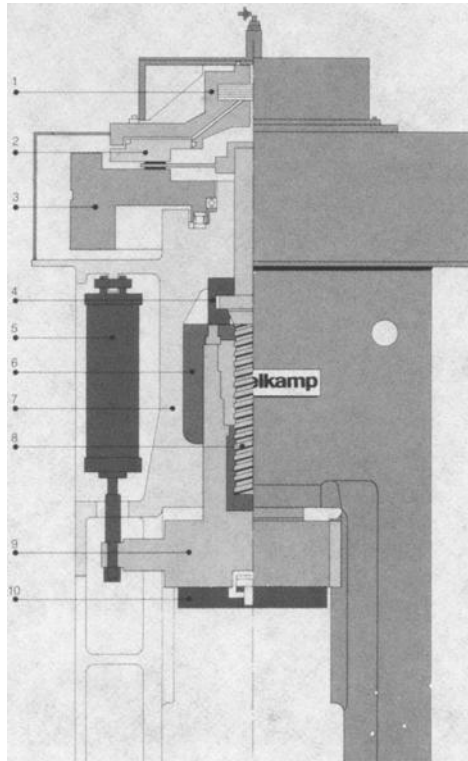


FIG. 24—Sketch of internal design of screw press. (Courtesy of Schirmer-Plate-Siempelkamp Hydraulic Presses.)

characteristics similar to a hydraulic press while retaining mechanical press characteristics:

1. Full or adjustable tonnage is available at any position of the stroke.
2. Energy per blow is approximately 2 to 3 times that available from a conventional screw or crank-type forging press.
3. Energy transfer rate is uniform throughout stroke.
4. Ram speed is identical to a mechanical press.



FIG. 25—Typical parts forged on high-energy screw press. (Courtesy of Schirmer-Plate-Siem-pelkamp Hydraulic Presses.)

An 800-metric ton press is shown in Fig. 23. A sketch of the internal design is shown in Fig. 24. Typical parts forged on these presses are shown in Fig. 25. Approximately 35 presses of this design have been installed in the last few years, with tonnages from 315 to 2500 metric tons (350 to 2750 tons). Larger sizes will be installed in the next few years.

Conclusion

The demands of the new sophisticated forging techniques have required the use of various forms of computer technology and innovative press designs by press and control engineers to make possible the forging of difficult, hard-to-work alloys. In addition, the design and performance of the presses and controls themselves have been greatly improved through the use of available new technologies such as the finite-element method of calculation of structures and the use of new and powerful servohydraulic control technologies. Forging is now a modern technology, not a "blacksmith art," using the latest developments in a machine design, machine-building computers, and servotechniques to make possible the working of new materials.

References

- [1] Novelli, O. and Shipley, R. J., *Precision Metal*, Oct. 1984, pp. 17-18.
- [2] Altan, T., Oh, S., and Gegel, H., *Metal Forging—Fundamentals and Applications*, American Society for Metals, Metals Park, OH, 1983, pp. 244-246.
- [3] Altan, T., Oh, S., and Gegel, H., *Metal Forging—Fundamentals and Applications*, American Society for Metals, Metals Park, OH, 1983, pp. 316-319.
- [4] "Near Net Shape—A Reality for Aircraft Forgings," Wyman-Gordon Co., Worcester, MA, 1981.
- [5] "Aluminum Precision Forgings," Martin Marietta Aluminum, Torrance, CA, 1984.
- [6] "Forging Presses," Schirmer-Plate-Siempelkamp, Krefeld, W. Germany, 1984.

Forging Force Requirements with Special Regard to Shear Resistance of the Forge Material

REFERENCE: Javorik, L. J., "Forging Force Requirements with Special Regard to Shear Resistance of the Forge Material," *Steel Forgings*, ASTM STP 903, E. G. Nisbett and A. S. Melilli, Eds., American Society for Testing and Materials, Philadelphia, pp. 476–503.

ABSTRACT: The purpose of this development project was to precalculate forging forces. This is important not only to design the most economical machine to do the job, but also because knowledge of the exact forging force enables us to carry out the desired metallurgical change in the material.

While the work on strength, work hardening, the effect of speed on the virtual strength of the material, temperature, and friction offers little novelty and serves mostly as a summary, the formulas developed are still the results of a new and independent theoretical and experimental work; emphasis was put on developing a theory to calculate shear resistance offered by the forge material because the author found no publication dealing with this subject in spite of the fact that such forces by shear characteristically range around one third of the total forging force requirement.

The author faced the difficulty that all regular (bidirectional) shear formulas are strongly restricted in their range of validity, and, if this limited range is exceeded, the formulas suffer greatly in accuracy. Therefore, the author briefly explains existing shear theories and their ranges of validity and gives new and revised formulas for the ordinary bidirectional shear that no longer are restricted by location thickness, or by other dimensions of the material. Then the author uses the newly developed general shear theory, converting the theory to monotool shear calculation as is the case in forging.

KEY WORDS: Bauschinger effect; bidirectional shear; new and improved shear theory; shear stresses, duality principle; shear theories; forging experiments; monotool shear; friction increasing virtual strength; shear from bending; basic strength of material; shear resistance of the forge material; synthesis of forging forces; temperature effect on strength; work hardening

Nomenclature

- A Cross-sectional area
- c Transfer factor (a material constant that reduces shear stresses inwardly in case of direct shear) for the metals tested, 47.244/m
- F Force
- G Shear modulus (see Young's modulus in normal stress)

¹ President, Inventive Engineering, Oregon, IL 61061.

G_s	Secant modulus in shear
I	Area moment of inertia ($\int yx^2 dx$)
L	Length
L_r	Length in radial forging
M_s	Static moment of area ($\int xy dx$)
p	Pressure (force per unit of area)
t	Thickness
V	Shearing force
v	Speed (mostly as speed of deformation)
w	Width
x	Coordinate codirectional with the force
y	Coordinate perpendicular to the force
α	Angle (as die angle)
γ	Deformation angle caused by shear stresses
ϵ	Specific deformation
μ	Friction coefficient
σ	Internal pressure, that is, normal stress
σ_t	Tensile stress or strength
σ_u	Ultimate strength in normal stress
σ_{ur}	Ultimate tensile strength
σ_y	Yield strength
τ	Tangential (shear) stress or strength
$\tau_{ultimate}$	Ultimate tangential stress or strength

While a complete enumeration of all factors governing any phenomenon is usually an impossible task, this author believes that six major factors can give us a reasonably good figure on the force required for a given forging process. These six major factors are:

1. Basic strength of the material (tensile ultimate).
2. Work hardening (true stress).
3. The effect of temperature.
4. Friction resistance between the die and the material influenced by material thickness (flow resistance).
5. The effect of forging speed.
6. Shear resistance of the material in forging if the tools are not congruent with the surface of the material or if they are narrower than the part in forging.

As Topics 1 through 5 are discussed in literature, their presentation will be only for the sake of completeness and thus will be short. The author has not seen shear resistance caused by a single tool, such as in forging, discussed elsewhere. Moreover, added work to discuss actual shear stress distribution throughout the cross section subject to dual tool shearing and thus refine the calculation of load

capacity of a sheared element in dual shear also could be considered to have some novelty and merit; therefore, this topic will be discussed in more depth.

Strength of the Material in Compression

If we test a material in tension, the well-known $\sigma - \epsilon$ diagram will be obtained as shown with the solid line on the upper portion of Fig. 1. The conventional stress on this curve is generated by dividing the load at any point of the relative elongation by the original cross section of the specimen. The true stress is, however, greater than that. The dotted line shows the true stress curve of the specimen in tension.

In compression, the opposite is true. The true stress at any point of the diagram is lower than the virtual stress recorded by the testing laboratory (dotted line at lower part of diagram, true stress in compression). If we could make tools without friction, the thickening would be uniform. When true stress would cease to increase, this could be considered the true stress ultimate of the material in compression [1].

According to Mohr, tension and compression specimens should fail in diagonal shear (Fig. 2), and for mild steel such failure should occur in tension and in compression at the same load level. This seems to be the case for harder materials only. Soft, short steel specimens in compression could go to extreme values of measured strength. The author favors 1:3 side-to-height ratios. In this case,

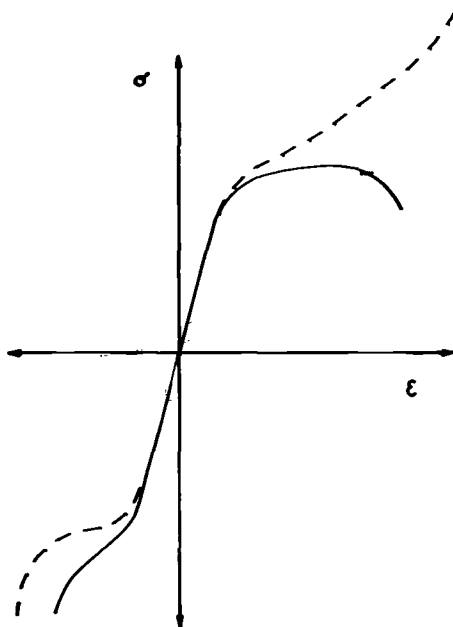
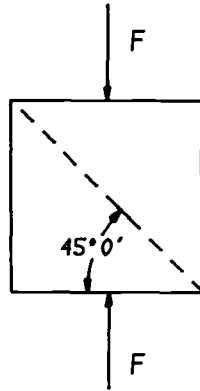


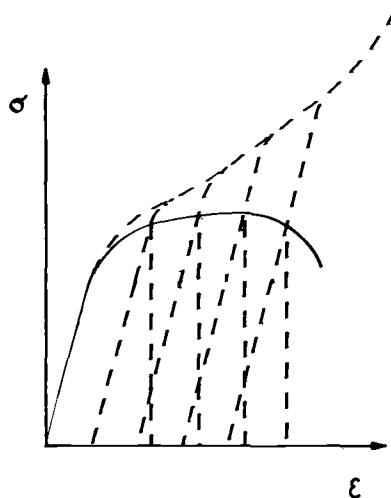
FIG. 1—Conventional and true stress.

FIG. 2—*Shear by compression.*

weakening the specimen by buckling is about on the same level as virtual strength increase due to friction between dies and the specimen. With this setup, compression and tension ultimates appear to be about equal.

Work Hardening

If we interrupt the tension test at several given points of relative elongation, ϵ_1 , ϵ_2 , etc., as shown in Fig. 3, and restart it as the setup was, we obtain increased yield strength, but the envelope will be the regular $\sigma - \epsilon$ diagram. However, if we reevaluate the data for the reduced cross section before we start over again, we obtain a true stress diagram for the envelope of a multitude of curves. The

FIG. 3—*True stress.*

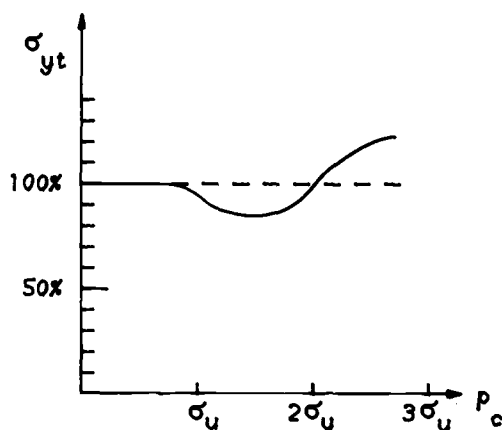


FIG. 4—Bauschinger: the full story.

steady increase in stress levels as elongation continues is commonly called “work hardening.” Because stress in tension cannot go over the ultimate, work hardening by tension cannot increase the ultimate of true stress. In compression, however, several times higher than the ultimate can be applied. As a result, not only can the compressive ultimate be increased, but even the tensile ultimate [1]. This seemingly contradicts the Bauschinger effect [2,3], but extends its interpretation rather than contradicting it [1] as demonstrated in Fig. 4.

For treatment pressure not much higher than the ultimate, the yield in the opposite direction is decreased, but, for treatment pressures double or triple the ultimate, the yield and the ultimate in both directions is increased. Even in high temperature forging this was true.

It also was found that when the material was confined in compression, high applied pressure produced very little deformation in compression, yet the increase in properties was the same. Beliefs to the contrary probably are due to misinterpretation of Bridgeman [4,5].

The Effect of Temperature

Besides improved chances to cure cracks, the main purpose of forging steel while hot is to reduce its strength, increase its elongation, and improve its formability in general. Our topic is reduction of strength. This is presented on Fig. 5 for mild steel. This is a $\sigma - \tau$ diagram, but, because σ and τ are coordinated once we established a curve for σ , we also can obtain the data for τ . It is the observation of this author that these ratios do not change with temperature.

Another question is how this ratio of σ/τ varies according to authors:

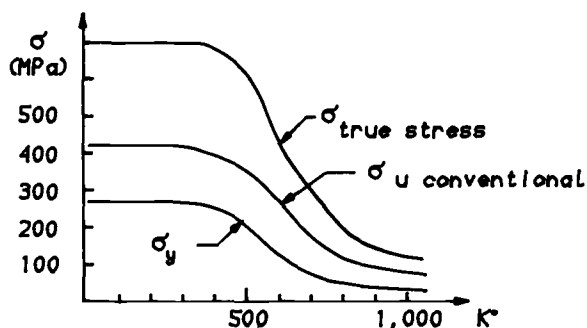


FIG. 5—Temperature dependence of properties of mild steel as a function of temperature.

Mohr and Guest state it for 2; Mises and Hencky claim $\sqrt{3} = 1.73$. It is the author's observation that the ratio is even lower than that (1.4), but, because this is not the topic of this paper, we shall use the most widely accepted 1.73 in our investigation. The rest of the parameters change proportionally with the strength as a function of temperature except friction, which may be a little higher than for cold forging ($\mu = 0.3$), and the strength versus deformation speed, which simply has to be newly established for any temperature in question.

Effect of Friction

Because the volume of the material does not change in forging when compressed, it has to flow outward. The friction between the material and the die surface tends to prevent this. Hence, the well-observed barrel shape when tools are wider than the material. In some forging operations, however, a pressure drop may occur inside of the material. If this effect is larger than the effect of friction, the opposite situation may occur. The friction coefficient between the die and the material may be as large as 0.15, even 0.2 in cold forging, and may approach 0.3 in hot forging.

By calculating the added force requirements as a result of material flow against friction, first we examine a one-dimensional flow. This is the case when the material is very wide in one direction; then, all the flow takes place in the narrower direction. Figure 6 shows that the situation is symmetrical, sufficient to analyze half of it.

Assuming that material is completely pliable, at $y = 0$, $p_o = \sigma_o$, or, simply, $p = \sigma$; that is, the pressure needed equals the strength of the material. Thus, the force pushing the material outward, $F = tw\sigma$. For width of unity, $F = t\sigma$. The increase in pressure inward along x is dp . Through a small distance $\Delta x \rightarrow dx$, it relates to the already existing pressure p as the increase in friction force relates to the existing outward force. Therefore, if $L \ll w$, that is, for a one-dimen-

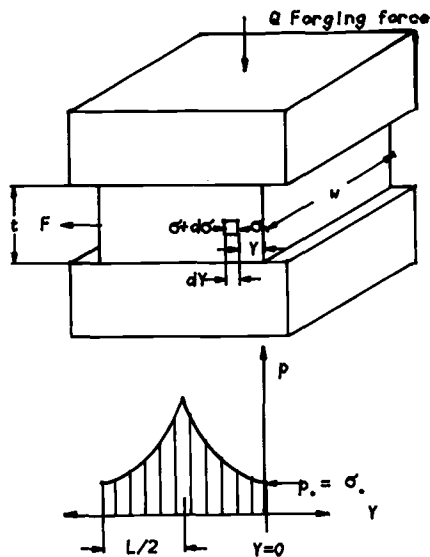


FIG. 6—Force buildup in unidirectional flow during forging.

sional flow

$$\frac{dp}{p} = \frac{\mu}{p} \frac{p dy}{t/2} = \frac{2\mu}{t} dy$$

Integrating this for $x]_o^{L/2}$ and for $P]_o^{P_{\max}}$ we get

$$\int_{p_o}^{P_{\max}} \frac{dp}{p} = \int_o^{L/2} \frac{2\mu}{t} dy$$

Thus

$$\ln(p) \Big|_{p_o}^{P_{\max}} = \frac{2\mu y}{t} \Big|_o^{L/2}$$

So that

$$P_{\max} = p_o e^{\mu L/t} \quad (1)$$

The average pressure, on the other hand, is the La Grange integral of the

pressure function

$$p_{\text{average}} = \frac{\int_0^{L/2} p_o e^{2\mu y/t} dy}{L/2} = \frac{tp_o}{L\mu} (e^{\mu L/t} - 1) \quad (2)$$

Thus, the virtual increase of strength because of friction is

$$\frac{p_{\text{average}}}{p_o} = \frac{t}{L\mu} (e^{\mu L/t} - 1) \quad (3)$$

For a two-dimensional flow such as compressing a cylindrical rod axially, the La Grange integral has to be formed for an area of a circle, rather than for a straight line

$$\frac{p_{\text{average}}}{p_o} = \frac{\int_0^R p_o e^{\mu \frac{y}{(R/2)}} (R - y) \pi dy}{R^2 \pi} = (2/R^2) \frac{t}{4\mu^2} (e^{2\mu R/t} - 1) - \frac{tR}{2\mu} \quad (4)$$

Tests were made measuring forging force on the same kind of cylindrical specimen (same area, $D = 2R$) but with different D/t ratios (different heights). Because tests were made dry, they should agree with the results of the previous equation when plotted, calculated with $\mu = 0.2$.

D/t	$D \gg t$	1	2	4	8
Load to production, 20% shortening, kN	95.2	104.5	109.4	133.7	185.2
Force increase, %	0	10	15	40	94

The test data in this table are in excellent agreement with the data derived from Eq 4 as shown on Fig. 7 for 0.2 friction coefficient.

Finally, we should attempt to modify the equation of one-dimensional flow (Eq 3) to describe the case for a radial forging machine. (See Fig. 23 and a more detailed description in "Conclusions.") Here twelve dies attack the billet and squeeze it radially; this, in turn, expands axially as shown in Fig. 8.

A crude but still useful approximation is: $L = 4L_r$ and $t = D$. Based on the analogy of bound versus free area ratio

$$\frac{2(L/2) w}{tw} = \frac{D\pi L_r}{(D^2\pi/4)}$$

$$L/t = (4L_r)/D$$

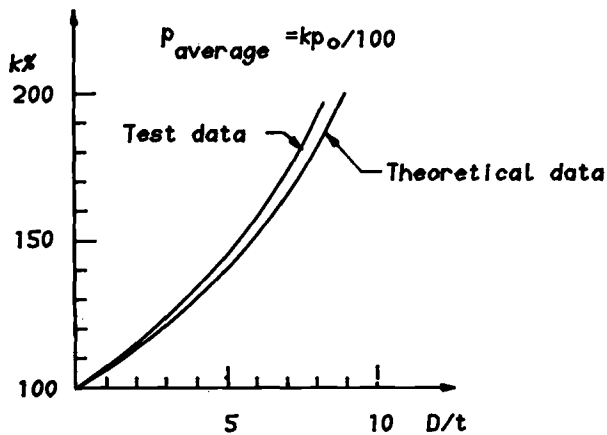


FIG. 7—The effect of friction.

With these changes Eq 3 converts to

$$\frac{p_{average}}{p_o} = \frac{D}{4L_r\mu} (e^{4\mu L_r/D} - 1) \quad (5)$$

All these equations assume flat dies. We also have a sloped portion on the die as shown on Fig. 8. For this portion, instead of μ we have to write $\tan [\arctan (\mu - \alpha)]$, where α is the slope angle.

The Effect of Forging Speed

The time dependence of total strain and the dependence of material strength on the speed of strain are long since known. Nadai reports [3] experiments done by F. H. Norton where hollow cylinders at 838 K were subjected to 11.15 MPa

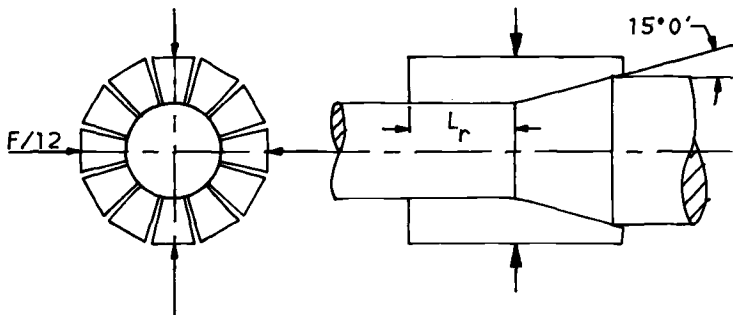


FIG. 8—Schematic of radial forging.

for as long as for 4000 h; a quasiuniform rate of deformation occurred. Such phenomenon of creep need not be discussed.

Davis and Austin report [6] that (conventional) ultimate tensile strength of mild steel increases from 414 to 455 and to 555 MPa, respectively, as deformation speed is increased from 0.0254 to 0.254 to 25.4 m/s, respectively. As more authors agree that this time dependence is a logarithmic function, this author feels that the just-mentioned function (strength of cold mild steel as a function of speed) can be best described by the following equation

$$\sigma_2 = \sigma_1 [1 + 0.05 \ln(v_2/v_1)] \quad (6)$$

For example,

$$414 [1 + 0.05 * \ln(10)] = 461.7$$

and

$$414 [1 + 0.05 * \ln(1000)] = 557$$

Both results are close to the reported figures of 455 and 555, respectively.

Because our main interest is hot forging, we made experiments with 1200 K low-carbon steel and received the data recorded in Fig. 9.

We have found that this phenomenon is best described by this equation

$$\sigma_2 = \sigma_1 [1 + 0.126 \ln(v_2/v_1)] \quad (7)$$

Strain Rate, mm/s	$\sigma_{\text{Ultimate Con.}}, \text{ MPa}$	$\sigma_{\text{Ultimate True Stress, MPa}}$
0.00424	46.06	72.39
1.65	80.77	126.99
57.6	116.77	183.71

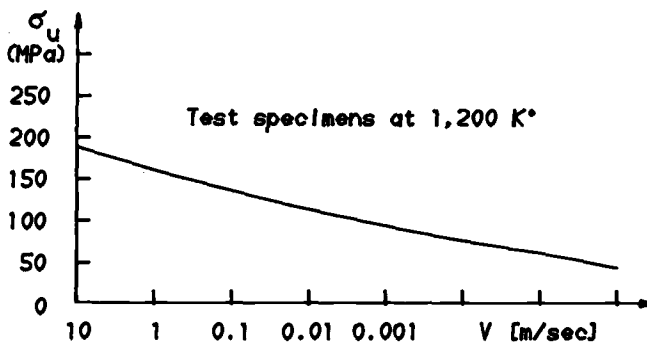


FIG. 9—Ultimate tensile strength versus speed of deformation.

For example: $46.06 (1 + 0.126) * \ln (165/0.424) = 80.72$ and $80.72 (1 + 0.126) * \ln (5.76/0.165) = 116.85$, which is substantially close to measured 116.8 MPa q.e.d.

The Effect of Shear

Theory

If the surface of the material to be forged is not congruent with the forging tool (Fig. 10A) or if it extends behind the edges of the forging tool (Fig. 10B), forging forces have to overcome the shear strength of the material.

This can be visualized by putting parallel lines on the sides of the specimen perpendicular to the force. As the load is applied, these lines will deviate from the original direction with an angle γ . According to the most basic shear theory

$$\tau = G\gamma \quad (8)$$

However, this is a more suitable representation of this basic shear equation

$$\tau = G_s * \tan \gamma \quad (9)$$

While the value of the secant modulus (G_s) may be considered constant to a certain portion of the curve (Fig. 11), theoretically it is defined differently for

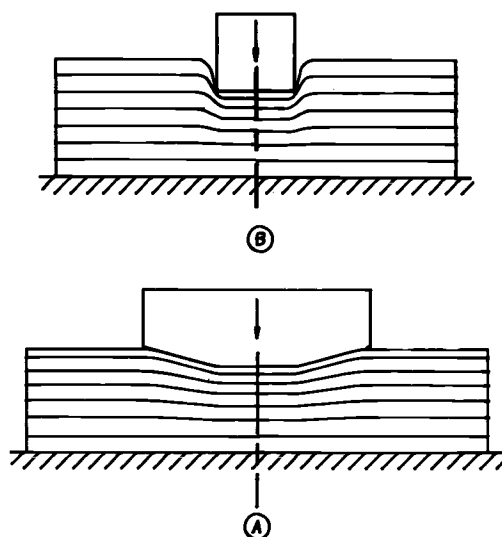
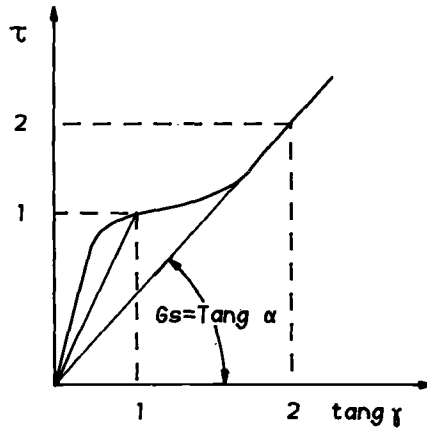


FIG. 10—Deformation of lines due to shear stresses.

FIG. 11— τ versus $\tan \gamma$ diagram.

each point of the curve as

$$G_{s1} = \tau_1 / \tan \gamma_1$$

or

$$G_{s2} = \tau_2 / \tan \gamma_2$$

Because of the obvious difficulties involved in this method, the author found very little reference, if any, in literature to where this method was experimentally or theoretically used. A good example of such prudent thinking can be seen in a 1984 issue of *Materials Engineering* [7]; but here, too, the lines do not represent actual stress trajectories but rather a grid network as used in the finite-element method that reflects anticipation, not actually calculated shear distribution.

Surveying further present-day shear theories:

1. They do not make an effort to calculate single tool shear stresses such as caused by the forging of a material.
2. They do not involve the sharpness of the tools in their analyses.
3. They properly calculate secondary shear stresses (shear stresses due to bending) for certain assumptions and properly end up with the formula

$$\tau = FM_s/Iw \text{ (or } \tau = VM_s/Iw \text{)} \quad (10)$$

4. Referring to the duality principle, some decades back Eq 10 was used to calculate direct shear (as, for example, shear in a rivet), too. However, most (if

not all) authors recently switched to the formula

$$\tau = F/A \text{ (or } \tau = V/A \text{)} \quad (11)$$

But, they do so without setting up restrictions to the duality principle, according to which Eqs 10 and 11 could not coexist.

For such reasons, it is imperative, before setting up an extended shear theory with a general and unrestricted range of validity, which would include calculation of shear stresses as caused by a single tool forging device, to summarize existing shear theories and point out their simplifying assumptions; only then will we set up a general shear theory with no or with lesser restrictions and assumptions.

The shear theory, as it is commonly referred to, is stated by Eq 10 and is proven to be correct for the tacit assumptions its author obviously had in mind, because if we substitute the values of

$$M_s = w (t/2)(t/4)$$

and $I = wt^3/12$, we get $\tau = 1.5 V/A$, and elementary considerations looking at Fig. 12 also result (for the center of the rectangular beam) in the same

$$\tau = \int_0^x w(\sigma_{\max}) \frac{(t/2) - x}{(t/2)} \frac{dx}{wL} = 12 \frac{F}{w} \left[\frac{(t/2)x - x^2/2}{t^3} \right] \frac{1}{t^3} \quad (12)$$

For $x = t/2$, Eq 12 boils down to

$$\tau = 1.5 F/A \text{ (q.e.d.)} \quad (13)$$

For circular cross sections [8]

$$\tau = 1.33 F/A \quad (14)$$

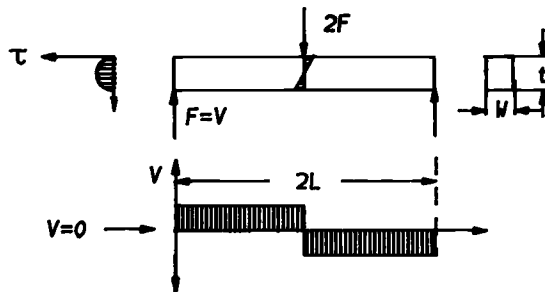


FIG. 12—Normal stresses produce tangential stresses.

Can we also prove that the shear stress in perpendicular direction (vertical direction) at the same point will be the same? If we integrate the shear stress curve in the vertical direction, and we end up with the shear force ($V = F$), then, indeed, we shall prove another statement of the classical shear theory (which is commonly referred to as the duality principle)

$$2 * \int_0^{(t/2)} \int_0^x \left[w^2 \frac{(t/2) - x}{(t/2)} \frac{6 VL}{wt^2} \right] \frac{dx}{wL} \quad (15)$$

Indeed, after a lengthy, but relatively simple integration, the result of Eq 15 ends up in

$$2w \int_0^{(t/2)} \tau dx = F = V \quad (16)$$

What did we prove? Did we prove that shear stresses in an element loaded with a perpendicular force V in both directions are defined by Eq 10? No, we have proven that in a homogeneous isotropic beam of uniform radius of curvature without overhang, the shear stresses far from the support points in both directions are identical and are defined by Eq 10. Let us have a few examples proving that these assumptions are real and that these restrictions do exist.

The author has built a beam that was sliced horizontally in the middle, but not all the way through; however, it had two overhangs, and the slit in the middle stopped in the overhangs short of the ends of the beam as shown in Fig. 13.

When loaded to failure point, the beam failed in shear as shown by the arrow. It should be noted that at this point the shear stress by Eq 10 should be zero because V is zero.

Let us consider a similar beam without the slot, but with a total length L_T and supported at two points spaced at a length L_S ; thus, at each end there is an equal overhang. In case of an absolutely inelastic beam, the failure load will still be

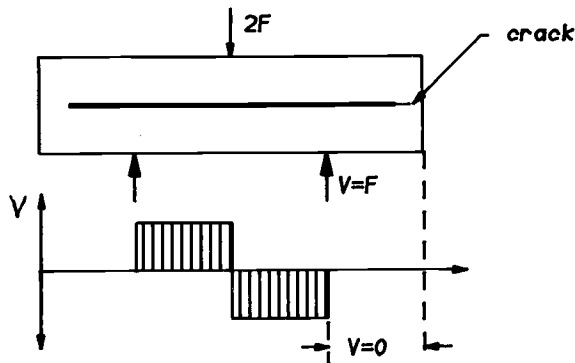


FIG. 13—A beam that doesn't follow Eq 13.

properly given by Eq 10 and 13: $\tau = 1.5V/A$ (for a rectangular beam); but, for a perfectly plastic beam, the horizontal shear stresses will be reduced as given by equation

$$\tau = 1.5(V/A)(L_S/L_T) \quad (17)$$

If we have a practical case where the beam is elastoplastic, the actual stress would be in between.

Because it would depend on many factors, we only can give a general formula for it

$$\tau = 1.5 (V/A * [f (L_S/L_T)])$$

It also is known from literature [8–12] that because $V = dM/dx$, where the moment is constant, the value of V is zero; thus, shear stresses are also zero.

The last statement assumes, however, a straight beam (or a beam with uniform curvature). If a straight beam goes into a curvature, the Navier type stress distribution is replaced by Grashof type, the neutral axis is shifted, and the differences of X directional stress integral before and after the point of change in curvature has a finite value. This divided by the distance of these points ($w = 1$), if the change is sudden, should result in failure level shear stresses for an absolutely rigid beam. Naturally, a beam is never absolutely rigid, so while the theoretical importance of this statement is undisputable, its practical importance is to be regarded in view of other practical aspects.

These claims are hard to believe; for example, that vertical shear stresses would be reduced by adding an overhang to the beam, as well as the recent trend of literature giving two different formulas for primary and for secondary shear; this makes it about time that someone take a closer look at the validity range of the duality principle.

Timoshenko properly proves [11] that a free body element in a beam in bending is kept in balance against rotation by shear stresses only (thus $\tau_x dy dx = \tau_y dx dy$) because the moments from the normal stresses $\sigma_x dy dx (2/3) dy$ and $\sigma_y dx dy (2/3) dx$ are of a higher order of infinitesimal. While this is absolutely correct to a place far from the support points, it is no longer true close to the support points, that is, as the length of the beam is reduced to quasizero as in the case of a sheared rivet or in the case of forging with a sharp tool as shown on Fig. 10B. The difference between Figs. 10A and 10B is in the sharpness of the tool as it can be realized if the reader considers that for an absolute sharp tool $\gamma = 90^\circ$. But because of the size limitations of this paper, only the case of absolutely sharp tools will be discussed. In this case, $d\sigma/dy$ can theoretically be assumed to be infinity (if the tool is absolutely sharp and absolutely rigid), and, especially in the case of dual tool single cross-section shear, the total shearing force may load the edge of the free body, producing a moment of Vdy , which is a lower order infinitesimal than the moment produced by shear stresses. (In each case, $Z = W = 1$

was considered.) In summary, the action of the y directional normal stresses can be neglected, but the action of the x directional normal stresses can be neglected only if we are far from the attack points (See Fig. 14.).

This indicates that

1. The balance of normal stresses close to the edge of the die is no longer negligible. Thus, the duality principle is no longer valid.

2. $\tau_x \neq \tau_y$, but $\tau_x \gg \tau_y$.

3. As the shear stresses are linear with the derivative of the surface pressure p (or σ_x) according to y

$$\tau = K dp/dy \quad (18)$$

where K is a constant. Because, the closer we get to the surface, the larger the value of dp/dy ; the stresses are maximum at the surface (rather than as proven for indirect shear, zero at the surface). This is in good agreement with the observation that a material in direct shear first shears at the surface and not in the center!

4. It is also obvious, as numerous literatures spell out [12,13] that the pressure in x direction spreads out from the edge of the tool, which applies a pressure on the surface. Thus, while on the surface the pressure goes from maximum to quasizero in a very short distance (y) as we go laterally, going more and more inward; the value of $d\sigma_x/dy$ is becoming smaller and smaller and thus the shear stresses are becoming smaller and smaller. Consequently, the newer representation of direct shear, as can be found in more recent literature [8-11] and as expressed by Eq 12, is a uniform stress distribution founded on an oversimplification.

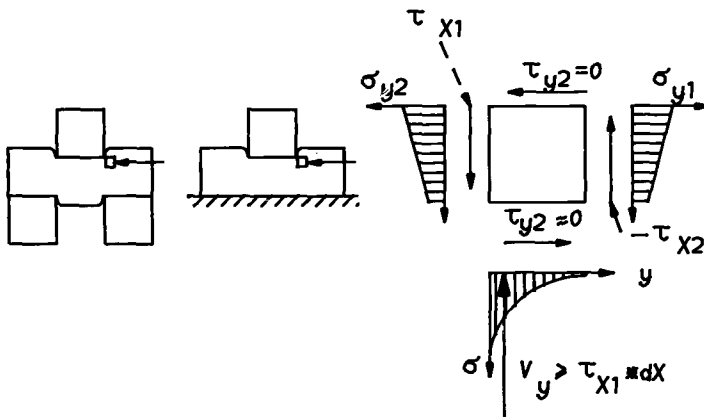


FIG. 14—Free body at die edge.

The true shear stress distribution in direct shear is actually simple if not outright obvious

$$dp = cpdx \quad (19)$$

Namely, Eq 19 states that the pressure drop in the material (progressing downward in x direction) equals the amount of pressure spread throughout the same distance dx [12,13]

From Eq 19

$$\int_{p_1}^{p_2} \frac{dp}{p} = \int_{x_1}^{x_2} c \, dx \quad (20)$$

$$\ln (p_2/p_1) = c (x_2 - x_1) \quad (21)$$

Here c is a constant representing the amount of spreading of the pressure underneath the tool. We shall refer to it as the "transfer factor."

From Eqs 18 and 21

$$p_2/p_1 = \tau_2/\tau_1 = e^{c(x_1-x_2)} \quad (22)$$

For the general case:

$$\tau = \tau_o e^{cx}$$

and for max: (23)

$$\tau_{\max} = \tau_o e^{ct}$$

So, the entire shear resistance of the cross section is

$$V = w \int_0^t \tau \, dx = \frac{w\tau_o}{c} (e^{ct} - 1) \quad (24)$$

Thus

$$\tau_o = \frac{Vc}{w(e^{ct} - 1)} \quad (25)$$

and

$$\tau_{\max} = \frac{Vc}{w(1 - e^{-ct})} \quad (26)$$

Thus, for the entire shear load capacity

$$V = \tau_{\text{permissible}} * w \frac{1 - e^{-ct}}{c} \quad (27)$$

$$\tau_{\text{average}} = V/wt \quad (28)$$

Therefore, from Eqs 26 and 28

$$\frac{\tau_{\text{max}}}{\tau_{\text{average}}} = \frac{ct}{1 - e^{-ct}} \quad (29)$$

It is an important test for the correctness of the just-presented mathematics that if $t \rightarrow 0$, that is, for very thin specimens, the value of Eq 26 approaches the value obtained from Eq 28. So that the just-presented equations do not really contradict the present day practice, but extend the accuracy of shear calculation to a wider range of thicknesses. While the just-presented equations have extended validity for the case of general (dual tool) shear, we shall now convert them for the case of forging application (monotool shear).

From Eq 23

$$\tau = \tau_{\text{max}} e^{-cx} \quad (30)$$

If we are forging on an infinitely thick anvil, the same size as the specimen and the same flexibility as the specimen, this equation properly defines stress distribution at any point of the specimen and of the anvil. Thus, the force requirements for such a situation is defined by

$$V = (\Sigma L) \int_0^t \tau_{\text{ultimate}} * e^{-cx} dx = (\Sigma L) \frac{\tau_{\text{ultimate}}}{c} (1 - e^{-ct}) \quad (31)$$

Where L means the total length of the line sheared.

If, however, as is most often the case, we are forging on an anvil which can be considered absolutely rigid with respect to the part in forging by the principle of the mirroring theorem of stresses, the values given by Eq 31 will be reduced at any point of x by the amount of stresses that would be present in case of an elastic anvil at the point determined by the mirrored distance of the point x around the plane of the anvil.

$$\tau = \tau_{\text{max}} [e^{-cx} - e^{-c(2t-x)}] \quad (32)$$

Again, checking the boundaries gives us assurance of the correctness of the equation: the stresses at the anvil have to be zero. Indeed, for $t = x$, the value of Eq 32 is zero.

From this, the total shear force per unit of length of the die

$$\frac{V}{\Sigma L} = \tau_{\max} \int_0^t (e^{-cx} - e^{-c(2t-x)}) dx = \tau_{\max} \left[-\frac{e^{-cx}}{c} \right]_0^t + \left[\frac{e^{(cx-2ct)}}{c} \right]_0^t \quad (33)$$

Where τ_{\max} is the shear stress at the surface.

Having finished the presentation of existing and of newly developed shear theories, it would be useful to take a look at Fig. 15, which presents the assumed shear distribution for the cases just discussed:

Figure 15A = secondary shear; shear in a rectangular beam due to bending.

Figure 15B = bidirectional shear assuming uniform shear stress distribution.

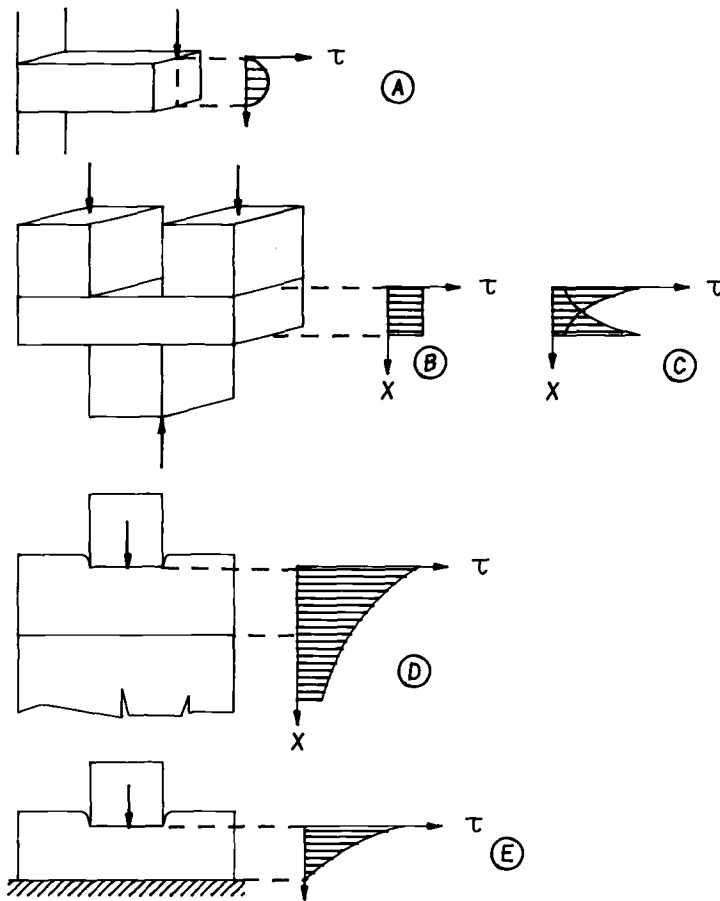


FIG. 15—Shear stress distribution for the cases discussed.

Figure 15C = same as Fig. 15, but with the real shear stress distribution.

Figure 15D = single tool shear assuming an anvil of identical flexibility.

Figure 15 = same as Fig. 15D, but with a rigid anvil assumption.

We deliberately left for last the value of c because the author feels that it is a material property and may deviate as a function of material properties, brittleness, temperature, etc. In any event, the most logical and the safest way to establish a value for c is by experiments. Throughout the limited number of experiments the author carried out for the material and temperatures examined (cold aluminum, cold and hot mild steel), in spite of expectations, c turned out to be pretty much the same number in the value of $47.21/m$.

Experiments

Bidirectional Shear of Various Thicknesses of Aluminum Plates—All specimens were 12.7 mm wide. The three tests were made with 12.7, 25.4, and 38.1-mm-high specimens. We have accepted test data for the single-thickness (12.7-mm) specimen on face value. It failed under 206.1 MPa, of average stress. From this, we calculated with Eq 29 the maximum shear stress for zero thickness. It turned out to be 273.9 MPa. If the formula established for such bidirectional shear is correct, we should have sheared the double and triple thickness under an average stress of 159.5 and 127.0 MPa, respectively. Experimental data were in excellent agreement as the actual average shear stress at failure turned out to be 163.5 and 130.3 MPa, respectively! For the sake of clarity, we will show at least one of these points to be calculated

$$\tau_{\text{average for 38.1 mm height}} = 273.9 \frac{1 - e^{-47.2 * 0.0381}}{47.2 * 0.0381} = 127.0 \text{ MPa}$$

The actual shear failure occurred at a load that constituted an average stress of 130 MPa, a deviation of about 2 to 3%. When, at the same time, present day practice [9–12] presents a formula that would make us calculate the three-times-thicker element with the same average shear stress, in spite of the fact that the shear resistance of the 38.1-mm-thick material exhibited 62% of the value (130 against 206 MPa) of the three-times-thinner material in the case of the given actual dimension (see Fig. 16).

Inside Distribution of Shear Stresses—In the case of forging, we have to know the actual shear stress distribution inside the material and to be able to integrate it to establish total force requirement. First, this was done in a dual shear operation because it also was vital to prove the validity of the just-presented new shear theory. Figure 17 shows an aluminum specimen in multiple bidirectional shear, with lines perpendicular to the shearing force drawn on its surface. The angular

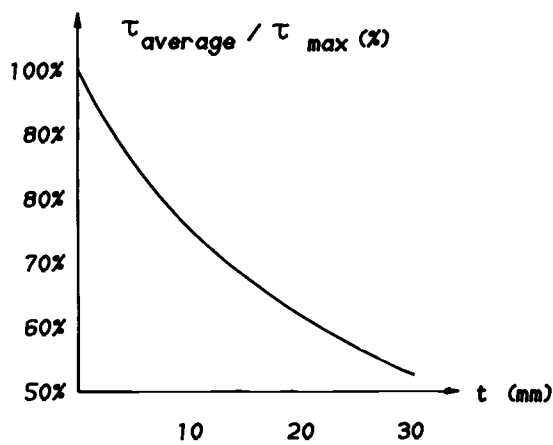


FIG. 16—Reduction in load capacity per unit of area as a function of thickness.

deviations, γ , were measured and recorded; the tangents were tabulated, also, and, in a separate series of tests, G_s -values, as a function of $\tan \gamma$, were established by surveying the τ versus $\tan \gamma$ curve by a very thin specimen where shear stress distribution can be assumed uniform and by composing from this the G_s versus $\tan \gamma$ curve as shown in Fig. 11. With this the $\tau = f(x)$ curve was established as shown on Fig. 18. The curve with the solid line shows a stress pattern caused by one tool and the curve with the dotted line, the stress pattern caused by the other tool as a reaction force. Small circles show the test data; the curves themselves show the calculated values. Obviously, the situation is symmetrical, so that the actual maximum shear stress in the material is defined by the curve having the greater value. It also is important to note that the area between one curve and the upper portion of the horizontal line representing $\tau_{\text{average}} = 184.8$ MPa is to be the same as the area between the same curve and down from this horizontal line which requirement is properly fulfilled. The curve is made by establishing maximum shear strength for a very thin specimen (316.4 MPa) and then using Eq 30

$$\tau = 316.4 e^{-47.2x}$$

Depth, mm	$\gamma_{\text{Average}}^\circ$	Tan γ	G_s , MPa	$\tau = \text{Tan } \gamma * G_s$	$\tau / \tau_{\text{Middle}}$
2.0	42.33	0.911	344.7	314.0	1.82
3.8	30.00	0.577	468.8	270.5	1.57
5.5	27.17	0.513	482.6	247.6	1.44
7.1	23.33	0.431	482.6	208.0	1.21
9.1	22.67	0.418	482.6	201.7	1.19
11.4	21.00	0.384	482.6	185.3	1.07
12.4	19.67	0.357	482.6	172.3	1.00

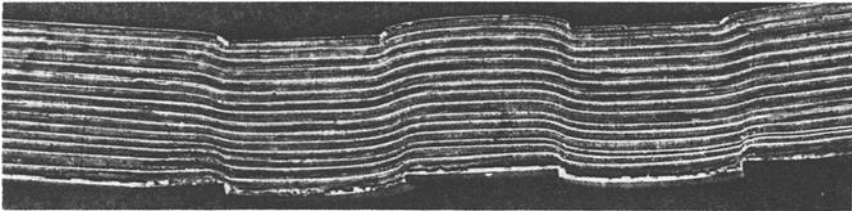


FIG. 17—Shear deformation pattern on a 12.7-mm-wide, 25-mm-high aluminum specimen under 184.8 MPa average shear stress.

It also is important to note that the integrated stress area under any of the two curves is equal to the integrated stress area of the average stress.

Forging Against Rigid Anvil—A similar piece of aluminum of the same material was forged down by 2.03 mm after a similar set of lines was applied to it, as shown on Fig. 19. The applied force that produced this deformation was 146.3 kN. This would have meant 293-MPa surface pressure on the surface of the aluminum specimen if shear resistance would not have reduced the surface pressure, which it obviously did. Again, the angular deformations of the lines was measured and recorded. The G_s values, as a function of the deformation angle, were established. They turned out quite similar (482.6 MPa) because the deformation angles were relatively low as a result of the monotool shear.

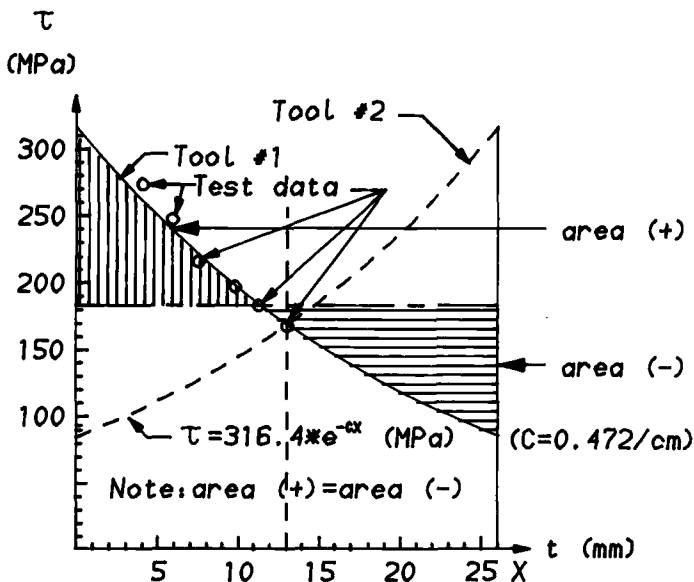


FIG. 18—Actual stress distribution inside a sheared specimen.

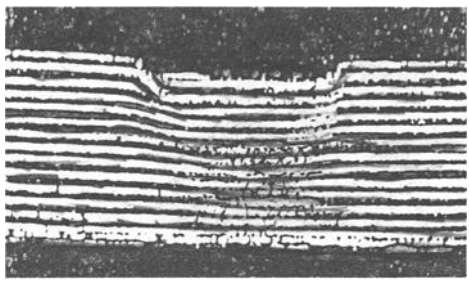


FIG. 19—Aluminum specimen forged from 24.9 to 22.9 mm.

Depth, mm	γ°	Tan γ	$\tau = G_s \tan \gamma$, MPa
1.3	20.5	0.374	180.7
3.8	17.0	0.305	147.5
5.1	15.0	0.267	129.3
7.1	14.0	0.249	120.3
8.6	12.5	0.221	106.6
9.6	11.0	0.194	93.8
11.4	9.5	0.167	80.7
12.9	8.5	0.149	72.1
13.9	7.5	0.132	63.5
15.7	6.0	0.106	52.7
17.3	4.0	0.070	33.7
18.5	2.5	0.044	21.1
20.3	2.0	0.035	16.8
22.8	0.0	0.0	0.0

These stress values have been recorded with circles on Fig. 20, and the results from the theory using Eq 32 also have been recorded (graph). The agreement is very good! It is important to note that, because our closest point to the surface was at 1.3 mm, the actual stress value at the surface, calculated by Eq 32, was close, so that one point on the graph was taken for granted; but, of course, if the equation used would not follow properly the actual behavior of the material, the rest of the points would have deviated from the test results—but they did not. The stress at the surface was 220.5 MPa (against 180.7 at a depth of 1.3 mm). From this, the actual numerical equation we used was

$$\tau = 220.5 (e^{-47.2x} - e^{-47.2(2*0.0229-x)})$$

The total length of the shearline was 25.4 mm. Using Eq 33, or simply carrying out a planimetry, or using a computerized numerical integration program, we ended up with a total shear force of 51.6 kN. Deducting this from the 146.3 kN total force previously quoted, we got for actual compressive force: 94.7 kN.

A very convincing proof that the presented shear theory and the resulting formulas are correct is: If we cut a specimen from the same aluminum, engaging

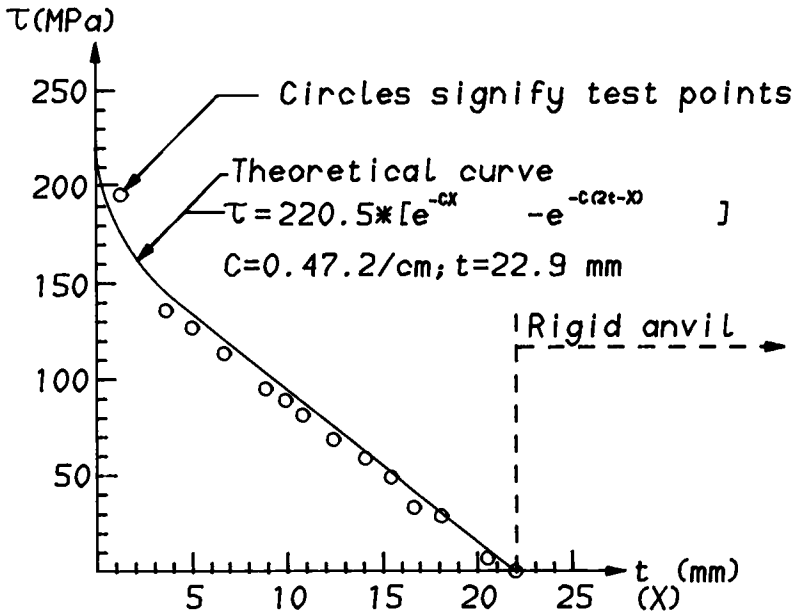


FIG. 20—Internal stress distribution in an aluminum specimen forged on a rigid anvil.

the forging tool, with a surface smaller than the surface of the forging tool so that shear resistance was eliminated, and we compressed it to the same height and by the same amount, we found that it took 94.4 kN, which is in good agreement with the calculated 94.7 kN.

Bidirectional Shear of a Hot Low-Carbon (Mild Steel) Specimen—Specimen size: 12.7 mm wide, 25.4 mm tall; temperature: 1255 K. The quadruple bidirectional shear took a total of 91.7 kN to produce the deformations shown in Fig. 21.

This meant 45.8 kN/25.4 mm of length or 1.8 MN/m of the sheared specimen. This meant, in average stress, 71.0 MPa. The tracer lines were produced by milling very narrow and very shallow grooves in the metal and then, after the

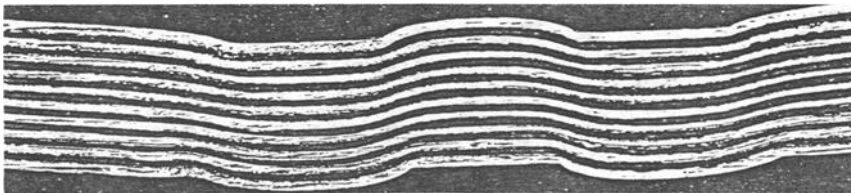


FIG. 21—Deformation pattern exhibited by a hot mild steel specimen in bidirectional shear.

test, coloring the extruding surface white. As a result of machining, the lines are exactly equidistant, so that we do not show depth in the table that follows. To reduce the length of this paper, we concentrate on the demonstration of $\tau_{\max}/\tau_{\text{average}}$ only. According to Eq 29, for the size in question, with the same $c = 47.2/\text{m}$ value, $\tau_{\max}/\tau_{\text{average}} = 1.717$.

The deformation of the lines is shown by the following table.

γ	35	20	18	17	16	17.5	18	19	35	Average
$\tan \gamma$	0.70	0.36	0.32	0.30	0.29	0.31	0.32	0.34	0.70	0.384

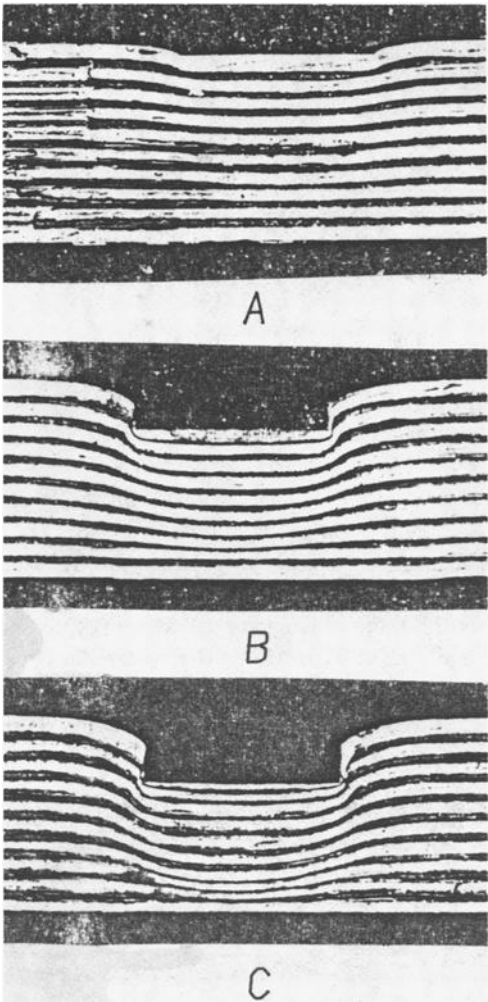


FIG. 22—Single tool shear (forging) of hot low-carbon specimens: A = 284; B = 385; C = 426 MPa.

Thus $\tan \gamma_{\max} / \tan \gamma_{\text{avg}} = 0.70 / 0.384 = 1.84$.

Because we had soft, hot material, G_s did not seem to change much, if any; therefore, the just-mentioned number 1.84 can be considered on its face value as the figure for $\tau_{\max} / \tau_{\text{average}}$. As such, this proves again the validity of the theory just presented as 1.84 is within 7% of 1.717.

Single Tool (Forging) Experiments of Hot Low-Carbon (Mild Steel)—Specimen size, as usual, is 12.7 mm wide and 25.4 mm high. Temperature is the same: 1255 K.

Figures 22A, B, and C show photos of similarly prepared low-carbon steel specimens, with similar size and similar temperature as described in the section entitled, “Bidirectional Shear of a Hot Low-Carbon (Mild Steel) Specimen.” The forging force applied to them in the same sequence was: A: 91.7 kN, producing 2.54-mm deformation; B: 114.6 kN, producing 6.3-mm deformation; and C: 137.5 kN, producing 9.1-mm deformation. These created normal stresses (if there would be no shear present) are: $A = 284$; $B = 355$, and $C = 426$ MPa. Now we compressed specimens identical with those tested, but shorter than the tool (no shear), to the same permanent deformation. We got: $A = 206.7$; $B = 227.4$; and $C = 255.7$ MPa.

These normal stress numbers compared with the just-recorded total stress numbers show that the shear resistance of these samples demanded: $A = 27\%$; $B = 36\%$; $C = 40\%$ of the total forging force, respectively. This leads us to the conclusion that shear resistance in forging, although showing a slight increase with the depth of forging deformation (bite), is characteristically about one third of the total forging force, as this figure was repeatedly obtained throughout our numerous tests. The exact figure can be calculated by the method and equations just presented.

Machine Forging

How the analytical methods discussed can be put into practice are discussed in following paragraphs, showing the forging process of a mild steel specimen on a 30-MN total radial force 12 die Grotne forging machine. Figure 23 shows the hot material, part of which is already forged, moving upward out of the machine. Forging was done in one pass, and the diameter of the material was reduced from 152.4 to 101.6 mm. The ultimate tensile strength of this material was given to us at this temperature (1200 K) by the testing laboratory: 80.7 MPa. The true stress of the material was, however, 127 MPa (work hardening). However, these figures were obtained with a very low testing speed: 1.65 mm/s. For 58 mm/s, they increased to 116.7 and 183.6 MPa, respectively. For our actual forging speed (12.7 mm/s), interpolation gave us 151.6 MPa true stress.

The dies are shown in Fig. 24. The dimensions so given, for 12 dies, result in a 0.029-m² squeeze area and in a 2.438-m shear length. Thus, the resistances described in earlier paragraphs commanded a total radial force of $F = 151.6 \times 0.029 = 4.4$ MN.

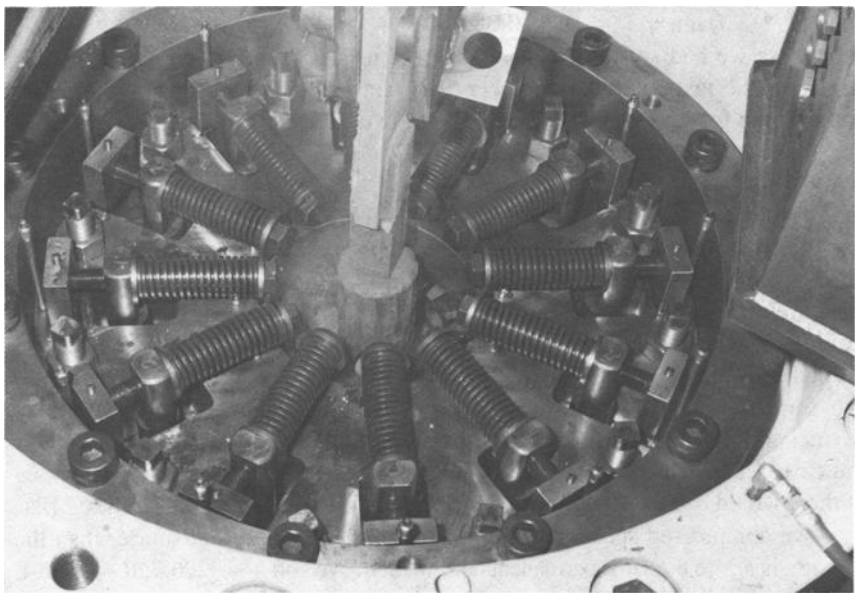


FIG. 23—Hot forging in process.

While this figure included the natural strength, work hardening, and the effect of temperature and forging speed, the effect of friction was calculated by Eq 5 with the following input data: $D = 101.6$ mm, $L_r = 50.8$ mm, and $\mu = 0.3$

$$\frac{p_{avg}}{p_o} = \frac{0.1016}{4 * 0.0508 * 0.3} * e^{(4*0.3*0.0508/0.1016)} = 1.37$$

Therefore, the actual increment of forging force due to friction is 37% of 4.4 MN, that is, 1.6 MN.

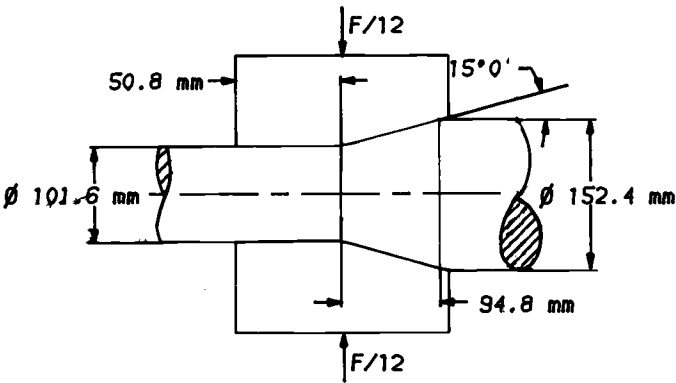


FIG. 24—Schematic of radial forging.

Please note that the actual angle of the leading part of the dies was so chosen as to match the actual friction coefficient (15°), thus the effect of friction for this conical portion was neglected.

Shear strength of the material was assumed to be $\tau = \sigma/\sqrt{3}$, as most commonly recommended by literature [9,10,13]. Thus, $\tau_u = 151.6/\sqrt{3} = 87.5$ MPa. Because the setup had a mirror-image symmetry, it was considered as if half would be forged on a rigid anvil, this way producing a height of $101.6/2 = 50.8$ mm. Therefore, the total shearing force for the 2.438-m total length, according to Eq 33, was calculated to be

$$V = 2.438 * 87.55 \int_0^{0.0508} [e^{-0.472x} - e^{-47.2(0.1016 - x)}] dx = 3.41 \text{ MN}$$

Forging force "budget," in MN:

Conventional ultimate	2.34
Work hardening	1.34
Speed	<u>0.72</u>
Subtotal (from lab)	4.40
Friction	1.63
Shear	<u>3.41</u>
Total	9.44

This compares well to the measured figure of 9.34 MN.

References

- [1] Javorik, L., "The Effect of Axial Compression," Technical Conference Machine Tool Show, Machine Tool Builder's Assn., McLean, VA.
- [2] Bauschinger, J., *Mitteilungen Tech. Lab Munchen*, Vol. 13, 1880.
- [3] Nadai, *Theory of Flow and Fracture of Solids*, McGraw Hill, 1950.
- [4] Bridgeman, P., "The Effect of Hydrostatic Pressure on Fracture," *Journal of Applied Physics*.
- [5] Bridgeman, P., *Studies on Large Plastic Flow*, 1895.
- [6] Davis, R., and Austin, R., *Developments in High Speed Metalforming*, Indiana Press.
- [7] Bittence, J., "Laboratories Are Busy," *Materials Engineering*, 1984.
- [8] Belluzzi, O., *Science of Structures*, Topografia Galavotti, Bologna.
- [9] Marks, L., *Mechanical Engineering Handbook*, McGraw Hill, New York, 1967.
- [10] Dubel's: *Pocketbook for Machine Builders*, Springer Verlag, New York, 1967.
- [11] Muttonyanszky, A., *Stress Analysis*, Tankonyvkiadó, Budapest, 1957.
- [12] Timoshenko, S., *Theory of Elasticity*, McGraw Hill, New York, 1951.
- [13] Boldizsar, T., *Banyaszati Zsebkönyv*, Muszaki könyvkiadó Budapest.
- [14] Donald, E. P., "A Practical Guide to Bolt Analysis," *Machine Design*, 1981.

Forging of Long-Stroke Crankshafts by the TR Method

REFERENCE: Rut, T., "Forging of Long-Stroke Crankshafts by the TR Method," *Steel Forgings, ASTM STP 903*, E. G. Nisbett and A. S. Melilli, Eds., American Society for Testing and Materials, Philadelphia, 1986, pp. 504–519.

ABSTRACT: The manufacture of long-stroke crankshafts lends itself to new methods of forging and equipment. Lately, at the Metal Forming Institute in Poznan, Poland, a very efficient method and the necessary equipment have been developed for single throws for semibuilt, shrink-fitted crankshafts. Furthermore, the method also is well-adapted for forging single crank throws carrying a half main journal on each side. The method enables the forging of single crank throws with the optimal shape of crank webs and with minimum weight. Thanks to a special design development, the horizontal upsetting force is about 2.5 times larger than the nominal press capacity. Such a very high-efficiency forging device permits the forging of large crank throws on a relatively small forging press. Furthermore, with a background of accumulated experience, a new forging method for fully forged, long-stroke crankshafts has been developed at the Metal Forming Institute. By this method, each crank arm is formed separately in new, specially designed forging equipment.

KEY WORDS: long-stroke crankshaft, TR device, TR forging method, RTA—superlong-strokes engines, semibuilt, shrink-fitted crankshafts, single crank throws, long-stroke crankshafts fully forged, solid-type crankshafts.

There is full interdependence between the further progress of metal forging and the development of the required equipment; that means, for a new forging process, it is necessary to design new forging devices.

Fully Forged Crankshafts

The largest size of crankshaft which could be forged hitherto with continuous grain flow was limited to about a 1200-mm stroke. Only two sources, both located in Japan, have the equipment to make crankshafts of this size. One utilizes the RR method and the other the TR method² [1–3] on a hydraulic 80-MN forging press. Such size limitation results from the required press load, the daylight of the press, and the distance between columns.

The TR method [4, 5] equipment for fully forged solid crankshafts is used in Japan. Forging a Sulzer-type RLA56 crankshaft is shown in Fig. 1. The Burmeister-and-Wain-type crankshafts L35MC and the Sulzer RTA-38 also can be

¹ Manager—Forging Dept., Metal Forming Institute, 61-120 Poznan, Poland.

² Initials of the inventor, T. Rut.

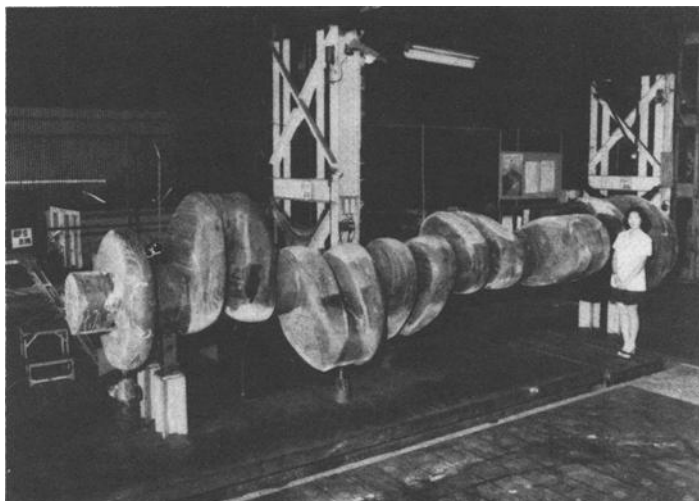


FIG. 1--- *Crankshaft forging (Sulzer Type RLA56) weighing 37.4 tons forged by the TR method.*

solid, fully forged by this TR equipment, which is used extensively in Europe and the Far East.

The Burmeister-and-Wain "ultralong-stroke" (L-MC type) marine diesel engines, the largest being the L90MC type (2925-mm stroke), and the Sulzer RTA "superlong-stroke" engines, the largest being the RTS-84 type (2400-mm stroke), are typical examples of the new generation of long-stroke diesel engines.

Design requirements for superlong-stroke engines, such as high firing pressure and a long stroke, would normally result in a relatively large and heavy engine, with significantly increased production costs. Therefore, traditional design principles have been subjected to critical review.

One of the main purposes of the revised forging method is to decrease production costs, for example, by reduction of the overall dimensions such as cylinder distance, total engine length, etc. In this respect, the thickness of the webs can be reduced as compared to a semibuilt-up shaft.

The monoblock design permits a reduction in the distance between the cylinders by about 5%. The reduced overall dimensions of the crank web enlarge the space above the crankshaft, which facilitates dismantling the crosshead. This, in turn, allows a reduction in the connecting rod length by about 10% in favor of a smaller engine height.

Burmeister and Wain have decided to introduce the welding process as an assembling method for crankshaft components. This welded crankshaft would be made using one forging per cylinder, with every crank throw carrying a half main journal on each side, so that the welds are placed in the middle of all main journals.

At Poznan, very efficient equipment and a method of forging [6-8] have been developed for single throws for semibuilt crankshafts (Fig. 2a) and already have

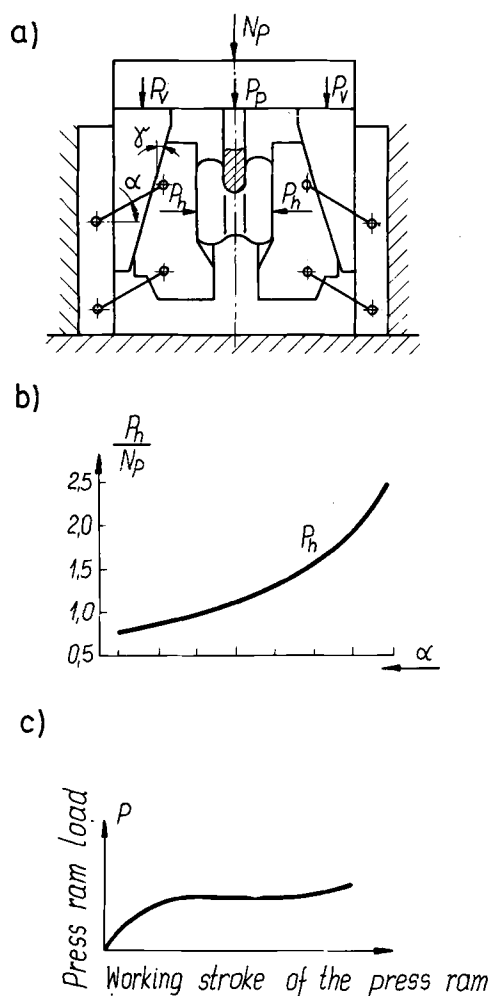


FIG. 2- Forces acting in the device: (a) layout of forces; (b) diagram of the calculated value of the upsetting force ratio (P_h) on the nominal press capacity (N_p) plotted against the connector inclination angle α ; (c) diagram of a press ram load plotted against the working stroke of the press ram.

been introduced on an 80-MN forging press. In consequence, the method also is well adapted for forging a single crank throw carrying a half main journal on each side, as shown schematically in Fig. 3. The TR method [9,10] enables single crank throws to be forged with optimal shape of crank webs and with a minimum weight.

Description of the Forging Operation

Attention is drawn to some new features of the mechanisms used in the drive transmission. The forging device, Fig. 3, uses a two-stage translation of the

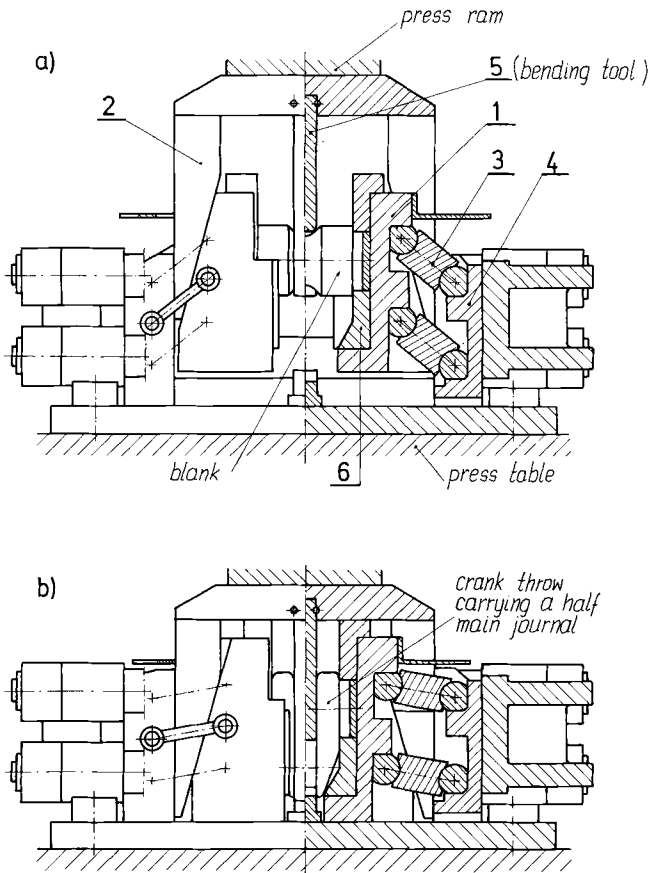


FIG. 3—Forging device adapted to the forging of crank throws carrying half journal on both sides (schematically shown): (a) View shows the device in the open position when the bending tool and the blank have touched each other (left hand side of figure shows elevation; right hand side shows sectional view); (b) View shows the device in the closed position at the end of the working stroke (left hand shows elevation; right hand side shows sectional view).

vertical press ram movement into a transverse force causing the closure of die holders (1). The first stage takes place on a wedge (2), the movement of which is constant along the entire length of a working stroke. The second stage takes place by means of articulated connectors (3) applied between a stationary body (4) and countermoving holders (1). This transmission changes during a working stroke, and the transmission ratio is compatible with a tangent function of the angle between the direction of press force action and a longitudinal axis of connectors (3). This method of associating two transmissions, each having different performance characteristics, enables selection of the required movement of forging tools in accordance with actual needs.

Another feature of the drive transmission mechanisms, also shown in Fig. 3, is the fact that the punch (5) as well as the shaped material are both the elements

transmitting a part of the press thrust force on the dies (6) and their holders (1), causing their motion towards each other in a direction transverse to the motion of the press. That is why the wedge shafts (2) are relieved to a great extent, because they transmit only a part of the force required to drive the die holders (1). Because of this arrangement, the horizontal upsetting force is about 2.5 times larger than the nominal press capacity (Fig. 2b).

Figure 2a shows schematically the same forging device as shown in Fig. 3 and the distribution of forces acting on certain parts of the device. From Fig. 2a, the equilibrium of forces gives the formula estimating the horizontal upsetting force P_h

$$P_h = \frac{(1 - \mu \cdot \tan \gamma)\omega + [\tan \gamma + (2 - \omega)\mu]\cot(a + \rho) 0.5N_p}{\tan \gamma + 2 \mu} \quad (1)$$

where

N_p = press capacity,

P_p = joggling force,

P_v = force acting on the wedge,

γ = angle of the wedge inclination,

μ = friction coefficient, and

ρ = friction angle.

$$\omega = 1 - \frac{P_p}{N_p} \quad (2)$$

The factor ω estimates the part of the press pressure which acts on the wedges.

Owing to the fact that the inclination of the connectors diminishes during the working stroke, the necessary increase in the upsetting force P_h is obtained virtually without changing the press ram load. This force P_h , must exceed the actual forging resistance. Thanks to the very high efficiency of the forging device, large crank throws can be forged now on relatively small forging presses.

Figure 2c shows the diagram of a press ram load plotted against the working stroke of the press ram. The curve nearly parallel to the diagram axis means that the press ram load changes in small range during the whole working stroke; however, the shaping resistance of the just-forged crank throw is increasing. It is evidence of the correctness of the forging device design.

In order to investigate the influence of the new forging process upon the closing of internal cavities in crank throw forging, special tests were carried out at the Metal Forming Institute. The results have been described [7,11-13]. The test indicates that crank throws forged by means of the TR method have satisfactory mechanical properties at the positions of healed cavities.

It is expected that the response of the crankshaft producers will be positive and that this forging method may have a bright future. The design of the

forging device readily can be adapted for forging crank throws as components of welded crankshafts, and the same forging device can be used for the forging of crank throws for assembly by shrink-fitting. When the forging device is used for forging of crank throws carrying half journals only, the equipment design is simpler than the one described in our paper earlier.

Long-Stroke Crankshafts, Fully Forged

Though the welding technique can be a viable alternative to the shrink-fitting of joints in the shaft pieces, the manufacture of welded crankshafts has several disadvantages:

1. Possible limitations in welding of a low-alloy chromium molybdenum steel.
2. Some risk of inadequate welded joint quality.
3. The production of welded crankshafts demands the investments by the crankshaft producer both for a forging device and the welding equipment.

With this background, it is thought that production of the fully forged crankshafts may be expected to be a more straightforward job than that of assembling crankshafts by submerged arc welding.

The Metal Forming Institute in Poznan lately has developed, on the basis of previous experience, the new TR method of forging for fully forged, long-stroke crankshafts. The previous crank throw shaping method meant the bilateral upsetting of a bar portion and the simultaneous bending of its middle part. As mentioned earlier, using this earlier method, it is impossible to form a crank throw having a stroke longer than 1200-mm even on the largest hydraulic forging press (up to 120 MN).

By a new forging procedure, each crank arm is formed separately. A bar portion is clamped on both sides, and the crank arm is shaped by means of simultaneous upsetting and bending at the beginning of the operation and joggling at the end of the operation.

As results from the kinematics of the equipment, the relation of upsetting velocity to bending (joggling) velocity at the beginning of the forming operation is larger than the one at the end of crank-web-forming operation. Thanks to the upsetting predominance at the beginning of the crank web formation, the gathering of the material takes place. At the second phase of crank web forming, the bending (joggling) predominates; thus, it is a very advantageous sequence in the metal-forming process.

Working Sequence (Figs. 4 to 6)

Initial stage: The device is opened, and the upper toolholder (14) is shifted from its initial position by means of hydraulic cylinders (not shown on the drawing). The lower toolholder (6) is raised to its initial position by means of hydraulic cylinders (also not shown on the drawing) while the press table (1)

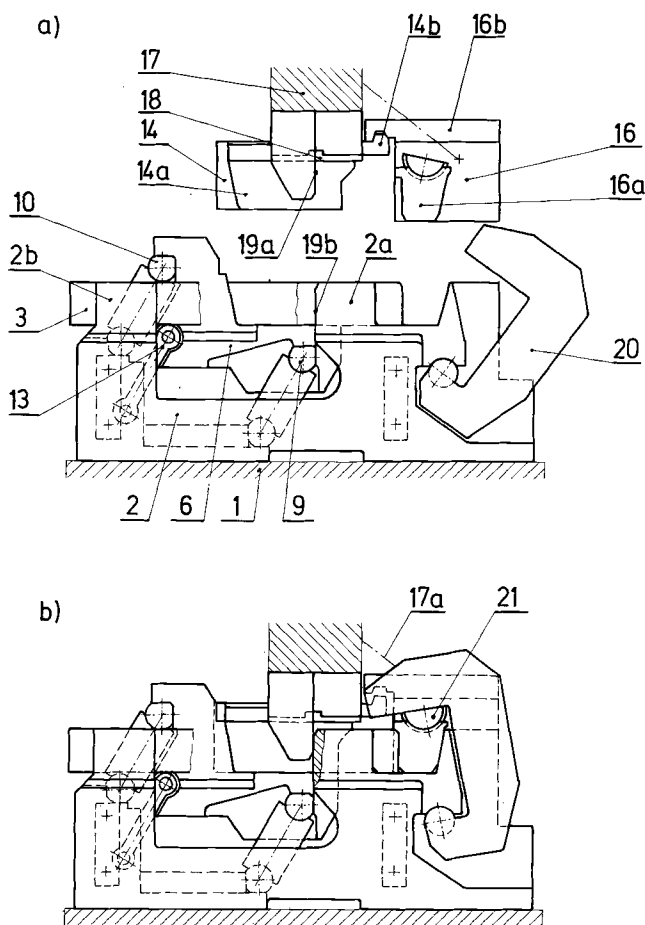


FIG. 4—View of the forging device: (a) When crosshead of the press is in top position; (b) In open position when die inserts and the blank has come to contact.

and the lower device assembly with a set of bottom die inserts are shifted out of the press.

A blank locally heated to forging temperature is put on the bottom tools, and then the lower assembly of the device is shifted under the press. The press is then put in motion, and the press crosshead (17) is lowered until the contact of the cover toolholder (16) with longitudinal beams (2) is achieved. The cover toolholder (16) is held down through self-aligning elements (21) to the longitudinal beams (2) by means of inclinable hook clamps (20) driven by hydraulic cylinders (not shown on the drawing). As a result, the forged bar is clamped between upper and bottom clamping die inserts. When the cover toolholder (16) is held down to the longitudinal beams (2) by means of hook clamps (20), the

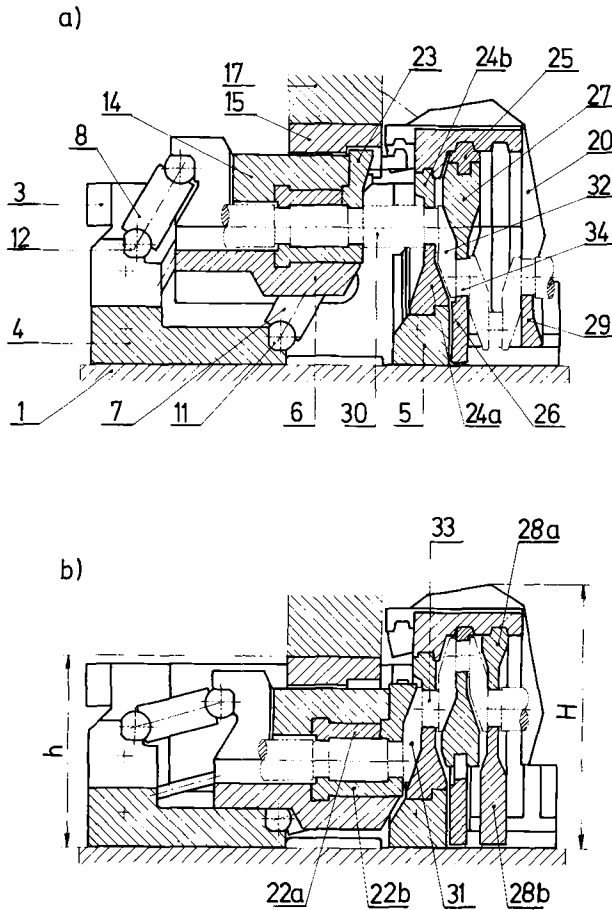


FIG. 5—Sectional view of the device shown in Fig. 4: (a) Before forming the second crank web of the same crank throw; (b) After forming the first crank web of the next crank throw.

tie (17a) is detached to enable the press crosshead downward movement to be continued. Further movement of the press crosshead (17) causes the contact between the upper and lower die holders (14 and 6).

Because the lower die holder (6) is kept in its top position by means of hydraulic cylinders (not shown on the drawing), the forged bar is clamped between upper and lower clamping dies (22a and 22b) automatically.

During the working stroke, the press crosshead (17) drives via the head (15) the upsetting-joggling mechanism. As a result of the action of this mechanism, a part of the forged bar (30) is simultaneously upset and joggled between face dies; thus, a crank web is formed. It is worth noting that the same press power which is applied to drive the upsetting-joggling mechanism is used simultaneously for clamping the workpiece.

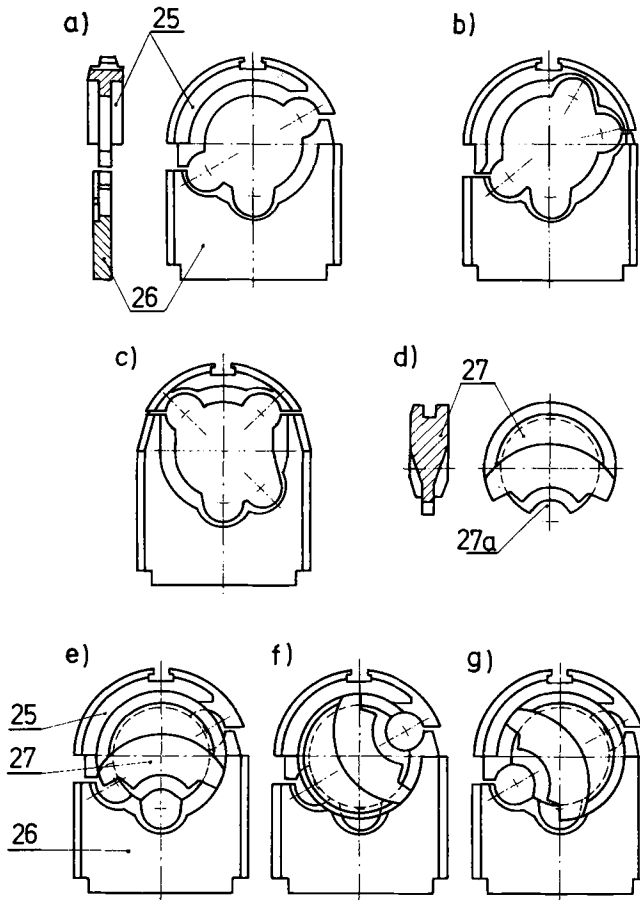


FIG. 6—Angle die insert set: (a) Top and bottom angle die insert designed for a six-throw crankshaft; (b) Top and bottom angle die insert designed for a seven-throw crankshaft; (c) Top and bottom angle die insert designed for an eight-throw crankshaft; (d) Web supporting plate; (e) Angle die inserts (shown in Fig. 6a), the web supporting plate placed as shown in Fig. 5a; (f) and (g) The angle die insert set shown in Fig. 6e (web supporting plate situated for fixing the proper angle of torsion between the finished crank throw and the just-forged crank throw).

When the lower die holder (6) abuts on the bumper, the forming of the crank web is complete, after which the press crosshead (17) with the device head (15) is raised to enable the hook clamps (20) to unlock and release the cover toolholder (16). Then, the upward moving of the press crosshead can be continued until the cover toolholder (16) rests on support (14b) protrusions (16b). At this moment, the cover toolholder has to be hung on the tie (17a), and the press crosshead (17) together with the device head (15) and cover toolholder (16) can be raised to its top position. The forged piece is taken out after moving the press table out of the press. After the forging operation for the first crank web, the clamping die inserts (not shown on the drawing) have to be removed.

During forging of the second crank web of the same crank throw, the crank pin is placed into the impression of the face die insert (24a) and the adjacent journal is placed in the impression of the angle die insert's bottom part (26a) (Fig. 6). Then the supporting plate (27) is set into the bottom part of the angle die insert (26) in such a way that the impression (27a) of the web supporting plate (27) rests on the main journal. Thus, the parallelism of both crank webs of the just-forged crank throw is ensured.

The angle between the completed crank throw and the next throw to be forged is fixed by a corresponding impression in the bottom or top part of the angle die insert. Thus, when forging the first crank web of the next crank throw, the adjacent crank pin is placed into the corresponding impression in the bottom or top part of the angle die insert. The supporting plate (27) is set onto the impression of the bottom part of the angle die insert (26) such that the impression (27a) will come in contact with the crank pin. Also, when forging the first crank web of the second or next crank throw, the journal supporting plate (28b) should be mounted (Fig. 5b).

Crank web forming operations are continued with further local heating to the forging temperature until the required number of throws has been produced for the crankshaft. The forging procedure is such that separate straightening operations are rarely required.

Advantages of the New Forging Method

During the working stroke of the device head (15), the horizontal force appears. It is equal to the friction force between device head (15) guides (18) and upper toolholder guides (14). This force is transmitted through the vertical guides (19a and 19b). It is anticipated that, using the device shown in Fig. 4 for a given press, crankshafts with about double the crank stroke can be forged compared to the crankshafts forged in the device according to the earlier design.

The horizontal upsetting force of the device shown in Fig. 4 is about double that of the original TR device. This force can be calculated in a simplified way according to the formula:

1. For the original TR device

$$P_{h1} = 0.5 (N_p - P_p) (\cot \alpha - \mu) \quad (3)$$

2. For the new device according to Fig. 4

$$P_{h2} = (N_p - P_p) (\cot \alpha - \mu) \quad (4)$$

where

N_p = capacity of the press,

P_p = joggling force,

α = connector inclination angle, and

μ = coefficient of friction which appears between sliding elements of the device.

The efficiency of the forging device calculated as P_h/N_p depends mainly on the value of the connector inclination angle assumed for the end of the forging operation.

Thanks to the technological and design features of the new forging equipment, the connector inclination angle by the end of the forging operation can be smaller than in the original TR device, that is, $P_{h2} > 2P_{h1}$.

Crankshaft forging devices applied up to now demand separate angle die inserts for nearly every crank throw of a given crankshaft. This inconvenience is eliminated by using a newly designed angle die insert which consists of the top part fastened to the cover tool holder and the bottom part placed in the longitudinal beam impressions and the web's supporting plate (27) (Fig. 6).

A newly invented angle die insert permits the forging of all crank throws of a given crankshaft using the same die inserts. Besides, the web supporting plate (27) can be used for the forging of crankshafts of the same type irrespective of the number of crank throws. It is worth noting that the new die insert design needs fewer tools, thus reducing the production costs.

A special small experimental forging device was built to investigate the forging process and the device itself. Figure 7 shows the model crankshaft forging made of steel. Grain flow of a single crank arm from Fig. 7 is shown in Fig. 8.

By the tensiometric measurements of forces during the experimental forging, the distribution of forces and stresses acting on some parts of the device and the tools were estimated for the experimental forging by means of actual tensiometric measurements made during the process.

In the case of long-stroke crankshafts, both the axial length of the main journals and the crank pins are close; this is a common feature for many crankshaft types.

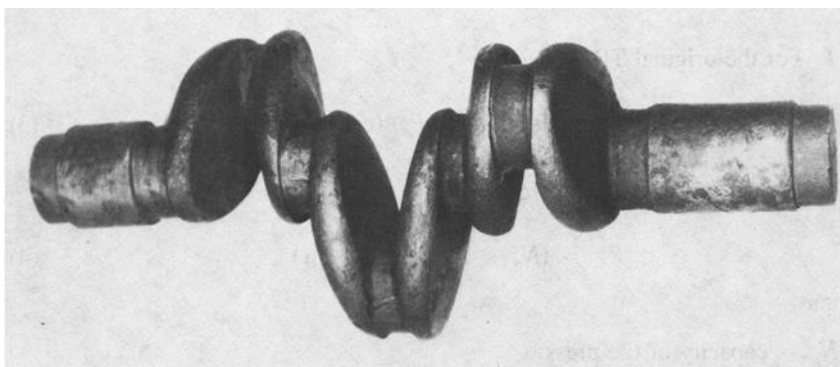


FIG. 7 --Model crankshaft made of steel. The journal diameter is 50 mm.

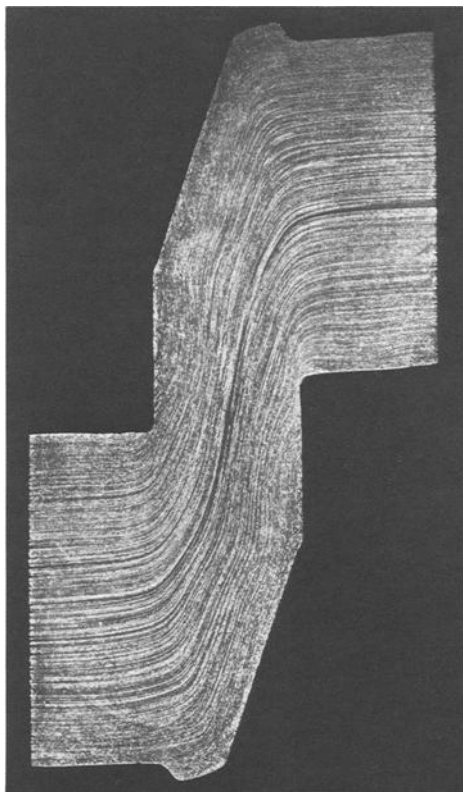


FIG. 8—Grain flow of the crank web of the model forging with 50-mm journal diameter.

Assuming, for forging only, the same length of journal and pin and also the symmetrical web shapes, the front die insert will be stronger against bending.

Some leading engine manufacturers already have decided to redesign the crank arm shape to obtain the optimum crank throw shape from the manufacturing point of view to take advantage of the new method. These requirements lead to an assurance of minimum crank throw weight both in manufacturing and design.

Assuming that a blank will be rough-machined before forging, the machining of forged throws could be limited only to the journal and pin surfaces and partially to the side surfaces of webs. Other web surfaces could be left as forged, thus holding machining costs to a minimum. The surfaces left in the as-forged condition should, however, be cleaned by grinding, as is done for cast throws or for fully forged, RLA56-type crankshafts.

From the technical point of view, the new forging method permits forging even the largest crankshafts as solid pieces using, for example, a 100-MN forging press. Limitations come rather from the weight of the forging device. It now seems to be reasonable that the new method could be used for fully forged

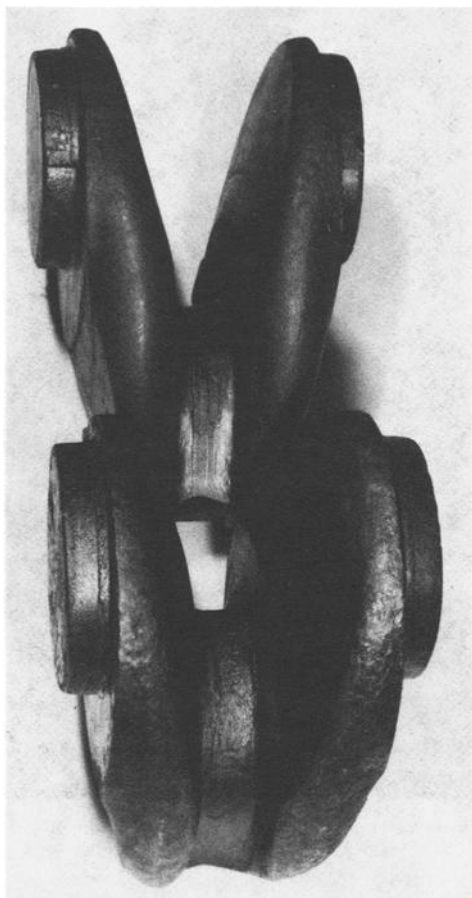


FIG. 9—Model forging of a single crank throw with half journals, made from lead and with a journal diameter of 50-mm.

crankshafts up to about a 2000-mm stroke. The same forging device (designed for fully forged crankshafts) could be used also for the forging of single crank throws with half journals (Fig. 9) for welded crankshafts such as the Type L-MC.

Determination of the Smallest Admissible Angle of the Connector Inclination α on Account of Strain Rate

During the crank web forming in the forging device (Fig. 4), the angle of connector inclination α diminishes. This angle reaches the smallest value at the end of the forming operation. When the angle α diminishes, the value of the ratio of the upsetting travel increment ds to the increment of the joggling radius dr (when $\alpha = 0$, the ratio $ds/dr = 0$) also decreases.

It results from Fig. 10a that for the adequately small increment of values ds and dr and the correspondingly large value of the radius R , it can be assumed that the arms of the angle α are, respectively, perpendicular to the arms of the angle β (dr and dp). On this basis, we can recognize the equality of angles $\alpha = \beta$. Therefore

$$\frac{ds}{dr} = \tan \beta = \tan \alpha \quad (5)$$

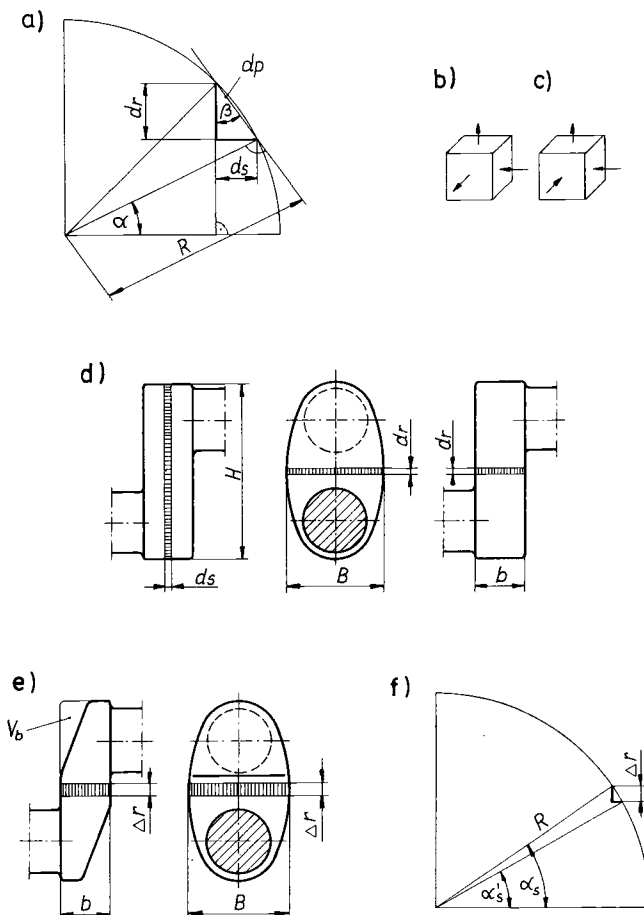


FIG. 10—Determination of the smallest admissible angle of the connector inclination α on account of the strain state, where: (a) is the polar diagram of the relation ds/dr to the angle of the connector inclination α ; (b) and (c) are the states of strain; (d) is volumes displacement during formation of the crank web as the effect of change of the values ds and dr ; (e) is volumes displaced during the crank web forming under the effect of the bevelling shaping; (f) is the polar diagram of the relation Δr to the connector angle inclination α .

When instantaneous values of ds/dr are too small, a change of the strain state in the just-formed crank web may occur. The fundamental state of strain (Fig. 10b), characteristic for the upsetting with the simultaneous joggling operation, can pass into the state of strain shown in Fig. 10c. It may take place at the moment when, as the angle of the connector inclination α diminishes, the width of the crank B, after reaching its maximum, will start to decrease. The limiting angle α is the angle at which the instantaneous upsetting does not influence the change of the crank width. With this assumption, we state the equation of the displaced volume (Fig. 10d)

$$V_s = V_r = ds \frac{\pi B H}{4} = dr \cdot B \cdot b \quad (6)$$

where from

$$\frac{ds}{dr} = \frac{4 B b}{\pi B H} = \frac{4b}{\pi H} \quad (7)$$

After substituting, according to Eq 5, we get

$$\tan \alpha_s = \frac{4b}{\pi H} \quad (8)$$

$$\alpha_s = \arctan \frac{4b}{\pi H} \quad (9)$$

The angle α_s is the minimum angle admissible on account of the desired state of strain.

For a crank web with symmetrical bevels, the bevel volume V_b (Fig. 10e) also influences the smallest admissible angle of connector inclination α_s on account of strain state. When forming the crank web, the material adjacent to the crank web bevels is displaced mainly to the middle part of the crank web.

Assuming the simplification that the whole Volume V_b is displaced to the middle part of the crank web, according to the superposition we can take into consideration the following relations (see Figs. 10e and 10f)

$$2 V_b = b B \Delta r \quad (10)$$

$$\Delta r = \frac{2V_b}{b \cdot B} \quad (11)$$

but also

$$\Delta r = R(\sin \alpha_s - \sin \alpha'_s) \quad (12)$$

where from

$$\alpha'_s = \arcsin \left[\sin \left(\arctan \frac{4b}{\pi H} \right) - \frac{2V_b}{bBR} \right] \quad (13)$$

The angle α'_s is the minimum admissible angle on account of the desired state of strain in the case when the crank web with symmetrical bevels is forged.

Based on the results from the just-mentioned testing and using experience gathered up to now with crankshaft forging processes and TR forging-device designs, the design of a device for the forging of long-stroke crankshafts is practicable. The engine producers, therefore, may choose now among semibuilt crankshafts assembled by shrinking, solid-type crankshafts assembled by welding and a solid-type crankshaft as fully forged. Research work toward further development of the described forging methods is ongoing at the Metal Forming Institute in Poznan.

References

- [1] Rut, T., "Multi-connector Equipment for Forging Crankshafts and Upsetting Bar Stock by the TR-Method," in *Annales of the International Institution for Production Engineering Research (CIRP)*, Pergamon Press, Elmsford, NY, 1968.
- [2] Rut, T., "Verfahren zum Schmieden von Kurbelwellen," *Ind. Anz.*, Nr 34, 1969.
- [3] "A New Forging Method for Crankshafts, Bars," *Machinery* (New York), Vol. 76, 1970, No. 6.
- [4] Rut, T., "Better Crankshafts from Two-Way Forging," *Engineer*, 1971, April.
- [5] Rut, T., "Anwendungsmöglichkeiten des TR-Schmiedeverfahrens," *Stahl u. Eisen*, 1977 Heft 4, 24. Feb.
- [6] Rut, T., "New Forging Process for Conventional Presses," *Machinery and Production Engineering*, 3 Nov. 1976.
- [7] Rut, T., "New Forging Method of Semi-Built-Up Crankshafts," The 8th International Forge-masters Meeting, Kyoto, Japan, Oct. 1977, Steel Castings and Forging Associates of Japan.
- [8] Rut, T., "Neues Verfahren für das Schmieden von Kurbelkröpfungen halbgebauter Kurbelwellen," *Industrie—Maschinen Report International*, 5A/1979, Wien.
- [9] Rut, T., "New Forging Process for Conventional Presses," *Equipment and Technology International*, Vol. 3, No. 1, 1979.
- [10] Rut, T., "New Forging Processes For Conventional Presses. The TR-Method," The 10th International Drop Forging Convention, London, June, 1980, National Association of Drop Forgers and Stampers.
- [11] Rut, T., "Neues Verfahren für das Schmieden von Kurbelkröpfungen halbgebauter Kurbelwellen," *VDI-Z*, Hef 7/1980.
- [12] Tomlinson, A. and Stringer, I. D., "The Closing of Internal Cavities in Forgings by Upsetting," *Journal of the Iron and Steel Institute*, March 1958.
- [13] Tateno, M. and Shikano, S., "Study on Closing of Internal Cavities in Heavy Forgings by Not Free Forging," International Forging Conference, Paris, May 1963, Chambre Syndicate de la Grosse Forge, Francaise.

General Industrial Forgings

Manufacture and Application

Cryogenic Mechanical Properties of A286 Alloy and 304LN Stainless Steel Used in Fabrication of Support Struts for Superconducting Magnets

REFERENCE: Abe, T., Kohno, M., Suzuki, A., and Scanlan, R. M., "Cryogenic Mechanical Properties of A286 Alloy and 304LN Stainless Steel Used in Fabrication of Support Struts for Superconducting Magnets," *Steel Forgings, ASTM STP 903*, E. G. Nisbett and A. S. Melilli, Eds., American Society for Testing and Materials, Philadelphia, 1986, pp. 523–539.

ABSTRACT: A286 alloy and 304LN stainless steel were chosen for support struts used in the construction of a mirror fusion testing facility, which is subjected to the cryogenic temperature. Electroslag remelting technology (ESR) was adopted to manufacture A286 alloy. A program was initiated to investigate the cryogenic mechanical properties with emphasis on the effect of the grain size of A286 alloy.

The test results revealed that: (1) A286 alloy showed little effect of grain size on the tensile properties, while the fracture toughness properties were affected by the grain size, especially at 4 K; (2) 304LN stainless steel produced almost the same tensile and fracture toughness properties as A286 alloy.

The temperature dependence of the mechanical properties of 304LN stainless steel and A286 alloy also is discussed. The support strut forgings produced excellent quality, and the proof load test results were indicative of the no plastic deformation during applications.

KEY WORDS: A286 alloy, 304LN stainless steel, electroslag remelting (ESR), cryogenic mechanical property, J_{IC} , grain size, proof load test.

The support struts are used to fix the magnet array to the vacuum vessel in the construction of a tandem mirror fusion testing facility (MFTF-B) in Lawrence Livermore National Laboratory (LLNL). Since the superconducting magnets are cooled to the cryogenic temperature, high tensile and toughness properties with nonmagnetic characteristics are required for the materials in this environment. The selected materials for the support struts are 304LN austenitic stainless steel and the iron base superalloy A286.

¹ Manager, Material Engineering, Forging Dept., Kobe Steel, Ltd., Takasago, Japan.

² Senior metallurgist, Takasago Plant, Kobe Steel, Ltd., Takasago, Japan.

³ Acting general manager, Steel Casting and Forging Div., Kobe Steel, Ltd., Wakihamu, Japan.

⁴ Metallurgist, Lawrence Livermore Laboratory, Livermore, CA 94550.

The manufacturing work on the support struts included all steps, from selection of raw materials to final machining, including tests and inspections. The required tests and inspections are mechanical property tests at both room temperature and cryogenic temperature, ultrasonic and liquid penetrant examinations, and proof load tests after final assembly.

At present, few cryogenic mechanical property data for A286 alloy have been reported [1,2]. Furthermore, the electroslag remelting process (ESR) utilized in this work is an alternative for the vacuum arc remelting (VAR) in manufacturing A286 alloys and provides advantages in forgeability and in electrode-to-forging yield. This paper describes the manufacturing experience and the quality test results of the support struts for MFTF-B. The cryogenic tensile and toughness properties of A286 alloy made by the ESR and 304LN stainless steel are reported in this paper. A286 alloy is discussed in terms of the relationship between grain size and the mechanical properties.

Support Struts

Figure 1 shows the magnet support system [3]. The total number of main coils is 26. In addition to these main coils, there are 16 trim coils. The total magnet system weighs about 1 500 000 kg (1500 tonnes) and is mechanically grouped into five independent systems to minimize both the axial loads on the vessel and the heat leaks from the vessel to the magnet. The yin-yang coils (M1 and M2) are the heaviest coils of the entire system and are supported by three support struts (SS) as shown in Fig. 1.

The middle eight solenoids are paired in four modules, each of which is supported by two support struts. Other main coils have two support struts, also. The trim coils are supported by their adjacent transition coils.

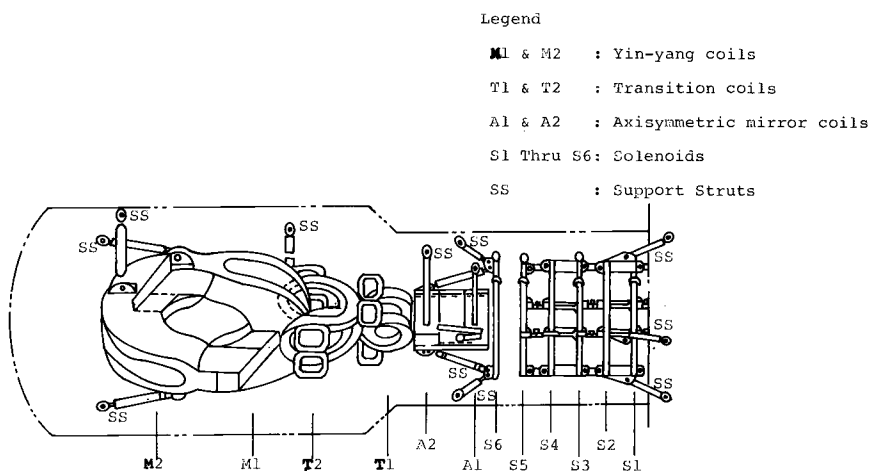


FIG. 1—Magnet support system of MFTF-B.

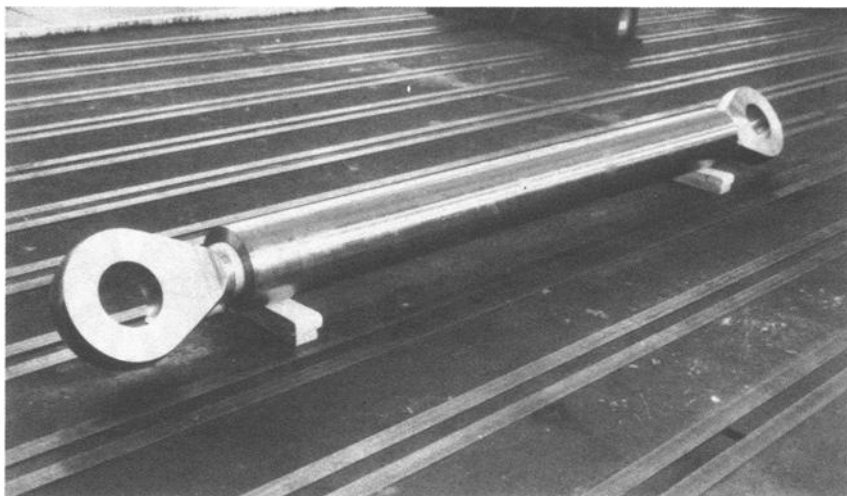


FIG. 2—Support strut.

Figure 2 shows a support strut. The strut consists of a turnbuckle tube made by 304LN steel and rod ends made by A286 alloy. The rod ends have spherical bearings at the center and are threaded at both ends for attaching to the turnbuckle tubes. These support struts vary from 1110 to 4940 mm in length and from 75 to 265 mm in tube diameter. In addition to these support struts, the support system requires the links and the pins to be made from 304LN steel and A286 alloy, respectively.

Preliminary Investigation

The required mechanical properties for the support struts are listed in Table 1. Since only limited data were available, preliminary tests were conducted on ESR'd A286 alloy with emphasis on the effect of the grain size.

A 2000 kg (2-ton) ESR ingot 480 mm in diameter was manufactured and forged into a 840-mm-diameter and 220-mm-thick disk. In the ESR of A286 alloys containing active titanium and aluminum, it is important to develop the optimum slag composition and melting conditions. The development of the ESR technology of A286 alloy is reported elsewhere [4]. The ESR material has higher ductility than the VAR materials; in addition, the ESR ingot surface is smooth and sound enough to eliminate surface conditioning prior to forging operations. Consequently, ESR materials produce superior forgeability compared with VAR materials [5].

A coupon was removed from the edge of the disk to conduct the following tests.

TABLE 1—Mechanical property requirements (minimum values).

Orientation ¹	Tensile Properties				Fracture Toughness, K _{Ic} , MPa√m
	Tensile Strength, MPa	0.2% Yield Strength, MPa	Elongation, %	Reduction of Area, %	
Room temperature property, L & T	1000	621	12	15	...
Cryogenic property (4 K), L & T	1310	862	12	15	99
			A286		
			304LN		
Room temperature property, L	586	241	30	40	...
Cryogenic property, L	1380	690	16	20	132

¹ L = parallel to principal working direction; T = transverse to principal working direction.

Samples

Three samples having different ASTM grain size numbers, 1.5, 3.0, and 6.0, were tested. Samples were prepared by controlling the final forging conditions, that is, Grain Size Numbers 1.5, 3.0, and 6.0 samples received a forging reduction of 10% at 1150°C, 10% at 1100°C, and 50% at 1100°C, respectively.

The heat treatment applied for the samples was oil quenching from 980°C and hardening treatment at 720°C for 16 h. Tables 2 and 3 summarize the history of the samples. The tension and Charpy impact specimens were removed in parallel to the principal working direction. The notch of Charpy impact specimens was perpendicular to the surface. The J_{Ic} specimens were oriented in the L-T⁵ per ASTM Method for Plane-Strain Fracture Toughness of Metallic Materials (E 399-81). The size of Charpy impact specimens was per ASTM Methods and Definitions for Mechanical Testing of Steel Products (A 370-77), Fig. 11, Type A.

Test Equipment and Procedure

The tension and fracture toughness tests at 4 K were performed in a Kobe-developed, multiple-specimen-type testing apparatus [6]. The apparatus permits ten tension specimens (Fig. 6, Specimen 1 per ASTM Method A370-77) or five J_{Ic} specimens [1 compact tension (CT) type per ASTM Method for J_{Ic} , a Measure of Fracture Toughness (E 813-81)] on a turret disk to be cooled simultaneously in the cryostat, and mechanical tests to be performed in sequence without the need to warm the cryostat to ambient temperature.

J -integral test techniques were used to obtain useful fracture toughness data per ASTM E 813-81, as valid K_{Ic} data could not be obtained by the criteria of ASTM E 399-74 unless specimens of quite large thickness were employed, which will be not representative of the cross-sectional thickness found in actual cryogenic structures. Single specimen compliance unloading techniques were employed after confirming the compatibility with the multiple specimen technique. Charpy impact tests at 4 K were conducted using a cooling capsule set on the Charpy impact test machine, in which the specimen was cooled and held for 1 min at 4 K by liquid helium [7].

Results

The tensile properties versus the grain size are presented in Fig. 3. The tensile strength increased with increase of the grain size number, but the yield strength decreased slightly. The dependence of the yield strength on the grain size is quite small, and the behavior observed is attributed to factors other than grain size. The precipitation conditions might be different among the specimens. The elongation and reduction of area values appeared to be proportional to the grain size number.

⁵ L = parallel to the principal working direction; T = transverse to the principal working direction.

TABLE 2—*Preliminary investigation. Chemical composition of tested materials (weight %), A286 alloy.*

C	Si	Mn	P	S	Ni	Cr	Mo	V	Ti	Al	B
0.046	0.40	1.20	0.012	0.001	25.20	15.15	1.30	0.27	2.30	0.27	0.0082

TABLE 3—*Preliminary investigation. History of A286 alloy samples.*

Ingot	Total Reduction from Ingot	Final Forging Conditions		Heat Treatment	ASTM Grain Size No.
		Heating, °C	Reduction, %		
2000-kg (2-ton) ESR	11: 1	1150	10	980°C × 1h, OQ, +720°C × 16h, AC	1.5
		1100	10		3.0
		1100	50		6.0

NOTE: OQ = oil quench; AC = air cool.

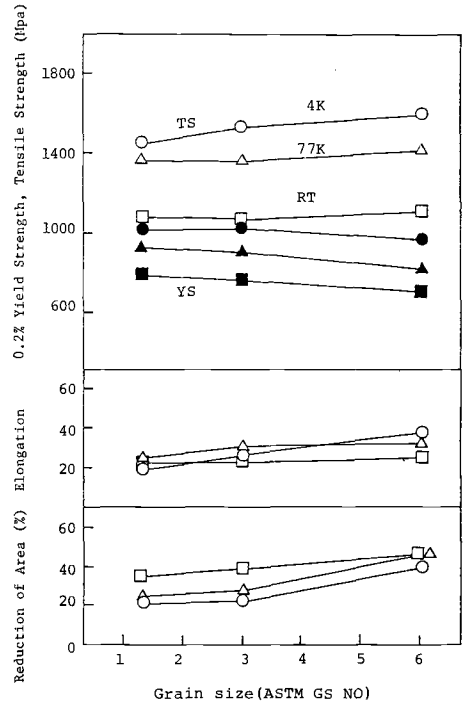


FIG. 3—Effect of grain size on tensile properties of A286 alloy at 4, 77, and 293 K.

Figure 4 shows the Charpy impact test results. The grain size effect is indicated by the decrease in the Charpy impact value with decrease in the grain size number. This behavior was confirmed at three different test temperatures of 4, 77, and 293 K. The impact values were not influenced by the test temperature. $K_{Ic}(J)$ -values are presented in Fig. 5. K_{Ic} -values are converted from the J_{Ic} test results per ASTM E 813-81, that is, $K_{Ic}^2 = J_{Ic}E$, where E = Young's modulus. $K_{Ic}(J)$

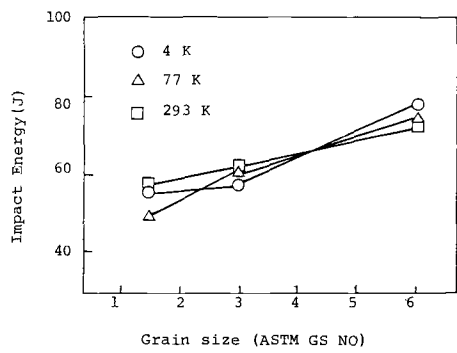


FIG. 4—Effect of grain size on Charpy impact energy at 4, 77, and 293 K.

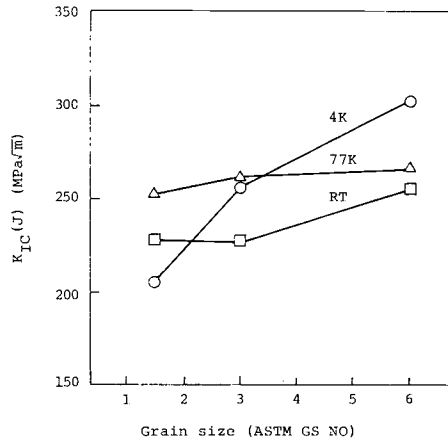


FIG. 5—Effect of grain size on fracture toughness K_{IC} (J) of A286 alloy at 4, 77, and 293 K.

decreased with decrease in the grain size number at every temperature. The 4 K test results produced the largest decrease. For further investigation of the behavior observed in the 4 K test, microstructural characterization and fracture mode analysis were carried out. Fractured surfaces of 4 K specimens were checked by scanning electron microscope (SEM). The dimple pattern is observed on every specimen. The fracture in the finest grain specimen (Grain Size No. 6) was predominantly transgranular, while the other specimens exhibited the mixed mode of intergranular and transgranular. Grain boundary carbide was observed in all specimens, but in the specimen having a grain size number of 1.5 there were large-chained carbide in some local areas. From these results, the significant decrease in K_{IC} (J)-value was attributed to both the large grain size and the chained carbide precipitation at the grain boundary during specimen preparation.

The ESR A286 alloy in the present study showed excellent tensile and fracture toughness properties, meeting the specification requirements as shown in Table 1 even at a grain size of 1.5.

Manufacturing of the Support Struts

Figure 6 illustrates the manufacturing process for the support strut.

A286 Alloy Forging

ESR ingots 8000-kg (8-ton)-type (diameter 725 mm) were utilized as materials for the rod ends. A286 alloys exhibit no grain-refining effect due to the heat treatment; hence, the forging condition governs the grain size. The target grain size of the A286 support strut parts was a grain size number of 3 or finer for the superior mechanical properties and for good ultrasonic sound propagation, though the preliminary test results showed that a grain size of 1.5 or finer was sufficient

A 286 Rod End

304 LN Turnbuckle Tube

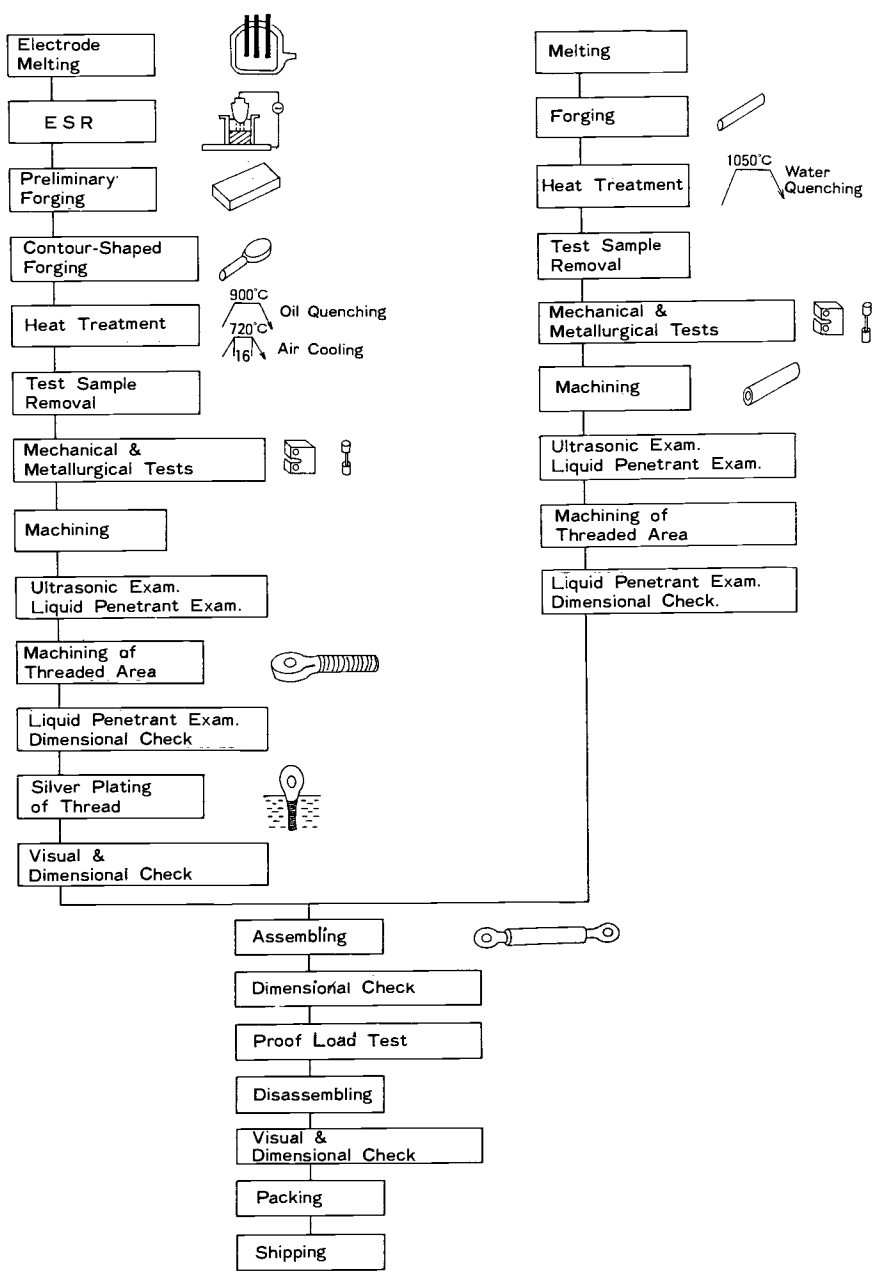


FIG. 6—Manufacturing procedure of support struts.

to meet the specification requirements. To obtain this fine grain structure, the heating temperature was limited to the 1050°C max, and the forging operation was conducted within a temperature range of 1050 to 900°C [8]. The rods ends were first forged into a plate and then contour-forged as close as practicable to the final shapes. A minimum forging reduction of 3 or more was obtained through the forging operations. The heat treatment consisted of oil quenching at 900°C followed by the hardening treatment at 720°C for 16 h.

304LN Steel Forgings

A vacuum oxygen decarburization process was applied to Grade 304LN forgings, ASTM Specification for Steel Forgings, Alloy, for Pressure and High-Temperature Parts (A 336-83). The turnbuckle tubes were forged into a bar shape with a temperature limit of 1050°C max to obtain fine structure and then center-bored by machining. The heat treatment applied was a solution annealing at 1050°C with water quenching.

Quality Test Results

Chemical Composition and Metallurgical Properties—Table 4 shows the chemical composition of the A286 forgings. The check analysis results on the ESR ingots are indicated in the average of the several ingots made from one parent heat. All heats surpassed the chemical composition requirements of ASTM Specification for Precipitation Hardening Iron Base Superalloys Bars, Forgings, and Forging Stock for High-Temperature Service (A 638-82), Grade 660. The inclusion contents of the forgings were measured per ASTM Practice for Determining the Inclusion Content of Steel (E 45-81), Method D. Inclusions observed were predominantly globular, and cleanliness was quite good. The occasional Type A and D inclusions were found.

The forgings were free from Type B and C inclusions. The actual grain size was measured on the eleven A286 forgings. The results varied from 4.0 to 6.0, and most parts were Grain Size Number 5.5.

The chemical composition of the 304LN forgings surpassed the ASTM requirements. The inclusion rating results of 304LN steels revealed that all forgings were free from Type A, B, and C inclusions.

The occasional Type D inclusions were found, and the worst inclusions were rated 1½. The actual grain size also was observed, and the largest grain sizes were 3.0 at the center and 3.5 at a quarter thickness on the round bar shape after the heat treatment.

Mechanical Properties—In Figs. 7 and 8, tension and fracture toughness test results of A286 forgings are graphically indicated along with the data points obtained from the tests on the effect of grain size. The test results for 304LN forgings also are shown in Figs. 7 and 8. As no tests were conducted on the actual forgings at 77 K, only the laboratory test data were plotted. The tensile and yield strengths increased with decrease in the test temperature for both

TABLE 4—Chemical composition of A286 rod ends.

	C	Si	Mn	P	S	Cr	Ni	Mo	Ti	Al	V	B
Min	13.50	24.00	1.00	1.90	...	0.10	0.003
Max	0.08	1.00	2.00	0.025	0.025	16.00	27.00	1.50	2.35	0.35	0.50	0.010
ASTM A 638, Grade 660												
Heat A	0.05	0.57	1.23	0.012	0.001	14.83	25.22	1.30	2.27	0.29	0.31	0.004
Heat B	0.05	0.59	1.20	0.013	0.001	14.94	25.10	1.33	2.30	0.26	0.31	0.004
Heat C	0.04	0.44	1.16	0.017	0.001	15.13	25.22	1.33	2.32	0.26	0.30	0.004

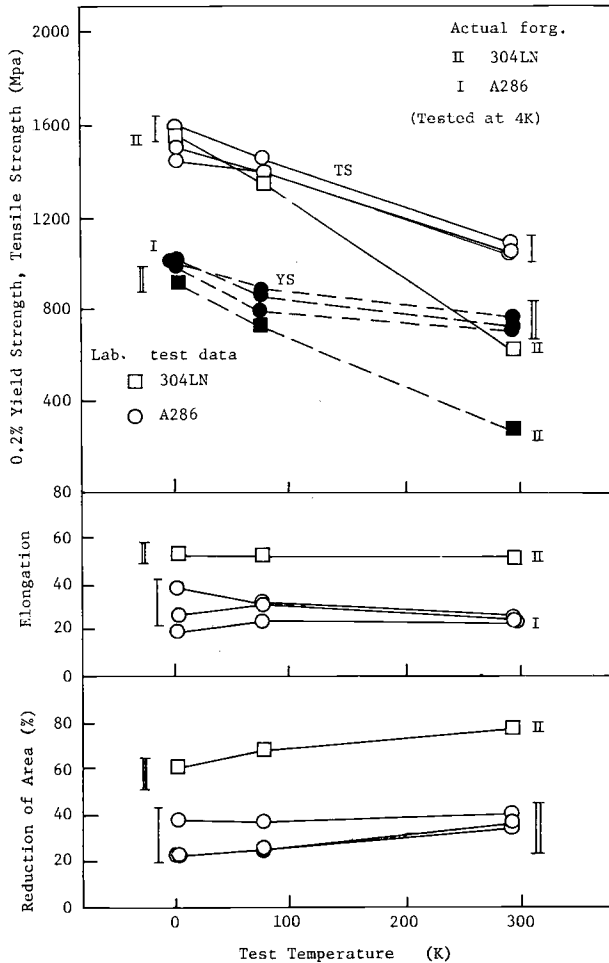


FIG. 7 Tensile properties of 304LN steel and A286 alloy.

forgings. The 304LN forgings experienced the larger increment in the strength at reduced temperatures compared with the A286 forgings. This type of behavior is attributed to the stability of the austenitic structure. A286 alloy contains sufficient nickel to stabilize the austenitic phase at cryogenic temperatures, where 304LN steel is not sufficiently stable with respect to martensitic transformation. 304LN forgings provided almost the same strength levels as A286 forgings at 4 and 77 K. Elongation values remained nearly constant from 4 to 293 K for both forgings. Reduction of area decreased slightly with decrease in temperature, and the 304LN forgings exceeded the A286 forgings at the whole temperature range.

The effect of the specimen orientation on the fracture toughness property of A286 forgings was noted. The laboratory test data for the A286 alloy indicated

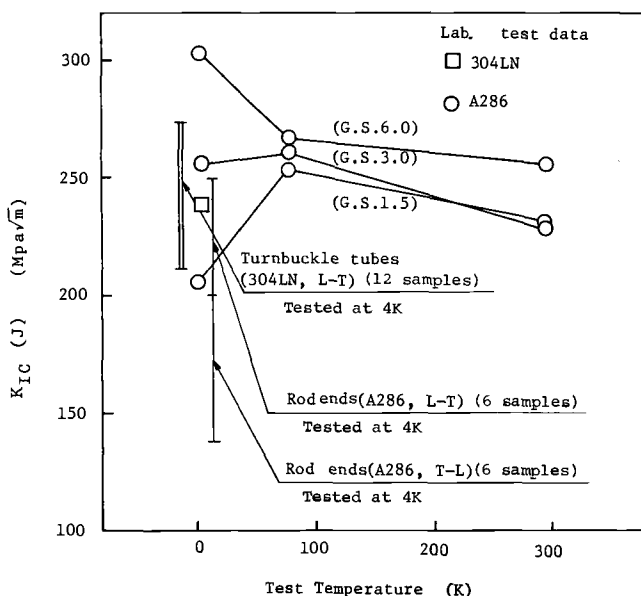


FIG. 8—Fracture toughness $K_{IC}(J)$ of 304LN steel and A286 alloy.

the different temperature dependencies of the fracture toughness properties on the grain size effect. $K_{IC}(J)$ of Grain Size Numbers 1.5 and 3.0 increased slightly at 77 K from 293 K then, decreased at 4 K, while $K_{IC}(J)$ of Grain Size Number 6.0 increased with decrease in temperature. This fact is attributed to the difference in the carbide precipitation mentioned previously. Valid J_{IC} data of the 304LN forgings were not obtained at 77 and 293 K because of their quite high fracture toughness properties.

In Fig. 9, the $K_{IC}(J)$ values at 4 K are shown as a function of the yield strength at the same environment. Data for the austenitic 304-type stainless steels are referenced in the figure by a hatched band [9]. The present results for 304LN forgings are located at the upper side of the band. A286 forging data scattered with their center at the midpoint of the band. The 304LN forgings showed nearly the same cryogenic mechanical properties as A286 forgings, and, however, the strengths decreased significantly at room temperature.

Therefore, the room temperature design stress may govern the material selection for cryogenic components.

As expected, both A286 and 304LN forgings showed excellent quality and surpassed the specification requirements. The actual product data are compatible with the laboratory test results.

Nondestructive Examination

All forgings were subjected to ultrasonic examination (UT) and liquid penetrant examination (PT). UT was performed using a 4-MHz straight beam probe and

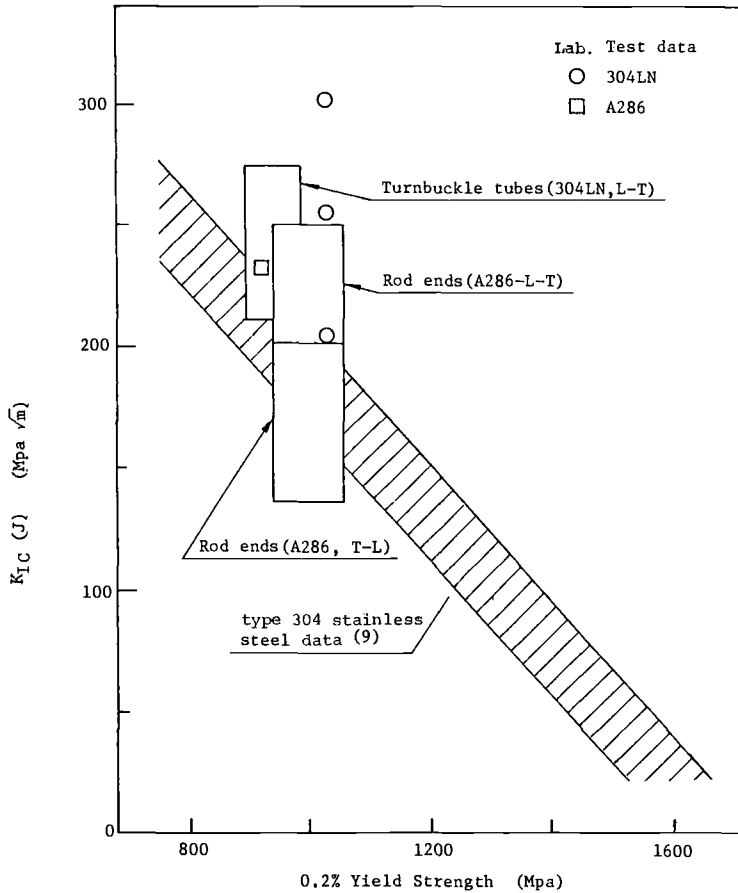


FIG. 9—Fracture toughness versus yield strength for 304LN steel and A286 alloy.

a 4-MHz twin-crystal straight beam probe with an acceptance standard not to exceed the amplitude distance correction curve from the 2-mm flat-bottomed holes. The angle beam UT also was carried out on the turnbuckle tubes. All forgings produced quite good penetrability and were completely free from indications over the 1-mm flat-bottom hole size. The acceptance standard of the PT was settled at 1.6 mm, and no unacceptable indications were found in any forgings.

Proof Load Tests

All support struts were subjected to the proof load tests. The tensile and compression loads were applied per the applicable loading conditions of the support struts in the system. The peak stress during testing coincided with 1/1.5 of the specification yield strength. Strain gages were attached at both ends of

the turnbuckle tubes to obtain a stress-strain curve. A chart showing the load versus total displacement between the pins also was monitored. A 1 000 000 (1000-ton) and a 600 000 (600-ton) machine also were used where the strut size and required load would allow. The results showed the complete elastic deformation mode, and no permanent strain remained.

Conclusions

The A286 forgings made by the ESR process and the 304LN forgings produced excellent quality and surpassed all specification requirements at both room temperature and cryogenic temperature for the support struts.

1. The effect of grain size on the tensile properties of the A286 forgings was small within the temperature range from 293 down to 4 K, while the fracture toughness decreased with the coarseness of the grains, especially at 4 K.

2. The A286 and 304LN forgings produced almost the same strengths at the cryogenic temperature. Both materials increased the tensile and the yield strengths with decrease in temperature.

3. The Charpy impact property of the A286 forgings remained constant over the temperature range from 293 down to 4 K, while the 304LN forgings showed an apparent decrease with a temperature decrease.

4. The A286 forgings showed a substantial temperature dependence of the fracture toughness. No valid fracture toughness data of the 304LN forgings were obtained at 77 and 293 K due to its quite high toughness. Both forgings produced almost the same fracture toughness at 4 K.

Acknowledgement

The authors gratefully acknowledge T. Horiuchi, R. Ogawa, and M. Shimada of the Asada Research Laboratory, Kobe Steel, Ltd. for their advice, contributions, and cooperation in the conduct of this work. Special acknowledgement is extended to the Lawrence Livermore National Laboratory for their permission to publish this work.

References

- [1] Dalder, E. N. C. et al., in *Advances in Cryogenic Engineering-Materials*, Vol. 28, 1982, p. 883.
- [2] Read, R. P. et al., in *Advances in Cryogenic Engineering*, Vol. 22, 1977, pp. 68–79.
- [3] Wang, S. T. et al., "Progress on Axicell MFTF-B Superconducting Magnet Systems," IEEE 10th Symposium on Fusion Engineering, Philadelphia, PA, 5–9 Dec. 1983, Institute of Electrical and Electronics Engineers.
- [4] Okamura, M. et al., in *Proceedings*, Seventh International Conference on Vacuum Metallurgy, Tokyo, Japan, Nov. 1982, p. 1511.
- [5] Kohno, M. et al., in *Proceedings*, International Gas Turbine Congress, Tokyo, Japan, 23–29 Oct. 1983, pp. 773–778.
- [6] Horiuchi, T. et al., in *Proceedings*, Fifth International Cryogenic Engineering Conference, 1974, pp. 465–468.

- [7] Ogata, T. et al., *Journal of the Iron and Steel Institute of Japan*, Vol. 69, 1983, No. 6, p. 135.
- [8] Kohno, M. et al., "Heavy Disk of Heat Resistant Alloy for Gas Turbine," International Forging Conference, Dusseldorf, 4-9 May, 1981, pp. 4.1, 1-22.
- [9] Reed, D. T. et al., "Materials Studies for Magnetic Fusion Energy Applications at Low Temperatures-III," NBSIR 80-1627, National Bureau of Standards, Boulder, Colorado, 1980, p. 17.

DISCUSSION

*W. Childs*¹ (*written discussion*)—(1) Were the microstructures shown (SEM) in the etched or unetched condition? (2) Was there a continuous grain boundary phase present in the material with a grain size of 6? (3) Did you say there was a film present in the Grain Size 6 material and that it was not titanium carbide?

T. Abe, M. Kohno, A. Suzuki, and R. M. Scanlan (authors' closure)—(1) Etched by nitrohydrochloric acid. (2) No, there was not. (3) There was no film present in the Grade Size 6 material, but there were chains present in the Grade Sizes 1.5 and 3.0 material. The chains seem to be titanium carbide.

¹ Turbodyne Division, Dresser Industries, Inc., Wellsville, NY 14895.

Steel Forgings for a Tension Leg Platform Anchoring System—The Design and Management Contractor's Experience of Their Manufacture and Testing

REFERENCE: Whitehouse, P. J., "Steel Forgings for a Tension Leg Platform Anchoring System—The Design and Management Contractor's Experience of Their Manufacture and Testing," *Steel Forgings, ASTM STP 903*, E. G. Nisbett and A. S. McIlilli, Eds., American Society for Testing and Materials, Philadelphia, 1986, pp. 540–549.

ABSTRACT: The specification and manufacture of a number of special forgings against severe schedule constraints for a novel offshore application provided an interesting experience of coordination between forging works, machine shops, and a design and management contractor. The two major types of HY80 forgings and their significant design and service features are described. The background to the material and manufacturing route selection procedure is outlined. The findings of investigative work to determine the influence of post heat treatment cooling rates on the toughness of the material are briefly presented. Procedural aspects of the fabrication processes used to complete the components are included. Comparative data on the surface and midsection toughness of other thick-walled HY80 forgings at different testing temperatures are presented.

KEY WORDS: industrial forgings, low-alloy steel, residual stresses, embrittlement, fabrication

The tension leg platform (TLP) is a new type of oil production platform in which a floating structure is moored by vertical tension legs to foundation structures on the seabed. Excess buoyancy keeps the legs in tension at all times.

The world's first TLP was installed in the North Sea Hutton field in July 1984. Vickers Design and Projects was awarded the contract for the design and supply of mooring system components, including the anchor connectors and associated test rigs. In total, 21 sets of hardware were manufactured, a prototype and 20 production sets including 4 spares. Each leg of the 16 installed is designed to cope with a maximum load of 30.4 MN.

¹ Project manager, Design and Projects Division, Brown & Root, Ltd., Hampshire, England.

All mooring system components were designed to offer a 20-year service life without intermediate maintenance. Material choices were to be justified by existing environmental performance data. Where necessary this was to be supplemented by test programs to obtain final design approval.

The anchor connector provides the means by which the tension leg assembly is connected to the seabed foundation. It is capable of remote insertion and locking under its own weight and is released hydraulically to permit retrieval of the tension leg assembly. The two major components of the anchor connector are:

1. The anchor body, which forms the main structural component of the anchor assembly. It is also the hydraulic cylinder within which a ram is pushed downwards during unlatching.
2. The spring collet, which is external to and surrounds the anchor body. During latching it moves up a flange until the collet fingers lock over the flange. The anchor is raised until the fingers contact a conical load reaction ring in the foundation structure.

A view of the anchor connector is shown in Fig. 1.

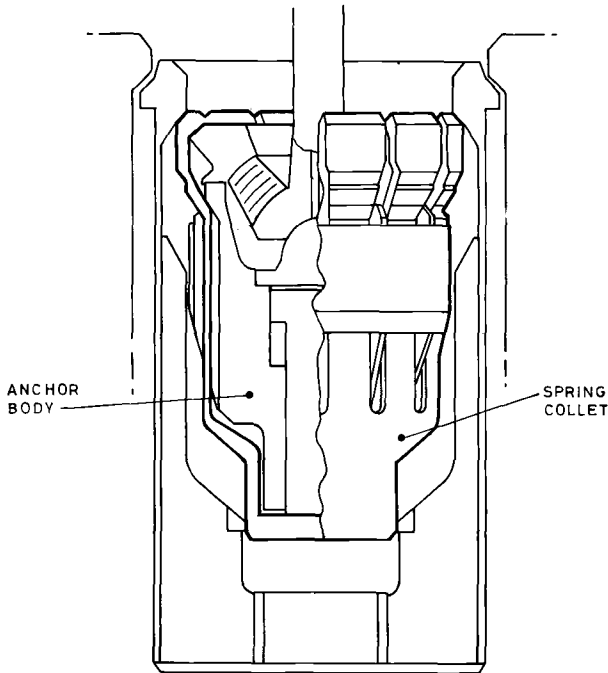


FIG. 1—Anchor connector.

Design Methodology

Hand calculations and standard stress concentration formulae initially gave extreme stresses in the components under various service conditions. At this time the urgency was to fix a minimum material strength level and an outline shape from which the finish-machined profile, when determined, could be obtained.

With the prototype and later the initial production components in manufacture, finite-element analysis and photoelastic modelling were utilized to determine the final machining profile for the prototype part. This was released on the basis of predicted compliance with design safety factors and fatigue damage accumulation limits.

Proof testing of the assembled prototype in a large purpose-built test rig provided strain gage information to corroborate the analytical data. In practice there was a high degree of agreement between theoretical and practical work. Component design justification reports were then produced; these reports integrated in-service stresses, the environmental performance characteristics of the material, material mechanical properties, and also nondestructive examination levels (maximum initial defect sizes) to show that overall design requirements had been satisfied. At this point final design approval could be obtained for completion of production component machining and fabrication activities. The logic of this design sequence is depicted in Fig. 2.

Spring Collet

This is a hollow cylindrical component which is cut axially along part of its length to form twelve fingers.

Material Selection

Initial analysis showed that a material yield strength of approximately 550 MPa was necessary. In-service stresses would be low, but the critical loading case was associated with finger deflections during anchor actuation. Consideration of candidate quenched and tempered steels led to the selection of a material grade

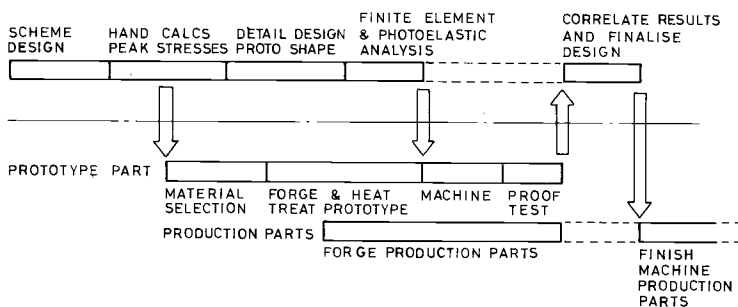


FIG. 2—Design process.

TABLE 1—Basic details of component forging specification, chemical composition, weight %.

	C	Mn	P	S	Si	Ni	Cr	Mo	V	Cu	Ti	Al
Minimum	...	0.10	0.20	2.50	1.40	0.45
Maximum	0.18	0.40	0.02	0.008	0.35	3.50	1.80	0.60	0.03	0.20	0.02	0.05

NOTE: Proof stress, 0.2%: 550 to 650 MPa. Charpy V-notch energy (at -40°C): 50 J minimum average per set; 45 J minimum individual.

based on Military Specification: Steel Forgings, Alloy, High Yield Strength [MIL-S-23009A (SHIPS) HY80 and HY100]. The exact specification reflected the heavy sections of the component during heat treatment. Table 1 gives details.

Manufacturing Method

Fabrication, casting, and forging were potential manufacturing methods. It was important to minimize changes from prototype to production components. Fabrication from subcomponents was precluded by schedule considerations. Casting potentially offered some commercial advantages. The choice of castings when integrity requirements might change as a result of design finalization, and when there is no time for extensive weld repair qualification and completion, was not attractive. Forging was the selected manufacturing process.

Forging Route

Discussion with various manufacturers led to consideration of three potential forging routes at comparable costs:

1. Solid forging.
2. Reverse extrusion in a shaped die.
3. Mandrel forging with one end closed in.

Reverse extrusion was a feasible solution and was judged to be comparable technically to the hollow forging option. However, the time scale for production of the extrusion dies was too great for manufacture of the prototype by this method. This would have invalidated the correlation of test data and general manufacturing experience between prototype and production items. The additional time to rough machine solid forgings prior to heat treatment presented a schedule problem.

Mandrel forging was selected. A ladle refined and degassed primary melted ingot was cogged and upset prior to hollow punching. It was drawn down and expanded to full diameter prior to closing in one end. See Fig. 3.

Heat Treatment

The major concern with this component related to the final machining operation, when the individual fingers are formed by a slotting operation. With actual

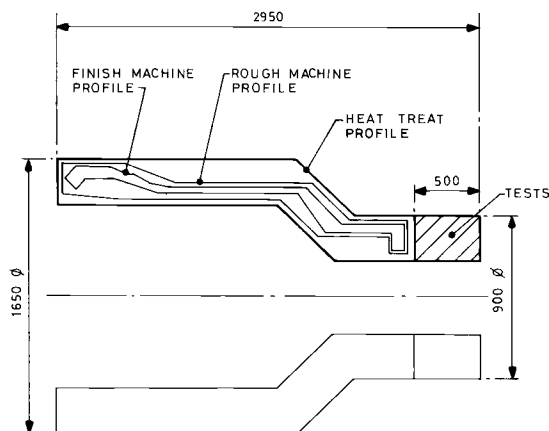


FIG. 3—Spring collet forging details.

finger positions limited to within 3 mm radially of their nominal position, unwanted displacements caused by residual stresses were a potential problem. This could have resulted in machining difficulties and required a “setting” operation on individual fingers to overcome the distortions. From a dimensional standpoint, low cooling rates from the tempering treatment were desirable. Against this there was the possibility of loss of toughness due to intergranular embrittlement.

Furnace cooling at a rate of approximately 20°C/h was used for the prototype. Mechanical testing showed some impact energies to be marginal against specification requirements. This led to an investigation of impact energy and fracture appearance transition temperature against cooling rate. This was to be used as a basis for modifying the treatment cycle for early production components, by then progressing through manufacture. These tests were conducted on surplus material from the prototype forging prolongation. Results are shown in Fig. 4. Measurements on the prototype spring collet showed a maximum movement of any single finger tip from its nominal position of 0.8 mm.

At this stage the second and third forgings had been processed at cooling rates up to 32°C/h. A review with the forging supplier of the impact results and further machining results led to selection of a 40°C/h furnace cooling rate. At this level, finger movements and forging properties were acceptable for the remainder of the program.

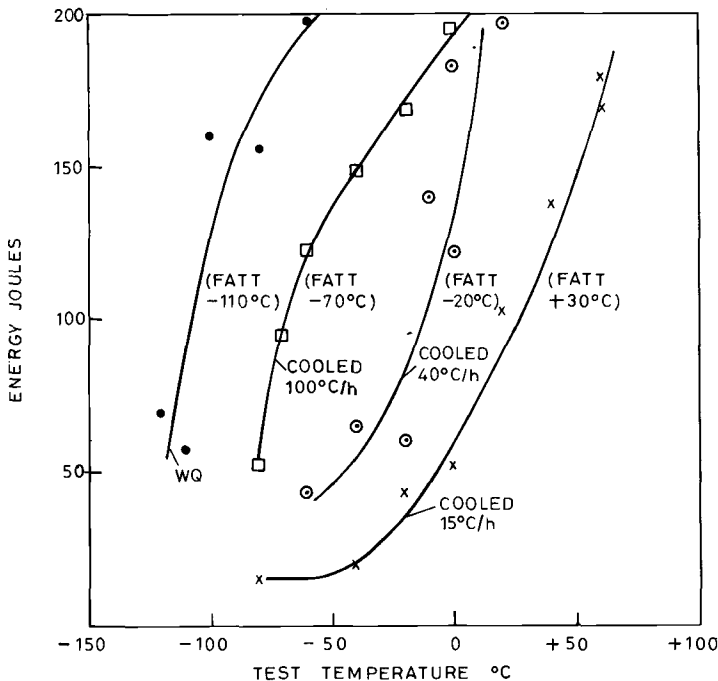
Mechanical Testing

The spring collet heat treatment profile had a wall thickness of 230 mm. The most highly loaded region has a finished thickness of 40 mm. Specimens for production items had to be located for economic reasons in a small diameter prolongation; the specimens were located at mid-wall positions which would, in places of the finished part, be the surface of the collet. This is a variation from

the practice of MIL-S-23009A (SHIPS) where impact tests are near the surface of the heat treatment profile. There was no exactly applicable toughness data available to us or the manufacturer prior to commencing the program. The testing temperature of -40°C was chosen as a temperature appropriate to primary special structural steel for components of heavy wall thickness, as per Rules of Design Construction and Inspection of Offshore Structures—Det Norske Veritas 1977 and other comparable specifications.

On the prototype, additional specimens were taken adjacent to the most critical region of the part. Correlation with prolongation results was satisfactory. All parts used duplicate tension and impact specimens from diametrically opposite locations; in conjunction with approved thermocouple locations during the furnace cycles, this gave an assured uniformity of properties.

At the conclusion of prototype tests, a decision was made to increase the anchor unlatching loads by increasing the collet spring stiffness. This was to be achieved by cold setting the fingers inward from their machined positions by an



MIDWALL CIRCUMFERENTIAL SPECIMENS. ORIGINAL TREATMENT WATER QUENCH 920°C , TEMPER 615°C , COOLED $15^{\circ}\text{C}/\text{h}$. RETEMPER IN LABORATORY & COOL AT RATES INDICATED.

FIG. 4—Effect of cooling rate on collet material (Charpy V-notch).

amount determined by analysis. Uniformity of initial finger positions was just as important as it had been before the design change.

The concurrent testing and manufacturing program was structured to cope with machining profile alterations on the collet, but this was the only change required on the anchor after the prototype stage.

Anchor Body

This is a pressure vessel with a large variation in wall thickness of the finished component from 385 to 75 mm. External axial webs are added at twelve circumferential locations to support protective rings.

Material Selection

The component is only significantly stressed at its extreme ends during hydraulic pressurization. It must have a high mass to facilitate anchor latching under self weight. Peak stresses were initially shown to justify a material of the same strength level as the collet, with the additional requirement of good weldability for web attachment.

Manufacture, Heat Treatment, and Mechanical Testing

Casting was discounted because schedule considerations would not permit weld repair of the critical areas, either due to the presence of internal defects or surface-breaking defects on major sealing and bearing surfaces.

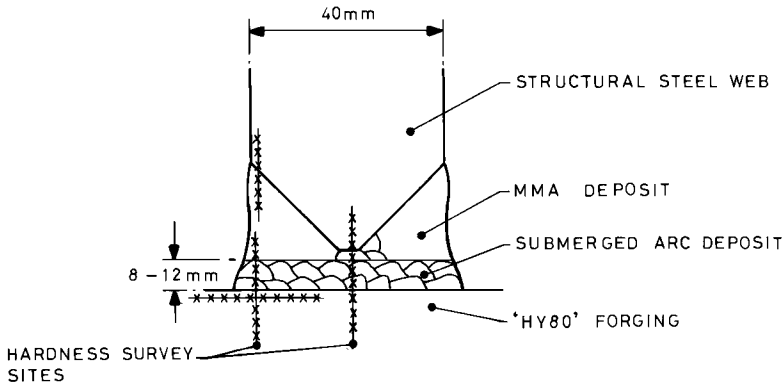
All suppliers indicated that they would manufacture the part as a solid forging, boring it out prior to heat treatment. Again, mechanical specimens were taken from a midwall location of the test prolongation.

Fabrication

Discussion with the customer indicated that they would require a maximum hardness of 300 Vickers hardness number (VHN) within the weldment zone, this limit being fixed on the basis of a potentially sour service environment. Additionally, the certifying authority (Lloyds Register of Shipping) indicated that they would expect the part to receive a postweld heat treatment (PWHT) cycle.

The eventual procedure selected was a combination of a submerged arc buttering layer with manual metal arc main runs. Procedure details and typical results from test plates are given in Fig. 5. Cooling rates from postweld heat treatment were controlled to avoid embrittlement, as confirmed by tests on surplus test material which accompanied the prototype through PWHT. It was not possible to achieve less than 320 VHN without PWHT.

Postweld treatment was limited to a 2-h soak period at least 15°C below the final tempering temperature. This was shown to reduce the maximum VHN below 300, which was not otherwise possible even with strict bead positioning and sequencing.



SUBMERGED ARC DEPOSITS	120°C PREHEAT, 150°C MAXIMUM INTERPASS ENERGY INPUT 1.2 - 2.2 kJ/mm
MMA DEPOSITS	100°C PREHEAT, 200°C MAXIMUM INTERPASS ENERGY INPUT 1.7-2.0 kJ/mm FIRST TWO PASSES 2.0-2.5 kJ/mm REMAINING PASSES
PWHT	2 HOURS AT 15-20°C BELOW FINAL TEMPERING TEMPERATURE. COOL AT > 40°C/HOUR
ACTUAL VHN MAXIMUM	285-310 KILOGRAMME LOAD (320 ACHIEVED BEFORE PWHT, AT TOE OF WELD)

FIG. 5—Body fabrication procedure.

Weldment Examination

All web to body welds were subject to magnetic particle inspection for surface defects, with no cracklike indications being permitted. Additionally, all welds were ultrasonically examined for freedom from internal flaws, using both compression and shear waves to scan the fusion faces and the entire internal volume. The rejection level was a signal amplitude exceeding that from a 4-mm flat-bottomed hole in the test block and with a length above 20 mm or any discontinuities interpreted as lack of fusion, incomplete penetration, or cracks. There were no incidents of weld repairs being required during the production program.

HY80 Toughness

Other HY80 components manufactured in this program were in the primary tensile load path of the platform mooring system. The principal processing difference was that the parts were given accelerated cooling from the tempering treatment.

In addition to near surface impact specimens taken in accordance with MIL-S-23009A, midsection toughness also was evaluated at -40°C , as for the two

TABLE 2—Typical surface and midwall impact energies for HY80 type forgings (longitudinal Charpy V-notch tests)^a

Component-type and Wall Thickness	Near Surface, −84°C			Midwall, −40°C		
	CV Avg	CV Max, J	CV Min	CV Avg	CV Max, J	CV Min
A, 400 mm	144	169	119	175	184	159
B, 190 mm	187	200	175	219	229	208
C, 160 mm	230	250	218	240	250	230

^a All components were subjected to accelerated cooling from temper cycle.

components just described. Data showed that the material displayed comparable toughness at −40°C at the midwall of sections up to 400 mm to tests at −84°C some 30 mm from the heat treatment surface. Typical values are summarized in Table 2 for information.

Conclusions

Manufacture of high integrity forgings to a tight time scale while retaining flexibility for design or specification changes requires very close liaison between client, design contractor, and forging supplier. It has proved possible to accommodate both design and processing changes within this program by appropriate scheduling and with cooperation from all parties. The HY80-type material has been found to have an excellent heat treatment response in sections up to 400 mm thick.

Acknowledgments

The author is grateful to the management of the participating companies in the Hutton Field Development for permission to publish this paper. The participating companies are: Conoco (UK), Ltd. (Operator); Britoil plc; Gulf Oil Corp.; Amoco (UK) Exploration Co.; Enterprise Oil, plc; Mobil North Seal, Ltd.; Amerada Hess (UK), Ltd.; and Texas Eastern North Sea, Inc.

DISCUSSION

B. Durginan (written discussion)—(1) What was the actual stress relief temperature for the manual metal arc and submerged arc welds, and what were the toughness requirements and results from the welds? (2) What chemistry controls were imposed on the H4-80 base metal and weld metal?

P. J. Whitehouse (author's closure)—(1) Typically 590 to 600°C. Toughness requirements were the same as the forging—50 J minimum average of 3 Charpy V notch tests at −40°C. HAZ properties in the HY80 were typically 100 to 120

J, as were the all-weld metal properties. (2) The HYBO chemistry is given in Table 1. There was no chemistry control applied to the weld metal as a weld procedure approval requirement. The submerged arc wire composition was: C = 0.12; Mn = 1.5; Si = 0.2; S = 0.01; P = 0.01. The manual metal arc electrode was an all-positional, basic-coated type giving all metal properties as follows: C = 0.05; Mn = 1.60; Si = 0.40; S = 0.01; P = 0.01.

¹ Babcock & Wilcox, Barberton, Ohio.

General Industrial Forgings

Test Methods and Forging Assessment

John G. Gensure,¹ Albert S. Melilli,² and Stephen M. Brueggemann³

High-Sensitivity, Immersion, Ultrasonic Testing of Steel Forgings

REFERENCE: Gensure, J. G., Melilli, A. S., and Brueggemann, S. M., “**High-Sensitivity, Immersion, Ultrasonic Testing of Steel Forgings,**” *Steel Forgings, ASTM STP 903*, E. G. Nisbett and A. S. Melilli, Eds., American Society for Testing and Materials, Philadelphia, 1986, pp. 553–572.

ABSTRACT: Present industry-wide standards covering ultrasonic inspections of forgings such as ASTM Recommended Practice for Ultrasonic Examination of Heavy Steel Forgings (A 388-80) specify the contact method of inspection. Sensitivity settings vary as to inspection technique—longitudinal or shear wave (straight or angle beam). Normally, the sensitivity is established using a back reflection or test sample technique in order to resolve equivalent flat-bottom hole (EFBH) sizes of 3.175 mm (0.125 in.) at the centerline or bore surface of the forging. The assumption is made that most indications will be oriented parallel to the direction of the longitudinal axis of cylindrical forgings and in a circumferential plane of ring forgings.

On occasion, discontinuities occur in forgings that are different than normal, requiring changes in normal procedures and techniques. Size, orientation, location, and distribution require special considerations. This paper outlines how a high-sensitivity, immersion, ultrasonic technique is utilized to inspect a group of gear component and miscellaneous forgings suspected of having internal hydrogen flakes. The technique is successful in locating the discontinuities and distinguishing between the flakes and other types of discontinuities, specifically nonmetallic inclusions.

KEY WORDS: ultrasonic testing, immersion, high sensitivity, longitudinal and shear wave (angle beam), transducer, test block, nonmetallic inclusion, hydrogen flakes

Present industry-wide standards covering ultrasonic examination procedures such as ASTM Recommended Practice for Ultrasonic Testing of Steel Forgings (A 388-80) specify the contact method of inspection. The method is chosen because it is simple, convenient, and provides adequate sensitivities with reasonably accurate results. The forging can be examined at almost any suitable location, allowing the transporting of portable inspection equipment to the component. Both longitudinal and shear-wave (angle beam) inspections can be per-

¹ Materials engineer, Corporate Engineering and Manufacturing, General Electric Co., Bridgeport, CT 06601.

² Manager, Materials and Processes, General Electric Co., Lynn, MA 01910.

³ Specialist, Nondestructive Testing, General Electric Co., Lynn, MA 01910.

formed conveniently using the procedures. Examination frequencies are chosen and specified to accommodate the required sensitivity levels within the forgings to be evaluated. Utilized are ultrasonic instruments that are calibrated, accurate, portable, and durable with variable frequency adjustments. Permanent records are normally manually produced by the inspector.

Search units are chosen which provide the best combination of penetration and resolution to locate discontinuities within the volume to be inspected. Size and frequency of the search unit will vary depending upon the type of examination, longitudinal or shear wave, and size of component to be evaluated. Other factors influencing the choice of the search unit are surface condition, radius of curvature, material acoustic characteristics, near field effects, and discontinuity morphology including number, size, shape, and location. Examinations are performed employing an established size and frequency search unit. Evaluations can be made using additional sizes or frequencies. Industry standards usually specify a 2 or 2.25-MHz frequency search unit for longitudinal beam inspections and a 1-MHz frequency for shear-wave inspections.

The selected frequency used for shear-wave inspection is approximately one half of the frequency used for longitudinal beam inspections. This combination results in a reasonably similar sensitivity during inspection of the same component. Sensitivity is dependent upon acoustic wave length. Wave length is proportional to velocity and inversely proportional to the frequency. Within the same alloy steel, the velocity of a longitudinal wave is twice that of a shear wave [1]. The following equations apply [2]

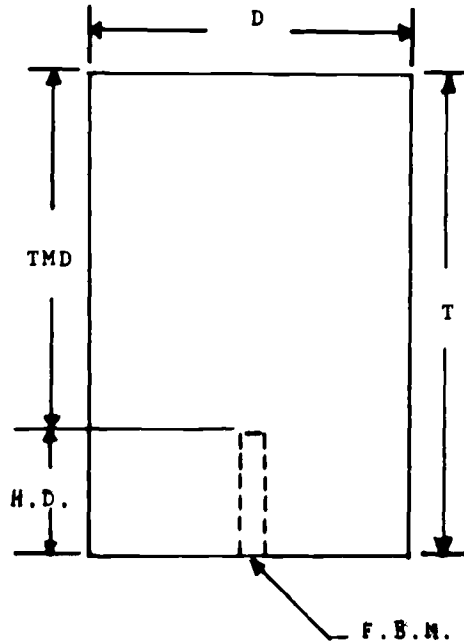
$$\begin{aligned}\lambda &= V_l/F \\ \lambda &= V_s/F\end{aligned}\tag{1}$$

where

- λ = wave length, mm,
- V_l = longitudinal wave velocity, m/s,
- V_s = shear wave velocity, m/s, and
- F = frequency, MHz.

By changing the frequencies used during longitudinal and shear wave inspections, the value of the wave length remains constant.

Sensitivity levels for longitudinal beam inspections are sufficient to resolve indications with minimum equivalent flat-bottom hole (EFBH) diameters of 3.175 mm (0.125 in.) at the centerline or bore surface of cylindrical forgings. Smaller discontinuities can be resolved closer to the transducer entry surface. The sensitivity may be established using standard reference blocks such as ASTM Recommended Practice for Fabrication and Control of Steel Reference Blocks Used in Ultrasonic Inspection [E 428-71 (1980), Block Number 8] (Fig. 1), custom fabricated-reference blocks, or by utilizing the back reflection method. Displays and presentations on the cathode ray tube (CRT) screen vary depending upon the



Flat Bottom Hole	Diameter	Thickness	Test Metal Distance	Hole Depth
1/32 in. to 1/16 in.	50.8 mm	25.4 to 184 mm in 6.35-mm increments	6.35 to 165 mm in 6.35-mm increments	19 mm

NOTE: Material: 4340 aircraft quality alloy steel; specification: manufactured in accordance with ASTM Practice for Fabricating and Checking Aluminum Alloy Ultrasonic Standard Reference Blocks (E 127-82a) and ASTM Recommended Practice for Fabrication and Control of Steel Reference Blocks Used in Ultrasonic Inspection [E 428-71 (1980)].

FIG. 1—Calibration block details.

method utilized, as shown in Fig. 2. Using a reference standard, a 38-mm (1.5-in.) or 51-mm (2-in.) sweep-to-peak height is established. Reporting levels are a percentage, 25 or 50% of the reflection height.

Employing the normal back-reflection technique, reflections from the back wall surfaces are set at 38 or 51-mm (1.5 or 2-in.) sweep-to-peak height. The reporting level using the normal back reflection technique is 10% of the established screen height setting. Discontinuities of EFBH sizes of 3.175 mm (0.125 in.) minimum normally will be reported using this procedure. The thickness of the forging to be inspected, the length of sound travel, and the size of the discontinuities to be resolved may influence the size of the search unit to be utilized.

Angle-beam or shear-wave inspections are normally performed on hollow or ring-type forgings only. A 45° angle-beam search unit is used for this inspection

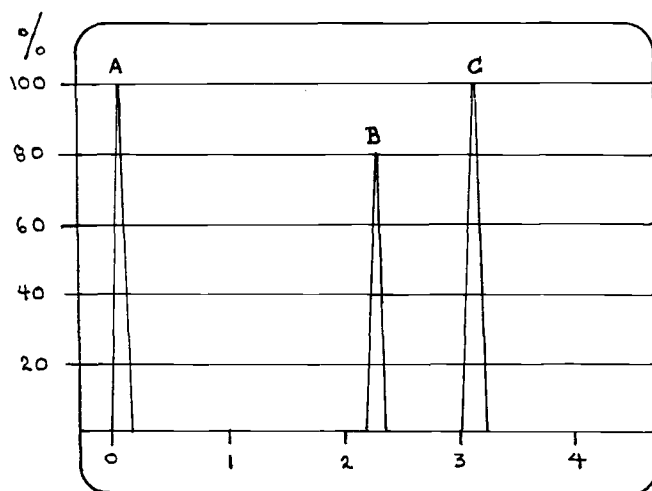


FIG. 2—Calibration block presentation with ASTM E 428 flat-bottomed hole. CRT: A = front surface echo; B = response from 8/64-in. flat-bottomed hole; C = back surface echo.

technique. Instrument sensitivity levels are established utilizing a notch standard which is generated on the inside diameter surface. The instrument is calibrated to obtain a 75% full-screen height reflection from a rectangular or 60° V-notch. Specified depth of the V-notch is created in the axial direction, and the sound beam is propagated in the circumferential direction.

When performing inspections using either technique, a manual, hand-scanning method usually is employed with a maximum scanning rate of 152 mm/s (6 in./s). The forgings may be stationary or rotating. In order to ensure complete coverage, the search unit is indexed using a 15 to 25% overlap minimum with each pass. Actual required overlap considering the minimum discontinuity reporting level is not established. An oil base couplant is used between the search unit and entry surface.

Scanning is performed while observing the reflection on the CRT screen. The numbers, sizes, and location of discontinuities are reported manually as a result of the observation. Automatic gating may be employed.

Capabilities

Evaluations using the techniques outlined contain certain limitations which should be considered when interpreting results. Initial pulse and near field effects have to be considered. Presentations from the initial pulse at 2.25 MHz encompass an equivalent distance of approximately the first 13 to 19 mm (0.5 to 0.75 in.) below the entry surface depending upon the transducer diameter. Representations on the CRT screen from indications within this area will be obscured by the initial pulse. Normally the ultrasonic inspection is performed in the rough-machined condition; therefore, a portion of this area which cannot be inspected will

TABLE 1—*Search unit near field length in low-alloy steels.*

Search Unit Frequency, MHz	Diameter, mm (in.)	Near Field Length, mm (in.)
2.25	12.7 (0.5)	15 (0.59)
2.25	19.05 (0.75)	34.3 (1.35)
2.25	25.4 (1.0)	61.5 (2.42)
2.25	28.6 (1.125)	78 (3.07)
2.0	24.0 (0.95)	54.9 (2.16)
5.0	12.7 (0.5)	34.3 (1.35)
5.0	19.05 (0.75)	77.5 (3.05)
5.0	25.4 (1.0)	137.7 (5.42)

be removed during finish machining. A surface inspection using other techniques can be effective in inspecting the portion of the zone which remains after machining. In addition, this area of solid forgings can be examined from the opposite entry surface.

The near field of a search unit is dependent upon the size and frequency. In low-alloy steels, the near field lengths for several different search units are listed in Table 1 [3]. Near field length increases with increasing frequency and size. Without covering the details concerning the propagation of sound waves, within the near field there exists fields of maximum and minimum of acoustic pressure. Discontinuities in the area of minimum acoustic pressures within this interference field must be of a relatively large size in order to be detected and resolved. A constant sensitivity level for inspections within the near field is impossible. Similar to areas masked by the initial pulse in solid forgings, this area can be inspected from the opposite entry surface.

In order to improve the ability to evaluate the size of a discontinuity, the propagation of sound waves essentially should be normal to the plane of the major ligament of the discontinuity. In cylindrical forgings, discontinuities normally are parallel to the direction of the longitudinal axis. By performing the inspection using longitudinal beam technique with the sound waves propagating in a radial direction, the ability to determine the size of a discontinuity is maximized.

Inspection coverage can be an additional problem. Operator technique is relied on to ensure the required overlaps during manual scanings. Although normally effective, the inspector's concentration is divided between the component being examined and the CRT screen presentation. In addition, when inspections are performed at higher sensitivities to resolve discontinuities of smaller EFBH sizes, a 25% search unit overlap may be insufficient to detect indications near the minimum size specified. For example, if discontinuities with an EFBH diameter of 1.5875 mm (0.0625 in.) minimum are to be located, indexing the search unit with a 6.35-mm (0.25-in.) overlap may be inadequate to detect the indications.

Indications with EFBH sizes of 3.175 mm (0.125 in.) diameter may not be always detected when using a normal back reflection such as 75% of screen height and a reporting level which is 10% of the sensitivity setting. Consider the

example of inspecting a solid forging 400 mm (15 in.) in diameter while referring to average distance gain size (AVG/DGS) diagrams modified for a 2.25-MHz, 25.4-mm (1-in.)-diameter transducer for EFBH diameter conversion [4]. At a 10% reporting level, discontinuities will be less than the minimum acceptable EFBH size diameter of 3.175 mm (0.125 in.) only to a depth of 140 mm (5.5 in.) (Fig. 3). At midradius, a 10% reporting level equates to an EFBH diameter of 4.4 mm (0.172 in.). At the back wall, a 10% reporting level equates to an EFBH size of 7.9 mm (0.312 in.).

The longitudinal beam testing technique may be unacceptable for detecting even large size discontinuities oriented with the major axis in the radial direction. Employing this technique, the edge of the discontinuity would be intercepted; therefore, the reflective surface area may be insufficient to return a detectable signal. An inspection using the shear wave technique likely would be required to determine the radial extent of the discontinuity.

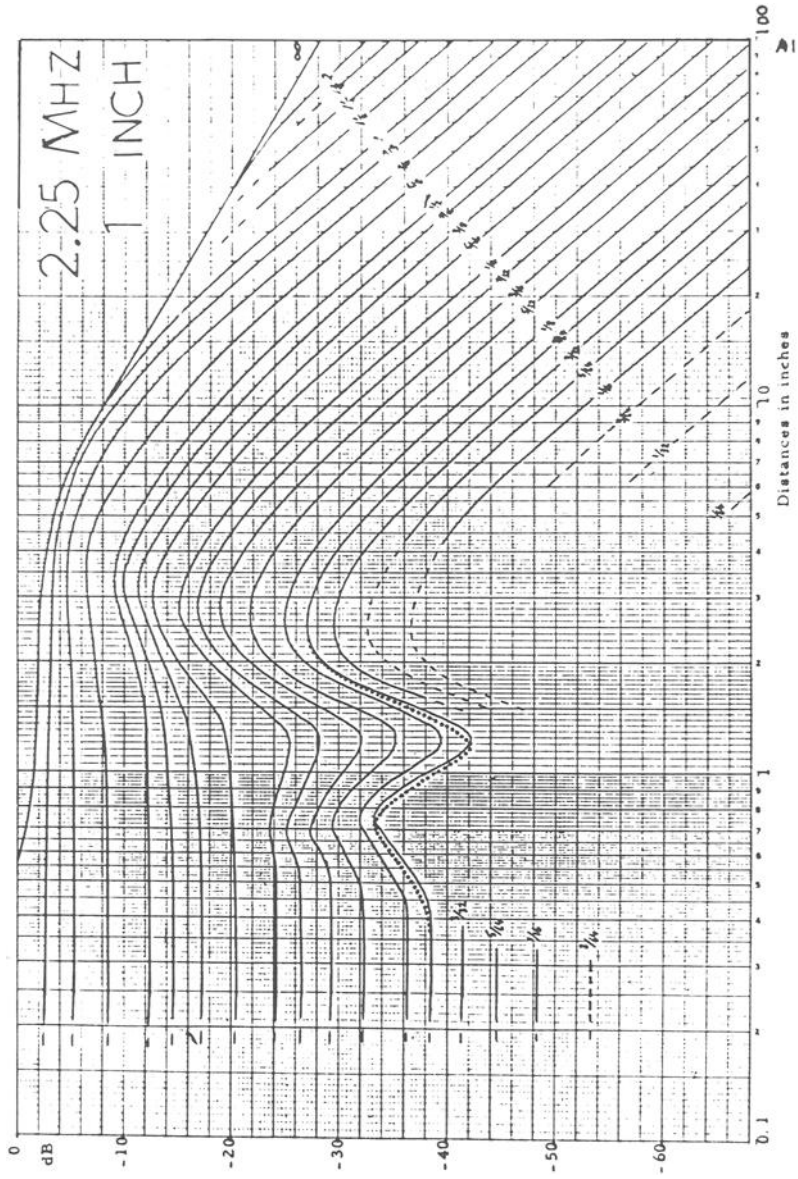
Internal Flaws

This user recently encountered forgings for gear rotor applications which contained several different internal discontinuities. Sectioning for macro- and microexaminations disclosed two types of defects. Several forgings contained nonmetallic inclusions, some of which were elongated along the longitudinal axis. The nonmetallics were generally located near the centerline of the forging. Discontinuities in other forgings were cracklike in nature and were suspected to be associated with a hydrogen flaking condition. These discontinuities occurred in numerous orientations but generally in a radial direction.

The discontinuities were located throughout the cross section from the centerline to the surface of the forgings. Several forgings with bores also contained the cracklike discontinuities. Indications in some of these forgings were on the bore surface while others appeared on the peripheral surface. We suspect that some of the hollow forgings may have had defects near the centerline which were removed during boring.

The group of forgings presented a multifaceted problem:

1. Gear teeth are machined in many of the forgings approximately 3 mm (0.125 in.) below the peripheral surfaces as inspected. The gear tooth area is one of the critical areas of the forging, making it necessary to ensure that an adequate inspection is performed within this area.
2. It is important to determine which forgings contained discontinuities suspected to be associated with hydrogen flakes.
3. During ultrasonic inspection, it is necessary to distinguish between CRT screen presentations caused by nonmetallic inclusions and those that are the result of hydrogen flakes.
4. Determination of the size of indications is important.
5. Determination of indication number, location, orientation, and direction is important.



6. The discontinuities related with hydrogen flakes and many of the nonmetallic inclusions were not detectable when ultrasonically inspected using normally established techniques.

7. Size and shapes of forgings were: shafts—150 mm (6 in.) diameter; solid pinions—500 mm (20 in.) diameter; hollow pinions—800 mm (32 in.) outside diameter with 200-mm (8-in.)-diameter bores.

High Sensitivity, Immersion Techniques

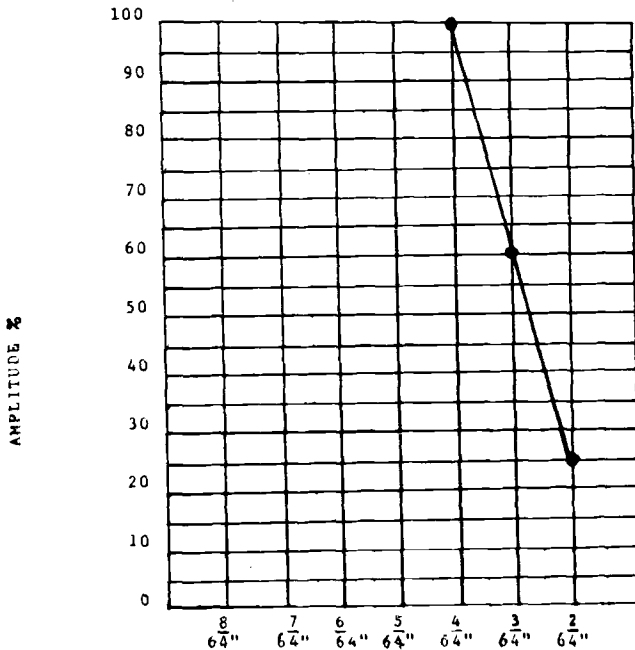
In order to maximize the ability to detect the discontinuities in the group of forgings, several new techniques are required. Sensitivity levels have to be increased. A procedure which minimizes initial pulse and near field effects is required. A shear-wave inspection to detect radially oriented discontinuities is included. The search unit index increment is decreased. Comparisons between discontinuity presentations are made. An immersion ultrasonic testing system as described in Table 2 is utilized when performing the inspections.

Using the longitudinal beam technique, higher sensitivity levels are required to detect hydrogen flakes in the forging. Because of the radial orientation of the flakes, the ultrasonic beam intersects the discontinuities essentially on edge. Only minor reflections are obtained from these edge surfaces; therefore, detection and size determination are difficult. Sensitivity for longitudinal beam inspections are established using the flat bottom hole in an ASTM E428-4340-4 alloy steel test block. Sensitivity settings and inspections are performed using a 19-mm (0.75-in.)-diameter, 5-MHz search unit. A 100% CRT screen height presentation is established from the 1.5875-mm (0.0625-in.)-diameter flat bottom hole. Equipment automatic gating is utilized with a 25% of sensitivity reporting level which is equivalent to the reflection from a 0.7938-mm (0.03125-in.), flat bottom hole diameter (Fig. 4).

TABLE 2—Immersion ultrasonic system description.

<i>Instrument:</i>	Sonic mark IV with positive mode flaw alarm system; — 15 MHz frequency selector, distance echo calibration module and delay and material thickness controls.
<i>Tank Dimensions:</i>	1524 m length by 1524 m width by 1727 m diameter.
<i>Capacity:</i>	Weight = 7.2 metric tons; length = 1143 m; diameter = 1220 mm.
<i>Ring Rotator:</i>	Rubber-coated, ring end stop thrust bearing, manual job control, variable speed control of 0 to 20 rpm with tachometer mounted in control panel readout in inches per second. Parallelism with "X" axis of tanks maintained at ± 1 mm.
<i>Bridge:</i>	Motorized step index in "X" axis; two directions adjustment and digital readout on control panel. Accurate to ± 0.025 mm. Bridge index terminates when flaw gate level triggered. Manual index in "Y" axis with digital readout on control panel.
<i>Manipulator:</i>	Motorized step index in "Z" axis with adjustment and digital readout on control panel; motorized transducer angulation (120°) and rotation (360°) with digital readout on panel. Uncontrolled motion does not exceed 2 mm at extreme conditions, index accuracy ± 0.025 mm, and backlash during normal operations does not exceed $1/4^\circ$.
<i>Transducers:</i>	Panametrics 5.0-MHz, 19-mm diameter, resolution-type immersion transducer, and 2.25 MHz, 19-mm diameter, standard-type immersion transducer.

INSTRUMENT MAKE: <u>SONICS</u>	TRANSDUCER MAKE: <u>PANAMETRICS</u>
INSTRUMENT MODEL: <u>MARK IV</u>	TRANSDUCER MODEL: <u>R-102</u>
INSTRUMENT S/N: <u>18854</u>	TRANSDUCER S/N: <u>A3028A-38796</u>
TEST BLOCK S/N: <u>7075-T651</u>	METAL TRAVEL: <u>8"</u>
TARGET FBH: <u>7/64"</u>	WATER PATH: <u>7 1/2"</u>
FREQUENCY: <u>5.0 MHZ</u>	SENSITIVITY DB: <u>36</u>
DATE: <u>8/4/63</u>	
TECHNICIAN: _____	



FLAT BOTTOM ROLL SIZE

FIG. 4—Area versus amplitude plot (linearity).

Metal travel of the test blocks is varied depending upon the thickness range of the forging being inspected. To evaluate discontinuities, various metal travels of standard test blocks are utilized. When necessary, blocks with different flat bottom hole sizes will be used.

The material chemistry of the test block is similar to the chemistry of the forgings, and, because of similar processing, acoustic characteristics are similar. Surface effects are discounted because the forgings are machined prior to inspection and the surface finishes are controlled for inspection. Surface roughness and conditions are within reasonable limits. Effects of curvature are not considered because the diameters involved are large enough that the entry surface is considered essentially flat. By utilizing immersion testing, the effects of the entry surface conditions are reduced.

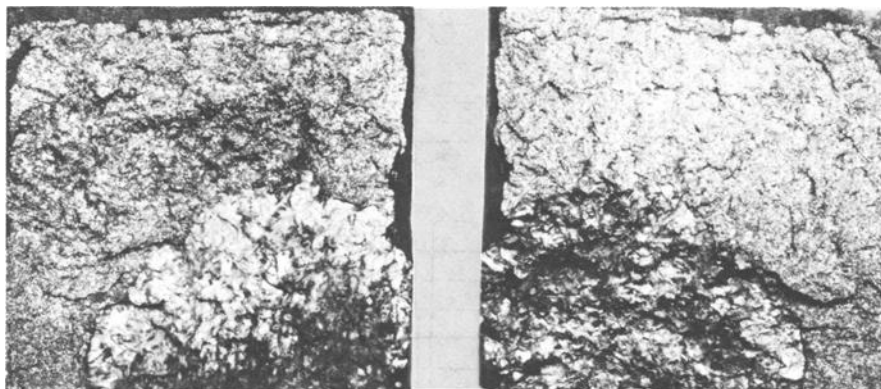


FIG. 5—Hydrogen flake broken open to show fracture surfaces. ID surface from the bottom, X4 (reduced one fifth for reproduction).

It is possible to reduce the effects of initial pulse by frequency selection. Using the immersion technique, the extended near field portion of the sound beam will be located in the water path. Because of the final location of the gear teeth near the entry surface, detection of even the smallest flaws is important in this area. The technique allows detection of an almost uniform minimum flaw size beginning approximately 3 mm (0.13 in.) below the entry surface. Finish-machining plus surface inspections will eliminate or establish the conditions within uninspectable areas.

Hydrogen flakes are suspected and verified to have ligaments with radial orientations as shown in Fig. 5, viewed parallel to the radial direction. Shown is a hydrogen flake beginning at the bore surface oriented radially for a depth of at least 13 mm (0.5 in.). In order to improve detecting, a shear-wave inspection was added to supplement the longitudinal beam test. Since the requirement is to

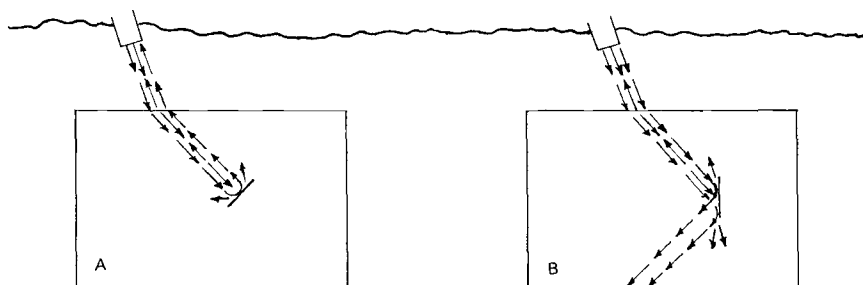


FIG. 6—Comparisons of discontinuities at normal orientation versus radial orientation: (A) discontinuity normal to sound energy, almost total reflection of energy back towards transducer; (B) discontinuity at 0° with respect to 45° sound energy path, almost no energy reflected back towards transducer.

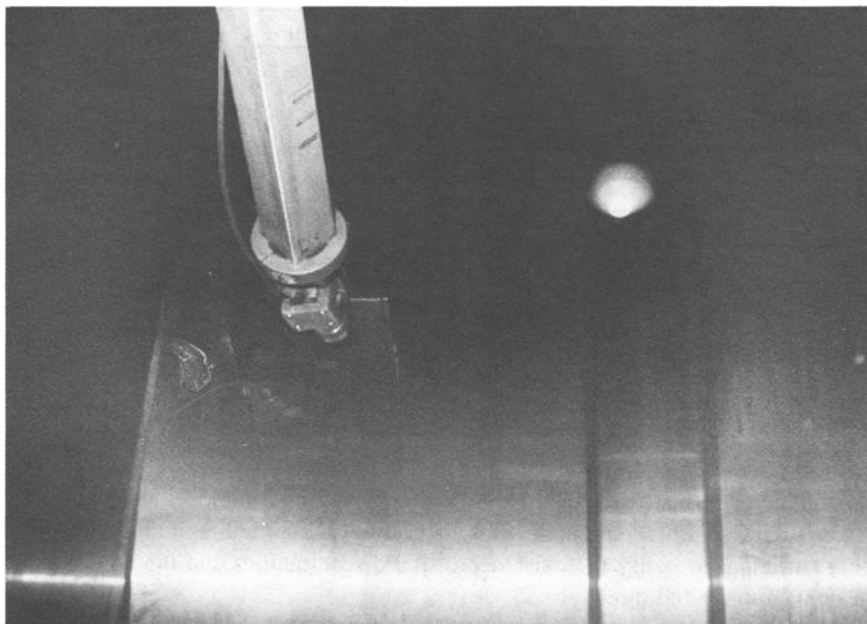


FIG. 7—Transducer setup for shear wave test.

determine the existence of radially oriented flaws, a correlation with an EFBH size is not essential.

Actual correlation of angle-beam reflections with standard hole sizes are difficult to attain. Sensitivity settings must be sufficient to detect relatively small energy responses. Because of the intercept angles, the energy responses returning along original sound wave propagation paths, which will be detected by the search unit, represent only a small percentage of the original energy of propagation. Depending upon the location and actual orientation of the discontinuity, a large percentage of the reflecting energy may be undetectable. Consider a smooth reflector, radially oriented at the midthickness of the section examined as shown in Fig. 6. Approximately 90% of the reflecting energy will propagate at an angle of 90° from the original shear-wave angle. This portion of the energy will not be detected by the search unit. Detection utilizing a second off-set transducer is difficult because the actual reflection angle will vary depending upon the location and orientation of the discontinuity. Detectability of a discontinuity is most probable when the direction of the propagation of the reflecting signal is along the original wave propagation path.

Shear-wave inspections are conducted using a 19-mm (0.75-in.)-diameter, 2.25-MHz transducer. A full screen height reflection is set from the hole in an ASTM E428-4340-4 standard steel test block using the longitudinal wave propagation technique. Maintaining this sensitivity setting, as shown in Fig. 7, the search unit is angled at 19° toward the long axis of the forging. Circumferential

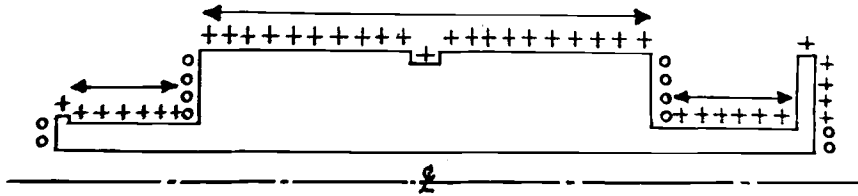


FIG. 8—Ultrasonic scan methods: +++ = longitudinal wave test from OD using 5.0-MHz frequency; 000 = longitudinal wave test from faces using 2.25-MHz frequency; <-> = axial shear wave test—two opposite directions—45° refracted angle—2.25-MHz frequency.

scans are made indexing the transducer along the length of the forging in one direction, then repeated opposite the original direction of indexing as displayed in Fig. 8. For reporting, instrument gates are set at 25% of the sensitivity setting or full screen height. In cylindrical forgings and in cylindrical forgings containing bores, circumferential shear-wave propagation is not always possible. Since the orientations of hydrogen flakes are random when considering the longitudinal and transverse directions, peripheral inspections along the longitudinal direction are sufficient to verify the existence of the discontinuities and the approximate extent in the radial direction.

Search unit index increments must be reduced in order to detect the size discontinuity required. With sensitivity established using a 1.5875-mm (0.0625-in.)-diameter, flat-bottom hole and the flaw alarm gated at 25% of the established level, effective beam measurements must be taken over an 0.79-mm (0.0315-in.)-diameter, flat-bottom hole to ensure detecting (Fig. 9).

By using a controlled indexing increment system for the search unit, once established the necessary overlap is maintained. One shortcoming is the increased time for inspection. Since the indexing also can be manually adjusted and the transducer angled for optimum response, the determination of the size of the discontinuity may be maximized.

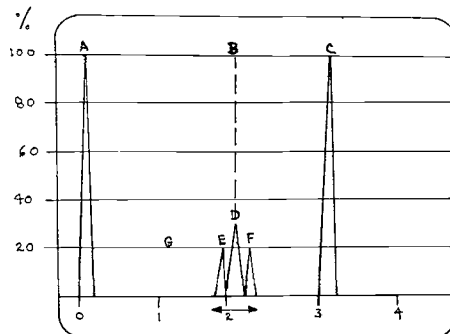


FIG. 9—CRT: A = front surface echo; B = response from 4/64-in. flat bottom hole; C = back surface echo; D = response from 2/64-in. flat bottom hole; E-F = transducer movement over FBH 20%, 25%, 20%; 80% of this distance is scan index increment; G = flaw alarm gate level.

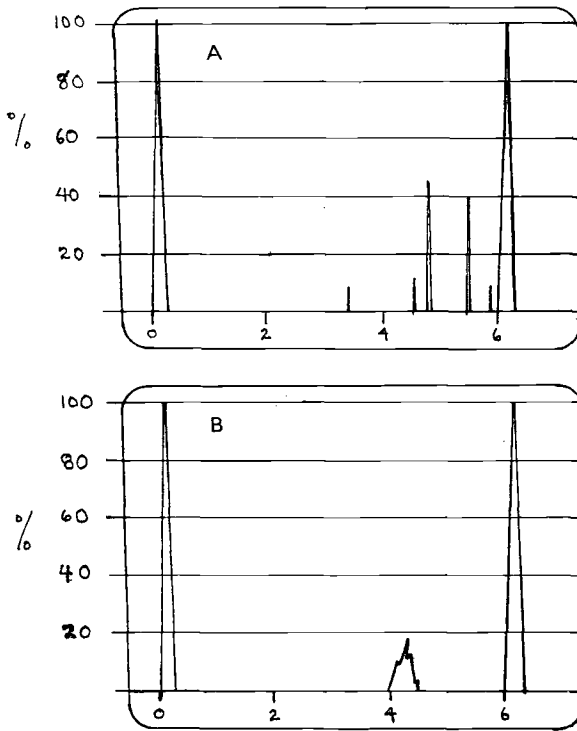


FIG. 10—CRT presentation of inclusions versus flakes: (A) inclusions; (B) flake.

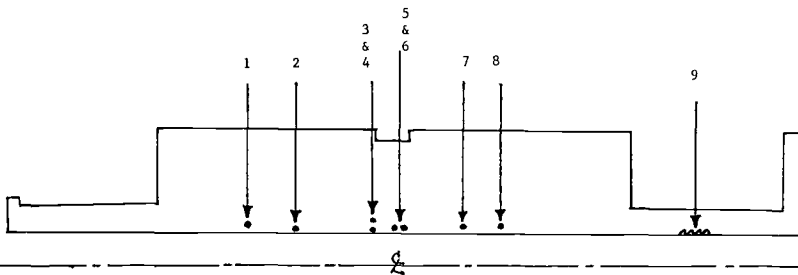


FIG. 11—Indication location. NOTE: Indications Nos. 1 through 8 were detected during longitudinal wave examination using 5.0-MHz, 3/4-in.-diameter transducer. Indication No. 9 was detected during shear wave examination only using 2.25-MHz, 3/4-in.-diameter transducer. The ultrasonic profile of this forging exhibited indications along the entire length from surface of bore to 50 mm into the forging. Bore magnetic particle inspection (MPI) examination showed indication No. 9 as being cracklike discontinuities.

TABLE 3—*High sensitivity indication detail.*^a

Indication No.	Section Thickness, mm	Distance From Bore, mm	Distance Reference "A," mm ^b	Amplitude Response, %	EFBH, 1/64 in.
1	173	26	216	10	-2
2	173	11	254	10	-2
3	137	9	371	48	+3
4	137	20	371	20	+2
5	137	13	406	100	-5
6	137	10	431	35	+3
7	173	18	483	20	+2
8	173	18	508	30	+3
9	38	5	908 to 959	100	-5

^a With probe optimized over indications, no loss of back echo occurred.

^b Reference "A," from end opposite coupling.

Forgings within the group in question were known to contain at least two types of discontinuities, nonmetallic inclusions and hydrogen flakes. It is important to be able to distinguish between these defects. Of the two, hydrogen flakes are of greater concern. As indicated, the orientation of this type of discontinuity made detectability difficult and size determination improbable. In addition, the orientation of the discontinuities are a concern to the design engineers because the defects are located essentially normal to one of the directions of the principal stresses. When hydrogen flakes occur in a forging, they usually occur in large numbers. Because of close proximities between indications, the probability of the linking of discontinuities during possible in-service growth becomes a serious problem.

As displayed in Fig. 10, during the course of evaluating the indications detected in the forgings (Fig. 11 and Table 3), differences in profile and CRT presentations were noted, suggesting that two types of discontinuities were present. At the high sensitivity inspection level, the nonmetallic inclusions were very sharp, single point spikes which exhibited no travel or elongation and which appeared and disappeared very quickly on the CRT. The indications were congregated at or near the center bore. Indications which were the result of nonmetallic inclusions could not be detected utilizing the shear wave mode due to their probable axial planar orientation. The hydrogen flakes appeared as broad uneven spikes holding or traveling along the CRT, random in nature and distributed through the cross section of the forging from the center bore to the outside diameter. The heaviest concentration of the hydrogen flakes was near the center bore and dispersed at random away from the bore. Unlike nonmetallic inclusions, the hydrogen flakes could be detected utilizing the shear wave mode test.

Testing Procedure

Employing the sensitivity and evaluation techniques outlined, inspections are performed using equipment presently available at the authors' facilities as shown

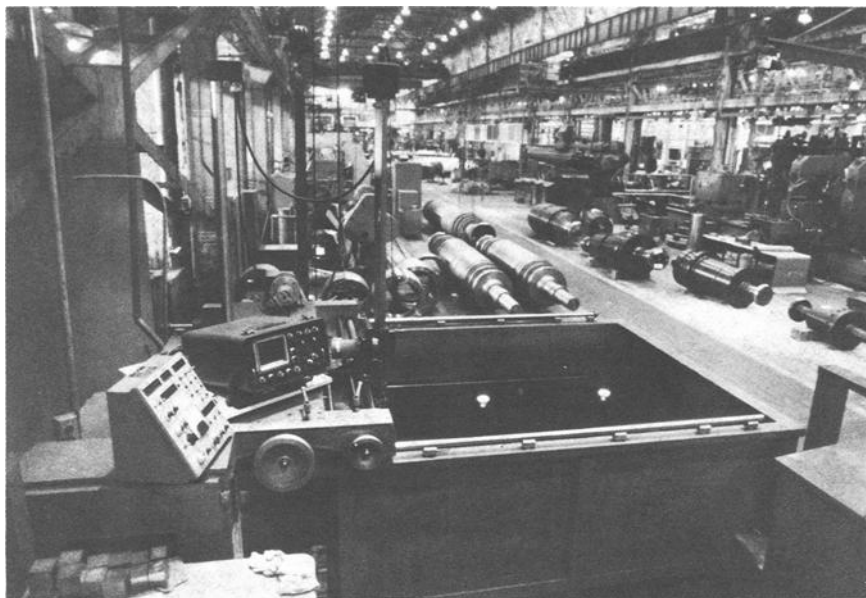


FIG. 12—Immersion testing facility showing tank, ultrasonic instrument, and bridge with manipulator.

in Fig. 12. The forgings are placed in an immersion tank on power-driven rollers. Rotational speed can be adjusted as required. The forgings are fully submerged, and the search unit is located above the entry surface, suspended from a bridge which spans the width of the tank as shown in Fig. 13. The manipulator search tube is adjustable to obtain the correct water path distance for the various transducers utilized. The system employs a microprocessor that indexes the bridge and search unit a preset amount after each rotation. The bridge can be jogged manually and the search unit angled to optimize indications for evaluation. The calibration blocks are placed in the water on a level stand, and once calibrated for amplitude responses and correct water path, the instrument delay controls are locked to maintain the same water path for the test as used during calibration. For longitudinal inspections, the search unit can be zeroed or normalized and for shear-wave inspections placed at the desired angle by an electrical control with a digital readout on the control panel. The rotation rollers can be jogged mechanically to assist in indication evaluation. As can be seen in Fig. 14, the CRT presentation is monitored continuously with all digital readouts conveniently located to allow the operator to know what the system is doing at any given instance. The system is equipped with stop or alarm circuitry which stops the bridge index mechanism when an indication response breaks the level of the flaw gate.

Typically, forgings are scanned from all peripheral surfaces a total of three



FIG. 13—Closeup view of immersion facility.

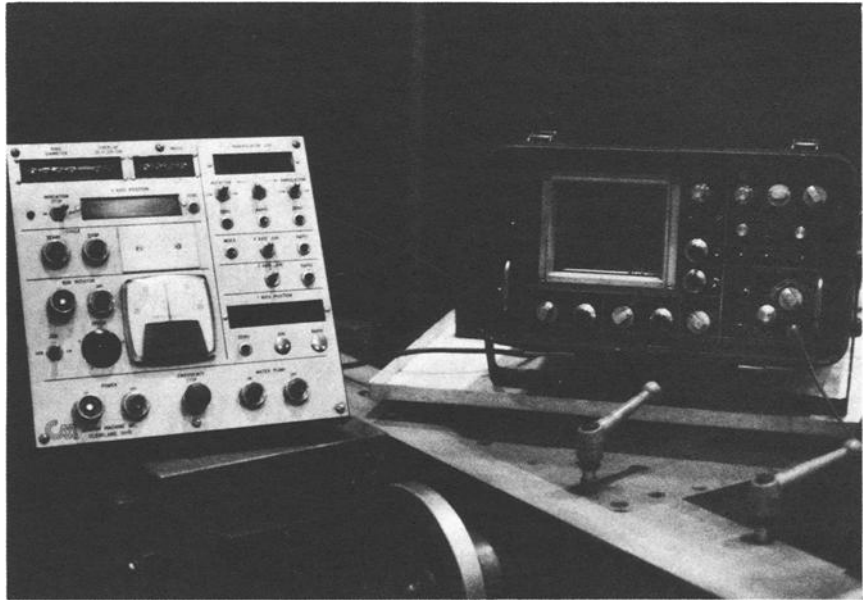


FIG. 14—Control panel and ultrasonic instrument display.

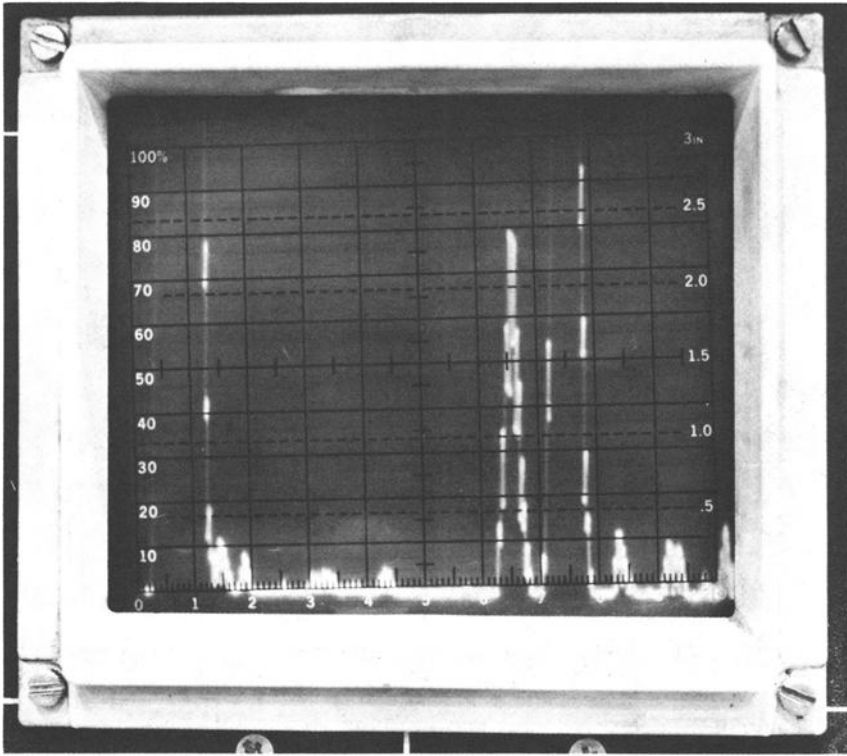


FIG. 15—CRT display of reflections from flat-bottom hole in test block.

times, once using the longitudinal beam technique and twice using the shear-wave technique. A CRT presentation reporting the reflection from a flat bottom hole in a test block is displayed in Fig. 15. Presentations in a defect-free area of the forging are displayed in Fig. 16. The reflection on the left of the CRT represents the first echo reflection of the sound beam water-to-steel interface using the longitudinal wave technique. The right of the screen represents the inside diameter of the forging or the steel-to-water interface. In immersion testing, the initial pulse is shifted through the use of the delay control, and the time from pulse through water is not displayed.

Figure 17 shows actual locations where hydrogen flakes were encountered in a pinion forging. This forging was sectioned for macro- and microscopic examinations as displayed in Fig. 17.

After sectioning, additional ultrasonic evaluations were made on block samples to pinpoint the location of discontinuities. Additional sections were made, and the defects displayed in Fig. 5 and Fig. 18 at 8X magnification confirmed the existence of flakes. The defect was oriented radially from the bore surface. The

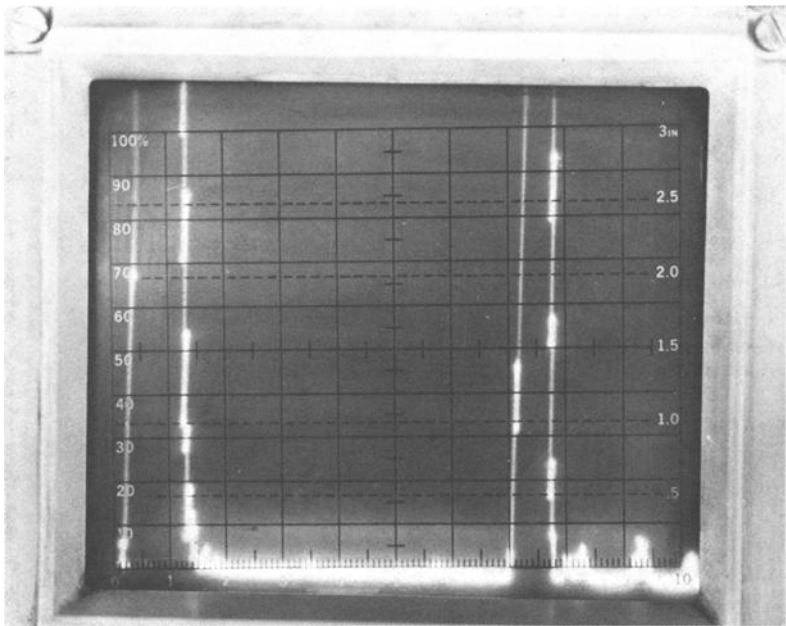


FIG. 16—CRT display in a defect-free area of the forging.

total length of the defect is approximately 13 mm (0.5 in.). Upon sectioning the hydrogen flake normal to the radial direction, the cracklike defect as shown in Fig. 19 was clearly displayed. The length as shown is 25 mm (1 in.). As indicated by these two photographs, it is easy to understand how the hydrogen flakes were difficult to resolve using the longitudinal wave technique and the normal sensitivity setting. One also can understand how the discontinuities can be found using the shear-wave technique.

Summary

Techniques capable of locating and detecting flaws in forgings using high-sensitivity, immersion ultrasonic inspection are outlined. The techniques were

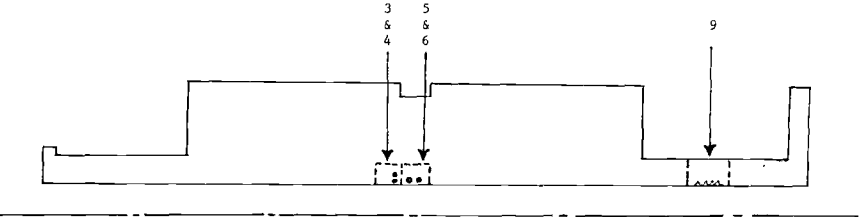


FIG. 17—Sectioning locations. NOTE: Sections are 50 by 50 mm.

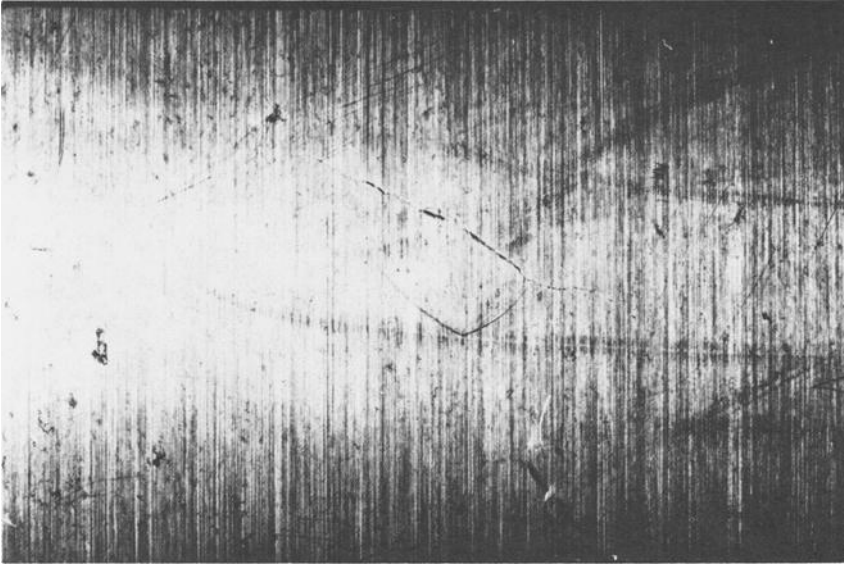


FIG. 18—*Hydrogen flake as visually found on the bore surface, X8 (reduced one third for reproduction).*



FIG. 19—*Polished and etched transverse section of flake shown in Fig. 18, X12 (reduced one third for reproduction).*

developed to evaluated forgings which contained both nonmetallic and hydrogen discontinuities.

References

- [1] "Velocity Tables Condensed," Automation Industries, Inc., Boulder, CO, reference series for ultrasonic nondestructive testing, Vol. 2, 1970.
- [2] Krauthramer, J. et al., *Ultrasonic Testing of Materials*, Springer-Verlag, New York, Heidelberg, Berlin, 1969, p. 6.
- [3] Krauthramer, J. and Krauthramer, H., "Data Sheets for Ultrasonic Flaw Detectors and Probes," 1969.
- [4] Krauthramer, J. et al., *Ultrasonic Testing of Materials*, Springer-Verlag, New York, Heidelberg, Berlin, 1969, p. 79.

Hydrogen—Its Occurrence, Determination, and Control in Steel Forgings

REFERENCE: Murphy, E. L. and Steiner, J. E., “**Hydrogen—Its Occurrence, Determination, and Control in Steel Forgings**,” *Steel Forgings, ASTM STP 903*, E. G. Nisbett and A. S. Melilli, Eds., American Society for Testing and Materials, Philadelphia, 1986, pp. 573–582.

ABSTRACT: The history of hydrogen-related problems in heavy steel forgings is traced. Hydrogen embrittlement and its manifestation as “fisheyes” and lowered ductility in tension specimens is discussed. Flaking, its occurrence, detection, and control, past and present, is reviewed. Recommendations for hydrogen control in specifications of ASTM Subcommittee A01.06 on Steel Forgings and Billets are presented.

KEY WORDS: hydrogen, steel forgings, hydrogen embrittlement, fisheyes, flaking, flake detection, hydrogen control, hydrogen analysis

Upon initial consideration, presenting a paper on hydrogen in steel forgings in 1986, about 30 years after the introduction of vacuum degassing, may seem like a questionable endeavor. However, the facts are that in the last few years several reports have been made at meetings of ASTM Subcommittee A01.06 on Steel Forgings and Billets on hydrogen-related problems in forgings, and requests by affected members have been made to include hydrogen controls in some of our specifications. Because of vacuum degassing, many members have not previously experienced any of these hydrogen-related problems. Therefore, it seems appropriate to discuss this subject.

In the early part of this century, problems of so-called thermal cracking or hairline cracking (flaking) were encountered in alloy steel ordnance forgings (gun barrels and armor plate) [1] and also in high-carbon steel railroad products (rails, forged wheels, and locomotive tires). Generally, these defects were not recognized until after failure of the product and subsequent investigation. In these early days, no association of these defects was made with hydrogen in the steel. In the 1930s the recognition of hydrogen as the major cause of flaking became prevalent throughout the industry. Subsequently, various controls were initiated

¹ Consultant—Forgings, Engineering Materials & Processes, Inc., Pittsburgh, PA 15217.

in an effort to keep hydrogen out of the steel. None proved very effective until the introduction of vacuum degassing in the mid- to late 1950s.

During the 1940s and early 1950s, there were two major hydrogen-related problems, embrittlement and flaking, with flaking being by far the most serious. The industry approach to resolving these problems was by attempting to minimize the hydrogen pickup in melting and casting. These efforts were aimed particularly at eliminating moisture from scrap, alloy additions, slag-making additions, refractories used in both pouring and casting, and, where possible, furnace atmosphere control. These precautions helped to some degree but did not eliminate the hydrogen problems, which persisted, especially with basic electric furnace-melted steel. For turbine and generator rotor forgings, the thrust to lower sulfur content and improved overall cleanliness of the steel led eventually to abandonment of open hearth steel and to the use of the electric furnace for making these ingots. In addition, designs of electric generating equipment steadily moved to higher capacity units, thus increasing rotor forging diameters and weights. These factors made the hydrogen problems more difficult to control.

Hydrogen Embrittlement

Hydrogen embrittlement caused low ductility in tension specimens. Figure 1 shows the effect of hydrogen on radial ductility in Ni-Mo-V forgings. The test bar fracture surfaces occasionally exhibited one or more shiny areas, commonly called fisheyes or, in older days, snowflakes. Figure 2 shows a typical embrittled fisheye fracture. These are not defects in the steel from which the specimen was taken, but brittle fracture areas resulting from the combination of hydrogen and

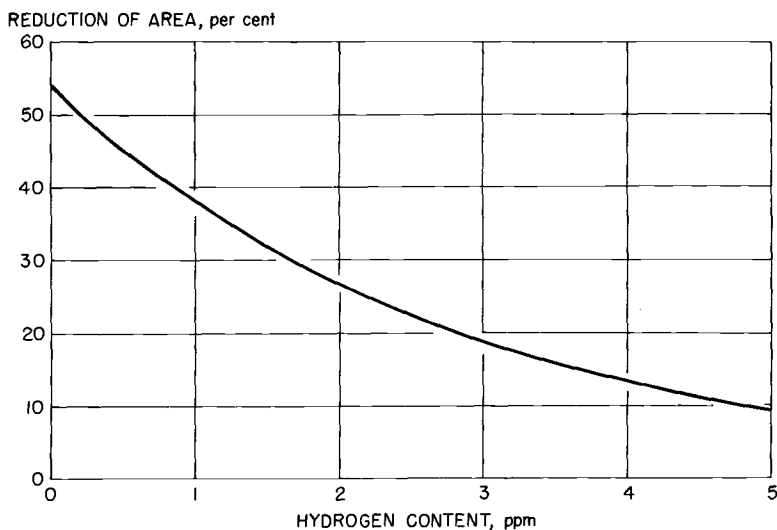


FIG. 1—Effect of hydrogen on radial ductility of Ni-Mo-V forgings.

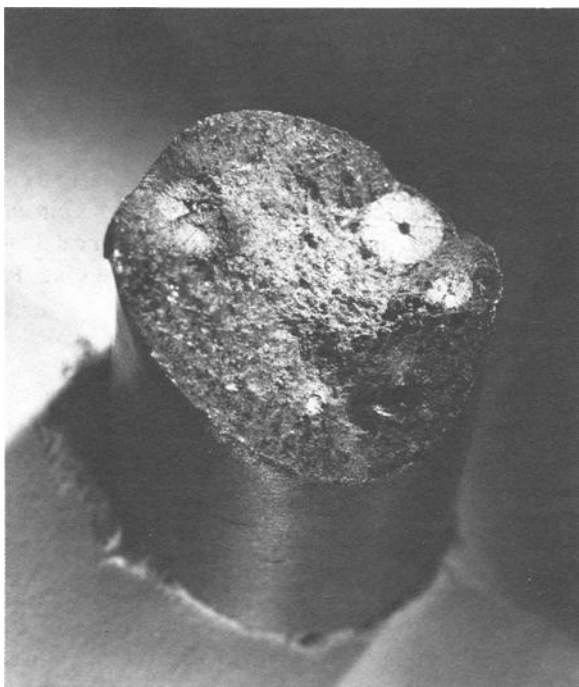


FIG. 2—*Fisheyes in fracture of a broken tension test.*

stress beyond the elastic limit applied in tension testing. The nucleation sites of these brittle fracture areas are frequently small nonmetallic inclusions.

Low temperature stress relief of tension specimens eliminates the manifestation of embrittlement and restores normal ductility. Considerations of this factor resulted in a rationalization on the part of many that the embrittlement was caused by residual stresses in the specimen resulting from removal of the coupon from the forging and machining of the test bar. Consequently, it became common practice to age or stress relieve tension test bars prior to testing. The *Manual of Open Die Forgings* [2], published in 1949, states:

The setting up of a certain amount of residual stresses is perhaps unavoidable in the removal of tension test coupons and their subsequent machining for testing. In order to relieve these stresses, it is considered desirable by some to age the specimens by keeping them for 24 h after machining and before testing, or by boiling them in water or in oil at 300°F [149°C] for a period. There is considerable justification for the belief that such practices give test results more truly indicative of the forging itself, and forging manufacturers sometimes properly so condition test bars.

Until the introduction of vacuum casting, the aging of tension test bars was a common and accepted practice in the forging industry. Thus, the problem of low ductility caused by embrittlement was resolved. In reality, however, the basic

problem of hydrogen embrittlement, recognized or not, still remained. In retrospect, this type of embrittlement was not a dangerous problem. We know of no reported service failures of forgings attributable to such embrittlement. With modern vacuum cast steels, the aging of specimens is unnecessary and is no longer practiced.

It will undoubtedly come as a surprise to many to learn that all current ASTM A01.06 product specifications still permit aging of tension specimens. Our specifications cite ASTM Methods and Definitions for Mechanical Testing of Steel Products (A 370-77) as the reference standard for tension testing. Paragraph 6.4 of this standard states:

Unless otherwise specified, it shall be permissible to age tension test specimens. The time-temperature cycle employed must be such that effects of previous processing will not be materially changed. It may be accomplished by aging at room temperature 24 to 48 h or in shorter time at moderately elevated temperatures by boiling in water, heating in oil or in an oven.

Flaking

Control of flaking in large forgings was a difficult and persistent problem prior to the introduction of vacuum degassing. It became even more difficult as forging diameters increased and melting shifted to the basic electric furnace.

A thermal flake may be defined [3] as “a tight crack formed by combined action of hydrogen and stress, always fully contained within a steel section, generally appearing as a disk unless directional stresses or localized weaknesses change the shape.” Note that both hydrogen and stress must be present for flaking to occur. The stress can be thermal stress from cooling, transformation stresses, or a combination of both. Note also that flakes are contained within the section, that is, they do not intercept the forging surface. Figure 3 shows transverse macroetched sections through heavily and lightly flaked Ni-Mo-V forged steel blocks. Note that heavy flaking consists of a large number of small flakes, while lighter flaking shows a small number of much larger flakes. This is characteristic.

The critical part of processing flake-sensitive forgings is to get them to room temperature after hot working without developing flakes. Recognizing the role of stress in flaking, forging manufacturers devised many variations of lengthy preliminary heat treatments consisting of one or several austenitizing treatments followed by slow cooling through the transformation range, usually ending with a long temper, then slow cooling to room temperature. As an example, the preliminary heat treatment of a low-alloy Ni-Cr-Mo tube sheet forging 24 in. thick comprised three austenitizing treatments and a temper that took a total of 36 days. Such heat treatments were very costly. They were generally, but certainly not always, successful in preventing flaking.

Before the introduction of ultrasonic testing to the heavy forging industry in the late 1940s, there was really no very good inspection method to ensure that a forging was flake-free. Since flakes are internal and do not appear on the

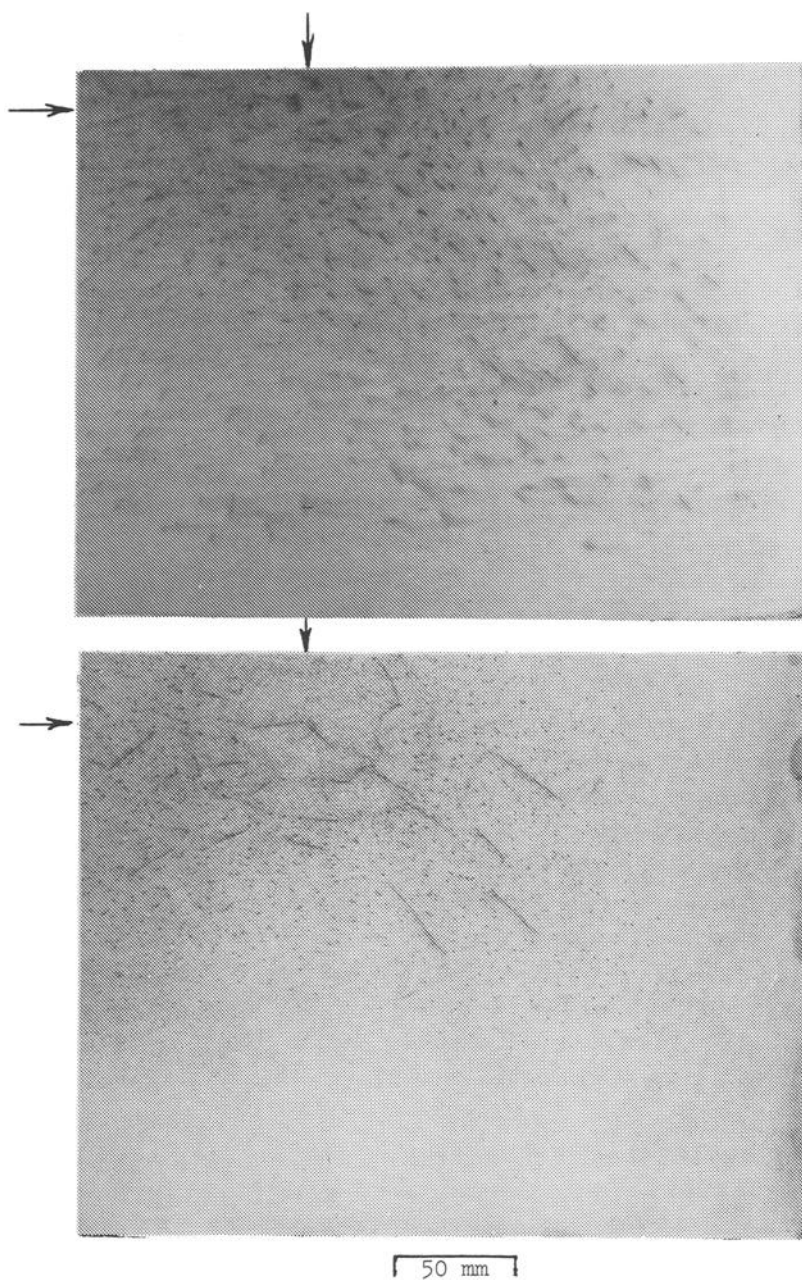


FIG. 3—Transverse macroetched section through heavily and lightly flaked Ni-Mo-V rotor steel blocks. Arrows point to centers of blocks.

forging surface, detecting them was difficult. Positive identification depended on locating and gaining physical access to the flakes. Methods of identification included: (1) deep etching, (2) metallographic examination (either of these methods might require destruction of the forging) and (3) magnetic particle or dye penetrant examination of exposed surfaces that were originally internal in the forging, for example, bore surfaces, fillets, and cutouts between wheels of a turbine forging. If a forging had no machined-exposed internal surfaces (such as a solid shaft), it is unlikely that the flakes would have been detected.

Ultrasonic testing eventually provided a rather positive method of detecting internal defects such as flakes. After the introduction of ultrasonic testing, the next several years were a time of learning for everyone in the forging industry. During this period only the most obviously bad forgings were rejected, and destructive examination usually confirmed the validity of the decision. Each producer and consumer attempted to categorize and correlate indication amplitude, shape, and frequency with actual defects in forgings by trepanning samples and where possible examining these visually and under low and high magnifications. These activities were later coordinated under ASTM Subcommittee A01.06 jurisdiction. The first ASTM Subcommittee A01.06 standard for ultrasonic examination of heavy steel forgings was published in 1955 [Recommended Practice for Ultrasonic Examination of Heavy Steel Forgings (A 388–55T)]. Through many revisions, this is still the industry standard.

With experience it became recognized that ultrasonic indications from flakes have these characteristics:

1. Sharp, peaked indications. The indication amplitude and back reflection loss depend on the severity of the flaking.
2. Numerous indications are present, and their location is generally from near quarter thickness to the center.
3. Indications do not appear at or near any forged surface.
4. Because of their random orientation, some flakes may appear as travelling indications, that is, they travel across the screen with relative movement of the transducer and the forging. Large flakes generally show this type of response.

Vacuum Processes—Hydrogen Control

From the late 1950s to the present, most large forging ingots have been cast using the vacuum stream degassing process, which entails pouring into a mold in a vacuum chamber evacuated to less than 1 mmHg (1 torr). The molten steel stream, when exposed to the vacuum, breaks up into small droplets from which hydrogen is readily exhausted. There is no further exposure of the molten steel to moisture. Thus, vacuum stream degassing is very effective, usually resulting in hydrogen contents of 1 ppm or less.

The vacuum lift processes, Dortmund-Hoerder (D-H) and Reinstahl-Haereaus (R-H), are frequently used for smaller forging ingots. These processes are time-

dependent because successive portions of the steel are exposed to the vacuum for a number of cycles or a period of time to achieve the desired low hydrogen content. To achieve the desired pouring temperature, these processes require superheating of the tapped steel to compensate for temperature loss during the degassing period. With proper low vacuum levels and adequate cycling, these processes provide satisfactory low hydrogen contents. Because the ingots are poured in air, there is a normal pickup of about 0.5-ppm hydrogen during teeming, even when argon shielding is employed.

In the more than 25 years since the introduction of vacuum degassing to large forging ingots, hydrogen problems have disappeared almost entirely. Based on reports and actions in our ASTM A01.06 forging subcommittee, which reflects the state of the industry in this country, the following observations can be made:

1. There have been no reported instances of hydrogen-related problems in any of the large forgings made from vacuum stream degassed ingots.
2. Until fairly recently, there were not reported hydrogen problems with forgings made from vacuum lift processed ingots. Within the last few years, there have been a few reported and verified instances of flaking in smaller forging from ingots made by these processes. This does not reflect on the ability of the processes to obtain the desired low hydrogen contents. Rather it is a confirmation that these processes have more points of control that require constant monitoring and evaluation.

As a result of these few instances of flaked forgings, requests were in ASTM Subcommittee A01.06 for revision of some specifications aimed at preventing a recurrence. Requests ranged from:

1. Additional restriction and definition of process control parameters for vacuum lift processes.
2. Specifying maximum hydrogen limits.
3. Analyzing and reporting hydrogen content when requested through a supplementary requirement.

Ballot items for Nos. 1 and 3 are presently in process of ballot for Specification for Vacuum-Treated Carbon and Alloy Steel Forgings for Turbine Rotors and Shafts (A 470-84). (NOTE: Ballot items 1 and 3 have been incorporated into A 470-84.)

Determination of Hydrogen Content of Steel

During the 1940s and 1950s determination of hydrogen content in steel was rather erratic. Methods of analysis were not standardized, and variations in sampling methods were a source of large discrepancies in results. Obtaining samples of liquid steel for analysis was difficult and not standardized. Sampling, handling

and preservation were not uniform and contributed greatly to the scatter in results. Determination of hydrogen by sampling from the forging was even more chaotic. To prevent evolution of hydrogen, it was necessary to keep the area cool while the test coupon was being cut out of the forging and to immediately chill the sample after it was removed. These controls were not always applied effectively. A bigger problem with hydrogen determination by sampling from the forging is where to locate the test sample. Near surface, midradius, and center sample locations give widely varying results. Figure 4 shows transverse distribution of hydrogen in a 49-in.-diameter Cr-Mo-V forging from near surface to center. Note that the hydrogen at the center is almost five times that at near surface. This forging was made from an air cast electric furnace ingot made before vacuum degassing was available.

Today equipment for obtaining hydrogen samples from molten steel is available that is simple to use, reproducible, and positive with regard to ensuring no hydrogen loss. Coupled with the modern automatic analyzing machines that give an accurate digital readout of hydrogen content in a few minutes, this equipment comprises a system for rapid, accurate, and reproducible determination of hydrogen in molten steel. Automatic analyses are just as efficient for analysis of samples taken from forgings; however, the problems of sample location and removal are still present.

With modern equipment, hydrogen content of molten steel can be accurately determined. What we are really concerned with, however, is hydrogen levels in the forgings. There is some hydrogen segregation during ingot solidification and some hydrogen loss during forging and heat treatment. Thus a direct correlation of hydrogen in the molten steel to hydrogen in the forgings is not practical.

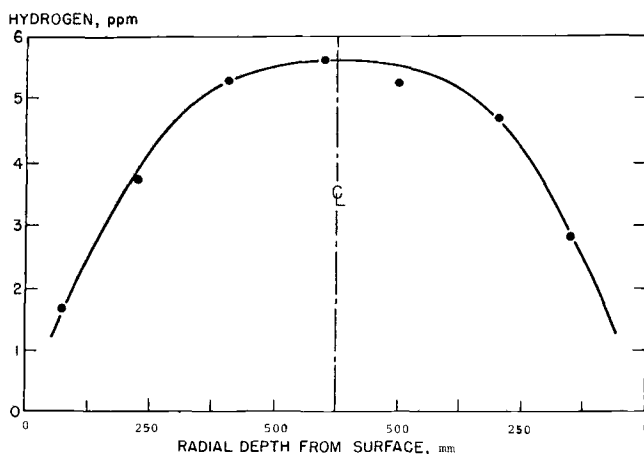


FIG. 4—Transverse distribution of hydrogen in a 1250-mm (49-in.)-diameter Cr-Mo-V rotor forging.

Determining molten steel hydrogen, however, can be a very valuable tool for process control and is generally used for this purpose.

How should we in the ASTM A01.06 Forgings subcommittee approach the question of hydrogen control in our specifications? After reviewing all pertinent factors, the following points are recommended for consideration:

1. Continue to use process control parameters as the primary method of precluding hydrogen problems. *Rationale:* Process control parameters in our specifications for vacuum stream degassing have proven successful. For the 22 years of existence of the specifications, there have been no reported instances of hydrogen problems. There have been a few recently reported problems with forgings made from vacuum lift process ingots, but overall the experience has been excellent. Additional control parameters for these processes have been proposed for modification of the specifications and are in ballot process at present. Approval is expected and these additions should appear in our specifications shortly. (NOTE: these additions have been incorporated into A 470-84.)

2. We should not consider adding hydrogen limits to our specifications. *Rationale:* Each grade of steel has a different safe hydrogen level. These levels have not been defined or determined. The problems of sample location and procurement previously discussed also make this approach impractical.

3. If it is felt necessary to specify that a hydrogen analysis be made and reported, it should be done through a supplementary requirement. It is suggested that such analyses be restricted to liquid metal samples. *Rationale:* Process controls have proven successful in controlling hydrogen problems. Addition of mandatory hydrogen analyses to our specifications would be unproductive and unnecessary. The problems of hydrogen analyses from samples from forging have been previously discussed.

Conclusion

The hydrogen problem, largely solved almost 30 years ago, persists today in sporadic occurrences of flaking. Specification limits on hydrogen content of flake sensitive steels are under consideration. Because of the practical difficulties and metallurgical complexity of sampling for hydrogen in solid steel products, it appears that specifications for hydrogen content should be directed toward liquid steel sampling, and this only through a supplementary specification requirement. Control through process specifications should be considered where practical. Process control and not specific hydrogen content limits appears most reasonable.

References

- [1] Foley, F. B., "A Problem in Ordnance—Flakes and Cooling Cracks in Forgings," *Metals and Alloys*, Oct. 1940.
- [2] *Manual of Open Die Forgings*, Open Die Forging Industry, New York, NY, Oct. 1949, p. 44.
- [3] Steiner, J. E., "Control of Flaking and Other Hydrogen Problems in Heavy Forgings," First International Conference on Current Solutions to Hydrogen Problems in Steel, Washington, DC, 1-5 Nov. 1982, American Society for Metals, Metals Park, OH 44073, p. 55.

DISCUSSION

*W. H. Childs, Jr.*¹ (*written discussion*)—Mr. Murphy indicated that recent problems with hydrogen have been linked to the vacuum lift process. He also said something to the effect that this resulted in the realization that the control points in the vacuum lift must be monitored more closely. My question is: What are those control points, where is the hydrogen coming from, and how do you monitor for it?

E. Murphy and J. Steiner (authors' closure)—The major control points are vacuum pressure level and number of lift cycles. The latter is controlled largely by steel temperature. Thus, we suspect that, if a batch of steel is on the cold side of the desired temperature range at the beginning of degassing, the operator will have a great temptation to minimize the time and hence the efficacy of degassing.

The hydrogen is introduced into the steel in the melting process. Contents of from 4 to 6 ppm in the furnace ladle after tap are typical of basic electric arc furnace steel.

Hydrogen is monitored by sampling at that point in processing of interest to the investigator.

¹ Turbodyne Division, Dresser Industries, Inc., Wellsville, NY 14895.

Failure Analysis of Hot Forging Dies

REFERENCE: Ebara, R. and Kubota, K., “**Failure Analysis of Hot Forging Dies,**” *Steel Forgings, ASTM STP 903*, E. G. Nisbett and A. S. Melilli, Eds., American Society for Testing and Materials, Philadelphia, 1986, pp. 583–592.

ABSTRACT: Impact failure of hot forging dies occurs frequently from surface cracks due to mechanical or thermal fatigue. However, useful information regarding failure analysis of hot forging dies is scarce because few data exist on the fracture behavior and fractography of hot forging die steels.

In this paper, what is mainly described is dynamic fracture toughness, low cycle fatigue behavior, and fracture surface appearances of hot forging die steels. A couple of quantitative analyzed examples of fracture toughness and temperature by use of stretched zone width measurement for hot forging die failure are described.

KEY WORDS: forging dies, dynamic fracture toughness, low-cycle fatigue, stretched zone, fractography, failure analysis

Hot forging die failure is caused by the inadequacy of such factors as die material properties, die design, and the forging operation. Many efforts have been made to prevent die failure and to improve die life. However, it is comparatively rare to find available information for practical applications. Therefore, fundamental investigations of failure analysis of hot forging dies were carried out. In this paper, what is described mainly is dynamic fracture toughness, low cycle fatigue properties, and fracture surface appearances of hot forging die steels. A couple of quantitative analyzed examples of fracture toughness and temperature by use of stretched zone width measurement for the press and hammer forging dies are described.

Fracture Appearances of Hot Forging Dies and Fractographic Approaches

The investigation process for failure analysis of hot forging dies is basically the same as for the failure of other machine components. However, it is rare to find analyzed examples of failed hot forging dies by fractography. The strongest reason seems to be because most die failure occurred impactly from the impression corner as exemplified in the case of the knuckle forging die (Fig. 1). And the

¹ Associate chief research engineer, Hiroshima Technical Institute, Mitsubishi Heavy Industries, Hiroshima 733, Japan.

² Assistant manager, Tokyo Motor Vehicle Works, Mitsubishi Motors Corp., Kawasaki 210, Japan.

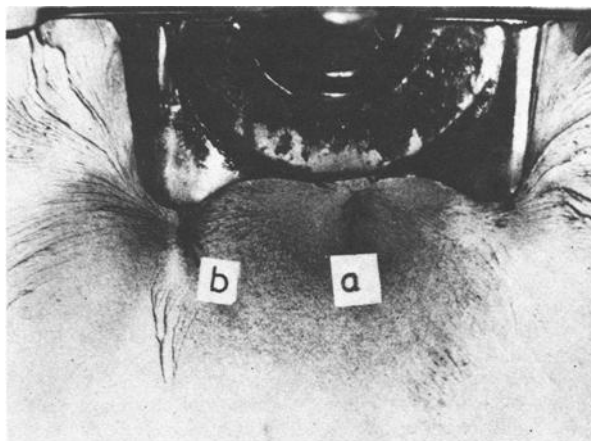


FIG. 1—The macroscopic fracture surface of a knuckle forging die for a motor vehicle, SKD62. Arrows a and b show crack initiation points.

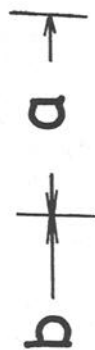
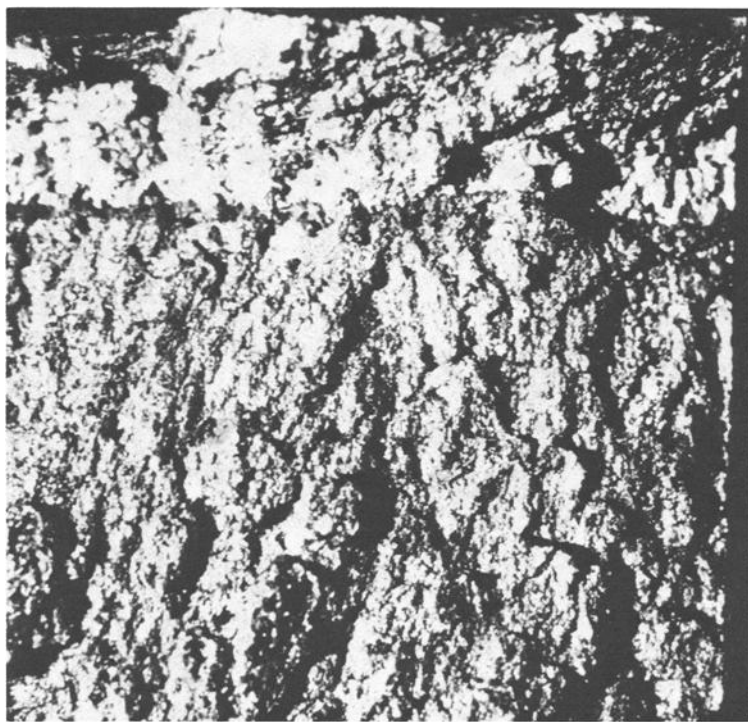


FIG. 2—The macroscopic fracture surface of a turbine blade die, SKT4: (a) subsurface layer; (b) brittle fracture surface.

impact fracture was easily identified without microfractography. However, low magnification observation frequently revealed that the impact failure occurred from surface cracks initiated at the impression corner (Fig. 2). Most of the cracks are relatively short and are due to mechanical or thermal fatigue. Moreover, generally, it is rare to find microfractographical data for high-hardness steels such as forging die steels. Therefore, the detailed observations were conducted on the fracture surface of mechanical or thermal fatigue, the stretched zone, and the impact fracture to clarify the reason of the die failure. And the information obtained from these observations might be deeply related to the prevention of die failure and the improvement of die life.

Fundamental Fracture Behavior and Microfractographs

Dynamic Fracture Toughness and Fracture Surface Appearances

Instrumented impact tests using the introduced fatigue crack Charpy V-notched specimen were conducted at room temperature (RT) to 500°C. The chemical composition and mechanical properties of tested materials are SKT4 and SKD62, as shown in Table 1. Complete details of the experimental procedure already have been provided in Ref 1. K_{Id} calculated by use of the Brown-Srawley equation [2] as a function of temperature is shown in Fig. 3. The K_{Id} was increased as testing temperature was increased. After attaining the maximum value of 49.6 MN/m^{3/2}, K_{Id} decreased as temperature increased. This inclination is similarly observed in the relationship between impact value, crack initiation and propagation energy, and static fracture toughness (K_Q) versus temperature. K_Q of the same material had about twice the value of K_{Id} [3]. Therefore, K_{Id} should be applied to evaluate the fracture toughness of a forging die that has a small crack in the surface layer. Ductile-brittle transition temperature (Ti) of steels is dependent on the kind of steel and is in the range of 100 to 150°C for hot forging die steels. Figure 4 shows the impact fracture surface of SKT4 steel for a hammer forging die. At RT, the fracture surface consisted of a mixed mode of cleavage and intercrystalline fracture.

TABLE 1—Chemical composition and mechanical properties of tested materials.

Surface Treatment	σ_c/σ_B	N_c
Ion nitriding (500°C × 30 h)	0.79 (931.6/1176.8)	3×10^3
Ion nitriding (450°C × 30 h)	0.73 (858.1/1176.8)	5×10^3
Tufriding (570°C × 12 h)	0.63 (735.5/1176.8)	7×10^3

NOTE: σ_c = stress expected for surface hardening effect (MPa); σ_B = ultimate tensile strength of SKD62 (MPa); σ_c = number of cycles expected for surface hardening effect; N = number of cycles; c = critical.

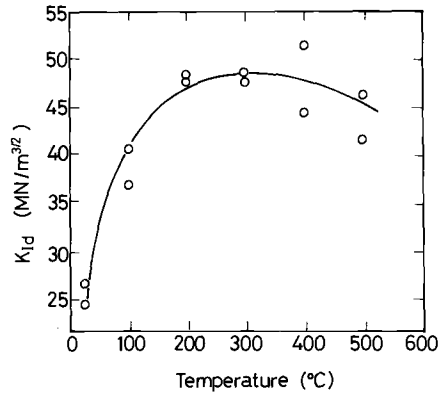


FIG. 3—Dynamic fracture toughness (K_{Id}) as a function of tested temperature, SKD62.

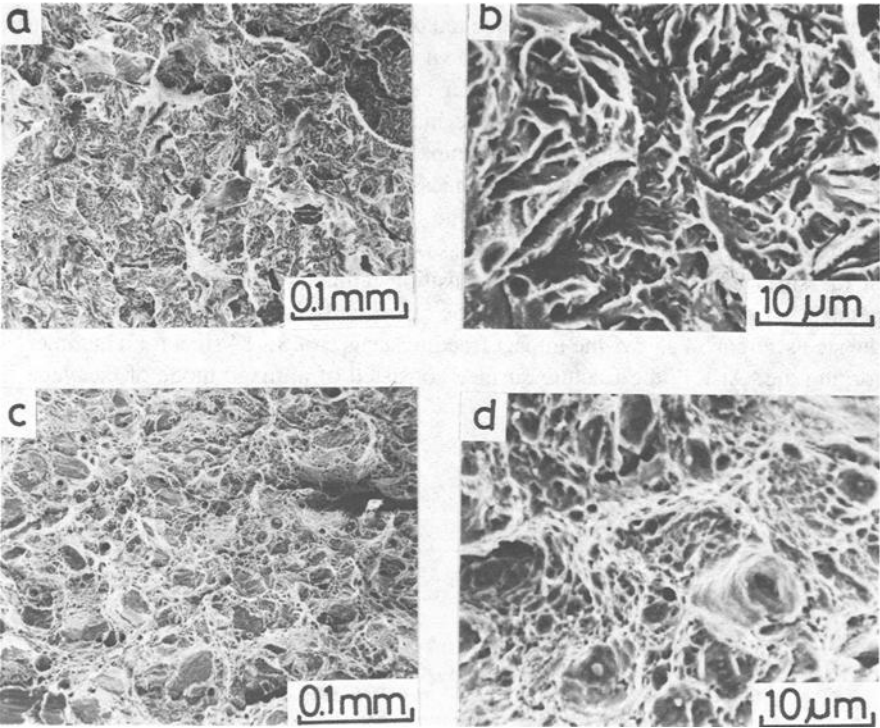


FIG. 4—Impact fracture surface, SKT4: (a) and (b) = RT; (c) and (d) = 300°C. Micrographs (b) and (d) are enlargements of (a) and (c), respectively.

Above 100°C, a dimple pattern was observed predominantly. Stretched zone also was found at the transition zone from fatigue to impact fracture surface (Fig. 5).

Relatively good correlation was found among stretched zone width, crack initiation energy, and testing temperature. Figure 6 shows K_{Id} as a function of stretched zone width.

Low-Cycle Fatigue Behavior and Fractography

As aforementioned, most of the die failure occurred at the impression corner. Therefore, it is important to decide the figure and dimension of the impression corner at the time of the die design. Surface-hardening treatments such as tuftride and ion-nitriding frequently are applied to the die surface to prevent die failure and to improve die life. Low-cycle fatigue tests were carried out by use of the

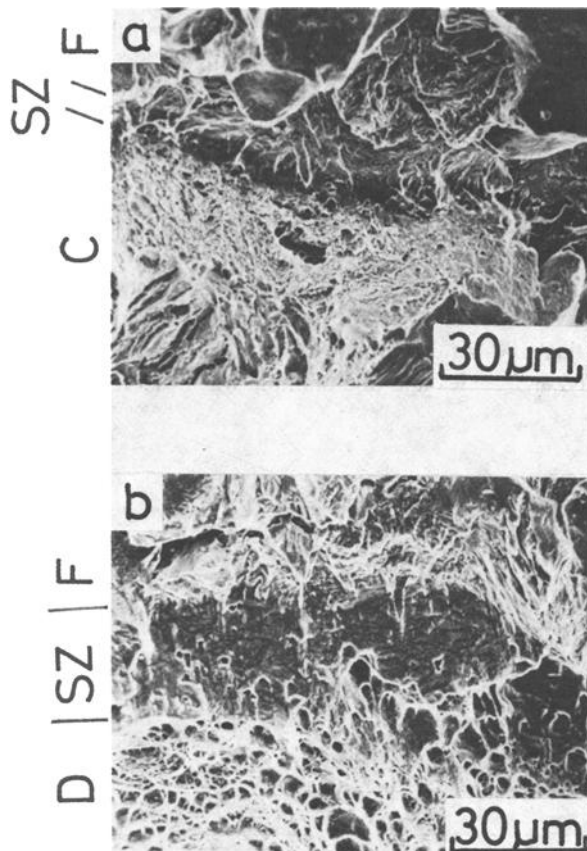


FIG. 5—Stretched zone, SKD62: (a) RT; (b) 400°C. F = fatigue; C = cleavage; D = dimple; SZ = stretched zone.

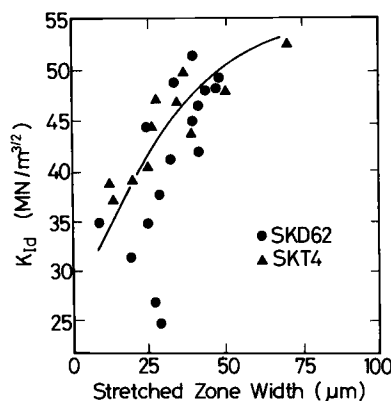


FIG. 6— K_{Id} as a function of SZW.

notched round bar specimen made of SKD62 [2] steel (Table 1) with and without surface-hardening treatment. The complete details of the experimental procedure have been described already in Ref 1. The results of low-cycle fatigue life tests are summarized in Fig. 7. The effect of the surface-hardening treatment cannot be recognized in the low-cycle range. Stress and the number of cycles expected for the surface-hardening effect are dependent on the kind of surface hardening. The number of cycles expected for the surface-hardening effect increases for ion-nitriding at 500°C, ion-nitriding at 450°C, and for tuftriding, in that order (Table 2). In the results of fracture surface observations, striation was not observed at a number of cycles lower than 10. Striation was identified at the number of cycles higher than 100. At the initiation area of fracture, the surface of the fatigue specimen failed at 7 cycles and microdimple was observed (Fig. 8). These phe-

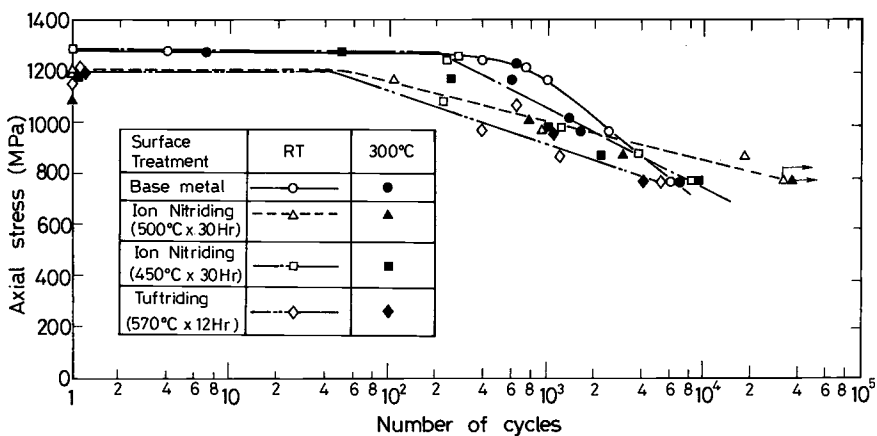


FIG. 7—Influence of surface hardening on low-cycle fatigue strength of SKD62.

TABLE 2—Surface-hardening effect on low-cycle fatigue strength of SKD62.

Materials	Chemical Composition, %								Mechanical Properties					
	C	Si	Mn	Ni	Cr	Mo	V	W	Yield Strength, MPa	Tensile Strength, MPa	Elongation, %	Reduction of Area, %	HB	Charpy 2-mm U-Notch Impact Energy, N · m
SKT4	0.51	0.27	0.65	1.45	1.99	1.36	0.16	...	1087.9	1332.9	18	9	401	49.0
SKSD62(1)	0.38	0.97	0.45	...	4.91	1.23	0.38	1.21	852.6	1283.9	11	38	401	27.4
SKSD62(2)	0.40	0.93	0.43	...	5.24	1.33	0.40	1.29	...	1176.1	376	...

NOTE: HB = brinell hardness.

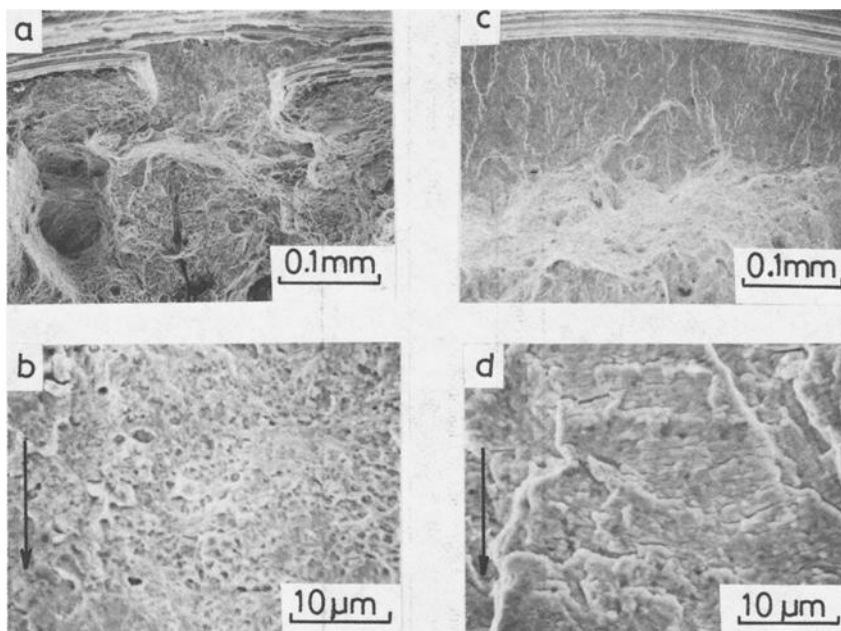


FIG. 8—Low cycle fatigue fracture surface: (a,b) axial stress ≈ 1274.9 MPa and number of cycles = 7; (c,d) axial stress = 1029.7 MPa and Number of cycles = 1.4×10^3 , (b) and (d) are enlargements of (a) and (c), respectively. Arrows show crack propagation directions.

nomena frequently are seen on the fracture surface of a low-cycle fatigue specimen. The data available for quantitative analysis of the fatigue fracture surface should be accumulated further.

Other Fracture Surface Appearances

It was reported that intercrystalline fracture predominantly appeared on thermal-shocked fracture surfaces [3]. However, little is known about thermal fatigue fracture surfaces. Fracture surface appearances of tensile and fracture toughness specimens also have been identified [4].

Quantitative Analysis by Stretched Zone Width (SZW) Measurement

As shown in Fig. 3, the highest toughness of die steel can be achieved near 300°C. Therefore, before forging, preheating is conducted to keep the die surface temperature at 300°C. However, during the hot forging operation, the die suddenly fails when the preheating of the die is insufficient. In such cases, the failure temperature was determined by the circumstances of the forging operation and the hardness distribution of the cross section of the failed die. However, if the stretched zone width should be measured, the temperature when the die fails could be determined by use of the relationship among stretched zone width,

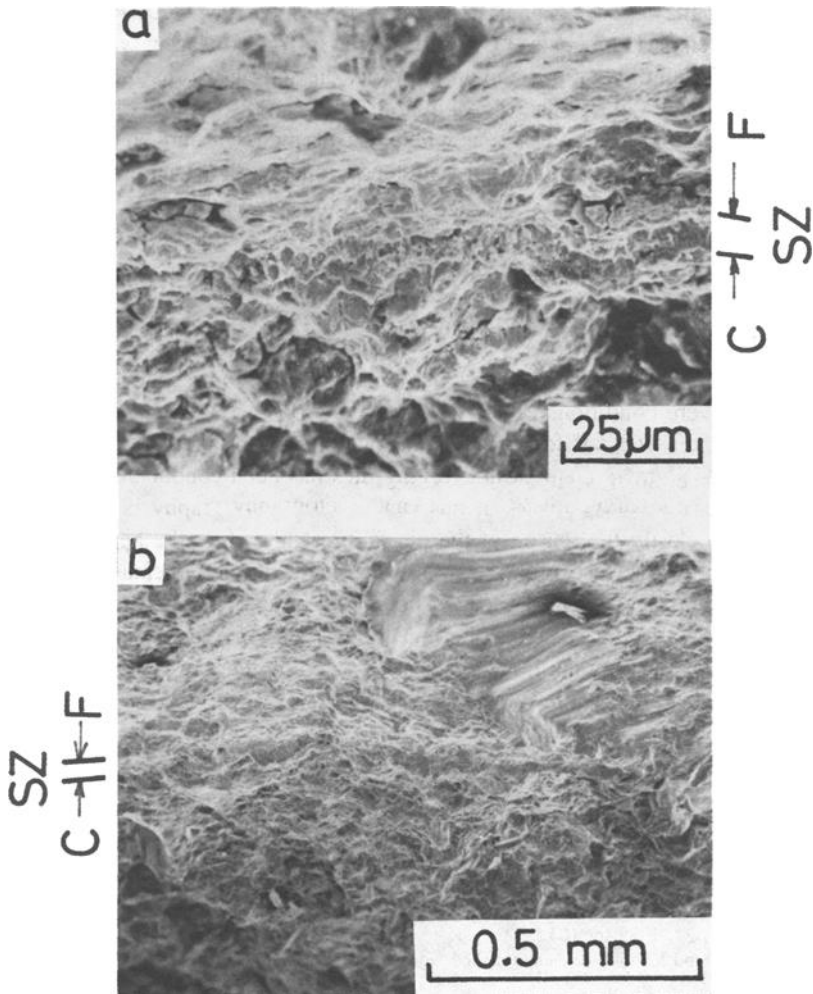


FIG. 9—Stretched zone observed on fracture surface of hot forging die: (a) connecting rod; (b) reverse gear.

dynamic fracture toughness, and temperature. Figure 9 shows the stretched zone observed on the fracture surface of the dies for connecting rod and reverse gear. The stretched zone could be identified clearly between the fatigue and the cleavage fracture surface. By use of the relationship shown in Figs. 3 and 6, dynamic fracture toughness K_{Id} and the temperature when the die fails can be determined by the following process. In the case of the connecting rod, $SZW = 12.5 \mu\text{m}$; $K_{Id} = 34.1 \text{ MN} \cdot \text{m}^{-3/2}$; and the failure temperature $\approx 55^\circ\text{C}$. In this case, preheating was insufficient, and the failure temperature was assumed to be lower than 100°C . Moreover, a crack was found on the die surface after ten forging operations.

While, in the reverse gear case, $SZW = 41 \mu\text{m}$; $K_{Id} = 47.4 \text{ MN} \cdot \text{m}^{-3/2}$; and failure temperature $= 200^\circ\text{C}$. In this case, sufficient heating was conducted before the forging operation, and an improper die setting was assumed to be the reason for the die failure. Therefore, in both cases, an assumption of temperature failure because of the stretched zone width measurement was judged to be correct. Failure temperature determination by stretched zone width measurement also was successful for flange yoke dies for hammer forging use. In this case, the stretched zone also was found, and the failure temperature was assumed to be 100°C . This was also the case in which preheating was insufficient.

Concluding Remarks

The hot forging techniques have a marked inclination to precision forging, and the more severe conditions of the forging operation are anticipated. Therefore, fracture and the wear of forging dies are overcoming problems to improve die life. So far, failure analysis of hot forging dies has been conducted by case-by-case experience. In this study, it has proved that fractography is an available technique to clarify the reason of the die failure and to find the key for die life improvement. However, information is still limited on fundamental fracture behavior and the fracture appearances of hot forging die steels. Further studies are needed, especially on wear and thermal fatigue. The prevention of die failure and the improvement of die life are possible by combining the scientific approach with accumulated experiences.

References

- [1] Ebara, R., Inoue, K., and Kubota, K., *Journal of the Society of Materials Science, Japan*, Vol. 29, 1980, p. 599.
- [2] Brown, W. F. and Srawley, J. E., *Plane Strain Crack Toughness Testing of High Strength Metallic Materials, ASTM STP 410*, 1966, p. 13.
- [3] Hirano, K., Kobayashi, H., and Nakazawa, H., *Journal of the Society of Materials Science, Japan*, Vol. 27, 1978, p. 104.
- [4] Ebara, R., and Kubota, K., unpublished work.

Author Index

A

Abe, T., 523
Albrecht, J., 178
Argo, H. C., 198
Austel, W., 385

B

Badeau, J. P., 425
Bellows, R. H., 219, 272
Bernabei, P., 275
Bertilsson, J.-E., 178
Blondeau, R. P., 367, 425
Bocquet, P. G., 87, 367
Brueggemann, S. M., 553

C

Callegari, L., 275
Cazenave, R. H., 258
Chang, H. S., 45
Chang, Y. S., 45
Cheruvu, N. S., 72, 201
Childs, W., 363, 539, 582
Curran, R. M., 9, 72, 103

D

Darden, W. S., 346
DeBadereau, A. G., 87, 425
Durginan, B., 548

E

Ebara, R., 583
Evans, J. H., 177
Ewald, J., 43, 103, 198, 214, 449

F

Finkler, H., 107

G

Gelpi, A., 328
Gensure, J. G., 553
Graham, O., 256
Grimm, W. W., 410

H

Handerhan, K., 449
Hartman, G. S., 44, 197, 217

I

Iwadate, T., 203

J

Jaffee, B., 256
Jaffee, R. I., 35, 124, 199
Javorik, L. J., 476
Juergen, E., 345

K

Kanno, N., 203
Kawaguchi, S., 203, 398
Kawai, M., 59
Kahare, A. K., 303
Kikuchi, H., 74
Kim, J. T., 45
Kim, W., 157
Kinoshita, S., 74
Kohno, M., 523

Körbe, H., 385

Koren, 154

Kramarow, N. M., 453

Krubsack, W. L., 346

Kubota, K., 583

Kuhlman, G. W., 346

L

Leone, S. G., 157

M

Mayer, K. H., 71

Melilli, A. S., 1, 157, 553

Meyer, E., 86, 103

Miyazaki, M., 59

Murphy, E. L., 573

N

Newhouse, D. L., 256

Nisbett, E. G., 1, 256, 362, 423

Nishiyama, H., 438

Novak, R. L., 196

O

Oakes, G., 154

Ohhashi, T., 203

Onodera, S., 398

P

Pishko, R., 346

Pisseloup, J., 87

Poitrault, I. S., 87, 425

Potthast, E., 107, 143

Pyo, M. R., 45

R

Rambaud, J. B., 258

Rut, T., 504

S

Saint-Ignan, J.-C., 367

Salinetti, T., 275

Sato, I., 398

Scanlan, R. M., 523

Scarlin, B., 178

Scepi, M., 275

Schönfeld, K., 143

Sikka, V. K., 303

Simkins, G. P., 256

Skamletz, T. A., 410

Stein, G., 237

Steiner, J. E., 35, 124, 141, 573

Suzuki, A., 74, 523

Suzuki, K., 398

Swaminathan, V. P., 71, 85, 124, 234

T

Tihansky, E. L., 439

Toney, S., 157

Tsukada, H., 398

W

Walker, D. N., 219

Watanabe, O., 59

Watkins, E. J., 439

Whitehouse, P. J., 540

Wiemann, W. J., 102, 141, 214, 327

Y

Yamada, M., 59

Z

Zawoysky, R. J., 219

Subject Index

A

- ABBOR computerized test system, 222, 224, 226
- Aging, 344
 in forging industry, 575–576
 isothermal, 134
 optimum temperature, 361
- Alloys (*See also* Steels)
 high-temperature, 453–454
 optimizing mechanical properties, 346–364
 processing improvements, 19–25
- Alpha-gamma transformations, 419, 421 (illus), 424
- Alumina inclusions, 283
- Aluminum
 additions, 283, 392, 395–396
 in ESR forgings, 142, 525
 fine-grained heats, 290
 grain size and, 277, 281, 424
 low, 37
 nitride, 290
 role, 42
 shear stress of, 495, 497, 498–499 (illus)
 treatment, 282–286, 290
- American Society of Mechanical Engineers (ASME)
 Code Case 1943 for Grade 91, 315
 Code Section I, 304
 Code Section III, Div. 1, 445
 Code Section VIII, 304
 Divs. 1 and 2, 296–297
- Diamond Jubilee annual meeting, 19 standards, 276
- Anchor
 body, 546–547
 connector, 541
- Annealing, post-forging, 388
- Antimony content
 embrittlement and, 165–167
 limits, 38
 role, 42
- Argon-oxygen decarburization (AOD), 36, 42, 306, 347
 AOD-vacuum arc remelting, 347, 354
- Arsenic content
 embrittlement and, 165–167
 limits, 38
 role, 42
- Association of Technical Supervisory Bodies (TUV), 413
- ASTM Committee A-1 on Steel
 Special Task Force on Large Forging, 20–21, 24
 Subcommittee A01.06, 20, 573, 576, 578, 579, 581
- ASTM Standards
 A 182–82a: 303
 A 213–83: 303
 A 262: 446
 A 293: 13, 21
 A 335–81a: 303
 A 336–83: 533
 A 370–77: 527, 576
 A 387/A 387M–83: 303
 A 388–55T: 578

ASTM Standards (*continued*)

- A 388-80: 553
- A 428-71 (1980): 554, 555 (illus)
- A 470-82: 21, 125, 204
- A 470-84: 579
- A 638-82: 533
- B 557-84: 349, 354
- E 8-85: 347
- E 45-81: 533
- E 399-83: 180, 204, 349, 527
- E 647-83: 205
- E 813-81: 180, 204, 316, 320, 527, 530

ASTM STP 463, 199

ASTM Symposia

- 68th Annual Meeting, 21
- Temper Embrittlement in Steels* (STP 407), 24

ASTM-ASME Joint Committee on the Effect of Temperature on the Properties of Metals, 12

Data and Publication Panel reports, 12-13

Austenite (*See also* Steels, austenitic)

- secondary, 148, 149
- transition, 168

B

- Bainite, 189, 201-202
- Basic-electric arc-furnace (BEF) process, 36-37, 42, 281
- Bore magnetic particle tests, 220, 224, 229
- Bore sonic tests, 224-229
 - development of, 25, 26, 222
- Bore visual tests, 220, 224, 229
- Brinell hardness, 160-162, 308, 309 (illus)
- British-Standards Institution (BSI) standards, 276, 282

C

Calcium-argon blowing (CAB) process, 418, 420 (illus), 423

Carbides, 201-202

- chromium, 72, 539
- distribution and shape, 193, 194, 195 (illus), 196, 201
- effect of tempering temperature on, 191 (illus)
- grain boundary, 531
- inclusions, 334, 337 (illus)
- titanium, 539

Carbon

- check/ladle ratio, 217
- distribution, 49 (illus), 51 (illus), 405-406
- effects on embrittlement, 430, 431 (illus), 438
- extractive replicas, 334
- in flaws, 163
- segregation, 46, 51-53, 206-207, 296, 368, 380
- segregation ratio, 52-56
- variation in, 217-218

Carbonitrides, 277

Carbon-molybdenum rotor forgings, 157-177

Central zone remelting (CZR), 125

Charpy impact energy, 133-134, 310, 311 (illus), 326-327

Charpy impact tests, 131, 207, 308-311

- of hot forging dies, 585
- of nuclear reactor shell, 382, 383 (illus)
- of superconducting magnets, 530

Charpy V notch energy values, 102

- of new ingots, 375, 377 (table)

Check analysis/ladle analysis, 217 (table)

Chlorides, 259

Chromium (*See also* Steels, Cr-Ni-Mo)

- carbides, 72, 539
- content, 145-146, 148, 153, 241, 242

Cleavage, mixed mode (*See also* Cracks; Flaws; Fractures), 585

Compression strength, 478-479, 480

Computer-controlled forging system, 459-462

preform, 469–472
 Cold expansion, 144, 250 (illus), 260, 269
 Coolant circuit (nuclear reactor), primary, 385–397
 Cooling rate, 91
 cracking during, 154
 critical, 193
 effects, 62, 66–67, 72, 93, 133, 196, 197
 FATT and, 102
 as function of forging properties, 193
 for large-diameter rotor forgings, 180
 toughness and creep strength and, 79
 Cooling transformation, continuous, 90, 111 (illus)
 Cooling treatment, step, 117–118, 134, 343
 Copper content
 control of, 141
 limits, 43–44
 Corrosion
 attack on nuclear cooling pump, 388
 behavior of 18-18-alloy, 266
 fatigue, resistance to, 243–244, 258–272
 tests, integranular, 446
 Corrosion-resistant alloys, 349–354, 359–364
 Corrosive agents, 259
 Crack initiation
 of 18-18 alloy, 266
 with start-stop cycles, 230, 231–233
 Crack propagation
 of 18-18 alloy, 266
 growth rates, 174, 210–211, 232
 rapid, 183
 resistance to in nuclear turbine forgings, 208
 from service-induced flaws, 158, 171, 173
 stable extension, 320
 transgranular, 172 (illus), 176
 Crack shrinkage, 391
 Crack size, critical, 233

Cracks, hydrogen-induced flake (*See also* Hydrogen, flake cracking), 407, 573–582
 Crank web, 511 (illus), 513, 515 (illus), 518
 Crankshafts
 connector inclination angle, 516–519
 forging operation, 506–509
 fully forged, 504–509
 long-stroke, 504–519
 Creep properties, 137–139
 ductility, 71–73, 137–138, 312
 of modified Cr-Mo forging, 313–315, 340–341
 rupture strength
 of Cr-Mo-Ni-W-V steel, 120–122
 of Cr-Mo-V steels, 108
 in HP rotor, 83, 85
 in HP-LP rotor, 59–73
 niobium and, 86
 temperature and, 78–79
 Creep rupture tests, 12
 of Cr-Mo-Ni-W-V steel, 120, 122
 of differentially heat-treated rotors, 82
 of HP-LP rotors, 62, 66, 70, 72, 73
 long-time, 142
 in retaining rings, 252
 Creep strength tests, 256
 Creep tests of saddle forging, 313–315
 Cryogenic mechanical properties, 523–539

D

DATAQ computerized boresonic system, 222, 224, 226
 Dehydrogenation, 281, 284
 Deoxidation (*See also* Sulfur, deoxidation; Vacuum carbon deoxidation), 392–396
 in electroslog refining, 442
 Deoxidizers, 283–286
 Dephosphorization, 44
 Desulfurization, 392, 394–396, 442, 446

Dies
 hot forging, 583–592
 types, 463

Discontinuities, 558–572
 sources of, 17

Disks, shrunk-on construction, 203

Dome (nuclear), cover, 399

Ductile-to-brittle transition, 148

Ductility
 of 18-18 alloy, 260
 improvement in, 21–23
 in long-time creep tests, 142

E

Edelstahlwerke Buderus AG, 410, 413

Electric Power Research Institute (EPRI)
 “Advanced Steelmaking Processes
 for Rotor Forgings,” 36
 “High Purity Steels for Utility Com-
 ponents,” 38

Palo Alto workshop, 245

San Antonio workshop, 200

steering committee meeting (1982),
 111, 121

Westinghouse Electric Corp. joint
 project, 125

Electricite de France
 research program, 262–264
 standards, 276

Electricity, cost of, 12

Electroslag remelting (ESR), 36, 42,
 108, 245
 electrodes, 440–442
 equipment, 439–440
 facility, 28
 ingot production, 442–443
 large ingot, 439–449
 in manufacture of production rings,
 267–269
 in mechanical properties testing,
 125–127, 134, 136–139, 142
 of superconducting magnets, 524, 525
 under pressure, 247, 249–250, 256

Electroslag hot topping practice, 29, 36,
 42, 125, 443

Elements, effects on “A” segregation,
 45–56

Embrittlement
 from ferrite, 246–247
 hydrogen, 243–244, 573–582
 long-term, 119
 nickel content and, 214
 reducing level of, 24–25
 relaxation, 390
 service-induced, 159
 temper, 39–40, 42
 effects, 91–93
 of HP-LP rotors, 59
 parameters influencing, 426–434
 resistance to, 343, 345
 sensitivity, 66
 sensitizing to, 39, 43
 toughness and, 168–169
 from tramp elements, 165–167
 temperature-induced, 396

Energy sources, 143

Equivalent flat bottom hole (EFBH) di-
 ameters, 554–555, 557

Erhardt process, 467

Exothermic hot topping, 36

Expansion tests, 241

F

Failure
 from flaws, 175
 of hot forging dies, 583–592
 in retaining rings, 242, 243
 in-service, 260

Fatigue (*See also* Fatigue tests), 259
 corrosion (*See* Corrosion fatigue)
 crack growth rate, 210, 211 (illus)
 low-cycle behavior, 587–590
 properties
 high-cycle and low-cycle, 135–139
 of modified Cr-Mo forgings, 341

Fatigue tests

- crack growth, 315–316
- low-cycle, 135, 205, 212 (illus), 587–588
- rotating beam high-cycle, 135
- Ferrites
 - austenetic, 253–255
 - chromium, 255
 - effect on embrittlement, 430 (table, illus)
 - proeutectoid, 168
- Ferroalloys, 247
- Ferrous oxide slag, 442–443, 446
- Finite-element method (FEM), 64, 65 (illus), 66
- Flanges, 399, 402 (illus), 404–405, 406 (illus), 408 (illus)
- Flaws (*See also* Cracks; Fractures; Inclusions)
 - critical size, 175, 231, 233
 - detectable size, 213
 - indication, 170–172
 - internal, 558–560
 - metallurgical analysis of, 157–177
 - service-induced, 158–159
 - size prediction, 163, 176, 177
- Forge material, shear resistance, 476–503
- Forge processing improvements, 19–25
- Forging
 - against rigid anvil, 497–499
 - automatic ring preform, 465–467
 - center core, 66, 69, 446–448
 - classification by process, 454, 455–456 (tables)
 - computer-controlled preform, 469–472
 - cooled down, 388
 - dies, 583–592
 - equipment, 453–475
 - of ERS ingot, 443–444
 - failure analysis, 583–592
 - force requirements, 476–503
 - hot dies, 583–592
 - isothermal and hot die, 456–462
 - of long-stroke crankshafts, 504–519
 - low-sulfur (*See* Low-sulfur melting practices)
 - machine, 501–503
 - mandrel, 543
 - nuclear reactor technology, 385–397
 - precision, 462–465, 592
 - preform, 465–467, 469–472
 - reverse extrusion, 543
 - single tool, 500 (illus), 501
 - solid, 543, 546
 - speed, 484–486, 502
 - techniques, 453–475
 - technology, 385–397
 - TR method, 504–519
 - warm die, 454
- Forging evaluation techniques
 - advances in, 25–28
- Forging presses (*See also* Forging, equipment; *specific presses*)
 - automatic cogging, 469
 - automatic preform, 469 (illus), 471 (illus)
 - high-speed energy screw-type, 473–475
- Forging Symposium in Terni, Italy, International, 386
- Forgings (*See also* Rotor forgings; Steels)
 - alloy steel
 - heat/corrosion resistant, 349–354, 359–361
 - specialty, 347, 354–358
 - stainless, 347–349, 358–359
 - cleanliness, 31
 - fabrication, 306–308
 - general industrial
 - equipment and process, 453–519
 - manufacture and application, 523–549
 - testing and assessment, 553–592
 - high-sensitivity, immersion testing of, 553–572
 - hydrogen in, 573–582
 - impression die, 454

Forgings (*continued*)

- heavy pressure vessel, 367–384, 402–409
 - modified 9Cr-1Mo steel, 303–327
 - nuclear reactor stainless steel, 439–449
 - for nuclear steam supply system components, 398–409
 - optimizing mechanical properties, 346–364
 - pressure vessel and nuclear processing, 367–449
 - seamless shell course forgings for, 275–300
 - steels for pressure retaining components, 303–364
 - sample, 66–68
 - for tension leg platform anchoring system, 540–549
 - turbine and generator
 - general retaining rings, 237–272
 - improvements in, 9–32
 - rotor assessment, 157–234
 - rotor manufacture, 59–103
 - rotor steel production processes, 35–44, 45–56
 - steels for rotors, 107–154
- Fractography, 583–585, 587–590
- Fracture appearance transition temperature (FATT), 24, 25 (illus)
- austenizing temperature and, 75, 78
 - in center core, 66, 69
 - cooling rate and, 62, 93
 - of Cr-Mo-Ni-W-V steel, 116–119
 - in generator rotors, 222, 232–233
 - grain size and, 117–118, 287, 288 (illus)
 - in high-risk rotors, 222
 - improving, 86, 98–99, 102, 395
 - impurities effect on, 94 (illus)
 - of nuclear turbine forgings, 207–208, 209 (illus)
 - shift, 142, 159
 - in tube sheet forgings, 413, 417, 418 (illus), 422–423, 438

- Fracture behavior, 585–592
- Fracture mechanics analysis, 159
 - of large generator rotor, 231–233
 - linear, 173–175
 - linear elastic, 229
 - of 3.5Ni rotor forgings, 183–187
- Fracture surface appearance, 583, 585–587
- Fracture toughness
 - of Cr-Mo-Ni-W-V steels, 121–122
 - of Cr-Mo-V steel, 134–135
 - effect of grain size on, 286–287
 - of 18-18 alloy, 164–166
 - of hot forging dies, 585–587
 - improvements in, 15, 30–31, 395
 - J-integral, 316–321
 - of 3.5Ni steel, 178–202
 - in nuclear reactors, 391, 392, 395
 - of retaining rings, 242–243, 264–266
 - specimen thickness and, 102–103
 - of superconducting magnets, 536–537, 538
 - after welding simulation, 287–290
- Fractures (*See also* Cracks; Flaws)
 - brittle, 169, 187
 - ductile dimple, 183
 - intercrystalline, 242, 585, 590
 - mixed-mode, 183, 187, 585
 - quasicleavage, 187
 - transcrystalline to intercrystalline, 242
- French laboratory Cr-Mo evaluation, 328–345
- French Nuclear Code (RCC.M), 382
- French Nuclear Program, 88
 - plants, 267
- Friction effects, 481–484, 502–503

G

- “Gatorizing” process, 457–459
- Generator (*See* Nuclear plants, generators; Retaining rings; Steam generators; Turbine-generators)

- Generator rotors, large
 - in-service inspection and evaluation, 219–234
 - service life, 219
 - tensile properties, 232
- Geothermic power stations, 143–154
- German Nuclear Committee (KTA), 391
- German specialty steel producers, 410–424
- Grain
 - austenitic growth kinetics, 286
 - coarsening, 79
 - fine-grain practice, 277, 299
 - growth, 419, 421 (illus)
 - refinement, 253, 392, 419
 - size, 321–327
 - controlling, 269, 282, 424
 - reducing, 86, 449
 - tensile properties and, 527
 - size effects, 60–61, 71, 81, 197, 288–289 (illus), 419, 525, 530–531, 536, 539
 - of FATT, 117–118
 - on toughness, 286–287

H

- Hardenability, 39–40
 - of Cr-Ni-Mo steel grade, 90
 - effect of nickel on, 75
 - effect of temperature on, 78
 - levels, 108
 - parameters influencing, 426–427, 431–434, 438
- Hardening
 - surface, 587–588, 589 (table)
 - through, 192–193
 - work, 479–480
- Hardness (*See also* Brinell hardness; Vickers hardness number)
 - of modified Cr-Mo forging, 308, 326
- Heat, geothermic, 143
- Heat-resistant alloys, 349–354, 359–364
- Heat stability test, 13
- Heat treatment (*See also* Thermal treatment)
 - of AF1410 alloy, 358
 - conditions, 62, 91
 - differential, 70, 74–86
 - for forged shells with heavy walls, 425–438
 - effect on mechanical properties, 63 (illus), 64, 68 (illus)
 - of HY80 steel alloy, 543–544, 546
 - mechanical properties and, 126–127
 - of nuclear components, 404–405
 - postweld (PWHT)
 - of anchoring system, 546
 - effects on mechanical properties, 91–93, 99 (table)
 - embrittlement due to, 95
 - final, 343
 - thermal cycle of, 89
 - quenched tempered (QT), 91, 93, 419, 423–424
 - of retaining rings, 242
 - simulation, 216
 - thick plate, 341–344
 - water-cooled tempering (WCT), 91, 93
- Heating ladle refining process (HLRP), 95, 97
- Heavy-section tube sheets, 410–424
- Heavy-wall reactor vessels (*See* Reactor vessels)
- High-sensitivity tests, 553, 560–572
- High-temperature tests, 14
- Hot tensile tests, 12
- Hot working, 269
- Hydraulic presses, 464
- Hydrogen (*See also* Embrittlement, hydrogen)
 - control, 578–579
 - determining content, 579–581, 582
 - elemental, 442
 - flake cracking, 407, 573–582
 - flaking, 558, 560, 562 (illus), 565 (illus), 566, 569, 571 (illus), 572

Hydrogen (*continued*)

- inclusions, 407
- low, 37
- role, 42
- in steel forgings, 573–582

I

Immersion tests, 553, 560–572

Impact properties

- in Cr-Mo forgings, 339
- in Cr-Mo-V steel, 129–135
- effect of impurities on, 95

Impact tests (*See also* Charpy impact tests), 14

- of Cr-Mo-Ni-W-V steel, 114–115, 120
- of Cr-Mo-V steel, 129
- on HP-LP rotors, 62

Impurities (*See* Steels, impurities)

Inclusions

- aluminum, 283
- analysis, 333–334
- content, 102
- frequency, 170
- hydrogen (*See also* Hydrogen), 407
- manganese-silicate, 175–176
- manganese-sulfide, 201–202
- nonmetallic, 169, 170–171, 172–173 (illus), 231, 292, 407, 558–560, 566
- oxide, 17, 334

Ingot

- cylindrical, 434–437
- in heavy pressure vessel forgings
 - conventional, 368
 - manufacturing, 400–402
 - mechanical properties, 407
 - new, 368–384
 - quality of, 405–408
- hollow, 291–292, 299, 371
 - chemical analysis, 378–381
 - mechanical testing, 382

- nuclear reactor shell from, 378–383, 434, 435 (illus)

large

- “A” segregation in, 45–56
- electroslag remelting, 439–449
- size and shape, 46–49
- solidification analysis, 17, 18 (illus)
- solidification shrinkage, 163–165, 175, 177

In-service inspection tests, 219, 223–234

- automated, 222
- historical development, 220–221
- of nuclear reactors, 399
- recommended procedure, 222–223
- trends, 223

Ion-nitriding, 587, 588

Isothermal aging, 134

Isothermal forging, 456–462

Isotropy, 245, 391, 418

J

Japan Steel Works

- Internal Pressure Bursting (IIB) test, 205, 210–211
- nuclear component forging processes, 399, 404 (illus)

J-integral tests, 527

K

Kerosene-and-whiting tests, 13

Kraftwerk Union (KWU), 399, 400, 410, 413

L

Ladle analysis, 217 (table)

Ladle furnaces (LF), 281

Ladle injection, 36, 42

Ladle refining furnace (LRF), 36–37, 42, 267

Ladle refining process, heating (HLRP), 431

Larson-Miller parameter (LMP) curves, 137, 138 (illus)
 Lawrence Livermore National Laboratory, 523
 Le Creusot Heavy Forge, 368–384, 426, 430, 431, 437
 Liquid melt, residual, 391
 Liquid penetrant examination, 536
 Longitudinal beam tests, 553, 558–562, 569–570
 Low-sulfur melting practices, 29, 126–127, 139–140

M

Magnetic particle tests, 13, 14
 of rotor center bore, 66
 Magnets, superconducting, 523–539
 Manganese levels
 decreasing, 37, 90
 effect on hardenability, 90, 91 (illus)
 effect on liquid density, 53–56
 embrittlement and, 429–430, 431 (illus)
 low, 44
 in retaining rings, 241, 242
 role, 38, 39–40
 Manganese-silicate inclusions, 175–176
 Manganese-sulfide inclusions, 136, 201–202
 degrading effects, 391
Manual of Open Die Forgings, 575
 Martensite
 microstructure, 343, 344
 tempered, 189, 192
 Mechanical properties (*See also under specific materials*)
 of advanced technology Cr-Mo-V forgings, 124–142
 cryogenic, 523–539
 improvement, 108
 Mechanical testing of anchor system, 544–546
 Melting media, 277

Metal Forming Institute, Poznan, 509, 519
 Microscopy (*See also* Scanning electron microscopy), 333–334
 Microstructure (*See also under specific materials*)
 effects of, 426–427
 investigations, 187–189, 190 (illus), 333–337
 Mirror fusion testing facility (MFTF-B), 523–524
 Molybdenum
 austenitic steels, 250–253
 carbides, 72
 effect on hardenability, 90, 91 (illus)
 effect on liquid density, 53–56
 Multiaxial presses, 465

N

Nickel (*See also* Steels)
 content, 145–146, 148, 153
 creep strength and, 75
 effect of addition, 60–64, 70, 72, 144
 embrittlement and, 214
 fracture toughness of, 178–202
 high, 38
 in retaining rings, 241, 242
 Niobium
 carbides, 62, 72
 creep strength and ductility and, 86
 effect of addition, 60–64, 70, 72
 inclusions, 334
 toughness and, 75
 Nitrates, 259
 Nitrogen
 as alloying element, 245–247, 249–255, 256
 inclusions, 334
 low levels, 37
 solubility in steels, 247–249
 Nondestructive tests, 220, 224, 231
 of ERS ingots, 444–445
 of superconducting magnets, 536–537

Nonmagnetic ring material (*See* Retaining rings, nonmagnetizable)

North Sea Hutton field, 540

Nuclear plants

generators, 258–272

German, 386

Obrigheim, 386

pressurized water reactor, 87–103

Stade, 386

Nuclear Regulatory Commission, 179

Nuclear steam supply system components, 398–409

Nuclear turbine forgings

fracture toughness, 208, 209–210 (illus)

integrity, 203–218

mechanical properties, 207–213

segregation in, 205–206

O

Oak Ridge National Laboratory (ORNL), 328

Offshore Structures—Det Norske Veritas 1977, Rules of Design Construction and Inspection of, 545

Oxygen

activity, 283–284

decreasing, 36–37

high, 44

Oxysulfides, 418

P

Periphery ultrasonic tests, 14, 26, 220–221, 229

Phosphorus content

chronological evolution, 97, 98 (illus)

distribution, 49 (illus)

effect on carbon segregation, 56

effect on ductility, 137

embrittlement and, 119, 429, 431

in flaws, 163

low, 21, 22 (table), 36–37, 95, 137
role, 40

segregation, 217–218

Pitting, 262

Porosity, 17

micro, 292

shrinkage, 231

in weldings, 256

Power generating industry, 237–257

corrosion resistance in, 258–272

heavy-section tube sheet technology, 410–424

Pressure vessels (*See* Reactor vessels)

Proof load tests, 537–538

Pump casing, integral forged, 385–397

Q

Quenching, 388

air and oil, 109, 122

liquid-medium, 160

R

Reactor vessels

boiling water reactor pressure vessel (BWRPV), 399

fabrication problems, 292–298, 299

forging processing and nuclear application, 367–449

heavy-wall, 275–300

new ingot applications, 367–384

pressurized water reactor pressure vessel (PWRPV), 399

specifications, 276–290

Reactors

components, 425

light water (LWR), 399

liquid metal fast breeder (LMFBR), 328–329, 340, 344

petrochemical, 425

pressurized heavy water (PHWR) vessel, 399, 400

primary coolant circuit, 385–397

steam supply system components, 398–409

“Recommended Practices for Ultrasonic Inspection of Large Rotor Forgings,” 20–21

Refining processes, secondary, 36

removal of sulfur in, 40

Retaining rings

- cold-expanded, 244
- corrosion-resistant, 258–272
- function and demands, 238–240
- future trends in, 271–272
- manufacture of, 267–269
- materials for, 237–257
- mechanical properties, 242–243, 269–271
- nonmagnetizable, 237–257, 259–260
- resistance to corrosion and embrittlement, 243–244
- service conditions, 259

Ring preform forging presses, 466

Rotor failure, technological impact, 35–36

Rotor forgings

- evaluation of, 80–84
- fracture toughness, 178–202
- high-pressure–low-pressure, integral, 59–73
- applications, 69–70
- high-temperature characteristics, 13
- manufacture, 79–80
- mechanical properties, 13
- metallurgical analysis of flaws in, 157–177
- microstructural investigations, 179, 187–189, 190 (illus)
- modern technology, 14–17
- 3.5Ni steel, 178–202
- simulated large diameters, 179–180
- specification trends, 35–44

Rotor steels, high purity, 37–38

Rupture ductility, trends in, 27 (illus)

Rupture strength, high-temperature trends, 27 (illus)

S

Scanning electron microscopy, 160

Segregation

- “A,” 45–56
- cleanliness, 129
- degrading effects of, 391
- high manganese-sulfide inclusions in, 125
- carbon (*See* Carbon, segregation)
- dendritic, 189
- in ERS ingots, 448
- macrosegregation, 291, 370–371, 373
- microsegregation, 392
- negative and positive, 51–52, 292, 380
- in nuclear turbine forgings, 205–206, 207 (illus)
- phosphorus, 217–218
- ratio, 48 (illus), 49, 50 (illus)
- sulfur, 127, 164, 217–218

Shear

- bidirectional, 495, 499–501
- distribution, 387, 490–494
- effect, 486–495
- failure, 495
- resistance, 476–503
- stresses, 488–494
- inside distribution of, 495–497

Shear-wave inspections, 553–555, 569–570

Shells

- flanges, 402, 404, 406 (illus), 408 (illus)
- forged, 425–438
- torus and, 399

Silicon

- decreasing, 37, 75
- deoxidation (SD), 23, 49–52, 139, 392, 395–396, 429–430
- effect on ductility, 137
- effect on embrittlement, 429
- effect on liquid density, 53–56

Silicon (*continued*)

- effect on tensile properties, 93–94, 296
- killing, 282–286
- low, 38
- modified alloy, 354
- role, 41

Simulation technique, 179–180, 194–195, 198–202

Solidification

- conditions, 368
- horizontal-oriented (*See* Solidification, LSD)
- of ingot, 46, 291
- liquid density change during, 53–56
- LSD (*Lingot a Solidification Dirigee*), 369–375, 384, 434–437
- shrinkage, 163–165, 175, 177
- vertical and horizontal-oriented, 369

Solution treatment, 269

Sonic tests (*See* Ultrasonic tests)

Spheroidization, 202

Spring collet, 542–546

Steam-turbine rating trends, 11 (illus)

Steel production (*See* Steelmaking process)

Steelmaking process

- advanced technology, 35–44
- effects on “A” segregation, 45–56
- effects on rotor specification trends, 35–44
- for heavy-wall reactor vessels, 276–290
- improvements, 17–19
- new processes, 28–31

Steels (*See also* Alloys; Forgings; *specific materials*)

- A286, 349–365
 - cryogenic mechanical properties, 523–539
- A-508 Class 2, 386, 390
- A-508 Class 3, 282–283, 388, 391, 414–415 (illus), 423–424
- acid open hearth (AOH), 13

AISI 329, 253–255

austenitic, 245–247, 250–255

austenitic Cr-Ni, 144, 388

basic open hearth (BOH), 13

bidirectional shear, 499–501

carbon, 14

segregation of, 51–56

carbon-molybdenum, 157–177

macrostructure and microstructure, 321–326

mechanical properties, 308–326

modified, 303–327

cleanliness, 35, 44, 75, 283, 296

Cr-Mn, 241–243

Cr-Mn-N, 241–243

Cr-Mo, modified

chemical composition, 329

evaluation by French laboratories, 328–345

hardness, 338–339

mechanical properties, 339–341

microstructure, 333–337

transformation points, 329–333

Cr-Mo-Ni-W-V, 107–123

Cr-Mo-V, 14, 28, 31

analysis, 24

compositions, 15–16

in differentially heat-treated forgings, 74–86

ductility, 21–23

mechanical properties, 124–142

nickel/niobium effects on, 62–64

toughness, 59

Cr-Ni-Mo

chemical composition, 150, 153

mechanical properties, 98, 99 (table)

soft-martensitic stainless, 143–154

specification requirements, 89

tensile properties, 152, 154

electric furnace (EF), 13

ferritic-austenitic, 253–255

ferritic chromium, 255

fracture toughness, 178–202

- heat/corrosion-resistant, 349–354, 359–361
- high-sensitivity, immersion, ultrasonic testing, 553–572
- high-temperature, 107, 119–122
- hot low-carbon, 499–501
- HY80, 543–549
- hydrogen effects on (*See also* Hydrogen), 573–582
- impurity levels, 36–37, 195, 375
 - effects of, 87–103
- Inconel 625, 349, 360
- mechanical property improvement, 108, 346–364
- metallurgical analysis of flaws, 157–177
- Mn-Cr-N (18-18 alloy), 259–272
 - corrosion behavior, 266, 267 (illus)
 - fracture toughness, 264–266
 - mechanical properties, 264
- Mn-Mo-Ni, 388, 391, 392
 - in nuclear power stations, 418–419, 423
- 0.5Mo-2.5Ni-V, 13
- 3.5Ni, 178–202
- Ni-Cr-Mo-V
 - creep rupture strength and temper embrittlement, 59
 - segregation in, 217
 - sensitizing to temper embrittlement, 39
 - toughness, 40–42, 214–215
- Ni-Mo-Cr, 390
- Ni-Mo-V, 13, 14, 29–30
 - analysis, 24
 - fracture toughness, 23
 - metallurgical analysis of flaws, 157–177
- nitrogen as alloying agent, 245–247, 249–255, 256
- nitrogen solubility in steels, 247–249
- nonmagnetizable, 240–243
 - for nuclear steam supply system components, 398–409
- optimization of grade, 87–103
- optimization of mechanical properties, 346–364
- quality, 35
- quenched and tempered, 189, 192–196
- retaining-ring, 245, 249–255
- SA 336 F22 grade, 373–377
 - chemical composition, 427–431
 - heat treatment, 425–438
 - microstructure, 426–427
- specialty, 347, 354–358
- stainless, 347–349, 358–359
- Type 304 stainless, 304, 439–449
 - cryogenic properties, 523–539
- Strain rate, 516–519
- Stress (*See also* Shear, stresses)
 - corrosion (*See also* Stress corrosion cracking), 259
 - flaking and, 576
 - in-service, 259, 542
 - relieving, 269, 390, 548, 575
 - residual, 83–84, 85
 - tangential, 231
 - thermal (*See also* Thermal cracking), 170, 173
 - transformation, 154
 - true, 478, 479 (illus), 501
- Stress corrosion cracking, 30, 154
 - of disks, 203
 - resistance to, 241, 243–244
- Stress corrosion tests, 260
- Stress intensity factor, 174
- Stress rupture, carbon-molybdenum rotor, 169–170, 176
- Stretched zone width (SZW) measurement, 590–592
- Sulfides
 - critical concentrations, 418
 - inclusions, 136
 - linear, 17

Sulfur content

chronological evaluation, 97, 98 (illus)

distribution, 448

effect on fatigue, 136

effect on liquid density, 55, 56

effect on mechanical properties, 126–127, 136, 139–140

in flaws, 163

grain growth and, 421 (illus), 423

low, 21, 22 (table), 36–37, 38, 95

print, 163, 167

reduction in, 392, 395–396

role, 40–41

segregation, 127, 154, 217–218

Superalloys, 238

Support struts fabrication, 523–539

T

Technischer Überwachungs-Verein (TUV) standards, 276

Temperature (*See also* Stress, thermal)

austenizing, 62–63, 64, 66, 67 (illus), 71–73

effect on FATT, 75, 78

effect on hardenability, 431–434, 438

effect, 480–481

on turbine rotor, 12–13, 75, 78–79, 108–122

failure, 590–592

hardening, 146

strength dependence on, 182

tempering, 146–148, 194, 196, 354, 356

transformation, 145, 149, 192–193

in modified Cr-Mo forgings, 329–333

suppression, 144

transition, 168

Tempering study, 347, 348 (table), 354

Tensile properties

in Cr-Mo forgings, 339–340

in Cr-Mo-V steel, 129–135

effect of silicon on, 93, 94 (illus), 296

of modified Cr-Mo forging, 311–313

Tensile strength

trends in, 27 (illus)

ultimate, 94 (illus), 271, 287, 296, 485

Tensile tests, 14

Tension leg platform anchoring system, 540–549

Tension testing standard, 576

Tension tests, 13

of Cr-Mo-Ni-W-V steel, 114

of Cr-Mo-V steel, 129, 154

of HP-LP rotors, 62

of 3.5Ni steel, 181–182

Thermal cracking (flaking) (*See also* Hydrogen, flaking), 573, 576

Thermal shock, 590

Thermal stability, 83, 85

Thermal treatment (*See also* Heat treatment), 347, 443–444

Thermomechanical processing, 346–364

Thickness and fracture toughness, 102–103

Tin content

embrittlement and, 119, 165–167

limits, 38

role, 42

Titanium, 525

carbide, 539

Toughness (*See also* Fracture toughness)

of HP-LP rotors, 59–73

of HY80 alloy, 547–548

properties, 108–109

TR method, 504–519

Trace elements (*See also* Tramp elements; *specific elements*)

embrittlement and, 119

reduction, 97, 108

Tramp elements (*See also specific elements*)

- role of, 42
- in temper embrittlement, 165–167
- Transformation structure, 413, 417–419, 424
- Trepanning equipment, center core, 25
- Tube sheets, heavy-section, 410–424
- Tubes, heavy-walled, 467–469
- Tuftsride, 587–588
- Turbine rotors
 - Cr-Mo-V forgings, 124–142, 157–177
 - development programs, 14–15
 - differentially heat-treated, 74–86
 - failures, 14
 - mechanics of, 16–17
 - full-integral, low-pressure forgings, 203–218
 - high-pressure, 107–123, 165–170
 - analysis for flaw indication, 170–172
 - fracture mechanics of flaws, 173–175
 - mechanical properties, 166 (table), 167–168
 - low-pressure, 163–165
 - mechanical properties, 166 (table)
 - manufacture of, 149–153
 - metallurgical analysis of flaws in forgings, 157–177
 - soft-martensitic stainless Cr-Ni-Mo steel, 143–154
 - welded polyblock, 87–103
- Turbine-generators
 - history of, 9–12
 - modern steam, 9–32
 - in power generation, 238

U

- Ultrasonic tests, 20–21 (*See also* Bore sonic tests; Periphery ultrasonic tests)
 - of bore surface indications, 160, 162–163

- of Cr-Mo-Ni-W-V steel, 11
- detecting internal defects, 577–578
- of ERS ingot forgings, 445, 447 (table), 448, 449
- for flaw size, 160, 162–165, 171–172, 176, 177
- high-sensitivity, immersion, 553–572
- of large generator rotors, 229–230
- of near-bore zone, 158
- of rotor center bore, 66, 160
- of steel forgings, 553–572
- of superconducting magnets, 536–537

V

- Vacuum arc degassing (VAD), 373
- Vacuum arc remelt (VAR), 347
 - furnace, 28
- Vacuum carbon deoxidation (VCD), 23–24, 41–42, 125
 - effect on segregation, 49–56, 72
 - of forged reactor pump casing, 392–396
 - hardenability and, 86
 - impurities and, 93, 95
 - reduction of, 72
 - in mechanical properties testing, 125–140
 - in reactor forgings, 281–290, 299
 - temper embrittlement and, 75, 86
 - toughness and, 62
- Vacuum casting, 575–576
- Vacuum induction melted (VIM)–vacuum arch remelting, 347, 349
- Vacuum lift process, 578–579, 582
- Vacuum stream degassing (VSD), 37, 42, 281, 299
- Vanadium
 - carbides, 72
 - effect on carbon segregation, 46, 56
 - in grain size control, 424
- Vickers hardness number, 546
- Voids, 164

Voids (*continued*)

irregularly shaped, 177
microshrinkage, 292

W

Water (as corrosive), 259
Welded polyblock turbine rotors,
87–103, 198
Welding problems, 256
Weldment examination, 547, 548

Y

Yield strength
effect, 189, 164, 196
of 18-18 alloy, 260, 261 (illus)
ratio to ultimate tensile strength, 271
of superconducting magnets, 536–537
in tube sheets, 413–417

Z

Zirconium, 283

ISBN 0-8031-0465-0